Εθνικό & Καποδιστριακό Πανεπιστήμιο Αθηνών
Τμήμα Βιολογίας
Τομέας Βοτανικής

Μελέτη των ρυθμιστικών μηχανισμών στόχευσης και ενδοκύτωσης διαμεμβρανικών μεταφορέων πουρινών σε ενα πρότυπο γενετικό σύστημα

Διδακτορική Διατριβή

Γεωργία-Μαρία Καραχάλιου
Βιολόγος

Αθήνα, 2014

Συμβουλευτική Επιτροπή:

Γ. Διαλλινάς, Αναπληρωτής Καθηγητής Πανεπ. Αθηνών (Επιβλέπων)

Σ. Ευθυμιόπουλος, Αναπληρωτής Καθηγητής Πανεπ. Αθηνών

C. Scazzocchio, Καθηγητής Imperial College

Εξεταστική Επιτροπή:

C. Scazzocchio, Καθηγητής Imperial College

Χ. Δελιδάκης, Καθηγητής Πανεπιστήμιο Κρήτης

Γ. Διαλλινάς, Αναπληρωτής Καθηγητής Πανεπ. Αθηνών

Σ. Ευθυμιόπουλος, Αναπληρωτής Καθηγητής Πανεπ. Αθηνών

Δ. Χατζηνικολάου, Επίκουρος Καθηγητής Πανεπ. Αθηνών

Δ.Ι. Στραβοπόδης, Επίκουρος Καθηγητής Πανεπ. Αθηνών

Ι.Π. Τρουγκάκος, Επίκουρος Καθηγητής Πανεπ. Αθηνών

National & Kapodistrian
University of Athens
Faculty of Biology
Department of Botany

Study of regulatory mechanisms of targeting and endocytosis of membrane purine transporters in a model genetic system

Doctoral Dissertation

Georgia-Maria Karachaliou

Biologist

Athens, 2014

Advisory committee:

G. Diallinas, Associate Professor University of Athens (Supervisor)

S. Efthimiopoulos, Associate Professor University of Athens

C. Scazzocchio, Professor Imperial College

Examining committee:

C. Scazzocchio, Professor Imperial College

C. Delidakis, Professor University of Crete

G. Diallinas, Associate Professor University of Athens

S. Efthimiopoulos, Associate Professor University of Athens

D. Hatzinikolaou, Assistant Professor University of Athens

D.J. Stravopodis, Assistant Professor University of Athens

I.P. Trougakos, Assistant Professor University of Athens

This dissertation is dedicated to my wonderful parents,
Dimitris & Elli

Preface

The experimental work for this dissertation was conducted under the supervision of Assoc. Prof. George Diallinas in the *Aspergillus* Genetics and Molecular Biology laboratory of the Faculty of Biology, University of Athens. It consists of three independent parts, the common denominator of which are the use of UapA as a prototype cargo and the principal aim to unravel its endocytic and exocytic processes. The work presented herein reflects the joint effort of the author and other members of the *Aspergillus* Genetics and Molecular Biology group, the individual projects of whom are also related to the elucidation of the mechanisms of transporter intracellular trafficking. More specifically, experiments presented in Chapter 3 were performed in collaboration with Vassilis Bitsikas (then an undergraduate student), Christos Gournas (then an PhD student) and George Diallinas, while experiments presented in Chapter 4 were performed in collaboration with Dr. Sotiris Amillis, Minoas Evangelinos (then an undergraduate student), Alexandros Kokotos (then an undergraduate student), Vassilis Yalelis (then an undergraduate student) and George Diallinas. The precise contribution of each partner will be described in detail in the corresponding chapters. Experiments in Chapter 5 were exclusively performed by the author. The experimental work of the author demonstrated herein is a major part of the results obtained during her post-graduate academic years. Other projects that have been undertaken by the author during this period, and not pertaining directly to the thesis subject, are largely represented in the attached peer-reviewed publications in the appendix of this manuscript.

Acknowledgements

This dissertation has been a unique and life-changing experience. Despite being a personal challenge, a number of people have made a significant contribution in bringing it to completion. Therefore, I seize this opportunity to acknowledge the people who have supported me through all these years.

First and foremost, I would like to express my gratitude to my supervisor Assoc. Prof. George Diallinas, who introduced me to the world of science. With his enthusiasm and passion for research he established a stimulating working environment. Open-minded and promoting creativity, he was always willing to discuss about thoughts and ideas, no matter how basic or crazy they might have been. I wish to thank him for all the inspiring and intriguing conversations that for me were the driving force to evolve scientifically, for the valuable suggestions and his continuous guidance and supervision. His ingenious approaches to solve scientific problems compensated for the lack of resources and equipment and are a paradigm of how knowledge and critical spirit can walk you through difficulties. I also want to express my appreciation to him for giving me the opportunity to live unforgettable experiences, for educating me not only about science, but also about life and for teaching me how to «tell stories».

I wish to express my appreciation to Prof. Claudio Scazzocchio, my «scientific grandpa», for being one of the most inspiring people I have ever met. Not only does he possess deep knowledge, but he also has an impressive ability and eagerness to share it. I particularly thank him for his valuable advice and for constructive comments on this manuscript • I would like to thank Assoc. Professor Spiros Efthimiopoulos for his positive attitude and kind assistance whenever it was asked • I specially thank Assist. Prof. Dimitris Hatzinikolaou for his personal concern and for always being available and giving me constructive scientific advice • I wish to thank Prof. Christos Delidakis, Assist. Prof. Dimitris Stravopodis and Assist. Prof. Ioannis Trougakos for kindly agreeing to participate in my examining committee.

I wish to acknowledge Dr Sotiris Amillis, Vassilis Bitsikas, Minoas Evangelinos, Alexandros Kokotos, Dr Christos Gournas and Vassilis Yalelis for our close and fruitful collaboration in a major part of this work. I particularly want to thank Sotiris for his guidance, intellectual support and sharing of ideas • I would specially like to express my appreciation to Maria Galinou, a dearest friend, for her

continuous support, encouragement and concern • I wish to thank Fivos Borbolis and Katerina Galanopoulou for sharing ideas and collaborating in other projects of our group at my very early days in the lab and at the very end of my dissertation, respectively • I am also thankful to Aimilia Krypotou and older lab members Dr Vasso Kosti, Joana Sa Pessoa, Andreas Pavlidis, Eleni Fotinou, Dr Anna Vlanti, Dr Ioannis Papageorgiou and Dr Areti Pantazopoulou for engaging discussions, sharing their own experiences and kindly assisting me in many ways • Special thanks to Dr George Zacharioudakis for all the inspiring scientific conversations that made me think outside the box.

I would like to thank other members of the Department of Botany, Pantelis Livanos, Andreas Andreou, Dr Panayota Stathopoulou, Dr Stathis Katsifas and Dr Alexandros Savvidis for their kind support and generosity.

I am indebted to Prof. Margarida Casal for giving me the opportunity to elaborate part of this work in her lab and making me feel Braga was my home. I consider myself very lucky for having worked in such an inspiring environment and having collaborated with so many beautiful people • Special thanks to all my lab colleagues there for their warm welcome in the lab and in their lives.

I owe special thanks to my dear friend Asjad Basheer for always having my back, providing me with all the papers I didn't have access to and most of all for being very close to me, even though very far away • A special reference to all my friends for their constant encouragement and understanding.

I am most grateful to Thanos Katsikas, for his infinite patience and for all the emotional support and caring he provided. His faith, optimism and humour have comforted me more times than I can recall.

I cannot finish without saying how grateful I am to my parents; for their love, their encouragement and for always inspiring me to do my best in all matters of life. Without their continuous support at every possible level, this work would not have been completed. Therefore, I dedicate this dissertation to them with all my heart.

«Instruction does much, but encouragement everything»
Johann Wolfgang von Goethe, Letter to A. F. Oeser (9 November 1768)
In Early and miscellaneous letters of J. W. Goethe, including letters to his mother.
With notes and a short biography (1884) George Bell & Sons, London. pp 26-28

Περίληψη

Οι ευκαρυωτικοί διαμεμβρανικοί μεταφορείς ανταποκρίνονται σε περιβαλλοντικά και αναπτυξιακά σινιάλα τόσο στο μεταγραφικό όσο και στο μετα-μεταφραστικό επίπεδο. Η έκφραση των μεταφορέων ρυθμίζεται αυστηρά με την ταχεία *de novo* σύνθεση και στόχευση τους στη πλασματική μεμβράνη, αλλά και την ακόμη πιο ταχεία απομάκρυνσή τους απο αυτήν μέσω της διαδικασίας της ενδοκύτωσης, ως απόκριση στην παρουσία ιόντων αμμωνίου ή περίσσειας υποστρώματος. Ο εκτενώς μελετημένος μεταφορέας ουρικού οξέος-ξανθίνης UapA του *Aspergillus nidulans* χρησιμοποιήθηκε για τη διερεύνηση τριών βασικών ερωτημάτων που σχετίζονται με τους μηχανισμούς που διέπουν την ενδοκυτταρική διακίνηση των μεταφορέων. Συγκεκριμένα, μελετήθηκαν οι συνέπειες του υπερτονικού στρες στην φυσιολογία των μυκήτων και την ενδοκύτωση των μεταφορέων τους, οι μηχανισμοί που ρυθμίζουν την ουβικουιτινίωση των μεταφορέων με σκοπό την απομάκρυνση τους από την πλασματική μεμβράνη και την καταστροφή τους στα χυμοτόπια, και ο ρόλος του ολιγομερισμού στην διακίνηση των μεταφορέων προς και από την πλασματική μεμβράνη.

Χρησιμοποιώντας στελέχη του *A. nidulans* που εκφράζουν διαμεμβρανικούς μεταφορείς σημασμένους με την πράσινη φθορίζουσα πρωτεΐνη (GFP), μελετήσαμε (σε συνεργασία με τους Β. Μπίτσικα, Χ. Γουρνά και Γ. Διαλλινά) την άμεση εμφάνιση στατικών φθοριζουσών κηλίδων στο επίπεδο της πλασματικής τους μεμβράνης, μετά από έκθεση σε υπερτονικές συνθήκες. Οι φθορίζουσες κηλίδες που παρατηρήθηκαν δεν αντιστοιχούν σε μικροπεριοχές της μεμβράνης ειδικές για μεταφορείς, αλλά αντικατοπτρίζουν ένα μάλλον γενικό φαινόμενο που σχετίζεται με την αναδιοργάνωση της μεμβράνης. Αυτό φάνηκε από τον συνεντοπισμό τους με άλλα μόρια που σχετίζονται με τη πλασματική μεμβράνη, όπως το πεπτίδιο ομόλογο της πλεξτρίνης (PH) και η t-SNARE SsoA, ή με λιπόφιλους δείκτες, όπως η FM4-64 και η φιλιπίνη. Επιπλέον, οι κηλίδες αυτές δεν εμφανίζουν χαρακτηριστικά γνωρίσματα λιπιδικών σχεδίων ή άλλων μεμβρανικών μικροπεριοχών. Εικόνες από συνεστιακό μικροσκόπιο που έχουν επεξεργαστεί με αλγόριθμους απο-αλληλεπικάλυψης (deconvolution) δείχνουν ότι οι φθορίζουσες αυτές κηλίδες αντιστοιχούν σε εκτεταμένες εγκολπώσεις της μεμβράνης. Οι μεταφορείς παραμένουν πλήρως λειτουργικοί κατά τη διάρκεια του φαινόμενου της εντοπισμένης πλασμόλυσης. Η εμφάνιση αυτών των εγκολπώσεων συνοδεύεται

εντούτοις από μειωμένο ρυθμό ανάπτυξης και πλήρη παρεμπόδιση τόσο της ενδοκύτωσης των μεταφορέων μέσω κλαθρίνης, όσο και της ενδοκύτωσης ρευστής φάσης της FM4-64. Τα παραπάνω φαινόμενα είναι παροδικά και άμεσα αναστρέψιμα μετά την απομάκρυνση από το υπερτονικό περιβάλλον, ενώ εξαρτώνται άμεσα από τη συγκέντρωση των υπερτονικών διαλυμάτων που έχουν χρησιμοποιηθεί. Το υπερτονικό στρες δεν επηρέασε την τοπολογία πρώιμων (SlaB) και όψιμων (AbpA) ενδοκυτικών παραγόντων, αλλά τροποποίησε σε μεγάλο βαθμό την τοπολογία της τροπομυοσίνης, υποδεικνύοντας ότι η παρεμπόδιση της ενδοκύτωσης των μεταφορέων και των λιπόφιλων χρωστικών γίνεται έμμεσα, μέσω δυναμικής τροποποίησης της ακτίνης. Παράλληλα, η δράση της λατρουνκουλίνης Β στην ενδοκύτωση, ενός παράγοντα αποπολυμερισμού της ακτίνης, ενίσχυσε περαιτέρω τις παραπάνω παρατηρήσεις. Παρόμοια φαινόμενα παρατηρήθηκαν και στον *Saccharomyces cerevisiae*, γεγονός που υποδεικνύει ότι οι ασκομύκητες αποκρίνονται στις υπερτονικές συνθήκες χρησιμοποιώντας παρόμοιους μηχανισμούς.

Προκειμένου να διαλευκανθούν οι μηχανισμοί που ρυθμίζουν την ουβικουιτινίωση των μεταφορέων και την απομάκρυνσή τους από τη μεμβράνη, μελετήσαμε (σε συνεργασία με τους Σ. Αμίλλη, Μ. Ευαγγελινό, Α. Κοκοτό, Β. Γιαλελή και Γ. Διαλλινά) το ρόλο όλων των πρωτεϊνών που ομοιάζουν με αρρεστίνες του *Aspergillus nidulans*, σχετικά με την ανάπτυξη, τη μορφολογία, την ευαισθησία του οργανισμού σε φάρμακα, και κυρίως την ενδοκύτωση του μεταφορέα UapA. Μία μόνο αρρεστίνη, η ArtA, βρέθηκε να είναι απαραίτητη για την εξαρτώμενη από τη HulA^{Rsp5} ουβικουιτινίωση και ενδοκύτωση του UapA, ως απόκριση στην παρουσία αμμωνιακών ιόντων ή υποστρωμάτων. Περαιτέρω γενετική ανάλυση έδειξε ότι τα κατάλοιπα 545-563 του καρβοξυτελικού άκρου του UapA, που περιλαμβάνουν και ένα σημαντικό δισόξινο μοτίβο, είναι απαραίτητα για την ενδοκύτωσή του, γεγονός που υποδεικνύει ότι αυτή ενδεχομένως είναι η περιοχή αλληλεπίδρασης της αρρεστίνης και του μεταφορέα. Επιπλέον, τα PPXY μοτίβα του ArtA είναι απαραίτητα και επαρκή για την ουβικουιτινίωση και την ενδοκύτωση του UapA. Η δράση της ArtA εντοπίζεται πριν από αυτήν του όψιμου ενδοκυτικού παράγοντα SagA^{End3}, υποδεικνύοντας ότι η ουβικουιτινίωση του UapA λαμβάνει χώρα στην πλασματική μεμβράνη και όχι στα ενδοσώματα. Η ArtA ουβικουιτινιώνεται επίσης από τη HulA στη λυσίνη 343 και αυτή η τροποποίηση είναι σημαντική για την ουβικουιτινίωση και την ενδοκύτωση του UapA. Η ArtA

είναι απαραίτητη για την ενδοκύτωση και άλλων μεταφορέων ειδικών για πουρίνες (AzgA) και L-προλίνη (PrnB), αλλά όχι για το μεταφορέα ασπαρτικού/γλουταμικού (AgtA). Είναι αξιοσημείωτο ότι τα δεδομένα που έχουμε στη διάθεσή μας υποδεικνύουν ότι το ενδοκυτικό μονοπάτι που επάγεται από την παρουσία ιόντων αμμωνίου είναι διαφορετικό από αυτό που ακολουθείται υπό την παρουσία περίσσειας υποστρώματος. Το δεύτερο μονοπάτι, μάλιστα, φαίνεται να εξαρτάται άμεσα από τις δομικές αλλαγές που υφίσταται το μόριο του UapA κατά την κατάλυση της μεταφοράς.

Τα παραπάνω συμφωνούν με προηγούμενες παρατηρήσεις που έδειξαν ότι η ενδοκύτωση που επάγεται από την παρουσία περίσσειας υποστρώματος λαμβάνει χώρα μόνο εφόσον τα μόρια του μεταφορέα είναι λειτουργικά. Εντούτοις, μεταλλαγμένες ανενεργές μορφές του UapA μπορούν να ενδοκυτωθούν *in trans* όταν εκφράζονται παράλληλα με λειτουργικές μορφές του μεταφορέα στο ίδιο στέλεχος, το οποίο αποτελεί μια ένδειξη ότι ο UapA ολιγομερίζεται. Ο ολιγομερισμός του UapA επιβεβαιώθηκε χρησιμοποιώντας δύο ξεχωριστές προσεγγίσεις: την *in vivo* διμοριακή ανασύσταση φθορισμού (BiFC) και την παράλληλη ανοσοκατακρήμνιση διαφορικά σημασμένων UapA μορίων (pull-down assay). Επιπλέον, γενετικά δεδομένα που δείχνουν αλληλοεξαρτώμενη δράση ανενεργών UapA μορίων στην ενεργότητα μεταφορέων αγρίου τύπου, συμφωνούν με την ιδέα του ολιγομερισμού. Τα ολιγομερή του UapA φαίνεται να σχηματίζονται πρώτα στο ενδοπλασματικό δίκτυο (ΕΔ) και παραμένουν σταθερά και λειτουργικά στην πλασματική μεμβράνη. Η χρήση μεταλλαγμένων μορφών του UapA που παραμένουν στο ΕΔ συνέβαλε στον προσδιορισμό ενός αμινοτελικού μοτίβου καθώς και άλλων στοιχείων που επηρεάζουν τον ολιγομερισμό. Ενδιαφέρον παρουσιάζει το γεγονός ότι η επαγόμενη από το υπόστρωμα ενδοκύτωση φαίνεται να συμπίπτει με τον απο-ολιγομερισμό του μεταφορέα, κάτι που δεν ισχύει στην περίπτωση της ενδοκύτωσης που επάγεται από τα αμμωνιακά ιόντα. Όλα τα παραπάνω ευρήματα υποδεικνύουν ότι ο ολιγομερισμός του UapA είναι σημαντικός για την έξοδο του από το ΕΔ, τη στόχευσή του στη πλασματική μεμβράνη αλλά και την ενδοκύτωσή του, όπως άλλωστε έχει δειχθεί και για μεταφορείς στα φυτά και τα θηλαστικά.

Abstract

Eukaryotic transporters respond to environmental and developmental signals at both the transcriptional and post-translational levels. Their tight control includes rapid *de novo* synthesis and targeting to the plasma membrane (PM) and even more rapid down-regulation through endocytosis and vacuolar degradation, triggered by NH_4^+ or excess substrate. The extensively studied uric acid-xanthine transporter UapA of *Aspergillus nidulans* was used to address three questions concerning the mechanisms underlying intracellular trafficking of transport proteins: what are the effects of hypertonicity in fungal physiology and transporter endocytosis, which are the mechanisms regulating transporter ubiquitination and turnover, and what is the role of transporter oligomerization in membrane trafficking and endocytosis.

In particular, *A. nidulans* strains expressing GFP-tagged transporters were used to study the rapid appearance of cortical, relatively static, fluorescent patches in response to hypertonic treatment (in collaboration with V. Bitsikas, C. Gournas and G. Diallinas). Patch formation is not a transporter-specific effect, but rather reflects global membrane reorganization. This was shown by co-localization with other plasma membrane-associated molecules, such as a pleckstrin homology (PH) domain and the SsoA t-SNARE, or the lipophilic markers FM4-64 and filipin. Moreover, patches did not show characteristics of lipid rafts or any other membrane microdomains. Accordingly, deconvoluted microscopic images showed that fluorescent patches correspond to PM invaginations. Transporters remain fully active during this phenomenon of localized plasmolysis. Plasmolysis is, however, associated with reduced growth rate and a dramatic blockage of both clathrin-mediated endocytosis of transporters and fluid-phase internalization of FM4-64. These phenomena are concentration-dependent, transient and rapidly reversible upon wash-out of hypertonic media. Blockage of endocytosis by hypertonicity did not affect the cortical appearance of upstream (SlaB) or downstream (AbpA) endocytic markers, but dramatically modified the subcellular localization of tropomyosin, suggesting that hypertonicity acts indirectly on endocytosis by modifying actin dynamics. This was further supported by the effect of latrunculin B, an actin depolymerization agent, on endocytosis. Hypertonic conditions elicited similar phenomena in *Saccharomyces cerevisiae*, which suggests that they constitute basic homeostatic responses of ascomycetes to hypertonic stress.

In order to elucidate the mechanisms regulating transporter ubiquitination and internalization from the PM, the role of all arrestin-like proteins of *A. nidulans* was investigated in respect to growth, morphology, sensitivity to drugs and specifically for UapA turnover. A single arrestin, ArtA, was found to be essential for HulA^{Rsp5}-dependent ubiquitination and endocytosis of UapA in response to either NH_4^+ or substrates (in collaboration with S. Amillis, M. Evangelinos, A. Kokotos, V. Yalelis and G. Diallinas). Mutational analysis showed that residues 545-563 of the UapA C-terminal region, which includes a critical di-acidic motif, are required for efficient UapA endocytosis, thus suggesting that this might be the interaction interface between the arrestin and the transporter. Furthermore, PPXY motifs of ArtA are essential and sufficient for UapA ubiquitination and endocytosis. ArtA functions upstream from the late endocytic factor SagA^{End3}, indicating that UapA ubiquitination takes place in the PM rather than in an early endosomal compartment. ArtA is itself ubiquitinated by the same ubiquitin ligase (HulA) at residue Lys343 and this modification is critical for the efficiency of UapA ubiquitination and endocytosis. ArtA is also essential for vacuolar turnover of transporters specific for purines (AzgA) or L-proline (PrnB), but not for an aspartate/glutamate transporter (AgtA). Notably, evidence presented herein indicates that NH_4^+-induced and substrate-elicited endocytosis occur via two distinct pathways and the latter is dependent on conformational changes of UapA associated with transport catalysis.

This is consistent with previous observations showing that substrate-induced endocytosis operates only for functional UapA molecules. However, inactive UapA versions can be endocytosed *in trans* when co-expressed with active ones, an indication that UapA homo-oligomerizes. Oligomerization of UapA was confirmed using two different approaches: *in vivo* bimolecular fluorescence complementation (BiFC) and direct pull-down assays of differentially tagged UapA molecules. It was also supported by genetic evidence showing an apparent dominant-negative effect of inactive mutants on the activity of wild-type UapA. UapA oligomers seem to be initially formed in the ER and remain stable and functional in the PM. Using UapA showing ER-retention mutants, an N-terminal motif and other elements affecting oligomerization were identified. Interestingly, substrate-elicited endocytosis, unlike NH_4^+-induced, seems tocoincide with the dissociation of transporter oligomers prior to internalization. Therefore, UapA oligomerization, analogously to some plant and mammalian transporters, is critical for ER-exit, sorting to the PM and endocytosis.

Table of contents

<div align="right">

1

</div>

General Introduction

1.1 Ascomycota

1.1.1 Basic features

Ascomycota, the largest phylum of the Fungi Kingdom, consists of more than 6300 genera and 64000 species, ranging from unicellular yeasts to fairly large morels and truffles, as well as some of the common black and green moulds, the powdery mildews and the cup fungi (Kirk *et al.*, 2008; Figure 1.1A).
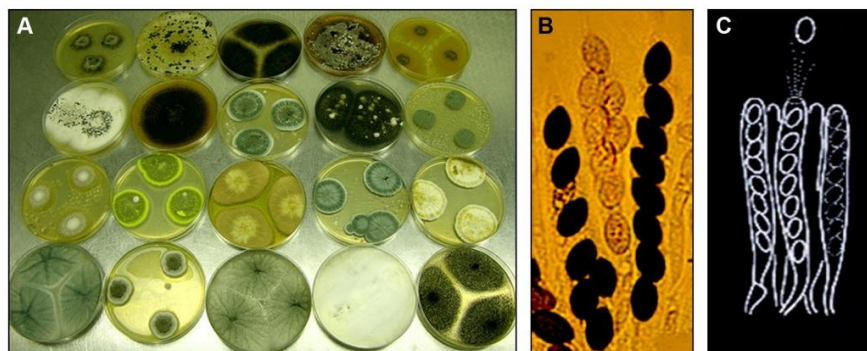
Figure 1.1. A. Various ascomycetes growing in axenic cultures (photograph by Dr. David Midgley, retrieved from http://goo.gl/1JLqM5). **B.** Asci of the hyphal ascomycete *Podospora* (photomicrograph by R. Vilgalys, retrieved from http://tolweb.org/Ascomycota). **C.** Diagram of the asci, the defining characteristic of Ascomycota, each of them carrying eight ascospores. The bursting of an ascus to release its ascospores is also illustrated.

The primary morphological feature that distinguishes members of Ascomycota from all other fungi is the ascus, a saclike cell containing the ascospores, which are produced by a combination of meiosis and a subsequent mitotic division (Alexopoulos *et al.*, 1996). Eight ascospores are typically formed within the ascus (Figure 1.1B and C), although this number may vary according to the species and may be as little as one ascospore per ascus (Esser and Stahl, 1976). Asci are usually produced in fruiting bodies called ascocarps, also known as ascomata. Besides this sexual cycle of reproduction, ascomycetes can also reproduce asexually (Figure 1.2B). In asexual reproduction, conidiospores are formed as a result of mitosis and are released in large numbers, allowing the fungus to disperse over a wide area.

Filamentous ascomycetes are characterized by a compartmentalized mycelium with distinctive walls, called septa (Figure 1.2A). Septa generate from the hyphal periphery and advance towards the centre. There, a small circular pore is formed, through which the plasma membrane (PM) and cytoplasm extend, and nuclei are permitted to migrate from one hyphal compartment to the next (Alexopoulos *et al.*, 1996; Figure 1.2C).
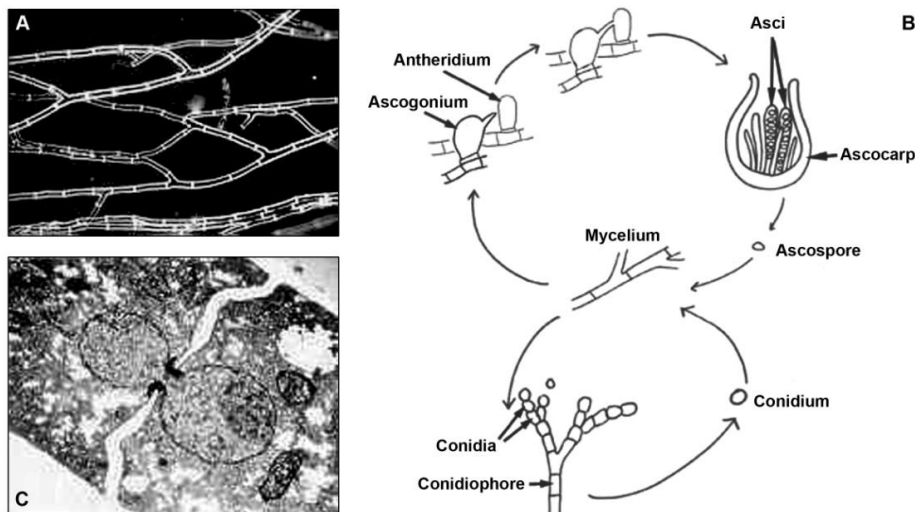
Figure 1.2. A. Hyphae of ascomycetes divided into compartments by septa placed at regular intervals. These miniature bulkheads give the hyphae some physical rigidity and limit loss of cytoplasm, if the hyphal wall is ruptured (retrieved from http://goo.gl/Q5GRjC). **B.** Ascomycetes may have two distinct reproductive phases, the sexual, where asci and ascospores are formed and the asexual, where conidiospore (conidia) production occurs at different times on the same mycelium (scheme by A. Edwards and G. Wyn Griffith, retrieved from http://goo.gl/9FVAoM). **C.** Septa are centrally perforated to allow movement of cytoplasm and nuclei between compartments. This transmission electron micrograph of a short segment of *Neurospora crassa* hypha shows a nucleus in the act of squeezing through the septal pore (photomicrograph by Beth Richardson, retrieved from http://goo.gl/Q5GRjC).

In the past, ascomycetes have often been grouped on fruit body type and ascus arrangement (Hemiascomycetes, Plectomycetes, Pyrenomycetes, Discomycetes, Loculoascomycetes). In recent years, molecular sequence data have changed the way this phylum is classified (Kirk *et al.*, 2008). Thus, based on a series of major phylogenetic studies, the phylum Ascomycota is divided in three subphyla, the Pezizomycotina (Ascomycotina), containing almost all ascomycetes that produce ascocarps, the Saccharomycotina, consisting of most of the true yeasts, and the basal group Taphrinomycotina (Lutzoni *et al.*, 2004; Kirk *et al.*, 2008). Nevertheless, fruit body-based taxa names are still occasionally used (Figure 1.3).
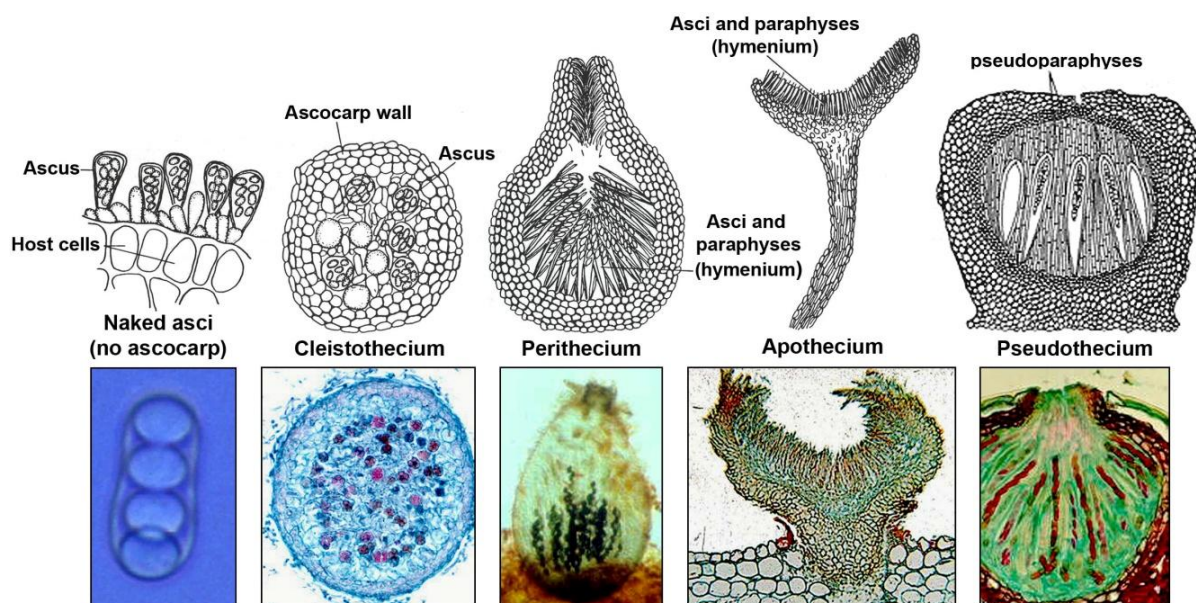
Figure 1.3. Diagrams (Alexopoulos *et al.*, 1996) and photomicrographs (retrieved from http://goo.gl/Q5GRjC) of the ways in which ascomycetes bear their asci. Naked asci (absence of an ascocarp) are characteristic of Hemiascomycetes, consisting of the yeasts and yeast-like fungi that have now been placed into the subphyla Saccharomycotina or Taphrinomycotina. The four different types of ascocarps found in ascomycetes, cleistothecium, perithecium, apothecium and pseudothecium, are borne by Plectomycetes, Pyrenomycetes, Discomycetes and Loculoascomycetes, respectively, all of which (except one genus) are now placed in the subphylum Pezizomycotina.

1.1.2 Ecology and importance of Ascomycota

Ascomycetes rival other groups of eukaryotic organisms in their ability to occupy a broad range of habitats. Corticolous, lignicolous, foliicolous, coprophilous and marine ascomycetes are present in ecosystems worldwide, even at some of the most extreme environments on earth, such as the inside of rocks on the frozen plains of Antarctica (Selbmann *et al.*, 2005) and the deep-sea sediments (Raghukumar *et al.*, 2010). While a few are entirely hypogean, others form long-lived symbiotic

associations with green algae or cyanobacteria (lichens), as well as with plants (mycorrhizae) and animals (Figure 1.4). They are important decomposers and have substantial roles in nutrient cycling, since they can break down large molecules, such as cellulose and lignin (Schoch *et al.*, 2009).
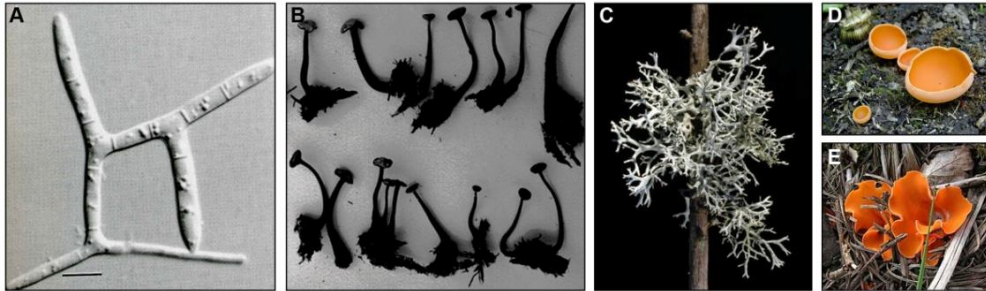
Figure 1.4. A. Highly branched conidium of the marine fungus *Varicosporina ramulosa* (Shearer, 1986; Zhang *et al.*, 2006). **B.** Ascostromata of coprophilus fungus *Poronia oedipus* dissected from horse dung (photograph by M. J. Richardson, retrieved from http://goo.gl/qnvpgB). **C.** The lichen *Pseudevernia furfuracea*, a symbiotic association of an ascomycete with a green alga (retrieved from http://goo.gl/imj8F9). **D, E.** Apothecia of the saprobic cup fungus *Aleuria aurantia* (photograph by J.H. Petersen/MycoKey, retrieved from http://tolweb.org/Pezizomycotina/29296).

Ascomycetes are also very important for food production. The fermentative ability of certain yeasts is the basis of the baking and brewing industries (Figure 1.5A). The enzymes produced by some species of the genus *Penicillium* play a significant role in the manufacture of the famous French cheeses Camembert, Brie and Roquefort, while *Aspergilli* have been used since more than 2000 years in the orient for the production of local specialties, such as soyu (soy sauce), miso (fermented soybean paste) and sake (rice wine) (Scazzocchio, 2009). Morels (*Morchella*) and truffles (*Tuber*) are also known as some of the most sought-after fungi delicacies (Figure 1.5B).

A huge array of metabolic products, such as antibiotics, organic acids, enzymes and vitamins, is provided by ascomycetes. The most famous case may be that of penicillin, an antibiotic which triggered a revolution in the treatment of bacterial infectious diseases in the 20th century. Fleming's penicillin-producer was recently identified as *Penicillium rubens* (Houbraken *et al.*, 2011). Moreover, some species can be relatively easily genetically engineered to produce useful proteins, such as insulin produced in *Saccharomyces cerevisiae* (Kjeldsen, 2000) and human growth hormone in *Pichia pastoris* (Apte-Deshpande *et al.*, 2009).

However, along with their benefits and positive contributions, ascomycetes can also be very harmful. Some secondary metabolites they secrete are responsible for

food contaminations, which result in food spoilage and in some cases may lead to fatal intoxications (Scazzocchio, 2009). Aflatoxin B1, a mycotoxin produced by *Aspergillus flavus*, is one of the most toxic and carcinogenic compounds known (Figure 1.5C). Furthermore, ascomycetes are widespread plant pathogens, causing great economic damages in agriculture (Dutch elm disease, powdery mildew), but are also responsible for human and animal infections, such as candidiasis (*Candida albicans*) and several dermatophyte (*Epidermophyton floccosum*) skin diseases (Berbee, 2001). *Aspergilli* are important opportunistic pathogens of individuals with compromised immune systems, causing a group of diseases collectively known as aspergilloses (Figure 1.5D-F).
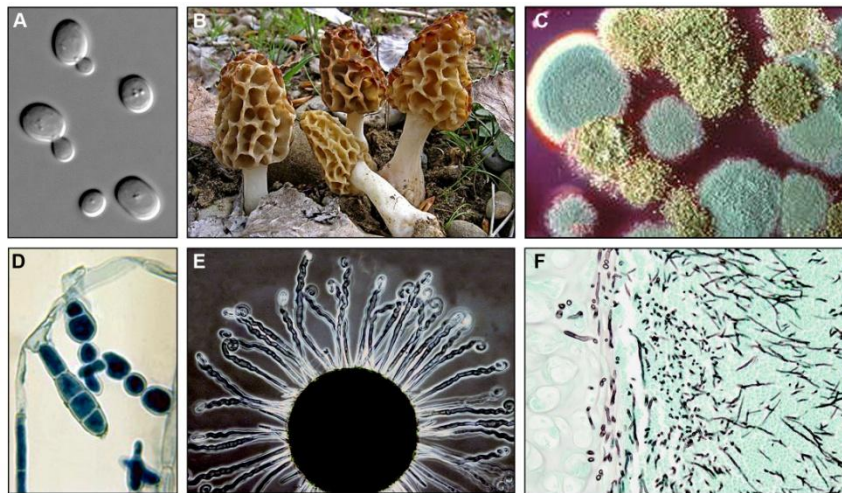
Figure 1.5. A. Cells of *Saccharomyces cerevisiae*, commonly called the brewer's yeast (retrieved from http://goo.gl/1qs5UB). **B.** The morel *Morchella rigida,* a highly prized gourmet delicacy (photograph by Paco Serrano, retrieved from http://goo.gl/UunM9W). **C.** Solid cultures of mycotoxin-producing ascomycetes. The yellowish colonies are of *Aspergillus flavus*, a producer of aflatoxin, while the green colonies are of *Penicillium*, another mycotoxin-producing genus (retrieved from http://goo.gl/VB9QxK). **D.** Macroconidia of the dermatophytic fungus *Epidermophyton floccosum*, a cause of tinea pedis (athlete's foot), tinea corporis (ringworm), tinea cruris (jock itch) and onychomycosis (photomicrograph by L. Ajello, retrieved from http://goo.gl/zkflrn) **E.** Cleistothecium of *Uncinula necator*, the causal agent of powdery mildew of grapes (photomicrograph by G. Barron, retrieved from http://goo.gl/xRIxJV). **F.** Histopathologic image of pulmonary invasive aspergillosis in a patient with interstitial pneumonia (retrieved from http://goo.gl/Iv9HX7).

Finally, fungi are eukaryotes, more closely related to metazoans than to plants; this is why ascomycetes can be useful models in molecular and cell biology (Scazzocchio, 2009). Moreover, several species have biological properties and genetic systems that make them ideally suited for basic biological research. Among them, *S. cerevisiae* and *A. nidulans* hold prominent positions in this field (Alexopoulos *et al.*, 1996).

1.2 *Aspergillus nidulans*

1.2.1 Basic Features

Aspergilli are homothallic, filamentous fungi belonging to the phylum Ascomycota. This genus was first described in 1729 by the priest and botanist Pietro Antonio Micheli and was named after an instrument called *Aspergillum*, which he used in the Roman Catholic mass to sprinkle holy water over the heads of the faithful. Figure 1.6 compares the original Micheli's drawing with modern observations of conidiophores (Scazzocchio, 2009).
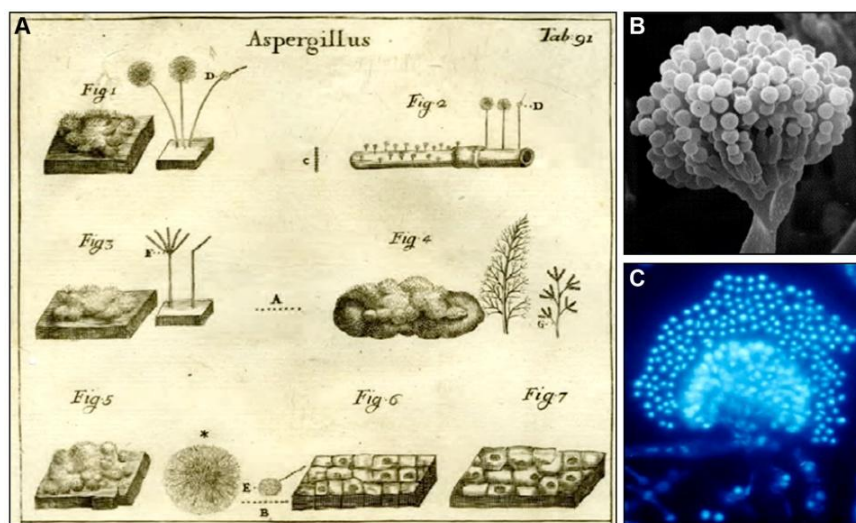
Figure 1.6. A. Scan of copper-engraving 91 from Micheli's *Nova plantarum genera*, showing his drawings of *Aspergillus* conidiophores (retrieved from Scazzocchio, 2009). Scanning electron micrograph (**B**) and epifluorescence micrograph (**C**) of a conidiophore of *A. nidulans*. Staining with DAPI reveals the nuclei of the conidia and of the subjacent structures of the conidiophores (photomicrograph by U. Kues and R. Fischer, 2006, retrieved from Scazzocchio, 2009).

 A. nidulans is commonly isolated from soil, plant debris, and house dust and is an opportunistic pathogen of immunocompromised individuals. It is recognized by its distinct conidiophores terminated by a swollen vesicle bearing flask-shaped phialides, which are borne on the intervening metulae. Conidia are produced in long chains, budding from the ends of the phialides, and have a green pigment in the wild type strain. The hyphal compartment that branches to give rise to the conidiophore is the foot cell (Figure 1.7A). *A. nidulans* is normally haploid, but can also be induced to grow as heterokaryon or vegetative diploid. It produces asexual conidiospores for rapid distribution in the environment and sexual ascospores for long-term survival in soil (Figure 1.7B). The asci, containing the ascospores, are dispersed in cleistothecia (see 1.1.1), which are surrounded by thick-walled nurse cells, called "hülle cells".
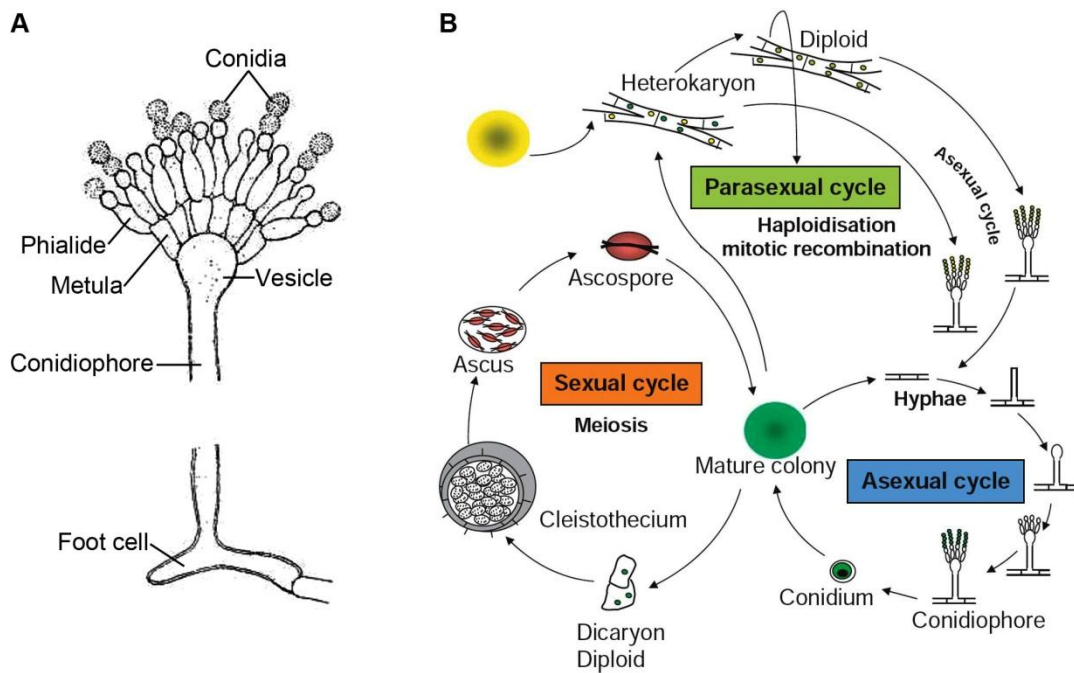
Figure 1.7. A. Diagram of the typical conidiophore of *A. nidulans*. See text for description (diagram adapted from Thom and Raper, 1945). **B.** The life cycle of *A. nidulans*. In the asexual cycle, *A. nidulans* forms haploid vegetative filamentous hyphae following germination of uninucleate conidia or binuceate ascospores. Vegetative hyphae differentiate to form conidiophores, on which conidia are produced (Todd *et al.*, 2007). In the sexual cycle, two nuclei divide synchronously as a dikaryon in a specialized structure. Eventually, the nuclei fuse to give a diploid, which does not divide as such but undergo meiosis followed by a post-meiotic mitosis. One last mitotic e yields eight binucleate ascospores in each ascus. Classical genetics procedures are facilitated by the fact that one cleistothecium derives from only one fertilization event. In the parasexual cycle, a heterokaryon is formed and nuclei fuse to yield a diploid, which does not undergo meiosis but divides as such. Breaking up of the diploid (haploidization) and mitotic recombination are additional genetic tools. Both diploids and heterokaryons can undergo the asexual cycle (Todd *et al.*, 2007; Scazzocchio, 2009; scheme by Stephane Demais, modified by Claudio Schazzocchio, retrieved from Scazzocchio, 2009).

The modern classification of Ascomycota, places *A. nidulans* in the subphylum Pezizomycotina, class Eurotiomycetes, order Eurotiales and family Aspergillaceae (Kirk *et al.*, 2008; Houbraken *et al.*, 2014). Moreover, unlike the past classification of *A. nidulans* as the anamorph of the teleomorph *Emericella nidulans*, the single-named, but pleomorphic, nomenclatural and taxonomical system classifies both anamorphic and telomorphic states in *Aspergillus*, while *Emericella* is considered synonymus to the latter (Houbraken *et al.*, 2014).

1.2.2 *A. nidulans* as a model organism

It was about 1946 in Glasgow, when an enthusiastic scientist named Guido Pontecorvo searched for a potentially ideal genetic organism, in order to raise the "resolving power of genetic analysis". After testing several microorganisms (e.g. *Aerobacter, Serratia*) for this purpose, he finally selected *A. nidulans*, despite the

scorn from his colleagues who thought that its homothallism would be a practical barrier (Cohen, 2000). The supposed difficulties due to homothallism turned into advantage with the discovery that segregation of autonomously expressed conidial color mutations could be used to identify crossed cleistothecia and by 1953 (Pontecorvo *et al.*, 1953), the utility of *A. nidulans* as a genetic organism had been comprehensively established (Cohen, 2000). Moreover, since the development of transformation protocols (Tilburn *et al.*, 1983), *A. nidulans* has also become a model microbial system for molecular biology and reverse genetics.

The sophisticated system of *A. nidulans* genetics, molecular and cell biology led to the analysis of multiple metabolic and cellular processes. The work of Pateman *et al.* (1964) on enzymes of nitrate assimilation in *A. nidulans*, initiated the use of this organism as a model system to study the control of gene expression (Scazzocchio, 2013). About a decade later, the main factors of nitrogen metabolite repression and carbon catabolite repression had been identified (Arst and Cove, 1973; Bailey and Arst, 1975).Work carried out in *A. nidulans* has also contributed to our understanding of the biochemistry and regulation of mitosis (Morris, 1975; Morris and Enos, 1992). One useful consequence of these regulatory studies was the characterization and development of the *alcA* alcohol dehydrogenase regulatable promoter, which is induced by alcohol and repressed by glucose, as an effective tool to control gene expression (Felenbok, 1991). Other important contributions include the dissection of the development of conidiophores (Timberlake, 1990), extensive work on transporter proteins (Diallinas, 2008a and references therein) and the recent work of Peñalva *et al.* (2012) on membrane trafficking, Golgi dynamics and endocytosis in *A. nidulans*. A significant step for *A. nidulans* research was the sequencing of its entire genome (Galagan *et al.*, 2005), which was calculated to be 30.07 Mb in size and to contain 10560 putative protein-coding genes (http://www.broadinstitute.org/annotation/genome/aspergillus_group/ GenomeStats.html)

A. nidulans has considerable advantages as a laboratory model organism. It has eight well-marked chromosomes with many color, auxotrophic and drug resistance markers. It is homothallic (there are no mating types), so any two strains can be mated. While it is normally haploid, heterokaryons and stable diploids can be produced for complementation analysis of mutations. It is also efficiently transformed in an integrative and site-specific fashion and can generate stable transformants. Thus, its genes can be cloned, altered, disrupted or deleted at will, at

their normal or any other location in the genome (Morris and Enos, 1992). The fact that its conidiospores are uninucleate enables the direct screening of mutants/transformants by plating on appropriate media. Moreover, mutations often result in detectable colony phenotypes. *A. nidulans* can also serve as a host for the functional heterologous expression of genes coming from other microorganisms or even higher eukaryotes (Argyrou *et al.*, 2001; Goudela *et al.*, 2008). Additionally, it grows rapidly on inexpensive media under a variety of nutritional conditions and produces conidia or ascospores that can be stored for long periods of time.

Even when compared to *S. cerevisiae*, whose wealth in genetic and biochemical tools and resources of all kinds cannot be matched by any other competitor, *A. nidulans* has several benefits to display. First, although it has almost twice the number of genes of *S. cerevisiae*, it has an almost complete absence of genetic redundancy, since, unlike the budding yeast, it has not undergone genome duplication. Also, the level of similarity between human and *A. nidulans* orthologs is usually higher than that between budding yeast and humans. On the practical side, the large size of the cells facilitates studies with conventional microscopy, as the organelles are less crowded than in the unicellular yeasts (Peñalva *et al.*, 2012). Most importantly, what clearly distinguishes *A. nidulans* is its polar lifestyle. Apical extension is highly demanding in special mechanisms for rapid protein exocytosis and endocytosis, which are dependent on the microtubule cytoskeleton (Taheri-Talesh *et al.*, 2008). Interestingly, the molecular mechanisms underlying fungal polarity are analogous or/and homologous to those found in the cells of higher eukaryotes, such as mammalian neurons.

Finally, *A. nidulans* is closely related to a large number of other *Aspergillus* species of industrial and medical significance, such as *A. niger*, *A. oryzae*, *A. flavus*, and *A. fumigates*, which have no sexual cycle but are exploited experimentally using technologies developed for *A. nidulans* (Scazzocchio, 2006).

1.3   *Saccharomyces cerevisiae*

1.3.1 Basic Features

S. cerevisiae is mankind's oldest domesticated organism and the world's premier commercial microorganism for biotechnological applications (Pretorius *et al.*, 2003; see 1.1.2). Legend has it that, many years ago, a Mesopotamian farmer found that the

water some grain had been soaking in had developed a funny taste. He woke the next day having made two important discoveries, beer and hangover. Whether this is just a tale or not, it is very likely that mankind's first encounter with alcoholic beverages was by chance.

Chemical analysis of ancient organics absorbed into pottery jars from an early Neolithic village in China have revealed that fermented beverages were produced as early as the 7000 BC (McGovern *et al.*, 2004). Moreover, *S. cerevisiae* DNA has been isolated from residue present inside an Egyptian wine jar that dates back to 3150 BC (Cavalieri *et al.*, 2003). In 1680, the Dutch naturalist Antonie van Leeuwenhoek observed yeast cells microscopically for the first time, although at the time he did not consider them to be living organisms, but rather starchy globular structures (Alba-Lois and Segal-Kischinevzky, 2010). It was about 150 years later that three pioneer scientists, Charles Cagniard-Latour, Theodor Schwann and Friedrich Kützing, showed independently that alcoholic fermentation was conducted by living yeasts and not by a chemical catalyst (Barnett, 1998). The role of yeast in the fermentation process was elucidated two decades later by French microbiologist Louis Pasteur (Pasteur, 1857).

S. cerevisiae naturally occurs in very diverse habitats, such as the soil, the aquatic environments, the surface of plants and the gastrointestinal tracts and body surface of insects and warm-blooded animals. Most often, it is found in areas where fermentation can occur, such as the surface of ripe fruits (Walker, 2009). It has a predominantly unicellular thallus, although it can form pseudohyphae, as a physiological response to nitrogen starvation or a stressful environment (Zaragoza and Gancedo, 2000).Vegetative cell division of *S. cerevisiae* occurs by budding, in which a daughter cell is initiated as an outgrowth from the parent cell, followed by nuclear division, cell wall formation and finally cell separation. Yeast can be found as a haploid or a diploid. Haploid cells have buds that appear adjacent to the previous one, whereas diploid cells have buds that appear at the opposite pole (Figure 1.8). Each mother cell usually forms no more than 20-30 buds and its age can be determined by the number of bud scars left on the cell wall (Sherman, 1997). Moreover, *S. cerevisiae* has two mating types, MATa and MATα. The conjugation of two haploid cells of opposite mating types leads, as in many other eukaryotes, to genetic recombination (Walker, 2009).
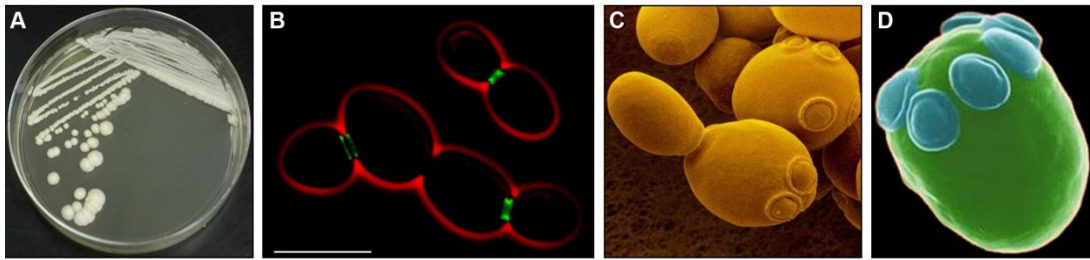
Figure 1.8. A. *S. cerevisiae* growing in an axenic culture (retrieved from http://goo.gl/QkxJA3). **B.** Fluorescent micrograph of *S. cerevisiae* with GFP-tagged septin, a protein critical for the formation and effectiveness of the diffusion barrier between the parent and the daughter cells. Red: outline of the cells (phase contrast), scale bar: 10μm (by Philippsen Lab, Biozentrum Basel, retrieved from http://goo.gl/1WNkHR). **C.** False color SEM micrograph of *S. cerevisiae* cells. The cell with the appearance of pinched in waistline is in the process of dividing (by D. Scharf, retrieved from http://goo.gl/tkFWmz) **D**. False color SEM micrograph of a haploid *S. cerevisiae* parent cell that has produced at least six daughter cells, as shown by the polar contiguous array of circular bud scars (blue) (by A. Cosney and J. Forsdyke; original version published in Harold, 1990; adapted version retrieved from http://goo.gl/lS1IEP).

The modern classification of Ascomycota, places *S. cerevisiae* in the subphylum Saccharomycotina, class Saccharomycetes, order Saccharomycetales and family Saccharomycetaceae (http://www.ncbi.nlm.nih.gov/Taxonomy/Browser/wwwtax.cgi?id=559292; Kirk *et al.*, 2008).

1.3.2 *S. cerevisiae* as a model organism

Although yeasts have greater genetic complexity than bacteria, they share many of the technical advantages that permitted rapid progress in the molecular genetics of prokaryotes. Properties that make *S. cerevisiae* a good model system for biological studies include rapid growth, dispersed cells, lack of pathogenicity, ease of replica-plating and mutant isolation, a well-defined genetic system, as well as a highly versatile DNA transformation system, the development of which made *S. cerevisiae* particularly accessible to gene cloning and genetic engineering techniques (Sherman, 1997). Plasmids can be introduced into yeast cells either as replicating molecules or by integration into the genome. In the latter case, integration proceeds only by homologous recombination, unlike most other organisms. Recombinant DNA with at least partial homologous segments can therefore be directed at will to specific locations in the genome. Thus, wild type genes can be conveniently replaced with altered or disrupted alleles, so as to study the function of certain proteins *in vivo*. Interestingly, disruption of some genes that were previously assumed to be essential, led to viable mutants with little or no abnormal phenotypes. Moreover, because of *S. cerevisiae* double nature, being stable both as a haploid and a diploid, recessive

mutations can be conveniently isolated in the haploid and complementation tests can be carried out in the diploid (Sherman, 1997).

S. cerevisiae has proved to be a valuable tool also for studies of other organisms. Examples are the development of the two-hybrid screening system for the general detection of protein-protein interactions (Fields and Song, 1989), the use of yeast artificial chromosomes (YACs) for cloning large DNA fragments (Murray and Szostak, 1983)and the use of yeast as a heterologous expression system for proteins from other eukaryotes, for the systematic analysis of their functions (Leung *et al.*, 2010). The importance of *S. cerevisiae* as a model organism is also illustrated by the fact that it was the first eukaryotic organism to have its genome fully sequenced (Goffeau *et al.*, 1996), which, combined with the current availability of a complete set of deletion mutants, has further enhanced the potential use of *S. cerevisiae* as a model for unraveling the basic cellular mechanisms of eukaryotic cells.

1.4   Nitrogen metabolism in fungi

1.4.1 General aspects of nitrogen metabolism in fungi

Nitrogen, one of the most abundant chemical elements on earth, is a fundamental component of nearly all of the macromolecules of living organisms, and thus an essential growth factor for all biological systems. Nitrogen metabolism has been extensively studied in fungi, for which the availability of several nitrogen sources is often a regulatory signal for activation or inactivation of the various regulatory pathways and is, consequently, of great significance for the morphological development, the production of secondary metabolites and, in the case of phytopathogenic fungi, the regulation of virulence determinants (Marzluf, 1997; Caddick, 2004). Moreover, nitrogen is implicated to a number of serious environmental issues, such as global warming, ozone depletion and eutrophication caused by nitrate-based fertilization in agriculture, which not only lead to ecological instability, but also consist a threat to human health (Giles, 2005). Therefore, beyond getting an insight into the molecular processes involved in nitrogen utilization, the study of nitrogen metabolism has a great ecological value.

Fungi can use a surprisingly diverse array of compounds as nitrogen sources, such as purines, nitrate, nitrite, ammonium and most amino acids (Figure 1.9A), and are capable of expressing upon demand the catabolic enzymes of many different

pathways. However, not all nitrogen sources are used in the same preference. It has been shown that certain nitrogenous compounds, such as ammonia, glutamine, glutamate and asparagine, are preferentially used, whereas others are utilized only when these so-called primary nitrogen sources are absent or in limiting amounts.

Utilization of any of the secondary nitrogen sources is highly regulated. The activation of the corresponding catabolic pathways is controlled at the level of transcription and often requires two distinct positive signals: a global acting signal indicating nitrogen derepression due to absence of a primary source and pathway-specific induction, which indicates the presence of a substrate or an intermediate of the pathway (Marzluf, 1997). For purine catabolism in *A. nidulans*, the *de novo* synthesis of a set of catabolic enzymes and permeases is required. This can only happen upon nitrogen derepression, mediated by AreA, a global GATA-type zinc finger transcription factor (Arst and Cove, 1973; Ravagnani *et al.*, 1997), and upon simultaneous induction with uric acid, mediated by the pathway-specific transcription factor UaY (Scazzocchio *et al.*, 1982); Figure 1.9; see also 1.5.6).
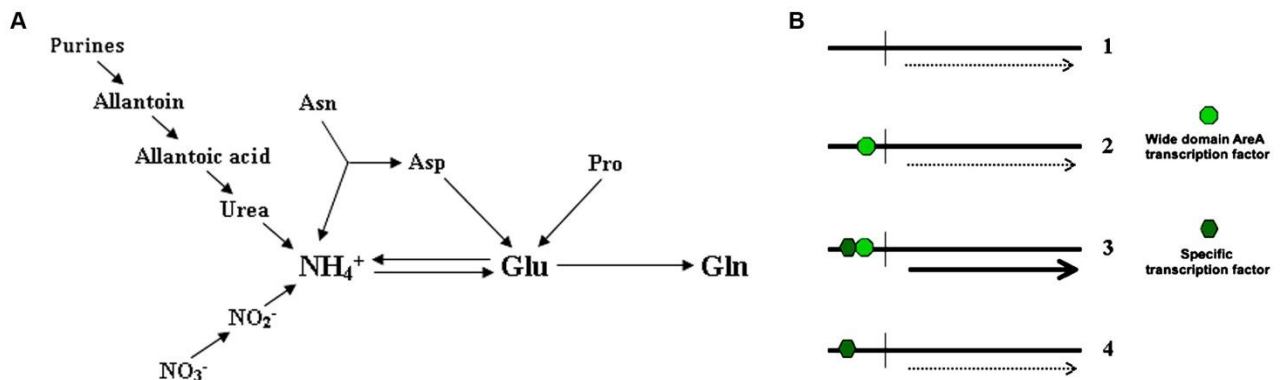
Figure 1.9. A. A schematic representation of relevant aspects of nitrogen metabolism. A wide variety of compounds are utilised by fungi as nitrogen sources, including purines, various amino acids, nitrate and nitrite. These are metabolised through ammonium (NH_4^+) and/or glutamate (Glu) to glutamine (Gln), the last two being utilized by the cell for the production of macromolecules. NH_4^+ and Gln are excellent nitrogen sources and their presence in the medium results in the repression of metabolic pathways required for the utilization of most other compounds(adapted from Caddick, 2004). **B.** General scheme of the transcriptional regulation of genes involved in the utilization of nitrogen sources in *A. nidulans*: (1) In the absence of a specific inducer and in the presence of a preferred, repressing nitrogen source (NH_4^+ or Gln), neither the specific transcription factor, nor the broad-domain transcription factor is activated; no or only basal transcription is seen. (2) In the absence of a specific inducer and in the presence of a non-repressive nitrogen source, only AreA is active; only basal transcription is seen. (3) In the presence of a specific inducer and in the absence of a repressing nitrogen source, both transcription factors are active; full transcription is seen. (4) In the presence of both a specific inducer and of a repressing nitrogen source, the specific transcription factor is active, but AreA is inactive; no transcription is seen (adapted from Scazzocchio, 2009).

1.4.2 Purine assimilation pathway

Bacteria, fungi, protozoa, plants, insects and mammalian tissues, all have the ability to take up purines. In most of these microorganisms, the uptake of purines fulfils two main functions. One is to scavenge exogenous preformed bases for nucleotide biosynthesis and the other is catabolic, since most fungi can use purines as fairly good nitrogen sources (De Koning and Diallinas, 2000). This is due to the degradation of purines, first to ureides (allantoin, allantoic acid) and eventually to urea, via several enzyme-catalyzed oxidations. The complete purine catabolic pathway (Figure 1.10) is present in most filamentous fungi and is the same as that of most bacteria and plants. In contrast, most yeasts have degenerate variations of the purine degradation pathway (Pantazopoulou and Diallinas, 2007).

More specifically, most yeasts lack xanthine dehydrogenase (HxA, also known as purine hydroxylase I), the major enzyme-oxidizing hypoxanthine to xanthine and xanthine to uric acid, and urease (UreA), the last enzyme-oxidizing allantoic acid to urea. Some yeasts however, like *Candida albicans* and *Schizosaccharomyces pombe*, can use purines as nitrogen sources through XanA (xanthine a-ketoglutarate-dependent dioxygenase) .*S. cerevisiae* lacks all the enzymes necessary for purine oxidation, but can still break down allantoin or allantoic acid to urea and ammonia. This is reflected in the evolution of its uptake systems, which include transporters specific for salvageable purines, while they lack transporters for the oxidized purines uric acid or xanthine (Pantazopoulou and Diallinas, 2007).

In *A. nidulans*, the complete purine utilization pathway has been described (Figure 1.10; Gournas *et al.*, 2011). Recently, the *in vivo* subcellular localization of seven key enzymes of this catabolic pathway, namely xanthine dehydrogenase (HxA), urate oxidase (UaZ), 5-hydroxy-isourate hydrolase (UaX), 2-oxo-4-hydroxy-4-carboxy ureido imidazoline carboxylase (UaW), allantoinase (AlX), allantoicase (AaX) and ureidoglycolate hydrolase (UglA), as well as, that of the alpha-ketoglutarate Fe(II)-dependent dioxygenase (XanA), has been identified. HxA, AlX, UaW, AaX and XanA are localized in the cytoplasm, while UaZ, UaX and UglA were found to be peroxisomal (Katerina Galanopoulou, Claudio Scazzocchio, Maria Eleftheria Galinou, Weiwei Liu, Fivos Borbolis, Mayia Karachaliou, Nathalie Oestreicher, Dimitris G. Hatzinikolaou, George Diallinas and Sotiris Amillis. Fungal Genetics and Biology. In revision).
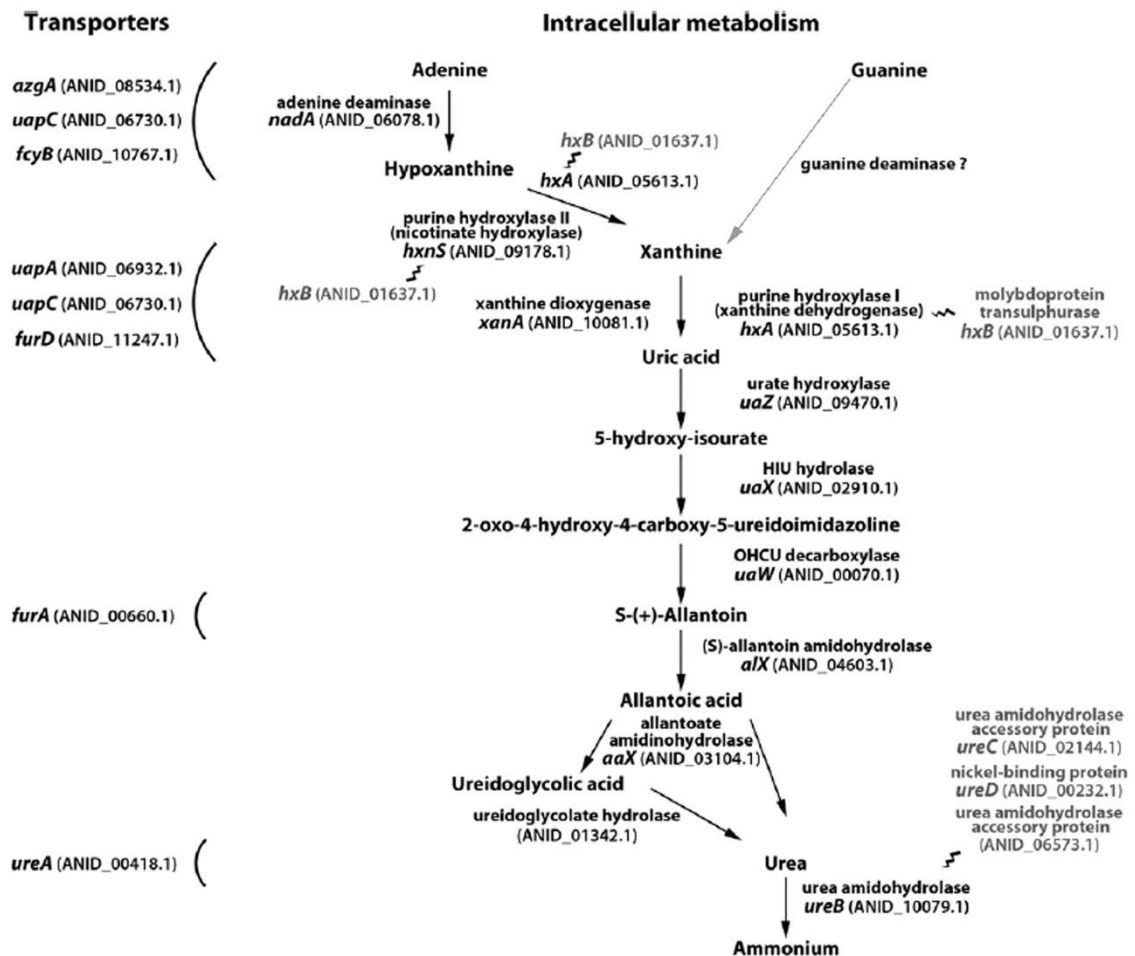
Figure 1.10. The complete pathway of purine degradation to ammonium in *A. nidulans*. Arrows connect the metabolic intermediates. Adjacent to each arrow the corresponding enzymatic reaction is shown, together with the name and identifier of the cognate gene. To the left of the figure, and opposite to their substrates, the transporters involved in the uptake of different metabolites are shown. The FcyB and FurD transporters play a minor role in the transport of purines, but are included for the sake of completion. In grey type, genes and their cognate proteins involved in co-factor synthesis or modification are shown. They are connected by a squiggly line to the relevant enzymes. Guanine is a nitrogen source for *A. nidulans* and thus it must be metabolised through this pathway. However, as no experimental work on the conversion of guanine, presumably to xanthine, is extant, nor has a guanine deaminase activity been characterized, a grey arrow indicates this predicted step (retrieved from Gournas *et al.*, 2011).

1.5   Nutrient transport across the plasma membrane

1.5.1 Biological membranes and membrane proteins

Biological membranes are indispensable to the life of the cell. The PM encloses the cell, defines its boundaries and maintains the essential differences between the cytosol and the extracellular environment. Inside the cell, the membranes of the endoplasmic reticulum (ER), Golgi apparatus, mitochondria, and other membrane-bounded organelles of eukaryotic cells maintain the characteristic differences between the contents of each organelle and the cytosol (Alberts *et al.*, 1994). Despite

their differing functions, all biological membranes have a common general structure, consisting of lipids, carbohydrates and proteins (Figure 1.11). The basic unit of the membrane is a bilayer formed by phospholipids and sphingolipids organized in two layers, with their polar headgroups along the two surfaces and their acyl chains forming a non-polar domain in between. Embedded in the lipid bilayer are sterols and integral membrane proteins, while peripheral membrane proteins are associated with the surface of the bilayer. Carbohydrates are solely externally attached to proteins (glycoproteins) or lipids (glycolipids).
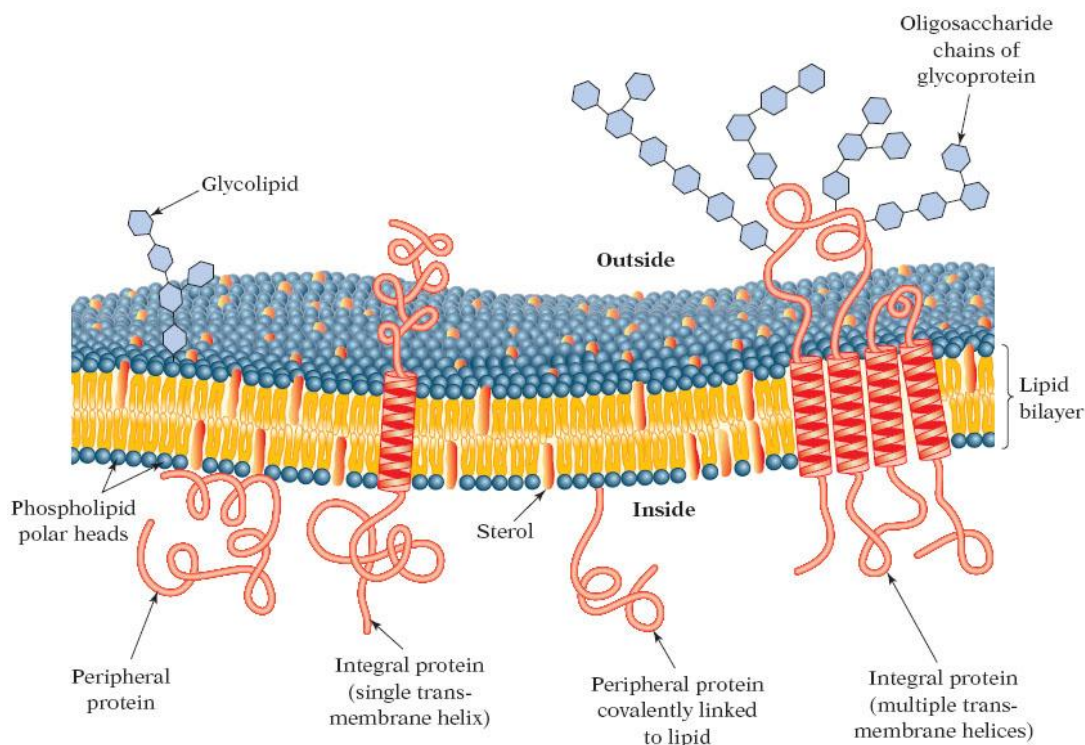
Figure 1.11. Components of biological membranes (retrieved from Nelson and Cox, 2004).

The understanding of lipid membrane structures and their role in cellular functions has developed significantly since the introduction of the classical fluid-mosaic model by Singer and Nicolson (1972). This model predicted that cellular membranes are fluid, homogenous and characterized by random distribution of their molecular components, resulting in lateral and rotational freedom. A large number of experimental data, however, converge toward the idea that membrane components move both in the transverse direction across the bilayer and the lateral direction in the plane of this two-dimensional matrix. These movements enable interactions among proteins and between proteins and lipids, to provide temporal associations that are important to membrane functions (Luckey, 2008). Moreover, transbilayer

(flip-flop) motions of lipids have been shown to have a role in the maintenance of membrane asymmetry (Gurtovenko and Vattulainen, 2007).

It has also become evident that several lipid environments with different physical properties may coexist in membrane bilayers. A widely accepted example of this heterogeneity is the existence of lateral domains within the bilayer, enriched in sphingomyelin and cholesterol (Figure 1.12). These nanosized domains, called lipid rafts (Simons and Ikonen, 1997), have been suggested to provide the membranes with characteristic physical properties and to take part in various dynamic cellular processes, such as membrane trafficking, signal transduction and regulation of the activity of membrane proteins. In agreement to that, recent atom-scale computer simulations for lipid rafts have shown that the elastic and dynamic properties of the membranes depend strongly on their lipid composition. Changes in these elastic properties are likely to influence conformational state, dynamic sorting and thus functionality of membrane proteins (Niemela *et al.*, 2007).
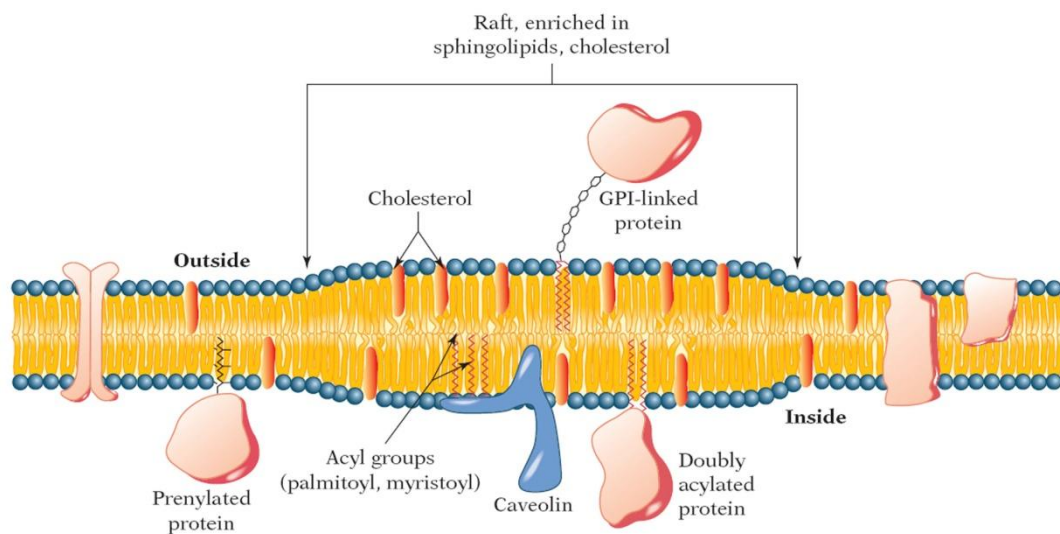
Figure 1.12. Lipid rafts. Membranes have stable but transient microdomains that are enriched in cholesterol and sphingolipids, along with glycosylphosphatidylinositol (GPI)-linked proteins and proteins anchored by acyl groups (retrieved by Nelson and Cox, 2004).

Novel aspects of membrane structure also include the high density of proteins in the bilayer, which makes it a molecularly "crowded" space with important physiological consequences, as well as the existence of proteins that bind the membranes on a temporary basis, thus establishing a continuum between the purely soluble proteins, never in contact with membranes, and those who cannot exist unless bilayer-bound (Goñi, 2014).

The biological importance of membrane proteins is clearly reflected in two numbers. First, about 30% of eukaryotic genome is predicted to encode for membrane proteins (Engel and Gaub, 2008) and second, membranes contain up to 80% (w/w) of proteins (Luckey, 2008). Membrane proteins perform a wide range of essential cellular functions, most of which are regulated by a variety of membrane protein interactions. Channels, pores, pumps and transporters facilitate the exchange of membrane-impermeable molecules between cellular compartments and between a cell and its extracellular environment. Transmembrane receptors sense changes in the cellular environment and, typically through associated proteins, initiate specific cellular responses. Owing to their central role in almost all physiological processes, membrane proteins constitute more than 60% of approved drug targets and their three-dimensional (3D) structures are eagerly sought to assist in structure-based drug design (Yildirim *et al.*, 2007; Salom and Palczewski, 2011).

1.5.2 Principles of membrane transport

Membranes are responsible for the selective permeability of cell envelopes that enables cells to take up nutrients and exclude harmful agents. The permeability properties are determined by the lipid and protein components of membranes. In general, the lipid bilayer is readily penetrated by non-polar molecules, but is nearly impermeable to ions and hydrophilic compounds (Figure 1.13), thus enabling the conservation of electrochemical gradients that are critical for cell metabolism. The movement of those substances across the membrane is assisted by specialized membrane proteins or protein complexes. Surprisingly, some small polar molecules are capable of permeating the bilayer without the aid of transport proteins (Luckey, 2008).
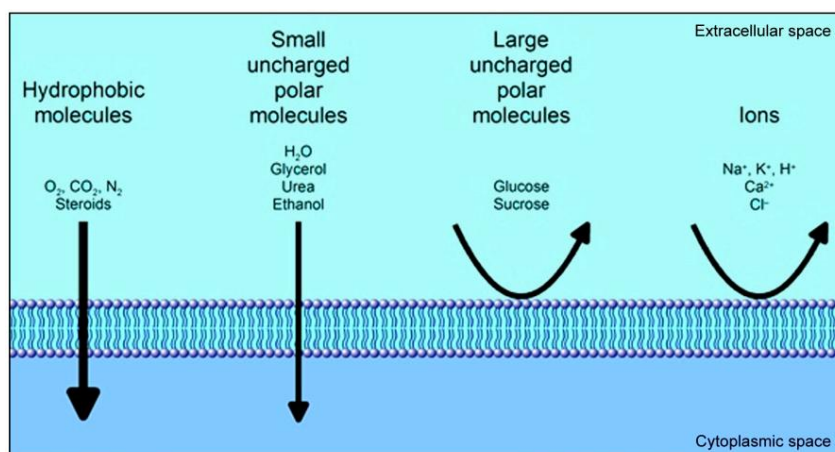
Figure 1.13. Permeation through pure lipid bilayers (adapted from http://www.physiologyweb.com).

Based on its energetics, a transport system can be classified as passive or active. Passive transport may be through the lipid bilayer (simple diffusion) or mediated by a channel (passive diffusion) or a facilitative transporter (facilitated diffusion or uniport). Passive transport systems are energy independent, since substances cross the lipid bilayer down their electrochemical gradient (Figure 1.14).
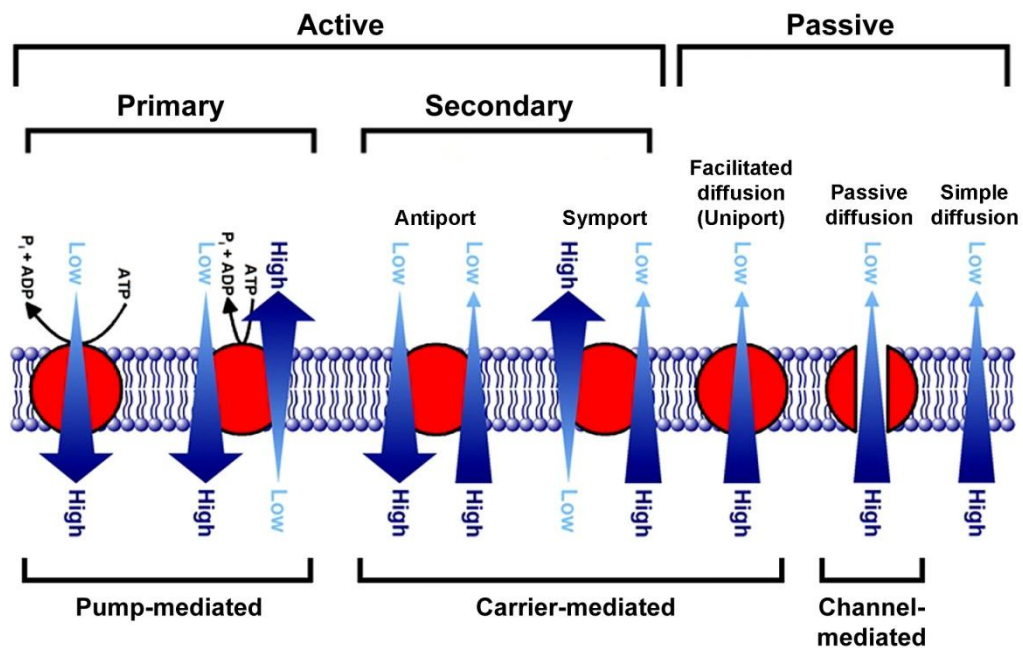
Figure 1.14. Overview of the mechanisms of membrane transport (adapted from http://www.physiologyweb.com).

In contrast, transport is considered active when the solute is transported against its chemical and/or electrical gradient. Active transport is also mediated by transporters (also called carriers or permeases) and can be divided in two types based on the type of energy used. Primary active transport uses a primary source of energy, such as adenosine-triphosphate (ATP) hydrolysis, light absorption or electron force. The resulting membrane potential can be used in turn to drive other cellular processes, such as the formation of action potentials in neurons or the transport of nutrients and metabolites by secondary active transporters. Primary active transporters are also referred to as pumps.

Secondary active transporters, on the other hand, use electrochemical potentials of co-substrates as an energy source. They do that by coupling the movement of the substrate to be transported against the electrochemical gradient to the movement of an ion, usually H^+ or Na^+, downhill the electrochemical gradient, which is an energy-releasing procedure. It is thus a "secondary" process in the sense that the source of

energy must be first generated by ATP-dependent (primary transport) mechanisms (Forrest *et al.*, 2011). Secondary active transporters can be symporters, that transport two or more chemical species in the same direction or antiporters that catalyze the exchange of one or more chemical species for another (Figure 1.14). They exhibit a huge diversity of amino acid sequences, 3D structures and substrates. At the level of primary structure, amino acid sequence analyses suggest that there are more than 100 distinct families of secondary active transporters (Krishnamurthy *et al.*, 2009).

The main difference between channels and carriers is that channel proteins do not need to bind the substrate. Instead, they form hydrophilic selective gated pores that extend across the lipid bilayer and allow specific solutes (usually ions of appropriate size and charge) to flow rapidly down chemical and electrostatic gradients. Carriers, on the other hand, bind the specific substrate and undergo a series of conformational changes in order to transfer the bound solute across the membrane, downhill (facilitated diffusion) or uphill (active transport) electrochemical gradients. Not surprisingly, transport through channel proteins occurs at a significantly faster rate than transport mediated by carrier proteins (Dahl *et al.*, 2004; Diallinas, 2008a).

1.5.3 Structural and functional features of secondary active transporters

In recent years, the availability of 2D and 3D structures obtained by X-ray and EM crystallography, as well as contributions from computational and theoretical approaches, have greatly enhanced our understanding of the molecular function of transporters. Since 2002, when the first crystal structure of a secondary transporter at atomic resolution was obtained (bacterial multidrug efflux transporter AcrB; Murakami *et al.*, 2002), there is a growing amount of well-resolved 3D structures, providing structural information on membrane-bound transporters. Despite these advancements, however, the number of well-resolved transporter structures is still rather limited in comparison to the numerous high-resolution structures available for soluble enzymes. Moreover, static pictures, even of high resolution, cannot explicitly describe the dynamic aspects of carrier function and thus the inherently dynamic process of transport is still not completely understood (Forrest *et al.*, 2011).

All described secondary active transporters are integral membrane proteins with 4-14 (most commonly 10-12) transmembrane α-helices connected by intracellular and extracellular loops. Surprisingly, transporters of functionally and evolutionary distinct protein families with no primary amino acid sequence similarity

and different substrate specificities have repeatedly been found to exhibit similar folds, such as the MFS (Major Facilitator Superfamily), the NhaA or the LeuT folds (see later). Moreover, several symporters and antiporters have been shown to share common structural folds, indicating that protein architecture does not dictate the mode of transport (Diallinas, 2008a; Forrest *et al.*, 2011).

A prominent feature of most available structures is an occurring internal structural symmetry, where two or more repeated structural elements (repeats) are related to each other by a distinct symmetry axis. The conformational changes that transporters undergo appear to involve symmetry-related movements of those structural repeats. In some cases, such as the MFS fold, the repeats show sequence homology, suggesting that they resulted from a gene duplication event. The symmetry axis runs perpendicular to the membrane plane and in between the repeats, straight through the center of the carrier, dividing it into two distinct N- and C-terminal halves (Forrest *et al.*, 2011; Figure 1.15A). In other cases, however, no sequence homology is observed. The symmetry axis runs parallel to the membrane plane and through the repeats (rather than between them). Therefore, the repeats have inverted topologies and their helices are interwoven (Figure 1.15B).
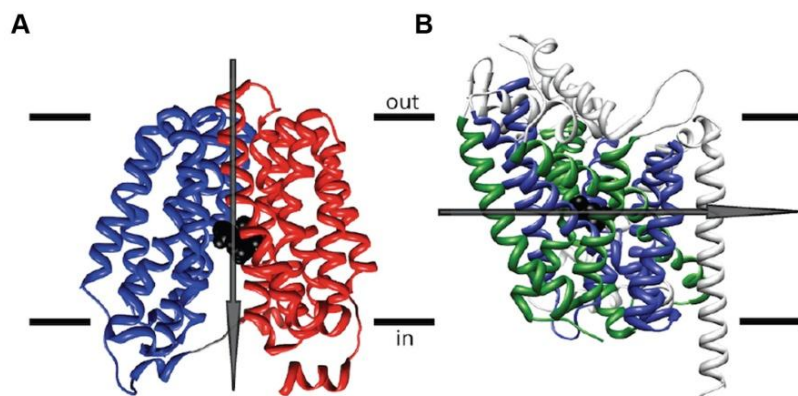
Figure 1.15. Internal structural symmetry within secondary active transporters. **A.** Sideview of bacterial H+/lactose symporter LacY. The six α-helices from each of the two structural repeats are depicted in blue and red, respectively. **B.** Sideview of a monomer of the bacterial Na^+/ Leu symporter LeuT. The five α-helices from each of the two structural repeats are depicted in blue and green, respectively. Both domains exhibit strong intertwining. Symmetry-unrelated helices are depicted in white. The symmetry axis is shown as an arrow. Bound substrates, thiogalactoside (LacY) and leucine (LeuT) are displayed as black spheres. The membrane plane is shown as black lines (adapted from Kebbel, 2013).

Most transporters are found in dimeric forms (e.g. bacterial Na^+/ Leu symporter LeuT; Yamashita *et al.*, 2005; Figure 1.16B), although there are examples available for other oligomeric states, such as monomers (e.g. bacterial H^+/lactose symporter
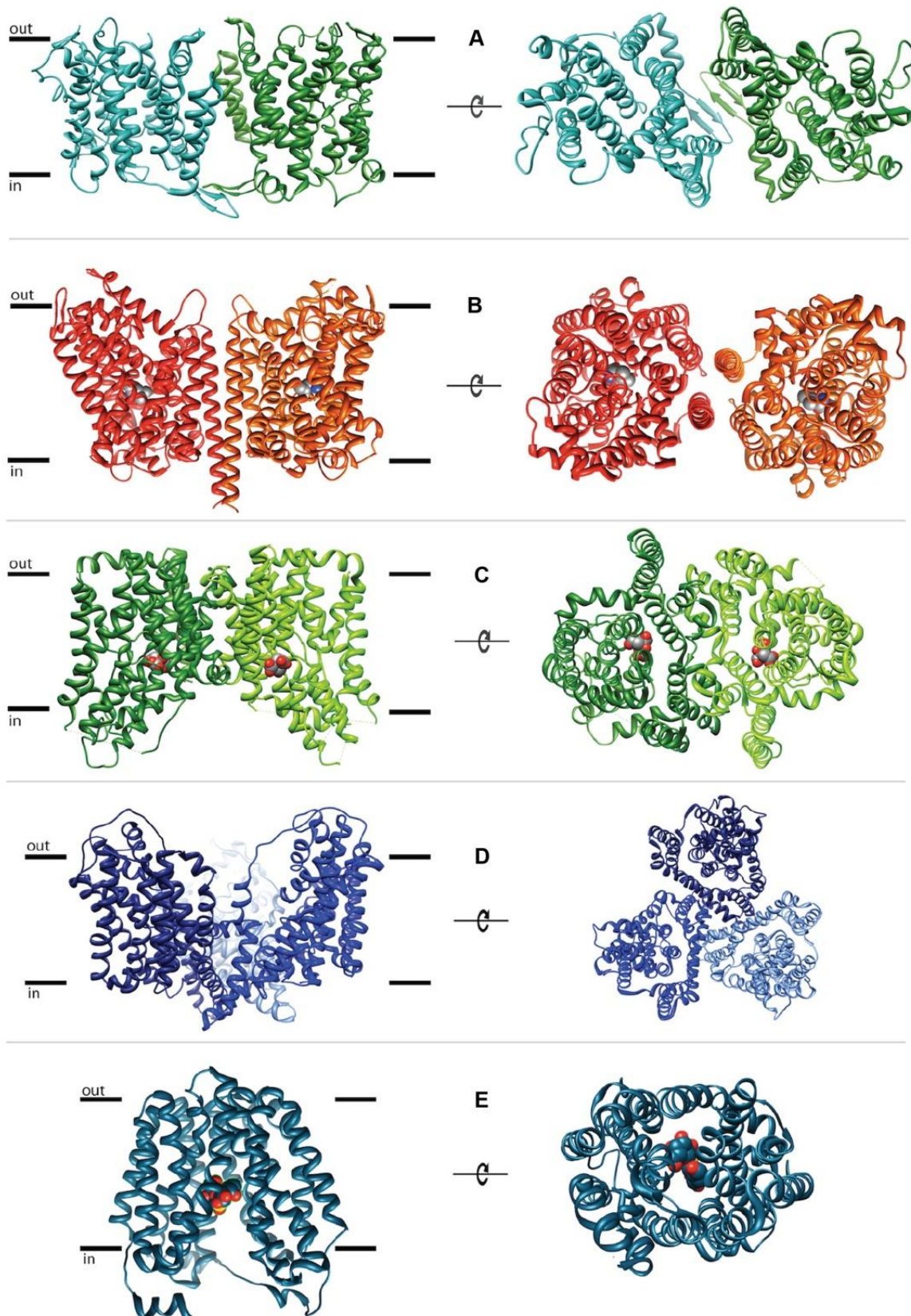
Figure 1.16. Structural diversity of secondary active transporters. Sideview (left) and topview (right) of (**A**) NhaA, (**B**) LeuT, (**C**) V*c*INDY, (**D**) GltPh and (**E**) LacY, a paradigm for the MFS family. Monomers within higher oligomers are depicted in different colors. Bound substrates are displayed as spherical structures, where available. The membrane plane is shown as black lines (retrieved from Kebbel, 2013).

LacY; Abramson *et al.*, 2003; Figure 1.16E) and trimers (e.g. bacterial Na^+/aspartate symporter GltPh; Yernool *et al.*, 2004; Figure 1.16D). The interaction interface between monomers can be formed by β-sheets, as exclusively found in NhaA (bacterial H^+/ Na^+ antiporter; Hunte *et al.*, 2005; Figure 1.16A) or by up to seven α-helices (e.g. bacterial Na^+/dicarboxylate symporter V*c*INDY; (Mancusso *et al.*, 2012; Figure 1.16C). In addition, several transporters have been crystallized in the presence of native or artificial substrates (Figure 1.16B, C), which were bound in the center of each monomer, close to the middle of the membrane plane.

In respect to function, transport is characterized by Michaelis-Menten kinetics, similar to enzymatic reactions. Transporters are "saturable", meaning that at high substrate concentrations all of the transporter molecules have their binding sites occupied and the rate of transport reaches a maximum (V_{max}). Each transport protein binds specific substrates and has an affinity constant (K_m) for each of those substrates that is equal to the concentration of the solute when the transport velocity is half its maximum value.

1.5.4 The model of "alternating access" for secondary transporters

As a basic mechanistic explanation for the transport function of secondary active transporters, the model of "alternating access" has been supported by numerous kinetic, biochemical and biophysical studies. According to this model, the transporter cycles through a set of defined conformational states providing a unique structural framework for efficient substrate transport.

The principle of secondary transport for an importing symporter is illustrated in Figure 1.17A. Here, the substrates first bind to the empty transporter in the outward facing conformation, where the binding site is only accessible from the outer side (Figure 1.17A,B). This is followed by the closure of outer molecular gates to hinder substrate diffusion. The gate closure is facilitated by the substrate-induced rearrangement of single amino acid side chains or by the bending of single α-helices and/or helical hairpins as found for LacY and LeuT, respectively. The transport cycle then proceeds by a substantial conformational change from the closed outward facing to the closed inward facing conformation (Figure 1.17A,D). During this structural switch the transporter passes through the closed occluded form (Figure 1.17A,C), where the substrates are inaccessibly buried within the protein. This is followed by the opening of the inner molecular gates that enables the release of the substrates
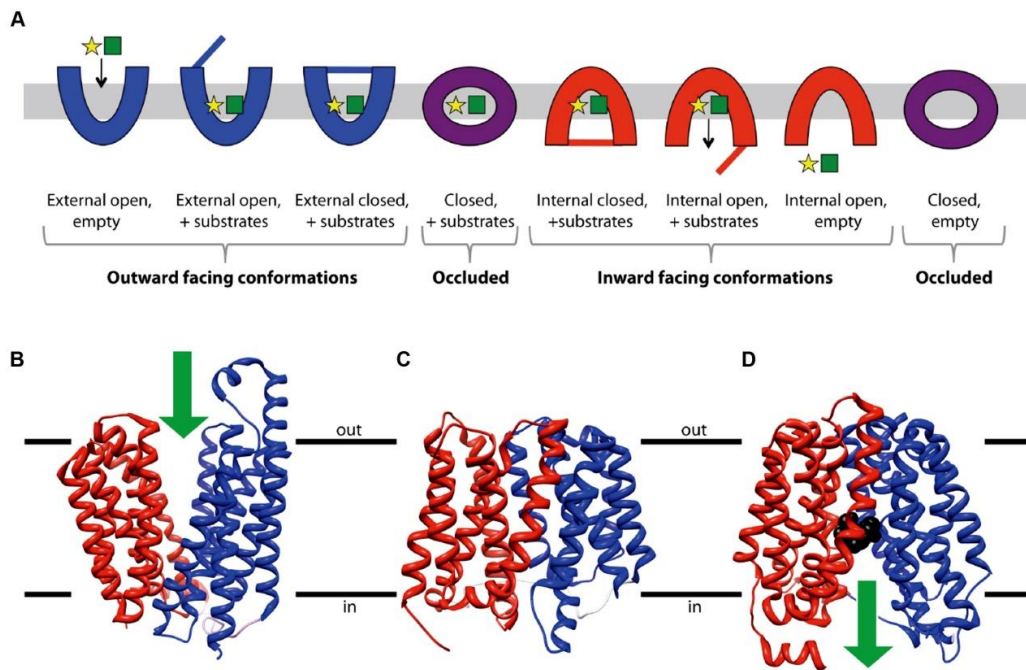
Figure 1.17. The principle of secondary symport by the "alternating access" mechanism. **A.** Secondary active transporters exhibit three main conformations: outward-facing (blue), occluded (purple) and inward-facing (red). Substrate binding at one side of the membrane induces the closure of outer molecular gates, followed by a substantial conformational change, which eventually leads to the inward-facing conformation. Opening of the inner molecular gates enables the substrates to be released. Main substrates and co-substrates are shown as yellow stars and green rectangles (modified version from Kebbel, 2013, original published in Forrest *et al.*, 2011). **B.** V-shaped outward-facing conformation of FucP (Dang *et al.*, 2010). **C.** Occluded state of EmrD (Yin *et al.*, 2006). **D.** A-shaped inward-facing conformation of LacY. All three belong in the MFS. The symmetry-related N- and C-terminal halves (blue and red) rock against each other. Where available, substrates are shown as black spheres. Green arrows show substrate diffusion routes (retrieved from Kebbel, 2013).

from the transporter protein into the cytosol. The transport cycle is completed by the switching of the transporter from the empty internal form, back to the empty external conformation, where the protein is ready to start further cycles (Diallinas, 2008a; Forrest *et al.*, 2011). In the case of an antiporter, a single substrate is transported during the conversion from the closed outward facing to the closed inward facing conformation, while the co-substrate is transported in the returning step.

The transition from the outward to the inward-facing state requires a substantial conformational change of the carrier protein, which usually occurs via rocking movements of its structural repeats. A rocker-switch mechanism has been described for LacY and other proteins of the MFS fold (Figure 1.17A-C). Two other variations of this mechanism exist, the "rocking bundle" mechanism available for the LeuT fold (Forrest and Rudnick, 2009) and the less common "gating mechanism" for GltPh (Reyes *et al.*, 2009). All three mechanisms, however, are in good agreement with the "alternating access" model.

1.5.5 Fungal nucleobase transporters

Nucleobases (purines and pyrimidines) and nucleobase analogues are highly hydrophilic compounds that do not readily diffuse across lipid bilayers (Figure 1.18). Thus, their transport is mediated by specific transmembrane transport proteins. Nucleobase transporters have been identified in bacteria, fungi, protozoa, algae, plants and mammals. The universality of specific purine-pyrimidine transport systems reflects the importance of nucleobases, not only in nucleotide and nucleic acid biosynthesis, but also in cell signaling, nutrition, response to stress and cell homeostasis (De Koning and Diallinas, 2000). Moreover, nucleobase analogues are widely used as antimetabolites against a host of different diseases and infections, ranging from antitumour and leukaemia chemotherapy (5-fluorouracil, 6-mercaptopurine, thioguanine) and antiviral compounds (acyclovir, ganciclovir, carbovir) to antibiotics and drugs against parasitic disease (allopurinol, pyrimethamine) and even for the prevention of organ transplant rejection (azathioprine) and the treatment of gout (allopurinol; Rundles *et al.*, 1966; Elion, 1989; Kolb, 1997).
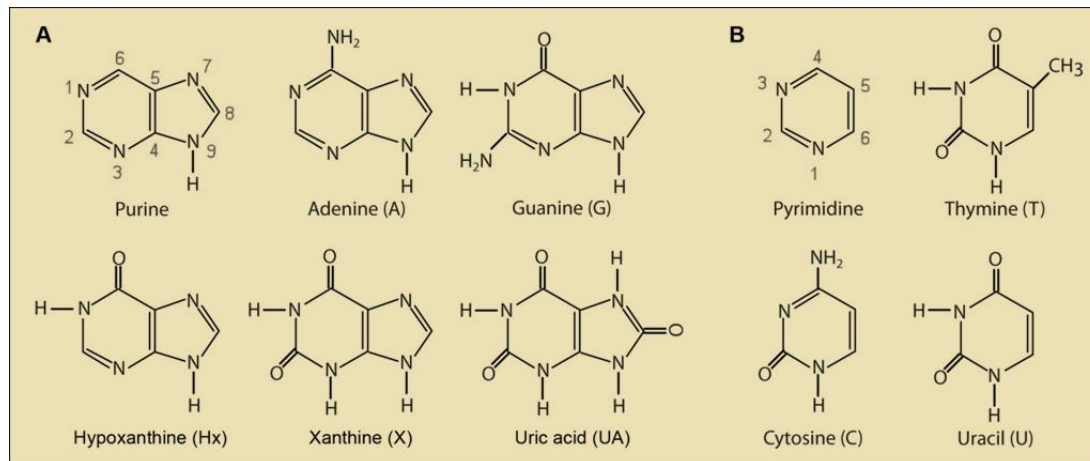
Figure 1.18. Structural formulas of (**A**) purines and (**B**) pyrimidines transported by fungal nucleobase transporters (adapted from http://goo.gl/SH45rB).

Early genetic and biochemical studies established the presence of highly specific nucleobase transporters in fungi (Darlington and Scazzocchio, 1967). Most fungi can use purines, but not pyrimidines, as fairly good nitrogen sources (see 1.4.2). The lack of growth on purines or the use of purine or pyrimidine toxicity, caused either by an excess of a base (e.g. uric acid, uracil) or by a cytotoxic analogue (e.g. oxypurinol, allopurinol, 8-azaguanine, 5-fluorouracil), provided a powerful tool

to select mutants and identify the corresponding genes (Pantazopoulou and Diallinas, 2007; Katerina Galanopoulou, Claudio Scazzocchio, Maria Eleftheria Galinou, Weiwei Liu, Fivos Borbolis, Mayia Karachaliou, Nathalie Oestreicher, Dimitris G. Hatzinikolaou, George Diallinas and Sotiris Amillis. Fungal Genetics and Biology. In revision).

Cloning and genome sequencing showed that the fungal nucleobase transporters belong to three evolutionary distinct protein families: the Nucleobase Cation Symporter family 1 (NCS1), also known as the Purine-Related Transporter family (PRT), the AzgA-like family and the Nucleobase-Ascorbate Transporter family(NAT), also known as the Nucleobase Cation Symporter family (NCS2). All these families are classified as secondary active transporters catalyzing the symport of purines with protons. Three criteria have been used for classifying transporters into these families. Firstly, an overall sequence identity >21% and sequence similarity >40%. Secondly, similar hydropathy profiles compatible with 9–14 putative α-helical transmembrane segments (TMS). Thirdly, the presence of several conserved short sequence motives located at similar topological positions (De Koning and Diallinas, 2000; Pantazopoulou and Diallinas, 2007).

The NCS1/PRT family

Members of this family are, in general, 419–635 amino acid residues long and most probably possess 12 putative TMSs and cytoplasmic N- and C-termini. At least some of them have been shown to function as H^+ symporters. Based on the fact that some NAT/NCS2 symporters have similarities to NCS1/PRT members, the two families are considered to be distantly related. The NCS1/PRT family is restricted to prokaryotes, fungi and plants and includes transporters for purines, cytosine, uridine, allantoin, pyridoxine or thiamine (http://www.tcdb.org/browse.php). In 2008, the crystal structure of a bacterial member of the NCS1 family, namely the Mhp1 benzyl-hydantoin permease from *Microbacterium liquefaciens*, was reported (Weyand *et al.*, 2008). Mhp1 contains 12 transmembrane helices, 10 of which are arranged in two inverted repeats of five helices, resulting in a topology very similar to that of LeuT (see 1.5.3).

In *A. nidulans*, the NCS1 transporters FurA and FurD, homologues of yeast Fur4p and the FcyB, homologue of yeast Fcy2p, have been functionally characterized (Amillis *et al.*, 2007; Vlanti and Diallinas, 2008; Hamari *et al.*, 2009).

FurA is an allantoin transporter, whereas the FurD protein is able to recognize with high affinity uracil, thymine and several 5-substituted analogues of uracil, and with moderate-affinity uric acid and xanthine (Table 1.1). FcyB mediates high-affinity transport of adenine, hypoxanthine, guanine and cytosine, but has a rather low-capacity, thus acting basically as a cytosine supplier and only secondarily as a purine carrier. High-capacity purine uptake in *A. nidulans* is catalyzed by another transporter, called AzgA (see below). Based on the Mhp1 crystal structure a 3D of the FcyB has been constructed. The model consists of 12 transmembrane, α-helical segments (TMSs) and cytoplasmic N- and C-tails. A distinct core of 10 TMSs is made of two intertwined inverted repeats (TMS1-5 and TMS6-10) that are followed by two additional TMSs. TMS1, TMS3, TMS6, and TMS8 form an open cavity that is predicted to host the substrate binding site (Krypotou *et al.*, 2012).

Table 1.1. Families, specificity and kinetics of fungal nucleobase transporters (adapted from Pantazopoulou and Diallinas, 2007).

Fungus/transporter	Family	Physiological substrates [$K_{m/i}$ (μM)]	Other ligands < 100 μM [$K_{m/i}$ (μM)]	Transport capacity
A. nidulans				
UapA	NAT/NCS2	X [7], UA [8]	2TX [63], 3MX [28], 8MX [100], OX [103], ALL*	H
UapC	NAT/NCS2	X[4], UA[136]	1MX [< 50], 2TX [< 50], 3MX [~100], 8MX [~100], OX [38], ALL*	M
AzgA	AZGA-like	HX[1.5], AD[3], GU[3]	PU [99], 6TPU [78], 2,6DAPU [2], 8AZX [11]	H
FcyB	NCS1/PRT	AD[7], HX[20], CY[20], GU[12]	ND	L
FurD	NCS1/PRT	UR [0.4]	THY [3.3], 1MUR [4], 2TUR [8], 4TUR [14], 5FUR [0.5], 6AZUR [2], 6MUR [15], X [94], UA [99]	H
A. fumigatus				
UapC	NAT/NCS2	X[5.5], UA[89]	8MX [50], 1MX [60], 2TX [65], 3MX [100], OX [103],	H
AzgA	AZGA-like	AD[3.5], HX[6], GU[8]	2,6 DAPU [3], PU [40], 6TPU [48], 9MGU [69]	M
FcyB[†]	NCS1/PRT	ND	ND	L
FurD[†]	NCS1/PRT	ND	ND	H
S. cerevisiae				
Fcy2p	NCS1/PRT	AD[1.8], HX[2.5], CY [1.8], GU[ND]	ND	H
Fur4p	NCS1/PRT	UR [2.5], URD [ND]	5FUR, 5FURD[‡]	H
C. albicans				
Xut1p	NAT/NCS2	X [4], UA [50]	2TX [30], 2TUA [97], 3MX [22], 6TUA [84], 8MX [80], 8AZX [55], OX [4],	H
Fcy21p	NCS1/PRT	HX[4], AD[16], GU[53], CY [4]	3MAD [22], 3DAZG [72], 5MCY [20], 5FCY [35]	H
Fur4p[§]	NCS1/PRT	ND	ND	H

*Allopurinol affinity cannot be determined due to non-Michaelis–Menten kinetics (M. Koukaki, G. Diallinas, unpublished data). Based on genetics and growth tests allopurinol is formally shown to be a substrate of UapA and UapC and that concentrations as low as 2 μM lead to allopurinol sensitivity.
[†]FcyB and FurD orthologues of *Aspergillus fumigatus* have only been recognized *in silico* based on the *Aspergillus nidulans* proteins.
[‡]Based on growth tests.
[§]A Fur4p orthologue of *Candida albicans* has only been recognized *in silico* based on the *Saccharomyces cerevisiae* protein.
X, xanthine; UA, uric acid; AD, adenine, HX, hypoxanthine; GU, guanine; CY, cytosine; UR, uracil; 1MX, 1-methylxanthine; 2TX, 2-thioxanthine; 3MX, 3-methylxanthine; 8MX, 8-methylxanthine; OX, oxypurinol; ALL, allopurinol; PU, purine; 6TPU, 6-thiopurine; 2,6DAPU, 2,6-diaminopurine; 8AZX, 8-azaxanthine; THY, thymine; 1MUR, 1-methyluracil; 2TUR, 2-thiouracil; 4TUR, 4-thiouracil; 5FUR, 5-fluorouracil; 6AZUR, 6-azauracil; 6MUR, 6-methyluracil; 9MGU, 9-methylguanine; 2TUA, 2-thiouric acid; 6TUA, 6-thiouric acid, 3MAD, 3-methyladenine; 3DAZG, 3-deazaguanine; 5MCY, 5-methylcytosine; 5FCY, 5-fluorocytosine; URD, uridine; FURD, 5-fluorouridine. H, M and L stand for high, moderate or low capacity of transport, respectively, as this is judged by calculated V_m or/and growth tests. ND, not determined.

The AzgA-like family

AzgA-like proteins are 423–594 amino acids long and are predicted to possess 10–12 TMSs. Based on overall primary and secondary sequence comparisons, AzgA-like proteins are grouped as a separate subfamily within the MFS (http:// www.tcdb.org/). However, AzgA also shares some common features with NAT/NCS2, a family clearly grouped outside the MFS. Moreover, AzgA does not possess the two-fold symmetry present in MFS proteins; therefore, can be considered an independent family. The AzgA-like family includes homologues in bacteria, archaea, fungi and plants, but only the *A. nidulans* and *A. fumigatus* proteins have been characterized as hypoxanthine–adenine–guanine/H^+ symporters (Cecchetto *et al.*, 2004; Goudela *et al.*, 2006). Fungal proteins share up to 35% and 44% identity with bacterial and plant homologues, respectively, while identities among fungi vary from 45% to 75%.

The AzgA protein of *A. nidulans* is a 580-amino-acid protein consisting of 12 TMSs. It has been functionally characterized (Cecchetto *et al.*, 2004; Goudela *et al.*, 2006; Pantazopoulou *et al.*, 2007) as a high-affinity, high-capacity transporter, specific for adenine, guanine, hypoxanthine, 8-azaxanthine and 2,6-diaminopurine (Table 1.1). It also transports efficiently the analogues purine and 8-azaguanine. Very recently, AzgA has been shown to be topologically similar to the NAT/NCS2 family, implying that AzgA-like proteins constitute a distant sub-group of the latter (Krypotou *et al.*, 2014).

The NAT/NCS2 family

NAT members usually are 414-650 amino acids long and are predicted to contain 12-14 α-helical TMSs and cytoplasmic N- and C-termini (http://www.tcdb.org /browse.php). NATs contain two highly conserved motifs; the NAT signature motif, [Q/E/P]-N-X-G-X-X-X-T-[R/K/G] (where X is a hydrophobic amino acid residue) located in an amphipathic region just upstream of TMS9 and the QH motif in the middle of TMS1, known to be critical for function of well-studied examples of this family. Another characteristic of the NATs is the presence of some almost absolutely conserved single polar/charged amino acids (Diallinas and Gournas, 2008).

The NAT is a ubiquitous family consisting of proteins derived from Gram-negative and Gram-positive bacteria, archaea, fungi, plants and animals (http://www.tcdb.org /browse.php). It is subdivided into three sub-families in respect to substrate specificity. The first, present in bacteria, fungi and plants, is specific for

the oxidized purines xanthine and/or uric acid. The second that is specific for uracil, is present only in bacteria, since fungal uracil transporters belong to the NCS1/PRT (see above). The third sub-family is present in vertebrates and is specific for L-ascorbic acid. No function is known for metazoan homologues outside the vertebrates (Diallinas and Gournas, 2008). All known bacterial, fungal and plant NATs are high-affinity H^+ symporters, while the mammalian SVCTs use Na^+ for L-ascorbate symport (Liang *et al.*, 2001).

Aspergillus nidulans has two NAT/NCS2 members, called UapA and UapC. Both are extensively characterized with respect to transcriptional regulation, post-translational down-regulation by endocytosis and sorting in the vacuoles, expression during asexual and sexual development and structure–function relationships. UapA is analyzed in detail in section 1.5.6. UapC (Diallinas *et al.*, 1995; Ravagnani *et al.*, 1997; Valdez-Taubas *et al.*, 2000; Valdez-Taubas *et al.*, 2004) is a 580 amino acid protein and a very similar paralogue of UapA (62% identity). UapC has a high affinity for xanthine and a moderate affinity for uric acid and other xanthine analogues (Table 1.1). It also has a very low affinity ($K_m > 500$ μM) and very low capacity for binding of other purines, not recognized by UapA, such as adenine or hypoxanthine (Helen Tsilivi and George Diallinas, unpublished results; Pantazopoulou and Diallinas, 2007).

A single *A. fumigatus* UapA/UapC homologue (61% and 80% identity, respectively) has been characterized kinetically by expression in an *A. nidulans* strain carrying deletions of its endogenous purine transporter genes (Goudela *et al.*, 2008). This carrier resembles UapC with respect to its substrate affinity and specificity (Table 1.1) but has a high transport capacity, similar to UapA. Xut1, a *Candida albicans* UapA homologue (55% identity) is a high-capacity transporter with a high affinity for xanthine and a moderate affinity for uric acid (Table 1.1; Goudela *et al.*, 2005). Most fungi possess UapA/C homologues, usually one in each species; *S. cerevisiae* and several other members of Saccharomycetaceae, however, do not have any NAT/NCS2 protein, reflecting their lack of enzymes involved in xanthine or uric acid utilization (Wong and Wolfe, 2005; Claudio Scazzocchio, unpublished results). Several protozoa have also been found to lack NAT/NCS2 transporters (Gournas *et al.*, 2008).

Recently, the first crystal structure of a member of the NAT family, namely the uracil/ H^+ symporter UraA from *Escherichia coli*, was obtained (Lu *et al.*, 2011).

UraA was crystallized in complex with uracil at a resolution of 2.8 Å and revealed a novel structural fold of 14 TMSs divided into two inverted repeats, with a critical pair of anti-parallel β-strands located between TMS3 and TMS10. It was also reported that the structure is spatially arranged into a core domain and a gate domain.

NAT-mediated purine or pyrimidine uptake in microorganisms and plants seems to serve both catabolic and anabolic needs, but recent evidence suggests that NAT-mediated uric acid redistribution in plant vascular tissues (Maurino *et al.*, 2006) or fungal conidiospores (Pantazopoulou *et al.*, 2007) might play a critical role for development and reproduction. In mammals, NAT-mediated ascorbic acid transport is essential for brain development (Sotiriou *et al.*, 2002). Eukaryotic NATs are tightly regulated, in response to physiological and developmental signals, both at the transcriptional (see 1.4.1) and the post-translational level. The latter is mainly exerted by regulated endocytosis and probably recycling to the PM (Gournas *et al.*, 2008).

1.5.6 UapA, the prototype member of NAT

UapA, the prototype member of NAT, is one of the most extensively studied eukaryotic carriers with respect to regulation of expression and structure–function relationships. Historically, *uapA* was among the first eukaryotic transporter genes to be genetically identified (Darlington and Scazzocchio, 1967) and cloned (Diallinas and Scazzocchio, 1989; Gorfinkiel *et al.*, 1993) Since then, the ease of genetic manipulation of *A. nidulans* enabled the selection or construction of a great variety of *uapA* mutants through classical or reverse genetics, which were subsequently analysed biochemically in great detail with simple kinetic studies.

UapA structure and function

UapA is a high affinity (7-8 μM), high capacity H^+ symporter specific for the uptake of the oxidized purines, xanthine and uric acid. Several purine analogues, such as 2-thioxanthine, 3-methyloxanthine, 8-methyloxanthine, oxypurinol and allopurinol, have also been shown to act as substrates or ligands, albeit with lower affinity (Table 1.1; Goudela *et al.*, 2005; Koukaki *et al.*, 2005). In addition, kinetic analyses of UapA-mediated transport using more than a hundred different UapA mutants, combined with genetic approaches, have revealed specific amino acid residues that are involved in purine specificity, binding and transport. Five of those, Q408, G411,

T416, R417 and the irreplaceable N409, belong to the NAT motif ^{408}**QN**N**G**VIAL**TR**^{417} (Koukaki *et al.*, 2005).

Based on its primary structure, UapA is predicted to have its 574 amino acids distributed in 12 α-helical TMSs, separated by hydrophilic loops and a segment of amphipathic nature, and thus ambiguous topology, between TMS8 and TMS9. Within this segment lays the NAT signature motif. Moreover, the N- and C-termini are predicted to be cytoplasmic (Koukaki *et al.*, 2005; Papageorgiou *et al.*, 2008). However, the recent release of the crystal structure of the NAT member UraA of *E. coli* (Lu *et al.*, 2011), allowed the construction of a 3D topological model of UapA. The model corresponds to a cytoplasm-facing conformer made of 14 TMSs divided into two inverted repeats (TMS1-7 and TMS8-14). The structure is spatially arranged into a core and a gate domain, consisting of TMS1-4/8-11 and TMS5-7/12-14, respectively (Figure 1.19A; Amillis *et al.*, 2011; Kosti *et al.*, 2012).

In addition, advanced molecular simulations allowed the outlining of a possible substrate translocation mechanism, as well as possible selectivity gates at the outward and inward ends of the translocation pathway. The proposed pathway starts from the centrally located major substrate binding site (F155, E356, A407, Q408) and is followed by subsequent poses of xanthine docking towards the cytoplasmic face of the transporter, close to residues D360, A363, G411, T416, R417, V463 and A469 (Figure 1.19B; Kosti *et al.*, 2012).
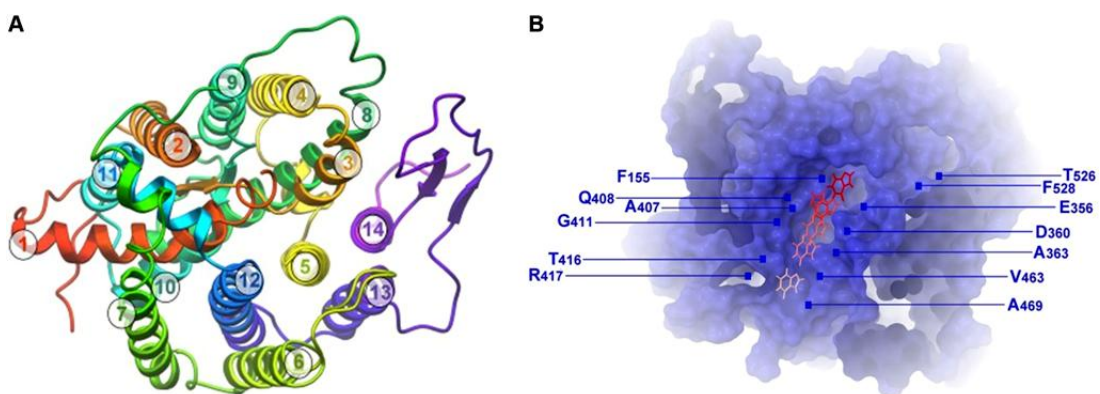
Figure 1.19. Theoretical structure of UapA. **A.** Top view of UapA 3D model, indicating core (TMS1-4/8-11) and gate (TMS5-7/12-14) domains and TMS numbering (retrieved from Kosti *et al.*, 2012). **B.** A xanthine translocation pathway in the cytoplasm-facing UapA model. Residues F155, Q408, E356 and A407 define the major substrate binding site, whereas T526 and F528 indicate a putative outward-facing gate (retrieved from Kosti *et al.*, 2012).

Regulation of UapA expression

The regulation of UapA expression has also been studied in great detail. In resting conidiospores, mRNA steady-state level of *uapA* gene is undetectable or very low. The transcription of *uapA* is developmentally activated during the isotropic phase of conidiospore germination, prior to the first nuclear division and polarity establishment, and leads to the appearance of transport activity within a short time delay (30-60 min). *uapA* transcriptional activation seems to be dependent on the general transcription factor AreA, but is independent of the pathway-specific transcriptional regulator UaY (see also 1.4.1) and is not affected by the temperature, the pH or the absence of a carbon or a nitrogen source. In fact, the only requirement for the early *de novo* transcriptional activation of *uapA* during germination is hydration of the dormant conidiospores, suggesting that *A. nidulans* uses its transporters both for sensing the environment and for the transport of solutes. Interestingly, genes encoding enzymes necessary for purine catabolism (*uaZ, hxA*) are not transcriptionally activated during the isotropic growth phase of germination, but only at later stages of mycelium development (Amillis *et al.*, 2004).

Once germination is completed, regulation of UapA expression occurs through both transcriptional and post-translational mechanisms. Transcription of *uapA* is subject to purine induction and nitrogen metabolite repression (see also 1.4.1). In the absence of purines, when a non-repressing nitrogen source (urea, NO_3^-, proline) is used in the medium, *uapA* is transcribed at basal levels. Purines, through their oxidation to uric acid, induce *uapA* transcription several fold. This is mediated by the positive-acting pathway-specific regulatory protein UaY that contains a typical zinc binuclear cluster domain, through which it binds to the promoter regions of *uapA* (Scazzocchio *et al.*, 1982; Suarez *et al.*, 1995). However, this is only possible in the absence of a primary nitrogen source (NH_4^+ or Gln), since their presence drastically represses *uapA* expression by inactivating the global GATA-type zinc finger transcription factor AreA (Arst and Cove, 1973; Ravagnani *et al.*, 1997).

Apart from the transcriptional control, ammonium-elicited down-regulation occurs also post-translationally via ubiquitination, endocytosis and targeting of UapA to the endosomal/vacuolar pathway for degradation. Recently, it has been shown that such a post-translational control is also elicited by the substrates of the transporter (Gournas *et al.*, 2010). The regulation of UapA endocytosis will be discussed in more detail in section 4.1.

UapA subcellular localization

The subcellular localization of the UapA has been extensively studied using Green Fluorescent Protein (GFP) tags (Pantazopoulou and Diallinas, 2006; Vlanti *et al.*, 2006; Pantazopoulou *et al.*, 2007; Papageorgiou *et al.*, 2008; Leung *et al.*, 2010; Gournas *et al.*, 2010; Kosti *et al.*, 2010). UapA-GFP is not expressed in resting conidiospores and only becomes evident after 4 h of germination at 25°C (equivalent to 2 h germination at 37°C). Interestingly, after 6 h of germination at 25°C, UapA-GFP is localized in cytoplasmic rings corresponding to the ER membrane. At later stages of germination and in mycelia, UapA-GFP appears in the PM and in the vacuoles, as a result of its constitutive degradation. The ER rings are not apparent anymore, suggesting that UapA exits rapidly from the ER membrane (Figure 1.20; Pantazopoulou and Diallinas, 2007).
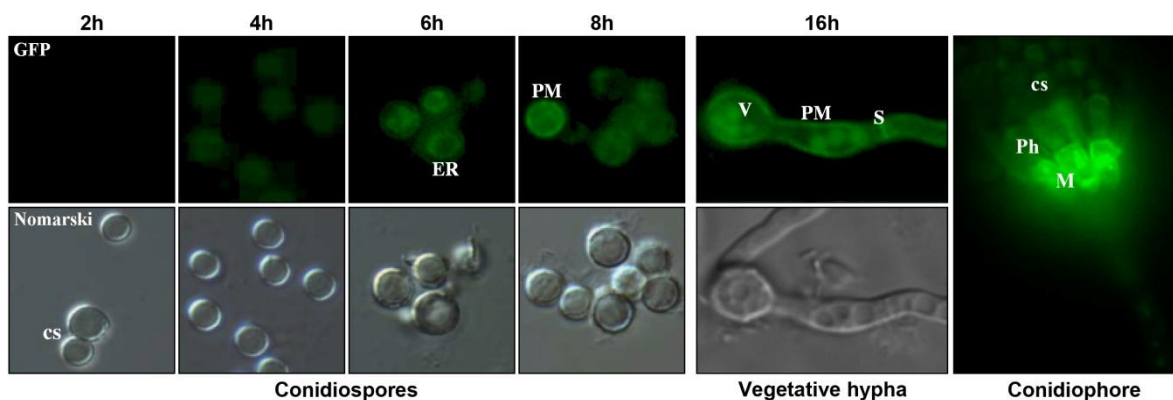
Figure 1.20. Expression of UapA-GFP in conidiospores, a vegetative hypha and a conidiophore, as visualized by epifluorescence microscopy. Growth was in minimal media with a non-repressing nitrogen source, at 25°C. Under the conditions used, 2 h correspond to the isotropic growth phase (conidiospore swelling, nuclear decondensation and changes in surface properties reflected by increased adhesion), 4–6 h coincide with the first nuclear division, polarity establishment and maintenance, 8 h is just prior germ tube emergence (Pantazopoulou *et al.*, 2007). cs, conidiospores; ER, endoplasmic reticulum; PM, plasma membrane; V, vacuoles; S, septa; Ph, phialidae; M, metulae (adapted from Pantazopoulou and Diallinas, 2007)

The expression of UapA-GFP was also tested in the sexual and the asexual reproduction structures of *A. nidulans*. The transporter was found to be expressed in the PM of ascogenous hyphae, in the outermost periphery of hülle cells and in the interconnecting hyphae of the latter. Interestingly, UapA-GFP is not expressed in the conidiophore stalk and the vesicle, but is highly expressed in the periphery of the metulae and to a lesser extent in the phialidae, while it was absent in the conidiospores. (Figure 1.20; Pantazopoulou *et al.*, 2007). We recently obtained

evidence that UapA localization is shared with its paralogue UapC, but not AzgA, suggesting that only purine transporters specific for uric acid and xanthine have a function in the compartments of the conidiophore of *A. nidulans*. Moreover, it was shown that through the activity of the UapA and UapC that are expressed in the asexually differentiated aerial cells, metabolically produced uric acid is actively transported from the mycelium to the conidiospores. This is the first time transporters are shown to mediate solute redistribution within fungal cells, in addition to their role as suppliers of nutrients from the growth medium (Katerina Galanopoulou, Claudio Scazzocchio, Maria Eleftheria Galinou, Weiwei Liu, Fivos Borbolis, Mayia Karachaliou, Nathalie Oestreicher, Dimitris G. Hatzinikolaou, George Diallinas and Sotiris Amillis. Fungal Genetics and Biology. In revision).

Upon treatment with NH_4^+, UapA-GFP internalizes from the PM and is sorted to the vacuoles for degradation. This is evident after 30 min of treatment and is clearly visible after 1 h in NH_4^+. After 2 h all UapA-GFP has disappeared from the PM and appears only in the vacuoles (Figure 1.21). Rapid internalization of UapA-GFP has also been observed in response to the substrates of the transporter, but seems to be mediated via a distinct regulatory mechanism (for details see 4.1; Gournas *et al.*, 2010).
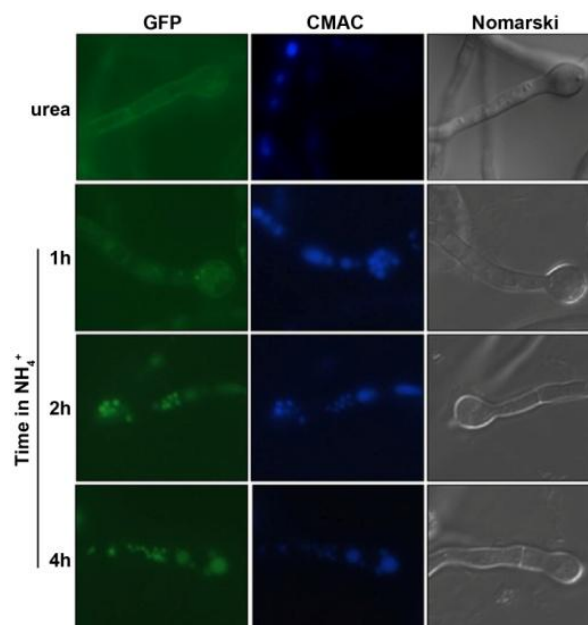
Figure 1.21. The effect of NH_4^+ on the expression of UapA-GFP. Epifluorescence microscopy of a UapA-GFP strain shifted in ammonium for 1, 2 and 4 h, after 16 h of growth in minimal media with urea as a nitrogen source, at 25°C. A control sample in urea, not shifted to ammonium, is also shown. CMAC vacuolar staining and Nomarski of the same samples are shown in the middle and right panels, respectively (adapted from Pantazopoulou *et al.*, 2007).

1.6   Intracellular trafficking of membrane proteins

1.6.1 General aspects of vesicular transport

A characteristic feature of all eukaryotic cells is compartmentalization. The presence of membrane-bound intracellular compartments enables the efficient separation of cell functions, but also creates the need for communication between them. A major process of communication between the different cellular compartments is vesicular transport (Tokarev *et al.*, 2009).

In this process, cargo-loaded vesicles are formed at a donor compartment with the help of specific coat and adaptor proteins, such as COPI (coat protein complex I), COPII (coat protein complex II) and clathrin (Kirchhausen, 2000; Bonifacino and Lippincott-Schwartz, 2003). These coats are supramolecular assemblies of proteins that are recruited from the cytosol to the nascent vesicles. The coats deform flat membrane patches into round buds, thus leading to the release of coated transport vesicles (Figure 1.22). They also participate in cargo selection by recognizing sorting
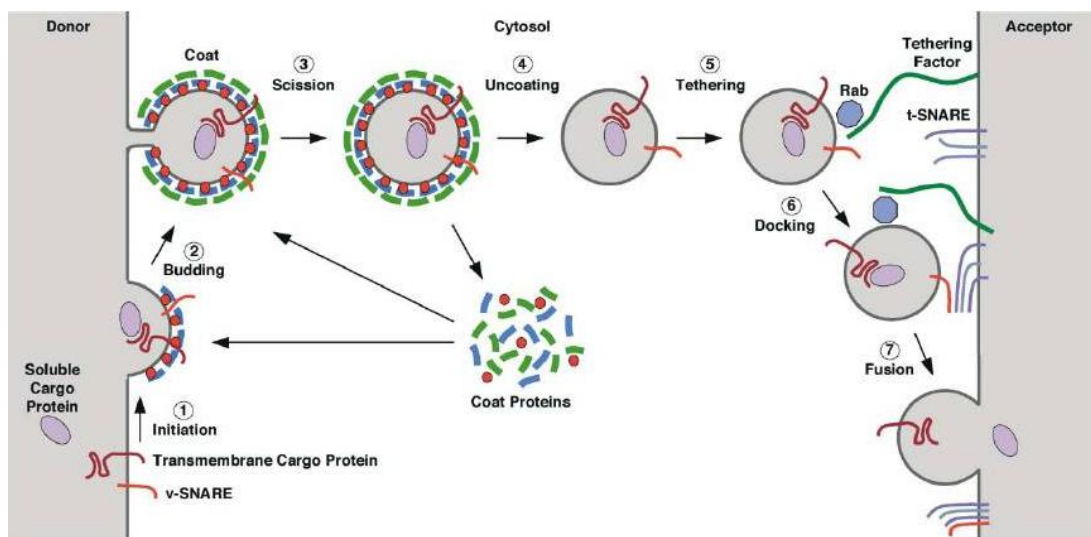
Figure 1.22. Vesicle budding and fusion. (1) Initiation of coat assembly. The membrane-proximal coat components (blue) are recruited to the donor compartment by binding to a membrane-associated GTPase (red) and/or to a specific phosphoinositide. Transmembrane cargo proteins and SNAREs begin to gather at the assembling coat. (2) Budding. The membrane-distal coat components (green) are added, cargo becomes concentrated and membrane curvature increases. (3) Scission. The neck between the vesicle and the donor compartment is severed either by direct action of the coat or by accessory proteins. (4) Uncoating. The vesicle loses its coat due to inactivation of the small GTPase, phosphoinositide hydrolysis and the action of uncoating enzymes, while cytosolic coat proteins are recycled. (5) Tethering. The "naked" vesicle moves to the acceptor compartment, possibly guided by the cytoskeleton, and becomes tethered by the combination of a GTP bound Rab and a tethering factor. (6) Docking. The v- and t-SNAREs assemble into a four-helix bundle. (7) This "trans-SNARE complex" promotes fusion of the vesicle and acceptor lipid bilayers. Cargo is transferred to the acceptor compartment, and the SNAREs are recycled (retrieved from Bonifacino and Glick, 2004).

signals present in the cytosolic domains of transmembrane cargo proteins (Bonifacino and Glick, 2004). The vesicles are then targeted to the appropriate acceptor compartment, to which they attach with the help of tethers and with which they fuse with the help of SNAREs [soluble NSF (N-ethylmaleimide-sensitive fusion protein) attachment protein receptor] (Figure 1.22). Thus, membrane-bounded vesicles serve as vehicles for the transport of proteins to their appropriate residence. The cytoskeleton is an integral component of cellular trafficking mechanisms, as the vesicles and endosomes move on actin filaments or microtubules (Tokarev *et al.*, 2009).

Protein transport within the cell happens via two major cellular pathways, the exocytic/secretory and the endocytic (Figure 1.23). The exocytic pathway moves cargo from the ER through the Golgi to the PM, while retrograde transport from the Golgi to the ER has also been observed. In the endocytic pathway, proteins are internalized from the PM via a set of endosomes, early and late, and are eventually targeted to the lysosome/vacuole. The two pathways are connected by bi-directional transport between the Golgi and the endosomes. Various proteins follow their own specific routes towards their destination; for example, secreted cargo and PM receptors and transporters are targeted to the PM, whereas newly synthesized endosomal and vacuolar proteins are sorted to the endosomes and the vacuoles, respectively (Tokarev *et al.*, 2009).
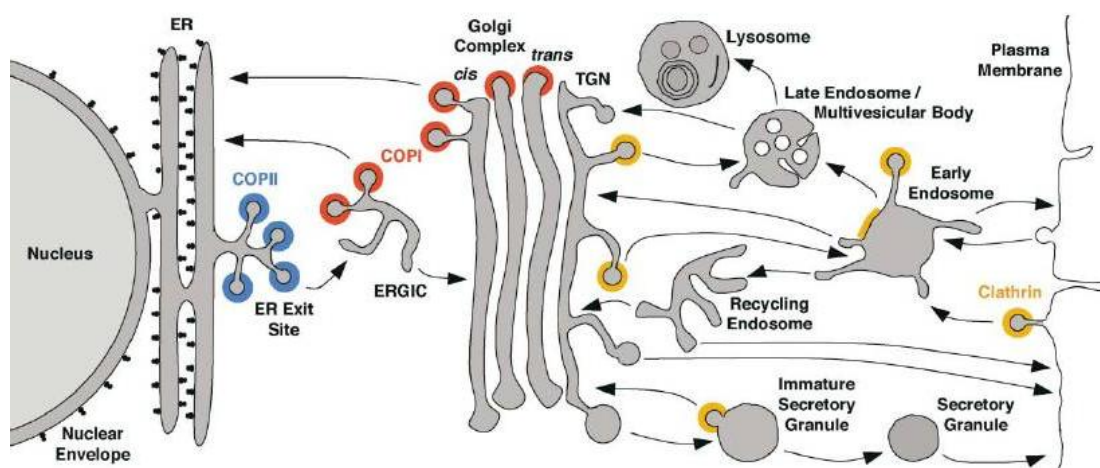
Figure 1.23. Scheme depicting the compartments of intracellular transport pathways. Transport steps are indicated by arrows. Colors indicate the known or presumed locations of COPII (blue), COPI (red), and clathrin (orange). Clathrin coats are heterogeneous and contain different adaptor and accessory proteins at different membranes. Additional coats or coat-like complexes exist but are not represented in this figure (retrieved from Bonifacino and Glick, 2004).

Vesicle budding at different stages of the exocytic and endocytic pathways is mediated by different coats and sorting signals. The first coats to be identified contained clathrin as their main constituent. Clathrin coats mediate vesicular transport at post-Golgi locations, including the PM, the *trans*-Golgi network (TGN) and the endosomes. Export from the ER to either the ER-Golgi intermediate compartment (ERGIC) or the Golgi complex is mediated by COPII, whereas COPI coat is involved in intra-Golgi transport and retrograde transport from the Golgi to the ER (Figure 1.23; Bonifacino and Glick, 2004).

1.6.2 Membrane protein translocation and quality control

Transmembrane proteins enter the ER co-translationally in a process known as translocation. Co-translational translocation begins with a targeting phase; the signal or transmembrane sequence of the growing polypeptide chain is recognized by a signal recognition particle (SRP), while it is still being synthesized on the ribosome. SRP is a cytoplasmic, 11S ribonucleoprotein particle comprised of 6 proteins and a single 7S RNA. After this, the ribosome–nascent-chain–SRP complex binds to the membrane, first by an interaction between SRP and its membrane receptor, and then by an interaction between the ribosome and the translocation channel. The translocation channel is formed from an evolutionarily conserved heterotrimeric membrane protein complex, called the Sec61 complex in eukaryotes. The channel allows hydrophobic TMSs of membrane proteins to move from its aqueous interior through the lateral gate and into the lipid phase. Hydrophilic segments between the TMSs move alternately from the ribosome through the aqueous channel to the external side of the membrane, or merge into the cytosol between the ribosome and the channel. The first TMS of a membrane protein can have its N-terminus on either side of the membrane, depending on the amino acid sequence of the protein, which often determines the orientation of subsequent TMSs (Rapoport, 2008; Fewell and Brodsky, 2009).

Following synthesis and translocation into the ER, nascent proteins must attain their proper conformations. The association of these proteins with the various chaperones and enzymes of the ER quality control machinery allows segregation of folding proteins, preventing their aggregation and giving them time to achieve proper folding while still in the permissive environment of the ER. Apart from achieving

proper folding, some proteins must assemble into complexes with other proteins before they are exported from the ER.

Newly-synthesized proteins undergo examination through an efficient and selective mechanism prior to their export from the ER to the Golgi apparatus. Improperly folded secretory proteins, whether they are nascent proteins that have yet to achieve proper conformation, misfolded proteins that can be refolded or terminally misfolded proteins, are retained in the ER. Although the retention of unfolded proteins in the ER primarily aims at allowing such proteins time to fold, accumulation of unfolded proteins in the lumen of the ER causes a heightened state of ER stress known as the unfolded protein response (UPR). Accumulation of misfolded proteins in the ER is a cause of a number of pathological states. The misfolded amyloid β protein, for example, is a known causative of Alzheimer's disease while retention of misfolded cystic fibrosis transmembrane conductance regulator (CFTR) and β-glucocerebrosidase is linked to cystic fibrosis and Gaucher's disease, respectively (Benyair *et al.*, 2011).

Once a protein has been identified as terminally mis-folded, in order to protect the cell from damage, it is routed to a specialized ER-derived quality control compartment (ERQC). ERQC is located around the centrosomes in mammalian cells, from where misfolded proteins are targeted to ER-associated degradation (ERAD). ERAD is a ubiquitin-mediated degradation pathway that apart from its central role as an avenue of cellular quality control, it is also used for the selective degradation of correctly folded proteins as a means of regulation of many cellular processes. Apart from the quality control mechanisms that operate in the ER ensuring that, until fully assembled, cargo proteins are retained and/or not recognized by the export machinery, a protein retrieval mechanism exists later in the secretory pathway, in the ERGIC and the Golgi complex (Hampton, 2002; Benyair *et al.*, 2011).

1.6.3 ER-exit and targeting to the Golgi

Once correctly folded and assembled, proteins are segregated from ER resident proteins and are exported from the ER to either the Golgi complex or the ERGIC. Prior to ER export, the majority of cargo proteins are actively concentrated in COPII-coated buds and vesicles. In *S. cerevisiae*, the formation of COPII vesicles appears to proceed throughout the ER, whereas in most other eukaryotes, COPII vesicle-mediated protein export is restricted to a specialized ER subdomain, called

transitional ER (tER) or ER exit site (ERES; Figure 1.23). Assembly of the COPII coat is initiated through activation of the small Ras-like GTPase Sar1. Conversion of Sar1-GDP to Sar1-GTP is mediated by Sec12, an ER-bound transmembrane guanine nucleotide exchange factor (GEF). Sec12 is strictly regulated to localize in the ER, and thereby Sar1 activation is restricted to the ER. The GDP-to-GTP transition triggers the exposure of the N-terminal amphipathic α-helix element of Sar1 that inserts into the ER membrane. Membrane-bound Sar1-GTP recruits Sec23-Sec24 heterodimer by binding to the Sec23 portion, and Sec23/24-Sar1 complex selects cargo to form a pre-budding complex. Subsequently, the pre-budding complex recruits Sec13-Sec31 heterotetramer, which provides the outer layer of the coat (Figure 1.24). Additional factors are known to contribute in the COPII assembly, such as the large ER membrane-associating peripheral protein Sec16 and the integral ER membrane protein Sed4, two factors that are likely to function together (Bonifacino and Glick, 2004; Sato and Nakano, 2007).
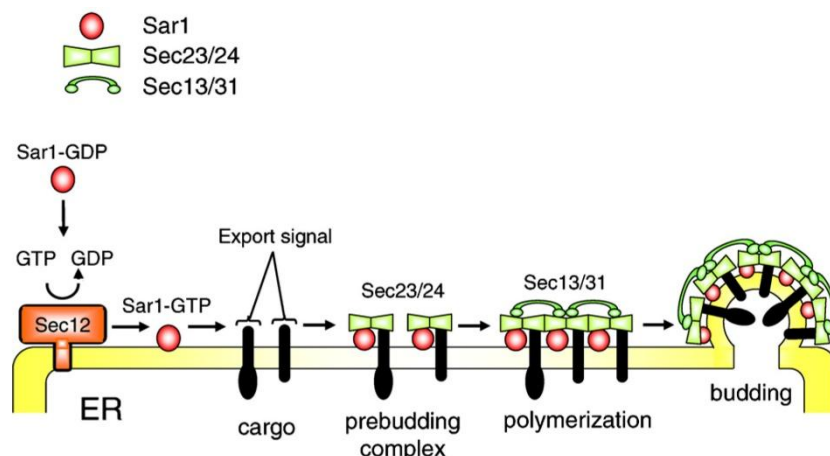
Figure 1.24. COPII vesicle formation and the selective uptake of cargo proteins. The COPII vesicle formation is initiated by GDP-GTP exchange on Sar1 catalyzed by the transmembrane GEF Sec12. Activated Sar1-GTP binds to the ER membrane and recruits the Sec23/24 subcomplex. The cytoplasmically exposed signal of transmembrane cargo is captured by direct contact with Sec24, forming the pre-budding complex. It is currently not clear whether the membrane-bound Sar1-GTP associates with cargo before the recruitment of Sec23/24 or lateral diffusion of Sar1-GTP-Sec23/24 complex captures cargo. These pre-budding complexes are clustered by the Sec13/31 subcomplex, generating COPII- coated vesicles (retrieved from Sato and Nakano, 2007).

The selective recruitment of cargo proteins in COPII vesicles is basically driven by ER export signals. Export signals of most transmembrane cargo proteins are thought to interact directly with the COPII coat subunits, but some transmembrane and most soluble cargo proteins bind indirectly to COPII through

transmembrane cargo receptors. Cargo receptors leave the ER together with their ligands, unload their cargo into the acceptor compartment and recycle back to the ER (Bonifacino and Glick, 2004; Sato and Nakano, 2007).

Genetic, biochemical, and structural analyses have demonstrated that most ER export signals interact with one of three binding sites on the COPII coat component Sec24.Several Sec24-binding motifs have been identified in the cytosolic domains of eukaryotic membrane proteins, the diversity of which explains the ability of COPII to package a wide variety of cargos. Some consist of di-acidic motifs fitting the consensus [D/E]X[D/E], whereas others of di-hydrophobic (FF, YY, LL or FY) , triple arginine or aromatic motifs. The majority of ER-exported membrane proteins, however, carry no known export signal in their sequence. Thus, either new signals remain to be identified or something else drives their recruitment into COPII vesicles. Since many membrane proteins form oligomers prior to export from the ER, combinatorial signals (i.e. oligomeric signals composed from many weakly interacting sequences) have been postulated to link oligomerization to efficient export (Barlowe, 2003; Sato and Nakano, 2007; Springer *et al.*, 2014). Indeed, oligomerization is required for the export from the ER of a yeast COPII-binding cargo receptor protein and its mammalian homologue (Sato and Nakano, 2003; Zheng *et al.*, 2010). Very recently, Springer *et al.* showed *in vitro* that oligomerization strongly enhanced protein uptake in COPII vesicles, independently of cytosolic COPII-binding motifs. As a mechanism for the induction of ER export by oligomerization, they proposed that oligomerization can generate a local membrane curvature that promotes vesicle formation and thus the oligomeric form is preferentially packaged into transport vesicles without direct protein-protein binding interactions (Springer *et al.*, 2014).

After their exit from the ER, COPII vesicles move cargo proteins to the ERGIC, a network of membranes that constitutes the gateway to the Golgi complex. Despite the intense research that has been taken in the field, it is not clear whether the ERGIC is a stationary compartment or, conversely, a transient structure formed by the fusion of ER-derived vesicles, which works as a carrier itself. ER to ERGIC transport is microtubule-dependent. Thus, anterograde and retrograde transport between these compartments is dramatically reduced in the presence of inhibitors of microtubule polymerization (Tomás *et al.*, 2010). From the ERGIC cargo proteins are eventually transferred to the Golgi via COPI transport vesicles.

1.6.4 Trafficking within the Golgi and targeting to the plasma membrane

In many eukaryotic cells, the Golgi apparatus consists of several stacked, flattened membrane sacs called cisternae. In each Golgi stack, the cisternae are polarized between the *cis* side, receiving cargo from the endoplasmic reticulum (ER), and the *trans* side, sending cargo forward to post-Golgi organelles. Notably, in most ascomycetes, including *S. cerevisiae* and *A. nidulans*, Golgi is not stacked, but is instead organized as a network of tubules and fenestrated cisternae, denoted Golgi equivalents (Breakspear *et al.*, 2007; Pantazopoulou and Peñalva, 2009).

There are two widely accepted models of how cargo proteins are transported through the Golgi stack: the vesicular transport (stable compartments) model and the cisternal maturation model. In the vesicular transport model, each stack is static with its own defined structure and a characteristic set of resident proteins. Cargo proteins are supposed to travel from one cisterna to the next in anterograde vesicles, whereas Golgi-resident enzymes are to be excluded from the vesicles and retained in the cisternae. Next, the cargo is sorted out of the stack into a vesicle that in turn fuses to the subsequent stack. Thus, cargo that enters on one face of the Golgi is transported in a series of vesicular transport steps to the other end.

In the cisternal maturation model, on the other hand, Golgi cisternae are considered to be transient structures, since the stacks themselves move from the *cis* side to the *trans* side of the apparatus. As they move, processing enzymes are sorted out into vesicles that then fuse with a younger stack. Thus, cargo proteins can be transported through the Golgi without exiting the cisternae (Simon, 2008; Ito *et al.*, 2012). While there are many experimental results consistent with either one or the other model, there are an equally large number of experiments demonstrating that neither model, on its own, sufficiently explains all of the results.

In 2008, Patterson *et al.* presented evidence for a third model of intra-Golgi transport, in which the Golgi stacks are a continuous structure and transmembrane cargos differentially partition between two different membrane environments: processing domains enriched in Golgi enzymes and export domains capable of budding transport intermediates. In particular, the stack-like organization of the Golgi, combined with the requirement of vesicular or tubule cargo transport across it and with the partitioning of lipids between two domains allows molecules in the system to sort spatially (Patterson *et al.*, 2008; Simon, 2008).

The *trans*-most face of the Golgi, the *trans*-Golgi network (TGN), is the penultimate compartment along the secretory pathway. Thus, membrane traffic from the TGN is the last and, potentially, rate-limiting step in the secretion. In TGN, proteins destined for secretion or to be presented on the PM are packed into secretory vesicles that subsequently fuse with the PM, either directly or via the endosomes, while other protein cargos are sorted to the endosomes and the lysosomes, or back to the ER. As described for upstream vesicular transport events of the secretory pathway, the selective packaging of cargos into transport vesicles in the TGN is also facilitated by specialized proteins and requires recognition of specific sorting signals within the cargo (Ponnambalam and Baldwin, 2003; Starr *et al.*, 2012).

Sorting between the TGN, endosomes and lysosomes is usually induced by tyrosine-based or di-leucine-based sorting signals and is mediated by clathrin, the adaptor protein complexes (APs), Golgi-localized gamma ear-containing ARF-binding proteins (GGAs) and epsin-related proteins. There are four AP complexes in mammalian cells and three in *S. cerevisiae* and *A. nidulans*. The AP-1 complex mediates trafficking between the TGN and endosomes, the AP-2 mediates endocytosis, the AP-3 directs proteins toward lysosomes in mammalian cells and the vacuole in yeast and the AP-4 may be involved in lysosomal and/or basolateral protein sorting and in the selective transport of cargo from the TGN to the endosomes (Robinson, 2004; Traub, 2009; Sotiris Amillis and George Diallinas, unpublished results). The existence of a fifth AP complex, AP-5, was recently reported in late endosomal compartment in HeLa cells (Hirst *et al.*, 2011).

Protein transport from the TGN to the PM is mediated by a less well-understood process, as there are limited examples of cytosolic signals within cargos recognized by coat protein complexes. In some cases export signals may not exist and TGN-to-PM traffic may be governed by the length of the transmembrane span and in turn be dictated by differences in the lipid composition of the TGN and the PM. In other cases, however, signals are necessary for efficient TGN-to-PM transport, such as a di-acidic motif at the N-tail of chitin synthase III (Chs3), an integral yeast membrane protein that is transported to the PM through the exomer pathway. Proteins found to be implicated in TGN-to-PM traffic are the dynamin-2 GTPase, heterotrimeric G-proteins and proteins belonging to the Rab family GTPases and the AGC serine/threonine protein kinase family (Ponnambalam and Baldwin, 2003; Starr *et al.*, 2012).

1.6.5 Endocytic internalization of membrane proteins

The accurate distribution and recycling of transmembrane proteins is vital to ensure correct functioning of the cell. Membrane proteins are upregulated or downregulated in response to environmental and developmental signals, not only at the level of secretion towards the PM, but also via direct vacuolar sorting or endocytosis. Endocytosis is the process by which eukaryotic cells internalize PM lipids and associated proteins in vesicles that fuse with the endosomal system. Subsequent segregation into different endosomal domains determines whether a given cargo recycles to the PM, traffics to the TGN or follows the endocytic pathway to the vacuole/lysosome, thus undergoing degradation (Peñalva, 2010).

Endocytosis occurs by a variety of mechanisms, among which clathrin-mediated pathway is the one that has been most extensively studied and is well-understood (Figure 1.25). During this highly coordinated process, clathrin is the most abundant protein in the coat of the endocytic vesicles and it provides the scaffold that orchestrates protein sorting, membrane deformation and budding. Sorting into clathrin-coated pits and formation of clathrin-coated vesicles are mediated by adaptor proteins. The variety of transmembrane cargos concentrated into clathrin-coated vesicles at the PM requires the use of diverse sorting signals, and diverse adaptors to recognize them. This variety prevents competition for entry and allows plasticity in the selection of cargo for internalization (Kirchhausen, 2000; Reider and Wendland, 2011).

Endocytic adaptors are divided into two main groups: multimeric adaptor proteins, such as the tetrameric AP-2 complex, and non-classic adaptor proteins, such as the clathrin-associated sorting proteins (CLASPs). AP-2 accumulates at newly forming pits in parallel with clathrin and binds to certain sorting motifs in the cytoplasmic tails of the cargo proteins. AP-2 is also responsible for the recruitment of clathrin to the membrane and thus for the initiation of coat formation. CLASP adaptors are mono- or dimeric and vary in structure and binding properties. These include ubiquitin-binding adaptor proteins, such as epsin 1 (EPN1/Ent1), epsin 2 (EPN2/Ent2) and the epidermal growth factor receptor pathway substrate 15 (EPS15), the arrestin adaptor family (see also 1.6.7) and the newly discovered muniscin family of endocytic adaptors. Endocytic adaptors vary greatly in size (~300-3000 amino acids) and structure, but possess similar properties. In addition,
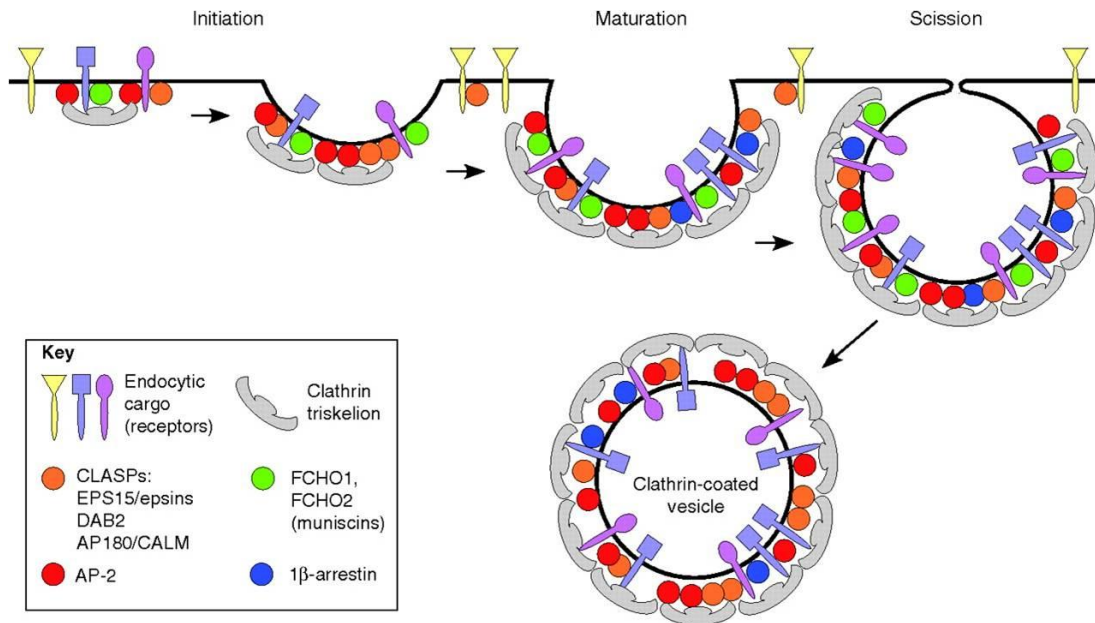
Figure 1.25. Diagram of clathrin-dependent endocytosis. Clathrin-dependent endocytosis begins when adaptor and clathrin complexes associate with cognate cargo, thus initiating the formation of a coated pit. As the pit matures, additional adaptor and scaffold proteins join the pit, providing a structural platform that helps regulate and synchronize interactions between the adaptors and the other endocytic proteins. Increasing membrane deformation attributed to BAR-domain-containing proteins (such as the muniscins) as well as from forces generated by polymerization of cytoskeletal elements, eventually leads to vesicle scission, which liberates a clathrin-coated vesicle into the cytoplasm. Examples of different cargos are given in different colors. Blue and purple cargos contain sorting motifs that bind to clathrin-associated adaptors. This type of cargo can therefore be incorporated into the forming clathrin-coated pit. Yellow cargo, by contrast, is internalized through an alternative clathrin-independent pathway that might involve a select subset of CLASP adaptors (retrieved from Reider and Wendland, 2011).

some of the endocytic adaptors described do not bind clathrin and are possibly mediating other non-clathrin based routes, such as caveolin-mediated internalization. Most of the clathrin adaptor proteins contain regions that interact with some or all of four types of binding partners: lipids, cargo, clathrin and accessory proteins (Figure 1.26). Cooperation between these interactions is required for efficient recruitment of adaptors to the PM and is crucial for progression of the internalization process (Kirchhausen, 2000; Reider and Wendland, 2011).

The large GTPase dynamin plays a dual role in clathrin-mediated endocytosis, functioning at early stages as a fidelity monitor to regulate clathrin-coated pit maturation and at later stages to directly catalyze membrane fission and clathrin-coated vesicle formation (Mettlen *et al.*, 2009). Vesicle release is followed by transient actin polymerization, which is thought to drive vesicles away from the surface. Additionally, actin is implicated at other stages of endocytosis, including organization of sites of coated pit formation, coated pit assembly and constriction

or/and scission of clathrin-coated vesicles. The central role of actin cytoskeleton in endocytosis is evident in *S. cerevisiae*, where treatment with actin polymerization inhibitors dramatically blocks internalization. In addition, many factors required for proper cortical actin organization in yeast are also important for endocytosis. These include the epsins Ent1 and Ent2, the EH domain proteins End3 and Eps15-related Pan1, amphiphysins Rvs161 and Rvs167, the intersectin-like Sla1, the Hip1/R homologue Sla2, the actin regulatory protein Arp2/3, the actin-binding protein Abp1, as well as kinases such as Ypk1/2, which is related to protein kinase B (PKB) and serum- and glucocorticoid-induced protein kinase (SGK), and actin-regulating kinases Ark1 and Prk1 (Newpher *et al.*, 2005).
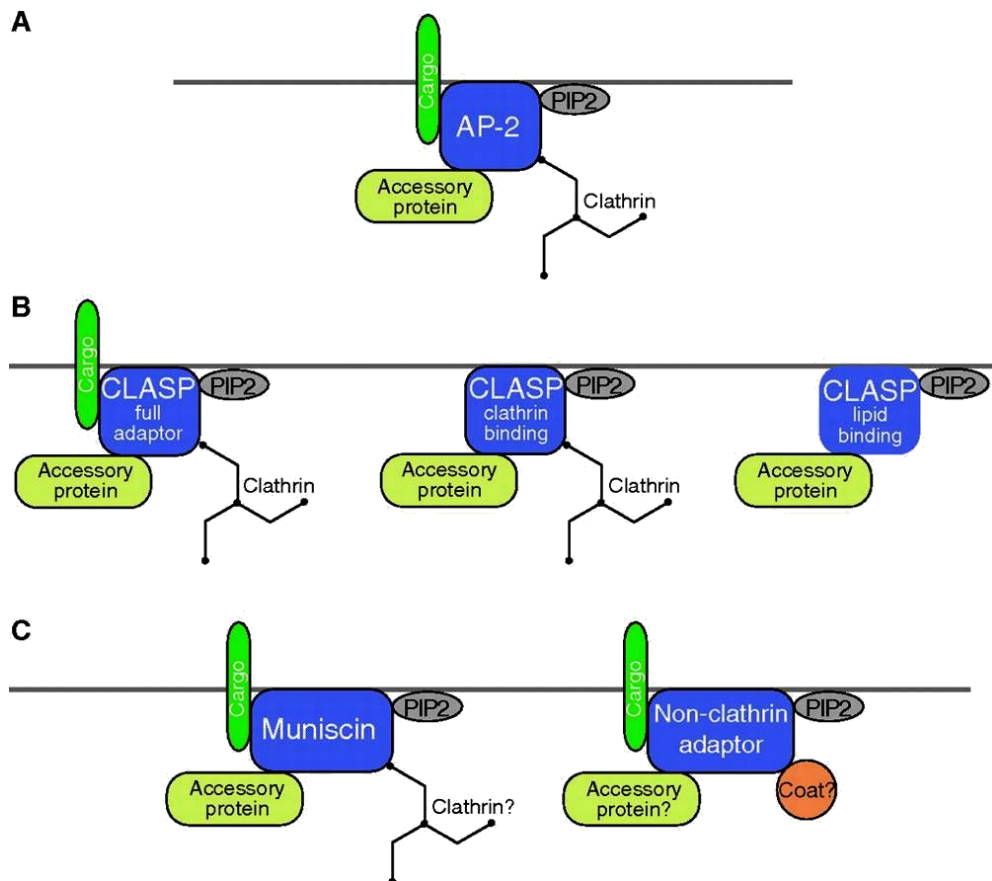
Figure 1.26. Schematic representations of different classes of adaptor proteins and their association with respective binding partners. **A.** AP-2 and CLASP (full adaptor) proteins bind to lipids, cargo, accessory proteins and clathrin. **B.** By contrast, other CLASP proteins are known to bind only some of these four partners. For example, some may not bind cargo, whereas others may not bind directly to clathrin. **C.** The recently described muniscin adaptors bind cargo, as well as lipids and accessory proteins. Another, new class of adaptors that selects cargo for internalization through non-clathrin pathways has been discovered recently. These non-clathrin adaptors bind to cargo and lipids, and some may also associate with currently unknown coat and accessory proteins. PIP2, PtdIns (4,5)P2 (retrieved from Reider and Wendland, 2011).

Most of the proteins known to be involved in endocytic internalization localize in punctuate cortical structures that often partially or fully co-localize with cortical actin patches, which are believed to form at sites of endocytosis. Real-time microscopy of fluorescently labelled endocytic patch proteins has provided insight into the dynamics of these factors during endocytosis in yeast. Initially Sla1, Sla2, Pan1, and Las17 are recruited to cortical sites. This is followed by the assembly of actin, Arp2/3 complexes, and Abp1. As vesicles appear to pinch off, the early patch proteins are released and actin/Abp1 patches move rapidly away from the cortex (Kaksonen *et al.*, 2003; Newpher *et al.*, 2005).

In contrast, the subcellular localization of endocytic factors in *A. nidulans* hyphae is significantly different. Hyphal cells of filamentous fungi represent an extreme example of polarized growth. After a period of isotropic expansion, the germinating fungal spore establishes a polarity axis, which leads to the emergence of a germ tube that grows by apical extension, resulting in the characteristic tubular morphology of the hyphal cell. Given that hyphal extension involves the continuous delivery of secretory vesicles to the apex, there should be a mechanism of continuous membrane recycling through an endosomal compartment, ensuring that excess membrane and vesicle fusion machinery proteins are efficiently redistributed (Araujo-Bazán *et al.*, 2008). A similar model has been proposed for the basidiomycete *Ustilago maydis*, in which endocytosis predominates in the apical regions of hyphae, where an endosomal compartment is involved in hyphal growth by mediating apical membrane/protein recycling (Steinberg, 2007). In agreement to that, fluorescence microscopy showed that AbpA, SlaB and AmpA, the *A. nidulans* orthologues of Abp1, Sla2 and Rvs167, as well as actin patches, are strongly polarized and form an 'endocytic ring' that embraces the hyphal tip, leaving an area of exclusion at the apex. This indicated that endocytosis is particularly active in these regions. The importance of endocytosis in the polarized hyphal extension of *A. nidulans* is supported by the fact that deletion of *slaB* is lethal, while *slaBΔ* conidia rescued from heterokaryons are able to establish polarity but arrest in apical extension shortly after germ-tube emergence, which would be consistent with a defect in polarity maintenance (Araujo-Bazán *et al.*, 2008).

1.6.6 Traffic across the degradation pathway

Once released from the PM, endocytic vesicles reach an endosome, where cargo-specific sorting takes place. Cargo can be routed to the TGN, to recycling endosomal carriers that bring the cargo back to the PM or to the endocytic pathway toward the degradation organelles (metazoan lysosomes and fungal vacuoles). Vesicle attachment and fusion to the endosomal membrane are mediated by intracellular vesicle trafficking proteins that fall into four major categories: (i) vesicle-anchored (v-) and target-membrane–anchored (t-) soluble N-ethylmaleimide–sensitive factor (NSF) attachment protein receptors (SNAREs), which bring the two membranes together and catalyze fusion by assembling into tight SNARE complexes through α-helical sequences called SNARE motifs, (ii) NSF and NSF attachment proteins (SNAPs), which disassemble SNARE complexes to recycle the SNAREs for another round of fusion, (iii) Rab GTPases and multi-component vesicle tethering complexes, which coordinate vesicle attachment and the subsequent assembly of cognate v-SNARE and t-SNARE complexes and (iv) Sec1/Munc18 (SM) proteins, which are soluble factors that may act with the SNARE proteins before and after vesicle attachment (Carr and Rizo, 2010).

The endosomal compartments involved in the degradation pathway are the early endosomes (EE), the late endosomes (LE), the multivesicular bodies (MVBs) and the lysosome/vacuole. Rather than being vesicle mediated, traffic between EE and LE occurs by maturation (Figure 1.27). During this process, EE, which receive biosynthetic traffic from the Golgi, progressively undergo changes in lumenal pH and composition as they fuse homotypically to give rise to gradually larger organelles. Simultaneously, portions of endosomal membranes bud inward, thereby delivering lipids and their associated proteins into the lumen of the organelle. Thus, maturation results in organelles that are larger than EE and display a characteristic multivesicular appearance. These multivesicular "late" endosomes undergo further fusion between themselves and with the vacuoles/lysosomes, thus making their cargo accessible to digestion by the vacuolar/lysosomal hydrolases (Abenza *et al.*, 2012).

The maturation of early into late endosomes is mediated by the class C core vacuole/endosome tethering complex (CORVET). Progressive acidification of endosomal compartments is accomplished by V-ATPase, a highly complex, multi-subunit proton pump, whereas the formation of intra-lumenal vesicles is performed by the endosomal sorting complex required for transport (ESCRT) machinery. Once

endosomes reach a certain maturation stage, CORVET is substituted by the homotypic fusion and vacuole protein sorting (HOPS) complex, and LE become competent to undergo fusion with lysosomes/vacuoles. A hallmark of early-to-late endosome maturation is Rab conversion, in which Rab5 present on EE is replaced by the late endosomal Rab7. *A. nidulans* has two Rab5 paralogues, the RabA and RabB. RabA localizing to EE plays a minor role in the endocytic downregulation of PM cargo. RabB, on the other hand, is the sole recruiter to endosomes of the prototypical Rab5 effectors AnVps19, AnVps45 and AnVps34, coordinates acquisition of degradative identity in EE with incoming Golgi traffic, mediates EE movement and is the major promoter of homotypic EE fusion, thus playing a pivotal role in the early-to-late endosome transition (Figure 1.27; Abenza *et al.*, 2010; Solinger and Spang, 2013).
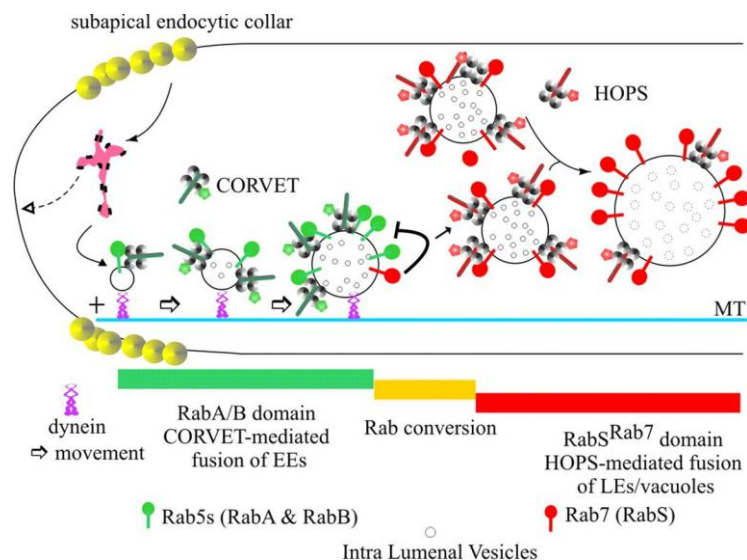
Figure 1.27. A model for endosomal maturation in *A. nidulans*. Endocytosis predominates in the tip. Endocytic vesicles reach a hypothetical endosomal compartment that would act as a sorting endosome, organized as a mosaic of domains (magenta). This mosaic possibly includes domains from which membrane and cargo can recycle to the PM, segregating from other domains in which the two Rab5s—RabA and RabB—determine «degradative early endosome (EE) identity» (i.e. the identity of membranes destined to the vacuole). Degradative EE become loaded on dynein and undergo Rab5-dependent movement on microtubules (MT). RabB is the major player in establishing this degradative identity, as it is required for EE movement and mediates recruitment of Vps45 and Vps34 to endosomes (not depicted). Vps45 enables endosomes to accept Golgi traffic required for maturation, whereas Vps34 synthesizes phosphatidyl inositol-3-phosphate, the landmark of degradative endosome identity, initiating the MVB pathway at the stage of EEs. RabB and, less efficiently, RabA recruit CORVET, mediating homotypic fusion between EEs. As endosomes increase their size, they decrease their motility and acquire their final composition, thus becoming late endosomes (LEs). Then RabS^Rab7 substitutes Rab5s. Finally, LEs undergo further fusion between them and with vacuoles in a HOPS-dependent manner. The negative feedback loop that may help to release Rab5s from endosomes is depicted (retrieved from Abenza *et al.*, 2012).

1.6.7 Regulation of transporter endocytosis

Ubiquitin as an endocytic signal

Transmembrane transport proteins play a crucial role in all cells by conferring to plasma and internal membranes selective permeability to a wide range of ions and small molecules. These transport proteins are very often subject to tight regulation allowing cells to adapt to different nutrient needs or stress conditions and protecting cells from self-poisoning, a particular problem with compounds such as heavy metals, which are essential for cell physiology but toxic in excess. Such a control occurs at the level of protein trafficking, including secretion towards the PM, direct vacuolar sorting, endocytosis, endosomal recycling and turnover in the vacuole/lysosome. The major regulatory mechanism of endocytic trafficking is ubiquitination, an evolutionarily conserved process from fungi to mammals (Dupré *et al.*, 2004; Miranda and Sorkin, 2007; Lauwers *et al.*, 2010). Ubiquitination is the only characterized signal promoting the internalization of yeast transporters from the PM, although the existence of an ubiquitin-independent mechanism has also been documented (Strochlic *et al.*, 2008). In mammalian cells, only some of the several internalization pathways that exist are regulated by ubiquitin (Traub, 2009).

Protein ubiquitination is a post-translational conjugation of ubiquitin to a target protein by the formation of an isopeptide bond between the C-terminal glycine of ubiquitin and the amino group of a lysine residue in the target protein. Ubiquitin is a 76-amino acid protein, highly conserved throughout evolution and found in all eukaryotic organisms and cell types. It is conjugated to the protein substrate via the sequential activity of three enzymes. First, a ubiquitin-activating enzyme, E1, activates ubiquitin in an ATP-dependent reaction. Ubiquitin is then transferred to a ubiquitin-conjugating enzyme (E2) and finally to a ubiquitin-protein ligase (E3) of the HECT family, which catalyzes the transfer of ubiquitin to the substrate. Alternatively, ubiquitin can be directly transferred from E2 to the substrate with the help of an E3 enzyme of the RING family, acting as a platform for substrate recognition (Dupré *et al.*, 2004; Lauwers *et al.*, 2010; see also Figure 1.29A). In several cases it has been demonstrated that ubiquitination of a given substrate involves several E3s. For example, ubiquitination and downregulation of the EGFR (epidermal growth factor receptor) appear, in some cases, dependent on both the HECT ligase AIP4 and the RING finger protein Cbl3, which are described to interact

(Courbard *et al.*, 2002). E3 enzymes account for the high specificity of the ubiquitination reaction, which is also evident by the fact that the yeast genome encodes a single E1, eleven E2 and 54 E3 enzymes (Lauwers *et al.*, 2010).

Target proteins can be modified with a single ubiquitin molecule on one (mono-ubiquitination) or several lysines (multi-mono-ubiquitination). Alternatively, given the fact that ubiquitin itself carries conserved lysine residues, ubiquitin molecules can be ligated to one another to form ubiquitin chains (poly-ubiquitination; Figure 1.28). All seven lysine residues (K6, K11, K27, K29, K33, K48, K63) are capable of conjugating ubiquitin, but Lys48- and Lys63-linked chains are the most abundant. K48-linked poly-ubiquitin chains adopt a close conformation and target proteins for degradation by the 26S proteasome, whereas K63-linked poly-ubiquitin chains are more elongated and are involved in various cellular processes including DNA repair, stress responses and endocytic trafficking of PM proteins.
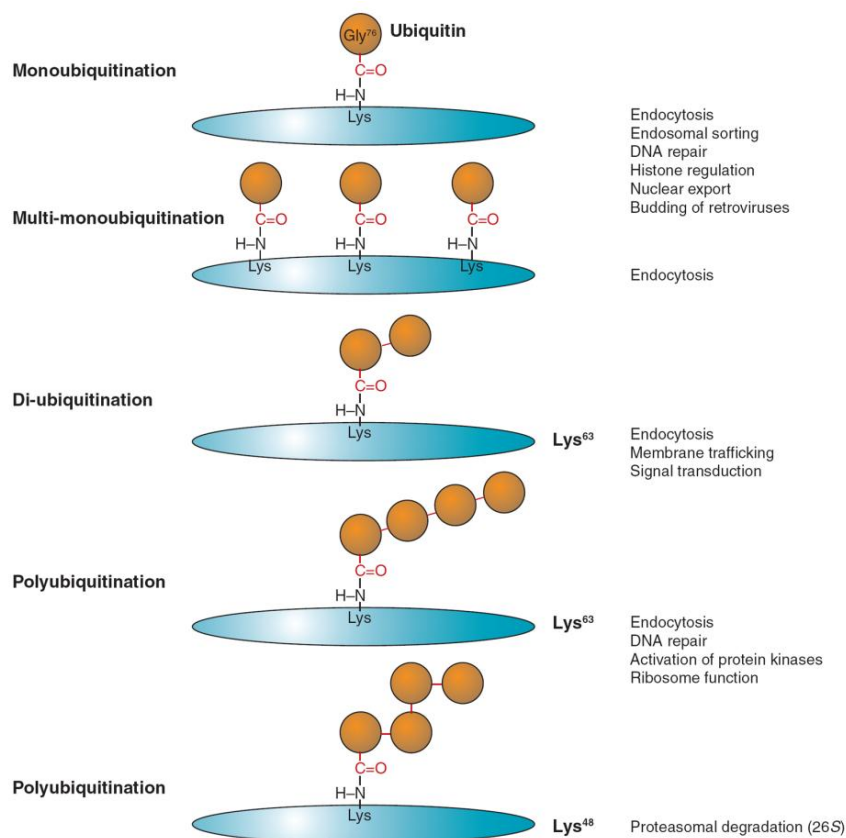
Figure 1.28. Types of ubiquitin conjugation. Gly76 of ubiquitin is covalently attached to the ε-amino group of lysines in the substrate. Substrates can be modified with a single ubiquitin molecule at a single (mono-ubiquitination) or multiple (multi-mono-ubiquitination) lysine residues. Further ubiquitin conjugation to the lysine residues of ubiquitin results in di- or poly-ubiquitination. Shown are the most frequently detected ubiquitin chains linked through Lys63 or Lys48 of ubiquitin. Lys48- or Lys63-linked chains have closed and extended conformation, respectively, resulting in different mechanisms of recognition by ubiquitin binding domains (retrieved from Miranda and Sorkin, 2007).

The ubiquitination of a given protein mostly affects its interaction network, either by preventing pre-existing interactions through steric obstruction or by providing a new interface for interaction via the ubiquitin moieties. Indeed, ubiquitin is recognized by ubiquitin-binding proteins possessing one or several ubiquitin-binding domains (UBD), such as the epsin/ Eps15-like adaptors in yeast. Ubiquitin-binding proteins interact non-covalently with ubiquitin and mediate the sorting of PM cargos into invaginating endocytic vesicles. Although mono-ubiquitination on a single lysine is often a sufficient signal for transporter internalization, the presence of several ubiquitin moieties accelerates this process, possibly by mediating higher affinity interaction with the endocytic ubiquitin-binding receptors (Miranda and Sorkin, 2007; Léon and Haguenauer-Tsapis, 2009; Lauwers *et al.*, 2010). For example, the internalization efficiency of the uracil permease (Fur4) and the general amino acid permease (Gap1) of *S. cerevisiae* are proportional to the number of ubiquitin monomers linked to these cargos (Springael *et al.*, 1999; Blondel *et al.*, 2004).

Ubiquitination serves as a signal not only for internalization from the PM, but also for sorting of cargos into the MVB pathway. This is mediated by the ESCRT machinery, comprising of five multi-subunit complexes (ESCRT-0,-I,-II,-III and Vps4-Vta1). At least one component of each of the ESCRT-0,-I and -II possesses a UBD, which interacts with the conjugated ubiquitin. Recent studies have demonstrated that K63-linked ubiquitin chains are required for this late step of endocytosis (Lauwers *et al.*, 2010). Gap1 for example, when modified with a single ubiquitin moiety is internalized at a normal rate, while the apparent internalization defect seen when K63-linked ubiquitination is defective is due to recycling of the endocytosed permease to the cell surface (Springael *et al.*, 1999). Another example is Jen1, one of the two monocarboxylate-proton symporters of *S. cerevisiae*. In fact, Jen1 is one of the few examples for which K63-linked ubiquitin chains were shown to be required for correct trafficking at two stages of endocytosis: endocytic internalization and sorting to MVBs (Paiva *et al.*, 2009).

Finally, ubiquitination is a reversible modification and ubiquitin molecules are recycled after cleavage of the isopeptide bond by specific proteases named deubiquitinating enzymes (DUBs). Doa4 ubiquitin isopeptidase is required for the recycling of ubiquitin from ubiquitinated substrates in *S. cerevisiae*. In a *doa4Δ* mutant, ubiquitin is strongly depleted and this phenotype can be partially suppressed

by inactivation of vacuolar proteolysis or endocytosis (Swaminathan *et al.*, 1999). CreB is another enzyme with deubiquitinating activity, found in *A. nidulans*, which is also involved in carbon catabolite repression (Lockington and Kelly, 2002).

Rsp5 ubiquitin ligase

The link between ubiquitin and endocytosis in yeast was first discovered by Kölling and Hollenberg (1994), while working with Ste6, the ATP-binding cassette (ABC) transporter for secretion of the pheromone a-factor. Using a mutant with impaired endocytic internalization, they observed that it accumulated ubiquitinated forms of the transporter in the PM fraction. Soon after that, two other groups supported the existence of ubiquitin-dependent endocytosis by two different approaches. Hicke and Riezman (1996) discovered that the endocytic signal identified in a C-terminally truncated form of Ste2, the receptor for α-factor, was in fact a ubiquitination signal, while Hein *et al.* (1995) cloned the gene *NPI1*, responsible for the downregulation of Fur4 and Gap1 and found out that it encoded the ubiquitin ligase Rsp5.

In *S. cerevisiae* the ubiquitination of transporters is exclusively carried out by the HECT (homologous to E6-AP carboxyl-terminus) ubiquitin ligase Rsp5, which is the only member of the Nedd (neural precursor cell expressed developmentally downregulated) 4/ Nedd4-like family of ubiquitin ligases in yeast. In humans there are nine members of this family, whereas plants have no Nedd4-like genes whatsoever. The C-terminal half of Rsp5 contains a HECT domain that catalytically ligates ubiquitin to proteins and functionally classifies Rsp5 as an E3 ubiquitin-protein ligase. The N-terminal half consists of four domains: a C2 domain, which binds membrane phospholipids and is presumed to act as membrane localization module, and three WW domains. The WW domains, named after two conserved tryptophan residues spaced 20–22 amino acids apart, are small protein interaction modules composed of 40 amino acids that fold into three-stranded, anti-parallel β-sheets. These constitute hydrophobic pockets that interact with proline-rich regions forming a [P/L]PXY (PY) motif. Whereas these domains allow direct binding of Rsp5 to some of its substrates, the transporters under Rsp5 control do not possess any PY motifs. Rsp5 in fact binds via its WW domains to PY sequences displayed by accessory proteins acting as specific adaptors for cargo ubiquitination (Chang *et al.*, 2000; Sullivan *et al.*, 2007; Lauwers *et al.*, 2010; Becuwe, Herrador, *et al.*, 2012).

Chromosomal deletion of *NPI1/RSP5* has shown that this gene is essential for cell viability. For this reason a viable *npi1/rsp5* strain with reduced expression of *NPI1/RSP5* is being used to study Rsp5 (Hein *et al.*, 1995). *A. nidulans* has a single orthologue of Rsp5, called HulA (HECT ubiquitin ligase). Deletion of the C2 domain of HulA results in a viable strain that grows and conidiates very poorly and has a trafficking defect (Boase and Kelly, 2004; Gournas *et al.*, 2010).

Adaptor proteins of Rsp5 ubiquitin ligase

Transporter ubiquitination and endocytosis must occur rapidly after an extracellular event (e.g. rapid change in substrate availability), implying that all the components of the endocytic machinery are present and functional at any given time. On the other hand, this pulse of endocytosis must be very transient. A way of reconciling these two requirements and finely tuning the endocytic fate of transporters is the tight regulation of specific cargo availability toward the ubiquitin ligase in charge of its ubiquitination. Recent studies illustrate that such regulation is obtained by the combinatorial use of various adaptor proteins and post-translational modifications (Figure 1.29B-E). Besides mediating the physical interaction of ubiquitin ligases with their substrates, adaptors have also been reported to affect the localization or the catalytic activity of their cognate ligases, while they often are themselves subject to a complex regulation. Therefore, ubiquitin ligase adaptor proteins represent an additional layer of specificity in the ubiquitination cascade (Léon and Haguenauer-Tsapis, 2009).

To date, Rsp5-dependent ubiquitination of transporters has only been described to occur via adaptor proteins containing PY motifs that interact with the WW domains of the enzyme. Among the adaptors of Rsp5, some act mainly at the level of endosomes and/or the Golgi (see later Table 1.2) and generally include one or several transmembrane domains (Merhi and André, 2012). The adaptor protein Bsd2 was initially observed as essential for the MVB sorting of the metal transporter Smf1 (Liu *et al.*, 1997; Hettema *et al.*, 2004). Two other redundant PY-motif-containing proteins, named Tre1/Tre2, assist Bsd2 in bringing Rsp5 in close proximity to Smf1 (Stimpson *et al.*, 2006). Therefore, two sets of adaptors are required for Smf1 ubiquitination. Another set of endosomal adaptors, the pair of homologous proteins Ear1/Ssh4, are required for proper Golgi-to-vacuole sorting of the Gap1 and the siderophore transporter Sit1. Also, the absence of Ear1/Ssh4 does not influence the

rate of internalization of Fur4 from the PM, but prevents its proper MVB sorting. This suggests that successive ubiquitination reactions occur on a cargo along the endocytic pathway but, at least for some transporters, with the use of different adaptors (Léon *et al.*, 2008).
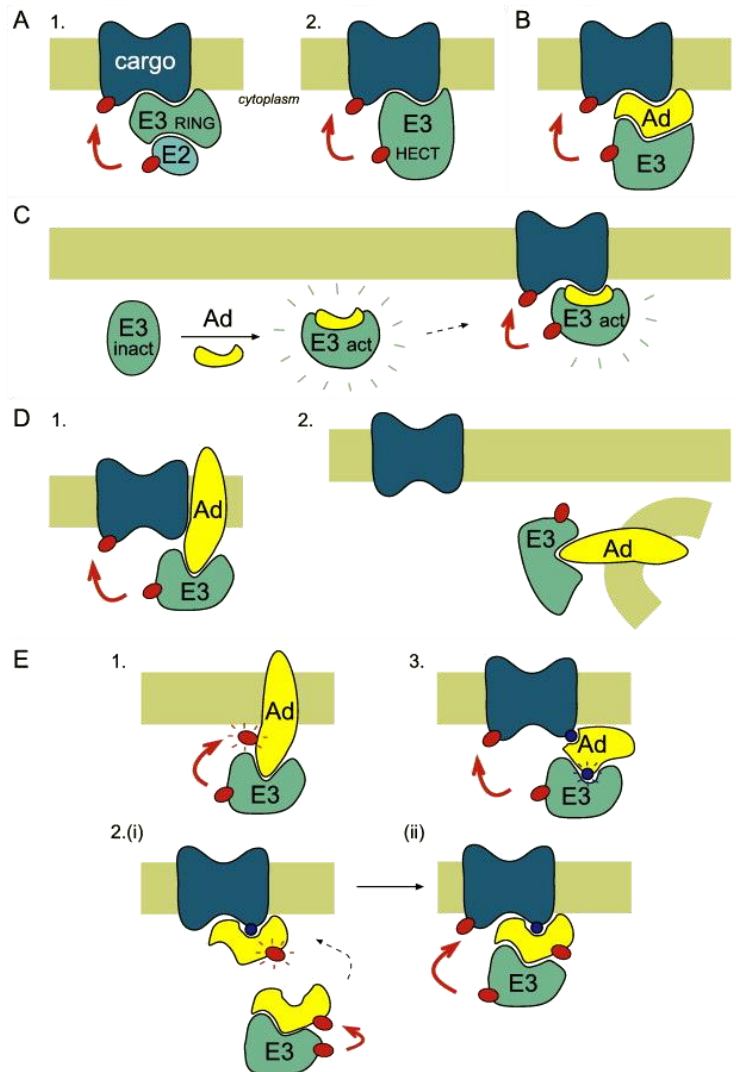
Figure 1.29. Models of the regulation of ubiquitin ligase (E3) function by adaptor proteins. **A.** Direct recognition of the substrate by the E3. (1) RING E3s (e.g. c-Cbl) act as scaffolds between the substrate and the activity-bearing E2. (2) HECT E3s (e.g. Nedd4) interact with the substrate and perform the ubiquitination reaction. **B.** Role of adaptor proteins (Ad) in mediating the interaction of E3s with substrates. The adaptor can also be a membrane protein. In some cases, cargo ubiquitination is contingent upon its prior phosphorylation (see panel E(3)). **C.** Role of adaptor proteins in the activation of E3. **D.** Role of adaptor proteins in the regulation of E3 localization. (1) Recruitment in the vicinity of the substrate (e.g. Bsd2, Tre1/Tre2). (2) Adaptors can also regulate E3 availability by keeping the E3 away from the substrate. **E.** Post-translational modifications of adaptor proteins. (1) Most adaptor proteins are ubiquitinated by the E3, which may influence its localization or affect its stability (e.g. PY-containing adaptors). (2) Ubiquitination of adaptors is required for their function. The E3 in charge of adaptor ubiquitination (i) or cargo ubiquitination (ii) can be the same (e.g. yeast arrestins/Rsp5) or different. (3) Adaptor modification, such as phosphorylation, can be required for E3 recruitment (retrieved from Léon and Haguenauer-Tsapis, 2009).

Arrestin-related proteins (also coined α-arrestins) are globally hydrophilic Rsp5 adaptors promoting ubiquitination at the PM and, as the name implies, they are similar to β-arrestins. β-arrestins, which were first described as proteins binding to G-protein coupled receptors (GPCRs) and arresting signaling by blocking receptor interactions with cognate G-proteins, are now known to participate in endocytosis and signaling of seven-transmembrane receptors (7TMR) by linking them to the endocytic internalization machinery (Shenoy and Lefkowitz, 2005; Merhi and André, 2012). On the basis of phylogenetic and structural analyses, both ancestral α-arrestins and more recently evolved β-arrestins constitute sub-classes of the arrestin family of proteins, but they have one important difference: β-arrestins contain tail domains with conserved clathrin-interacting motifs, whereas α-arrestins contain tail domains with PY motifs.

The α-arrestins are expressed in all eukaryotes except plants, which interestingly do not harbor Nedd4-like genes either. Six members of α-arrestins have been identified in humans, the arrestin-domain-containing 1-5 (ARRDC1–5) and the thioredoxin-interacting protein (TXNIP). In yeast, despite the presence of GPCRs, no gene encoding β-arrestins can be found. Instead, the *S. cerevisiae* genome encodes ten arrestin-related trafficking adaptor proteins (ARTs; Art1-10) and two distant homologues, the Bul1 and Bul2 (Nikko and Pelham, 2009; Reider and Wendland, 2011; Becuwe, Herrador, *et al.*, 2012). Notably, Bul1 and Bul2 were found to be functionally redundant with some of the ART proteins (Nikko and Pelham, 2009).

Arrestin-related proteins were initially identified in *A. nidulans* and named CreD, ApyA (Boase and Kelly, 2004) and PalF (Herranz *et al.*, 2005). In all cases, a connection with the ubiquitin pathway was established; CreD and ApyA were shown to interact physically with HulA, the Nedd4 homologue in *A. nidulans*, whereas PalF was found to be ubiquitinated *in vivo*. CreD is highly similar to yeast adaptors Art4/Rod1 and Art7/Rog3. The *creD* gene was genetically defined by a mutation (*creD34*) that suppresses the phenotypic effects of mutations in *creC* and *creB*, two genes encoding a de-ubiquitinating enzyme and a WD40-motif-containing protein, respectively, which form a complex essential for carbon catabolite repression. ApyA was identified as a homologue of CreD, sharing high amino acid identity (Boase and Kelly, 2004). PalF, homologue of the yeast Art9/Rim8, was shown to bind to the seven-transmembrane and putative pH sensor, PalH, which points out the similarity of PalF with mammalian β1.6.7-arrestins. Interestingly, unlike other fungal arrestins

mediating endocytic downregulation of PM transporters, PalF plays a positive role in ambient pH signaling. Activation of PalH by alkaline pH leads to PalF ubiquitination, which has been proposed to be the sole molecular trigger required for transmitting the alkaline pH signal to the downstream elements of the pathway (Hervás-Aguilar *et al.*, 2010; Becuwe, Herrador, *et al.*, 2012).

The family of arrestin-related trafficking adaptors (ARTs) was first defined in yeast by Lin *et al.* (2008), as a family of adaptor proteins that mediate endocytic downregulation by recruiting Rsp5 to specific PM cargos. They share a central arrestin core with sometimes long extensions on either side, increasing their size up to about 1100 amino acids for the longest members (Aubry and Klein, 2013). ARTs have been studied systematically in respect to their role on the ubiquitination and endocytosis of several transporters (Table 1.2) and the general model emerging is that different arrestin-like proteins recognize different transporters, or the same transporter in response to different stimuli, thus adding another layer of complexity to the system.

For example, Art1/Ldb19/Cvs7 is required for lysine-induced endocytosis of the lysine permease Lyp1, while Art2/Ecm21 is required for cycloheximide-induced endocytosis of the same transporter. Thus, Lyp1 internalization can be triggered by two different stimuli, and these two distinct pathways require different ARTs for endocytosis (Lin *et al.*, 2008). On the other hand, Fur4 and tryptophan transporter Tat2 are able to use the same arrestins (Art2/Ecm21 and Art8/Csr2) for both stress- and substrate-induced turnover (Nikko and Pelham, 2009). Art3/Aly2 and to a lesser extend Art6/Aly1 mediate substrate-induced endocytosis of the aspartic acid/glutamic acid transporter Dip5 (Hatakeyama *et al.*, 2010); strikingly, however, the same adaptors do not influence Gap1 endocytosis, but promote its recycling from endosomes to the TGN and/or PM (O'Donnell *et al.*, 2010). As in *A. nidulans*, the yeast PalF homologue Art9/Rim8, which lacks canonical PPXY elements, has a unique role in pH regulation (Peñalva *et al.*, 2008), whereas Art5 was shown to mediate the substrate-induced endocytosis of the inositol transporter Itr1 (Nikko and Pelham, 2009). Recently, Art4/Rod1 was identified as an essential component of the glucose-induced endocytosis of the lactate transporter Jen1 (Becuwe, Vieira, *et al.*, 2012). Finally, possible functions of Art7/Rog3 and Art10 remain to be revealed.

Table 1.2. Examples of Rsp5 adaptors of yeast transporters (adapted from Lauwers *et al.*, 2010).

Transporter (substrate)	Conditions of vacuolar targeting	Adaptors
Can1 (arginine)	Cycloheximide	Art1[a]
Ctr1 (copper)	Substrate excess	Bul1[a], Bul2[a]
Dip5 (glutamate/aspartate)	Substrate excess	Art3[a], Art6[a]
Fur4 (uracil)	Cycloheximide	Bul1[a], Bul2[a], Art1[a], Art2[a], Art8[a], Bsd2[b], Ear1[b], Ssh4[b]
	Substrate excess	Bul1[a], Bul2[a], Art1[a], Art2[a], Art8[a], Bsd2[b]
Gap1 (amino acids)	Ammonium or substrate excess	Bul1[a,b], Bul2[a,b], Ear1[b], Ssh4[b], Art3[b], Art6[b]
Hxt6 (hexoses)	Cycloheximide	Art8[a]
	Substrate excess	Art4[a]
Itr1 (inositol)	Substrate excess	Art5[a], Bsd2[b]
JenI (lactate)	Glucose	Art4[a]
Lyp1 (lysine)	Cycloheximide	Art2[a]
	Substrate excess	Art1[a]
Mup1 (methionine)	Substrate excess	Art1[a]
Sit1 (ferroxiamines)	Absence of substrate	Ssh4[b], Ear1[b], Tre1[b], Tre2[b]
Smf1 (manganese)	Substrate excess	Bsd2[b], Tre1[b], Tre2[b]
	Stresses	Bsd2[b] Art2[a], Art8[a], Bsd2[b], Tre1[b], Tre2[b] Ear1[b], Ssh4[b]
Tat2 (tryptophan)	Cycloheximide	Bul1[a,b], Bul2[a,b], Art2[a], Art8[a], Bsd2[b]
	Substrate excess	Bul1[a,b], Bul2[a,b], Art1[a], Art2[a], Art8[a], Bsd2[b]

[a]Adaptors acting at the plasma membrane; [b]adaptors acting at the Golgi-endosome

Notably, addition of PY motifs to the tail of the arginine permease Can1 is sufficient for its internalization, bypassing the need for Art1. This indicated that Art1 is not needed for interactions with other endocytic proteins; it only functions as ubiquitin adaptor and not as true endocytic adaptor that links cargo to clathrin (Lin *et al.*, 2008). On the other hand, the closely related Art3 and Art6, were shown to directly interact with clathrin and clathrin adaptor protein (AP) complexes, suggesting that, like their β-arrestin relatives, α-arrestins possibly promote cargo incorporation into clathrin-coated vesicles (O'Donnell *et al.*, 2010).

Regulation of arrestin-like Rsp5 adaptors

The interaction of Rsp5 adaptors with their cognate cargos is regulated in a timely manner with respect to the presence of extracellular signals. Three reports have recently provided the first molecular insights into the nutrient-induced activation of arrestin-related proteins, through a switch in post-translational modifications (MacGurn *et al.*, 2011; Becuwe, Vieira, *et al.*, 2012; Merhi and André, 2012). In the absence of preferred carbon or nitrogen sources, arrestin-like proteins Art1, Art4 or Bul1/2, controlling the ubiquitination and turnover of Gap1, Jen1 or Can1, respectively, are phosphorylated and remain inactive (Figure 1.30). In the case of Art4 or Bul1/2, it was shown that under such poor nutrient conditions, the relevant arrestin-like proteins bind to 14-3-3 proteins, a family of conserved eukaryotic proteins involved in diverse cellular functions, including signaling, which interact with many other proteins when these are phosphorylated. Binding to 14-3-3 proteins inhibits Art4 and Bul1/2 capacity to elicit Jen1 or Gap1 downregulation (Becuwe, Vieira, *et al.*, 2012; Merhi and André, 2012).
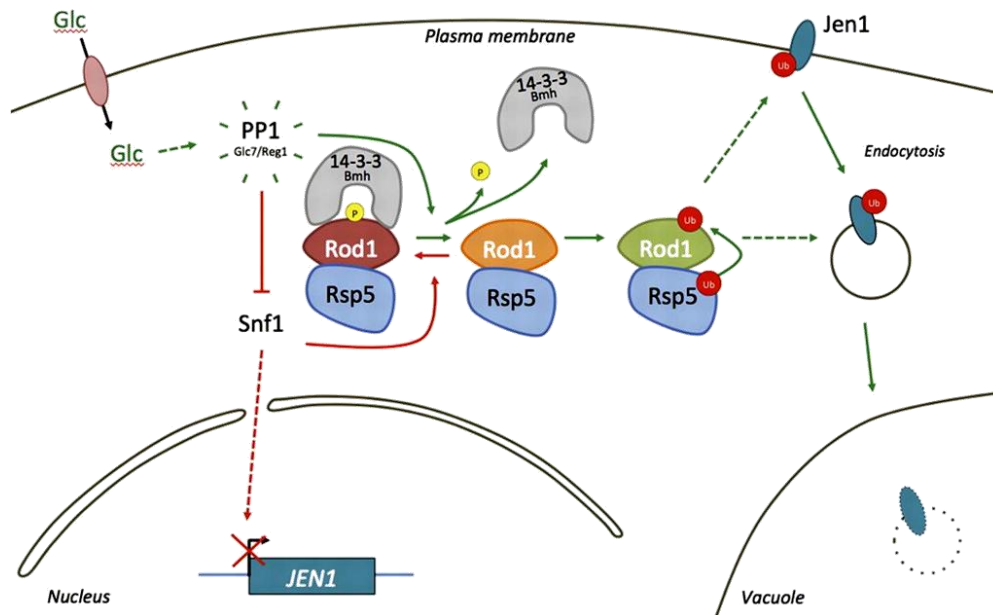
Figure 1.30. Model for the regulation of transporter endocytosis by intracellular signaling through arrestin-related protein activation. When yeast cells are grown in lactate medium, Snf1, the yeast AMPK homologue, is active and phosphorylates Art4 to inactivate it (red arrows). Glucose addition triggers Jen1 endocytosis, which depends on Art4 activation through its PP1-mediated de-phosphorylation and subsequent Rsp5-mediated ubiquitination, which are coordinated by 14-3-3 proteins (green arrows). The subcellular compartment at which Art4 acts on Jen1 endocytosis may be the PM, or internal compartments (dashed lines). Noteworthy, the Snf1/PP1 pathway also controls the transcriptional reprogramming of cells in response to glucose fluctuation, including the expression of the *JEN1* gene, illustrating a robust physiological regulation in which transcriptional and post-translational events are coordinated (retrieved from Becuwe, Vieira, *et al.*, 2012).

Upon shift to rich carbon or nitrogen sources, Art1, Art4 or Bul1/2 are de-phosphorylated, probably released from 14-3-3 proteins and recruited for catalyzing the ubiquitination of their cognate cargos (Figure 1.30). In the case of the Art1 and Bul1/2, their phosphorylation involves the Npr1 kinase, which is itself negatively regulated by the target of rapamycin complex 1 (TORC1) pathway. The TORC1 is a highly conserved multi-protein kinase complex that senses various cellular and environmental cues including nutrient availability, energy status, and growth signals and responds by coordinating activities associated with cell growth and proliferation (MacGurn *et al.*, 2011; Merhi and André, 2012). On the other hand, phosphorylation of the Art4 seems to be mediated by Snf1, the yeast homologue of AMP-activated kinase (AMPK). De-phosphorylation of Bul1/2 and Art4 was shown to be dependent on the Sit4 phosphatase and the protein phosphatase 1 (PP1) Glc7/Reg1, respectively (Becuwe, Vieira, *et al.*, 2012; Merhi and André, 2012).

One more arrestin-like protein, the Art3, was found to be phosphorylated, but the physiological role of this modification remains unknown (O'Donnell *et al.*, 2010; Hatakeyama *et al.*, 2010). In addition, its closely related arrestin-like protein Art6 was very recently found to be de-phosphorylated by the Ca^{2+}- and calmodulin-dependent phosphoprotein phosphatase calcineurin/PP2B. De-phosphorylation of Art6 by calcineurin is required for Art6-mediated trafficking of Dip5 to the vacuole, but it does not alter Rsp5 binding, ubiquitination or stability of the adaptor and it does not regulate the ability of Art6 to promote the intracellular sorting of Gap1. These results suggest that de-phosphorylation of Art6 serves as a regulatory switch to promote Art6-mediated trafficking to the vacuole (O'Donnell *et al.*, 2013).

Another aspect of the emerging mechanism underlying the control of arrestin-like protein action is their ubiquitination. In all cases tested (Art1, Art2, Art3, Art4, Art8, Art9, Bul1 and Bul2), adaptor ubiquitination is Rsp5-dependent and essential for their function (Kee *et al.*, 2006; Lin *et al.*, 2008; Herrador *et al.*, 2010; Hatakeyama *et al.*, 2010; Becuwe, Vieira, *et al.*, 2012; Merhi and André, 2012). Therefore, arrestin-like proteins are adaptors as well as targets of the same ubiquitin ligase. Studies on Art1, Art4 and Bul1/2 revealed that this ubiquitination is required for proper permease downregulation (Figure 1.30) and that there seems to be a cross-talk between the phosphorylation/de-phosphorylation status and the ubiquitination levels of arrestin-like proteins. Interestingly, Art1 ubiquitination appears to be constitutive in the conditions tested (Lin *et al.*, 2008), whereas Art4 or Bul1/2

ubiquitination is induced by glucose or ammonium and may therefore provide an additional step for its regulation (Becuwe, Vieira, *et al.*, 2012; Merhi and André, 2012). The signal-dependent ubiquitination of arrestin-related proteins has been also described in filamentous fungi (see also earlier in 1.6.7; Herranz *et al.*, 2005; Hervás-Aguilar *et al.*, 2010) and is reminiscent of β-arrestin ubiquitination in mammalian cells in response to agonist treatment; however, the precise mechanism by which this occurs is still unknown (Becuwe, Vieira, *et al.*, 2012).

Apart from the regulation of adaptor activity by post-translational modifications, an additional regulatory mechanism that has been proposed is the physiological control of the location of Rsp5 adaptors, that is, a change in their intracellular localization in response to environmental changes and their recruitment to the compartments at which they perform their function. To date, such a mechanism has only been reported for Art1 (Lin *et al.*, 2008). Under non-stress conditions, Art1-GFP localized mainly to the late Golgi and to the cytoplasm, while PM signal was weak but still detectable. Interestingly, when cells were stressed by cycloheximide, an enrichment of Art1-GFP at the PM was observed, which is consistent with stress-induced, Art1-mediated internalization of Can1. A striking redistribution of Art1-GFP to the PM was also observed upon shift to a rich medium.

In addition, the subcellular localization of another three adaptors has been observed microscopically, but without any evidence for signal-specific relocation/recruitment. Art9-GFP appeared in cortical punctate structures and this localization was strictly dependent on the interaction of the adaptor with the ESCRT-I subunit Vps23 (Herrador *et al.*, 2010). Art3-GFP and Art6-GFP exhibited both diffuse cytoplasmic fluorescence and localized to multiple intracellular foci. In particular, a significant portion of the adaptors localized to endosomes. They also partially co-localized with t-SNAREs that mediate fusion of vesicles trafficking between early endosomes and the TGN, with a component of the ESCRT III complex (present at the MVBs) and with clathrin-coated vesicles (O'Donnell *et al.*, 2010).

1.7   Membrane protein interactions

1.7.1 General aspects of protein-protein interactions

Protein-protein interactions (PPIs) are physical contacts with molecular docking between proteins that occur in a cell or in a living organism *in vivo*. They are involved in the regulation and execution of all biochemical pathways within a cell, in bacteria, fungi, plants, and mammals. Because of their essential role in cellular regulation, impairment of PPIs is associated with a large number of human diseases, including cancer, neurodegenerative diseases, and various metabolic diseases. Not all possible interactions will occur in any cell at any time. Instead, interactions depend on cell type, cell cycle phase and state, developmental stage and environmental conditions, and they are efficiently regulated by post-translational modifications, presence of co-factors or presence of other binding partners. Through these interactions, macromolecular complexes are formed that function in the correct place and time (Park *et al.*, 2008; De Las Rivas and Fontanillo, 2010).

There are several advantages of multi-subunit complexes in comparison to a single large protein with multiple sites. First, it is more convenient to have one gene encoding a protein with different interacting partners, such as some of the eukaryotic RNA polymerase subunits, rather than having the gene for that subunit reiterated for each different polymerase. Second, translation of large proteins can cause a significant increase in errors; if such errors occur, they are more economically eliminated by preventing assembly of that subunit into the complex than by eliminating the whole protein. Third, multi-subunit assemblies allow synthesis at one locale, followed by diffusion and assembly at another; this results in both faster diffusion, since the monomers are smaller, and compartmentalization of activity (if assembly is required for activity). Fourth, homo-oligomeric proteins that have an advantage over monomers are easily selected in evolution, if the oligomers interact in an anti-parallel fashion; in this case, a single-amino-acid change that increases interaction potential has effects at two such sites. Finally, another advantage of multi-subunit complexes is the ability to use different combinations of subunits to alter the magnitude or type of response (Phizicky and Fields, 1995).

Proteins bind to each other through a combination of non-covalent forces, such as hydrogen bonding, ionic interactions, van der Waals forces and hydrophobic packing. The fact that PPIs imply physical contact between proteins does not mean

that such contacts are static or permanent. The cell machinery undergoes continuous turnover and reassembly. Protein interactions are fundamentally characterized as stable or transient, and both types of interactions can be either strong or weak. Stable interactions are those associated with proteins that are purified as multi-subunit complexes, and the subunits of these complexes can be identical or different. Hemoglobin and core RNA polymerase are examples of multi-subunit interactions that form stable complexes. Because these complexes are much easier to study, most of the available experimental data (such as crystal structures) have been obtained from stable complexes. However, transient interactions are equally important; they play major roles in signal transduction, electron cascades, protein modification, transport, folding, trafficking and other essential cellular processes. Transient interactions can be strong or weak, and fast or slow. As the name implies, transient interactions are temporary in nature and typically require a set of conditions to promote them, such as post-translational modifications, conformational changes or localization to discrete areas of the cell (Phizicky and Fields, 1995; Szilágyi *et al.*, 2005; De Las Rivas and Fontanillo, 2010).

Protein-protein interactions can have a number of different measurable effects. First, they can alter the kinetic properties of proteins. This can be reflected in altered binding of substrates, altered catalysis, or altered allosteric properties of the complex. Second, PPIs are a common mechanism to allow substrate channeling, by moving the substrate between domains or subunits, resulting in the intended final product, without having been released into solution. Third, they can result in the formation of a new binding site or they can change the specificity of a protein for its substrate, through the interaction with different binding partners. In addition, PPIs serve a regulatory role by either activating or inactivating a protein or by controlling its trafficking and dynamic subcellular localization. Transporter internalization due to ubiquitination by ubiquitin ligase and the oligomerization of some transporters prior to their export from the ER are both fine examples of cellular mechanisms where PPIs are indispensable. Finally, aberrant interactions can contribute to pathogenesis, as in the case of HIV interactions with the endocytic machinery (Pawson and Gish, 2005).

1.7.2 Challenges of studying membrane protein interactions

Understanding how proteins enter and leave countless associations in the cell is a hard task, since the biological network is enormously complex and the association between proteins is often extremely transitory. Things get worse when it comes to the analysis of interactions between membrane proteins. Because of the hydrophobic nature of these proteins, conventional biochemical and genetic assays are often of limited use.

The two-hybrid system, for example, has limitations in respect to identifying partners for membrane proteins. Because the PPI that leads to the reconstitution of an active transcription factor must occur on the promoter of the reporter gene, the interacting proteins have to be located in the nucleus. However, transmembrane proteins tend to be insoluble and form aggregates if not present within membranes. Therefore, although certain membrane protein interactions have been detected successfully with the two-hybrid assay (Bourette *et al.*, 1997; Hellyer *et al.*, 1998), the identification of integral membrane protein interactions with cytoplasmic or other membrane proteins is best carried out using other methodologies. Furthermore, atomic-resolution structures have been determined for only a small number of integral membrane proteins. These proteins are difficult to crystallize for X-ray analysis for two main reasons; first, the hydrophobic nature of membrane proteins, which makes them very difficult to handle and very sensitive to aggregation, and second, their lack of natural abundance.

In order to overcome these limitations, novel methodologies for the identification and analysis of membrane protein interactions have been introduced, as well as alterations to previously existing methods, including various biochemical techniques for examining interactions *in vitro* and fluorescence complementation-based methodologies for monitoring interactions *in vivo*. For example, the limitation of the low abundance of membrane proteins is addressed by enhancing the expression of the protein of interest with the use of strong promoters and/or by using a heterologous expression system, such as *E.coli*, *S. cerevisiae* or *Pichia pastoris* (Midgett and Madden, 2007). Further adjustments include the use of mutant proteins with increased stability, protease deficient cell lines and GFP-tagged proteins that will allow rapid assessment of the expression levels by simple fluorescence measurements (Leung *et al.*, 2010; Alguel *et al.*, 2010). A major advance in terms of expression has been the development of cell-free expression systems for the

production of membrane proteins (Liguori *et al.*, 2007; Schwarz *et al.*, 2008). This type of approach involves the *in vitro* production of proteins from a DNA or mRNA template. By its very nature, the system removes the problem of cytotoxicity and also simplifies protein isolation as the number of contaminant proteins is markedly reduced. Besides that, the expressed membrane proteins are maintained in a soluble state in detergent micelles post-translationally, since there is no native membrane environment for insertion.

In addition, taking into account the hydrophobic nature of the transmembrane domains of integral membrane proteins, and in order to solubilize and eventually purify them, a vast excess of detergents must be added. Detergents are amphiphilic molecules that form micelles above their critical micellar concentration. The detergent micelles take up the membrane proteins and cover their hydrophobic surface with their alkyl chains in a belt-like manner, whereas detergent polar head groups face the aqueous environment (Figure 1.31). Thus, detergents serve as mimics of lipid bilayers because of their self-assembling properties (Ostermeier and Michel, 1997). The major bottleneck to obtain well-ordered crystals for crystallization is to select the appropriate detergent. Mild detergents are widely used for membrane protein manipulation, but many membrane proteins tend to denature and aggregate when solubilized with these agents, making it difficult to conduct functional studies, spectroscopic analysis or crystallization. Moreover, some detergents may interfere with protein interactions. To address that, new classes of amphiphiles with properties
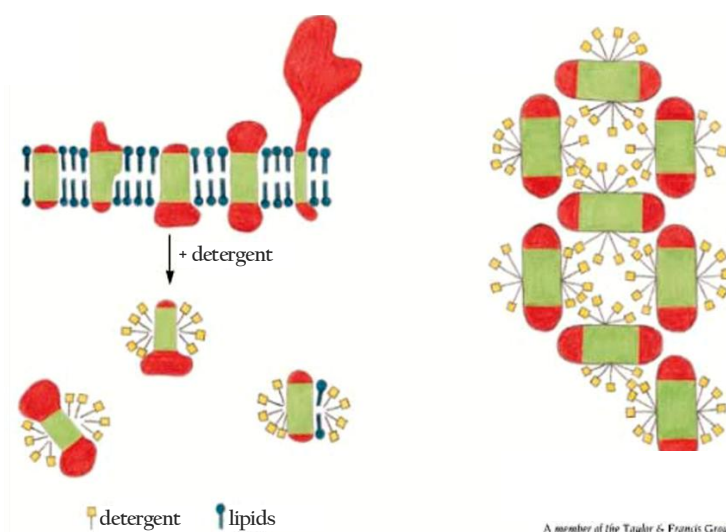
Figure 1.31. Detergent micelles take up the membrane proteins and help their solubilization by covering their hydrophobic surface (green), while leaving the hydrophilic parts (red) exposed (adapted from http://www.chemie.uni-hamburg.de/bc/betzel/Mesters_SPC1_3.pdf).

tailored for membrane proteins are being developed (Privé, 2007; Chae *et al.*, 2010). Cao *et al.* (2011) recently presented the crystal structure of ChbC from *Bacillus cereus* that transports diacetylchitobiose. ChbC was shown to be a homodimer, with an expansive interface formed between the amino-terminal halves of the two protomers.

1.7.3 Methods for the identification of membrane protein interactions

Multiple and diverse methods have been developed for the identification of membrane protein interactions and a combination of these techniques is usually being employed to validate and eventually characterize them. Physical methods have been extensively used and are considered very accurate. Crystallography can give a clear image of the structure of a protein complex, although the procedure of getting a crystal is quite laborious.

Affinity-based methods, such as protein affinity chromatography, affinity blotting and coimmunoprecipitation (CoIP), take advantage of the fact that when a cell is lysed under non-denaturing conditions, many of the PPIs that exist within the intact cell are conserved. These methods can be also used for detecting PPIs that can be reproduced *in vitro*. They are considered very sensitive but, like crystallography, they require the putative interacting proteins to be purified and dissolved in a solution. In general, stable PPIs are easier to isolate by affinity-based methods, because the protein complex does not disassemble over time. Weak or transient interactions can also be identified provided they have first been stabilized by chemical cross-linking, which promotes their survival during the procedures of the analysis (Phizicky and Fields, 1995; Vitale, 2002; Sudakin, 2005). Examples of affinity-based methods being used for the study of membrane protein interactions include the oligomerization of the human serotonin transporter (SERT) and the human dopamine transporter (DAT), which were demonstrated by CoIP (Kilic and Rudnick, 2000) and a pull down assay (Torres *et al.*, 2003), respectively.

Other methods focus on monitoring and characterizing specific biochemical and physicochemical properties of a protein complex. Isothermal titration calorimetry is a milder technique that allows the accurate determination of the binding affinity between a protein and its binding partner, as well as the changes in enthalpy (ΔH) and entropy (ΔS). Thus in a single experiment, a complete thermodynamic profile of the molecular interaction can be determined (Trankle and

Herrmann, 2005). Native electrophoresis, the electrophoretic analysis of intact protein complexes under non-denaturing conditions, is a fast, low-cost, but not very sensitive approach for the isolation and analysis of membrane protein complexes. One limitation of this method is that, like other biochemical methods, it is more efficient for the detection of stable protein complexes and can only be used for dynamic interactions after *in vivo* cross-linking of the interacting proteins (Wittig and Schägger, 2009). Recently, new methods have been developed to analyze protein interactions at a single molecule level. Atomic force microscopy (AFM) is a powerful tool allowing a variety of surfaces to be imaged and characterized at the atomic level. Thus, information concerning the state of oligomerization (dimer, higher order oligomer) can be obtained. The native arrangement of rhodopsin, which was shown to form paracrystalline arrays of dimers in mouse rod disc membranes, was revealed with the use of this technology (Figure 1.32; Fotiadis *et al.*, 2003).
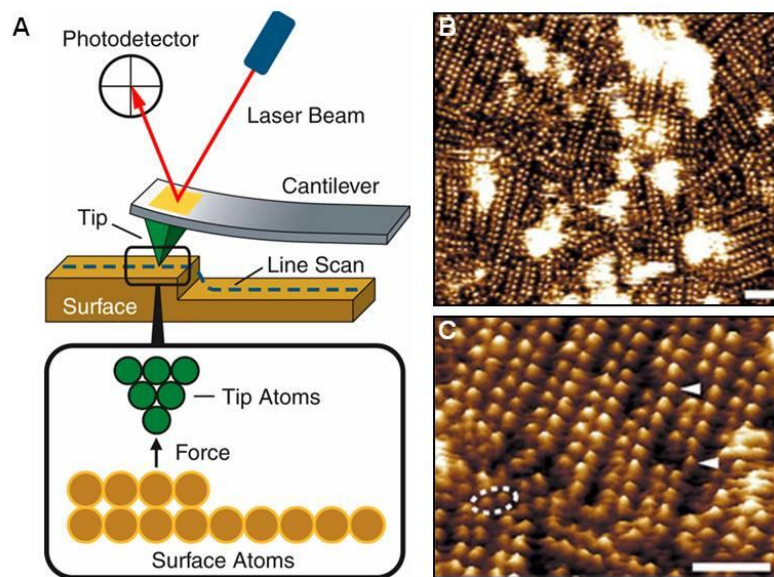
Figure 1.32. A. Schematic representation of AFM setup (retrieved from http://goo.gl/H1Ncug). AFM operates by rastering a sharp tip that is attached to a low spring constant cantilever across the sample. An extremely low force is maintained on the cantilever, thereby pushing the tip against the sample as it rasters. A laser beam aimed at the back of the cantilever–tip assembly reflects off the cantilever surface to a split photodiode, which detects the small cantilever deflections and converts them into an analogue image of the sample surface (Blanchard, 1996). **B.** Topograph obtained using AFM, showing the paracrystalline arrangement of rhodopsin dimers in the native mouse disc membrane. Scale bar: 50nm (adapted from Fotiadis *et al.*, 2003). **C.** Magnification of a region of the topograph in (B), showing rows of rhodopsin dimers, as well as individual dimers (inside dashed ellipse), presumably broken away from one of the rows, and occasional rhodopsin monomers (arrowheads). Scale bar: 15nm (adapted from Fotiadis *et al.*, 2003).

Over the past years, researchers have developed alternative yeast-based systems that retain the advantages of the original yeast two-hybrid system, but are also capable of detecting interactions involving membrane proteins. The reverse Ras recruitment system is based on the PPI-dependent PM localization of Ras, which is required for downstream signaling events of the Ras pathway in yeast that ultimately lead to cell growth (Broder *et al.*, 1998). The G-protein fusion technology is another yeast-based interaction approach appropriate for detecting membrane protein interactions, in which inactivation of a G-protein signaling pathway serves as the reporter readout (Ehrhard *et al.*, 2000). In the split-ubiquitin system, ubiquitin is split into two parts and each of them is fused to the putative interacting proteins. A reporter protein is also fused to one of the ubiquitin halves. Interaction of the proteins leads to ubiquitin reconstitution, resulting in the release of the reporter protein by the ubiquitin-specific proteases (Stagljar and Fields, 2002). Synthetic genetic approaches can also be used for high throughput screenings and can reveal a perplexing array of potential interacting partners for any target protein. It is now known, however, that this type of anonymous screening approach can yield high levels of false-positive or false-negative results and, therefore, interactions must also be confirmed by independent methods.

A breakthrough in the methods analyzing membrane protein interactions was the development of fluorescence complementation-based techniques. These methods enabled the detection of PPIs *in vivo*, but also the identification of the subcellular localization of the protein complexes. A robust technique in this respect is fluorescence resonance energy transfer (FRET), a dipole-dipole coupling process, through which energy is transferred from a donor fluorophore (CFP) to an acceptor fluorophore (YFP) in a distance-dependent manner. Thus, excitation of the donor produces a sensitized emission from the acceptor, while simultaneously quenching the fluorescence of the donor (Verveer *et al.*, 2005). FRET has been used for the validation of human dopamine transporter (DAT) oligomerization (Sorkina *et al.*, 2003). A variety of FRET detection methods exist, including donor fluorescence recovery after acceptor photobleaching (DFRAP) and fluorescence life-time measurements (FLIMs), whereas a variation using a luminescent donor protein has also been developed (bioluminescence resonance energy transfer–BRET). Moreover, bimolecular fluorescence complementation (BiFC) has proved very efficient and

precise, provided the appropriate controls are used, in order to eliminate the chance for false-positive results (see later).

For organisms for which powerful genetic analysis methods exist, classical genetic approaches can be used to indirectly access interactions. For example, identification of extragenic suppressors that restore the activity of a mutant gene often reveals mutations in genes whose products physically interact with the protein containing the original defect. Suppressors may either restore the original contact or may create a novel interaction compensating for the primary mutation in an indirect way. Synthetic lethal screens yield mutations that, in combination with another pre-existing non-lethal mutation, result in the inability of the organism to grow; this phenotype is commonly due to alterations in interacting proteins. Overproduction of certain proteins can lead to the suppression of mutations in interacting proteins. In other cases, overproduction disrupts a cellular process by altering the balance of the different components of a complex structure, or the overproduced protein is non-functional and acts in a dominant-negative manner. The existence of such dominant-negative phenotypes can lead not only to the detection of an oligomeric interaction, but also to the determination of the interaction domain of a protein (Guarente, 1993; Phizicky and Fields, 1995). Genetic approaches have been fruitful in several cases, such as the DAT transporter (Torres *et al.*, 2003).

Computational and conservation analyses are useful tools for the prediction of membrane protein interactions and/or their interaction interfaces. Close homologues almost always interact in the same way and PPIs place certain evolutionary constraints on protein sequence and structural divergence. Many interactions are conserved (interologs) even between remotely related species, such as yeast and worm. Data related to protein interactions are stored in protein-interaction or domain-interaction databases and can be used for the prediction of putative partners or interaction domains of a given protein of interest. Also, interaction networks are constructed and the interaction maps obtained for one species can be used to predict interaction networks in other species, to identify functions of unknown proteins, and to get insight into the evolution of protein interaction patterns (Shoemaker and Panchenko, 2007). Therefore, computational and conservation analyses, combined with experimental data, allow us to obtain a more complete picture of the membrane protein interactome.

Among the aforementioned methods for the identification and analysis of membrane protein interactions, affinity chromatography and BiFC were extensively used in this study and are described below in detail.

Column affinity chromatography

Affinity chromatography is a standard method of separating biochemical mixtures passing through a chromatographic column, based on a highly specific interaction. The stationary phase of the column is typically a gel matrix, often of sepharose resin. First, an already purified protein is covalently coupled to the resin, while passing through the column. The protein extract of potentially interacting proteins is subsequently loaded to the column. Most proteins pass through the column or are readily washed off under low-salt conditions; proteins that are retained can then be eluted by high-salt solutions, cofactors, chaotropic solvents, or sodium dodecyl sulfate (SDS). If the extract is labelled *in vivo* before the experiment, labelled proteins can be detected with high sensitivity, while unlabeled polypeptides derived from the covalently bound protein can be ignored (Phizicky and Fields, 1995; Sudakin, 2005).

A variation of this method that was used in this study is the immobilized metal ion affinity chromatography. This technique is based on the specific covalent bond of histidine to metals. It works by allowing proteins with an affinity for metal ions to be retained in a column containing immobilized metal ions, such as cobalt, nickel or copper. Since, many naturally occurring proteins do not have an affinity for metal ions, a poly-histidine tag can be introduced into the relevant gene. Therefore, when a crude protein extract is loaded on the column, only the His-tagged proteins along with their interacting partners will be retained on the matrix. His-tagged proteins are then eluted by adding a competitive molecule, such as imidazole, and the interacting proteins that were pulled down together with the former are subsequently identified. This procedure is also referred to as a pull-down assay.

There are four distinct advantages of protein affinity chromatography as a technique for detecting PPIs. First, and most important, protein affinity chromatography is very sensitive. With appropriate use, it can detect interactions within range of the weakest interaction likely to be physiologically relevant. Second, this technique tests all proteins in an extract equally; thus, extract proteins that are detected have successfully competed with the rest of the population of proteins.

Third, it is easy to examine both the domains of a protein and the critical residues within them that are responsible for a specific interaction, by preparing mutant derivatives. Fourth, interactions that depend on a multi-subunit tethered protein can be detected, unlike the case with protein affinity blotting. One potential problem derives from the very sensitivity of the technique. Since it detects interactions that are so weak, independent criteria must be used to establish that the interaction is physiologically relevant. Detection of a false-positive signal can arise for a number of reasons. For example, a protein of the extract may bind to the matrix non-specifically; for this reason, it is desirable to make a control experiment, with a protein extract devoid of a His-tagged protein. Also, the proteins may interact with high specificity even though they never encounter one another in the cell. The most famous example of this type is the high affinity of actin for DNase I (Phizicky and Fields, 1995).

Bimolecular fluorescence complementation

BiFC is a standard technique that enables direct visualization of protein interactions in living cells. It is based on the generation of fluorescent signal from two non-fluorescent fragments of a fluorescent protein (FP; Figure 1.33). Yellow fluorescent protein (YFP) is widely used for this purpose (also called split-YFP assay), but other variations exist. The two YFP halves are genetically fused to the proteins under study and if an interaction between these proteins occurs, the YFP protein is reconstituted and emits fluorescence.
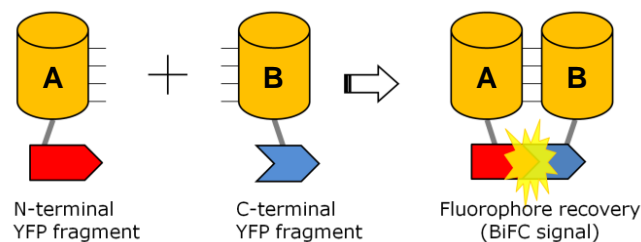
Figure 1.33. Bimolecular fluorescence complementation (BiFC). The fluorescent protein YFP is split into two parts, YFP_N and YFP_C (red and blue interlocking shapes). Two potentially interacting proteins (cylinders) are fused to YFP_N and YFP_C, respectively. The association of protein A and B brings YFP_N and YFP_C into proximity, allowing the refolding of a functional YFP. The fluorescence intensity of the refolded YFP reflects the interaction of A and B (adapted from Haider *et al.*, 2011).

One of the big advantages of this method is that it allows the detection of PPIs *in vivo* and even the visualization of the subcellular localization of the protein

complex under different conditions, without the need for staining. BiFC can be considered a sensitive technique since the complementation process produces a new fluorescent signal, whereas resonance energy transfer variations produce changes in fluorescence that already exists. Additionally, there is the possibility to generate complemented FPs by the association of fragments coming from different FPs. These new complemented FPs possess distinct spectral properties when compared to the native ones. This principle, called multi-color BiFC, can in theory allow the stoichiometry calculation of a multi-protein interaction (Kerppola, 2006; Ciruela, 2008). On the other hand, some limitations of this method are the inherent irreversible association of the fluorescent-protein fragments that has been observed in several cases and the intrinsic ability of the fluorescent-protein halves to spontaneously associate under certain circumstances (Magliery *et al.*, 2005; Ciruela, 2008).

In spite of its limitations, there is no doubt that this straightforward fluorescence-based method is a powerful tool for the study of PPIs in living cells. It has already been used for the visualization of interactions between many different proteins in a wide variety of cell types and organisms. One example is the use of split-YFP in live cells for the demonstration of the homodimerization of zinc transporters (Lasry *et al.*, 2014). Split-YFP has also been used for the detection of interactions between two proteins involved in the initiation and maintenance of polarized growth in *A. nidulans* (Takeshita *et al.*, 2008).

1.7.4 Understanding the biological role of membrane protein interactions

The verification of its existence is the first step on the road to understanding the biological significance of an interaction. Further questions of interest remain to be answered, such as where, how, under which conditions do these proteins interact *in vivo* and what are the functional implications of these interactions. In particular, it is well established that many proteins migrate between different cellular compartments, in response to internal or external stimuli (e.g. changes in cellular environment). Therefore, it is important to understand how the pattern of interactions changes in different physiological conditions. In addition, the subcellular localization where the interaction occurs is of great significance; usually, it is determined with the use of fluorescence complementation-based analyses and/or cell fractionation biochemical assays (Pugacheva and Golemis, 2005).

Another issue to be addressed is the identification of the specific binding domain(s) on each protein that mediate the interaction. These domains can be small binding clefts or large surfaces and can be just a few peptides long or span hundreds of amino acids; the size of the binding domain influences the strength of the binding. To establish the sequences of the interacting partners that contribute energy to the interaction, structure-function analyses are carried out by assessing the interactions between truncated and mutated forms of the proteins, guided by predictions of critical domains that sequence analysis has revealed. These studies can also reveal the possible effect of the interaction on the activity of each partner, as well as the role of the interaction for the development and the function of the cell or the organism (Pawson and Gish, 2005; Pugacheva and Golemis, 2005).

PPIs within the membrane milieu are mainly mediated through transmembrane domains. Non-covalent association of transmembrane domains is mediated by several motifs including: (i) a GXXXG motif, which is the most common motif for interaction of two transmembrane helices and was first found in the glycophorin A transmembrane domain (Lemmon *et al.*, 1994; Russ and Engelman, 2000); (ii) a polar-XX-polar motif, in which polar amino acids include Ser, Thr, Glu, Gln, Asp, and Asn, through the formation of hydrogen bonds; (iii) an aromatic-XX-aromatic motif, in which Trp gives the best dimerization; (iv) a Gly zipper (GXXXGXXXG) motif, found as the primary interaction interface for the homodimers of myelin protein zero, which is the major integral membrane protein of peripheral nerve myelin in higher vertebrates (Plotkowski *et al.*, 2007); (v) Ser/Thr rich sequences, which were initially identified by a randomized library of transmembrane interfaces (Dawson *et al.*, 2002) and (vi) a Leu zipper, an interaction motif in which there is a cyclical occurrence of leucine residues every seventh residue over short stretches of a protein in α-helix. These leucine residues project into an adjacent leucine zipper repeat by interdigitating into the adjacent helix, forming a stable coiled-coil. Because of the tight molecular packing, leucine zippers provide stable binding between transmembrane helices (Oates *et al.*, 2010). In addition, the leucine zipper may have functional roles, such as to transmit signals by altering binding properties (Phizicky and Fields, 1995; Fink *et al.*, 2012).

1.7.5 Oligomerization of transmembrane transporters

Accumulating evidence suggests that transporter oligomerization constitutes an evolutionary conserved mechanism for the fine regulation of transporter function and/or intracellular trafficking. Many transport proteins are now considered to exist and function as oligomers. In addition to those transport complexes made up of subunits with four or six transmembrane domains (Takahashi *et al.*, 1985; Saier, 1994; Yerushalmi *et al.*, 1996; Schroers *et al.*, 1998), larger proteins, such as glutamate (Haugeto *et al.*, 1996) and glucose transporters (Hebert and Carruthers, 1991), as well as most of the studied members of the Neurotransmitter:Sodium Symporter (NSS) Family have been inferred to be oligomeric (Korkhov *et al.*, 2004). Examples of the latter are the serotonin transporter (SERT; Kilic and Rudnick, 2000; Schmid *et al.*, 2001), the γ-aminobutyric acid (GABA) transporter 1 (GAT-1; Schmid *et al.*, 2001; Korkhov *et al.*, 2004), the norepinephrine transporter (NET; Kocabas *et al.*, 2003) and the dopamine transporter (DAT; Milner *et al.*, 1994; Berger *et al.*, 1994; Hastrup *et al.*, 2001; Torres *et al.*, 2003; Sorkina *et al.*, 2003; Chen and Reith, 2008; Li *et al.*, 2010). Among them, DAT is the most extensively studied in respect to its oligomerization.

Early radiation inactivation studies indicated the existence of DAT assemblies containing at least two protomers (Milner *et al.*, 1994; Berger *et al.*, 1994). More direct evidence for a quaternary organization of DAT has been obtained with cross-linking techniques (Hastrup *et al.*, 2001; Hastrup *et al.*, 2003; Chen and Reith, 2008), co-purification experiments with differentially tagged DATs (Torres *et al.*, 2003; Chen and Reith, 2008), as well as FRET microscopy and CoIP (Sorkina *et al.*, 2003). In particular, it has been proposed that DAT forms dimers of dimers with two distinct symmetrical interfaces in transmembrane domains 4 and 6 (Hastrup *et al.*, 2001; Hastrup *et al.*, 2003), although evidence from other studies points to TMS2 (Torres *et al.*, 2003). On the other hand, SERT was shown to appear in a variety of oligomerization states, revealing molecular associations larger than dimers and demonstrating the coexistence of different degrees of oligomerization in a single cell. Notably, the oligomeric state of SERT complexes is stably determined before being integrated into the PM (Anderluh *et al.*, 2014).

DAT and GAT-1 form oligomers already in the ER (Scholze *et al.*, 2002; Sorkina *et al.*, 2003). This is a prerequisite for newly formed transporters to pass the stringent quality control mechanisms of the ER, while this quaternary structure is

also the preferred state for transporters in the PM. Only properly assembled transporters are able to recruit the coat proteins needed for ER-to-Golgi trafficking and this is probably because oligomerization results either in the complementation of an ER export signal or in the masking of an ER retention signal (Farhan *et al.*, 2006). As expected, mutations that disrupt oligomer formation result in ER retention of transporters (Scholze *et al.*, 2002; Torres *et al.*, 2003). In addition, experiments with dominant-negative mutants of DAT revealed a reduction in DAT activity as a result of the formation of non-functional oligomeric complexes at the cell surface (Torres *et al.*, 2003).

In a FRET study, exposure to phorbol 12-myristate 13-acetate (PMA) or amphetamine caused DAT to accumulate in vesicular structures. Positive FRET signals were detected within these vesicular structures, suggesting that endocytosed DAT exists in oligomerized form. The vesicular structures carrying positive FRET signals were limited in amphetamine-treated cells compared with those in PMA-treated cells, suggesting a differential role of oligomerization in PMA- and amphetamine-induced DAT endocytosis (Sorkina *et al.*, 2003). In contrast, in two recent reports dopamine and amphetamine appeared to dissociate DAT oligomers, shifting the distribution of surface DAT towards a smaller ratio of oligomers to monomers, as seen with both CoIP and cross-linking experiments (Chen and Reith, 2008; Li *et al.*, 2010).

1.8   Principal aims

The main target of this dissertation is to study the regulatory mechanisms of intracellular trafficking of purine transmembrane eukaryotic transporters. Gaining insight into the regulation of expression of fungal nucleobase transporters and understanding the conditions of maximal expression in the PM, apart from satisfying basic scientific curiosity, might also provide ideas and contribute to the development of targeted pharmacological therapies against pathogenic fungi. In addition, it was recently demonstrated in a bacterial species that an endocytosis-like process occurs (Lonhienne *et al.*, 2010). Given the homology between fungal and bacterial nucleobase transporters, knowledge obtained from fungal proteins could possibly enable the use of existing or novel purine analogues also as antibacterial drugs.

A. nidulans, which grows exclusively by apical extension, provides an excellent system for the study of intracellular trafficking. One of the advantages of

using this organism for studying endocytic mechanisms is that *A. nidulans* early endosomes, unlike those of *S. cerevisiae*, display characteristic long-distance bidirectional motility and thus are readily distinguished from static late endosomes and Golgi cisternae (Taheri-Talesh *et al.*, 2008; Abenza *et al.*, 2009; Gournas *et al.*, 2010). Particularly for the study of purine transport and metabolism, *A. nidulans* provides unique advantages related to growth phenotypes, genetic screens and already available strains. Moreover, the major uric acid-xanthine symporter of *A. nidulans*, UapA, has been extensively studied at the molecular, cellular and biochemical level (see 1.5.6) and a plethora of characterized mutations exist. These, along with other advantages analysed herein (see 1.2.2), prompted us to select *A. nidulans* as a model organism for our study and UapA as the model cargo.

The experimental work of this dissertation consists of three independent parts, the prevalent aim of which was to elucidate the mechanisms regulating the endocytic and exocytic pathways of membrane purine transporters. The aims of each individual part are analyzed in the corresponding chapters of this manuscript (sections 3.2, 4.2 and 5.2). Briefly, the first part (Chapter 3) focuses on the phenomenon of the appearance of UapA in cortical patches upon hypertonic treatment and the effect of hypertonicity on fungal physiology and UapA endocytic internalization. The second part (Chapter 4) aims at the elucidation of the mechanisms regulating UapA endocytosis and vacuolar degradation and specifically on the identification of the ubiquitin ligase adaptor that is responsible for UapA ubiquitination and turnover, and the unraveling of its mode of function. The last part (Chapter 5) is dedicated to the demonstration of UapA homo-oligomerization and the study of its possible roles in the sorting to the PM and the endocytosis of the transporter.

2

Materials & Methods

2.1 Strains, culture media, growth and storage conditions

2.1.1 Strains used in this study

Table 2.1. List of strains used in chapter 3

Strain Genotype	References
Aspergillus nidulans	
uapA-GFP uapA∆ uapC∆:: pyrG^{Af} azgA∆ pabaA1	(Pantazopoulou *et al.*, 2007)
alcA$_p$-uapA-GFP uapA∆ uapC∆:: pyrG^{Af} azgA∆ pabaA1	(Gournas *et al.*, 2010)
uapA-mrfp azgA-gfp uapA∆ uapC∆:: pyrG^{Af} azgA∆ pabaA1	this study
azgA-gfp uapA∆ uapC∆:: pyrG^{Af} azgA∆ pabaA1	(Pantazopoulou *et al.*, 2007)
prn397::prnB-gfp-trpCC-term prnC pabaA1 argB2 yA2	(Tavoularis *et al.*, 2001)
furD-GFP uapA∆ uapC∆:: pyrG^{Af} azgA∆ furD∆::riboB cntA∆:riboB nkuA∆::argB pantoB100 pantoB	Borbolis and Diallinas, unpublished
argB2::argBBglII gpdA$_p$-gfp-(PHdomainPLC∆1)2 pabaA1 yA2	(Pantazopoulou and Peñalva, 2009)
ssoA::[ssoAp-gfp-ssoA]-pyrG^{Af} nkuA∆::bar pyroA4	(Taheri-Talesh *et al.*, 2008)
slaB-gfp-pyrG^{Af} argB2 nkuA∆::argB pyroA4	(Araujo-Bazán *et al.*, 2008)
slaB-gfp-pyrG^{Af} uapA-mrfp nkuA∆::argB pabaA1	this study
abpA-mrfp-pyrG^{Af} pabaA1 yA2	(Araujo-Bazán *et al.*, 2008)
alcA$_p$-K572R-gfp uapA∆ uapC∆:: pyrG^{Af} azgA∆ pabaA1	(Gournas *et al.*, 2010)
yA:: pyro^{Af} tpmA$_p$-gfp-tpmA pyrG^{Af} -mcherry-synA nku∆::argB nicA2 fwA1	(Taheri-Talesh *et al.*, 2008)
Saccharomyces cerevisiae	
BY4742 MATa his3∆1 leu2∆0 lys∆0 ura3∆0 / URA3 GAL-FUR4-GFP	(Dupré and Haguenauer-Tsapis, 2003)
MATa ura3-52 JEN1-GFP	(Paiva *et al.*, 2009)

Table 2.2. List of strains used in chapter 4

Strain Genotype	References
pabaA1	wild-type reference strain
TNO2A7: nkuAΔ::argB pyrG89 pyroA4 riboB2	(Nayak *et al.*, 2006)
uapAΔ uapCΔ::pyrG^{Af} azgAΔ argB2 pabaA1	(Pantazopoulou *et al.*, 2007)
uapAΔ::uapA-gfp uapCΔ:: pyrG^{Af} azgAΔ pabaA1 riboB2	this study
alcA$_p$-uapA-gfp uapAΔ uapCΔ:: pyrG^{Af} pabaA1	(Gournas *et al.*, 2010)
alcA$_p$-uapA-gfp uapAΔ uapCΔ:: pyrG^{Af} pabaA1 riboB2	this study
prnB-gfp argB2 pabaA1 yA2	(Tavoularis *et al.*, 2001)
agtA-gfp:: pyrG^{Af} pyroA4	(Apostolaki *et al.*, 2009)
azgA-gfp uapAΔ uapCΔ:: pyrG^{Af} azgAΔ pabaA1	this study
artAΔ:: riboB^{Af} nkuAΔ::argB pyrG89 pyroA4 riboB2	this study
artBΔ:: pyrG^{Af} nkuAΔ::argB riboB2 pyroA4 pyrG89	this study
artCΔ:: riboB^{Af} nkuAΔ::argB pyrG89 pyroA4 riboB2	this study
artDΔ:: riboB^{Af} nkuAΔ::argB pyrG89 pyroA4 riboB2	this study
artEΔ:: riboB^{Af} nkuAΔ::argB pyrG89 pyroA4 riboB2	this study
artFΔ:: riboB^{Af} nkuAΔ::argB pyrG89 pyroA4 riboB2	this study
artGΔ:: riboB^{Af} nkuAΔ::argB pyrG89 pyroA4 riboB2	this study
apyAΔ:: riboB^{Af} nkuAΔ::argB pyrG89 pyroA4 riboB2	this study
creD34 riboB2	(Boase and Kelly, 2004)
creDΔ:: pyrG^{Af} nkuAΔ::argB pyrG89 pyroA4	this study
palFΔ:: pyroA^{Af} inoB2 (pyroA4?)	Munera-Huertas T., Tilburn J., Arst, H., unpublished
sagAΔ:: riboB^{Af} nkuAΔ::argB pyrG89 pyroA4 riboB2	this study
sagAΔ:: riboB^{Af} uapAΔ uapCΔ:: pyrG^{Af} nkuAΔ::argB (pyrG89?) (riboB2?) pabaA1	this study
prnBΔ::prnB-gfp artAΔ:: riboB^{Af} nkuAΔ::argB pabaA1 (pyrG89?) (riboB2?) (argB2?) yA2	this study
agtAΔ::agtA-gfp:: pyrG^{Af} artAΔ:: riboB^{Af} (pyrG89?) (riboB2?) pabaA1 yA2	this study
azgA-gfp uapAΔ uapCΔ:: pyrG^{Af} azgAΔ pabaA1	this study
azgA-gfp artAΔ:: riboB^{Af} uapCΔ:: pyrG^{Af} azgAΔ (pyrG89?) (riboB2?) pabaA1	this study
azgA-gfp artAΔ:: riboB^{Af} uapAΔ uapCΔ:: pyrG^{Af} azgAΔ (pyrG89?) (riboB2?) pabaA1	this study
azgA$^{uapA-tail}$-gfp::argB argB2 uapAΔ uapCΔ:: pyrG^{Af} azgAΔ pabaA1	this study
azgA$^{uapA-tail}$-gfp::argB artAΔ:: riboB^{Af} (pyrG89?) (riboB2?) (argB2?) pabaA1	this study
uapAΔ::uapA-gfp artAΔ:: riboB^{Af} uapCΔ:: pyrG^{Af} nkuAΔ::argB (pyrG89?) (riboB2?) pabaA1	this study
uapAΔ::uapA-gfp artBΔ:: pyrG^{Af} uapCΔ:: pyrG^{Af} nkuAΔ::argB (pyrG89?) pabaA1	this study
uapAΔ::uapA-gfp artCΔ:: riboB^{Af} uapCΔ:: pyrG^{Af} (pyrG89?) (riboB2?) pabaA1	this study
uapAΔ::uapA-gfp artDΔ:: riboB^{Af} uapCΔ:: pyrG^{Af} (pyrG89?) (riboB2?) nkuAΔ	this study
uapAΔ::uapA-gfp artEΔ:: riboB^{Af} uapCΔ:: pyrG^{Af} nkuAΔ::argB (pyrG89?) (riboB2?) nkuAΔ	this study
uapAΔ::uapA-gfp artFΔ:: riboB^{Af} uapCΔ:: pyrG^{Af} (pyrG89?) (riboB2?) pabaA1 nkuAΔ	this study
uapAΔ::uapA-gfp artGΔ:: riboB^{Af} uapCΔ:: pyrG^{Af} nkuAΔ::argB (pyrG89?) (riboB2?) nkuAΔ	this study
uapAΔ::uapA-gfp apyAΔ:: riboB^{Af} uapCΔ:: pyrG^{Af} (pyrG89?) (riboB2?) pabaA1	this study
uapAΔ::uapA-gfp creD34 uapCΔ:: pyrG^{Af} riboB2 pabaA1	this study
uapAΔ::uapA-gfp palFΔ:: pyroA^{Af} uapCΔ:: pyrG^{Af} (pyroA4?)	this study
alcA$_p$-uapA-gfp artAΔ:: riboB^{Af} uapAΔ uapCΔ:: pyrG^{Af} nkuAΔ::argB (pyrG89?) (riboB2?) pabaA1	this study
alcA$_p$-uapA-gfp sagAΔ:: riboB^{Af} uapAΔ uapCΔ:: pyrG^{Af} nkuAΔ::argB (pyrG89?) (riboB2?) pabaA1	this study
sagAΔ::gpdA$_p$^{mini}:sagA-gfp:: pyrG^{Af} nkuAΔ::argB pyrG89 pyroA4 riboB2	this study
sagAΔ::sagA-gfp:: pyrG^{Af} nkuAΔ::argB pyrG89 pyroA4 riboB2	this study
alcA$_p$-uapA-gfp nkuAΔ::argB ArtAΔ:: riboB^{Af} nkuAΔ::argB pyrG89 pyroA4 riboB2	this study
alcA$_p$-uapA-gfp nkuAΔ::argB ArtAΔ::ArtA-P435A/V436A/Y437A::pyrG89 nkuAΔ::argB pyroA4 riboB2	this study
alcA$_p$-uapA-gfp nkuAΔ::argB ArtAΔ::ArtA-P445A/G446A/Y447A::pyrG89 nkuAΔ::argB pyroA4 riboB2	this study
alcA$_p$-uapA-gfp nkuAΔ::argB ArtAΔ::ArtA-P435A/V436A/Y437A/P445A/G446A/Y447A::pyrG89 nkuAΔ::argB pyroA4 riboB2	this study
alcA$_p$-uapA-gfp nkuAΔ::argB ArtAΔ::ArtA-K343R::pyrG89 nkuAΔ::argB pyroA4 riboB2	this study
uapA-K572R-gfp::argB uapAΔ azgAΔ uapCΔ:: pyrG^{Af} pabaA1	(Gournas *et al.*, 2010)
uapA-Δ547-571-gfp uapAΔ azgAΔ uapCΔ:: pyrG^{Af} pabaA1	this study

Strain Genotype	References
uapA-Δ564-571-gfp uapAΔ azgAΔ uapCΔ:: pyrG^Af pabaA1	this study
uapA-E545A/V546A/E547A-gfp uapAΔ azgAΔ uapCΔ:: pyrG^Af pabaA1	this study
alcA_p-uapA-E545A/V546A/E547A-gfp uapAΔ azgAΔ uapCΔ:: pyrG^Af pabaA1	this study
uapA-artAPY-gfp uapAΔ azgAΔ uapCΔ:: pyrG^Af pabaA1	this study
uapA-artA-P435A/V436A/Y437A/P445A/G446A/Y447A-gfp uapAΔ azgAΔ uapCΔ:: pyrG^Af pabaA1	this study
uapA-artAPY-gfp hulA::pyr4-hulAΔC2 uapAΔ azgAΔ uapCΔ:: pyrG^Af argB2 pyroA4	this study
hulA::pyr4-hulAΔC2 uapAΔ uapCΔ:: pyrG^Af azgAΔ pyroA4 argB2	(Gournas *et al.*, 2010)

Table 2.3. List of strains used in chapter 5

Strain Genotype	References
pabaA1	wild-type reference strain
uapA-K572R-gfp::argB uapAΔ azgAΔ uapCΔ:: pyrG^Af pabaA1	(Gournas *et al.*, 2010)
uapA100 pabaA1 pyroA4	(Ravagnani *et al.*, 1997)
uapAΔ azgAΔ uapCΔ:: pyrG^Af pantoB100	C. Gournas & G. Diallinas, unpublished
uapA100 uapCΔ? azgAΔ pyroA4	this study
uapA-K572R-gfp uapA100 uapCΔ? azgAΔ	this study
alcA_p-uapA-His uapAΔ uapCΔ:: pyrG^Af azgAΔ pabaA1	(Lemuh *et al.*, 2009)
alcA_p-uapA-GFP uapAΔ uapCΔ:: pyrG^Af azgAΔ pabaA1	(Gournas *et al.*, 2010)
alcA_p-uapA-GFP uapAΔ uapCΔ:: pyrG^Af azgAΔ pantoB100	this study
alcA_p-uapA-His alcA_p-uapA-GFP uapAΔ uapCΔ:: pyrG^Af azgAΔ	this study
uapAΔ uapCΔ:: pyrG^Af azgAΔ argB2 pabaA1	(Pantazopoulou *et al.*, 2007)
uapA-yfpN uapAΔ uapCΔ:: pyrG^Af azgAΔ pabaA1	this study
uapA-yfpC uapAΔ uapCΔ:: pyrG^Af azgAΔ pabaA1	this study
uapA-yfpC uapA-yfpN uapAΔ uapCΔ:: pyrG^Af azgAΔ pabaA1	this study
uapAΔ uapCΔ:: pyrG^Af azgAΔ pabaA1	(Pantazopoulou *et al.*, 2007)
alcA_p-uapA-yfpN uapAΔ uapCΔ:: pyrG^Af azgAΔ pabaA1	this study
alcA_p-uapA-yfpC alcA-uapA-yfpN uapAΔ uapCΔ:: pyrG^Af azgAΔ	this study
uapA-GFP uapAΔ uapCΔ:: pyrG^Af azgAΔ pabaA1	(Pantazopoulou *et al.*, 2007)
uapAΔ::uapA-GFP uapCΔ:: pyrG^Af pabaA1 pantoB100	C. Gournas & G. Diallinas unpublished
uapAΔ uapCΔ:: pyrG^Af azgAΔ pabaA1 argB2 riboB2	(Pantazopoulou *et al.*, 2007)
uapAΔ::uapA-GFP uapCΔ:: pyrG^Af azgAΔ pabaA1 argB2 pantoB100	this study
uapAΔ::uapA-GFP alcA_p-uapAN409D uapCΔ:: pyrG^Af azgAΔ pabaA1 pantoB100	this study
uapA-D44A/Y45A/D46A/Y47A-GFP uapAΔ uapCΔ:: pyrG^Af azgAΔ pabaA1	Amillis & Diallinas, unpublished
alcA_p-uapA-D44A/Y45A/D46A/Y47A-yfpC alcA-uapA-D44A/Y45A/D46A/Y47A-yfpN uapAΔ uapCΔ:: pyrG^Af azgAΔ	this study
alcA_p-uapA-D44A/Y45A/D46A/Y47A-yfpC alcA-uapA-yfpN uapAΔ uapCΔ:: pyrG^Af azgAΔ	this study
uapA-I74D-GFP uapAΔ uapCΔ:: pyrG^Af azgAΔ pabaA1	(Amillis *et al.*, 2011)
alcA_p-uapA-I74D-yfpC alcA-uapA-I74D-yfpN uapAΔ uapCΔ:: pyrG^Af azgAΔ	this study
alcA_p-uapA-I74D-yfpC alcA-uapA-yfpN uapAΔ uapCΔ:: pyrG^Af azgAΔ	this study
uapA-TMS14Δ-GFP uapAΔ uapCΔ:: pyrG^Af azgAΔ pabaA1	(Vlanti *et al.*, 2006)
alcA_p-uapA-TMS14Δ-yfpC alcA-uapA-I74D-yfpN uapAΔ uapCΔ:: pyrG^Af azgAΔ	this study
alcA_p-uapA-TMS14Δ-yfpC alcA-uapA-yfpN uapAΔ uapCΔ:: pyrG^Af azgAΔ	this study
alcA_p-uapA-D44A/Y45A/D46A/Y47A-GFP uapAΔ uapCΔ:: pyrG^Af azgAΔ	this study
alcA_p-uapA-D44A/Y45A/D46A/Y47A-His alcA_p-uapA-D44A/Y45A/D46A/Y47A-GFP uapAΔ uapCΔ:: pyrG^Af azgAΔ	this study
alcA_p-uapA-His alcA_p-uapA-D44A/Y45A/D46A/Y47A-GFP uapAΔ uapCΔ:: pyrG^Af azgAΔ	this study
uapA-G301A/G305A/G313A-GFP uapAΔ uapCΔ:: pyrG^Af azgAΔ pabaA1	V. Yalelis, S. Amillis & G. Diallinas, unpublished
alcA_p-uapA-G301A/G305A/G313A-His alcA_p-uapA-G301A/G305A/G313A-GFP uapAΔ uapCΔ:: pyrG^Af azgAΔ	this study
alcA_p-uapA-His alcA_p-uapA-G301A/G305A/G313A-GFP uapAΔ uapCΔ:: pyrG^Af azgAΔ	this study
alcA_p-uapA-D44A/Y45A/D46A/Y47A-His alcA_p-uapA-G301A/G305A/G313A-GFP uapAΔ uapCΔ:: pyrG^Af azgAΔ	this study
alcA_p-uapA-G301A/G305A/G313A-His alcA_p-uapA-D44A/Y45A/D46A/Y47A-GFP uapAΔ uapCΔ:: pyrG^Af azgAΔ	this study

2.1.2 Culture media and growth conditions

Two different types of media were used for the growth of fungal cultures, the complete medium and the minimal medium. The complete medium was enriched to contain all the elements required for fungal growth, thus enabling all strains to grow normally, independently of their auxotrophies. Minimal medium contained the minimum nutrients possible for fungal growth. As a result, it was always combined with the appropriate nutritional supplements, according to the auxotrophic requirements of each strain, and a nitrogen source, according to the desired conditions. Supplements and nitrogen sources were used at 1:100 or 1:10 dilutions of the stock solution. Growth media were used in liquid or solid form, according to the purpose of the culture. For a solid growth medium, 1-2% agar was added to the liquid medium, before autoclaving. Media and chemical reagents were obtained from Sigma-Aldrich, BD, Oxoid or AppliChem.

Aspergillus nidulans

Table 2.4. Culture media for the growth of *A. nidulans*

	Complete medium (CM)	Minimal medium (MM)	Sucrose medium (SM)
Salt solution	20 mL	20 mL	20 mL
Vitamin solution	10 mL	–	
D-Glucose	10 g	10 g	10 g
Casamino acids	1 g	–	–
Bactopeptone	2 g	–	–
Yeast extract	1 g	–	–
Sucrose	–	–	342,4 g
H_2O_{dist}	up to 1 L	up to 1 L	up to 1 L

Table 2.5. Solutions used in *A. nidulans* culture media

Salt solution		Vitamin solution		Trace Elements in 1 L H_2O	
KCl	26 g	p-aminobenzoic acid	20 mg	$N\alpha_2B_4O_7$ x 10 H_2O	40 mg
$MgSO_4$ $7H_2O$	26 g	D-pantothenic acid	50 mg	$CuSO_4$ x 5 H_2O	400 mg
KH_2PO_4	76 g	pyridoxine	50 mg	FeO_4P x 4 H_2O	714 mg
Trace elements	50 mL	riboflavin	50 mg	$MnSO_4$ x 1 H_2O	728 mg
Chloroform	2 mL	biotine	1 mg	Na_2MoO_4 x 2 H_2O	800 mg
H_2O_{dist}	up to 1 L	H_2O_{dist}	up to 1 L	$ZnSO_4$ x 7 H_2O	8 mg

The pH was adjusted to 6.8 with the use of NaOH 3N. Nitrogen sources were used at the final concentrations: urea 5 mM, $NaNO_3$ 10 mM, Ammonium L-(+)-tartrate 10 mM. Purines were used at 0.1 mg/mL. Amino acids were used at 5 mM. 8-Aza-guanine was used at 0.2-0.4 mM in the presence of $NaNO_3$ as sole nitrogen source. Allopurinol was used at 1-3 µM with hypoxanthine as sole nitrogen source. Acryflavine was used in CM at 0.0005-0.001% (w/v). Neomycin sulfate was used at 2 mg/mL. Uracil and uridine were used at 5 mM and 10 mM respectively.

A. nidulans cultures were inoculated with conidiospores harvested from sporulating culture plates with the use of sterile toothpicks or an inoculation loop. Solid cultures were incubated in 37°C or 25°C for 2-5 days and liquid cultures were incubated at 37°C or 25°C, 150 rpm. The duration of the incubation varied with the purpose of the culture. Derepression of proteins expressed under the control of the strong ethanol-inducible, glucose-repressible alcohol dehydrogenase (*alcA*) promoter was achieved with the use of 0.1% (w/v) fructose as a sole carbon source, while their induction was achieved by addition of 0.4% (v/v) ethanol in derepressing media (see also 2.3.1 and 2.9.1).

Saccharomyces cerevisiae

Table 2.6. Culture media for the growth of *S. cerevisiae*

	Complete medium (YPG)	Minimal media (MM)
D-Glucose	2 g	2 g
Bactopeptone	2 g	–
Yeast extract	1 g	–
H_2O_{dist}	up to 100 mL	up to 100 mL

Table 2.7. Stock solutions of the supplements used for *S. cerevisiae* mutant strains.

Supplement / Nitrogen source	Stock solution (in 50mL H_2O)	Dilution used
YNB w/o amino acids & NH_4^+	0.85 g	1:10
YNB w/o amino acids	3.35 g	1:10
Histidine	100 mg	1:100
Leucine	300 mg	1:100
Lysine	250 mg	1:100
Uracil	112 mg	1:100
Urea	1.5 g	1:100

Yeast minimal media were supplemented with yeast nitrogen base (YNB). Nitrogen source was either included in YNB (NH_4^+) or added separately (urea).Solid cultures were usually inoculated with cells harvested from culture plates with the use of an inoculation loop. The cells were streaked on the appropriate solid medium and the cultures were incubated for 2-3 days at 30°C. In the case of liquid cultures, an aliquot of saturated liquid culture or cells harvested from a single colony of a culture plate were mixed in a test tube with 5 mL of the appropriate liquid medium. Liquid cultures were incubated at 30°C, 220 rpm. The duration of the incubation varied with the purpose of the culture.

Escherichia coli

For the growth of bacterial cultures (strain DH5a) Luria-Bertani (LB) medium (Bacto Tryptone 10 g, NaCl 10 g, BactoYeast Extract 5 g for 1L) was used. The pH was adjusted to 7.0 with the use of NaOH 3N. For the selection of transformed colonies, ampicillin was added in 100 μg/mL concentration. Bacterial cultures were incubated overnight at 37 °C. Liquid cultures were additionally agitated at 200 rpm.

2.1.3 Storage conditions

Agar plates were stored at 4°C, where fungi could be preserved, without a serious loss of viability, for some weeks. For long-term storage, glycerol stocks were prepared. *A. nidulans* conidiospores from a fresh CM plate were harvested in 500μL PBS buffer (NaCl 8 g, KCl 0,2 g, Na_2PO_4 1,44 g, KH_2PO_4 0,24 g, pH 7.4 with 1 N HCl) in a sterile eppendorf tube and 500 µl of glycerol was added. For *S. cerevisiae*, an aliquot (950 μL) of a fresh liquid culture was transferred in sterile eppendorf tubes and mixed with 400 μL of 100% glycerol. For *E.coli*, an aliquot (500 μL) of a fresh liquid culture was transferred in sterile eppendorf tubes and mixed with 500 μL of 100% glycerol. In all cases, the eppendorf tubes were mixed well and stored for long periods at -80°C.

For reviving stored cultures, an aliquot of the stock was streaked on appropriate media. A single colony was selected and was analyzed with growth tests (see 2.2), to verify that it carried the auxotrophies described in the genotype and no contamination had occurred.

2.2   Genetic crosses and progeny analysis

Meiotic crossing is used for the construction of multiple mutant strains for genetic analysis (Todd *et al.*, 2007). *A. nidulans* is homothallic, meaning that it is self-fertile, but crosses can be initiated by hyphal fusions between homokaryons with genetically different nuclei. The resulting heterokaryons are not stable, but can be forced to maintain a balanced ratio of the component nuclei by including complementing auxotrophic mutations in the parental nuclei and forcing growth without the corresponding supplements (Casselton and Zolan, 2002). The result of a karyogamic event is the formation of cleistothecia. In order to obtain strains on a desired genetic background, the following experimental procedure was performed.

2.2.1 Preparation of a genetic cross

Petri dishes containing minimal media with the appropriate supplements were inoculated with spores from two different parental strains, in pairs, with a distance of 0.5, 1.5 and 2.5 cm between them. The cultures were incubated for 2 days at 37°C. Small parts of media in the contact area of the mycelia of the two strains were removed with a sterile scalpel and transferred in small Petri dishes, containing minimal media with nitrate, as nitrogen source, and only the supplements required from both parental strains. Therefore, only heterokaryons were able to produce the missing supplements and grow on the plates. The plates were incubated for 1-2 days at 37°C and were subsequently sealed with adhesive tape and incubated for further 14-20 days at 37°C. After that time, cleistothecia usually appeared.

2.2.2 Selection of cleistothecia

The plates were unsealed and single cleistothecia (usually 4) were selected with a sterile needle. Surrounding cells were removed by rolling the cleistothecia on an agar plate. Finally, each cleistothecium was burst open by mechanical forces and the ascospores were released in an eppendorf tube containing 1 mL of sterile H_2O_{dist}. An aliquot (~10μL) of each ascospore suspension was plated on minimal media selecting against both parental types and was incubated for two days at 37°C, so that only recombinant progeny would grow. Different dilutions of the suspension from one recombinant cleistothecium were plated in order to obtain single colonies. Single colonies were, then, selected and analyzed for their genetic background.

2.2.3 Progeny analysis

Growth tests in *A. nidulans* genetics are performed in order to characterize unknown strains, by comparing their growth with that of well-studied control strains, under different conditions (temperature, pH, nitrogen or carbon sources, supplements, toxic analogues and antibiotics). Replica plates with the appropriate media were used in the pursuit of distinct phenotypes. When analyzing the nutritional profile of the progeny, the so-called dropout plates contained minimal medium with all the auxotrophies supplemented except one. In other cases, replica plates contained minimal medium with all the auxotrophies supplemented but with a different nitrogen source or toxic analogue in the medium of each plate. Growth tests gave some evidence on the genotype of the studied strains, but further genetic analysis was, usually, required for their complete genetic characterization. For example, the presence of UapA transporter in the genetic background of a newly constructed strain could be determined by its growth on uric acid as a sole nitrogen source. However, the distinction between a wild-type UapA and a UapA-GFP strain required the use of fluorescence microscopy (see 2.3), while the detection of the presence or the absence of UapC transporter required the use of polymerase chain reaction (see 2.5.1).

2.3   Fluorescence microscopy

2.3.1 Sample preparation

Samples for fluorescence microscopy of *A. nidulans* strains were prepared as follows. Sterile cover slips (22 mm) were placed in small Petri dishes (35 mm) and 2 mL of minimal media 0.1% glucose pH 4.6, containing the appropriate supplements and urea or $NaNO_3$ as a nitrogen source, were added on top of them. Conidiospore solutions were prepared and an aliquot of 10 μL was pipetted in the middle of each cover slip and mixed well with the minimal media. The culture was then incubated at 25°C, for 12-17 h, protected from light, and when needed shifted to various conditions for 2–4 h. For the observation of proteins expressed under the control of the $alcA_p$ promoter mycelia were grown for 14-16 h in derepressing media (minimal media supplemented with urea or $NaNO_3$ and 0.1% (w/v) fructose as a sole carbon source; see also 2.1.2). Repression of expression was achieved in minimal media supplemented with urea or $NaNO_3$ and 1% (w/v) glucose. Induction of expression was achieved by addition of 0.4 % (v/v) ethanol in derepressing media, either for 2 h

or overnight. The cover slip with the mycelia was removed from the Petri dish with the use of a toothpick and was placed upside down on a microscope slide. Excess medium outside the cover slip was removed with filter paper.

In yeast, Jen1p-GFP expression was induced by 4 h growth in minimal media supplemented with 0.5% lactate and its endocytosis was elicited by 20-60 min incubation with 1% glucose (Paiva *et al.*, 2009). Fur4p-GFP expression was induced by 16 h growth in minimal media with 2% galactose (Leung *et al.*, 2010) and its endocytosis was induced by incubating with 40 µg/mL uracil for 2 h. Both strains were incubated protected from light, at 30°C, 220 rpm. Samples were then 10-fold concentrated (OD_{600} ~3-6) and 7 µL of each were mixed with an equal volume of Low Melting Agarose 1.2% on the surface of a glass slide and covered with a cover slip.

Staining with FM4-64 was according to Peñalva (2005). In particular, cover slips with germinated conidia were placed on top of plastic covers, covered with 0.1 mL of 10 mM FM4-64 in minimal media, incubated on ice for 15 min, washed with 2-3 mL minimal media, and transferred to fresh 2-3 mL medium for 0–30 min chase time. Staining with CMAC (7-amino-4-chloromethyl coumarin; Molecular Probes, Inc, USA) was according to Pantazopoulou *et al.* (2007). Cover slips with germinated conidia were placed on top of plastic covers, covered with 0.1 mL of 1/1000 dilution of CMAC (5 mg/ml stock solution), incubated at 25°C for 20 min, washed with 2-3 mL minimal media, and transferred to fresh 2-33 mL medium for 20 min. Staining with filipin was performed by addition of 0.1 mL minimal media supplemented with 25 mg/mL filipin on cover slips with germinated conidia, on top of plastic covers, 15 min prior to observation. Calcofluor white staining, used for detecting the presence and deposition of polysaccharides (chitin and b-1,3-glucan) in the cell walls of yeast and mycelial fungi, was performed according to Slaninová *et al.* (2000). Cells were stained for 5 min on coverslips with a solution of Calcofluor (0.001% (w/v) in relevant growth medium), washed and immediately observed in the fluorescence microscope. Lat-B was used as described in Taheri-Talesh *et al.* (2008), at a final concentration of 20-40 mg/mL (50-100 mM). The drug was added from a 10 mM stock in DMSO. For endocytosis, uric acid (0.1 mg/mL), NH_4Cl (10–50 mM) or ammonium L-(+)-tartrate (10-20 mM) were added for 1-4 h before observation. For hypertonic treatment, sucrose, NaCl or other agents were added as indicated in the relevant figures.

2.3.2 Microscopic observation and image processing

Samples were then observed on an Axioplan Zeiss phase-contrast epifluorescence microscope with appropriate filters and the resulting images were acquired with a Zeiss-MRC5 digital camera using the AxioVs40 V4.40.0 software. At CIB-CSIC (Madrid), an inverted Leica DMI6000B microscope with motorized z-focus and a Leica EL6000 external light source was used for epifluorescence excitation. The microscope was driven by Metamorph (Invitrogen, Carlsbad, CA, USA) software using a DMI6000-specific driver. Images were acquired using HCX _63 1.4 numerical aperture (NA) or _100 1.4 NA objectives and a Hamamatsu ORCA ER-II cooled-charge coupled device camera (Hamamatsu Photonics, Massy, France). The microscope was equipped with Semrock Brightline GFP-3035B and TXRED-4040B filter sets (Semrock, Rochester, NY, USA). Maximal intensity projections were obtained from z-stacks using the Metamorph 3D plugin. For Laser Confocal Microscopy at the Medical School of Universidade do Minho, an inverted FLUOVIEW confocal laser scanning microscope, version FV1000 Viewer (Ver.2.0b) was used (http://www.olympusfluoview.com/). A confocal laser DMR upright microscope and a wide-field time-lapse Olympus IX-81 Cell-R imaging system for Live Cell Imaging System were also used (http://www.pasteur.gr). The Confocal system operates with the Image acquisition and analysis Leica Confocal Software LCS.

Image processing, contrast adjustment and color combining were made using the Adobe Photoshop CS4 Extended version 11.0.2 software or the ImageJ software. Images were converted to 8-bit grayscale or RGB and annotated using Photoshop CS4 before being saved to TIFF. When indicated, images were deconvoluted using the blind deconvolution algorithms of ImageJ 1.37 (http://rsb.info.nih.gov/ij).

2.4   DNA manipulations

2.4.1 Preparation of genomic DNA from *A. nidulans*

CM culture plates were incubated for 4 days in 37°C. Conidiospores from 1/4 of a plate were harvested in 25 mL of minimal media containing NH_4^+ as a nitrogen source and any supplements required (depending on the auxotrophies carried by the strains used). Liquid cultures were incubated overnight at 37°C, 150 rpm. The next day the culture was filtered through blutex, squeezed between two papers to remove

excessive liquid and immediately frozen in liquid nitrogen. The mycelia were pulverized in a mortar with a pestle in the presence of liquid nitrogen and ~200 mg of the fine powder were transferred in a 2mL eppendorf tube. The mycelia powder was resuspended in 800 µL of DNA extraction buffer (Tris-HCl 0.2 M pH 8.0, Sodium Dodecyl Sulfate (SDS) 1%, Ethylenediaminetetraacetic acid (EDTA) 1mM pH 8) mixed by vortexing and incubated on ice for 5-20 min. 800µL of pure phenol were added and the mixture was shaken vigorously at room temperature (RT). The tube was then centrifuged for 5 min at 12000 rpm, RT and the upper phase, containing the DNA, was transferred to a new eppendorf tube. Equal volume of chloroform was added and the tube was shaken vigorously and centrifuged for 5 min at 12000 rpm, RT. The upper phase was recovered and transferred to a new 1.5 mL tube. The DNA was then precipitated by adding equal volume of isopropanol and 1/10 volume of 3 M sodium acetate (pH 5.3). The mixture was gently mixed (by inverting the tube several times) and was then centrifuged for 10 min at 12000 rpm, RT. The pellet was washed with 200 µL of 70% EtOH, without mixing. The EtOH was removed with a pipette, after spinning for 2 min. The pellet was dried for 5 min at 50°C and was finally dissolved in 100µl of sterile distilled water, containing 0.2 mg/mL RNaseA and incubated at 37°C for 30 min. Agarose gel electrophoresis was performed to an aliquot (2-3 µL) of the DNA solution, in order to analyse the quantity and quality of the extracted DNA.

2.4.2 Restriction Endonuclease Digestion

Restriction endonucleases bind and cleave DNA at specific target sequences. DNA was digested with restriction endonucleases to yield DNA fragments of convenient sizes for downstream manipulations. In particular, the appropriate amount of DNA was incubated with 1 u restriction enzyme, 1x restriction enzyme buffer and distilled water to a final volume of 20 µL at the enzyme's optimal temperature and for the time period specified by the manufacturer (TaKaRa, Fermentas, NEB). Digested DNA was then analysed by agarose gel electrophoresis.

2.4.3 Agarose gel electrophoresis

Agarose gel electrophoresis was used for the analysis of the size and conformation of DNA in a sample, quantification of DNA, and the separation and extraction of DNA fragments. 1% agarose was dissolved in 1x TAE buffer (Table 2.8) by warming up

the solution in the microwave. After cooling down to 70°C, 0.5 mg/mL ethidium bromide (EtBr) were added and the solution was poured into a casting tray and left to harden. DNA samples were mixed with loading buffer and were loaded in the gel. To determine the size of the fragments, a molecular weight marker was loaded along with the samples. Gels were run at 55-100V, depending on downstream applications. When adequate migration had occurred, the gel was exposed to UV light with a UV transilluminator and DNA bands were visualized and photographed due to the intercalating fluorescent dye (EtBr).

2.4.4 Southern Blot

Southern blot is used to detect specific sequences in a DNA sample. It combines agarose gel electrophoresis for size separation of DNA and transfer to a nitrocellulose membrane by capillary action for subsequent detection by probe hybridization. In this work, Southern blot was mainly performed to analyze *A. nidulans* transformants (see 2.7) in respect to the type of plasmid integration and the number of integrated copies. The method used is an adapted version of the one described in Sambrook and Russel (2001).

DNA digestion and gel preparation

Genomic DNA was isolated from *A. nidulans* transformants and 4-6 μg DNA of each were used to prepare a DNA digestion reaction in 50 μL total volume (for hybridization with 2 probes). To ensure complete digestion of DNA samples, the restriction enzyme was added in two steps; that is, overnight incubation with half the amount of enzyme, followed by addition of the other half and another 2 hours of incubation. DNA fragments were separated in 0.8% agarose gels (one for each probe) running at 55 V for 5-6 h in freshly made 1x TAE buffer (Table 2.8). A picture of the gels was captured with a ruler standing beside the marker, and the bottom right corner of the gels was cut off in a different fashion to mark them. The gels were exposed to UV radiation for 5 minutes to reduce the size of larger DNA fragments in order to facilitate their transfer at the nitrocellulose membrane, since fragments longer than 10 kb do not transfer efficiently. The DNA was denatured by submerging the gels in denaturation solution (Table 2.8) for 30 min with gentle shaking at RT. Gels were then submerged in neutralization solution (Table 2.8) and incubated for another 30 min with gentle shaking at RT.

Table 2.8. Solutions used in Southern blot analysis

Solutions	Composition for 1 L
TAE (50x)	242 g Tris Base, 57.1 mL glacial CH_3COOH, 100 mL 0.5 M EDTA pH 8.0
Denaturation	1.5 M NaCl, 0.5 M NaOH
Neutralization	1.5 M NaCl, 1 M Tris-HCl pH 8.0
20x SSC	3 M NaCl, 0.3 M $N\alpha_3C_6H_5O_7$, pH 7.0 with NaOH
Church buffer	0.5 M Na_2HPO_4 / NaH_2PO_4 pH 7.0, 1% BSA, 7% SDS, 1 mM EDTA

Blotting

The gel was placed on two sheets of filter paper (Whatman), the ends of which were dipped in a bath of 20x SSC solutions (Table 2.8). A sheet of Amersham Hybond-N$^+$ nitrocellulose membrane (Amersham Biosciences) was placed on top of the gel, followed by two sheets of filter paper and a stack of paper towels. Around the membrane and before placing the filter papers, some plastic foil was placed, in order to keep the transfer of the buffer within the limits of the membrane. Pressure was applied evenly by adding a weight on top of the paper towels and the blot was left overnight at RT. Transfer efficiency was improved by removing the wet paper towels and replacing them with dry ones at least once during the transfer.

The next day, the membrane was peeled off the gel and was exposed to UV radiation (upside down) for 5 min, to permanently and covalently crosslink the DNA to the membrane. When not required for use immediately, the blots were covered in plastic wrap and stored at 4°C.

Radioactive probe labelling

Probe labelling was done by random priming, according to the BRL Multiprime DNA Labelling Kit. In particular, the desired sequence was amplified by PCR (see 2.5.1) and 250 ng of the gel extracted (see 2.6.1) PCR product were adjusted with H_2O_{dist} to a final volume of 21 μL. The DNA was denatured by boiling for 2 min and was immediately put on ice. The rest of the components (Table 2.9) were added to the solution along with H_2O_{dist} to a final volume of 50 μL. The reaction was incubated at 37°C for 1 h and was then purified by passing through a column (Pharmacia) to remove unincorporated nucleotides. The resulting probe solution was boiled for 2 min and immediately added in prehybridization Church buffer. After hybridization, the radioactive probe could be stored at -20°C and used again after boiling for 10 min and cooling down for 2 min.

Table 2.9. Composition of random priming reaction for probe labelling

Components	Final concentration
DNA probe	250 ng
Random hexamers (Sigma)	10 ng
dATP (BRL)	10 µM
dGTP (BRL)	10 µM
dTTP (BRL)	10 µM
^{32}P-[^{a}dCTP]	0.05 mCi
Klenow DNA polymerase	5 u
10x Klenow buffer	5 µL
H_2O_{dist}	up to 50 µL

Hybridization and developing

The membrane was incubated in Church buffer (Table 2.8) for 2 h at 65°C. The pre-hybridization Church buffer was replaced by Church buffer with the labelled probe and the membrane was incubated overnight (15-18 h) at 65°C. After hybridization, the membranes were washed with 2x SSC, 0.1% SDS at 65°C for 30 min and the liquid was discarded. This washing step was repeated 2 times. The final washing step was done with 0.2x SSC, 0.1% SDS at 65°C for 30 min. The probed membranes were finally covered with plastic foil and were placed in an autoradiographic cassette along with an X-ray film (Kodak X-omat). The cassette was kept at -80°C for ~2 h, and then kept at RT to defreeze. The film was developed in a dark room with Kodak developing reagents.

2.5   Polymerase Chain Reaction (PCR)

2.5.1 Standard PCR reactions

Conventional PCR reactions were performed using KAPATaq DNA polymerase (Kapa Biosystems). Provided that the amplified fragment would be used for cloning or transformation, a DNA polymerase with proofreading activity was used in order to lower error frequency. High fidelity PCR reactions were carried out using the Phusion® Flash High-Fidelity PCR Master Mix (New England Biolabs GmbH, Frankfurt, Germany) or the KAPA HiFi HotStart ReadyMix (Kapa Biosystems), according to manufacturer's instructions. Components and conditions of these PCR reactions are described in the tables below.

Table 2.10. Composition of conventional, high fidelity and site-directed mutagenesis PCR reactions

Components	Final concentration		
	Conventional	*High fidelity*	*Mutagenesis*
10x Polymerase buffer (with 1.5 mM MgCl$_2$)	1x	-	1x
dNTPs	200 μM of each	-	200 μM from each
2x Polymerase Ready Mix	-	1x	-
Forward primer	0.4 μM	0.3 μM	0.4 μM
Reverse primer	0.4 μM	0.3 μM	0.4 μM
DNA Polymerase	KapaTaq 1 u	-	Pfu 1.25 u
DNA template	10-20 ng	10 ng	10 ng
H$_2$O$_{dist}$	up to 25 μL	up to 25 μL	up to 50 μL

Table 2.11. Conditions used for conventional, high fidelity and site-directed mutagenesis PCR

Steps	*Conventional*		*High fidelity*		*Mutagenesis*	
	°C	**Duration**	**°C**	**Duration**	**°C**	**Duration**
1	95	5 min	95	3 min	95	3 min
2	95	30 sec	98	20 sec	95	30 sec
3	T_m-5	30 sec	60-75	15 sec	T_m-5	30 sec
4	72	1 min/kb	72	15 sec/kb	72	2 min/kb
5	*steps 2-4*	x25 cycles	*steps 2-4*	x25 cycles	*steps 2-4*	x25 cycles
6	72	10 min	72	1 min/kb	72	10 min
7	12	∞	12	∞	12	∞

2.5.2 *In vitro* site-directed mutagenesis

Mutations were constructed by site-directed mutagenesis according to the instructions accompanying the QuikChange® Site-Directed Mutagenesis Kit (Agilent Technologies, Stratagene). In particular, a pair of complimentary primers was designed for each mutation. Primers intended for mutagenesis were long (35-40 amino acids), with >50% GC-content and the mutation was located in the middle of the sequence, so that annealing to the complementary sequence of the template DNA would not be severely affected by the mismatch. Taking advantage of the redundancy of the genetic code, codon substitutions were designed in a way that the least possible number of mismatches would occur, while resulting codons would be frequently encountered in *A. nidulans* genome. Moreover, designed mutations preferably led to the introduction of a restriction site that would enable diagnostic digestion after mutagenesis (see later on). High fidelity PCR reactions for *in vitro*

site-directed mutagenesis were carried out using the Pfu DNA Polymerase (Thermo Scientific). Components and conditions used for this type of PCR are described in tables above. The following formula was used for estimating the T_m of the primers: $T_m=69,3+0,41(\%GC)-650/L-(\%mismatch)$.

After amplification the PCR product was incubated at 37°C for 2 h with 10 u (1 μL) of the restriction enzyme *Dpn*I (TaKaRa), which cleaves methylated (GA^m | TC) DNA strands, so that parental non-mutated plasmids were fragmented. The resulting solution was used to transform *E. coli* competent cells. Plasmid DNA from ampicillin-resistant colonies was prepared, digested with the appropriate restriction enzyme and/or sequenced. Plasmids with the desired mutation were finally transformed in *A. nidulans* (for more details see also sections 2.6 and 2.7).

2.6   Molecular cloning

This experimental procedure includes the cleavage of circular plasmid DNA with one or more restriction enzymes, its ligation *in vitro* to foreign DNA bearing compatible termini, transformation of *E. coli* with the products of the ligation reaction and screening of the transformed colonies for those carrying the desired DNA sequences. This method takes advantage of the fact that a single bacterial cell can be induced to take up and replicate a single recombinant DNA molecule (Sambrook and Russel, 2001).

2.6.1 Preparation of cloning vector and insert

The first step towards the generation of a recombinant DNA molecule was the preparation of the cloning vector and the DNA fragment of interest (hereafter referred to as "insert"). In particular, the insert was amplified by PCR using primers that add the desired restriction sites to its termini and was subsequently digested with the corresponding restriction endonucleases. A cloning vector that contains recognition sequences for the same restriction enzymes in its multiple cloning site was selected and subjected to digestion in order to generate sticky ends complementary to those of the digested insert (Sambrook and Russel, 2001). The digested vector and insert were purified from an agarose gel after migrating for an adequate amount of time using the Nucleospin Extract II kit (Macherey-Nagel). The corresponding DNA bands were quickly excised from the gel under low-strength UV

light exposure to limit DNA damage, transferred into an eppendorf tube and processed as described in the manufacturer's instructions.

In cases where the termini of the resulting linearized plasmid were complementary (e.g. when cloning with one restriction enzyme), the digested vector was treated with 30 u (1 μL) of calf intestine alkaline phosphatase (TaKaRa) for 5 min at 37 ^{o}C, before being loaded to the agarose gel. Removal of the 5'-terminal phosphate groups suppressed self-ligation of the linearized vector and improved ligation efficiency by diminishing the background of transformed bacterial colonies that carry "empty" vectors (Sambrook and Russel, 2001).

2.6.2 Generation of recombinant DNA

Generation of recombinant DNA was mediated by DNA ligase, an enzyme that covalently links the complementary sticky ends together. The purified vector and insert were mixed at a 1:3 concentration ratio and an aliquot of the mixture was used to prepare a ligation reaction along with 175 u (0.5 μL) of T4 DNA ligase (TaKaRa) and 1x ligase buffer in 10 μL total volume. The reaction was incubated at 25°C for 1.5 h and was then used to transform competent *E.coli* cells. A control ligation without an insert was also performed in parallel.

2.6.3 Introduction of recombinant DNA into *E. coli*

Preparation of competent cells

A trace of DH5a *E. coli* cells from the glycerol stock was streaked on an LB agar plate and was incubated at 37°C overnight. 5 mL LB medium were inoculated with a single colony from the plate and were incubated for 16 h at 37°C, 220 rpm. An aliquot of 0.5 mL of the saturated overnight culture was used to inoculate 400 mL LB medium in a 1 L flask and was incubated at 37°C, 260 rpm until an OD_{600} of 0.45-0.55 had been reached. The culture was then centrifuged at low speed (4.500 g), 4°C for 5 min and the supernatant was discarded. The cell pellet was gently resuspended in 0.4x original volume of ice-cold transformation buffer 1 (30 mM CH_3COOK, 10 mM $CaCl_2$, 50 mM $MnCl_2$,100 mM $RbCl_2$, 15% glycerol, pH 5,8 with 1 M CH_3COOH) and incubated on ice for an additional 5 min. The cells were collected by centrifugation at 4500 g for 5 min at 4°C, and were resuspended carefully in 1/25 original volume of ice-cold transformation buffer 2 (10 mM MOPS pH 6.5, 75 mM $CaCl_2$, 10 mM $RBCl_2$, 15% glycerol, pH 6.5 with 1 M KOH). The

cells were again incubated on ice for 15-60 min and aliquots of 200 μL were distributed in sterile eppendorf tubes and frozen in liquid nitrogen. The competent cells were then stored at -80°C.

E. coli transformation

About 0.01-0.5 μg of plasmid DNA was added in 200 μL of defrosted competent *E. coli* cells, mixed and incubated on ice for 20-45 min. The cells were subjected to heat shock by incubating the tube in a heat block at 42°C for 90 sec and moving the tube immediately on ice for 2 min. To allow expression of the ampicillin resistance gene of the plasmid, 1 ml of LB medium was added and the cells were incubated at 37°C for 45-60 min. The cells were harvested by centrifugation at 8000 rpm for 2 min. They were then resuspended in ~100 μL of LB medium and spread on LB agar plates containing ampicillin at a final concentration of 100 μg/mL. The plate was incubated overnight at 37°C. To check the transformation efficiency, competent cells were transformed with 1 ng of a control plasmid containing the ampicillin resistance gene and were plated on an LB ampicillin agar plate. The transformation efficiency could be estimated by comparing the number of colonies obtained with the control plasmid to the number obtained with the plasmid of interest (Positive control). A negative control to check antibiotic activity was performed by transforming competent cells with 2 μL of sterile water and plating them on an LB ampicillin agar plate. An absence of colonies on the plate indicated good antibiotic activity (Sambrook and Russel, 2001).

2.6.4 Preparation of Plasmid DNA from *E. coli*

For high purity plasmid DNA preparation the Macherey-Nagel Nucleospin Plasmid kit was used. For downstream applications that did not require high purity, an adaptation of the protocol described in Sambrook and Russel (2001) was used. In particular, 5 mL of LB medium with ampicillin were inoculated with a single bacterial colony carrying the desired plasmid and were incubated overnight at 37°C, 200 rpm.1-1.5 ml of the bacterial culture was centrifuged at 12000 rpm for 1 min and the pellet was resuspended in 200 μL of cell suspension buffer (50 mM Tris-HCl pH 8.0, 10 mM EDTA) by vortexing for about 1 min. 200 μL of cell lysis solution (200 mM NaOH, 1% SDS) were then added and mixed by inverting the tube, followed by 200 μL of neutralization buffer (3 M CH_3COONa pH 5.5). The cell suspension was

centrifuged at 12000 rpm for 5 min and the supernatant was collected in a new eppendorf tube. 500 μL of isopropanol were added and the content of the eppendorf was mixed and centrifuged at 12000 rpm for 5 minutes to precipitate the DNA. The DNA was washed with 70% (v/v) ethanol to remove co-precipitated salt and to replace the isopropanol with the more volatile ethanol, thus making the DNA easier to redissolve. The pellet was dried for 5 min at 50°C and was resuspended in 100 μL of sterile distilled water with 0.2 mg/mL RNase. An aliquot was used for diagnostic digestions or PCR that would confirm the successful cloning of the desired DNA sequence, as well as the orientation of insertion.

2.7 *Aspergillus nidulans* DNA Transformation

A. nidulans DNA Transformation was performed as described in Koukaki *et al.* (2003). In particular, conidiospores were harvested from a full CM culture plate and filtered through blutex. 200 mL minimal media (in a 1 L flask) with urea and appropriate supplements were inoculated with the spore solution and were incubated at 37°C for 4-4.5 h, 150 rpm. After 3.5 h of incubation an aliquot of the culture was regularly observed under the microscope for the appearance of germ tubes. Once the conidia were at the germinative phase, incubation was stopped and the culture was transferred into sterile falcons and centrifuged at 4000 rpm for 10 min. The pellet was resuspended in 20 mL of Solution I (Table 2.12) and was poured into a sterile 250 mL flask. About 200 mg of the lytic enzyme glucanex, together with a few crystals of Bovine Serum Albumin (BSA) were then added for the disruption of the cell wall and release of the protoplasts. The spore suspension was incubated for 5 min on ice, and then for 1.5-2 h at 30°C, 60 rpm. Protoplasts were concentrated by centrifugation at 4000 rpm for 10 min and washed with 10 mL of solution II (Table 2.12). The pellet (protoplasts) was resuspended in solution II, at a volume depending on the number of transformations desired. Protoplasts were distributed in eppendorf tubes and plasmid DNA was added (1.5-2 μg) followed by 1/4 of the total volume Solution III (Table 2.12). A control tube without plasmid DNA was included in order to evaluate whether the protoplasts and the solutions used were free of contaminations. Tubes were incubated on ice for 15 min, after which 500 μL of Solution III were added, mixed and incubated for another 15 min at RT. The tubes were then centrifuged at 6000 rpm for 10 min and protoplasts were washed with 1 mL of solution II and resuspended in 200 μL of the latter. Protoplasts were

transferred into falcons containing 4 mL of melted Top SM (sucrose minimal media, 0.35% agar; see Table 2.4), carefully mixed and quickly used to inoculate previously prepared SM plates (sucrose minimal media, 1% agar; see Table 2.4). Plates were incubated at 37°C for 4-5 days and transformants were isolated by streaking on minimal media and analyzed by growth tests.

Table 2.12. Solutions used for *A. nidulans* DNA transformation

Solutions	Composition in H_2O_{dist}
Solution I	1.2 M $MgSO_4$, 10 mM orthophosphate pH 5.8
Solution II	1 M Sorbitol, 10 mM Tris-HCl pH 7.5, 10 mM $CaCl_2$
Solution III	60% (w/v) PEG6000, 10 mM Tris-HCl pH 7.5, 10 mM $CaCl_2$

Newly made null mutant strains and *in locus* gene tagging were constructed by transformation in an *nkuA* DNA helicase deficient strain (TNO2A7; Nayak *et al.*, 2006), allowing only homologous recombination events, based on the *A. fumigatus* markers orotidine-5′-phosphate-decarboxylase (*pyrG^{Af}*, Afu2g0836) or GTP-cyclohydrolase II (*riboB^{Af}*, Afu1g13300), resulting in complementation of auxotrophies for uracil/uridine (*pyrG89*) or riboflavin (*riboB2*), respectively. Mutants of *uapA-gfp, uapA-YFP* and *uapA-His* were constructed by transformation of a strain lacking all major purine transporters *uapA*, *uapC* and *azgA* (ΔACZ) based on the *A. nidulans* markers ornithine-carbamoyltransferase (ANID_04409.3) and para-aminobenzoic acid synthase (ANID_06550), complementing the arginine auxotrophic mutation *argB2* and paba auxotrophic mutation *pabaA1*, respectively.

2.8   Kinetic analysis of transporters

Kinetic analysis of UapA activity was measured by estimating uptake rates of [³H]-xanthine uptake, as previously described in Koukaki *et al.* (2005) and Papageorgiou *et al.* (2008). Briefly, conidiospores from a fresh CM plate were harvested in 25 mL of minimal media containing urea and any supplements necessary, filtered with blutex and incubated at 37°C, 150 rpm.

[³H]-xanthine uptake was assayed at 37°C in germinating conidiospores of *A. nidulans*, just prior of germ tube emergence (4 h) or in germlings (6 h). The culture was centrifuged for 5 min, 6000 rpm and conidiospores were concentrated at 10^7 conidiospores/100 μL. The resulting spore suspension was distributed in eppendorf tubes (75 μL in each tube) and these were equilibrated for 10 min at 37°C. Initial

velocities were measured at 1 min of incubation with 25 μL (0.2 μM) of radioactive substrate. Reactions were terminated by adding excess (1000-fold) of ice-cold non-radiolabelled substrate. To remove non-incorporated radioactivity the spore suspension was washed twice with ice cold minimal media (6000rpm, 5 min). The supernatant was removed by sunction and the pellet was finally resuspended in 1 mL of scintillation solution (666 ml toluol, 2.66 g PPO, 0.066 g POPOP, 333 ml Triton-X-100. The eppendorf tubes were inserted in scintillation vials and radioactivity was measured in a scintillation counter.

Initial velocities were corrected by subtracting background uptake values obtained in the simultaneous presence of 1000-fold excess of non-radiolabelled substrate. The background uptake level did not exceed 15-20% of the total counts obtained in wild-type strains. The K_m (concentration for obtaining $V_m/2$) of UapA for xanthine was obtained directly by performing and analyzing (Prism3) uptakes at various concentrations. All experiments were carried out in triplicates. Radiolabelled xanthine (33.4 Ci/mmol) was purchased from Moravek Biochemicals (Brea, CA, USA).

2.9 Protein manipulations

2.9.1 Protein extraction from *A. nidulans*

CM culture plates were incubated for 4 days in 37°C. Conidiospores from a full plate were harvested in 100 mL of minimal media containing $NaNO_3$ as a nitrogen source and any supplements required (depending on the auxotrophies carried by the strains used). Liquid cultures were incubated for 14-16 h at 25°C, 150 rpm. In the case of proteins expressed under the control of the strong ethanol-inducible, glucose-repressible $alcA_p$ promoter, mycelia were then filtered through a sterile blutex, washed with sterile washing buffer (1x salt solution, pH 6.8) and shifted in inducing minimal media for 2-6 h (see also 2.1.2). When repression of expression was required, mycelia were washed again with sterile washing buffer and shifted back in standard minimal media for 0.5-2 h. Endocytosis was elicited by adding NH_4^+ tartrate or uric acid for 2-4 h. After incubation was finished, the culture was filtered through blutex, squeezed between two papers to remove excessive liquid and immediately frozen in liquid nitrogen. The mycelia were pulverized 5 times in a

mortar with a pestle in the presence of liquid nitrogen and ~400 mg of the fine powder were transferred in a 2 mL eppendorf tube.

Total protein extraction

The mycelia powder was resuspended in 1 mL of ice cold precipitation buffer (see table below), mixed by vortexing and incubated on ice for 10-30 min. The sample was then centrifuged for 10 min, at 13000 rpm, 4°C. The pellet was resuspended twice in ice cold acetone and the sample was centrifuged for 5 min at 13000 rpm, 4°C. The supernatant was discarded and the pellet was incubated at 60°C in a heat block until cracks appeared. The pellet was then resuspended in 500-600 μL of protein extraction buffer I and the sample was centrifuged for 10-15 min at 13000 rpm, 4°C. The supernatant was transferred in a pre-frozen eppendorf tube and was stored at -80°C for further use. Before loading in a gel for electrophoresis (see 2.9.5), protein levels of the samples were quantified and normalized (see 2.9.2). The samples were then incubated with 4x sample loading buffer for 10-20 min at 37°C (membrane proteins), or 5 min at 95°C (soluble proteins).

Table 2.13. Solutions used for total protein extraction

Solutions	Composition in H_2O_{dist}
Precipitation Buffer	50 mM Tris-HCl pH 8.0, 50 mM NaCl, 12.5% (v/v) trichloroacetic acid (TCA), 1 mM PMSF, 1 x Protease Inhibitors Cocktail (PIC)
Extraction Buffer I	100 mM Tris-HCl pH 8.0, 50 mM NaCl, 1% (v/v) SDS, 1 mM EDTA, 1 mM PMSF, 1 x PIC
4x sample loading buffer	40% (v/v) glycerol, 250 mM Tris-HCl pH 6.8, 0.02% (w/v) bromophonol blue, 8% (v/v) SDS, 20% (v/v) β-mercaptoethanol

Membrane enriched extraction for ubiquitination

For the detection of ubiquitinated forms of UapA, protein extraction was performed as in Galan *et al.* (1994). The mycelia powder was resuspended in 2 mL of ice cold extraction buffer III (see Table 2.14) with *N*-ethylmaleimide (NEM) 25 mM, mixed by vortexing and incubated on ice for 10 min. The sample was then centrifuged for 3 min, at 3000 rpm, 4°C to remove cell debris and the supernatant was transferred in a pre-frozen eppendorf tube. Membrane proteins were then precipitated by centrifuging the sample for 45 min at 13000 rpm, 4°C. The pellet was resuspended in 400 μL of extraction buffer III with 5 M Urea (freshly added). After 30 min incubation on ice, the sample was centrifuged for another 45 min at 13000 rpm, 4°C

and the pellet was resuspended in 320 μL extraction buffer III with NEM 25 mM and 80 μL TCA 50% (v/v). The sample was incubated on ice for 30 min and was then centrifuged for 30 min at 13000 rpm, 4°C. The pellet was washed by pipetting in and out (without resuspending) 400 μL of Tris Base 1 M, for the acidic pH of TCA. The pellet was finally resuspended in 100 μL 1 x ubiquitination sample buffer. Usually, 5-20 μL of the protein samples were used for electrophoresis, after 20 min incubation at 37°C.

Table 2.14. Solutions used for the extraction of ubiquitinated forms of UapA

Solutions	Composition in H_2O_{dist}
Extraction Buffer III	100 mM Tris-HCl pH 7.5, 150 mM NaCl, 5 mM EDTA pH 8.0, 1 mM PMSF, 1 x PIC
1 x ubiquitination sample buffer	250 mM Tris, 50 mM Tris-HCl pH 6.8, 50 mM NaCl, 2% (v/v) SDS, 10% (v/v) glycerol, 2 mM EDTA, 0.005% (w/v) bromophenol blue, 2% (v/v) β-mercaptoethanol

Membrane enriched extraction for purification

The membrane-enriched extraction protocol (adapted from Pantazopoulou *et al.*, 2007) was mainly used prior to membrane protein purification by affinity chromatography. To increase protein yield, the extraction procedure was performed in 6-10 eppendorf tubes, containing mycelia of the same strain. The mycelia powder was resuspended in 2 mL of ice cold extraction buffer II (see table below), mixed by vortexing and incubated on ice for 20-30 min. The samples were then centrifuged for 3 min, at 3000 rpm, 4°C to remove cell debris and the supernatants were transferred in pre-frozen eppendorf tubes. Membrane proteins were then precipitated by centrifuging the samples for 1 h at 13000 rpm, 4°C. The pellets were resuspended in 80-100 μL of ice cold solubilisation buffer. The suspensions were collected in one eppendorf tube and solubilised, as described in section below2.9.3.

Table 2.15. Solutions used for membrane-enriched protein extraction prior to purification

Solutions	Composition in H_2O_{dist}
Extraction Buffer II	10 mM Tris-HCl pH 7.5, 100 mM NaCl, 5 mM MgCl$_2$, 0.3 M Sorbitol, 1 mM PMSF, 1 x PIC
Solubilisation Buffer	50 mM NaH$_2$PO$_4$ pH 8.0, 150 mM NaCl, 1% (w/v) dodecyl-β-D-maltoside (DDM), 1 mM PMSF, 1 x PIC

2.9.2 Protein quantification

The determination of protein concentration in the total membrane protein extract was done using the method of Bradford (Bradford, 1976). The protein-dye complex causes a shift in the dye absorption maximum from 465 nm to 595 nm. The amount of absorption produced is proportional to the protein concentration. 2 mL Bradford Reagent (100 mg Coomassie Brilliant Blue G-250, 50 mL 100% EtOH, 100 mL H_3PO_4, 850 mL H_2O) were transferred in a cuvette and 2 μL of the protein extract were added and vortexed briefly. Prior to reading the absorbance, 2 mL of this reagent were used as a blank to calibrate the spectrophotometer. The optical density (OD) of the protein extract in this reagent was then read at 595 nm. Each sample was analyzed in duplicate. The protein concentrations were determined by comparing the obtained OD values against the BSA standard curve, generated by plotting the average absorbance versus various concentrations of BSA. In the case of the ubiquitination extraction protocol, where Bradford assay was not applicable, normalization of sample concentrations was performed by Coomassie staining.

2.9.3 Purification of membrane proteins

Membrane protein purification was performed by combining affinity chromatography of His-tagged recombinant proteins with gel filtration chromatography. The procedure followed is an adaptation of the method described in Lemuh *et al.* (2009).

Detergent solubilisation of protein extracts

Prior to chromatographic purification, membrane protein extracts are solubilised in the appropriate – for this particular protein – detergent; incorrect detergent usage results in protein aggregation or failure of protein solubilisation. For UapA purification, crude membrane protein extracts were solubilised by resuspending in solubilisation buffer containing 1% (w/v) DDM without glycerol (see Table 2.15). The sample was stirred gently for 30 min on ice and then centrifuged for 20 min at 12000 g, 4°C, to separate the solubilised from the insoluble proteins. The supernatant (solubilised proteins) was then transferred to a pre-frozen eppendorf tube and glycerol was added to a final concentration of 20% (v/v) and gently mixed. The detergent-solubilised protein sample was stored at -80°C for further use or loaded directly onto a column for purification.

Affinity chromatography

Affinity chromatography is based on selective non-covalent interactions between an analyte (the substance which is to be purified) and the stationary phase of a chromatographic column. It is very specific and is often used for the purification of fusion proteins labelled with appropriate epitope tags. His-tags, for example, have an affinity for nickel ions; this property allows His-tagged proteins to be retained in a column containing immobilized nickel ions. For elution, an excess amount of a compound able to act as a nickel ligand, such as imidazole, can be used. During the entire chromatography process the eluent is collected in a series of fractions. In this study, proteins of interest were genetically tagged with a sequence encoding for 10 histidine residues and were purified using the Protino Ni-NTA Columns (Macherey-Nagel GmbH). The mobile phase was delivered in a consistent flow rate of 1 mL/min via a pump. The column was first equilibrated with 10-20 column volumes of Ni-column wash buffer (50 mM NaH_2PO_4 pH 8.0, 300 mM NaCl, 0.01 % (w/v) DDM, 1 mM PMSF), containing 10 mM imidazole. A total of 1-4 mg of protein in 1 mL of detergent solubilisation buffer was applied to the column and 2.5 mL of the flow-through were collected and put on ice (fraction f_0). The column was washed abundantly (10-20 column volumes) with wash buffer containing 20 mM imidazole and subsequently with another containing 50 mM imidazole to remove unbound and loosely bound molecules. 2.5 mL of each eluent were collected and put on ice (fractions f_{20} and f_{50}). Bound protein was eluted with increasing concentrations of imidazole in the column wash buffer (250 mM, 350 mM, 500mM) and 2.5 mL of each eluent were collected and put on ice (fractions f_{250}, f_{350} and f_{500}). The column was washed abundantly with the 500mM imidazole wash buffer and filled with 30% (v/v) EtOH before storing at 4°C.

Desalting and concentration

Removal of salts and exchange of buffer in protein samples can be easily achieved by gel filtration, a chromatographic method in which particles are separated based on their size. In this work, Sephadex G-25 columns were used. 2.5 mL of each fraction eluted from the Ni-NTA column were loaded onto the Sephadex column, which was previously washed abundantly with distilled water. After the sample volume had completely entered the column, 3.5 mL of sterile distilled water were added to the column and the protein was eluted and frozen at -80°C. The frozen protein samples

were then concentrated by overnight lyophilization. The freeze-dried samples were resuspended in a buffer containing 50 mM NaH_2PO_4, 10% glycerol, 0.1% (w/v) DDM, 1 mM PMSF, 1 x PIC, adjusted to pH 7.5 and analyzed electrophoretically and immunologically.

2.9.4 Purification of soluble proteins

Purification of soluble proteins was performed by immunoprecipitation. For immunoprecipitation under denaturing conditions, total protein extracts were resuspended in extraction buffer IV (see Table 2.16). Immunoprecipitation buffer (IP) was added and the lysates were incubated with 4 µg anti-GFP under gentle agitation at 4°C for 2 h. This step was followed by addition of A-Protein Sepharose CL-4B beads (Sigma-Aldrich) and incubation under gentle agitation at 4°C for 12 h. The beads were washed twice with IP buffer, once with wash buffer I, once with wash buffer II and once with wash buffer III and were finally boiled for 5 min at 95°C in protein sample buffer. Immunoprecipitation of ArtA-GFP and ArtA-K343R-GFPwas performed by S. Amillis.

Table 2.16. Solutions used for immunoprecipitation under denaturing conditions

Solutions	Composition in H_2O_{dist}
Extraction Buffer IV	50 mM Tris-HCl, pH 7.5, 2 mM EDTA, 100 mM NaCl, 2% SDS, 20 mM NEM, 1 x PIC
Immunoprecipitation buffer (IP)	50 mM Tris-HCl, pH 7.5, 2 mM EDTA, 150 mM NaCl, 1% Triton X-100, 0.5% sodium deoxycholate, 20 mM NEM, 1 x PIC
Wash buffer I	50 mM Tris-HCl, pH 7.5, 2 mM EDTA, 250 mM NaCl, 0.5% Triton X-100, 0.05% sodium deoxycholate, 20 mM NEM, 1 x PIC
Wash buffer II	50 mM Tris-HCl, pH 7.5, 1 mM EDTA, 500 mM NaCl, 0.1% Triton X-100, 20 mM NEM, 1 x PIC
Wash buffer III	50 mM Tris-HCl, pH 7.5, 1 mM EDTA, 100 mM NaCl, 1 x PIC

2.9.5 SDS-PAGE

Sodium dodecyl sulfate polyacrylamide gel electrophoresis (SDS-PAGE) is used for separation of proteins based on their size. By subjecting the sample under denaturing and reducing conditions (SDS), proteins become unfolded and coated with SDS detergent molecules, acquiring a net negative charge that is proportional to the size of the polypeptide chain. When loaded into a gel and placed in an electric field, the negatively charged protein molecules migrate towards the positively charged electrode and are separated based on their molecular weight. Protein bands can then

be visualized by protein-specific staining of the gel or by immunoblotting (see 2.9.6 and 2.9.7, respectively) and their size can be estimated by comparison of their migration distance with that of a marker of known molecular weight.

Polyacrylamide gel preparation requires casting of two different layers of acrylamide; the lower layer (separating gel) is responsible for separating polypeptides by size, while the upper layer (stacking gel) is designed to stack the proteins into a thin layer before they enter in the separating gel. In particular, the solutions consisting the separating gel were mixed in a flask connected to a vacuum pump prior to addition of APS and TEMED and the mixture was degassed for 20-30 min. APS and TEMED were added in the degassed mixture and the resulting solution was slowly poured into glass plates with spacers, assembled according to the manufacturer's instructions (BIORAD). Above that, a thin layer of distilled water was added and the gel was allowed to polymerize at RT. The surface of the polymerized separating gel was washed with distilled water and dried with Whatman paper. The stacking gel was prepared and applied on top of the separating gel, along with a comb. After polymerization, the comb was removed, wells were washed and the gel was placed into an electrophoresis apparatus containing electrophoresis running buffer (25mM Tris, 192 mM Glycine, 0.1% SDS pH 8.3).

Table 2.17. Composition of separating and stacking layers of polyacrylamide gels

	Separating gel 10% (11 mL)	Stacking gel 4% (5 mL)
H_2O_{dist}	4.5 mL	3.65 mL
Acrylamide/Bisacrylamide 30 %	3.63 mL	0.667 mL
Lower Tris (1,5 M Tris-HCl, pH 8,8)	2.75 mL	–
Upper Tris (0,5 M Tris-HCl, pH 6,8)	–	0.625 mL
20 % (w/v) SDS	50 μL	25 μL
10 % (w/v) Ammonium persulfate (APS)	50 μL	25 μL
TEMED	10 μL	10 μL

The samples were prepared as described in each extraction method and were loaded into the wells. The gel was run at 80 V through the stacking gel and 100 V through the separating gel, until the dye of the loading buffer had reached the bottom of the gel. A protein ladder was also loaded and run in parallel to estimate protein size and to determine transfer efficiency during western blotting. In the case of the ubiquitination extraction protocol, the gel was run for ~6 h until the 75 kDa band of the ladder had reached the end of the gel.

2.9.6 Protein gel staining

Protein bands on a gel can be visualized by incubating the gel with a staining solution. The most commonly used methods are Coomassie staining and silver staining.

Coomassie staining

Coomassie staining was mainly used for comparative quantification of different protein samples in a polyacrylamide gel. The gel was completely immersed in Coomassie staining solution (0.25% (w/v) Coomasie Brilliant Blue-R250, 45% methanol, 10% glacial acetic acid, filtered through Whatman paper) and incubated under gentle agitation for 0.5-1 h, at RT, until it was completely stained. The gel was rinsed with distilled water and washed with destaining solution (30% methanol, 10% glacial acetic acid) 2-3 x 30 min on a shaker, until the protein bands were clearly visible.

Silver staining

Silver staining is a highly sensitive staining method and was used to detect low protein levels, such as proteins purified by affinity chromatography (see 2.9.3). The gel was fixed for 30 min (or overnight) in fixing solution and then incubated for 30 min in sensitizing solution. After being washed 3 x 5 min in distilled water, it was incubated in silver solution for 20 min in the dark, to avoid oxidation by light. After being rinsed twice with distilled water, it was incubated in developing solution, while observing the appearance of bands. Once the bands were clearly visible, the development was terminated by incubating the gel in freshly-made stop solution for 10 min and rinsing with distilled water. Silver stained gels could be preserved for months in preserving solution.

Table 2.18. Solutions used for silver staining polyacrylamide gels

Solutions	Composition in H_2O_{dist}
Fixing	40% (v/v) EtOH, 10% (v/v) glacial CH_3COOH
Sensitizing	30% (v/v) EtOH, 6.8% (w/v) CH_3COONa, 0.2% (w/v) $Na_2S_2O_3 \cdot 5H_2O$, freshly added 0.125% (v/v) glutaraldehyde
Silver	0.25% (w/v) $AgNO_3$, freshly added 0.015% (v/v) formaldehyde
Developing	2.5% (w/v) Na_2CO_3, freshly added 0.0074% (v/v) formaldehyde
Stop	1.5% (w/v) $C_{10}H_{14}N_2Na_2O_8 \cdot 2H_2O$ (Na$_2$EDTA)
Preserving	30% (v/v) EtOH, 4% glycerol

2.9.7 Western blot

The western blot is used to detect specific proteins in a protein extract. Proteins are separated by size using gel electrophoresis before being transferred to a PVDF or nitrocellulose membrane. Once immobilized on the membrane, the proteins can be probed with specific antibodies (primary) against either the protein itself or an epitope with which the protein has been tagged. Highly specific and sensitive detection of a protein is enabled by the use of secondary Horse Radish Peroxidase (HRP)-linked antibodies against the primary that catalyze a chemiluminescent reaction.

Table 2.19. Solutions used for western blot

Buffers	Composition in H_2O_{dist}
Transfer Buffer	25mM Tris, 192 mM Glycine, 20% methanol
TBS	20 mM Tris-HCl pH 7.5, 500 mM NaCl, 0.1% (v/v) Tween 20
TBS-Tween	10 mM Tris-HCl pH 7.5, 150 mM NaCl
TBS-Tween-Triton	20 mM Tris-HCl pH 7.5, 500 mM NaCl, 0.05% (v/v) Tween 20, 0.2% (v/v) Triton X-100

Protein transfer on PVDF membrane

After electrophoresis (see 2.9.5) the SDS gel was equilibrated in Transfer Buffer (see Table 2.19) for 30 min. In the meantime, the PVDF membrane (Macherey-Nagel GmbH) was activated by soaking in 100% methanol for 1 min and together with filter papers (Whatman) was immersed in transfer buffer. The gel was placed in a cassette on top of a sponge and a couple of filter papers, followed by the membrane, two more filter papers and another sponge. The cassette was inserted in a blotting apparatus, filled with ice-cold Transfer Buffer, and electric current was applied forcing proteins to migrate on the membrane. Transfer was usually performed at 100V for 1.5-2 h. The membrane was immersed in TBS-Tween buffer (see Table 2.19) and stored at 4°C for further use.

Ponceau S staining

Transfer efficiency can be tested by staining proteins on the PVDF membrane using Ponceau S reagent. Ponceau S specifically binds to protein bands giving them a characteristic red color. The membrane was immersed in Ponceau S solution, incubated with mild agitation for 2 min and washed with distilled water until bands were visible. The membranes were destained by washing in TBS-Tween.

Immunostaining and chemiluminescence

After protein transfer from an SDS-PAGE gel to a membrane, the remaining protein-free sites of the membrane must be blocked in order to prevent the primary or secondary antibody from binding non-specifically directly to the membrane that would result in high background signal. The choice of blocking solution, washing solutions as well as the downstream procedure followed, depended on the antibody used.

In particular, when detecting the GFP epitope, blocking was performed by incubating the membrane in 2% (w/v) non fat dry milk in TBS-Tween for 1 h, at RT, under gentle agitation. A primary mouse *anti-GFP* monoclonal antibody (Roche Diagnostics) was diluted in an aliquot of the blocking solution (1:2000) and the membrane was soaked in the resulting solution and incubated for 2 h, at RT, under gentle agitation. After 2-3 x 10 min washing in TBS-Tween buffer with vigorous agitation to remove non-specifically bound antibody, the membrane was incubated for 1 h with a secondary goat anti-mouse IgG HRP-linked antibody (Cell Signaling Technology Inc.) diluted in blocking buffer (1:1000-1:3500), at RT, under gentle agitation. Once again, the membrane was washed with TBS-Tween 3-5 x 10 min with vigorous agitation to remove non-specifically bound antibody.

In the case of actin detection, a primary mouse *anti-actin* monoclonal (C4) antibody (MP Biomedicals Europe) was used in 1:2500 dilution. The membrane was blocked with 3% (w/v) BSA in TBS-Tween and both primary and secondary antibodies were diluted in that blocking solution. The procedure was the same followed for anti-GFP.

To detect ubiquitin, a mouse primary anti-ubiquitin (Ub-P4D1 HRP Conjugate, Santa Cruz Biotechnology) antibody was used in 1:200 dilution. The downstream procedure and blocking solution were the same as for anti-actin antibody. However, to improve the accessibility of the blotted protein to the antibody, the membrane was incubated in freshly-made denaturing buffer (6M guanidium chloride, 20 mM Tris-HCl pH 7.5, 1mM PMSF, 5 mM β-mercaptoethanol) for 30 min at 4°C and washed 3 x 10 min with TBS-Tween, prior to blocking.

For 10 x His tag, immunodetection was performed using an anti-His (PentaHis HRP Conjugate, Qiagen) antibody. After washing twice in TBS buffer, the membrane was blocked in anti-His-HRP conjugate blocking buffer (supplied by the manufacturer) for 1 h, at RT, under gentle agitation. The membrane was washed 2 x 10 min with

TBS-Tween-Triton and 1 x 10 min with TBS and was then incubated for 1 h with the anti-His antibody 1:2000 diluted in blocking buffer, under gentle agitation. The membrane was washed again 2-3 x 10 min with TBS-Tween-Triton and 1-2 x 10 min with TBS. Anti-His-HRP conjugate, was chemically coupled to the HRP reporter molecule and did not require the use of a secondary antibody.

After the last washing step, the membrane was subjected to chemiluminescence reaction using the LumiSensor Chemiluminescent HRP Substrate kit (GenScript USA Inc), according to the manufacturer's instructions. Briefly, 1 mL of each of the solutions provided was transferred in an eppendorf tube and was left in the dark for 20-30 min, to reach RT. The membrane was dried in filter paper and covered for 90 sec with a 1:1 mixture of the two solutions. Excess substrate was removed by touching the side of the membrane on a filter paper. After being covered with plastic foil, the membrane was exposed to a film in an autoradiography cassette for 5 sec-20 min and developed in a dark room with Kodak developing reagents.

2.9.8 Determination of detergent resistance

Detergent extractability assay was performed as described in Grossmann *et al.* (2008). In brief, aliquots corresponding to 50 mg of membrane protein in 100 μL of 50 mM Tris-HCl, pH 7.5, 150 mM NaCl, 5 mM EDTA, were treated with increasing concentrations of Triton X-100 (0–0.8%) for 30 min, at RT. Non-solubilised material was pelleted by centrifugation (30 min, at 14000 rpm, 4°C) and washed with 100 μL of the corresponding buffers under the same conditions. The pellets were resuspended in 30 μL of sample buffer, dissociated at 37°C for 15 min and then resolved by SDS-PAGE. UapA-GFP was detected by a specific anti-GFP antibody on a Western blot. Extractability of UapA-GFP by Triton X-100 from PM was performed by C. Gournas.

3

Effects of Hypertonicity
in Transporter Endocytosis & Fungal Physiology

3.1 State of the art

Biological membranes were long considered to be a fluid mixture of lipids organized in a homogenous bilayer, which serves as a solvent for membrane proteins. In contrast, current models underscore the high lateral compartmentation of membranes, consisting of lipid microdomains, so-called rafts, which are enriched in sterols and sphingolipids, and in specific raft proteins. Owing to their insolubility in mild non-ionic detergents at 4°C, these microdomains are defined as detergent-resistant membranes (DRMs; (Kubler *et al.*, 1996; Simons and Ikonen, 1997; Brown and London, 1998; Wachtler *et al.*, 2003).

In *S. cerevisiae*, two different non-overlapping lateral PM compartments have been distinguished so far; the membrane compartment occupied by proton ATPase Pma1 (MCP) and the membrane compartment occupied by arginine transporter Can1 (MCC), which is also accommodating permeases specific for tryptophan (Tat2) and uracil (Fur4), as well as Sur7, a protein presumably involved in endocytosis. In the

resolution of fluorescence microscopy, MCC and MCP together cover the whole PM surface. However, in contrast to mammalian cells, yeast membrane domains are sufficiently large and distant from each other to be resolved. MCC consists of isolated patches about 300 nm in diameter, whereas MCP exhibits a complementary, network-like pattern (Grossmann *et al.*, 2007). Electron microscopy analysis suggested that MCC patches correspond to furrow-like invaginations in the PM of yeast (Strádalová *et al.*, 2009). MCCs contain a distinct lipid composition enriched in ergosterol, as visualized by staining with filipin, a fluorescent marker binding this lipid (Malínská *et al.*, 2003; Grossmann *et al.*, 2007), but also as supported by transporter extractability assays from membranes using Triton-X 100 (Grossmann *et al.*, 2007). The compartmentation of the PM into MCC and MCP is highly stable, but transporters dock within MCC patches in a reversible, membrane-potential dependent manner (Malinska *et al.*, 2004; Grossmann *et al.*, 2007).

Based on a number of observations relating the rate of transporter endocytosis with localization in MCC patches, it has been proposed that the biological function of MCC is to protect therein embedded transporters and other proteins from internalization and turnover (Grossmann *et al.*, 2008). This view contradicts other studies showing that MCC organization is, at least in part, mediated by large protein complexes called eisosomes, which were proposed to mark static sites of endocytosis (Walther *et al.*, 2006). Eisosomes have also been observed in other fungi, *Candida albicans*, *Schizosaccharomyces pombe*, *A. nidulans* and *Ashbya gossypii* (Alvarez *et al.*, 2008; Vangelatos *et al.*, 2010; Seger *et al.*, 2011; Kabeche *et al.*, 2011). One possible function of MCC and eisosomes is to regulate protein and lipid abundance by sorting them into distinct, spatially separated pools where they are stabilized or from which they can be either endocytosed, or protected from internalization, selectively.

3.2 Aim of study

In *A. nidulans*, all characterized transporters, belonging to widely different families, show a continuous rather than punctuate pattern (Scazzocchio *et al.*, 2011). However, in the course of previous work, we observed that some *A. nidulans* transporters tagged with GFP form fluorescent cortical patches, when the hyphae were washed in buffers containing relatively high salt concentrations (Andreas Pavlides and George Diallinas). This observation prompted us to investigate the conditions eliciting the
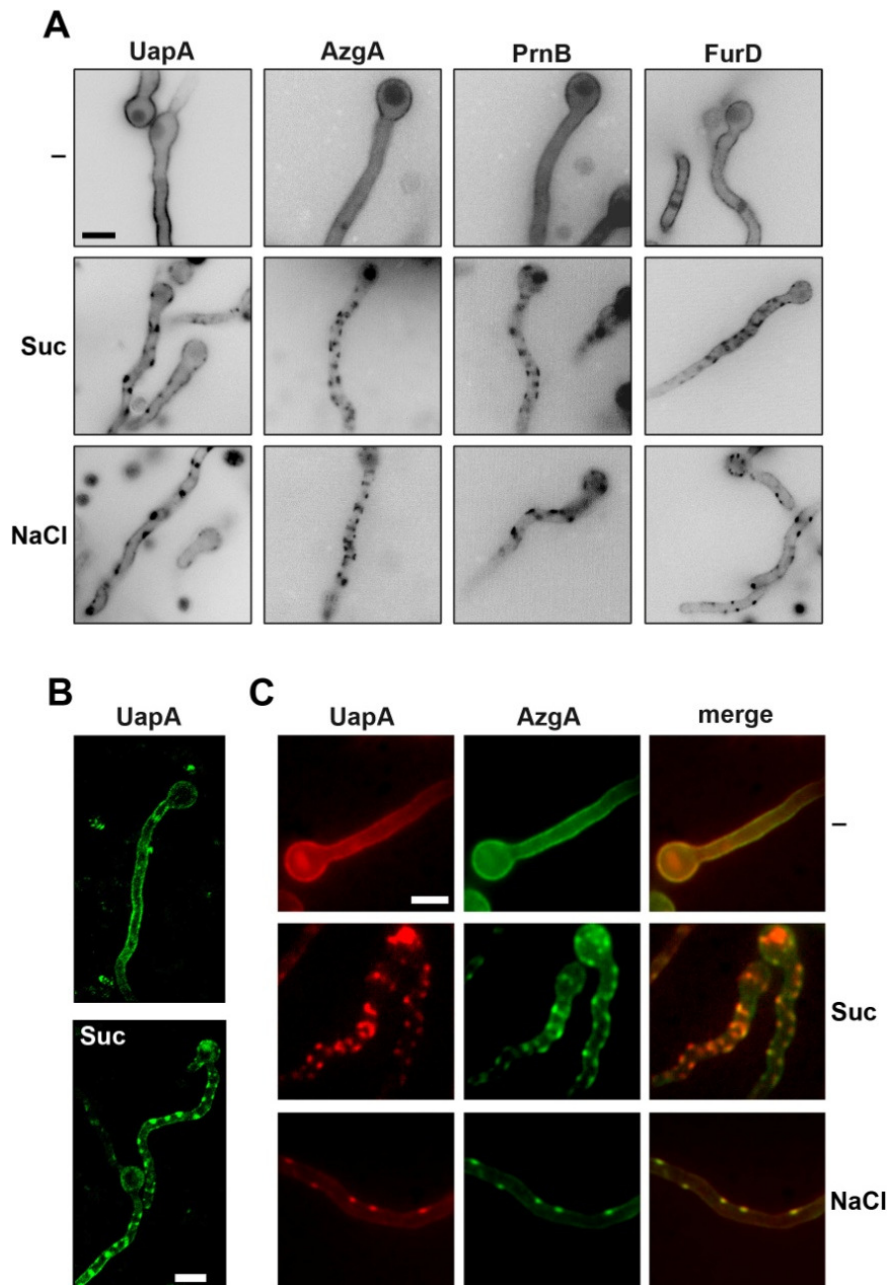
appearance of transporters in cortical patches and to examine the possibility of these patches corresponding to transporter-specific microdomains or membrane compartments similar to MCC. We also wanted to test the effect of hypertonic conditions on the physiology, the development and the endocytic mechanisms, of *A. nidulans*. Finally, we wished to explore whether this phenomenon is specific for our model organism or it can be reproduced in other fungal species. To this end, we examined the effect of hypertonic conditions in the model fungus *S. cerevisiae*, in respect to growth and transporter subcellular localization and endocytosis.

3.3   Results & Discussion

3.3.1 Hypertonic media elicit a cortical patchy appearance of transporters

Using functional GFP-tagged versions of seven *A. nidulans* transporters belonging to four evolutionary distinct protein families (NAT/NCS2, NCS1, AzgA-like, APC; http://www.membranetransport.org/), we have found that after transcriptional activation of the corresponding genes during conidiospore germination, transporter polypeptides show a rather uniform distribution along the PM of germlings and developing mycelia. A similar picture of uniform PM distribution was also observed in other *Aspergillus* transporters studied using GFP (Forment *et al.*, 2006; Apostolaki *et al.*, 2009). This contrasts the case of several *S. cerevisiae* transporters that appear to form discrete cortical foci, corresponding to MCC or MCP (see 3.1). A representative picture of transporter cellular expression in *A. nidulans* is shown in the upper panel of Figure 3.1A and B. In this figure, UapA (Gorfinkiel *et al.*, 1993) is a carrier specific for uric acid-xanthine (NAT family), AzgA (Cecchetto *et al.*, 2004) is carrier specific for adenine-guanine-hypoxanthine (AzgA-like family), PrnB (Tazebay *et al.*, 1997) is a proline permease (APC family) and FurD (Amillis *et al.*, 2007) is a uracil permease (NCS1 family).

The cellular expression of the *A. nidulans* GFP-tagged transporters was also examined in samples treated for 1-5 min with NaCl or sucrose. Under these conditions, we observed the rapid appearance of cortical fluorescent patches, as those shown in the lower panels of Figure 3.1A and B. By using a strain simultaneously expressing two of these transporters, UapA and AzgA, tagged with mRFP and GFP respectively, we showed that at least these permeases co-localize in the same patches (Figure 3.1C).

Figure 3.1. A. Hypertonic media elicit a cortical patchy appearance of *A. nidulans* GFP-tagged transporters observed by epifluorescence microscopy. Upper panel: Control samples (−) were grown for 13 h in minimal media (urea 5 mM, glucose 1%) at 25° C, which permit the induction of transporters during conidiospore germination (Pantazopoulou and Diallinas, 2007). Lower panels: Samples grown similarly as control samples, but then transferred to the same media containing 0.8 M Sucrose (Suc) or 0.5 M NaCl. Here and in several subsequent figures, images were converted to 8-bit inverted grayscale. The microscopy for A was performed by V. Bitsikas **B.** Confocal laser scanning microscopy of UapA-GFP cellular expression in control media (−) or after 1 min exposure to 0.8 M Sucrose (Suc). **C.** Epifluorescence microscopy of a strain expressing simultaneously UapA-mRFP and AzgA-GFP in control (−) or hypertonic (Suc, NaCl) media. Notice the overlap of red and green fluorescence (merge). Scale bars shown here and in subsequent figures correspond to 5 μm unless otherwise stated.

The kinetics of appearance of patches and most subsequent work were performed using a fully functional UapA-GFP transporter expressed from a strong controllable promoter (*alcA$_p$*) (Gournas *et al.*, 2010). Patch appearance depended on the concentration of sucrose or NaCl (Figure 3.2). The minimum concentrations of sucrose or NaCl eliciting the appearance of patches were determined to be 400 mM and 200 mM, respectively, in agreement with the relative hypertonic strength of these two solutes. Patches formed by the two solutes looked identical and their number and size depended on tonicity strength. The hypertonic effect imposed on mycelia was more evident at higher concentrations where hyphae became thinner, apparently due to water loss. The size of patches ranged from 0.5 through 2.3 μm.
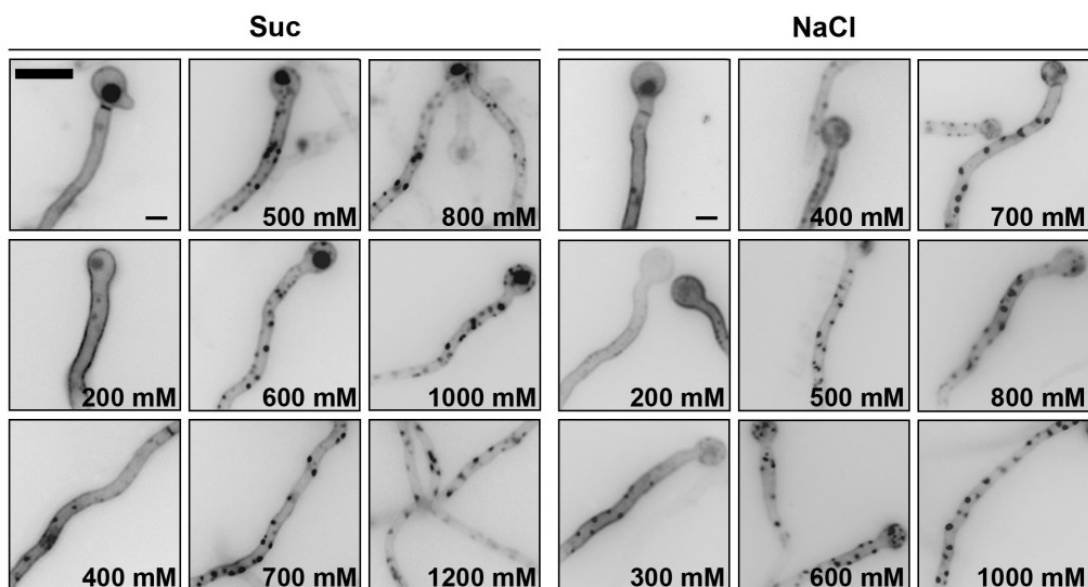
Figure 3.2. Kinetics of appearance of cortical patches in a strain expressing UapA-GFP from the alcA promoter (*alcAp*-UapA-GFP) in hypertonic media (1min) in response to tonicity strength. Samples were grown for 14-15 h in derepressing minimal media (urea 5 mM, fructose 0.1%), at 25°C, which permits the induction of UapA-GFP from *alcAp*.

Patches were shown to appear transiently, as they disappeared in overnight cultures in hypertonic media (Figure 3.3A). We estimated this recovery from the patchy appearance to take place after 4-8 h in sucrose (800 mM) or 2-4 h in NaCl (500 mM) (Figure 3.3A). Finally, patches disappeared rapidly (15 min) when sucrose or NaCl was washed-out (Figure 3.3B).
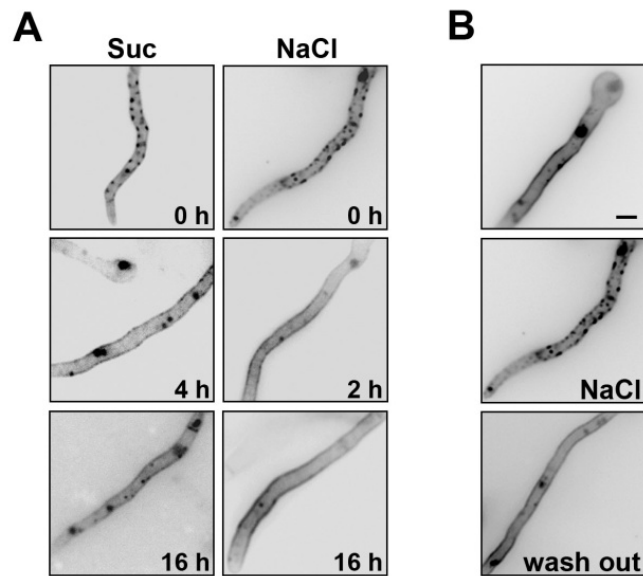
Figure 3.3. A. Disassembly of *alcAp*-UapA-GFP fluorescent patches after prolonged growth (4h or 16h) in hypertonic media (Suc or NaCl). **B.** Wash-out of *alcAp*-UapA-GFP fluorescent patches (NaCl) after 10 min transfer to control (-) media. The figure shows epifluorescence microscopy images. The scale bar shown is 10 μM.

Several other hypertonic media (LiCl, KCl, Na₂PO₄, NH₄Cl, sorbitol or mannitol) led to patchy distribution of UapA, whereas other stress conditions such as the presence of most divalent ions or heavy metals, protein synthesis blockage (cycloheximide), the presence of proton gradient uncouplers or extreme pH, had no effect (Figure 3.4).
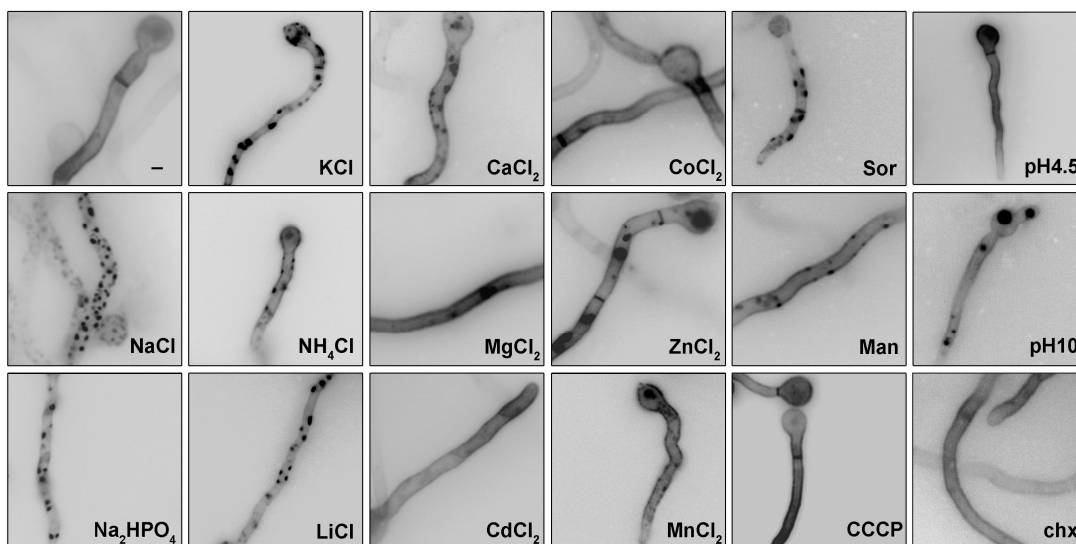
Figure 3.4. Examination by epifluorescence microscopy of UapA-specific fluorescent cortical patches after treatment with various salts (0.5 M), sugars (0.8 M), cycloheximide (chx; 20 μg/ml, 15 min prior to examination), different pH or the proton gradient uncoupler CCCP (30 μM, 15 min prior to examination). UapA-GFP is expressed from the *alcA* promoter (*alcAp*-UapA-GFP) as described in Figure 3.3. Notice that only monovalent ions and sugars (mostly Sor) lead to fluorescent patches. The microscopy for this figure was performed by V. Bitsikas and the author. Sor: Sorbitol; Man: Mannitol.

3.3.2 Patches correspond to PM invaginations rather than transporter-specific microdomains

Some patches, especially those produced under stronger tonicity, although clearly PM-associated, seem to extend beyond the membrane towards the cytoplasm. This was more clearly seen in deconvoluted Z-stack images, which strongly supported that patches correspond to membrane invaginations (Figure 3.5). This observation is in full agreement with two reports in *S. cerevisiae* (Slaninová *et al.*, 2000) and *Aspergillus repens* (Kelavkar *et al.*, 1993) directly showing, using transmission electron microscopy (TEM), that hypertonic media lead to PM invaginations, that can be extended deeply in the cytoplasm.
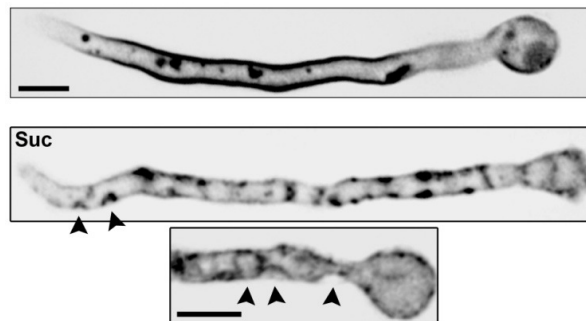
Figure 3.5. Fluorescent, UapA-GFP specific (*alcA*_p-UapA-GFP), patches correspond to PM invaginations (arrow heads) visible in deconvoluted images obtained with an inverted microscope. Maximal intensity projections obtained from z-stacks using the Metamorph 3D are shown. Two samples treated with sucrose (0.8 M) are shown compared with an untreated control. Microscopy and deconvolution for this figure was performed by A. Pantazopoulou and G. Diallinas.

We obtained independent evidence that fluorescent patches, initially observed using GFP-tagged transporters, are PM invaginations rather than specific transporter microdomains. This evidence is based on the following observations. First, similar patches were observed using two other PM-associated polypeptides. These are the pleckstrin homology (PH) domain of PLC-δ1, specifically recognizing the PM PI(4,5)P$_2$ lipids (Pantazopoulou and Peñalva, 2009) and the SsoA t-Snare, a protein that serves as a membrane-specific tag in the docking of transport vesicles to the PM (Taheri-Talesh *et al.*, 2008; Figure 3.6A). Second, similar patches were also observed in hypertonic conditions, using the lipophilic markers FM4-64 (Peñalva, 2005) or Filipin (Takeshita *et al.*, 2008; Figure 3.6B). Thirdly, since known PM microdomains have a distinct raft-like lipid composition, we tested the extractability of UapA by Triton X-100 from membranes. This biochemical approach is a standard
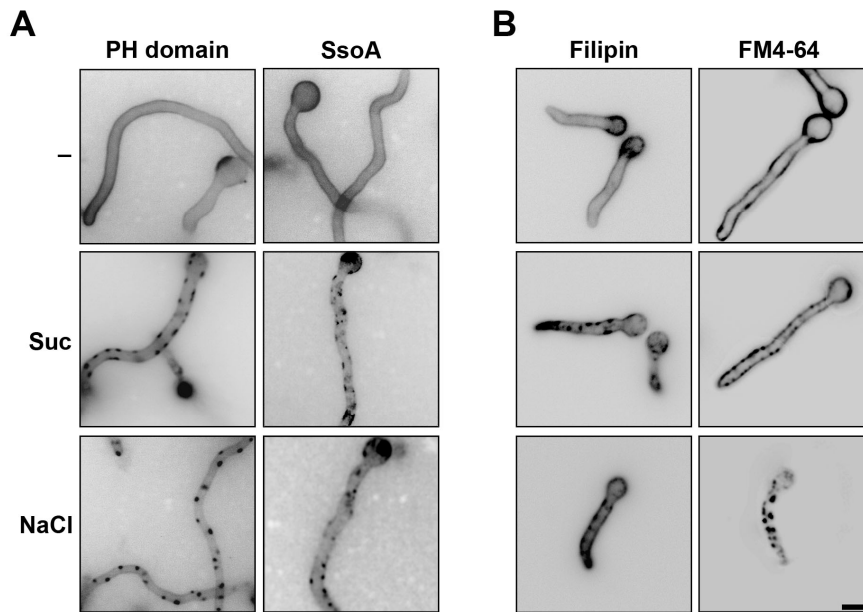
Figure 3.6. A. Fluorescent patches detected with membrane-associated molecular markers other than transporters in hypertonic conditions. 'PH domain' is a GFP-tagged duplication of the PLC-δ1 PH domain which acts as an exclusive marker for the PM through its high affinity binding of PI(4,5)P$_2$ lipids. SsoA is a GFP-tagged t-Snare exocytic protein that attaches to the inner leaflet of the PM. **B.** Filipin and FM4-64 are fluorescent lipophilic markers labelling the PM under specific conditions. Microscopy for Filipin and FM4-64 were performed by C. Gournas and V. Bitsikas, respectively.

assay used to detect partitioning of transporters in detergent resistant membranes (DRMs), which seems to be the biochemical equivalent of lipid-raft microdomains (Grossmann *et al.*, 2007). Figure 3.7C shows that UapA extractability was identical in standard and hypertonic media. Fourthly, direct transport measurements of radiolabelled ^{3}H-xanthine performed under hypertonic conditions showed that UapA-GFP remains fully functional, showing a K_m value (8 μM) and transport capacity nearly identical to the one obtained in standard media (Figure 3.7A).

Finally, using Calcofluor staining, a marker of cell wall material such as chitin or β-1,3-glucan, we showed that control samples exhibited a uniform fluorescence on their surfaces, whereas cells shifted to hyperosmotic medium showed cortical fluorescent patches. Several Calcofluor patches overlapped with UapA-GFP patches (Figure 3.7B). The intensity of Calcofluor or UapA-GFP fluorescence intensified with increased time of exposure to hyperosmotic conditions (not shown). These results strongly suggest that invaginated areas of the PM are rapidly filled with cell wall material, either through *de novo* synthesis or reorganization of pre-existing periplasmic material. Similar observations were reported in yeast (Slaninová *et al.*, 2000) and plants (Komis *et al.*, 2002). The simplest explanation of all the above

results is that fluorescent patches obtained with different markers represent PM invaginations, rather than specific microdomains with distinct lipid composition.

A

$K_m = 8\ \mu M$

% xanthine uptake rate

100
80
60
40
20
0

-    Suc   NaCl

B

UapA   Calcofluor

C

- Suc   + Suc

0   0.2   0.4   0.6   0.8   0   0.2   0.4   0.6   0.8

%Triton-X100
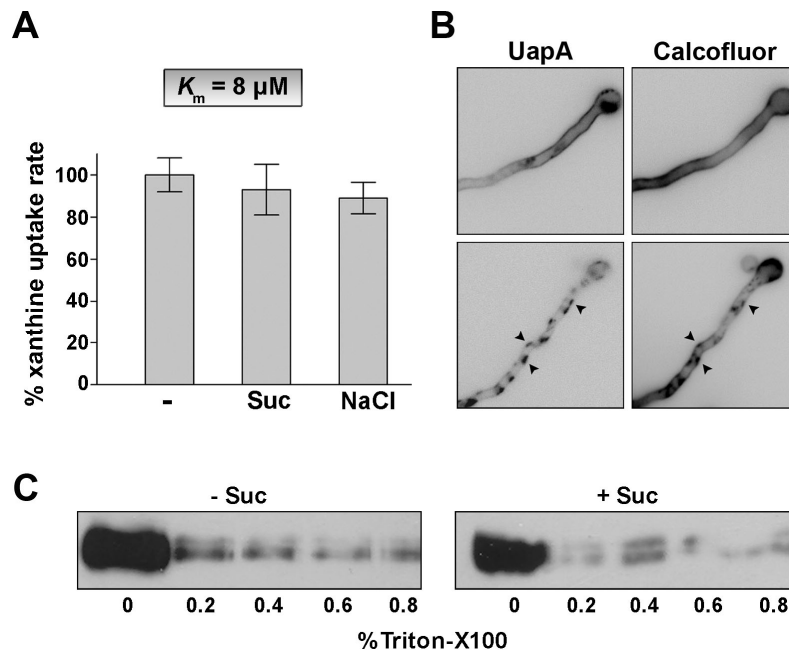
Figure 3.7. A. UapA-mediated (*alcA$_p$*-UapA-GFP) ^{3}H-xanthine transport capacity after exposure to hypertonic treatment (0.8 M sucrose or 0.5 NaCl, 10 min; performed by V. Bitsikas). The K_m value of UapA-GFP for xanthine, established in hypertonic media, is also shown (8 μM)..**B.** Calcofluor staining showing overlap of UapA-GFP patches with deposition of cell wall material (0.8 M sucrose). **C.** Extractability of UapA-GFP by Triton X-100 from PMs is identical in standard media before and after exposure to hypertonic treatment (0.8 M sucrose, 10 min; performed by C. Gournas)

3.3.3 Hypertonic media elicit transient blockage of endocytosis and growth arrest

Sucrose has been reported to be a specific clathrin-dependent inhibitor of receptor and transporter endocytosis in mammalian cells (Heuser and Anderson, 1989). This observation prompted us to investigate whether sucrose or other hypertonic media have an effect on endocytosis of UapA-GFP either in response to the presence of NH_4^+ ions or substrates (uric acid or xanthine). We observed that the addition of sucrose (0.8 M) or NaCl (0.5 M) prior to NH_4^+ or uric acid abolished the endocytosis and turnover of UapA-GFP (Figure 3.8A and B).

As expected, we also observed that in the presence of sucrose or NaCl, UapA-GFP molecules appeared in the PM patches described earlier. The block in transporter endocytosis and turnover was confirmed by western blot analysis, which showed the absence of free GFP in samples grown for the last hour in the presence of NH_4^+ or uric acid under hypertonic treatment (Figure 3.8C). The appearance of free GFP is a well-established marker of endocytosis and vacuolar turnover of UapA-GFP

and other GFP-tagged transporters (Gournas *et al.*, 2010). The blockage of UapA-GFP endocytosis was transient, as its internalization recovered with kinetics practically identical to those of patch disassembly after longer exposures to hypertonic media (Figure 3.8D). In addition, the minimal concentration of hypertonic solutes blocking UapA-GFP endocytosis was practically identical to that leading to plasmolysis (~0.45 sucrose, $\geq$ 0.2 M NaCl).
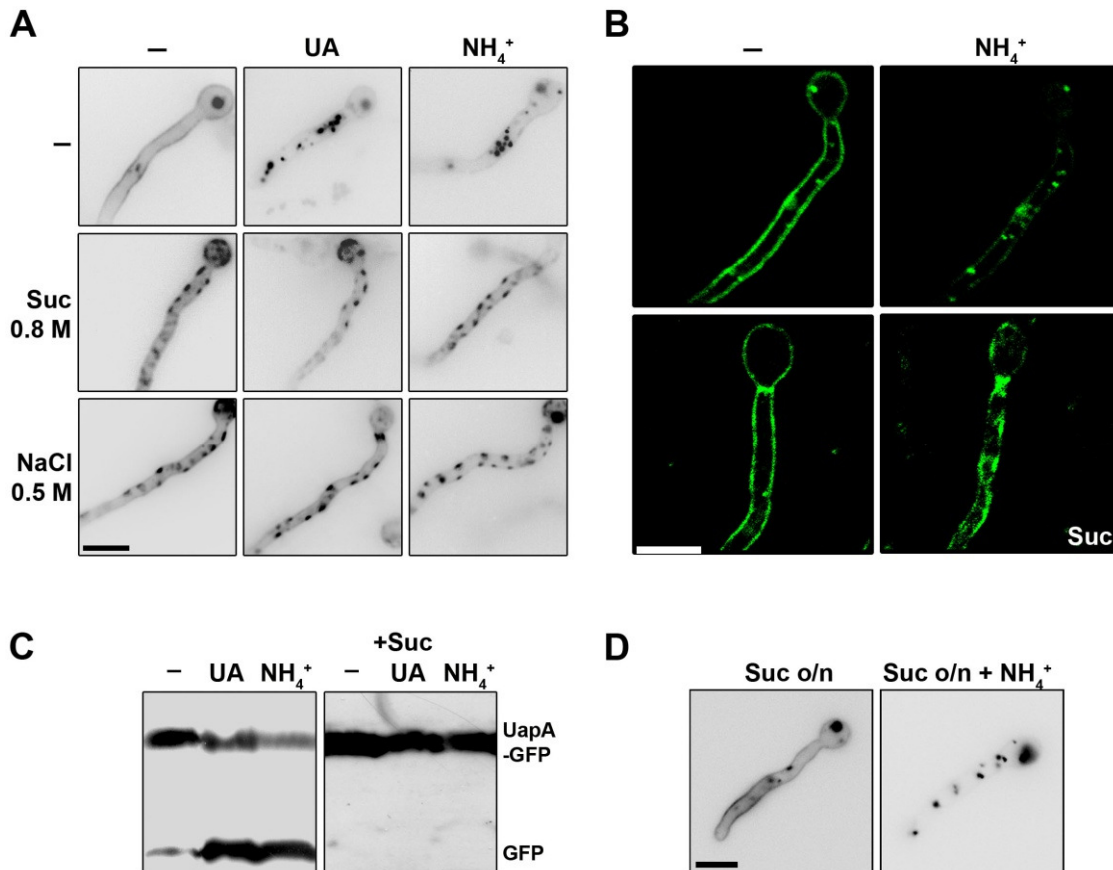
Figure 3.8. A. Hypertonic media elicit a blockage of UapA-GFP endocytosis. In control samples UapA-GFP (*alcA$_p$*-UapA-GFP) endocytosis is elicited upon transfer for 1h to standard media with either 1 mM uric acid (UA) or 20 mM ammonium ions (NH$_4^+$). Under these conditions UapA-GFP is internalized and degraded in the vacuoles (appearing as prominent fluorescent granules in the cytoplasm) through sorting in the MBV pathway. Here and in all subsequent figures, unless otherwise stated, hypertonic conditions are imposed by transfer to standard media with 0.8 M sucrose or 0.5 M NaCl. Notice that after hypertonic treatment there are UapA-GFP cortical fluorescent patches but no vacuoles visible in conditions that normally lead to UapA-GFP turnover. Microscopy was performed V. Bitsikas. **B.** UapA-GFP (*alcA$_p$*-UapA-GFP) endocytosis by NH$_4^+$ in a control sample and blockage of UapA-GFP endocytosis by NH$_4^+$ after hypertonic treatment, as seen with inverted confocal laser microscopy in a single hypha. **C.** Western blot analysis of membrane protein fractions corresponding to 2 h addition of uric acid (UA) or NH$_4^+$ and controls (-), probed with anti-GFP. The low mobility band corresponds to intact UapA-GFP (*alcA$_p$*-UapA-GFP) and the high mobility band to free GFP produced through vacuolar degradation of UapA. The western blot was performed by C. Gournas. **D.** Recovery of NH$_4^+$-elicited endocytosis of UapA-GFP (*alcA$_p$*-UapA-GFP) after prolonged growth (16 h) in hypertonic media.

In the course of the experiments described above, we noticed a significant delay in growth rate in samples exposed to hypertonicity. Figure 3.9A shows that this delay is maximal (40% reduction in colony radius) in media containing a non-catabolic carbon source such as fructose (0.1%), while it is more moderate (20% reduction) in carbon catabolite repressing (1% glucose) media. Figure 3.9B shows a quantification of this growth arrest expressed as reduction in average hyphal length after hypertonic treatment (20-40% reduction in germ tube length). The delay in growth recovered after longer exposures to hypertonic media, as did the appearance of fluorescent patches and the block in endocytosis (not shown).
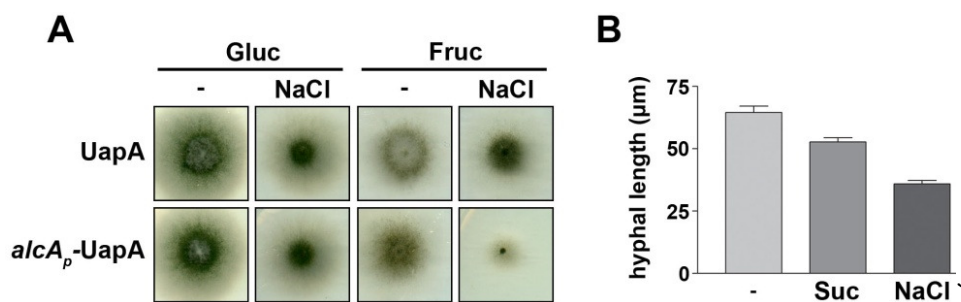
Figure 3.9. Hypertonic media elicit growth arrest of *A. nidulans.* **A.** Growth tests of two isogenic strains expressing UapA-GFP from either its native promoter (used for Fig. 1) or from the *alcA* promoter (used for all other figures). 0.5 NaCl was used for hypertonic treatment and tests were carried out in minimal media with fructose (0.1%) or glucose (1%) as carbon sources. NaCl led to a reduction of both the diameter of colonies and conidiospore production. The reduction of growth was stronger in fructose media. **B.** Reduction of hyphal length upon addition of either 0.8M sucrose or 0.5 M NaCl for 4h in the strain expressing *alcA$_p$*-UapA-GFP grown in fructose media. Measurements of hyphal length were performed by V. Bitsikas.

3.3.4 Hypertonicity affects actin dynamics and thus blocks endocytosis

A block in endocytosis can occur at several steps concerning the formation and internalization of the endocytic vesicle. To address this question we examined how basic elements of this process are affected by tonicity. In particular, we examined the cellular organization of well-characterized upstream (SlaB) and downstream (AbpA) endocytic factors, as well as that of tropomyosin (TpmA), tagged with either GFP or mRFP, under standard or hypertonic growth conditions. SlaB (Araujo-Bazán *et al.*, 2008) is a Sla2 *S. cerevisiae* orthologue (Wesp *et al.*, 1997), which acts as a well-characterized endocytosis regulator involved in the formation of early actin patch components (Newpher *et al.*, 2005). In particular, Sla2 regulates the association of the clathrin endocytic machinery with actin polymerization (Newpher and Lemmon, 2006).

AbpA (Araujo-Bazán *et al.*, 2008) is homologue of Abp1 in *S. cerevisiae*, which is a late endocytic vesicle formation component. It appears near the end of Sla2 lifetime, is localized exclusively to cortical endocytic actin filaments/patches (Huckaba *et al.*, 2004; Quintero-Monzon *et al.*, 2005) and does not associate with actin cables (Huckaba *et al.*, 2004). In *A. nidulans,* AbpA and SlaB are strongly polarized in hyphae, forming a ring that embraces the hyphal tip, leaving an area of exclusion at the apex (Araujo-Bazán *et al.*, 2008). AbpA localizes to highly motile and transient peripheral foci overlapping with actin patches, which predominate in the tip (Taheri-Talesh *et al.*, 2008). SlaB also localizes to peripheral foci, but these are markedly more abundant and cortical than those of AbpA (Araujo-Bazán *et al.*, 2008). Based on SlaB and AbpA cellular dynamics, it has been proposed that spatial association of exocytosis with endocytosis at the fungal tip underlies hyphal growth. Interestingly and unlike the case in *S. cerevisiae*, SlaB is an essential gene revealing a major role of endocytosis in filamentous fungal growth.

Tropomyosin (TpmA) is a major actin-binding protein that regulates actin mechanics (Stewart, 2001). A GFP-TpmA fusion has been used to image actin cables, which was not feasible with GFP-actin fusions, in *A. nidulans* (Pearson *et al.*, 2004; Taheri-Talesh *et al.*, 2008). GFP-TpmA is concentrated near the apex and at forming septa (Pearson *et al.*, 2004; Taheri-Talesh *et al.*, 2008), labels actin cables along the hyphae, but does not seem to co-localize with endocytic actin patches.

Figure 3.10A (upper panels) shows that, as expected, SlaB and AbpA form cortical foci which are mostly concentrated at the tip of hyphae, whereas TpmA has a rather diffuse localization in the cytosol, but also clearly labels actin cables along the hyphal axis and the tip region. The lower panels in Figure 3.10A show that neither sucrose nor NaCl affected the cortical and polar appearance of SlaB-GFP or AbpA-mRFP foci, whereas hypertonic media dramatically modified the cellular localization of GFP-TpmA. More specifically, fluorescence was not any longer associated with actin cables and the tips of the hyphae, but was apparent as diffuse cytosolic fluorescence and in scattered cortical foci along the axis of the hyphae. This picture constitutes strong evidence that hypertonic media modify actin dynamics, rather than the formation of cortical endocytic complexes *per se*, probably through immediate actin de-polymerization followed by rapid localized re-polymerization. A similar conclusion has been proposed for the effect of tonicity in plants (Komis *et al.*, 2002).
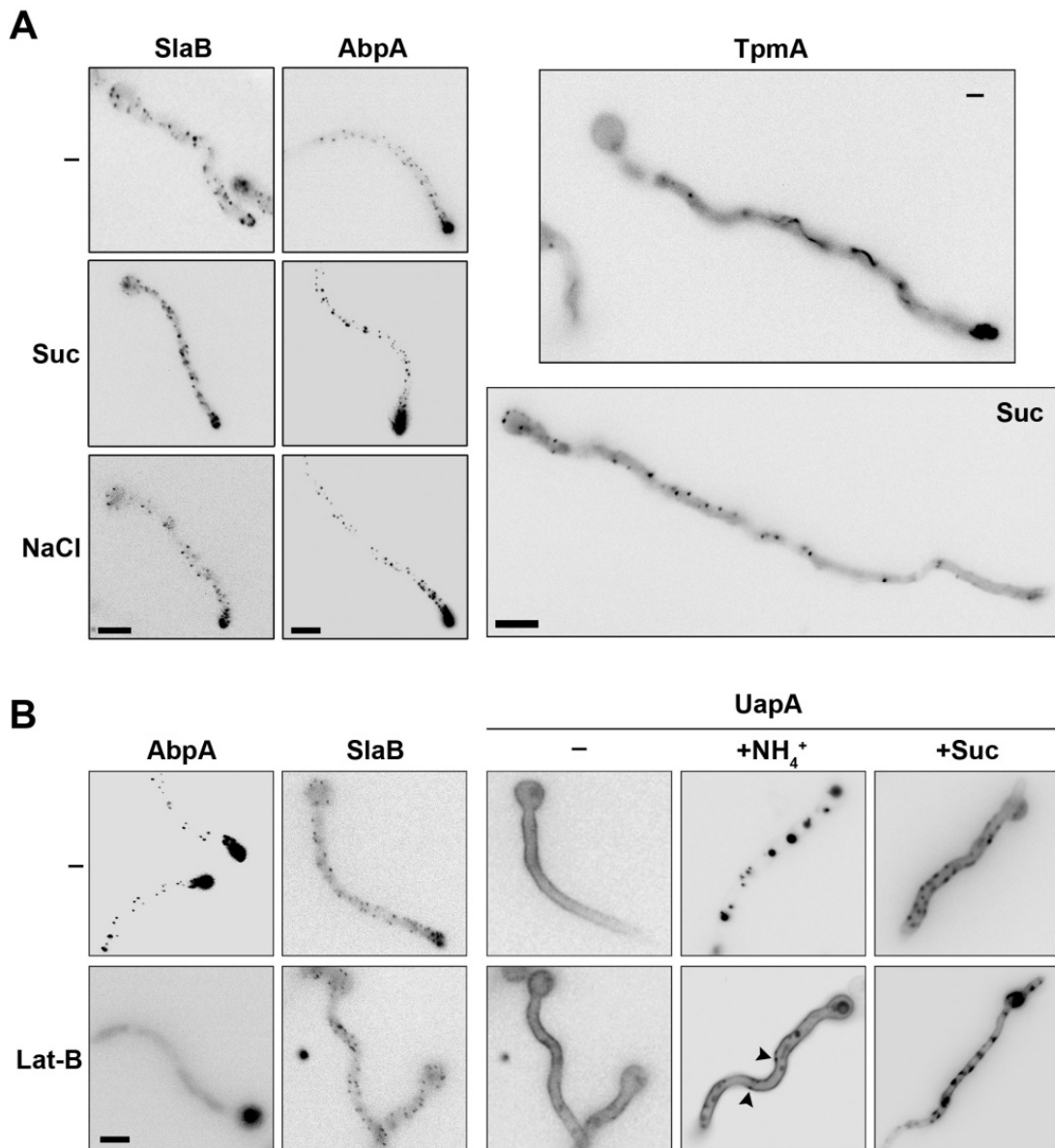
Figure 3.10. Hypertonicity and Lat-B effects on actin dynamics and the endocytic machinery. Microscopy was performed by V. Bitsikas. **A.** Cellular localization of SlaB, AbpA and of TpmA, tagged with either GFP or mRFP, under standard or hypertonic growth conditions. Samples were treated as previously described. SlaB-GFP and AbpA-mRFP form cortical foci which predominate at the tip of hyphae under all conditions. GFP-TpmA in standard conditions (-) labels diffusely the cytosol and more strongly actin-like cables along the hyphal length and the tip. In hypertonic conditions (Suc) labelling of the actin cables and the tip disappears and scattered cortical patches appear along the hyphal length. **B.** Effect of Lat-B (50 μM) on the subcellular localization of UapA (-GFP or -mRFP tagged) in standard (-), endocytic (NH_4^+) or hypertonic (Suc) conditions. The effect of Lat-B on AbpA-GFP and SlaB-GFP was also examined as a control. Lat-B leads to the disassembly of all AbpA patches as expected (Araujo-Bazán *et al.*, 2008), but has a minor effect on SlaB, as only the patches at the tip seem to disassemble. Lat-B has no effect on either the normal uniform localization of UapA in the PM in standard media (-) or on the appearance of UapA-specific fluorescent patches (plasmolysis) in hypertonic media (Lat-B+Suc). In contrast, Lat-B blocked the internalization of UapA by NH_4^+. Note that in the latter case, UapA cortical foci are also visible (arrows).

We also tested how actin de-polymerization triggered by Latrunculin B (Lat-B) (Taheri-Talesh *et al.*, 2008) affects plasmolysis and transporter endocytosis. As a control of Lat-B action we followed its effect on AbpA, but also on SlaB. Figure 3.10B shows that Lat-B led to complete disassembly of AbpA patches, as expected (Pantazopoulou and Peñalva, 2009), but had a moderate apparent effect on SlaB patches, more evident at the tip. This might be due to the fact that, unlike AbpA, SlaB regulates F-actin polymerization but contains a PI(4,5)P$_2$ binding domain that contributes to its PM localization. Lat-B had no effect on either the localization of UapA-GFP in the PM, or on the appearance of UapA-GFP cortical patches (plasmolysis), but blocked UapA-GFP endocytosis by NH$_4^+$ (Figure 3.10B). Therefore, both hypertonicity and Lat-B blocked endocytosis, suggesting that hypertonicity, similarly to Lat-B, might act through an effect on actin dynamics.

3.3.5 Hypertonic conditions elicit similar phenomena in *S. cerevisiae*

We tested the effect of similar conditions and studied the response of *S. cerevisiae* to hypertonicity. In these studies we used a strain expressing a functional GFP-tagged version of the lactate (Jen1) permease, a transporter that in standard media labels uniformly the PM. Jen1 is endocytosed and degraded through the MVB pathway in response to the presence of a preferred carbon source such as glucose. Figure 3.11 shows that both sucrose and NaCl lead to the appearance of prominent Jen1-specific fluorescent patches. These patches are clearly distinguishable from the Fur4p-specific MCC foci observed in the standard media, the former being larger and extended towards the cytoplasm as expected for PM invaginations.

In addition, Figure 3.11 shows that under hypertonic conditions, the endocytosis of Jen1 by glucose is totally blocked. As in *A. nidulans*, patch appearance and blockage of endocytosis showed similar kinetics and both phenomena recovered after 10-14 h in hypertonic media (not shown). Finally, similarly to *A. nidulans*, hypertonic media elicited a growth arrest (Figure 3.11), which has also been observed by others (Slaninová *et al.*, 2000; Hohmann *et al.*, 2007). A notable difference between the response of the two fungi to hypertonicity was that *S. cerevisiae* proved more resistant than *A. nidulans* to tonicity, that is, 2-fold higher concentrations of sucrose (1.6 M) or NaCl (1 M) were needed to elicit plasmolysis, blockage of endocytosis and growth arrest. Similar results were also obtained with a second *S. cerevisiae* transporter (Fur4; results not shown).
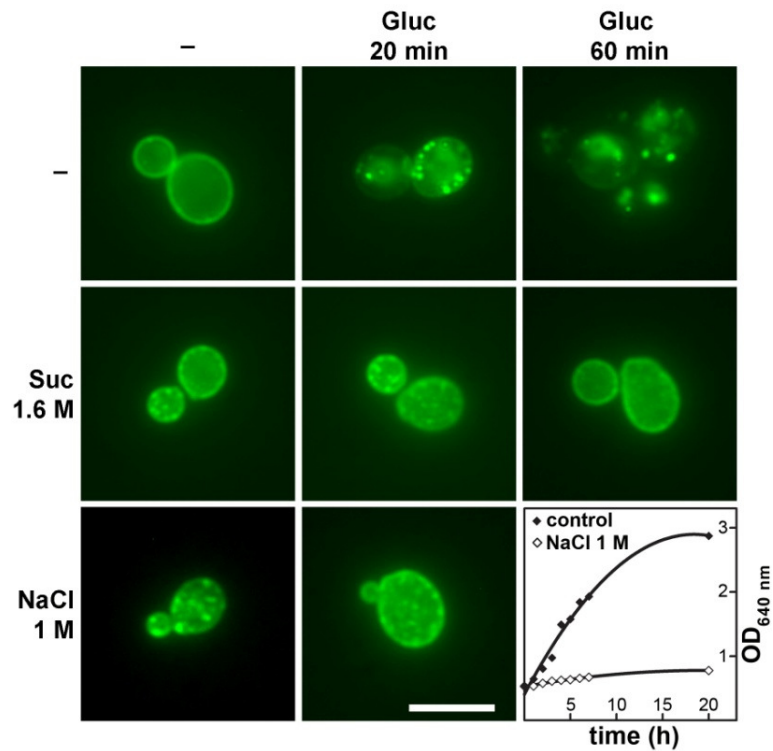
Figure 3.11. Hypertonic conditions elicit similar phenomena in *S. cerevisiae* as in *A. nidulans.* Epifluorescence microscopy images of a *S. cerevisiae* strain expressing a functional Jen1p-GFP chimeric transporter are shown. Jen1p-GFP is expressed uniformly in the PM under standard conditions of induction (-) but is rapidly internalized (20 min) and eventually degraded in the vacuole (60 min) upon addition of 1% glucose (Paiva *et al.*, 2009). Hypertonic treatment (1.6 M sucrose or 1 M NaCl) for 1 min leads to the appearance of mostly cortical fluorescent patches and shows no evidence of internalization or degradation of by glucose. The last panel shows the growth arrest elicited by addition of 1 M NaCl in the Jen1-GFP strain at an OD_{640nm} of 0.5. Scale bar: 10 µM.

4

Mechanisms of Regulation
of Transporter Ubiquitination & Endocytosis

4.1   State of the art

Similar to a number of *A. nidulans* (PrnB, UapC, AgtA) and *A. oryzae* (AoUapC) transporters involved in the uptake of amino acids and purines (Valdez-Taubas *et al.*, 2004; Pantazopoulou *et al.*, 2007; Higuchi *et al.*, 2009; Apostolaki *et al.*, 2009), UapA is down-regulated in response to ammonium ions (for details see 1.5.6). Recently, a novel downregulation mechanism was revealed; it was shown that UapA endocytosis and sorting into the endosomal degradation pathway is elicited not only by NH_4^+, but also by the presence of its substrates. Substrate-induced turnover is independent of UapA transcriptional induction or intracellular concentration of uric acid and it occurs at concentrations as low as 5 μM. Remarkably, substrate-elicited endocytosis, unlike NH_4^+-induced turnover, is absolutely dependent on UapA transport activity (see also 5.1; Gournas *et al.*, 2010).

Although the activity dependence clearly distinguishes this phenomenon from NH_4^+-induced endocytosis, both phenomena require UapA ubiquitination, which is mediated by HulA ubiquitin ligase, the only Rsp5 homologue of *A. nidulans*. Deletion of the C2 domain of HulA, dramatically blocked UapA ubiquitination and endocytosis, as evidenced by epifluorescence microscopy (Figure 4.1) and western blot analysis. Similar results were obtained by the substitution of the only Lys residue of the cytoplasmic C-terminal region of UapA (K572). In marked contrast, substitution of all five Lys residues located in the cytoplasmic N-terminal region of UapA (K21, K22, K59, K60, K73) did not have any effect in the internalization of the transporter, showing that HulA acts at a single Lys residue (Figure 4.1; Gournas *et al.*, 2010).

The convergence of broad-range and specific endocytic signals to a common ubiquitination mechanism suggested that different adaptors are recruited for each signal or that UapA is differentially modified when actively transporting its substrates or when NH_4^+ cellular levels increase (Gournas *et al.*, 2010). Therefore, the next step towards the elucidation of the mechanisms regulating UapA ubiquitination and endocytosis was the identification of the adaptor proteins involved in this procedure.
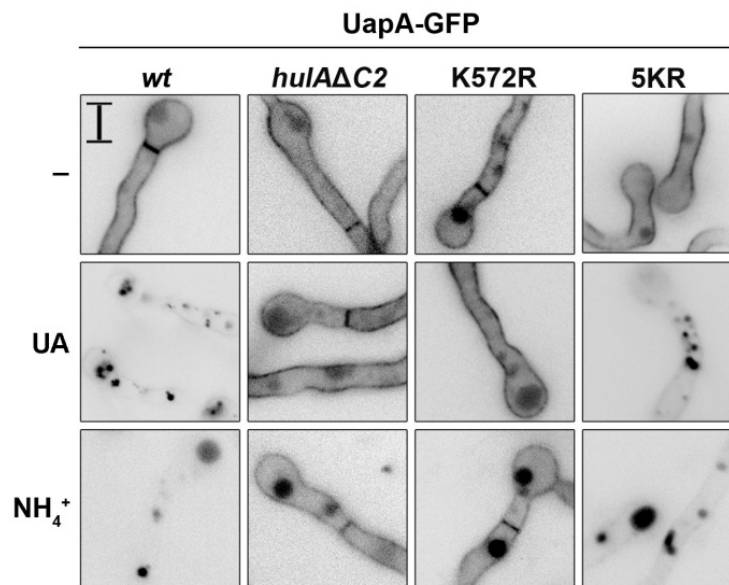
Figure 4.1. Epifluorescence microscopy of UapA-GFP subcellular localization under non-endocytic (-) or endocytic conditions (NH_4^+ or uric acid, UA) in strains bearing a deletion of the C2 domain of HulA or a substitution of the Lys572 located in the cytosolic C-terminal region of UapA or substitutions of all five Lys residues present in the cytosolic N-terminal region of UapA. Scale bar 5 μm (adapted from Gournas *et al.*, 2010).

Most of the advances in the study of intracellular trafficking have been achieved using the well-established prototype fungus *S. cerevisiae*. In order to take full advantage of the large collection of relevant mutations available, we established a heterologous system of UapA expression. The fact that *S. cerevisiae* lacks transporters of oxidized purines (xanthine and uric acid) made this model system appropriate for our purposes. Heterologously expressed UapA was fully functional and predominantly localized in the PM (Leung *et al.*, 2010). However, epifluorescence microscopy and uptake assays under standard endocytic conditions showed that UapA cannot be endocytosed in this system, at least under the conditions tested (Mayia Karachaliou and George Diallinas, unpublished observations). Hence, the investigation for the adaptor proteins involved in UapA turnover was carried out in *A. nidulans*.

4.2   Aim of study

In *S. cerevisiae*, Rsp5-dependent ubiquitination of transporters at the PM is mediated by arrestin-like adaptor proteins containing PY motifs that interact with the WW domains of the ubiquitin ligase. The aim of this part of the study was to examine whether arrestin-like proteins have an analogous role in *A. nidulans* and if so which proteins are specific for selected transporters and under which conditions. In this direction, we primarily wanted to identify the arrestin(s) that serve as HulA adaptors and are responsible for UapA ubiquitination and endocytosis in response to NH_4^+ or its substrates. Systematic knock outs led to the recognition of one arrestin-like adaptor, ArtA, involved in UapA endocytosis by both signals. Other questions raised include the identification of the interaction interface between the transporter and the adaptor, as well as the subcellular localization where these interactions occur. In addition, we wished to explore the importance of the PY motifs for the function of the ArtA and the possibility of its involvement in the ubiquitination of other *A. nidulans* transporters. Finally, it has been shown that in *S. cerevisiae* arrestin-like proteins are themselves ubiquitinated, which seems to be part of the mechanism regulating their action. Based on that, we investigated whether ArtA is ubiquitinated, in what conditions and what is the significance of this modification for UapA ubiquitination and endocytosis.

4.3   Results & Discussion

4.3.1 Phenotypic analysis of null mutants of genes encoding arrestin-like proteins in *A. nidulans*

A. nidulans has 10 genes coding for putative arrestin-like proteins, most of which contain PY elements (Figure 4.2). Three of them, *palF*, *creD* and *apyA* have been previously described (see 1.6.7). Seven more arrestin-like genes were identified and named *artA* (ANID_00056.1), *artB* (ANID_01089.1), *artC* (ANID_01743.1), *artD* (ANID_09105.1),   *artE*   (ANID_02447.1),   *artF*   (ANID_03302.1)   and   *artG* (ANID_05453.1). *In silico* analysis was performed by S. Amillis.
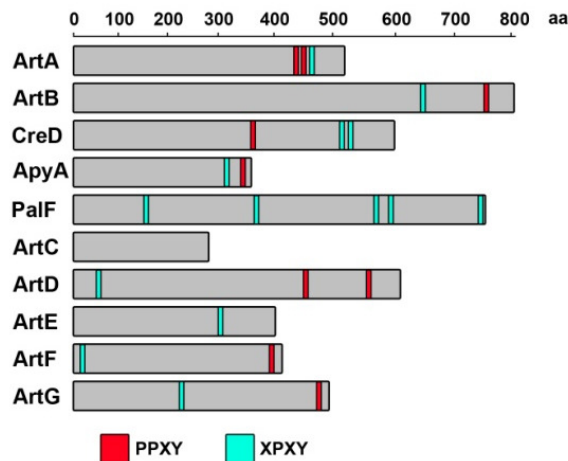
Figure 4.2. Schematical representation of the actual positions of putative PY elements in the *A. nidulans* arrestin-like protein sequences. Noticeably, ArtC has no canonical PY elements.

A comparison of the arrestin-like proteins of *A. nidulans* with the well characterized arrestin-like proteins of *S. cerevisiae* showed that ArtA is significantly more similar to the Art1/Ldb19/Cvs7 (21.4% identity) than to any other arrestin-like protein of *S. cerevisiae*. Art1 is an arrestin that is necessary for the endocytosis of several nitrogen-containing compounds, such as amino acids and uracil (Lin *et al.*, 2008; Nikko *et al.*, 2008; Léon and Haguenauer-Tsapis, 2009; Nikko and Pelham, 2009; MacGurn *et al.*, 2011). CreD is mostly similar to Art4/Rod1 and Art7/Rog3 (24.1-26.7% identity), the former being involved in the endocytosis of the glucose transporter Htx6p and of the lactate permease Jen1 (Nikko and Pelham, 2009; Becuwe, Vieira, *et al.*, 2012). The remaining ART proteins of *A. nidulans* share less clear-cut similarities with those of *S. cerevisiae* (identities up to 19.1%).

Null mutant strains for nine genes encoding arrestin-like proteins (*artA, artB, artC, artD, artE, artF, artG, apyA, creD*) were constructed by S. Amillis. The knock-

out mutant of the tenth arrestin, *palFΔ*, was a gift from Prof. H. Arst. All knock-out null mutants were viable and could thus be tested directly for their morphology and rate of growth in different temperatures (25°C and 37°C), pH values, nitrogen or carbon sources and toxic analogues of purines, pyrimidines and amino acids. Highlights of this analysis are shown in Figure 4.3. Increased sensitivity towards toxic compounds has been used to identify arrestin-like genes in *S. cerevisiae* (Lin *et al.*, 2008; Nikko *et al.*, 2008).
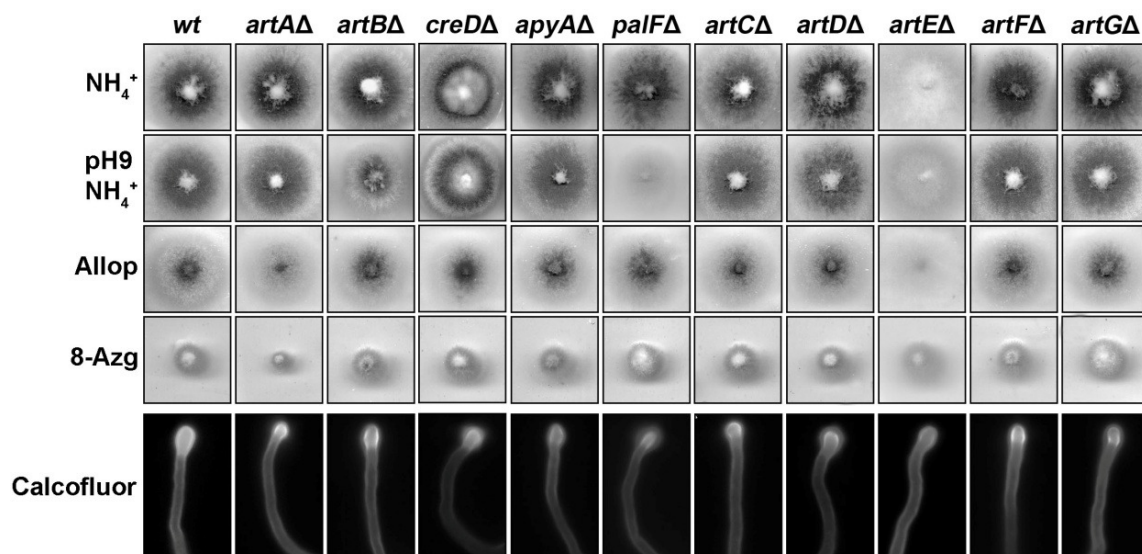
Figure 4.3. Growth phenotypes of arrestin null mutants. Minimal medium with 10 mM NH_4^+ as nitrogen source was used as a growth rate control. Hypoxanthine and sodium nitrate were used as nitrogen sources with the toxic analogues allopurinol (Allop) and 8-azaguanine (8-Azg), respectively. Growth tests were at 37°C and pH 6.8 and were performed by S. Amillis. In the lowest panel, vegetative microscopic samples of hyphal cells growing on minimal medium with glucose as carbon source and NH_4^+ as nitrogen source (16 h at 25°C) are shown after staining with Calcofluor white.

Among the ten arrestin knock-outs, *artEΔ* showed an inability to produce coloured asexual conidiospores, decorating the surface of the colony. Several of the knock-out mutants showed different growth rates on various nitrogen or carbon sources and especially in respect to resistance or sensitivity to the toxic analogues tested. In regard to UapA, which is the primary subject of this work, *artAΔ* showed increased sensitivity to allopurinol, a well established substrate of this transporter (Diallinas and Scazzocchio, 1989). *artAΔ* also showed increased sensitivity to 8-azaguanine, a substrate of the AzgA purine transporter (Cecchetto *et al.*, 2004). As will be shown below, ArtA is indeed responsible for the endocytic turnover of both UapA and AzgA, in full accordance with the increased sensitivity observed for the *artAΔ* mutant to allopurinol and 8-azaguanine (Figure 4.3). Finally, none of the

arrestin knock-outs showed altered polar growth or hyphal morphology, as evidenced by epifluorescence microscopic analysis of samples stained with Calcofluor white (Figure 4.3 lowest panel).

4.3.2 A single arrestin is necessary for UapA endocytosis in response to NH_4^+ or excess substrate

In order to investigate the role of all arrestin-like proteins in the endocytosis and/or MVB sorting of UapA, all relevant null mutants were crossed with a strain expressing a fully functional UapA-GFP version from its endogenous promoter (Gournas *et al.*, 2010). Genetic crosses were performed by S. Amillis. The strain expressing UapA-GFP was deleted for the homologous *uapC* gene, encoding a secondary uric acid/xanthine transporter (Diallinas *et al.*, 1995), so that uric acid or xanthine uptake was solely mediated by UapA. Isogenic progeny was selected and analyzed for UapA-GFP subcellular localization and endocytosis by epifluorescence microscopy. Results are summarized in Figure 4.4.

None of the arrestin knock-out deletions had any effect on the expression or localization of UapA-GFP in the PM, visible in the hyphal periphery and in the septa, under control conditions. Under endocytic conditions, imposed by the presence of NH_4^+ or excess substrate (uric acid), where UapA-GFP is normally internalized and sorted in MVBs/vacuoles (see wild-type control in Figure 4.4 and Figure 4.5), a single arrestin null mutant, *artA*Δ, showed no UapA-GFP vacuolar turnover. In all other arrestin knock-out deletion mutants UapA-GFP is turned-over similarly to the wild-type control in the presence of NH_4^+ or excess substrate. Given that we have previously shown that UapA-GFP vacuolar turnover occurs exclusively via endocytosis and not through direct sorting from the Golgi to the vacuole (Gournas *et al.*, 2010), our results strongly suggest that lack of a functional ArtA blocks UapA internalization from the PM.

To show more rigorously that ArtA controls UapA endocytosis and vacuolar turnover, *artA*$^+$ and *artA*Δ isogenic strains expressing UapA-GFP from the strong controllable *alcA$_p$* promoter (Gournas *et al.*, 2010) were constructed (by S. Amillis). These strains lack the genomic copies of *uapA* and *uapC* (i.e. *uapA*Δ *uapC*Δ) so that uric acid or xanthine uptake takes place through the integrated copy of *alcA$_p$*-UapA-GFP, expressed solely under de-repressed conditions (fructose as sole carbon source). In the presence of glucose (repressing carbon source) no UapA-GFP

expression or transport activity can be detected. Using the *alcA$_p$* system had two advantages. First, we could uncouple ammonium-elicited repression of *uapA* transcription from UapA endocytic turnover (Pantazopoulou *et al.*, 2007), and second, we could regulate UapA *de novo* synthesis prior or after imposing endocytic conditions (Gournas *et al.*, 2010).
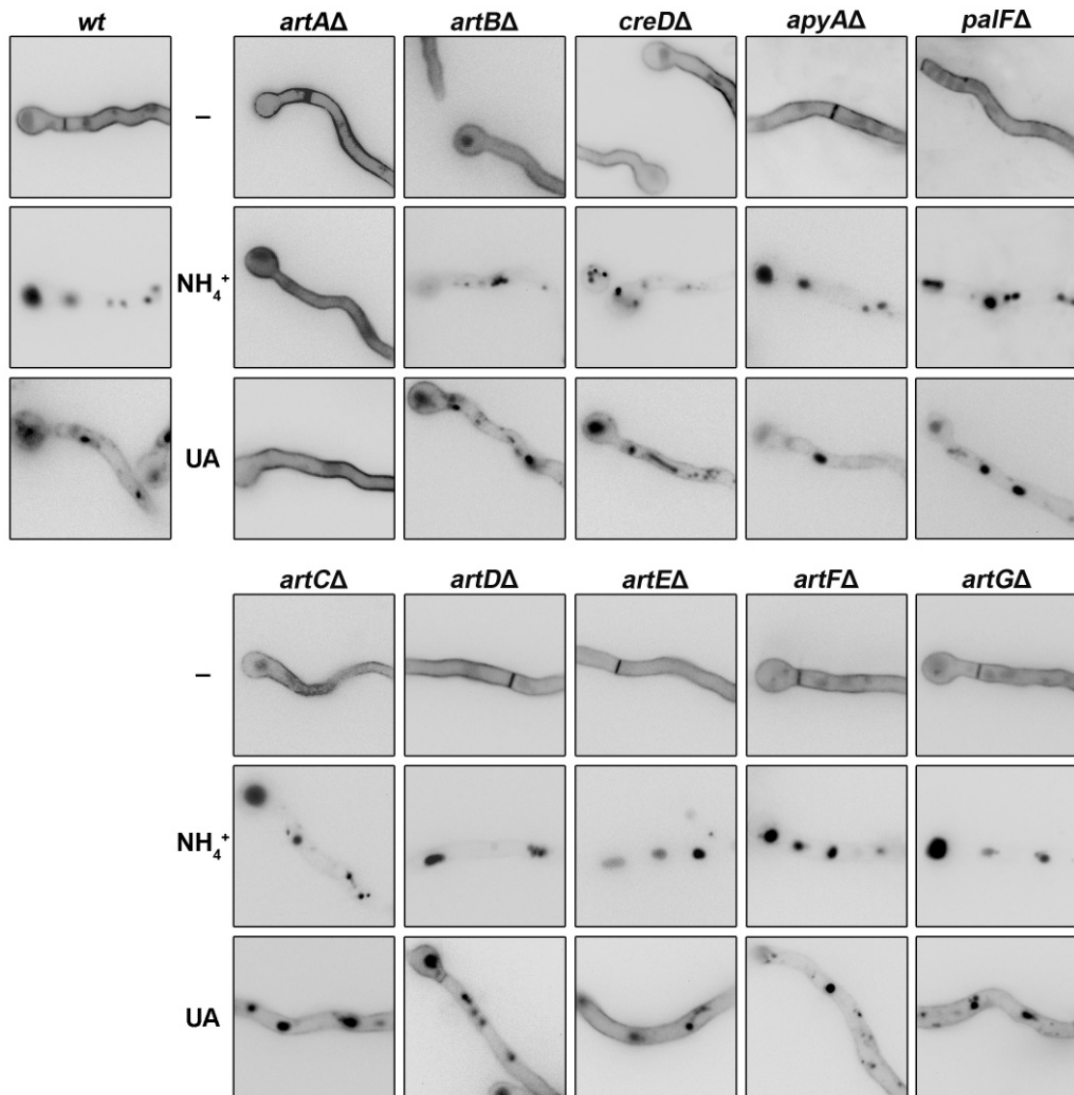
Figure 4.4. Epifluorescence microscopy of UapA-GFP subcellular localization under non-endocytic (-) or endocytic conditions (NH$_4^+$ or UA) in isogenic arrestin null mutants. Microscopy was performed by S. Amillis and the author.

We examined the effect of NH$_4^+$ or excess substrate into already synthesized UapA-GFP or to *de novo* made UapA-GFP in *artA$^+$* and *artA*Δ isogenic strains. In the first case, *alcA$_p$*-UapA-GFP expression was induced (4–6 h) in the presence of fructose/ethanol, then repressed by addition of glucose (1 hour), prior to ammonium or substrate addition. In the second case, ammonium or substrate was added to

cultures in which $alcA_p$-UapA-GFP expression was repressed by glucose, and then (> 30 min) UapA-GFP expression was induced by shifting the cells in fructose/ethanol (4–6 h). In both conditions the result was identical, showing that lack of a functional ArtA blocked UapA-GFP sorting into early endosomes and abolished vacuolar turnover (Figure 4.5). Early endosomes marked with UapA-GFP were identified by their unique bidirectional motility observed in an inverted microscope and co-localization with FM4-64, whereas vacuoles marked with UapA-GFP were identified by FM4-64 and CMAC (not shown).
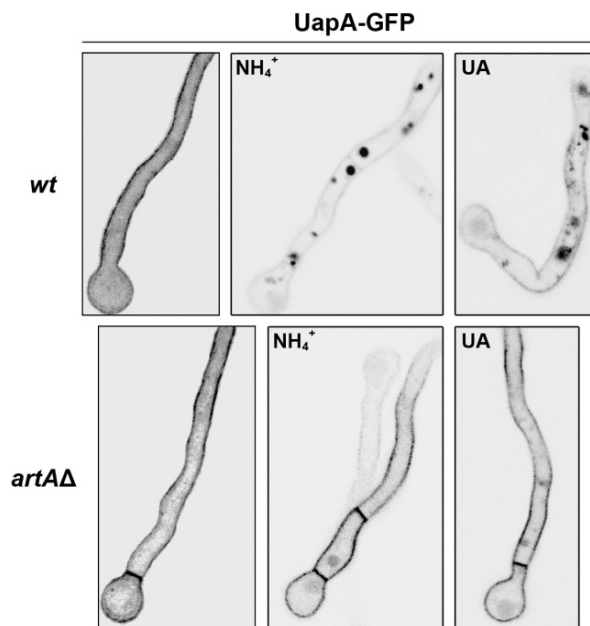
Figure 4.5. Confocal laser microscopy of UapA-GFP subcellular localization under non-endocytic (-) or endocytic conditions (NH_4^+ or UA) in isogenic $artA^+$ (wt) and $artA\Delta$ strains expressing UapA-GFP from the $alcA_p$. Microscopy was performed by G. Diallinas.

A western blot analysis confirmed that under both endocytic conditions UapA-GFP vacuolar turnover is significantly reduced in the $artA\Delta$ mutant (Figure 4.6A). Further evidence for the involvement of ArtA in UapA turnover was obtained by direct transport assays with radiolabelled xanthine. Figure 4.6B shows that, under endocytic conditions (NH_4^+), in the wild-type control ($artA^+$) the apparent xanthine uptake drops to 60%, whereas in the isogenic strain lacking ArtA ($artA\Delta$) xanthine uptake remains close to 100%. We also obtained independent *in vivo* evidence for an apparent increase in UapA activity in an $artA\Delta$ genetic background under endocytic conditions by a simple growth test using 2-thioxanthine. This xanthine analogue is

 taken-up by UapA and is metabolized to 2-thiouric acid, which inhibits a laccase necessary for the conversion of yellow to green pigment in conidiospores (Alderson and Scazzocchio, 1967; Darlington and Scazzocchio, 1967). As a result, strains expressing UapA produce yellow conidiospores in media containing 2-thioxanthine and a non-repressing nitrogen source (e.g. nitrate, L-proline). In the presence of NH_4^+, however, UapA transcription is repressed and thus 2-thioxanthine is not taken up by the cells, and consequently conidiospores remain green. In media containing NH_4^+, a strain expressing UapA from the $alcA_p$ promoter, which is not repressible by NH_4^+, shows a leaky phenotype (i.e. mixture of green and yellow spores), apparently due to NH_4^+-elicited UapA turnover. Figure 4.6C shows that in an $artA\Delta$ genetic background the effect of 2-thioxanthine is very strong even in NH_4^+-containing media, strongly suggesting that lack of ArtA reduces dramatically the turnover of UapA by endocytosis.
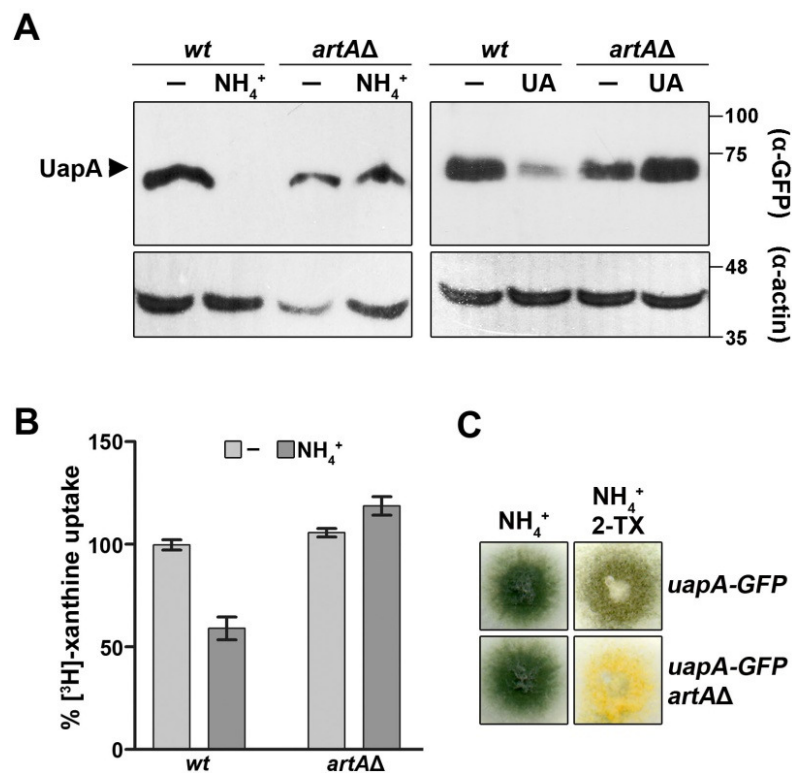
Figure 4.6. ArtA is involved in UapA endocytosis and vacuolar turnover. **A.** Western blot analysis of total protein extracts from $artA^+$ (wt) and $artA\Delta$ strains, expressing UapA-GFP from the $alcA_p$, using anti-GFP antibody. **B.** Uptake rate of ^{3}H-xanthine in $artA^+$ (wt) and $artA\Delta$ strains under non-endocytic (-) or endocytic conditions (NH_4^+). The uptake was performed by G. Diallinas. **C.** The 2-thioxanthine (2-TX) effect in $artA^+$ (wt) and $artA\Delta$ strains (see text).

4.3.3 ArtA is essential for UapA ubiquitination

We investigated whether ArtA is involved in the ubiquitination of UapA, as all evidence predicted. For that, we performed western blot analyses under conditions inhibiting the rapid de-ubiquitination of cargoes. Figure 4.7A shows that in the $artA^+$ strain the anti-GFP antibody detects a less motile form of UapA-GFP only after a relatively short shift in media containing NH_4^+ or substrate (uric acid), whereas in the isogenic $artA\Delta$ mutant such heavier forms are not visible. Similar less motile UapA-GFP-specific molecules have been previously detected and shown to correspond to UapA-GFP/ubiquitin conjugates (Gournas *et al.*, 2010). To further confirm this, we purified UapA-His molecules, through Ni^{2+} affinity chromatography, expressed in isogenic strains $artA^+$ and $artA\Delta$ and the purified UapA-His fraction was immunoblotted with His- and ubiquitin-specific antibodies (Figure 4.7B). Our results confirm that a functional ArtA is necessary for the formation of UapA-ubiquitin conjugates, similar to the need for a fully functional HulA ubiquitin ligase or the presence of Lys572 in the tail of UapA (Gournas *et al.*, 2010).
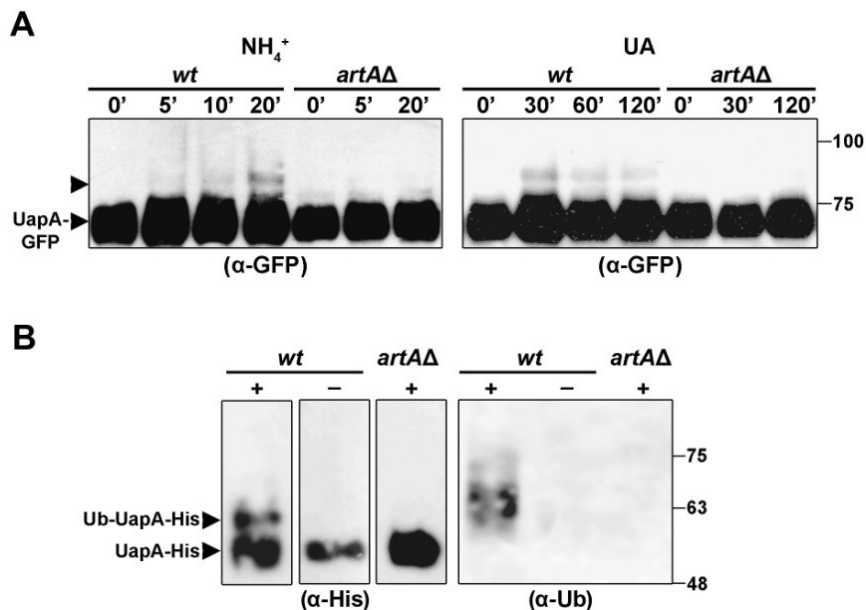
Figure 4.7. ArtA is essential for UapA ubiquitination. **A.** Western blot analysis of membrane-enriched protein extracts from $artA^+$ (wt) and $artA\Delta$ strains, expressing UapA-GFP from the $alcA_P$, under conditions detecting ubiquitination of UapA (see 2.9.7). Notice the ArtA-dependent appearance of less motile bands of UapA-GFP under endocytic conditions in membrane enriched fractions, which are not detected in the absence of a fully active HulA ubiquitin ligase ($hulA\Delta C2$) or with a UapA mutant lacking Lys572 (K572R). **B.** The less motile ArtA-dependent UapA-GFP signals can also be detected with anti-Ub antibody in purified UapA-His after 20 min treatment with NH_4^+.

4.3.4 The PY motifs are essential for ArtA function

In order to examine the function of the two canonical PPxY (PY) motives of ArtA, Ala substitutions were constructed using standard directed mutagenesis and were inserted to the genomic *artA* locus in a strain expressing UapA-GFP, through standard reverse genetics (A. Kokotos). Corresponding mutants were viable and showed wild-type growth and morphology, as expected, given that the *artAΔ* mutant shows no mutant phenotype. All mutants were analyzed microscopically in respect to $alcA_p$-UapA-GFP endocytosis by NH_4^+ or substrate. Figure 4.8A shows that Ala
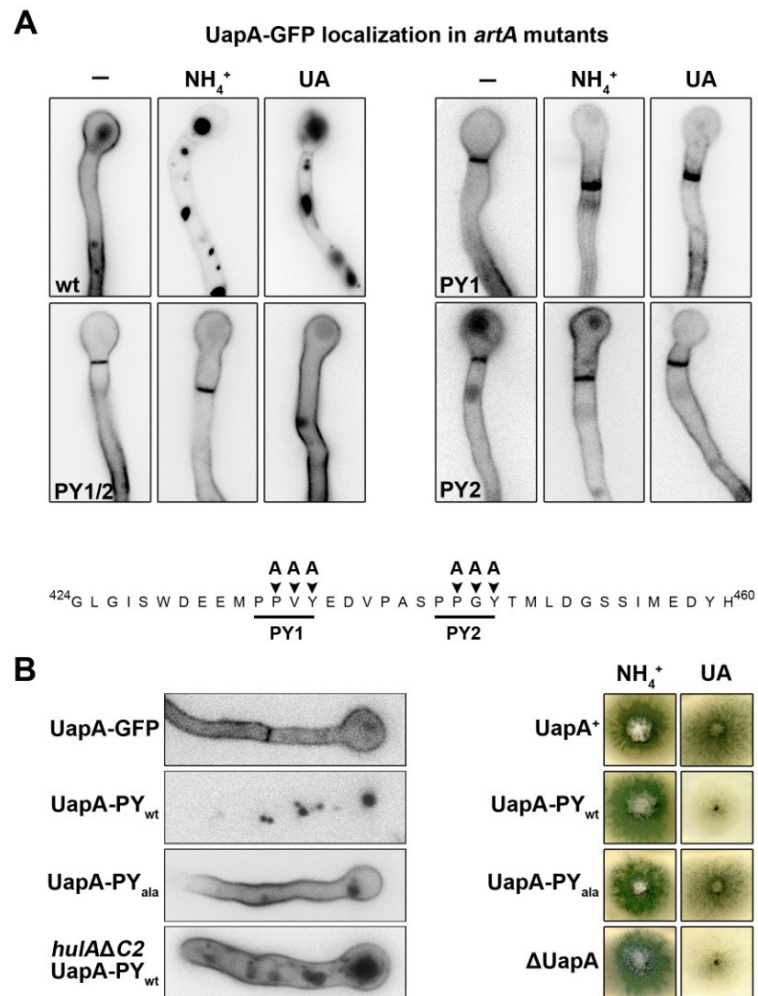
Figure 4.8. The PY motifs are essential for ArtA function. **A.** Epifluorescence microscopy of UapA-GFP subcellular localization under non-endocytic (-) or endocytic conditions (NH_4^+ or UA) in isogenic *artA* mutants expressing UapA-GFP driven under the *alcA* controllable promoter. Microscopy performed by A. Kokotos. PY1 stands for ArtA P435A/V436A/Y437A and PY2 for ArtA P445A/G446A/Y447A. **B.** Epifluorescence microscopy of UapA-PY$_{wt}$ and UapA-PY$_{ala}$ chimeras under non-endocytic conditions in *hulA$^+$* and in a *hulAΔC2* background, and UapA-mediated growth of the corresponding strains on UA as sole nitrogen source (performed by. M. Evangelinos).

substitutions of either one of the two PY motives (PY1 or PY2) totally blocked UapA endocytosis. *In vivo* evidence supporting the functionally essential role of the two PY motives was obtained using the 2-thioxanthine sensitivity test (not shown).

We obtained additional evidence that the PY motives are necessary and sufficient for HulA-dependent ubiquitination and turnover of UapA by constructing and analyzing mutants (M. Evangelinos) expressing chimeric fusions of UapA with a conserved 38-amino-acid sequence of ArtA including the two PY motives, either in their wild-type (UapA-PY$_{wt}$) or in a mutated version (UapA-PY$_{ala}$). Figure 4.8B shows that UapA-PY$_{wt}$ chimera is not functional (lack of growth on uric acid) due to constitutive targeting to the vacuole, whereas UapA-PY$_{ala}$ or UapA-PY$_{wt}$ expressed in a *hulAΔC2* background are functional, showing normal targeting to the PM.

The essentiality of the PPxY for ArtA-mediated UapA endocytosis was directly confirmed by western blot analysis. Unlike the result obtained in *artA*[+] genetic background, UapA-GFP protein steady state levels were not reduced in the presence of either NH$_4$[+] or uric acid, an observation also associated with low level of UapA-GFP vacuolar turnover, similar to the level obtained under non-endocytic conditions, as judged by the low amount of free GFP detected (Figure 4.9A). The requirement of the PPxY motives for HulA-dependent UapA ubiquitination was subsequently shown by an independent western analysis where no UapA-Ub conjugates could be detected in the strain expressing the *artA* allele mutated in its PPxY elements (Figure 4.9B).
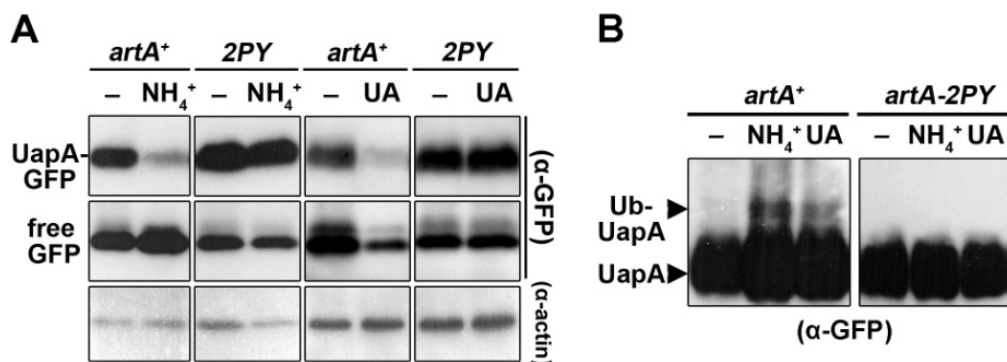
Figure 4.9. A. Western blot of total protein extracts of a wt (*artA*[+]) and an *artA* mutant strain carrying both PY1 and PY2 substitutions (2PY), expressing UapA-GFP under non-endocytic (-) or in the presence of UA or NH$_4$[+] for 2 h. **B.** Western blot analysis of UapA-GFP ubiquitination in membrane enriched fractions of a wt (*artA*[+]) and an ArtA-2PY strain, grown under endocytic (30 min, NH$_4$[+]) or control conditions.

4.3.5 HulA-dependent ubiquitination of ArtA at Lys343 is critical for ArtA function

We investigated whether ArtA itself is ubiquitinated and whether this has a role on UapA endocytosis. Figure 4.10 shows that anti-GFP antibody detects less motile forms of ArtA-GFP, which probably correspond to ArtA-ubiquitin conjugates. The steady state levels of ArtA-ubiquitin conjugates seemed moderately increased in response to NH_4^+, compared to control conditions or in response to substrates.
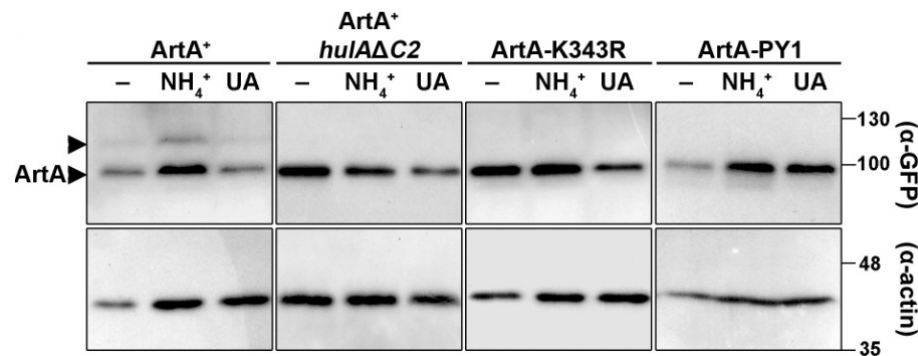
Figure 4.10. HulA-dependent ubiquitination of ArtA at Lys-343 is critical for ArtA function. **A.** Western blots of total protein extracts of isogenic wt, *hulAΔC2* and *artA* mutants PY1 and K343R under non-endocytic (-) or endocytic conditions (NH_4^+ or UA).

The increase in ArtA ubiquitination levels in response to the presence of NH_4^+ for increasing periods of time was confirmed by quantitative measurements of the relative ratios of ArtA-Ub/ArtA (Figure 4.11A). We subsequently showed that the less motile forms of ArtA-GFP cross-react with anti-Ubiquitin antibody (Figure 4.11B). Finally, we showed that ArtA ubiquitination requires an interaction with a fully functional HulA ligase, as judged by the absence of ArtA-Ub forms in *hulAΔC2* genetic background or when using an ArtA mutated in its PY motives (Figure 4.10). Based on sequence alignments of ArtA and Art1, we predicted that Lys343 might be the residue acting as an acceptor of ubiquitination in ArtA. To test this, a strain expressing ArtA-K343-GFP was constructed (by A. Kokotos). Results also shown in Figure 4.10 and Figure 4.11confirm that Lys343 is indeed the acceptor residue for ubiquitination. These results show that HulA-dependent ArtA ubiquitination at a single Lys residue occurs through the involvement of its PY elements, very probably through a direct interaction with the WW motifs of HulA.

A.

	NH$_4^+$			
	−	5'	15'	30'	60'
Ub-ArtA	0.1	2.3	1.5	2.6	1.2
ArtA	27.9	32.4	31.7	27.8	18.1
Total	28.0	34.7	33.2	30.4	19.3
Ratio	0.003	0.07	0.05	0.09	0.07

Figure 4.11. A. Time-course (left) and ImageJ semi- quantitative estimation (right) of NH$_4^+$-dependent increase in ArtA ubiquitination. **B.** Western blots of immunoprecipitated ArtA-GFP and ArtA-K343R-GFP under denaturing conditions in the presence (60 min, NH$_4^+$ or substrate) or absence (-) of endocytic stimuli, probed with anti-GFP (left panel) or anti-ubiquitin (right panel) antibodies. CoIP was performed by S. Amillis.

To investigate the role of ArtA ubiquitination, a strain expressing UapA-GFP in an ArtA-K343R genetic background was constructed (by A. Kokotos). In this strain, mutation ArtA-K343R severely inhibited UapA endocytosis, in response to both NH$_4^+$ and substrates (Figure 4.12). Western blot analysis showed that ArtA-K343R is a practically loss-of function mutation in respect to UapA turnover, as intact UapA-GFP levels remain high under endocytic conditions.
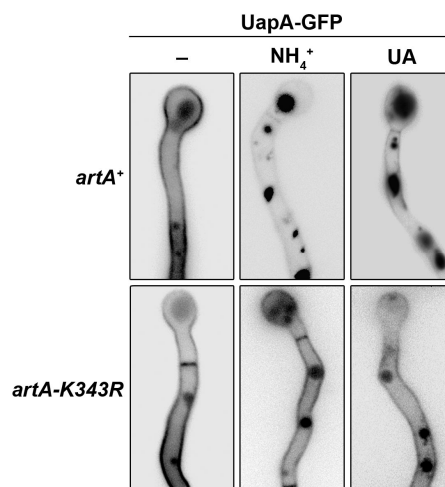
Figure 4.12. Role of ArtA ubiquitination in UapA endocytosis and turnover. Epifluorescence microscopy of UapA-GFP subcellular localization under non-endocytic (-) or endocytic conditions (NH$_4^+$ or UA) in a wt or an ArtA-K343R mutant expressing UapA-GFP.

In addition, the ratio of intact UapA-GFP/free vacuolar GFP is significantly higher, compared to the ratio found in an *artA*$^+$ background (Figure 4.13A). Notably, however, some UapA-GFP turnover was observed in the ArtA-K343R background, suggesting that ArtA ubiquitination is critical, but not absolutely essential for some UapA turnover. This observation was in agreement with a subsequent Western blot analysis showing that, although UapA ubiquitination is significantly reduced in an ArtA- K343R mutant, some minor fraction of UapA can still be ubiquitinated (Figure 4.13B).
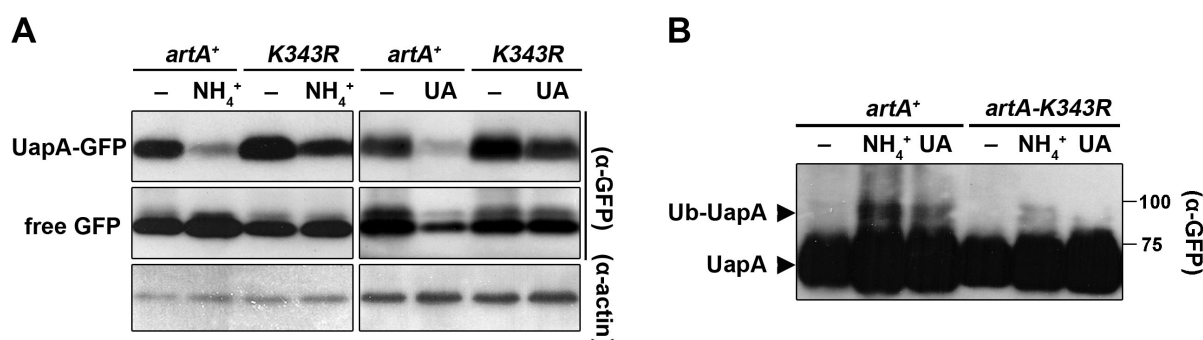
Figure 4.13. A. Western blot of total protein extracts of a wt (*artA*$^+$) and ArtA-K343R mutant strain, expressing UapA-GFP under non-endocytic conditions (-) or in the presence of UA or NH$_4^+$ for 2 h. **B.** Western blot analysis of UapA-GFP ubiquitination in membrane enriched fractions of a wt (*artA*$^+$) and an ArtA-K343R strain, grown under endocytic (30 min) or control conditions.
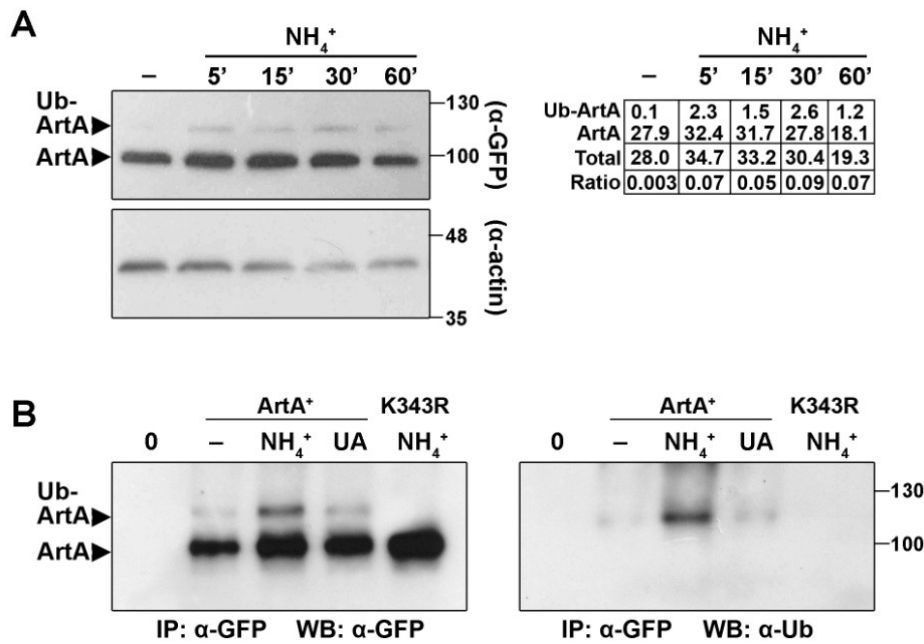
4.3.6 The C-tail of UapA contains a region essential for ArtA binding

Previous studies have shown that the UapA C-tail includes the single Lys residue (Lys572) necessary for HulA-dependent ubiquitination under endocytic conditions (Gournas *et al.*, 2010). This suggested that ArtA might interact with C-terminal region of UapA. To investigate this assumption, the C-terminal region of UapA was fused into the C-terminal region of AzgA, a purine transporter, which is fairly insensitive to NH$_4^+$-triggered endocytosis (Pantazopoulou *et al.*, 2007), and the resulting chimeric molecule was used for testing whether the UapA C-terminal region confers ArtA-dependent internalization of AzgA. Results in Figure 4.14 confirm that the UapA C-terminus promotes enhanced NH$_4^+$-elicited AzgA endocytosis and that this phenomenon is dependent on a functional ArtA protein. This strongly suggested that the C-terminal region of UapA contains a domain necessary and sufficient for ArtA binding.
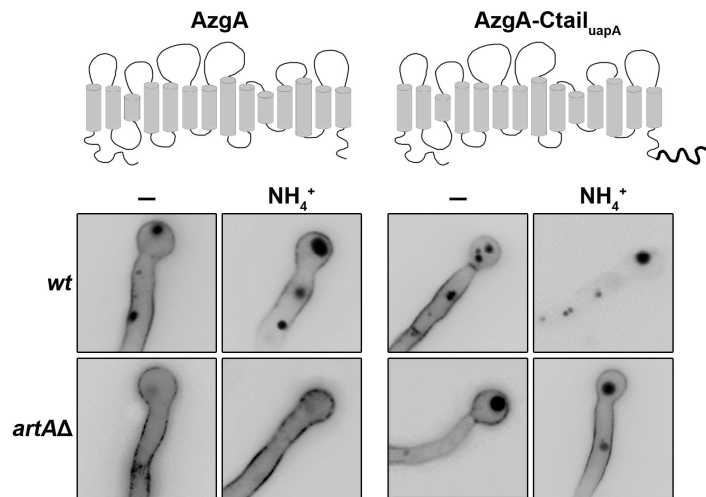
Figure 4.14. ArtA-dependent, NH$_4^+$-elicited, endocytosis of an AzgA-GFP version including the C-terminus of UapA, as shown by epifluorescence microscopy. Construction and microscopy by S. Amillis and V. Yalelis, respectively.

To further identify the region responsible for ArtA binding, we searched for UapA residues upstream from Lys572, which might prove necessary for UapA endocytosis. For this, two deletions corresponding to residues 564-571 and 547-571 (M. Evangelinos) and Ala substitutions of a di-acidic motif (E^{545}-V-E^{547}) were constructed (S. Amillis; Figure 4.15A). Microscopic analysis of corresponding mutants showed that solely the longer deletion (residues 547-571) and the mutated di-acidic motif led to a severe block of NH$_4^+$- or substrate-elicited UapA endocytosis (Figure 4.15B). Interestingly, di-acidic motives are known to be involved in membrane cargo trafficking and in particular in ER-exit or Golgi-to-vacuole transfer (Bonifacino and Traub, 2003; Renard *et al.*, 2010; Starr *et al.*, 2012), but are not known to interact with arrestin-like proteins or be related to ubiquitination of cargos. In this direction, we showed that an intact E^{545}-V-E^{547} element was necessary for UapA-GFP ubiquitination, and thus might be part of a putative ArtA binding site on the C-tail of UapA (Figure 4.15C). On the whole, our results showed that the region corresponding to residues 545-563 is required for UapA endocytosis, which in turn suggested that it might host the ArtA binding site.

4.3.7 The function of ArtA is a prerequisite for the formation of UapA-specific, SagA-dependent, pre-endocytic puncta

Considering that ArtA is involved in ubiquitination of UapA and that this modification constitutes the molecular signal for UapA endocytosis, we tested whether the effect of the *artAΔ* mutation is epistatic to a mutation blocking

endocytosis at a step downstream from cargo ubiquitination. For this, we decided to knock-out SagA (ANID_01023.1), the single End3 homologue of *A. nidulans* (38%, amino acid identity). In *S. cerevisiae,* End3 belongs to the family of proteins possessing an EH domain, members of which are implicated in endocytosis, vesicle transport, and signal transduction. End3 is part of the coat module protein complex along with Pan1, Sla1 and Sla2, otherwise known as the Pan1 complex, which acts downstream of cargo ubiquitination, but upstream of actin organization at endocytic sites (Tang *et al.*, 2000). Furthermore, End3 has been shown to be necessary for the internalization of all transporters tested up-to date.
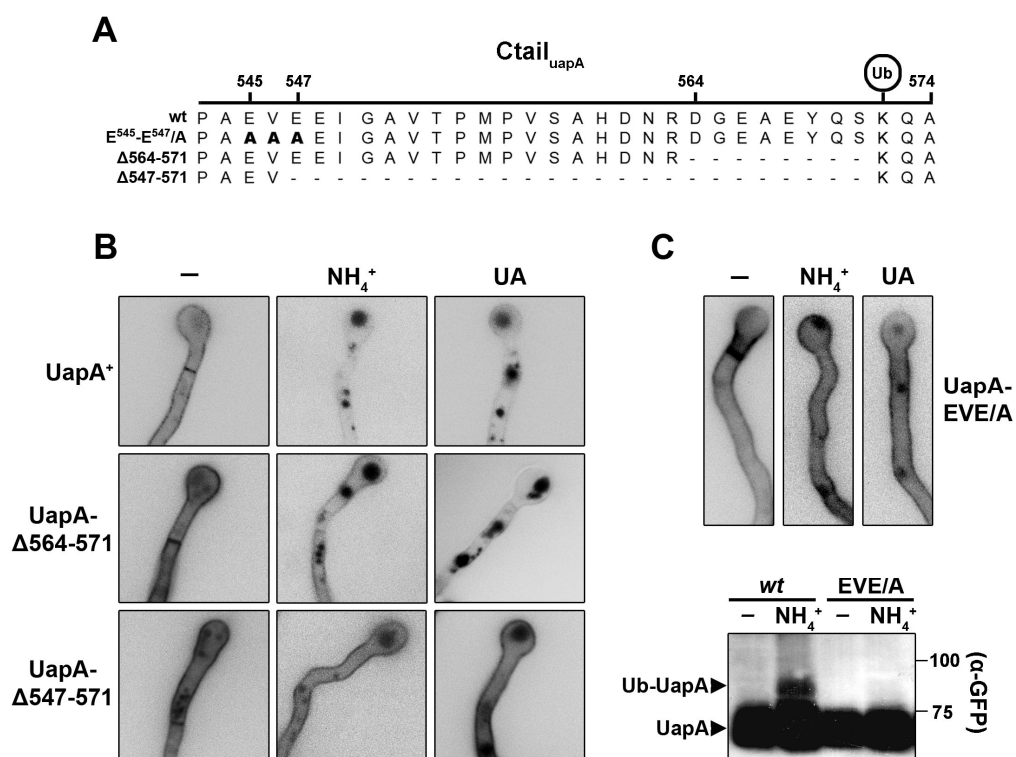
Figure 4.15. A. Schematic representation of UapA C-tail mutations analyzed for UapA endocytosis. Lys-572 acting as ubiquitin acceptor is indicated. **B.** Epifluorescence microscopy (M. Evangelinos) of UapA C-terminal truncations (Δ564–571, Δ547–571) under non-endocytic (-) or endocytic conditions (NH$_4^+$ or UA). **C.** Epifluorescence microscopy of mutation UapA-E545A/V546A/E547A (UapA-EVE/A) under non-endocytic (-) or endocytic conditions (NH$_4^+$ or UA) and western blot analysis of UapA-GFP ubiquitination in membrane enriched fractions of a wt and a UapA-EVE/A strain, grown under endocytic (30 min, NH$_4^+$) or control conditions, performed by S. Amillis.

The *sagA* gene has been genetically identified as a gene that only affects sensitivity to DNA-damaging agents (Jones *et al.*, 1999). An apparent loss-of-function mutation in *sagA* has no detectable mutant phenotype other than an increase in DNA alkylating agent sensitivity. A knock-out *sagA* mutant constructed for this work (by S. Amillis) had a moderately delayed rate of growth and increased

resistance to neomycin (Figure 4.16A). It also displayed a moderate defect in polarity maintenance, as evidenced by the increased bipolarity and early branching, as well as the partial loss of apical deposition of cell wall polysaccharides detected by staining with Calcofluor white (Figure 4.16B). Moreover, *sagA* proved to be essential for UapA endocytosis, as seen by western blot of UapA-GFP expression in the *sagA∆* mutant, under endocytic conditions. This is consistent with the production of yellow spores in the deletion mutant, in media containing NH_4^+ as a nitrogen source and 2-thioxanthine (Figure 4.16C; for details in 2-thioxanthine effect see 4.3.2). Finally, a functional GFP-tagged SagA protein showed punctuate cortical subcellular topology (Figure 4.16D), typical of other endocytic markers (Araujo-Bazán *et al.*, 2008).
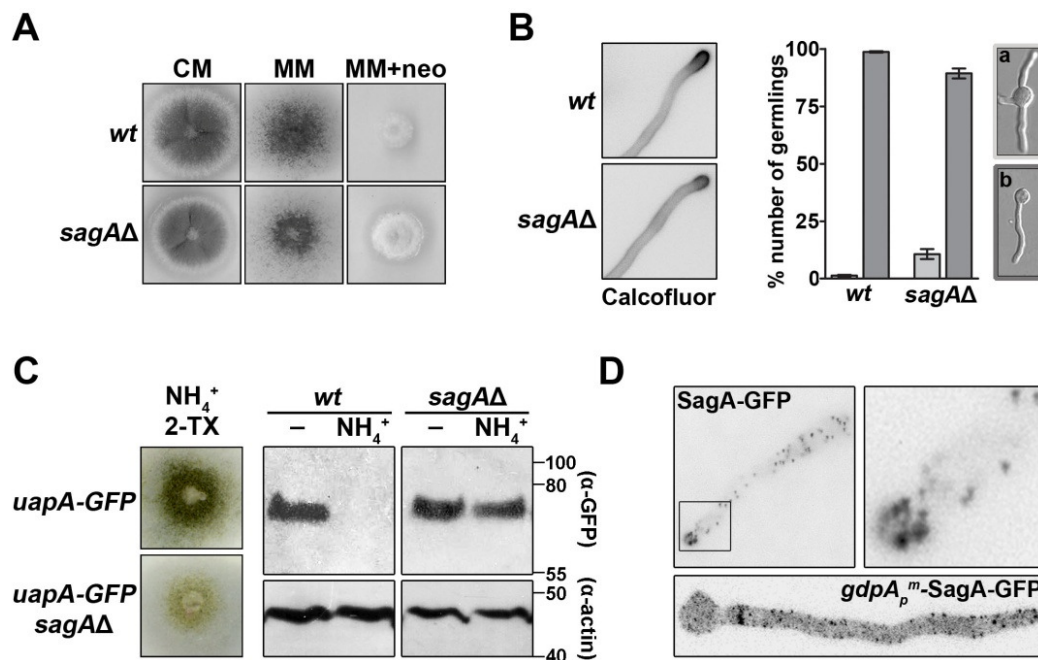
Figure 4.16. A. Growth tests at 37°C of the *sagA∆* mutant, showing a moderately delayed rate of growth at complete (CM) and minimal media (MM) and increased resistance to neomycin, as compared to the wild-type (performed by G. Diallinas). **B.** Epifluorescence microscopy (*left panels*) of the *sagA∆* mutant, displaying reduced apical deposition of cell wall polysaccharides compared to the wild-type, as evidenced by staining with Calcofluor white. *Right panels:* Quantitative analysis of the frequency of appearance of the bipolar and/or early branching phenotype (a) compared to the normal phenotype (b) in *sagA∆* and wild-type strains, observed under the microscope (Nomarski). **C.** *Left panels:* The 2-thioxanthine (2-TX) effect in *sagA⁺* (wt) and *sagA∆* strains. *Right panels:* Western blot analysis of UapA-GFP expression in the *sagA∆* mutant, under non-endocytic (-) or endocytic conditions. **D.** Epifluorescence microscopy (performed by S. Amillis and G. Diallinas) of the subcellular localization of SagA-GFP showing punctuate cortical subcellular topology, driven by the native and *gpdAₚᵐ* promoter.

We compared UapA-GFP subcellular localization in *artAΔ*, *sagAΔ* or *artAΔsagAΔ* null mutants by constructing the appropriate isogenic strains. Figure 4.17 shows that upon imposing an endocytic signal, either by NH_4^+ or substrates, there was a clear difference in the PM localization of UapA-GFP in the wild-type and in *artAΔ*, *sagAΔ* or *artAΔsagAΔ* mutant backgrounds. In wild-type, as expected, UapA-GFP was internalized into mobile structures, apparently early endosomes, and sorted to the MVB/vacuole for degradation. As a consequence the amount of UapA-GFP remaining in the PM was reduced. In the *artAΔ* mutant UapA-GFP remained stable in the PM, marking the periphery of cells in a relatively homogeneous manner, similar to the picture obtained in all three strains under non-endocytic conditions.

In the *sagAΔ* mutant, under endocytic conditions, UapA-GFP remained largely in or close to the PM, but in contrast to *artAΔ*, it also formed very distinctive cortical foci. Using an inverted fluorescent microscope we noticed that these puncta, which are very probably pre-endocytic membrane invaginations, are relatively static and remain attached to the PM, in mark contrast to the mobile early endosomes, seen in the wild-type strain. In the double mutant *artAΔ sagAΔ*, UapA-GFP remained extremely stable in the PM, without forming cortical patches, similar to the single *artAΔ* mutant. This result strongly suggested that ArtA is implicated in UapA endocytosis at a step taking place in the PM, upstream of the action of SagA and the formation of pre-endocytic invaginations containing UapA-GFP.
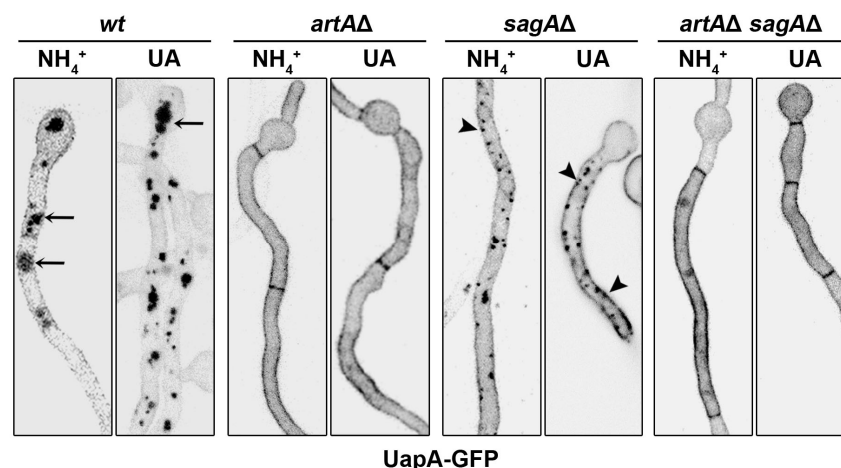
Figure 4.17. SagA and ArtA block UapA internalization at distinct steps of endocytosis. Confocal laser microscopy of UapA-GFP subcellular localization under endocytic conditions (NH_4^+ or UA) in isogenic wt, *artAΔ*, *sagAΔ* and *artAΔ/sagAΔ* strains expressing UapA-GFP.

To further confirm the above idea, we also tested whether blocking UapA ubiquitination by mutation K572R would have an effect on the formation of SagA-dependent, UapA-GFP-specific pre-endocytic invaginations. Figure 4.18 shows that, blocking UapA ubiquitination also blocked the formation of pre-endocytic invaginations containing UapA-GFP in the *sagA*Δ background. Our results confirm that UapA ubiquitination takes place in the PM rather than in an early endosomal compartment, such as early endosomes.
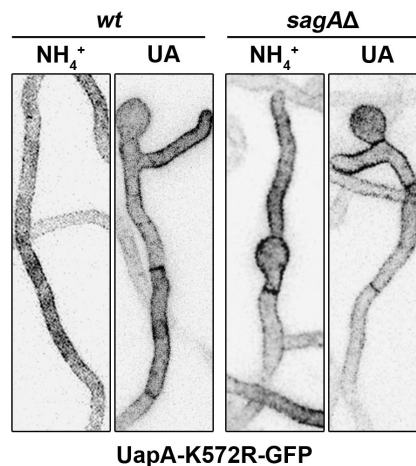
Figure 4.18. Confocal laser microscopy of UapA-K572R-GFP subcellular localization under endocytic conditions (NH_4^+ or UA) in isogenic wt and *sagA*Δ strains expressing UapA-GFP. Arrows indicate vacuoles. Arrowheads indicate immobile cortical puncta associated with the PM, only visible in the *sagA*Δ genetic background.

4.3.8 Specificity of ArtA in respect to transporter endocytosis

We finally investigated the substrate specificity of ArtA by examining what is the effect of deleting the *artA* gene on other transporters. We constructed *artA*Δ mutants expressing GFP-tagged transporters for L-proline (PrnB), L-glutamate (AgtA) or purines (AzgA), proteins that undergo NH_4^+-elicited (PrnB and AgtA; Tavoularis *et al.*, 2001; Apostolaki *et al.*, 2009) or substrate-triggered (AzgA; George Diallinas, unpublished observations) endocytosis. Notably, all these transporters belong to structurally and evolutionary distinct transporter families (Diallinas, 2008b). Figure 4.19 shows that ArtA is necessary for PrnB and AzgA endocytosis, but does not affect AgtA internalization.
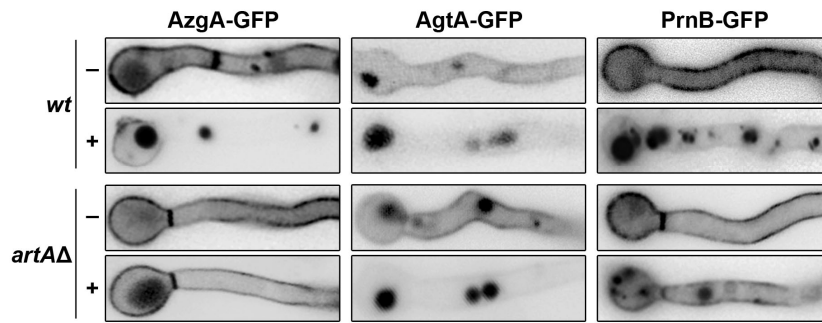
Figure 4.19. Specificity of ArtA in respect to the endocytosis of different transporter cargos. Epifluorescence microscopy of PrnB-GFP, AgtA-GFP, AzgA-GFP in *artAΔ* and *artA*[+] backgrounds under non-endocytic (-) or endocytic conditions (+). Endocytic conditions for PrnB and AgtA indicate addition of NH_4^+ and for AzgA addition of substrate (hypoxanthine) for 2 h. AgtA-GFP consistently gives a lower fluorescent signal compared to the other transporters tested. Notice that, unlike UapA-GFP or AzgA-GFP, AgtA-GFP and PrnB-GFP show a degree of constitutive turnover (appearance of GFP-labelled vacuoles) under non-endocytic conditions. For AgtA, this was recently shown to occur by direct sorting from the Golgi to the vacuole (Sotiris Amillis, unpublished observations). Constructions and microscopy were performed by V. Yalelis (PrnB-GFP) and the author (AgtA-GFP and AzgA-GFP).

5

Oligomerization of UapA
& its Role in Membrane Trafficking
& Endocytosis

5.1   State of the art

Efficient binding and transport of substrates are prerequisites for substrate-elicited endosomal sorting of UapA (see also 4.1; Gournas *et al.*, 2010). However, in the course of previous epifluorescence microscopic analyses of our group, it has been shown that PM–embedded inactive versions of UapA-GFP are internalized by uric acid in the presence of active untagged UapA molecules (Figure 5.1). This phenomenon of *in trans* endocytosis occurs even when the active UapA molecules themselves cannot be endocytosed, such as the UapA-K572R mutant. A possible explanation that has been proposed is the association of UapA molecules in an oligomeric complex (Gournas *et al.*, 2010).

The possibility of UapA existing in the membrane in the form of a dimer or an oligomer was further supported by the observation of higher molecular weight bands, migrating slower than the UapA monomers, in immunodetection experiments of the purified transporter. Moreover, those bands responded to purine induction and ammonium repression, in the same way monomeric UapA does, and were conspicuously absent in a negative control strain lacking *uapA* in its genetic

background (Njimoh Dieudonné Lemuh, George Diallinas and Dimitris Hatzinikolaou, unpublished observations). Finally, a putative oligomeric form of the transporter was observed in a denaturing gel, after several purification steps of UapA that had been heterologously expressed in *S. cerevisiae* (Leung *et al.*, 2010). In both cases, however, the constituents of the higher molecular weight bands have not been biochemically characterized.
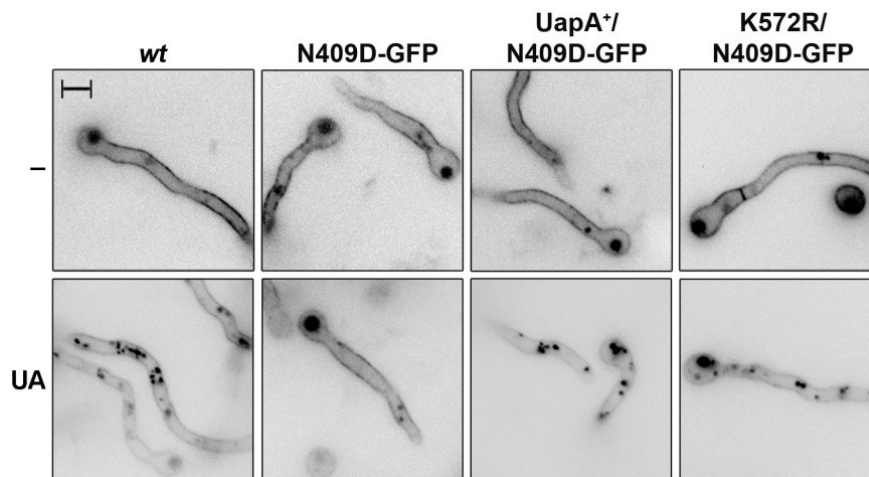
Figure 5.1. Substrate-induced endocytosis of inactive UapA molecules is triggered *in trans*. Epifluorescence microscopy of the subcellular localization of a non-functional UapA mutant (N409D-GFP) under non-endocytic (-) or endocytic conditions (UA) expressed either alone, or co-expressed with the wild-type UapA (UapA⁺) or the UapA version that cannot be ubiquitinated and thus endocytosed (K572R). Scale bar 5 μm (adapted from Gournas *et al.*, 2010).

5.2   Aim of study

The aim of this part of the study was to investigate the existence of UapA homo-oligomerization and its possible role in transporter cellular expression and/or function. UapA oligomerization was investigated by employing both indirect and direct methods, the latter including fluorescence complementation and pull-down assays. Other questions raised include the identification of the intracellular compartment in which UapA oligomeric complexes are formed and the identification of the interface involved in the interaction of the monomers. To this end, several ER-retained mutants were co-expressed with their corresponding wild-type versions and were analysed in respect to the ability of the latter to pull the former out of the ER and *vice versa*. Finally, by addressing these questions we also attempted to elucidate the involvement of oligomerization in transporter sorting, stability and endocytosis from the PM.

5.3 Results & Discussion

5.3.1 Non-functional UapA mutants have an apparent dominant-negative effect on wild-type UapA

Preliminary evidence for UapA oligomerization was obtained by investigating the possibility of mutant transporter molecules, devoid of uptake activity, to confer a dominant-negative effect on wild-type transporter function *via* their functional association. Asn409 is an absolutely essential amino acid for UapA transport activity *per se*. For example, mutant N409D does not exhibit detectable uptake activity, despite the fact that the protein is properly targeted to the PM, as evidenced by epifluorescence analysis (Koukaki *et al.*, 2005) and is capable of substrate binding (Papageorgiou *et al.*, 2008). To test the effect of this non-functional mutant version of UapA on wild-type UapA, the two UapA forms were co- expressed and [^{3}H] xanthine uptake assays and growth tests were performed under inducing conditions. In particular, a plasmid carrying *alcA$_p$-uapA-N409D* was generated (designated pAN510$_{exp}$:alcA-N409D; for details on the construction of this plasmid see 8.2) and was transformed in a *uapAΔ::uapA-GFP uapCΔ::pyrG^{Af} azgAΔ pabaA1 argB2 pantoB100* strain of *A. nidulans*. The growth of several transformants selected for arginine prototrophy, on minimal media with uric acid as the sole nitrogen source, under conditions inducing *alcA$_p$-uapA-N409D* expression, was significantly reduced compared to that of an isogenic control strain that does not express the mutant UapA version. Kinetic analysis of a selected transformant revealed an almost 50% decrease in uptake capacity as compared to that observed in a strain expressing the UapA-GFP alone (Figure 5.2).
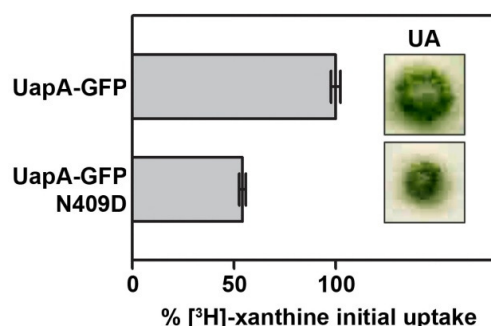
Figure 5.2. Radiolabelled [^{3}H]-xanthine (0.2 mM) uptake capacity, expressed as % initial uptake rate, and growth test comparing UapA-GFP activity in the absence and presence of UapA-N409D. In order to maximize the effect, the mutant UapA version was highly expressed *via* the *alcA$_p$* promoter. Results shown represent averages of several experiments, each experiment carried out in triplicate, with standard deviation <20%. Strains were grown on *alcA$_p$*-inducing minimal media, at 25°C.

One explanation of the apparent dominant-negative effect of the non-functional UapA on the wild-type transporter could be the formation of oligomeric complexes between wild-type and mutant proteins in the PM. This hypothesis is compatible with the idea of UapA homo-oligomerization and suggests that at least some of UapA molecules function as oligomers. A dominant-negative effect on transport activity has been reported in mammalian cells co-expressing mutant and wild-type forms of the dopamine transporter (DAT). In that case, loss-of-function mutant transporters that were targeted to the cell surface inhibited wild-type DAT uptake activity without affecting the membrane targeting of the latter (Torres *et al.*, 2003).

The effect of UapA-N409D on wild-type transporter activity is unlikely to be due to a decrease in the transcriptional expression levels of the latter, since the two UapA versions were expressed under different promoters and thus their transcriptional regulation was independent. Nevertheless, one could not exclude the possibility that the two UapA versions compete for PM sorting; thus, increased accumulation of the mutant molecules might indirectly lead to reduced translocation to the PM of the wild-type UapA, this being the cause of the reduction in growth and substrate uptake.

5.3.2 *In trans* endocytosis of non-ubiquitinated UapA versions

The observation of *in trans* endocytosis of inactive UapA molecules in the simultaneous presence of the UapA-K572R mutant, which cannot be ubiquitinated and thus internalized (Gournas *et al.*, 2010), prompted us to investigate the fate of this mutant, in the presence of functional UapA forms. A strain carrying the *uapA-K572R-GFP* was genetically crossed with one carrying the *uapA100* mutation, a duplication of 164 bp in the promoter region of the *uapA* gene, resulting in its constitutive and increased expression (Arst and Scazzocchio, 1975; Ravagnani *et al.*, 1997). A double mutant was selected from the progeny and was examined microscopically in the presence and absence of endocytic conditions. As indicated in Figure 5.3, co-expression of UapA-K572R-GFP with wild-type UapA over-expressed *via* the *uapA100* promoter resulted in the ammonium-elicited internalization of the former and its sorting to the vacuoles (lower panels), while when this mutant was expressed alone, it was predominantly localized in the PM (upper panels). Given the absolute requirement of this Lys residue for transporter ubiquitination and eventual endocytosis (Gournas *et al.*, 2010), the hypothesis that UapA oligomerization is responsible for the phenomenon of *in trans* endocytosis was further supported.
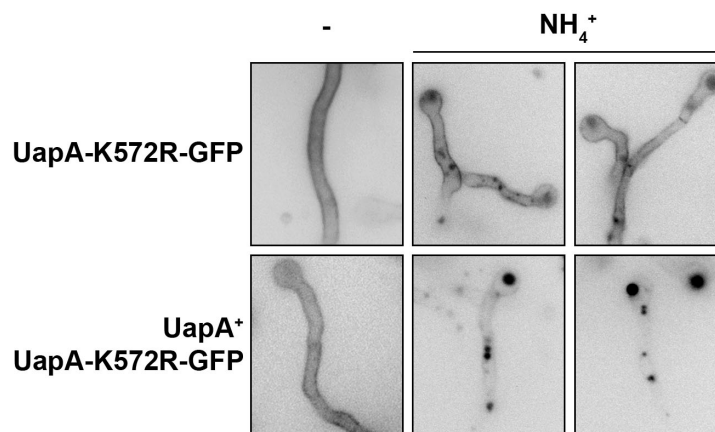
Figure 5.3. *In trans* endocytosis of a UapA mutant that cannot be ubiquitinated and thus endocytosed (UapA-K572R-GFP) due to its co-expression with a wild-type UapA. In order to maximize the effect, the wild-type UapA version was highly expressed *via* the *uapA100* promoter (see text).

5.3.3 Direct biochemical evidence for UapA oligomerization

To provide further evidence for homo-oligomerization, we performed a pull-down assay, a method commonly used to identify natural binding partners of a captured protein, using membrane protein extracts of a strain co-expressing differentially tagged UapA molecules (see 1.7.3). In particular, a strain carrying the *uapA* gene tagged C-terminally with a sequence encoding an epitope of 10 His residues (His_{10}) and expressed under the control of the strong regulatable promoter *alcA* was genetically crossed with a strain carrying *uapA* analogously tagged with the GFP epitope, and also expressed from $alcA_p$. From this cross we obtained a strain expressing simultaneously UapA-His and UapA-GFP (see later in Figure 5.8).

Total membrane proteins were prepared from this strain and solubilised with 1% DDM, which is the optimal concentration for UapA solubilisation, based on previously performed solubilisation assays (Lemuh *et al.*, 2009). The protein sample was purified with the use of a Ni-NTA column under non-denaturing conditions and the fractions obtained were resolved electrophoretically in an SDS polyacrylamide gel. Silver staining of the eluted fractions at 250 mM and 350mM imidazole showed a major band at ~55 kDa, which very probably corresponds to monomeric UapA-His (Figure 5.4A). The same analysis also showed the existence of other minor bands of slower mobility. Western blot analysis with anti-His antibody confirmed the identity of the major 55kDa band as being specific to UapA-His, and also showed that a minor band migrating close to the 100 kDa marker, is also UapA-His specific. In addition, in the f_{250} fraction, a very high molecular weight band (> 180kDa), was also detected as being UapA-His specific. The higher molecular weight bands observed in these

immunoblots might be oligomers or aggregates of UapA. Notably, pure monomeric UapA-His displayed higher electrophoretic mobility than the one predicted based on its amino acid sequence (63 kDa), which is a common phenomenon among purified hydrophobic proteins (Raunser *et al.*, 2006; Lemuh *et al.*, 2009).
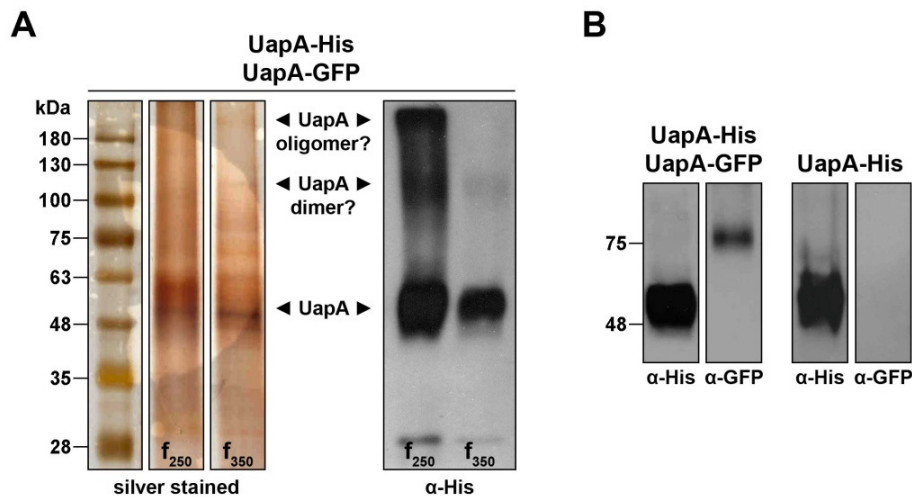
Figure 5.4. Pull down assay of membrane protein extracts from a strain co-expressing UapA-His and UapA-GFP and a control strain expressing UapA-His alone, all under the control of the *alcA$_p$*. Total membrane proteins were solubilized and applied to Ni-NTA columns. The columns were washed with increasing concentrations of imidazole (20 mM, 50 mM, 250 mM, 350 mM, 500 mM) yielding fractions f_{20}, f_{50}, f_{250}, f_{350}, f_{500}, respectively, and eluates were desalted and concentrated. Pure protein samples were resolved in reducing gels and were silver stained or immunoblotted. UapA-His eluted at 250 mM and 350mM imidazole, thus demonstrating its very strong affinity to the nickel column. **A.** Silver staining and western blot analysis of f_{250} and f_{350} obtained from the strain expressing both UapA-His and UapA-GFP. The prominent band over the 48 kDa marker corresponds to monomeric UapA-His. Two less prominent bands just over the 100 kDa and a band heavier than the 180 kDa marker are probably dimeric and oligomeric forms of UapA, respectively. **B.** Western blot analysis of f_{250} of the same strain with the anti-GFP antibody revealed that UapA-GFP co-purified with UapA-His (left panels), thus demonstrating a physical interaction between the two UapA versions, while f_{250} of the strain expressing UapA-His alone did not react with the anti-GFP antibody, as expected (right panels).

The high expression levels obtained through the *alcA$_p$* combined with the strong affinity of the His$_{10}$ epitope for Ni^{2+} (the binding strength increases with the number of His residues) enabled the development of an efficient and reproducible purification protocol for this highly hydrophobic protein. Moreover, the observation of putative oligomeric forms of UapA in reducing gels indicated that the interaction between the monomers is fairly strong. To rigorously show the physical association between UapA molecules, purified protein samples were immunoblotted with anti-GFP antibody. A prominent band migrating at the position corresponding to monomeric UapA-GFP (~75 kDa,) was detected (Figure 5.4B), thus demonstrating that UapA-GFP co-purified with UapA-His, as a result of a physical interaction between them.

5.3.4 *In vivo* evidence for UapA oligomerization

Bimolecular fluorescence complementation (BiFC), also referred to as split-YFP assay, allows the *in vivo* detection of oligomerization by ruling the reconstitution of a fluorescent protein that has previously been bisected (see 1.7.3). While biochemical methods of detection of protein-protein interactions require cell disruption and cannot guarantee that oligomers are not formed during cell lysis, the BiFC assay allows detection of oligomerization in intact living cells and with minimal perturbation of the normal cellular environment (Hu *et al.*, 2002). The rationale of using BiFC in this study, in addition to confirming UapA oligomerization, was to enable the detection of the subcellular localization of the oligomer formation.

The determination of UapA oligomerization in physiological conditions required the construction of chimeras co-expressing differentially tagged UapA molecules. Previous studies have shown that the fusion of GFP or mRFP to the C-terminus of UapA does not affect the functional properties of the transporter (Pantazopoulou *et al.*, 2007). Two forms of *uapA* were constructed bearing C-terminal fusions of either the 462 bp N-terminal part (YFP$_N$) or the 258 bp C-terminal part (YFP$_C$) of Yellow Fluorescent Protein (YFP). The generated plasmids (pAN510$_{exp}$-YFP$_C$ and pAN510$_{exp}$-YFP$_N$, respectively; see 8.2) were co-transformed in a strain lacking all major purine transporters (ΔACZ: *uapA*Δ *uapC*Δ *azgA*Δ). Transformants were selected for arginine prototrophy and e analyzed for the presence of both tagged *uapA* genes (*uapA-YFP$_C$* and *uapA-YFP$_N$*) by PCR (Figure 5.5A) and for functionality by growth tests (Figure 5.5C). The same strain was also transformed with each of the plasmids individually, and the resulting transformants were used as control strains in epifluorescence microscopy, in order to eliminate the possibility of false-positive fluorescence.

As seen in Figure 5.5B, co-expression of UapA-YFP$_C$ and UapA-YFP$_N$ resulted in co-localization of the two proteins in the PM and a positive YFP signal, similar to what was observed with UapA-GFP proteins, although devoid of any signs of constitutive degradation. YFP fluorescence was more easily detected in transformants with multiple plasmid integrations; this was reasonable since only hetero-olimers (formed by differentially tagged UapA) allow YFP fluorophore reconstitution, while monomers or oligomers, composed of either solely UapA-YFP$_C$ or solely UapA-YFP$_N$, are not microscopically visible (Figure 5.5B). In line with that, it has been reported that the fluorescence intensity produced by BiFC in living cells is generally less than 10% of that produced by intact fluorescent proteins, while the fluorescence

intensity of BiFC complexes that is produced *in vitro* is comparable to the intensity produced by intact fluorescent proteins (Hu *et al.*, 2002; Kerppola, 2006).
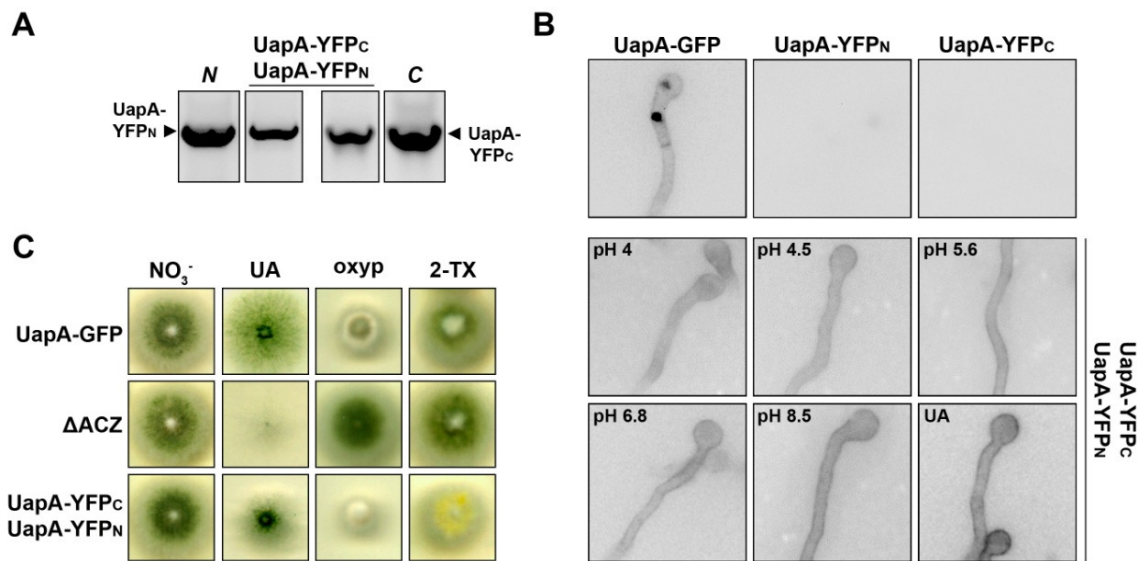
Figure 5.5. Functional UapA oligomers are present in the PM, as evidenced by BiFC analysis. **A.** Agarose-gel electrophoresis of the PCR products amplified from genomic DNA of the UapA-YFP$_C$ UapA-YFP$_N$ transformant, confirming the successful integration of both *uapA-YFP$_C$* and *uapA-YFP$_N$* constructs. Amplifications from plasmids pAN510$_{exp}$-YFP$_N$ (*N*) and pAN510$_{exp}$-YFP$_C$ (*C*) were used as positive controls of the corresponding PCR reactions. The primers used were complementary to the UapA ORF and to the YFP$_N$ (left panels) or the YFP$_C$ (right panels) fragments, respectively. **B.** Growth test of the UapA-YFP$_C$ UapA-YFP$_N$ transformant, as compared to the isogenic UapA-GFP control strain and an isogenic strain lacking all major purine transporters (ΔACZ). The effects of oxypurinol and 2-thioxanthine (2-TX) were stronger on the double transformant compared to the wild-type; this observation, along with a compact phenotype on uric acid (UA), implied that UapA is over-expressed or more stable in this transformant. **C.** Epifluorescence microscopic analysis of a strain co-expressing multiple copies of UapA-YFP$_C$ and UapA-YFP$_N$ (lower panels) showed detectable fluorescence of reconstituted YFP, similar to that obtained in the UapA-GFP control strain, but labelling exclusively the PM, in all pH tested. YFP signal was slightly boosted by the increase of the pH in the growth media and was notably enhanced by the induction of UapA promoter with uric acid (UA). Strains expressing UapA-YFP$_N$ or UapA-YFP$_C$ alone did not show any fluorescence (upper panels).

Fluorescent signal was prominent in the PM at all pHs tested, although fairly increased at higher pH values, and was significantly enhanced when uric acid was used as a nitrogen source, as a result of the induction of the promoter of *uapA*. The UapA-YFP$_C$ UapA-YFP$_N$ transformant showed similar to wild-type growth on nitrate, but also on uric acid. This latter observation showed that YFP$_C$ and YFP$_N$ tags did not affect UapA function. This was further supported by the fact that UapA-YFP$_C$ UapA-YFP$_N$ transformant also accumulated other known substrates of UapA, such as the oxypurinol or 2-thioxanthine. This was apparent as reduced growth on oxypurinol (Scazzocchio *et al.*, 1982) or strong yellow pigmentation of conidiospores on 2-

thioxanthine (Alderson and Scazzocchio, 1967; Darlington and Scazzocchio, 1967; see also 4.3.2). The rather compact growth on uric acid and the strong effect of oxypurinol or 2-thioxanthine further suggested that in the UapA-YFP$_C$ UapA-YFP$_N$ transformant, UapA is very probably over-expressed or more stable (Figure 5.5C).

In the BiFC experiments described above, UapA-YFP expression was driven by the endogenous promoter of *uapA*, which allows continuous but low level UapA synthesis. To enable high UapA expression levels, the strong and controllable *alcA* promoter was used. In particular, plasmids carrying *alcA$_p$-uapA-YFP$_C$* and *alcA$_p$-uapA-YFP$_N$* were generated (pAN520$_{exp}$:alcA-uapA-YFP$_C$ and pBS-argB:alcA-uapA-YFP$_N$, respectively; see 8.2) and introduced in the ΔACZ strain. Co-transformants were selected for arginine and p-aminobenzoic acid prototrophy and were further analyzed for the presence of both tagged *uapA* genes by PCR and Southern blot and for functionality by growth tests and uptake assays.

Using epifluorescence microscopy, a strong YFP signal was observed, associated exclusively with the PM of the double transformant (UapA-YFP$_C$ UapA-YFP$_N$), under inducing conditions for *alcA$_p$,* (0.1% Fructose, ethanol; Figure 5.6A). In
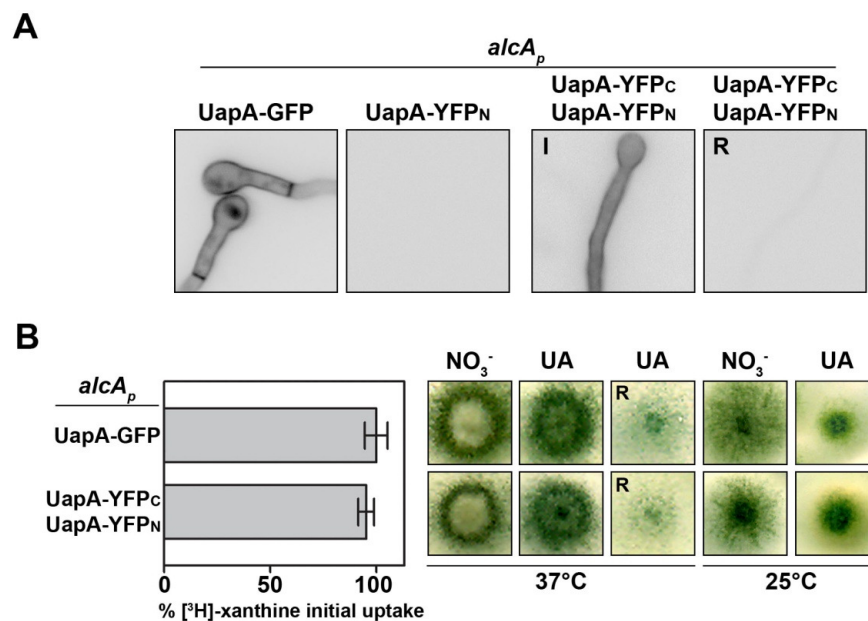
Figure 5.6. Functional expression of split-YFP-tagged UapA, driven by the *alcA$_p$*. **A.** Epifluorescence microscopic analysis of a control strain expressing UapA-GFP and a strain expressing UapA-YFP$_N$ only, both grown on *alcA$_p$*-inducing minimal media (left panels). Panels on the right display the presence and absence of fluorescence originating from YFP reconstitution in a strain expressing both UapA-YFP$_C$ and UapA-YFP$_N$ under inducing (I) and repressing (R) conditions, respectively. **B.** Radiolabelled [³H]-xanthine (0.2 mM) uptake capacity of the UapA-YFP$_C$ UapA-YFP$_N$ and an isogenic UapA-GFP control strain, expressed as % initial uptake rate. Results shown represent averages of several experiments, each carried out in triplicate, with standard deviation <20%. On the right, growth tests of the corresponding strains on *alcA$_p$*-inducing or repressing (R) minimal media, at 37°C and 25°C.

contrast, in the same strain, under repressing conditions (1% Glucose), there was no detectable YFP fluorescence. In addition, a strain expressing solely UapA tagged with YFP$_N$, the YFP fragment containing the tripeptide that ultimately forms the YFP fluorophore (Ghosh *et al.*, 2000), also did not show any fluorescence. This is consistent with previous observations of Takeshita *et al.* (2008) showing lack of fluorescence in strains expressing solely one of the YFP fragments in *A. nidulans* strains. The double transformant displayed a growth pattern similar to that of the control strain, which was also under the *alcA$_p$* control. Both strains showed a compact phenotype when grown on inducing minimal media with uric acid as a sole nitrogen source, at 25°C, as expected for strains over-expressing UapA or with more stable protein (Figure 5.6B). In agreement with this, the UapA-YFP$_C$ UapA-YFP$_N$ transformant showed very similar radiolabelled xanthine uptake capacity compared to a standard isogenic UapA-GFP control strain (Figure 5.6B).

5.3.5 Evidence that ER-retained mutants do not oligomerize

Transporters are co-translationally synthesized in the ER and traffic by a canonical vesicular, COPII-dependent transport through the *cis*-, medial and *trans*-Golgi before reaching the PM. A major question to ask was at which step of the exocytic process does UapA oligomerization take place? Answering this question was expected to assist in identifying the physiological role of UapA oligomerization. Our group has available several UapA-specific mutants that show complete or partial retention in the ER membrane, the latter being usually also associated with increased vacuolar turnover. In order to investigate the subcellular site of UapA oligomerization, three different mutants with impaired transport to the PM were examined using the BiFC assay. The rationale for selecting these mutants for further studies is outlined below.

i) An N-terminal motif necessary for ER exit

In the course of a systematic mutational analysis of the amino terminal region of UapA, a motif, G^{40}LIGDYDY^{47}, conserved in all fungal UapA-like transporters (Figure 5.7A), was recognized as necessary for proper targeting in the PM, since substitution of D44, Y45, D46, and Y47 with Ala residues (abbreviated DYDY/A) led to a complete retention of the transporter in the ER and lack of growth on uric acid (Sotiris Amillis and George Diallinas, unpublished observations; Figure 5.7B and C). Di-acidic motifs found in the cytosolic domains of transmembrane proteins have been

shown to serve as ER-export signals. These signals interact with the sec23-24 complex, which is responsible for the concentrated exit of transmembrane proteins from the ER (Bonifacino and Glick, 2004; Watanabe and Riezman, 2004). Therefore, ER-retention of DYDY/A mutant could be the result of deficient interaction of UapA N-tail with the ER export machinery.

ii) A mutation affecting the topology of TMS1

Ile74, which is predicted at the cytoplasmic limit of TMS1, has been shown to be a critical residue for UapA export from the ER. Ile74 replacement with Asp led to complete ER-retention, also reflected in the inability to grow with uric acid as a sole nitrogen source (Amillis *et al.*, 2011; Figure 5.7B and C). Classical selective screens for isolating revertants have led to the isolation of solely first site-suppressors of I74D. All isolated suppressors that fully restored UapA-GFP localization concerned the replacement of the Asp74 residue with small aliphatic residues (Ala, Gly or Val) (Amillis *et al.*, 2011). This observation suggests that the presence of a hydrophobic residue is crucial for the local topology of TMS1 and thus for proper UapA folding.

iii) A mutation deleting TMS14

An in-frame deletion of a 123 bp DNA fragment (including a 63 bp intron), corresponding to TMS14 of UapA, was shown to block transport in the ER. As a result, the deletion mutant (abbreviated TMS14Δ) was unable to grow on uric acid as a sole nitrogen source (Vlanti *et al.*, 2006; Kosti *et al.*, 2012; Figure 5.6B and C). Replacement of TMS14 with the TMS14 domain from XanQ, an *E. coli* homologue of UapA, restored the localization of the chimeric molecule in the PM of *A. nidulans,* but did not restore transporter function (Vlanti *et al.*, 2006). This result showed that a heterologous 14th TMS, even if it does not restore function, it is necessary for proper UapA folding. It should be noted that the lack of the last TMS might also result in an inverted, extracellular, orientation of the C-tail of UapA (Vlanti *et al.*, 2006).

We have used the above relevant mutants to test whether lack of a specific, cytoplasm-facing N-terminal motif or partial misfolding due to locally perturbed TMS are associated with UapA oligomerization. Plasmids carrying each of the $alcA_p$-$DYDY/A$-YFP_C, $alcA_p$-$DYDY/A$-YFP_N, $alcA_p$-$I74D$-YFP_C, $alcA_p$-$I74D$-YFP_N, $alcA_p$-$TMS14Δ$-YFP_C and $alcA_p$-$TMS14Δ$-YFP_N were generated and introduced in the ΔACZ ($uapAΔ$ $uapCΔ$ $azgAΔ$) strain in pairs (pAN520$_{exp}$:alcA-DYDY/A-YFP$_C$ together with pBS-argB:alcA-DYDY/A-YFP$_N$, pAN520$_{exp}$:alcA-I74D-YFP$_C$ together with pBS-

argB:alcA-I74D-YFP$_N$ and pAN520$_{exp}$:alcA-TMS14Δ-YFP$_C$ together with pBS-argB:alcA-TMS14Δ-YFP$_N$; see also 8.2). Co-transformants were selected for arginine and p-aminobenzoic acid prototrophy and were further analyzed by Southern blot for the presence of both tagged *uapA* genes and by growth tests for functionality. Epifluorescence microscopy was then used to examine the fate of oligomerization in all three ER-retained UapA mutants. Several transformants were examined for each mutant pair with ratios of plasmid integrations (YFP$_C$:YFP$_N$) ranging from 3:1 to 1:3.

As expected, transformants co-expressing YFP$_C$- and YFP$_N$-tagged UapA mutant forms under the *alcA$_p$* (DYDY/A-YFP$_C$ DYDY/A-YFP$_N$, I74D-YFP$_C$ I74D-YFP$_N$ and TMS14Δ-YFP$_C$ TMS14Δ-YFP$_N$) did not grow with uric acid as a sole nitrogen source (Figure 5.7C). All strains selected were also tested by epifluorescence microscopy and showed no sign of YFP reconstitution (Figure 5.7B). Given the fact that ER-localized YFP reconstitution has been previously reported (Zamyatnin *et al.*, 2006), there are two possible ways to explain the absence of fluorescence; first, UapA molecules might start interacting downstream from the ER, or second, the relevant mutations might interfere with UapA oligomerization.
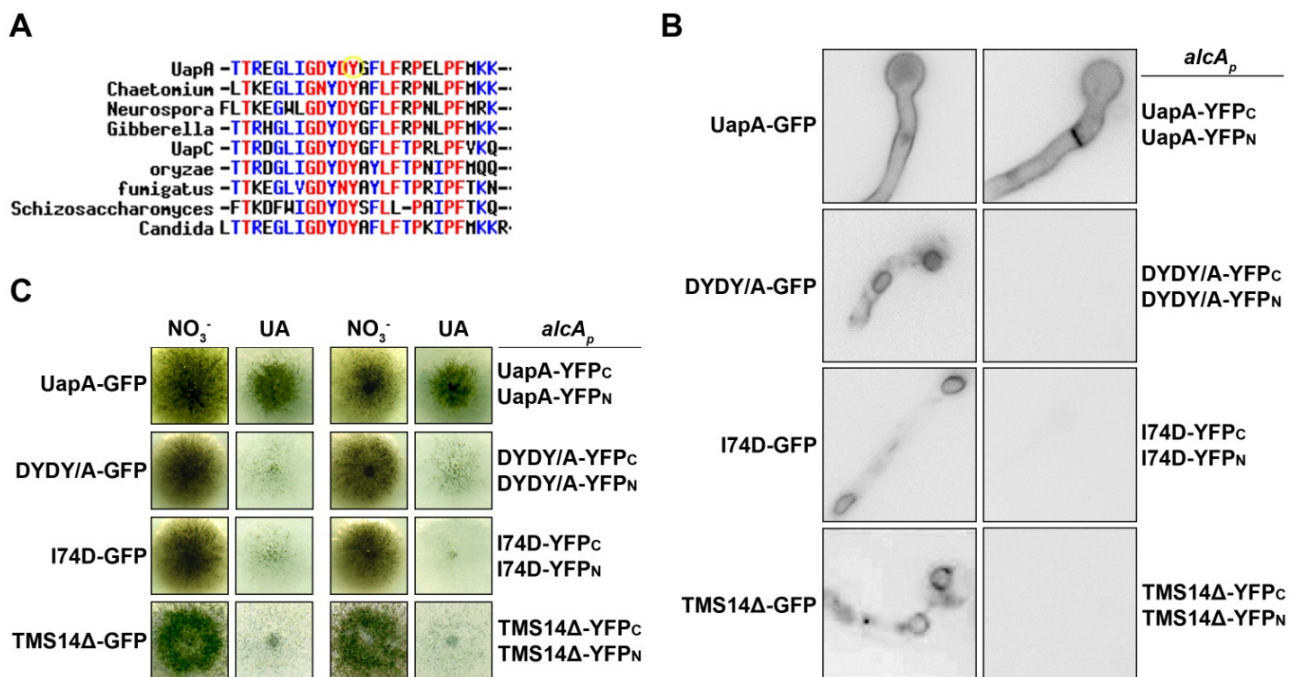
Figure 5.7. ER-retained mutants of UapA analyzed by BiFC. **A.** Sequence alignment of a part of the amino terminal region of UapA, showing conservation of the G^{40}LIGDYDY^{47} motif in fungal UapA-like transporters (performed by S. Amillis). Epifluorescence analysis (**B**) and growth tests (**C**) of strains co-expressing differentially tagged (YFP$_C$ or YFP$_N$) versions of ER-retained mutants, expressed under the *alcA$_p$*, and of their GFP-tagged versions, expressed under the endogenous UapA promoter. Strains were grown on *alcA$_p$*-inducing minimal media, at 25°C. The images of I74D-GFP and TMS14Δ are from Amillis *et al.*, 2011 and Vlanti *et al.*, 2006, respectively.

The apparent lack of YFP reconstitution in the strains expressing mutations that are very probably affecting the topology of TMS1 or TMS14, could well be due to partial disruption of the overall folding of UapA. However, lack of YFP reconstitution in the strain co-expressing the DYDY/A-YFP$_C$ with DYDY/A-YFP$_N$ is less easily rationalised due to disruption of UapA folding. In this case, the relevant mutations disrupt a highly conserved motif within the N-terminal cytoplasmic region of UapA, probably involved in transporter sorting rather than folding. This observation prompted us to investigate further, with a direct co-immunoprecipitation assay, whether DYDY/A mutants oligomerize.

Plasmids expressing the DYDY/A mutant under the control of the *alcA$_p$* and C-terminally tagged with the His$_{10}$ epitope or the GFP epitope *(alcA$_p$-DYDY/A-GFP)* were constructed (pBS-argB:alcA-DYDY/A-His and pAN520$_{exp}$:alcA-DYDY/A-GFP, respectively; see 8.2) and introduced in the ΔACZ strain. Co-transformants were selected for arginine and p-aminobenzoic acid prototrophy and the presence of both tagged *uapA* mutants was confirmed by Southern blot. As expected, DYDY/A-His DYDY/A-GFP transformants showed no growth when uric acid was used as sole nitrogen source, and when microscopically observed, they displayed the typical pattern of ER export-impaired mutants (Figure 5.8A). Moreover, an isogenic transformant expressing solely the *alcA$_p$*-driven DYDY/A-GFP (Figure 5.8A) confirmed that over-expression *via* the *alcA$_p$* did not change the phenotype observed by growth tests and epifluorescence microscopy of the original mutant (Figure 5.7).
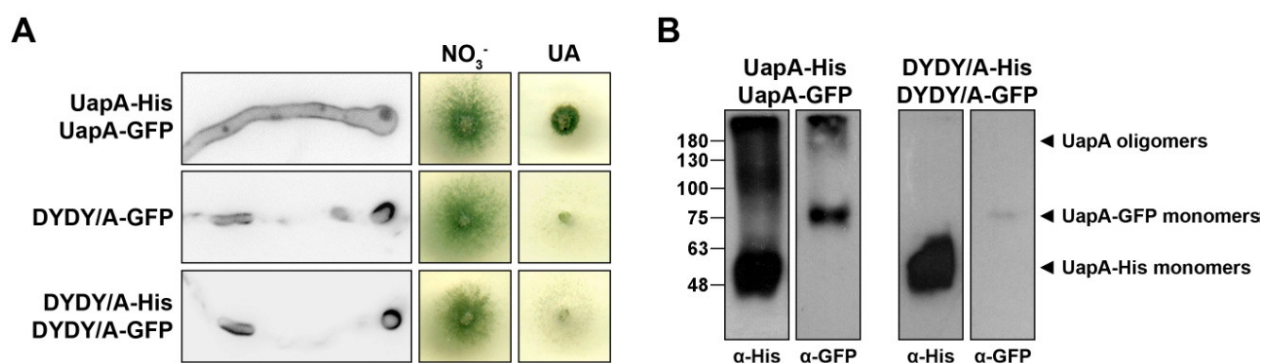
Figure 5.8. Evidence that DYDY/A mutant does not oligomerize. **A.** Epifluorescence microscopy and growth test at 25°C of the strain DYDY/A-His DYDY/A-GFP and the control strains DYDY/A-GFP and UapA-His UapA-GFP, all expressed under the control of *alcA$_p$*. **B.** Pull down assays of membrane protein extracts from strains co-expressing UapA-His with UapA-GFP (left panels) and DYDY/A-His with DYDY/A-GFP (right panels), all expressed under the *alcA$_p$*. In western blot analysis of f$_{250}$, DYDY/A-GFP in the double mutant strain, unlike UapA-GFP in the control strain, did not co-purify with the corresponding His-tagged version.

Total membrane proteins of the DYDY/A-His DYDY/A-GFP and its corresponding control strain were purified with the use of a Ni-NTA column under non-denaturing conditions and the fractions obtained were resolved electrophoretically in an SDS polyacrylamide gel. Western blot analysis of f_{250} revealed that while UapA-GFP co-purified with UapA-His in the control strain, DYDY/A-GFP reacted with the anti-GFP antibody only marginally, thus demonstrating dramatically reduced physical interaction between the two mutant versions (Figure 5.8B). Moreover, the anti-His blot of DYDY/A-GFP displayed only one prominent band, at the molecular weight of the monomer, unlike the control strain which also displayed less motile bands, probably corresponding to dimeric and oligomeric forms of the transporter. Thus, YFP reconstitution seems to be lost not only in strains expressing mutations that probably affect UapA folding through defective local topologies of specific transmembrane regions, but also due to mutations specifically blocking the ER-exit process.

5.3.6 In search of segments/residues critical for UapA oligomerization

To further understand the molecular basis of UapA oligomerization and identify domains essential for this, we tested the ability of each of the UapA ER-retained mutants studied here, to co-associate with the wild-type transporter. This strategy has been also used for the identification of the interaction interface of the human dopamine transporter (DAT) oligomers (Torres *et al.*, 2003). To this aim, we co-expressed each of the mutant forms with the corresponding wild-type partner and performed BiFC analysis. More specifically, the ΔACZ *(uapAΔ uapCΔ azgAΔ)* strain was co-transformed with pairs of plasmids, one carrying *alcA$_p$-uapA-YFP$_N$* (pBS-argB:alcA-uapA-YFP$_N$) and the other carrying *alcA$_p$-DYDY/A-YFP$_C$* or *alcA$_p$-I74D-YFP$_C$* or *alcA$_p$-TMS14Δ-YFP$_C$* (pAN520$_{exp}$:alcA-DYDY/A-YFP$_C$, pAN520$_{exp}$:alcA-I74D-YFP$_C$ and pAN520$_{exp}$:alcA-TMS14Δ-YFP$_C$, respectively). Co-transformants were selected based on arginine and p-aminobenzoic acid prototrophy and shown to display normal growth on uric acid (Figure 5.9A).

When wild-type and N-tail mutants (DYDY/A or I74D) were co-expressed, the distribution of the mutant transporter changed dramatically. In both cases, a strong fluorescent signal labelled the PM in a fashion similar to the wild-type (Figure 5.9B). Mutants were apparently able to associate with the wild-type transporter and the combination of the two forms led to a sort of "*in trans sorting*", where the presence of the wild-type enabled the trafficking of the mutant out of the ER and into the PM.

Additionally, in the DYDY/A-YFP$_C$ UapA-YFP$_N$ strain, prominent YFP signal was observed also in ring-like internal structures, typical of ER perinuclear membranes (Figure 5.9B). The perinuclear localization of those structures was confirmed by staining the nuclei with Hoechst dye and the vacuoles with CMAC (Figure 5.9C). This observation demonstrated that the mutant UapA version interfered with the normal delivery of the wild-type to the cell surface. A similar case has been described for the dopamine transporter (DAT), where DAT mutants with impaired targeting to the PM interfered with normal processing of the wild-type transporter to the PM (Torres *et al.*, 2003).
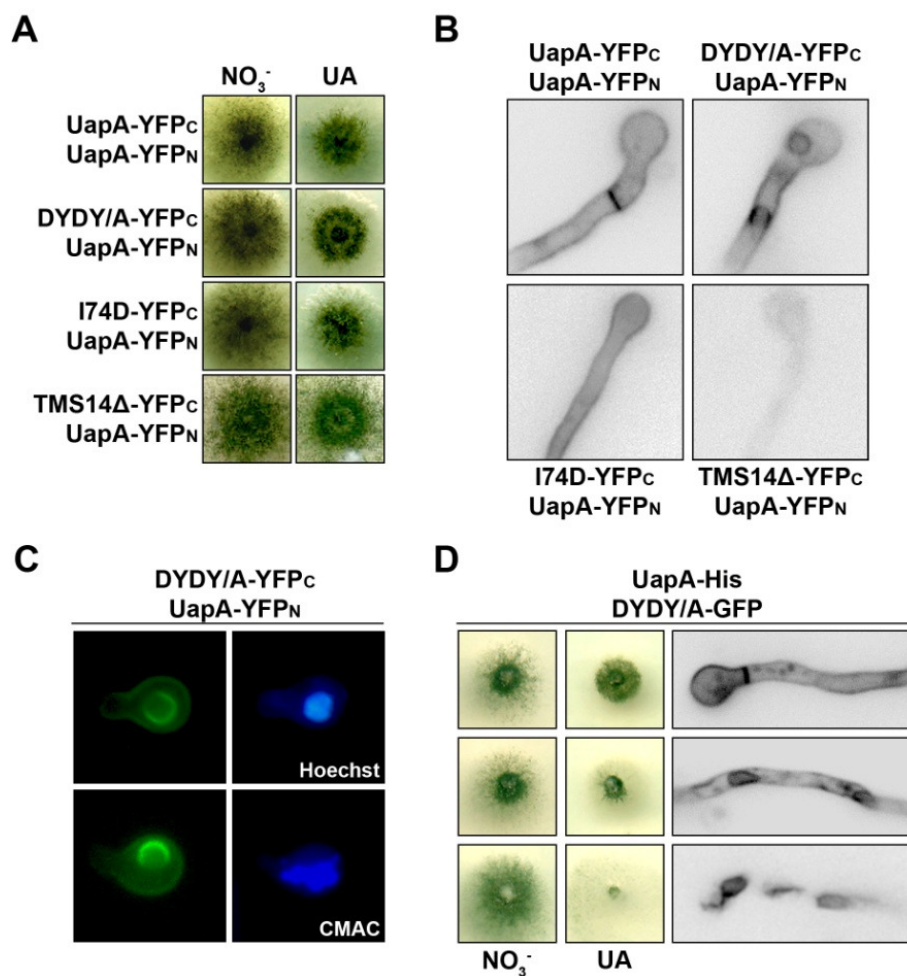
Figure 5.9. Examination of the ability of ER-retained mutants to associate with wild-type molecules. Growth tests (**A**) and epifluorescence microscopy analysis (**B**) of strains co-expressing YFP$_C$-tagged, ER-retained mutants with YFP$_N$-tagged wild-type molecules. **C**. Staining with Hoechst and CMAC dyes providing evidence that the YFP-labelled rings of the DYDY/A-YFP$_C$ UapA-YFP$_N$ strain are perinuclear, an image typical for ER membranes. **D**. Growth tests and epifluorescence microscopy of three DYDY/A-GFP UapA-His transformants. All UapA versions were expressed under the control of *alcA$_p$*. Strains were grown on *alcA$_p$*-inducing minimal media, at 25°C.

On the other hand, the deletion mutant (TMS14Δ) failed to co-associate with the full-length transporter. Although the TMS14Δ-YFP$_C$ UapA-YFP$_N$ strain displayed normal growth on uric acid, indicating that at least the wild-type UapA reached the PM, epifluorescence microscopy showed practically no fluorescence. We cannot conclude at this stage whether YFP reconstitution was blocked by the inverted orientation of the C-tail, where YFP fragments are fused, or UapA oligomerization was abolished by the lack of TMS14, which would imply that TMS14 is a part of, or indirectly affects, the interaction interface.

Finally, in order to confirm that the apparent *in trans* exocytic sorting of the DYDY/A mutant and the physical trapping of the wild-type in the ER were not dictated by the reconstitution of the YFP molecule, we repeated the experiment using the His$_{10}$ and GFP tags, instead. Interestingly, co-expression of *alcA$_p$*-driven DYDY/A-GFP with the *alcA$_p$*-driven UapA-His (pBS argB alcA-uapA-His; see 8.2), resulted in three different phenotypes, as evidenced by epifluorescence microscopy and growth tests, which possibly reflected the wild-type-to-mutant ratio of of relative expression. More specifically, DYDY/A-GFP was either localized solely in the PM and the strain exhibited normal growth on uric acid or it was localized both in the PM and the ER and the strain exhibited reduced growth on uric acid, or it was completely retained in the ER, leading to lack of growth on uric acid (Figure 5.9D). This is consistent with previous observations of Sorkina *et al.* (2003), where differential subcellular localization of the DAT transporter visualized by Fluorescence Resonance Energy Transfer (FRET) microscopy was proportional to the relative expression of each fluorescent partner.

The dominant-negative effect of the DYDY/A mutant on the targeting of the wild-type to the PM and the observation of ER-localized YFP reconstitution confirmed that oligomerization of newly synthesized UapA occurs already in the ER and suggested that proper UapA oligomerization is involved in the efficient transport of the transporter from the ER to the PM.

5.3.7 Investigating the role of TMS7 in UapA oligomerization

Within the G^{40}LIGDYDY^{47}motif, Tyr47 was found to play a key functional role. More specifically, Ala substitution of Y47 led to ER-retention of UapA (Sotiris Amillis & George Diallinas, unpublished results). Second-site suppressor mutations of Y47A were obtained and shown to map in TMS7 (V298A) and in the short, outward-facing,

α-helix linking TMS11-TMS12 (F437C). V298 is well conserved in eukaryotic NAT transporters known to be specific for nucleobases, whereas in bacterial NATs the analogous residue is more variable. F437 is also well conserved in eukaryotic NATs, but not so in bacterial homologues. The V298A mutation, which has a significant stronger suppressing effect of Y47A, was further shown to restore the sorting and PM localization of UapA-Y47A, albeit not fully (Vasillis Yalelis and George Diallinas, unpublished results). The suppressing effect of F437C on Y47A for the localization was only marginal. How mutations in central transmembrane or external α-helices restore UapA defective sorting due to mutations in a cytoplasmic N-terminal ER-exit motif, is not known.

Interestingly, in TMS7, in close proximity to the location of the V298A suppressor, we have observed the presence of a Gly-rich sequence, namely $G^{301}X_3G^{305}X_7G^{313}$, which conforms to the GX_3G motifs known to be critical for the non-covalent association of transmembrane α-helices and the stabilisation of membrane-associated dimerization and pore formation (Russ and Engelman, 2000; Fink *et al.*, 2012; see also 1.7.4). The UapA TMS7 Gly residues are well conserved in fungal NATs, but less so in mammalian homologues, and not at all in bacterial NATs. When all three Gly residues (G301, G305 and G313) were substituted by Ala, the resulting mutant (GGG/A) was retained in the ER and showed increased vacuolar turnover (Vassilis Yalelis, Sotiris Amillis and George Diallinas, unpublished results). Remarkably, mutation V298A also suppresses the ER-exit defect of UapA versions carrying G301, G305 or G313 Ala substitutions, similar to suppression of the Y47A mutation. Overall, these observations suggest the possible involvement of TMS7 in ER-exit and/or PM localization of UapA. Notably, TMS7 is predicted to be located towards the lipid phase of the PM in the UapA structure (Figure 1.19; Kosti *et al.*, 2012), an observation that favors the idea that this transmembrane segment might be part of an interface involved in UapA oligomerization, thus further linking the process of oligomerization to UapA exocytic sorting. This idea prompted us to test directly the ability for oligomerization of UapA mutants expressing a triple Ala substitution of the Gly residues in TMS7.

Plasmids expressing the *alcA$_p$-GGG/A-His* and *alcA$_p$-GGG/A-GFP* were constructed (pBS-argB:alcA-GGG/A-His and pAN520$_{exp}$:alcA-GGG/A-GFP, respectively; see 8.2) and introduced in the ΔACZ strain. Co-transformants were selected for arginine and p-aminobenzoic acid prototrophy and the presence of both

tagged *uapA* mutants was confirmed by Southern blot. As expected, transformants showed a growth phenotype similar to a negative control mutant (recipient strain ΔACZ) on uric acid as a sole nitrogen source, since mutant UapA was retained in the ER and/or sorted to the vacuoles (Figure 5.10A).

Pull down assays of total membrane proteins and western blot analysis of f_{250} revealed that a significant amount of GGG/A-GFP co-purified with GGG/A-His. In addition, apart from GGG/A-His and GGG/A-GFP monomers, prominent bands of higher molecular weight were also detected, possibly corresponding to oligomeric forms of the mutant transporter. Notably, the anti-GFP blot showed a significantly increased ratio of higher-to-lower molecular weight bands in the GGG/A mutant, compared to control strain (Figure 5.10B). These results suggest that the replacement of the Gly residues in TMS7 does not abolish oligomerization, but might affect the oligomer/monomer relative ratio of UapA, and thus impair export from the ER.
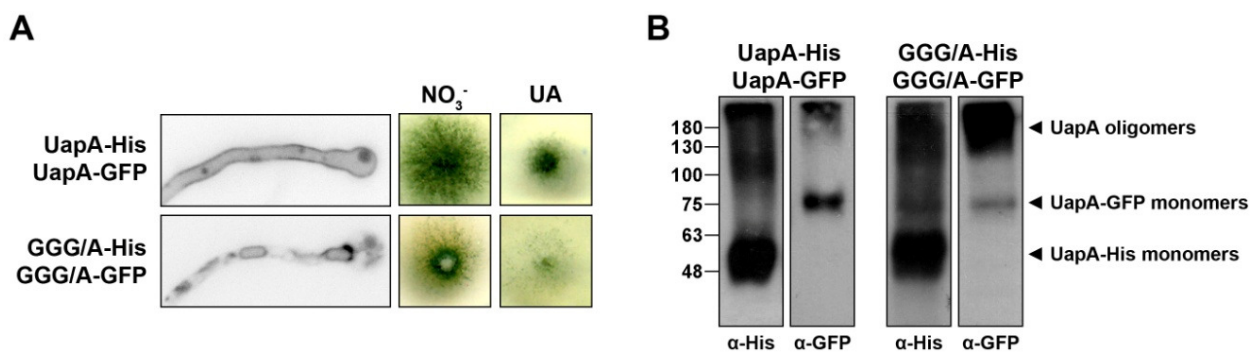
Figure 5.10. A. Epifluorescence microscopy and growth tests of the control strain UapA-His UapA-GFP, and the double mutant strain GGG/A-His GGG/A-GFP, all expressed under the control of *alcA$_p$*. Strains were grown on *alcA$_p$*-inducing minimal media, at 25°C. **B.** Pull down assays of membrane protein extracts from strains co-expressing UapA-His and UapA-GFP (left panels) or GGG/A-His and GGG/A-GFP (right panels), all expressed under the *alcA$_p$*. In western blot analysis of f_{250}, both UapA-GFP and GGG/A-GFP clearly co-purified with their His-tagged versions. Notably, the oligomer:monomer ratio of GGG/A-GFP is significantly elevated, compared to that of the control strain.

In accordance to what had been observed for DYDY/A, when GGG/A-GFP was co-expressed with the wild-type version UapA-His (both under the control of *alcA$_p$*), two phenotypes were obtained; one showing ER retention of GGG/A-GFP and lack of growth on uric acid and another showing PM labelling and ability to grow weakly with uric acid as a sole nitrogen source. Therefore, once again the wild-type appeared to have pulled the mutant version out of the ER and promoted its sorting into the PM (Figure 5.11).Thus, our results suggest that replacing the Gly residues of TMS7 with Ala has not abolished, at least, cross-oligomerization with wild-type UapA molecules.
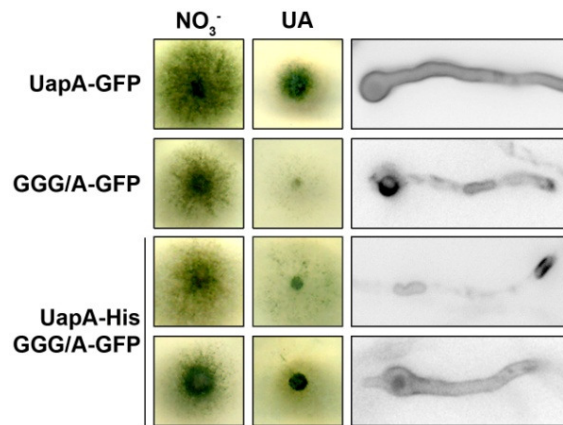
Figure 5.11. Epifluorescence microscopy and growth tests of the control strain UapA-His UapA-GFP, the double mutant strain GGG/A-His GGG/A-GFP and strains expressing both the mutant and the wild-type (UapA-His GGG/A-GFP), all expressed under the control of *alcA_p*. Strains were grown on *alcA_p*-inducing minimal media, at 25°C.

It has been reported that, although mutations changing the surface of the interface can destabilize the dimer, it is possible to restore dimerization by making compensatory changes to the opposing monomer (Lemmon *et al.*, 1992). To test the effect of one mutant transporter to the other, strains co-expressing DYDY/A-His with GGG/A-GFP or GGG/A-His with DYDY/A-GFP were generated. Interestingly, while GGG/A-GFP labelled almost exclusively the ER in the presence of DYDY/A-His, a significant fraction of DYDY/A-GFP was efficiently targeted to the PM in the presence of the GGG/A-His, in spite of some retention in the ER. However, despite the presence of the DYDY/A in the PM, the relevant strain did not show any growth on uric acid (Figure 5.12).
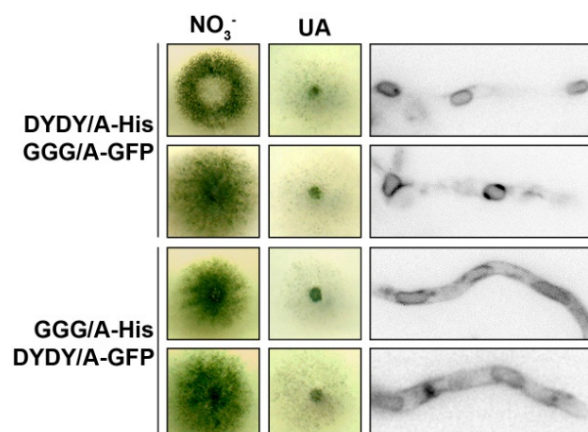
Figure 5.12. Growth tests and epifluorescence microscopy of strains co-expressing GGG/A and DYDY/A mutants, with the GFP epitope fused either to the former (upper panels) or the latter (lower panels). All mutants were expressed under the control of *alcA_p*. Strains were grown on *alcA_p*-inducing minimal media, at 25°C.

5.3.8 UapA PM oligomers dissociate upon substrate-elicited endocytosis

To test whether UapA remains oligomerized during endocytosis and sorting to the endosomal/MVB/vacuolar pathway, the PM internalization of $alcA_p$–driven UapA-YFP$_C$ / UapA-YFP$_N$ was induced by either NH_4^+ or uric acid and YFP reconstitution was observed by epifluorescence microscopy. Exposure to NH_4^+ caused sorting of YFP in endosomes, which occurred concomitantly with a decrease in PM fluorescence, similar to what was observed in the control strain (Figure 5.13A). The endosomal nature of YFP-labelled particles was supported by their co-localization with mobile FM4-64-labelled endosomes (Peñalva, 2005; Figure 5.13B). In contrast, upon uric acid addition YFP labelled exclusively the PM, and no fluorescence was observed in any internal structures. Interestingly, however, under this condition PM labelling was not uniform, but rather showed a foci-like labelling. Moreover, labelled areas displayed inconspicuous cortical puncta, that appeared like sites of endocytosis, where further internalization has been blocked (Figure 5.13A).

To ensure that over-expression by the $alcA_p$ was not implicated in these observations, the test was repeated with the strain co-expressing UapA-YFP$_C$ and UapA-YFP$_N$ driven by the endogenous UapA promoter. As expected, the subcellular localization displayed was comparable to the one observed with the $alcA_p$ (Figure 5.13C). Cortical punctuation, however, was only observed when the samples had been treated with 60μM uric acid, a concentration that is sufficient for stimulating UapA turn over, but inadequate for its transcriptional induction. On the other hand, upon incubation with 600μM uric acid, PM was uniformly labelled, probably as a result of the induction of UapA expression.

It has been reported that the generation of an intact YFP molecule under some conditions can be considered an irreversible process (Magliery *et al.*, 2005; Kerppola, 2006) and a stable interaction may be established between the two proteins fused to the YFP halves (Held *et al.*, 2008). If this is the case with the UapA-YFP chimeric constructs, the non-response to transport activity-dependent, substrate-elicited endocytosis, might, in principle, be due to lack of transport activity, resulting from the lack of dynamic de-oligomerization. However, we have previously shown, by growth tests and direct transport assays, that the strain expressing the two UapA-YFP constructs is fully capable of relevant transport activities (Figure 5.6). Thus, lack of internalization in the presence of uric acid should not be due to lack of transport activity. It rather seems to be due to either loss or reduction of UapA-YFP de-

oligomerization *per se*. In other words, if interaction of the YFP parts block de-oligomerization of UapA, this block is not critical for UapA function, but it is for efficient UapA internalization in the presence of substrates. Interestingly, this putative block in UapA de-oligomerization does not block NH_4^+-elicited endocytosis.
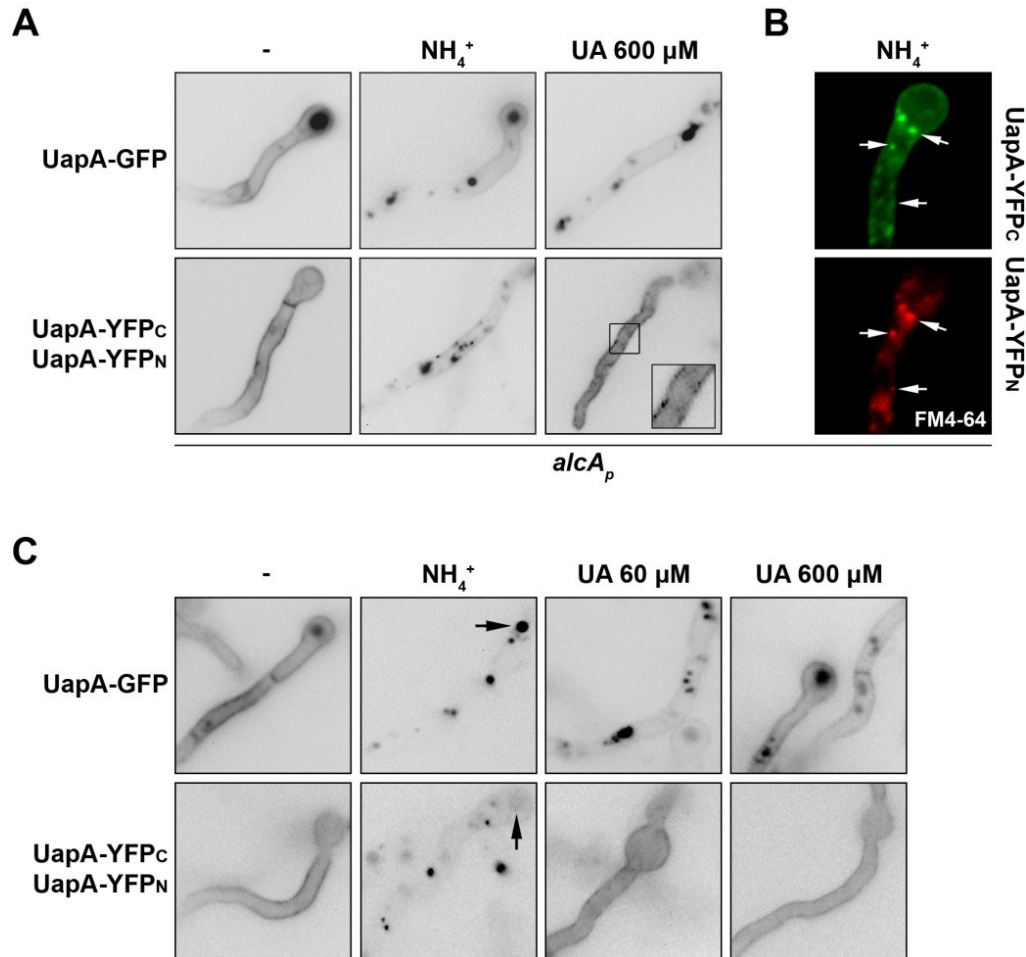
Figure 5.13. UapA oligomerization status upon induction of endocytosis, as observed by BiFC. **A.** Treatment with NH_4^+ for 4h after 1h transcriptional repression by glucose triggered UapA internalization in a similar to the wild-type fashion. Upon substrate incubation for 5h, however, no YFP-labelled internal structures were observed, while PM fluorescence was unevenly distributed (square), forming inconspicuous cortical puncta, associated with the PM and areas of decreased fluorescence. Inset, higher magnification image of a small region of the hypha (rectangle) **B.** UapA oligomers after 2 h incubation with NH_4^+ and simultaneously stained with FM4-64. Arrows highlight cytoplasmic granular bodies labelled with both YFP and FM4-64, which at the conditions used labels mainly the endosomes. **C.** Expression under the native promoter gave similar results in respect to endocytosis induced by NH_4^+ or uric acid (UA). Notably, unlike the intense and solid labelling of the lumens of larger vacuoles in the GFP-tagged control strain (arrow, upper panel), in the UapA-YFP$_C$ UapA-YFP$_N$ strain, YFP labelled the large vacuoles very faintly, mainly in the vacuolar membrane, possibly due to YFP dissociation in early stages of the degradation process (arrow, lower panel). Moreover, the uneven YFP labelling of the PM was only prominent upon addition of 60μM uric acid, a concentration that triggers endocytosis but does not stimulate transcriptional induction. Addition of 600μM uric acid restored the uniformity of YFP labelling in the PM, probably as a result of transcriptional induction of UapA expression, which was also demonstrated by reinforcement of PM fluorescence in the control strain.

De-oligomerization and substrate-elicited endocytosis as a consequence of transport activity has also been reported for dopamine transporter (DAT) oligomerization and endocytosis (Chen and Reith, 2008). Such phenomena of substrate-induced, activity-related, turnover of transporters might have evolved and been conserved from lower eukaryotes to metazoans as a fine negative feedback control for avoiding excess uptake of potentially toxic metabolites (Hicke and Dunn, 2003).

6

Concluding Remarks & Future Outlook

As it was illustrated in the introductory chapter of this study considerable work has been carried out towards elucidating the molecular mechanisms of intracellular trafficking of transmembrane proteins (Sato and Nakano, 2007; Lauwers *et al.*, 2010; Becuwe, Herrador, *et al.*, 2012; Springer *et al.*, 2014 and references therein). Whereas many major compartments and pathways are well defined, less is known about the dynamic nature of these processes and the molecular components responsible for their regulation. Through this study, essential components of the mechanism of intracellular trafficking of *A. nidulans* transporters were identified and aspects of their regulation by specific intracellular and extracellular signals were demonstrated. A model was generated in which there are two distinct molecular pathways for the regulation of UapA endocytosis, in response to broad range signals, such as NH_4^+, and specific signals (substrates), respectively. This study focused also on the blockage of endocytic mechanisms in hypertonic solutions, which is the result of major changes in the physiology of both *A. nidulans* and *S. cerevisiae*. Finally, it was demonstrated that UapA oligomerizes and that this oligomerization is dynamic and critical for UapA sorting and turnover.

The effects of hypertonic treatment on fungi have been extensively studied before. Yeast cells respond to increased tonicity by cell shrinkage, cessation of growth associated with diminished translational capacity (Teige *et al.*, 2001), rapid closure of the glycerol export channel Fps1 and remodeling of the actin cytoskeleton (Chowdhury *et al.*, 1992). These phenomena are transient and recover through gradual accumulation of the osmolyte glycerol (Blomberg and Adler, 1989), as a consequence of the activation of genes of the high-osmolarity glycerol (HOG) pathway (Brewster *et al.*, 1993). However, under extreme and persisting osmotic conditions the PM of *S. cerevisiae* is functionally and structurally reorganized irreversibly, which in turn leads to cell death (Dupont *et al.*, 2010). This work, along with another report in *S. cerevisiae* (Slaninová *et al.*, 2000), show with the use of TEM that response to hypertonicity also includes the rapid formation of deep PM invaginations or localized plasmolysis.

In agreement with these observations, it was shown *in vivo* that patches originally detected with transporters correspond to PM invaginations, rather than specific membrane microdomains, transiently elicited by hypertonic conditions. This phenomenon is associated with transient growth arrest and temporary but total block of transporter endocytosis in both *A. nidulans* and *S. cerevisiae*, as a result of the disassembly of actin cytoskeleton. Similarly to yeast (Dupont *et al.*, 2010) and unlike what has been observed in mammals (Daukas and Zigmond, 1985), hypertonic conditions have a dramatic effect also in fluid phase endocytosis, which might reflect differences in the molecular mechanisms employed by fungal and animal cells to respond to hypertonicity. Notably, conditions established herein can be used as tools to study transporter trafficking and endocytosis in *A. nidulans* and other filamentous fungi or even more complex cells*,* where genetic blocks in relevant genes are usually lethal or debilitating (Hein *et al.*, 1995; Araujo-Bazán *et al.*, 2008). This will permit us to address novel questions on transporter trafficking, recycling and turnover through alternative pathways.

As previously stated (Gournas *et al.*, 2010), the transport-dependence of substrate-elicited UapA endocytosis clearly distinguishes this phenomenon from NH_4^+-induced turnover. However, in both phenomena, UapA internalization is dependent on the ubiquitination of the transporter by the same ubiquitin ligase (HulA^{Rsp5}), which acts on the same Lys residue (K572) with the involvement of the same arrestin-like adaptor (ArtA). The fact that ArtA controls UapA ubiquitination

and endocytosis in response to both NH_4^+ and substrates leads to an apparent paradox. NH_4^+-elicited endocytosis is a broad range physiological response concerning probably most transporters involved in the uptake of nitrogenous compounds that can be used as secondary nitrogen sources, such as purines, amino acids or nitrate. The physiological rationale for this is that when NH_4^+ is present in the media as a primary nitrogen source, there is no need for taking up other nitrogenous compounds through their specific transporters, which are consequently internalized and turned-over. In contrast to NH_4^+-elicited, substrate-induced endocytosis is a highly specific signal, which seems to concern a single transporter in each case (Amillis *et al.*, 2007; Vlanti and Diallinas, 2008; Gournas *et al.*, 2010; George Diallinas and Sotiris Amillis, unpublished results). If arrestins respond to broad-range signals through their dephosphorylation, ubiquitination and recruitment to PM cargos, as reported in a number of recent publications (MacGurn *et al.*, 2011; Becuwe, Vieira, *et al.*, 2012; Merhi and André, 2012), how could this model account for the role of arrestin-like proteins in specific substrate-elicited endocytosis of a given transporter?

In *S. cerevisiae*, different arrestin-like proteins have been shown to recognize the same transporter in response to different stimuli (Lin *et al.*, 2008; Nikko and Pelham, 2009), whereas in the case of Fur4, five adaptors are involved in the endocytosis of the transporter both by substrates and by cycloheximide (Nikko and Pelham, 2009). Through the work of our laboratory, including my own, presented in this thesis, the regulation of two endocytic pathways by a single arrestin-like protein is described for the first time. The diversity of the two pathways is confirmed and the convergence of both endocytic signals to a common ubiquitination mechanism is justified by the differential modification of the adaptor (ubiquitination) occurring specifically when NH_4^+ cellular levels increase, rather than by the recruitment of different adaptors. Based on the experiments using UapA, a model is proposed (Figure 6.1) that might also be applicable to other transporters related to the uptake of secondary nitrogen sources. According to this model, in the presence of NH_4^+, ArtA is activated or recruited massively in the PM and thus promotes HulA-dependent ubiquitination of UapA. In contrast, in the presence of specific substrates, UapA undergoes dynamic rounds of alternating conformations associated with transport catalysis, which promote interactions with the endocytic machinery even in the absence of broad range signals activating arrestin adaptors.

Further aspects on adaptor regulation in *A. nidulans* remain to be elucidated, such as whether it occurs via a phosphorylation/de-phosphorylation cascade signaling pathway, which are the kinases/phosphatases involved in these modifications or whether there are other post-translational modifications involved, either on the adaptor proteins or the cargos. Moreover, a di-acidic motif at the C-tail of UapA was found to be involved in the ubiquitination and endocytosis of the transporter, indicating that this might serve as the interaction interface between the transporter and the adaptor. This raises the question of whether there are conserved motifs in transporters regulated by the same arrestins and if not, what is the mechanism of recognition of cargos by their cognate adaptors.
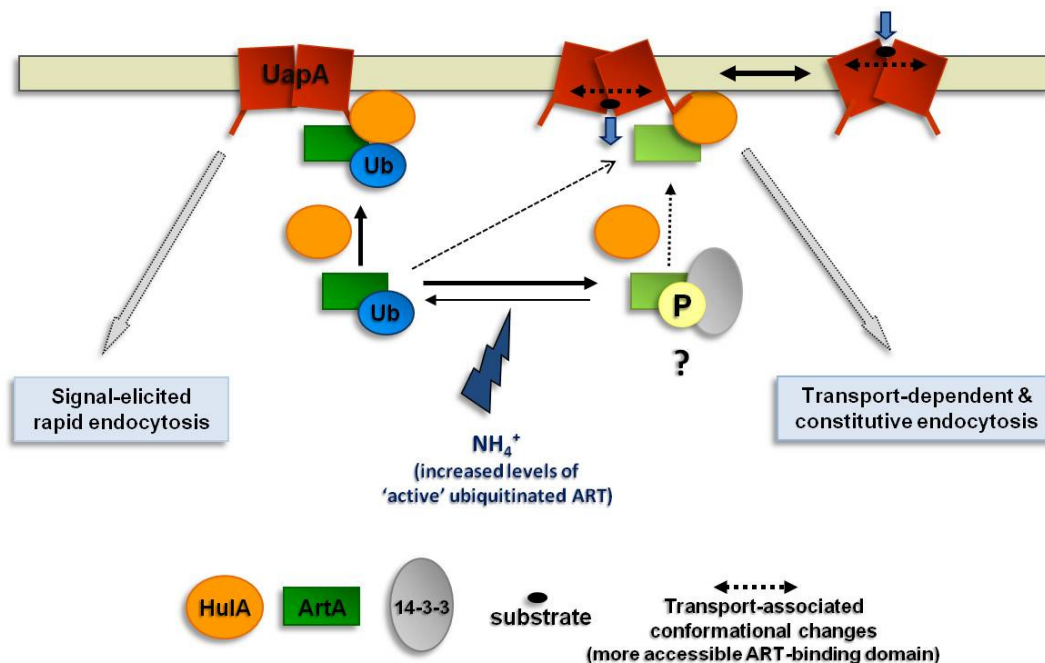
Figure 6.1. Model for the regulation of UapA ubiquitination and endocytosis. ArtA is in a constitutively ubiquitinated state with a low ratio of ubiquitinated (dark green) to non-ubiquitinated (light green) molecules, which increases several-fold in the presence of NH_4^+. The ubiquitinated ArtA mediates the interaction of UapA with HulA, which results in UapA ubiquitination and eventual internalization (left). In the presence of its substrates, conformational changes of UapA associated with its transport cycle (right) increase the affinity of the transporter for ArtA adaptor molecules, even for those that are not ubiquitinated, and thus UapA ubiquitination and turnover occur (adapted from G. Diallinas).

Our results also provide a possible explanation for the inability of UapA to be endocytosed when heterologously expressed in *S. cerevisiae* (Mayia Karachaliou and George Diallinas, unpublished observations). This could be the absence of *cis*-elements on UapA that are required for the endocytosis of a transporter in *S. cerevisiae*, such as specific motifs recognized by adaptors of Rsp5 ubiquitin ligase.

We showed here that apart from ArtA, at least one other factor, the SagA (homologue of End3 of *S. cerevisiae*), is necessary for the endocytosis of UapA in *A. nidulans*. Notably, among the transporters tested, SagA was found essential only for carriers specific for purines (Karachaliou *et al.*, 2013; Vassilis Yalelis, Sotiris Amillis and George Diallinas, unpublished observations). This specificity indicates that the regulation of endocytosis has a narrow specificity range and even though the conservation between the two proteins (Art1 and End3) and their *A. nidulans* homologues is high, small differences in their affinity for UapA are probably sufficient to hinder the interaction with the transporter. The expression in *S. cerevisiae* of all the components known to date to be essential for UapA endocytic internalization could serve as a workaround to enable the use of this heterologous system for trafficking studies. Nevertheless, the possibility that yet another protein essential for UapA endocytosis exists, cannot be excluded.

The observation of *in trans* endocytosis was the motive that prompted us to investigate whether UapA oligomerizes. We demonstrated UapA oligomerization using several direct and indirect approaches and showed that the physical interaction between the monomers is fairly strong, since it remains stable even in reducing conditions. Similar results were obtained very recently for the human vitamin C transporter 1 (hSVCT1), which is also a member of the NAT family (Boggavarapu *et al.*, 2013). Purification of hSVCT1 and low-resolution structure obtained by TEM and single particle analysis unveiled the existence of a major monomeric and minor dimeric population. UapA, however, was also observed to form higher order oligomers, which were diminished in a mutant that has lost the ability to oligomerize (DYDY/A), as evidenced by BiFC. This mutant bears substitutions of four amino acids forming a putative di-acidic motif at the N-tail of UapA, which were shown to be essential for ER export (Sotiris Amillis and George Diallinas, unpublished observations). Other ER-retain mutants (I74D, TMS14Δ) also failed to reconstitute the YFP fluorophore, unless one of the putative partners was a wild-type molecule. In that case, «*in trans* sorting» of the mutant protein to the PM occured, while some ER-retention of the oligomers was also observed. Taken together, we showed that UapA oligomer formation occurs already in the ER and that it is involved in the proper targeting of the transporter to the PM.

The exact role of UapA oligomerization in ER-exit is still unknown and could constitute the target of further research. One possible role has very recently been

proposed. Springer *et al.* (2014) showed that oligomerization induces local membrane bending, which in turn promotes COPII vesicle generation and eventual sorting to the PM. Other issues to be addressed include the determination of the oligomeric state at which most UapA molecules exist in the cell, the investigation of the possible existence of a dynamic equilibrium between different oligomeric states, as well as the identification of the possible role of oligomerization in UapA function.

An interesting and as yet standing question about UapA oligomerization is what the interaction interface between UapA monomers is. Genomic analysis of membrane protein families has shown that GXXXG (GX_3G) and GXXXXXXG (GX_6G) are among the most prevalent motifs mediating helix-helix interactions in membrane proteins. Moreover, these motifs are particularly well conserved in families corresponding to transporters and channels (Liu *et al.*, 2002). In line with that, we found that a conserved GX_3G motif in the TMS7 of UapA, which is predicted to be located towards the lipid phase of the PM (Figure 1.19; Kosti *et al.*, 2012), is possibly involved in UapA oligomerization.

Another UapA domain that is worth examining in the future for an involvement in the oligomerization of the transporter is the motif $G^{224}X_6GX_6GX_6GX_6G^{252}$ in TMS5. As seen in Figure 6.2, three out of four Gly residues that lie within or at the limits of TMS5 are highly conserved in fungi and bacteria, but not in higher eukaryotes, whereas the fourth one (Gly231) is absolutely conserved, with the
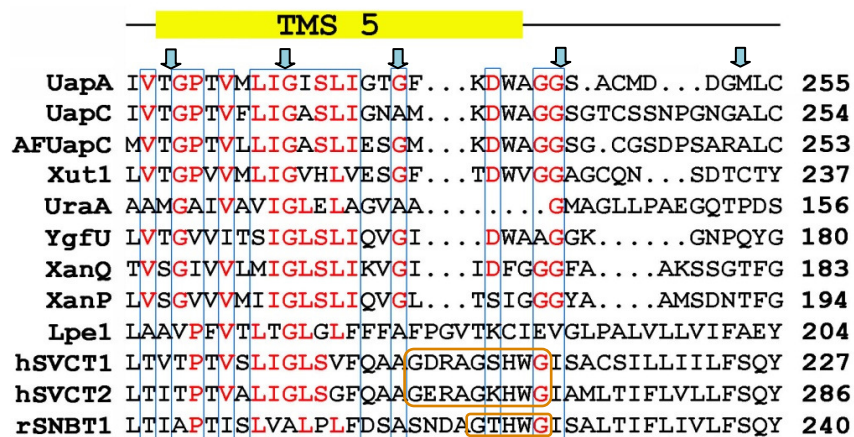
Figure 6.2. Multiple alignment of the putative TMS5 of UapA and selected NAT homologues. Highly conserved amino acids are shaded in blue boxes. Gly residues forming the $G^{224}X_6GX_6GX_6GX_6G^{252}$ motif in UapA are indicated (blue arrows). Putative GX_3GX_3G and GX_3G motifs of hSVCT and rSNBT1, respectively, are shaded in orange boxes. The listed NAT homologues include: UapA of *A. nidulans*; UapC of *A. nidulans*, AFUapC of *A. fumigatus*, Xut1 of C. *albicans*, UraA of *Escherichia coli*, YgfU of *E. coli*, XanQ of *E. coli*, XanP of *E. coli*, Lpe1 of *Zea mays*, hSVCT1 of *Homo sapiens*, hSVCT2 of *H. sapiens*, rSNBT1 of *Rattus norvegicus* (adapted from Krypotou and Diallinas, 2014).

exception of the rat sodium-dependent nucleobase transporter 1 (rSNBT1). Although the aforementioned motif is not present in higher eukaryotes, the human vitamin C transporters hSVCT1 and hSVCT2 contain a GXXXGXXXG motif, which has also been shown to mediate membrane protein interactions (Plotkowski *et al.*, 2007), while part of it (GXXXG motif) is also conserved in rSNBT1 (Figure 6.2).

Additionally, the residue I74, the substitution of which led to ER retention and abolishment of UapA oligomerization, lies at the cytoplasmic limit of TMS1, within a region that is rich in leucine residues. Four of these residues form a putative leucine zipper (L70X_6LX$_6$LX$_6$L91; Figure 6.3A), a common motif that has been shown to provide stable binding between α-helices (Oates *et al.*, 2010), which however is not conserved within the NAT family. Mutations replacing Leu with Ala residues within TMS1 (L77/84A and L77/84/91A) led to increased appearance of UapA in vacuoles, besides also being abundant in the PM, suggesting that the leucine zipper might have a role in the stability of the transporter in the membrane. Moreover, kinetic analysis showed that these mutations either increased (180% in L77/84A) or did not affect significantly (80% in L77/84/91A) UapA transport capacity for xanthine, which is consistent with their abundance in the PM (Pantazopoulou and Diallinas, 2006). Interestingly, according to the modeled structure of UapA, not only is TMS1 predicted to be to be located at the periphery of the molecule, but it is also in close proximity to TMS7 (Figure 1.19; Kosti *et al.*, 2012). Thus, it is likely that both TMSs are involved in the interaction interface of the oligomers.
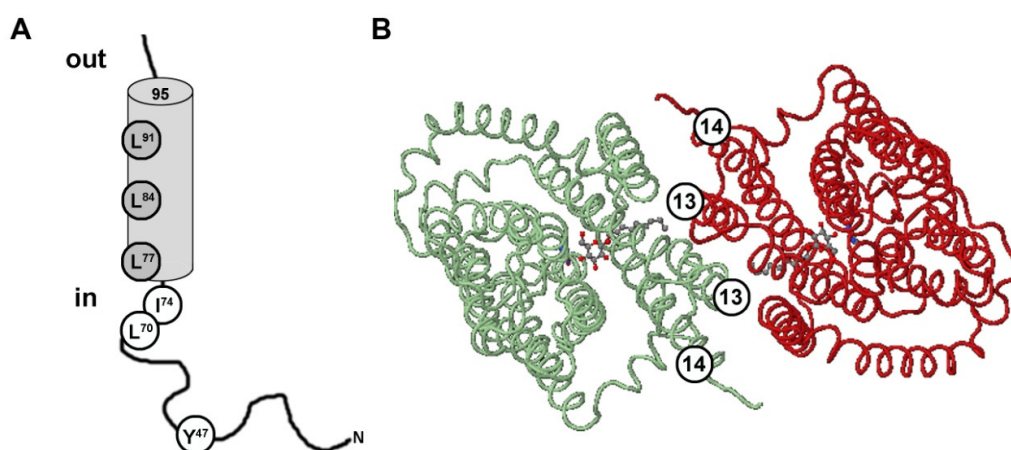
Figure 6.3. A. Speculative topology of TMS1 of UapA. The Leu residues forming a putative Leu zipper, as well as the I74 and Y47, which when substituted lead to complete ER retention, are depicted in circles. **B.** Predicted biological assembly of the uracil transporter UraA from *E. coli*, generated by PISA software based on the crystal structure of the monomer. Monomers within the dimer are depicted in different colors. Bound substrates are also displayed (retrieved from http://www.rcsb.org/pdb/explore.do?structureId=3qe7).

On the other hand, based on the crystal structure of the *E. coli* uracil/H$^+$ symporter UraA, which is the only resolved structure of a member of the NAT family, yet another domain can be proposed as a putative interaction interface between UapA monomers. In particular, although UraA was crystallized as a monomer, a software analyzing crystal structures and predicting their most likely biological form (PISA) suggests that UraA forms dimers and that the interaction interface lies within the TMS13 of each monomer (Figure 6.3B; http://www.rcsb.org/pdb/explore.do?structureId=3qe7). The TMS14 of the two monomers are tightly located at either side of the interacting domains, a conformation that might serve a supporting role for the TMS13 to acquire a topology that favors intermolecular interactions. An indirect role of TMS14 in the establishment of the dimer, could explain the lack of YFP reconstitution in the TMS14Δ mutant of UapA, even when one of the YFP-tagged partners was a wild-type molecule.

Last but not least, the present results strongly suggest that de-oligomerization of UapA is very probably a consequence of, rather than a prerequisite for, transport activity. Attachment of YFP epitopes did not affect UapA transport activity but apparently blocked its internalization by substrates, but not by NH$_4^+$, probably as a result of the stable reconstitution of the YFP molecule. This observation implied that while NH$_4^+$-elicited endocytosis proceeds with at least some UapA molecules being in oligomeric structures, addition of substrates elicits the dissociation of transporter oligomers, which in turn leads to their internalization and sorting to the endosomal/vacuolar pathway as monomers. This is in line with previous observations on dopamine transporter (DAT) oligomerization and endocytosis (Chen and Reith, 2008). Nevertheless, we cannot exclude the possibility that some UapA oligomers do dissociate and eventually internalize as monomers, this explaining the areas of decreased PM fluorescence in the sample treated with substrates. In that case, UapA de-oligomerization coincides with the dissociation of YFP parts and therefore, no fluorescent internal structures are observed. Notably, a block in constitutive endocytosis of YFP-tagged UapA was also observed, which is in accordance with our model suggesting that this type of internalization occurs via the substrate-induced endocytic pathway (Figure 6.1).

Combining this model with our results suggesting UapA de-oligomerization prior to its substrate-elicited internalization, one could speculate that the

conformational changes of UapA associated with its function are responsible for the disruption of the interaction between the UapA monomers and that this dissociation is responsible for making the transporter accessible also to non-ubiquitinated ArtA. However, this is just a hypothesis yet to be explored and to be supported by experimental data. A first step towards this could be the examination of the ubiquitination status of UapA molecules that are fixed in an oligomeric arrangement due to the stable reconstitution of YFP. In addition, other fluorescence complementation-based methods, such as FRET, could be employed for the observation of the oligomers *in vivo*, in order to avoid the tight reconstitution of the YFP parts. In conclusion, the substrate-induced turnover of transporters is generally believed to have evolved as a negative feedback control for avoiding excess uptake of potentially toxic metabolites (Hicke and Dunn, 2003) and UapA de-oligomerization by substrates and subsequent internalization appears to serve as a fine regulatory mechanism to this end.

7

References

Abenza, J.F., Galindo, A., Pantazopoulou, A., Gil, C., Ríos, V.D.L., Pen, M.A., *et al.* (2010) Aspergillus RabB Rab5 Integrates Acquisition of Degradative Identity with the Long Distance Movement of Early Endosomes. *Mol Biol Cell* **21**: 2756–2769.

Abenza, J.F., Galindo, A., Pinar, M., Pantazopoulou, A., los Ríos, V. de, and Peñalva, M. a (2012) Endosomal maturation by Rab conversion in *Aspergillus nidulans* is coupled to dynein-mediated basipetal movement. *Mol Biol Cell* **23**: 1889–901.

Abenza, J.F., Pantazopoulou, A., Rodríguez, J.M., Galindo, A., and Peñalva, M. a (2009) Long-distance movement of *Aspergillus nidulans* early endosomes on microtubule tracks. *Traffic* **10**: 57–75.

Abramson, J., Smirnova, I., Kasho, V., Verner, G., Kaback, H.R., and Iwata, S. (2003) Structure and mechanism of the lactose permease of *Escherichia coli*. *Science* **301**: 610–5.

Alba-Lois, L., and Segal-Kischinevzky, C. (2010) Beer and Wine Makers. *Nat Educ* **3**: 17.

Alberts, B., Bray, D., Lewis, J., Raff, M., Roberts, K., and Watson, J.D. (1994) Membrane structure. In *Molecular biology of the cell*. Garland Publishing, New York and London.

Alderson, T., and Scazzocchio, C. (1967) A system for the study of interlocus specificity for both forward and reverse mutation in at least eight gene loci in *Aspergillus nidulans*. *Mutat Res* **4**: 567–77.

Alexopoulos, C.J., Mims, C.W., and Blackwell, M. (1996) *Introductory Mycology*. 4th ed., John Wiley and Sons, New York.

Alguel, Y., Leung, J., Singh, S., Rana, R., Civiero, L., Alves, C., and Byrne, B. (2010) New tools for membrane protein research. *Curr Protein Pept Sci* **11**: 156–65.

Alvarez, F.J., Douglas, L.M., Rosebrock, A., and Konopka, J.B. (2008) The Sur7 protein regulates plasma membrane organization and prevents intracellular cell wall growth in *Candida albicans*. *Mol Biol Cell* **19**: 5214–25.

Amillis, S., Cecchetto, G., Sophianopoulou, V., Koukaki, M., Scazzocchio, C., and Diallinas, G. (2004) Transcription of purine transporter genes is activated during the isotropic growth phase of *Aspergillus nidulans* conidia. *Mol Microbiol* **52**: 205–16.

Amillis, S., Hamari, Z., Roumelioti, K., Scazzocchio, C., and Diallinas, G. (2007) Regulation of expression and kinetic modeling of substrate interactions of a uracil transporter in *Aspergillus nidulans*. *Mol Membr Biol* **24**: 206–14.

Amillis, S., Kosti, V., Pantazopoulou, A., Mikros, E., and Diallinas, G. (2011) Mutational analysis and modeling reveal functionally critical residues in transmembrane segments 1 and 3 of the UapA transporter. *J Mol Biol* **411**: 567–80.

Anderluh, A., Klotzsch, E., Reismann, A.W.A.F., Brameshuber, M., Kudlacek, O., Newman, A.H., *et al.* (2014) Single molecule analysis reveals coexistence of stable serotonin transporter monomers and oligomers in the live cell plasma membrane. *J Biol Chem* **289**: 4387–94.

Apostolaki, A., Erpapazoglou, Z., Harispe, L., Billini, M., Kafasla, P., Kizis, D., *et al.* (2009) AgtA, the dicarboxylic amino acid transporter of *Aspergillus nidulans*, is concertedly down-regulated by exquisite sensitivity to nitrogen metabolite repression and ammonium-elicited endocytosis. *Eukaryot Cell* **8**: 339–52.

Apte-Deshpande, A., Rewanwar, S., Kotwal, P., Raiker, V.A., and Padmanabhan, S. (2009) Efficient expression and secretion of recombinant human growth hormone in the methylotrophic yeast *Pichia pastoris*: potential applications for other proteins. *Biotechnol Appl Biochem* **54**: 197–205.

Araujo-Bazán, L., Peñalva, M.A., and Espeso, E.A. (2008) Preferential localization of the endocytic internalization machinery to hyphal tips underlies polarization of the actin cytoskeleton in *Aspergillus nidulans*. *Mol Microbiol* **67**: 891–905.

Argyrou, E., Sophianopoulou, V., Schultes, N., and Diallinas, G. (2001) Functional characterization of a maize purine transporter by expression in *Aspergillus nidulans*. *Plant Cell* **13**: 953–64.

Arst, H.N., and Cove, D.J. (1973) Nitrogen metabolite repression in *Aspergillus nidulans*. *Mol Gen Genet* **126**: 111–41.

Arst, H.N., and Scazzocchio, C. (1975) Initiator constitutive mutation with an "up-promoter" effect in *Aspergillus nidulans*. *Nature* **254**: 31–4.

Aubry, L., and Klein, G. (2013) True arrestins and arrestin-fold proteins: a structure-based appraisal. *Prog Mol Biol Transl Sci* **118**: 21–56.

Bailey, C., and Arst, H.N. (1975) Carbon Catabolite Repression in *Aspergillus nidulans*. *Eur J Biochem* **51**: 573–577.

Barlowe, C. (2003) Signals for COPII-dependent export from the ER: what's the ticket out? *Trends Cell Biol* **13**: 295–300.

Barnett, J. a (1998) A history of research on yeasts 1: Work by chemists and biologists 1789-1850. *Yeast* **14**: 1439–51.

Becuwe, M., Herrador, A., Haguenauer-Tsapis, R., Vincent, O., and Léon, S. (2012) Ubiquitin-mediated regulation of endocytosis by proteins of the arrestin family. *Biochem Res Int* **2012**: 1–12.

Becuwe, M., Vieira, N., Lara, D., Gomes-Rezende, J., Soares-Cunha, C., Casal, M., *et al.* (2012) A molecular switch on an arrestin-like protein relays glucose signaling to transporter endocytosis. *J Cell Biol* **196**: 247–59.

Benyair, R., Ron, E., and Lederkremer, G.Z. (2011) Protein quality control, retention, and degradation at the endoplasmic reticulum. *Int Rev Cell Mol Biol* **292**: 197–280.

Berbee, M.L. (2001) The phylogeny of plant and animal pathogens in the Ascomycota. *Physiol Mol Plant Pathol* **59**: 165–187.

Berger, S.P., Farrell, K., Conant, D., Kempner, E.S., and Paul, S.M. (1994) Radiation inactivation studies of the dopamine reuptake transporter protein. *Mol Pharmacol* **46**: 726–31.

Bitsikas, V., Karachaliou, M., Gournas, C., and Diallinas, G. (2011) Hypertonic conditions trigger transient plasmolysis, growth arrest and blockage of transporter endocytosis in *Aspergillus nidulans* and Saccharomyces cerevisiae. *Mol Membr Biol* **28**: 54–68.

Blanchard, C.R. (1996) Atomic Force Microscopy. *Chem Educ* **1**: 1–8.

Blomberg, A., and Adler, L. (1989) Roles of glycerol and glycerol-3-phosphate dehydrogenase (NAD+) in acquired osmotolerance of *Saccharomyces cerevisiae*. *J Bacteriol* **171**: 1087–92.

Blondel, M.-O., Morvan, J., Dupré, S., Urban-Grimal, D., Haguenauer-Tsapis, R., and Volland, C. (2004) Direct Sorting of the Yeast Uracil Permease to the Endosomal System Is Controlled by Uracil Binding and Rsp5p-dependent Ubiquitylation. *Mol Biol Cell* **15**: 883–895.

Boase, N.A., and Kelly, J.M. (2004) A role for creD, a carbon catabolite repression gene from *Aspergillus nidulans*, in ubiquitination. *Mol Microbiol* **53**: 929–40.

Boggavarapu, R., Jeckelmann, J.-M., Harder, D., Schneider, P., Ucurum, Z., Hediger, M., and Fotiadis, D. (2013) Expression, Purification and Low-Resolution Structure of Human Vitamin C Transporter SVCT1 (SLC23A1). *PLoS One* **8**: e76427.

Bonifacino, J.S., and Glick, B.S. (2004) The mechanisms of vesicle budding and fusion. *Cell* **116**: 153–66.

Bonifacino, J.S., and Lippincott-Schwartz, J. (2003) Coat proteins: shaping membrane transport. *Nat Rev Mol Cell Biol* **4**: 409–14.

Bonifacino, J.S., and Traub, L.M. (2003) Signals for sorting of transmembrane proteins to endosomes and lysosomes. *Annu Rev Biochem* **72**: 395–447.

Bourette, R.P., Myles, G.M., Choi, J.L., and Rohrschneider, L.R. (1997) Sequential activation of phoshatidylinositol 3-kinase and phospholipase C-gamma2 by the M-CSF receptor is necessary for differentiation signaling. *EMBO J* **16**: 5880–93.

Bradford, M.M. (1976) A rapid and sensitive method for the quantitation of microgram quantities of protein utilizing the principle of protein-dye binding. *Anal Biochem* **72**: 248–54.

Breakspear, A., Langford, K.J., Momany, M., and Assinder, S.J. (2007) CopA:GFP localizes to putative Golgi equivalents in *Aspergillus nidulans*. *FEMS Microbiol Lett* **277**: 90–7.

Brewster, J.L., Valoir, T. de, Dwyer, N.D., Winter, E., and Gustin, M.C. (1993) An osmosensing signal transduction pathway in yeast. *Science* **259**: 1760–3.

Broder, Y.C., Katz, S., and Aronheim, A. (1998) The ras recruitment system, a novel approach to the study of protein-protein interactions. *Curr Biol* **8**: 1121–4.

Brown, D.A., and London, E. (1998) Functions of lipid rafts in biological membranes. *Annu Rev Cell Dev Biol* **14**: 111–36.

Caddick, M.X. (2004) Nitrogen regulation in mycelial fungi. In *The Mycota III: Biochemistry and Molecular Biology*. Brambl, R., and Marzluf, G.A. (eds). Springer-Verlag Berlin Heidelberg, pp. 349–368.

Cao, Y., Jin, X., Levin, E.J., Huang, H., Zong, Y., Quick, M., *et al.* (2011) Crystal structure of a phosphorylation-coupled saccharide transporter. *Nature* **473**: 50–4.

Carr, C.M., and Rizo, J. (2010) At the Junction of SNARE and SM Protein Function. *Curr Opin Cell Biol* **22**: 488–495.

Casselton, L., and Zolan, M. (2002) The art and design of genetic screens: filamentous fungi. *Nat Rev Genet* **3**: 683–97.

Cavalieri, D., McGovern, P.E., Hartl, D.L., Mortimer, R., and Polsinelli, M. (2003) Evidence for *S. cerevisiae* fermentation in ancient wine. *J Mol Evol* **57 Suppl 1**: S226–32.

Cecchetto, G., Amillis, S., Diallinas, G., Scazzocchio, C., and Drevet, C. (2004) The AzgA purine transporter of *Aspergillus nidulans*. Characterization of a protein belonging to a new phylogenetic cluster. *J Biol Chem* **279**: 3132–41.

Chae, P.S., Rasmussen, S.G.F., Rana, R.R., Gotfryd, K., Chandra, R., Goren, M.A., *et al.* (2010) Maltose-neopentyl glycol (MNG) amphiphiles for solubilization, stabilization and crystallization of membrane proteins. *Nat Methods* **7**: 1003–8.

Chang, A., Cheang, S., Espanel, X., and Sudol, M. (2000) Rsp5 WW Domains Interact Directly with the Carboxyl-terminal Domain of RNA Polymerase II. *J Biol Chem* **275**: 20562–20571.

Chen, N., and Reith, M.E.A. (2008) Substrates dissociate dopamine transporter oligomers. *J Neurochem* **105**: 910–20.

Chowdhury, S., Smith, K.W., and Gustin, M.C. (1992) Osmotic stress and the yeast cytoskeleton: phenotype-specific suppression of an actin mutation. *J Cell Biol* **118**: 561–71.

Ciruela, F. (2008) Fluorescence-based methods in the study of protein-protein interactions in living cells. *Curr Opin Biotechnol* **19**: 338–43.

Cohen, B.L. (2000) Guido Pontecorvo ("Ponte"), 1907-1999. In *Perspectives on Genetics. Anecdotal, Historical and Critical Commentaries on Genetics.* Crow, J.F., and Dove, W.F. (eds). University of Wisconsin Press, pp. 497–501.

Courbard, J.-R., Fiore, F., Adélaïde, J., Borg, J.-P., Birnbaum, D., and Ollendorff, V. (2002) Interaction between two ubiquitin-protein isopeptide ligases of different classes, CBLC and AIP4/ITCH. *J Biol Chem* **277**: 45267–75.

Dahl, S.G., Sylte, I., and Ravna, A.W. (2004) Structures and Models of Transporter Proteins. *J Pharmacol Exp Ther* **309**: 853–860.

Dang, S., Sun, L., Huang, Y., Lu, F., Liu, Y., Gong, H., *et al.* (2010) Structure of a fucose transporter in an outward-open conformation. *Nature* **467**: 734–8.

Darlington, A.J., and Scazzocchio, C. (1967) Use of Analogues and the Substrate-Sensitivity of Mutants in Analysis of Purine Uptake and Breakdown in *Aspergillus nidulans*. *J Bacteriol* **93**: 937–40.

Daukas, G., and Zigmond, S.H. (1985) Inhibition of receptor-mediated but not fluid-phase endocytosis in polymorphonuclear leukocytes. *J Cell Biol* **101**: 1673–9.

Dawson, J.P., Weinger, J.S., and Engelman, D.M. (2002) Motifs of serine and threonine can drive association of transmembrane helices. *J Mol Biol* **316**: 799–805.

Diallinas, G. (2008a) An Almost-Complete Movie. *Science (80-)* **322**: 1644–1645.

Diallinas, G. (2008b) *Aspergillus* transporters. In *The Aspergilli. Genomics, Medical Applications, Biotechnology, and Research Methods.* Osmani, A., and Goldman, G.H. (eds). CRC Press, Boca Raton, FL. pp. 297– 316.

Diallinas, G., Gorfinkiel, L., Arst, H.N., Cecchetto, G., and Scazzocchio, C. (1995) Genetic and Molecular characterization of a gene encoding a wide specificity purine permease of *Aspergillus nidulans* reveals a novel family of transporters conserved in prokaryotes and eukaryotes. *J Biol Chem* **270**: 8610–8622.

Diallinas, G., and Gournas, C. (2008) Structure-function relationships in the nucleobase-ascorbate transporter (NAT) family. *Channels* **2**: 1–10.

Diallinas, G., and Scazzocchio, C. (1989) A gene coding for the uric acid-xanthine permease of *Aspergillus nidulans*: Inactivational cloning, characterization, and sequence of a *cis*-acting mutation. *Genetics* **122**: 341–350.

Dupont, S., Beney, L., Ritt, J.-F., Lherminier, J., and Gervais, P. (2010) Lateral reorganization of plasma membrane is involved in the yeast resistance to severe dehydration. *Biochim Biophys Acta* **1798**: 975–85.

Dupré, S., and Haguenauer-Tsapis, R. (2003) Raft partitioning of the yeast uracil permease during trafficking along the endocytic pathway. *Traffic* **4**: 83–96.

Dupré, S., Urban-Grimal, D., and Haguenauer-Tsapis, R. (2004) Ubiquitin and endocytic internalization in yeast and animal cells. *Biochim Biophys Acta* **1695**: 89–111.

Ehrhard, K.N., Jacoby, J.J., Fu, X.Y., Jahn, R., and Dohlman, H.G. (2000) Use of G-protein fusions to monitor integral membrane protein-protein interactions in yeast. *Nat Biotechnol* **18**: 1075–9.

Elion, G.B. (1989) The purine path to chemotherapy. *Science* **244**: 41–7.

Engel, A., and Gaub, H.E. (2008) Structure and mechanics of membrane proteins. *Annu Rev Biochem* **77**: 127–48.

Esser, K., and Stahl, U. (1976) Cytological and genetic studies of the life cycle of *Saccharomycopsis lipolytica*. *Mol Gen Genet* **146**: 101–6.

Farhan, H., Freissmuth, M., and Sitte, H.H. (2006) Oligomerization of neurotransmitter transporters: a ticket from the endoplasmic reticulum to the plasma membrane. *Handb Exp Pharmacol* **175**: 233–49.

Felenbok, B. (1991) The ethanol utilization regulon of *Aspergillus nidulans*: the alcA-alcR system as a tool for the expression of recombinant proteins. *J Biotechnol* **17**: 11–7.

Fewell, S.W., and Brodsky, J.L. (2009) Entry into the Endoplasmic Reticulum : Protein Translocation , Folding and Quality Control. In *Trafficking Inside Cells: Pathways, Mechanisms and Regulation*. Segev, N. (ed.). Landes Bioscience and Springer Science+Business Media, Chicago. pp. 119–142.

Fields, S., and Song, O. (1989) A novel genetic system to detect protein-protein interactions. *Nature* **340**: 245–6.

Fink, A., Sal-Man, N., Gerber, D., and Shai, Y. (2012) Transmembrane domains interactions within the membrane milieu: principles, advances and challenges. *Biochim Biophys Acta* **1818**: 974–83.

Forment, J. V, Flipphi, M., Ramón, D., Ventura, L., and Maccabe, A.P. (2006) Identification of the mstE gene encoding a glucose-inducible, low affinity glucose transporter in *Aspergillus nidulans*. *J Biol Chem* **281**: 8339–46.

Forrest, L.R., Krämer, R., and Ziegler, C. (2011) The structural basis of secondary active transport mechanisms. *Biochim Biophys Acta* **1807**: 167–88.

Forrest, L.R., and Rudnick, G. (2009) The rocking bundle: a mechanism for ion-coupled solute flux by symmetrical transporters. *Physiology (Bethesda)* **24**: 377–86.

Fotiadis, D., Liang, Y., Filipek, S., Saperstein, D.A., Engel, A., and Palczewski, K. (2003) Atomic-force microscopy: Rhodopsin dimers in native disc membranes. *Nature* **421**: 127–8.

Galagan, J.E., Calvo, S.E., Cuomo, C., Ma, L.-J., Wortman, J.R., Batzoglou, S., *et al.* (2005) Sequencing of *Aspergillus nidulans* and comparative analysis with *A. fumigatus* and *A. oryzae*. *Nature* **438**: 1105–15.

Galan, J.M., Volland, C., Urban-Grimal, D., and Haguenauer-Tsapis, R. (1994) The yeast plasma membrane uracil permease is stabilized against stress induced degradation by a point mutation in a cyclin-like "destruction box". *Biochem Biophys Res Commun* **201**: 769–75.

Ghosh, I., Hamilton, A.D., and Regan, L. (2000) Antiparallel Leucine Zipper-Directed Protein Reassembly : Application to the Green Fluorescent Protein. *J Am Chem Soc* **122**: 5658–5659.

Giles, J. (2005) Nitrogen study fertilizes fears of pollution. *Nature* **433**: 791.

Goffeau, A., Barrell, B.G., Bussey, H., Davis, R.W., Dujon, B., Feldmann, H., *et al.* (1996) Life with 6000 genes. *Science (80-)* **274**: 546, 563–7.

Goñi, F.M. (2014) The basic structure and dynamics of cell membranes: An update of the Singer-Nicolson model. *Biochim Biophys Acta* **1838**: 1467–1476.

Gorfinkiel, L., Diallinas, G., and Scazzocchio, C. (1993) Sequence and regulation of the uapA gene encoding a uric acid-xanthine permease in the fungus *Aspergillus nidulans*. *J Biol Chem* **268**: 23376–81.

Goudela, S., Karatza, P., Koukaki, M., Frillingos, S., and Diallinas, G. (2005) Comparative substrate recognition by bacterial and fungal purine transporters of the NAT/NCS2 family. *Mol Membr Biol* **22**: 263–75.

Goudela, S., Reichard, U., Amillis, S., and Diallinas, G. (2008) Characterization and kinetics of the major purine transporters in *Aspergillus fumigatus*. *Fungal Genet Biol* **45**: 459–72.

Goudela, S., Tsilivi, H., and Diallinas, G. (2006) Comparative kinetic analysis of AzgA and Fcy21p, prototypes of the two major fungal hypoxanthine-adenine-guanine transporter families. *Mol Membr Biol* **23**: 291–303.

Gournas, C., Amillis, S., Vlanti, A., and Diallinas, G. (2010) Transport-dependent endocytosis and turnover of a uric acid-xanthine permease. *Mol Microbiol* **75**: 246–60.

Gournas, C., Oestreicher, N., Amillis, S., Diallinas, G., and Scazzocchio, C. (2011) Completing the purine utilisation pathway of *Aspergillus nidulans*. *Fungal Genet Biol* **48**: 840–8.

Gournas, C., Papageorgiou, I., and Diallinas, G. (2008) The nucleobase–ascorbate transporter (NAT) family: genomics, evolution, structure–function relationships and physiological role. *Mol Biosyst* **4**: 1–13.

Grossmann, G., Malinsky, J., Stahlschmidt, W., Loibl, M., Weig-Meckl, I., Frommer, W.B., *et al.* (2008) Plasma membrane microdomains regulate turnover of transport proteins in yeast. *J Cell Biol* **183**: 1075–88.

Grossmann, G., Opekarová, M., Malinsky, J., Weig-Meckl, I., and Tanner, W. (2007) Membrane potential governs lateral segregation of plasma membrane proteins and lipids in yeast. *EMBO J* **26**: 1–8.

Guarente, L. (1993) Strategies for the identification of interacting proteins. *Proc Natl Acad Sci U S A* **90**: 1639–41.

Gurtovenko, A.A., and Vattulainen, I. (2007) Molecular mechanism for lipid flip-flops. *J Phys Chem B* **111**: 13554–9.

Haider, A.J., Briggs, D., Self, T.J., Chilvers, H.L., Holliday, N.D., and Kerr, I.D. (2011) Dimerization of ABCG2 analysed by bimolecular fluorescence complementation. *PLoS One* **6**: e25818.

Hamari, Z., Amillis, S., Drevet, C., Apostolaki, A., Vágvölgyi, C., Diallinas, G., and Scazzocchio, C. (2009) Convergent evolution and orphan genes in the Fur4p-like family and characterization of a general nucleoside transporter in *Aspergillus nidulans*. *Mol Microbiol* **73**: 43–57.

Hampton, R.Y. (2002) ER-associated degradation in protein quality control and. *Curr Opin Cell Biol* **14**: 476–482.

Harold, F.M. (1990) To Shape a Cell: an Inquiry into the Causes of Morphogenesis of Microorganisms. *Microbiol Rev* **54**: 381–431.

Hastrup, H., Karlin, a, and Javitch, J. a (2001) Symmetrical dimer of the human dopamine transporter revealed by cross-linking Cys-306 at the extracellular end of the sixth transmembrane segment. *Proc Natl Acad Sci U S A* **98**: 10055–60.

Hastrup, H., Sen, N., and Javitch, J.A. (2003) The human dopamine transporter forms a tetramer in the plasma membrane: cross-linking of a cysteine in the fourth transmembrane segment is sensitive to cocaine analogs. *J Biol Chem* **278**: 45045–8.

Hatakeyama, R., Kamiya, M., Takahara, T., and Maeda, T. (2010) Endocytosis of the aspartic acid/glutamic acid transporter Dip5 is triggered by substrate-dependent recruitment of the Rsp5 ubiquitin ligase via the arrestin-like protein Aly2. *Mol Cell Biol* **30**: 5598–607.

Haugeto, O., Ullensvang, K., Levy, L.M., Chaudhry, F.A., Honoré, T., Nielsen, M., *et al.* (1996) Brain glutamate transporter proteins form homomultimers. *J Biol Chem* **271**: 27715–22.

Hebert, D.N., and Carruthers, A. (1991) Cholate-solubilized erythrocyte glucose transporters exist as a mixture of homodimers and homotetramers. *Biochemistry* **30**: 4654–8.

Hein, C., Springael, J.Y., Volland, C., Haguenauer-Tsapis, R., and André, B. (1995) NPl1, an essential yeast gene involved in induced degradation of Gap1 and Fur4 permeases, encodes the Rsp5 ubiquitin-protein ligase. *Mol Microbiol* **18**: 77–87.

Held, M. a, Boulaflous, A., and Brandizzi, F. (2008) Advances in fluorescent protein-based imaging for the analysis of plant endomembranes. *Plant Physiol* **147**: 1469–81.

Hellyer, N.J., Cheng, K., and Koland, J.G. (1998) ErbB3 (HER3) interaction with the p85 regulatory subunit of phosphoinositide 3-kinase. *Biochem J* **333**: 757–63.

Herrador, A., Herranz, S., Lara, D., and Vincent, O. (2010) Recruitment of the ESCRT machinery to a putative seven-transmembrane-domain receptor is mediated by an arrestin-related protein. *Mol Cell Biol* **30**: 897–907.

Herranz, S., Rodríguez, J.M., Bussink, H.-J., Sánchez-Ferrero, J.C., Arst, H.N., Peñalva, M. a, and Vincent, O. (2005) Arrestin-related proteins mediate pH signaling in fungi. *Proc Natl Acad Sci U S A* **102**: 12141–6.

Hervás-Aguilar, A., Galindo, A., and Peñalva, M. a (2010) Receptor-independent Ambient pH signaling by ubiquitin attachment to fungal arrestin-like PalF. *J Biol Chem* **285**: 18095–102.

Hettema, E.H., Valdez-Taubas, J., and Pelham, H.R.B. (2004) Bsd2 binds the ubiquitin ligase Rsp5 and mediates the ubiquitination of transmembrane proteins. *EMBO J* **23**: 1279–88.

Heuser, J.E., and Anderson, R.G. (1989) Hypertonic media inhibit receptor-mediated endocytosis by blocking clathrin-coated pit formation. *J Cell Biol* **108**: 389–400.

Hicke, L., and Dunn, R. (2003) Regulation of membrane protein transport by ubiquitin and ubiquitin-binding proteins. *Annu Rev Cell Dev Biol* **19**: 141–72.

Hicke, L., and Riezman, H. (1996) Ubiquitination of a yeast plasma membrane receptor signals its ligand-stimulated endocytosis. *Cell* **84**: 277–87.

Higuchi, Y., Shoji, J., Arioka, M., and Kitamoto, K. (2009) Endocytosis is crucial for cell polarity and apical membrane recycling in the filamentous fungus *Aspergillus oryzae*. *Eukaryot Cell* **8**: 37–46.

Hirst, J., Barlow, L.D., Francisco, G.C., Sahlender, D.A., Seaman, M.N.J., Dacks, J.B., and Robinson, M.S. (2011) The fifth adaptor protein complex. *PLoS Biol* **9**: e1001170.

Hohmann, S., Krantz, M., and Nordlander, B. (2007) Yeast osmoregulation. *Methods Enzymol* **428**: 29–45.

Houbraken, J., Frisvad, J.C., and Samson, R.A. (2011) Fleming's penicillin producing strain is not *Penicillium chrysogenum* but *P. rubens*. *IMA Fungus* **2**: 87–95.

Houbraken, J., Vries, R.P. de, and Samson, R.A. (2014) Modern taxonomy of biotechnologically important *Aspergillus* and *Penicillium* species. In *Advances in applied microbiology*. Elsevier, pp. 199–249.

Hu, C.-D., Chinenov, Y., and Kerppola, T.K. (2002) Visualization of interactions among bZIP and Rel family proteins in living cells using bimolecular fluorescence complementation. *Mol Cell* **9**: 789–98.

Huckaba, T.M., Gay, A.C., Pantalena, L.F., Yang, H.-C., and Pon, L.A. (2004) Live cell imaging of the assembly, disassembly, and actin cable-dependent movement of endosomes and actin patches in the budding yeast, *Saccharomyces cerevisiae*. *J Cell Biol* **167**: 519–30.

Hunte, C, Screpanti, E., Venturi, M., Rimon, A., Padan, E., and Michel, H. (2005) Structure of a Na+/H+ antiporter and insights into mechanism of action and regulation by pH. *Nature* **435**: 1197–202.

Ito, Y., Uemura, T., Shoda, K., Fujimoto, M., Ueda, T., and Nakano, A. (2012) cis-Golgi proteins accumulate near the ER exit sites and act as the scaffold for Golgi regeneration after brefeldin A treatment in tobacco BY-2 cells. *Mol Biol Cell* **23**: 3203–14.

Jones, G.W., Hooley, P., Farrington, S.M., Shawcross, S.G., Iwanejko, L.A., and Strike, P. (1999) Cloning and characterisation of the sagA gene of *Aspergillus nidulans*: a gene which affects sensitivity to DNA-damaging agents. *Mol Gen Genet* **261**: 251–8.

Kabeche, R., Baldissard, S., Hammond, J., Howard, L., and Moseley, J.B. (2011) The filament-forming protein Pil1 assembles linear eisosomes in fission yeast. *Mol Biol Cell* **22**: 4059–67.

Kaksonen, M., Sun, Y., and Drubin, D.G. (2003) A pathway for association of receptors, adaptors, and actin during endocytic internalization. *Cell* **115**: 475–87.

Karachaliou, M., Amillis, S., Evangelinos, M., Kokotos, A.C., Yalelis, V., and Diallinas, G. (2013) The arrestin-like protein ArtA is essential for ubiquitination and endocytosis of the UapA transporter in response to both broad-range and specific signals. *Mol Microbiol* **88**: 301–317.

Kebbel, F. (2013) Structural and Functional Characterization of the Integral Membrane Proteins CitS and CCR5 by Electron Microscopy. Ph.D thesis, University of Basel. Switzerland. pp. 1–20.

Kee, Y., Muñoz, W., Lyon, N., and Huibregtse, J.M. (2006) The deubiquitinating enzyme Ubp2 modulates Rsp5-dependent Lys63-linked polyubiquitin conjugates in Saccharomyces cerevisiae. *J Biol Chem* **281**: 36724–31.

Kelavkar, U., Rao, K.S., and Ghhatpar, H.S. (1993) Sodium chloride stress induced morphological and ultrastructural changes in *Aspergillus repens*. *Indian J Exp Biol* **31**: 511–5.

Kerppola, T.K. (2006) Visualization of molecular interactions by fluorescence complementation. *Nat Rev Mol Cell Biol* **7**: 449–56.

Kilic, F., and Rudnick, G. (2000) Oligomerization of serotonin transporter and its functional consequences. *Proc Natl Acad Sci U S A* **97**: 3106–11.

Kirchhausen, T. (2000) Three ways to make a vesicle. *Nat Rev Mol Cell Biol* **1**: 187–98.

Kirk, P.M., Cannon, P.F., Minter, D.W., and Stalpers, J.A. (2008) *Dictionary of the Fungi*. 10th ed., Wallingford: CABI, .

Kjeldsen, T. (2000) Yeast secretory expression of insulin precursors. *Appl Microbiol Biotechnol* **54**: 277–86.

Kocabas, A.M., Rudnick, G., and Kilic, F. (2003) Functional consequences of homo- but not hetero-oligomerization between transporters for the biogenic amine neurotransmitters. *J Neurochem* **85**: 1513–20.

Kolb, V.M. (1997) Novel and unusual nucleosides as drugs. *Prog Drug Res* **48**: 195–232.

Kölling, R., and Hollenberg, C.P. (1994) The ABC-transporter Ste6 accumulates in the plasma membrane in a ubiquitinated form in endocytosis mutants. *EMBO J* **13**: 3261–71.

Komis, G., Apostolakos, P., and Galatis, B. (2002) Hyperosmotic stress induces formation of tubulin macrotubules in root-tip cells of Triticum turgidum: their probable involvement in protoplast volume control. *Plant Cell Physiol* **43**: 911–22.

Koning, H. De, and Diallinas, G. (2000) Nucleobase transporters (review). *Mol Membr Biol* **17**: 75–94.

Korkhov, V.M., Farhan, H., Freissmuth, M., and Sitte, H.H. (2004) Oligomerization of the {gamma}-aminobutyric acid transporter-1 is driven by an interplay of polar and hydrophobic interactions in transmembrane helix II. *J Biol Chem* **279**: 55728–36.

Kosti, V., Lambrinidis, G., Myrianthopoulos, V., Diallinas, G., and Mikros, E. (2012) Identification of the substrate recognition and transport pathway in a eukaryotic member of the nucleobase-ascorbate transporter (NAT) family. *PLoS One* **7**: e41939.

Kosti, V., Papageorgiou, I., and Diallinas, G. (2010) Dynamic elements at both cytoplasmically and extracellularly facing sides of the UapA transporter selectively control the accessibility of substrates to their translocation pathway. *J Mol Biol* **397**: 1132–43.

Koukaki, M., Giannoutsou, E., Karagouni, A., and Diallinas, G. (2003) A novel improved method for *Aspergillus nidulans* transformation. *J Microbiol Methods* **55**: 687–695.

Koukaki, M., Vlanti, A., Goudela, S., Pantazopoulou, A., Gioule, H., Tournaviti, S., and Diallinas, G. (2005) The nucleobase-ascorbate transporter (NAT) signature motif in UapA defines the function of the purine translocation pathway. *J Mol Biol* **350**: 499–513.

Krishnamurthy, H., Piscitelli, C.L., and Gouaux, E. (2009) Unlocking the molecular secrets of sodium-coupled transporters. *Nature* **459**: 347–55.

Krypotou, E., and Diallinas, G. (2014) Transport assays in filamentous fungi: kinetic characterization of the UapC purine transporter of *Aspergillus nidulans*. *Fungal Genet Biol* **63**: 1–8.

Krypotou, E., Kosti, V., Amillis, S., Myrianthopoulos, V., Mikros, E., and Diallinas, G. (2012) Modeling, substrate docking, and mutational analysis identify residues essential for the function and specificity of a eukaryotic purine-cytosine NCS1 transporter. *J Biol Chem* **287**: 36792–803.

Krypotou, E., Lamprinidis, G., Evangelidis, T., Mikros, E., and Diallinas, G. (2014) Modelling, substrate docking and mutational analysis identify residues essential for function and specificity of the major fungal purine transporter AzgA. *Mol Microbiol* Epub ahead of print.

Kubler, E., Dohlman, H.G., and Lisanti, M.P. (1996) Identification of Triton X-100 Insoluble Membrane Domains in the Yeast Saccharomyces cerevisiae: LIPID REQUIREMENTS FOR TARGETING OF HETEROTRIMERIC G-PROTEIN SUBUNITS. *J Biol Chem* **271**: 32975–32980.

Las Rivas, J. De, and Fontanillo, C. (2010) Protein-protein interactions essentials: key concepts to building and analyzing interactome networks. *PLoS Comput Biol* **6**: e1000807.

Lasry, I., Golan, Y., Berman, B., Amram, N., Glaser, F., and Assaraf, Y.G. (2014) In situ dimerization of multiple wild type and mutant zinc transporters in live cells using bimolecular fluorescence complementation. *J Biol Chem* **289**: 7275–92.

Lauwers, E., Erpapazoglou, Z., Haguenauer-Tsapis, R., and André, B. (2010) The ubiquitin code of yeast permease trafficking. *Trends Cell Biol* **20**: 196–204.

Lemmon, M. a, Flanagan, J.M., Treutlein, H.R., Zhang, J., and Engelman, D.M. (1992) Sequence specificity in the dimerization of transmembrane alpha-helices. *Biochemistry* **31**: 12719–25.

Lemmon, M.A., Treutlein, H.R., Adams, P.D., Brünger, A.T., and Engelman, D.M. (1994) A dimerization motif for transmembrane alpha-helices. *Nat Struct Biol* **1**: 157–63.

Lemuh, N.D., Diallinas, G., Frillingos, S., Mermelekas, G., Karagouni, A.D., and Hatzinikolaou, D.G. (2009) Purification and partial characterization of the xanthine-uric acid transporter (UapA) of *Aspergillus nidulans*. *Protein Expr Purif* **63**: 33–9.

Léon, S., Erpapazoglou, Z., and Haguenauer-Tsapis, R. (2008) Ear1p and Ssh4p are new adaptors of the ubiquitin ligase Rsp5p for cargo ubiquitylation and sorting at multivesicular bodies. *Mol Biol Cell* **19**: 2379–88.

Léon, S., and Haguenauer-Tsapis, R. (2009) Ubiquitin ligase adaptors: regulators of ubiquitylation and endocytosis of plasma membrane proteins. *Exp Cell Res* **315**: 1574–83.

Leung, J., Karachaliou, M., Alves, C., Diallinas, G., and Byrne, B. (2010) Expression and purification of a functional uric acid-xanthine transporter (UapA). *Protein Expr Purif* **72**: 139–146.

Li, Y., Cheng, S.-Y., Chen, N., and Reith, M.E.A. (2010) Interrelation of dopamine transporter oligomerization and surface presence as studied with mutant transporter proteins and amphetamine. *J Neurochem* **114**: 873–85.

Liang, W.J., Johnson, D., and Jarvis, S.M. (2001) Vitamin C transport systems of mammalian cells. *Mol Membr Biol* **18**: 87–95.

Liguori, L., Marques, B., Villegas-Méndez, A., Rothe, R., and Lenormand, J.-L. (2007) Production of membrane proteins using cell-free expression systems. *Expert Rev Proteomics* **4**: 79–90.

Lin, C.H., MacGurn, J.A., Chu, T., Stefan, C.J., and Emr, S.D. (2008) Arrestin-related ubiquitin-ligase adaptors regulate endocytosis and protein turnover at the cell surface. *Cell* **135**: 714–25.

Liu, X.F., Supek, F., Nelson, N., and Culotta, V.C. (1997) Negative Control of Heavy Metal Uptake by the *Saccharomyces cerevisiae* BSD2 Gene. *J Biol Chem* **272**: 11763–11769.

Liu, Y., Engelman, D.M., and Gerstein, M. (2002) Genomic analysis of membrane protein families: abundance and conserved motifs. *Genome Biol* **3**: research0054.

Lockington, R.A., and Kelly, J.M. (2002) The WD40-repeat protein CreC interacts with and stabilizes the deubiquitinating enzyme CreB *in vivo* in *Aspergillus nidulans*. *Mol Microbiol* **43**: 1173–1182.

Lonhienne, T.G. a, Sagulenko, E., Webb, R.I., Lee, K.-C., Franke, J., Devos, D.P., *et al.* (2010) Endocytosis-like protein uptake in the bacterium *Gemmata obscuriglobus*. *Proc Natl Acad Sci U S A* **107**: 12883–8.

Lu, F., Li, S., Jiang, Y., Jiang, J., Fan, H., Lu, G., *et al.* (2011) Structure and mechanism of the uracil transporter UraA. *Nature* **472**: 243–6.

Luckey, M. (2008) *Membrane Structural Biology: with biochemical and biophysical foundations*. Cambridge University Press, .

Lutzoni, F., Kauff, F., Cox, C.J., McLaughlin, D., Celio, G., Dentinger, B., *et al.* (2004) Assembling the fungal tree of life: progress, classification, and evolution of subcellular traits. *Am J Bot* **91**: 1446–1480.

MacGurn, J. a, Hsu, P.C., Smolka, M.B., and Emr, S.D. (2011) TORC1 regulates endocytosis via Npr1-mediated phosphoinhibition of a ubiquitin ligase adaptor. *Cell* **147**: 1104–1117.

Magliery, T., Wilson, C., Pan, W., Mishler, D., Ghosh, I., Hamilton, A.D., and Regan, L. (2005) Detecting protein-protein interactions with a green fluorescent protein fragment reassembly trap: scope and mechanism. *J Am Chem Soc* **127**: 146–157.

Malinska, K., Malinsky, J., Opekarova, M., and Tanner, W. (2004) Distribution of Can1p into stable domains reflects lateral protein segregation within the plasma membrane of living *S. cerevisiae* cells. *J Cell Sci* **117**: 6031–41.

Malínská, K., Malínský, J., Opekarová, M., and Tanner, W. (2003) Visualization of protein compartmentation within the plasma membrane of living yeast cells. *Mol Biol Cell* **14**: 4427–36.

Mancusso, R., Gregorio, G.G., Liu, Q., and Wang, D.-N. (2012) Structure and mechanism of a bacterial sodium-dependent dicarboxylate transporter. *Nature* **491**: 622–6.

Marzluf, G.A. (1997) Genetic regulation of nitrogen metabolism in the fungi. *Microbiol Mol Biol Rev* **61**: 17–32.

Maurino, V.G., Grube, E., Zielinski, J., Schild, A., Fischer, K., and Flügge, U.-I. (2006) Identification and expression analysis of twelve members of the nucleobase-ascorbate transporter (NAT) gene family in *Arabidopsis thaliana*. *Plant Cell Physiol* **47**: 1381–93.

McGovern, P.E., Zhang, J., Tang, J., Zhang, Z., Hall, G.R., Moreau, R.A., *et al.* (2004) Fermented beverages of pre- and proto-historic China. *Proc Natl Acad Sci U S A* **101**: 17593–8.

Merhi, A., and André, B. (2012) Internal amino acids promote Gap1 permease ubiquitylation via TORC1/Npr1/14-3-3-dependent control of the Bul arrestin-like adaptors. *Mol Cell Biol* **32**: 4510–22.

Mettlen, M., Pucadyil, T., Ramachandran, R., and Schmid, S.L. (2009) Dissecting dynamin's role in clathrin-mediated endocytosis. *Biochem Soc Trans* **37**: 1022–1026.

Midgett, C.R., and Madden, D.R. (2007) Breaking the bottleneck: eukaryotic membrane protein expression for high-resolution structural studies. *J Struct Biol* **160**: 265–74.

Milner, H., Béliveau, R., and Jarvis, S. (1994) The in situ size of the dopamine transporter is a tetramer as estimated by radiation inactivation. *Biochim Biophys Acta* **1190**: 185–187.

Miranda, M., and Sorkin, A. (2007) Regulation of Receptors and Transporters by Ubiquitination: New insights into surprisingly similar mechanisms. *Mol Interv* **7**: 157–167.

Morris, N.R. (1975) Mitotic mutants of *Aspergillus nidulans*. *Genet Res* **26**: 237–54.

Morris, N.R., and Enos, A.P. (1992) Mitotic gold in a mold: *Aspergillus* genetics and the biology of mitosis. *Trends Genet* **8**: 32–7.

Murakami, S., Nakashima, R., Yamashita, E., and Yamaguchi, A. (2002) Crystal structure of bacterial multidrug efflux transporter AcrB. *Nature* **419**: 587–93.

Murray, A.W., and Szostak, J.W. (1983) Construction of artificial chromosomes in yeast. *Nature* **305**: 189–193.

Nayak, T., Szewczyk, E., Oakley, C.E., Osmani, A., Ukil, L., Murray, S.L., *et al.* (2006) A versatile and efficient gene-targeting system for *Aspergillus nidulans*. *Genetics* **172**: 1557–66.

Nelson, D.L., and Cox, M.M. (2004) Biological membranes and transport. In *Lehninger Principles of Biochemistry*. W. H. Freeman & Company, .

Newpher, T.M., and Lemmon, S.K. (2006) Clathrin is important for normal actin dynamics and progression of Sla2p-containing patches during endocytosis in yeast. *Traffic* **7**: 574–88.

Newpher, T.M., Smith, R.P., Lemmon, V., and Lemmon, S.K. (2005) *In vivo* dynamics of clathrin and its adaptor-dependent recruitment to the actin-based endocytic machinery in yeast. *Dev Cell* **9**: 87–98.

Niemela, P.S., Ollila, S., Hyvonen, M.T., Karttunen, M., and Vattulainen, I. (2007) Assessing the Nature of Lipid Raft Membranes. *PLoS Comput Biol* **3**: 304–312.

Nikko, E., and Pelham, H.R.B. (2009) Arrestin-mediated endocytosis of yeast plasma membrane transporters. *Traffic* **10**: 1856–67.

Nikko, E., Sullivan, J. a, and Pelham, H.R.B. (2008) Arrestin-like proteins mediate ubiquitination and endocytosis of the yeast metal transporter Smf1. *EMBO Rep* **9**: 1216–21.

O'Donnell, A.F., Apffel, A., Gardner, R.G., and Cyert, M.S. (2010) Arrestins Aly1 and Aly2 Regulate Intracellular Trafficking in Response to Nutrient Signaling. *Mol Biol Cell* **21**: 3552–3566.

O'Donnell, A.F., Huang, L., Thorner, J., and Cyert, M.S. (2013) A calcineurin-dependent switch controls the trafficking function of α-arrestin Aly1/Art6. *J Biol Chem* **288**: 24063–80.

Oates, J., King, G., and Dixon, A.M. (2010) Strong oligomerization behavior of PDGFbeta receptor transmembrane domain and its regulation by the juxtamembrane regions. *Biochim Biophys Acta* **1798**: 605–15.

Ostermeier, C., and Michel, H. (1997) Crystallization of membrane proteins. *Curr Opin Struct Biol* **7**: 697–701.

Paiva, S., Vieira, N., Nondier, I., Haguenauer-Tsapis, R., Casal, M., and Urban-Grimal, D. (2009) Glucose-induced ubiquitylation and endocytosis of the yeast Jen1 transporter: role of lysine 63-linked ubiquitin chains. *J Biol Chem* **284**: 19228–36.

Pantazopoulou, A., and Diallinas, G. (2006) The first transmembrane segment (TMS1) of UapA contains determinants necessary for expression in the plasma membrane and purine transport. *Mol Membr Biol* **23**: 337–48.

Pantazopoulou, A., and Diallinas, G. (2007) Fungal nucleobase transporters. *FEMS Microbiol Rev* **31**: 657–75.

Pantazopoulou, A., Lemuh, N.D., Hatzinikolaou, D.G., Drevet, C., Cecchetto, G., Scazzocchio, C., and Diallinas, G. (2007) Differential physiological and developmental expression of the UapA and AzgA purine transporters in *Aspergillus nidulans*. *Fungal Genet Biol* **44**: 627–40.

Pantazopoulou, A., and Peñalva, M. (2009) Organization and dynamics of the *Aspergillus nidulans* Golgi during apical extension and mitosis. *Mol Biol Cell* **20**: 4335–4347.

Papageorgiou, I., Gournas, C., Vlanti, A., Amillis, S., Pantazopoulou, A., and Diallinas, G. (2008) Specific interdomain synergy in the UapA transporter determines its unique specificity for uric acid among NAT carriers. *J Mol Biol* **382**: 1121–35.

Park, H.R., Cockrell, L.M., Du, Y., Kasinski, A., Havel, J., Zhao, J., *et al.* (2008) Protein-Protein Interactions. In *Molecular Biomethods Handbook*. Walker, J.M., and Rapley, R. (eds). Humana Press, Totowa, NJ. pp. 463–494.

Pasteur, L. (1857) Mémoire sur la fermentation alcoolique. *Compte-rendus l'Académie des Sci* **45**: 1032–1036.

Pateman, J.A., Cove, D.J., Rever, B.M., and Roberts, D.B. (1964) A common co-factor for nitrate reductase and xanthine dehydrogenase which also regulates the synthesis of nitrate redutase. *Nature* **201**: 58–60.

Patterson, G.H., Hirschberg, K., Polishchuk, R.S., Gerlich, D., Phair, R.D., and Lippincott-schwartz, J. (2008) Transport through the Golgi apparatus by rapid partitioning within a two-phase membrane system. *Cell* **133**: 1055–1067.

Pawson, T., and Gish, G. (2005) Protein-Protein Interactions: A Common Theme in Cell Biology. In *Protein-Protein Interactions: A Molecular Cloning Manual*. Golemis, E.A., and Adams, P.D. (eds). Cold Spring Harbor Press, New York. pp. 1–11.

Pearson, C., Xu, K., Sharpless, K.E., and Harris, S.D. (2004) MesA, a novel fungal protein required for the stabilization of polarity axes in *Aspergillus nidulans*. *Mol Biol Cell* **15**: 3658–3672.

Peñalva, M.A. (2005) Tracing the endocytic pathway of *Aspergillus nidulans* with FM4-64. *Fungal Genet Biol* **42**: 963–75.

Peñalva, M.A. (2010) Endocytosis in filamentous fungi: Cinderella gets her reward. *Curr Opin Microbiol* **13**: 684–92.

Peñalva, M.A., Galindo, A., Abenza, J.F., Pinar, M., Calcagno-Pizarelli, A.M., Arst, H.N.J., and Pantazopoulou, A. (2012) Searching for gold beyond mitosis. Mining intracellular membrane traffic in *Aspergillus nidulans*. *Cell Logist* **2**: 2–14.

Peñalva, M.A., Tilburn, J., Bignell, E., and Arst, H.N. (2008) Ambient pH gene regulation in fungi: making connections. *Trends Microbiol* **16**: 291–300.

Phizicky, E.M., and Fields, S. (1995) Protein-protein interactions: methods for detection and analysis. *Microbiol Rev* **59**: 94–123.

Plotkowski, M.L., Kim, S., Phillips, M.L., Partridge, A.W., Deber, C.M., and Bowie, J.U. (2007) Transmembrane domain of myelin protein zero can form dimers: possible implications for myelin construction. *Biochemistry* **46**: 12164–73.

Ponnambalam, S., and Baldwin, S.A. (2003) Constitutive protein secretion from the trans-Golgi network to the plasma membrane. *Mol Membr Biol* **20**: 129–39.

Pontecorvo, G., Roper, J.A., Chemmons, L.M., Macdonald, K.D., and Bufton, A.W.J. (1953) The genetics of *Aspergillus nidulans*. *Adv Genet* **5**: 145–238.

Pretorius, I.S., Toit, M., and Rensburg, P. Van (2003) Designer Yeasts for the Fermentation Industry of the 21 st Century. *Food Technol Biotechnol* **41**: 3–10.

Privé, G.G. (2007) Detergents for the stabilization and crystallization of membrane proteins. *Methods* **41**: 388–97.

Pugacheva, E.N., and Golemis, E. (2005) Building a Better Web: Progress in the Concept and Methodology of Protein Interaction Studies. In *Protein-Protein Interactions: A Molecular Cloning Manual*. Golemis, E.A., and Adams, P.D. (eds). Cold Spring Harbor Press, New York. pp. 13–36.

Quintero-Monzon, O., Rodal, A.A., Strokopytov, B., Almo, S.C., and Goode, B.L. (2005) Structural and functional dissection of the Abp1 ADFH actin-binding domain reveals versatile in vivo adapter functions. *Mol Biol Cell* **16**: 3128–39.

Raghukumar, C., Damare, S.R., and Singh, P. (2010) A review on deep-sea fungi: occurrence, diversity and adaptations. *Bot Mar* **53**: 479–492.

Rapoport, T.A. (2008) Protein transport across the endoplasmic reticulum membrane. *FEBS J* **275**: 4471–8.

Raunser, S., Appel, M., Ganea, C., Geldmacher-kaufer, U., Fendler, K., and Kuhlbrandt, W. (2006) Structure and Function of Prokaryotic Glutamate Transporters from *Escherichia coli* and *Pyrococcus horikoshii*. *Biochemistry* **45**: 12796–12805.

Ravagnani, A., Gorfinkiel, L., Langdon, T., Diallinas, G., Adjadj, E., Demais, S., *et al.* (1997) Subtle hydrophobic interactions between the seventh residue of the zinc finger loop and the first base of an HGATAR sequence determine promoter-specific recognition by the *Aspergillus nidulans* GATA factor AreA. *EMBO J* **16**: 3974–86.

Reider, A., and Wendland, B. (2011) Endocytic adaptors-social networking at the plasma membrane. *J Cell Sci* **124**: 1613–22.

Renard, H.-F., Demaegd, D., Guerriat, B., and Morsomme, P. (2010) Efficient ER exit and vacuole targeting of yeast Sna2p require two tyrosine-based sorting motifs. *Traffic* **11**: 931–46.

Reyes, N., Ginter, C., and Boudker, O. (2009) Transport mechanism of a bacterial homologue of glutamate transporters. *Nature* **462**: 880–5.

Robinson, M.S. (2004) Adaptable adaptors for coated vesicles. *Trends Cell Biol* **14**: 167–74.

Rundles, R.W., Metz, E.N., and Silberman, H.R. (1966) Allopurinol in the treatment of gout. *Ann Intern Med* **64**: 229–58.

Russ, W.P., and Engelman, D.M. (2000) The GxxxG motif: a framework for transmembrane helix-helix association. *J Mol Biol* **296**: 911–9.

Saier, M.H. (1994) Computer-aided analyses of transport protein sequences: gleaning evidence concerning function, structure, biogenesis, and evolution. *Microbiol Rev* **58**: 71–93.

Salom, D., and Palczewski, K. (2011) Structural biology of membrane proteins. In *Production of Membrane Proteins: Strategies for Expression and Isolation*. Robinson, A.S. (ed.). Wiley-VCH Verlag GmbH & Co, pp. 249–273.

Sambrook, J., and Russel, D.W. (2001) *Molecular Cloning: A Laboratory Manual*. 3rd ed., Cold Spring Harbor Laboratory Press, New York.

Sato, K., and Nakano, A. (2003) Oligomerization of a Cargo Receptor Directs Protein Sorting into COPII-coated Transport Vesicles. *Mol Biol Cell* **14**: 3055–3063.

Sato, K., and Nakano, A. (2007) Mechanisms of COPII vesicle formation and protein sorting. *FEBS Lett* **581**: 2076–82.

Scazzocchio, C. (2006) *Aspergillus* genomes: secret sex and the secrets of sex. *Trends Genet* **22**: 521–5.

Scazzocchio, C. (2009) *Aspergillus*: A Multifaceted Genus. In *Encyclopedia of Microbiology.* Schaechter, M. (ed.). Elsevier, Oxford. pp. 401–421.

Scazzocchio, C. (2013) In praise of erroneous hypotheses. *Fungal Genet Biol* **58-59**: 126–131.

Scazzocchio, C., Sdrin, N., and Ong, G. (1982) Positive regulation in a eukaryote, a study of the *uaY* gene of *Aspergillus nidulans*: I. Characterization of alleles, dominance and complementation studies, and a fine structure map of the *uaY-oxpA* cluster. *Genetics* **100**: 185–208.

Scazzocchio, C., Vangelatos, I., and Sophianopoulou, V. (2011) Eisosomes and membrane compartments in the ascomycetes: A view from *Aspergillus nidulans*. *Commun Integr Biol* **4**: 64–8.

Schmid, J. a, Scholze, P., Kudlacek, O., Freissmuth, M., Singer, E. a, and Sitte, H.H. (2001) Oligomerization of the human serotonin transporter and of the rat GABA transporter 1 visualized by fluorescence resonance energy transfer microscopy in living cells. *J Biol Chem* **276**: 3805–10.

Schoch, C.L., Sung, G.-H., López-Giráldez, F., Townsend, J.P., Miadlikowska, J., Hofstetter, V., *et al.* (2009) The Ascomycota tree of life: a phylum-wide phylogeny clarifies the origin and evolution of fundamental reproductive and ecological traits. *Syst Biol* **58**: 224–39.

Scholze, P., Freissmuth, M., and Sitte, H.H. (2002) Mutations within an intramembrane leucine heptad repeat disrupt oligomer formation of the rat GABA transporter 1. *J Biol Chem* **277**: 43682–90.

Schroers, A., Burkovski, A., Wohlrab, H., and Krämer, R. (1998) The phosphate carrier from yeast mitochondria. Dimerization is a prerequisite for function. *J Biol Chem* **273**: 14269–76.

Schwarz, D., Dötsch, V., and Bernhard, F. (2008) Production of membrane proteins using cell-free expression systems. *Proteomics* **8**: 3933–46.

Seger, S., Rischatsch, R., and Philippsen, P. (2011) Formation and stability of eisosomes in the filamentous fungus *Ashbya gossypii*. *J Cell Sci* **124**: 1629–34.

Selbmann, L., Hoog, G. De, Mazzaglia, A., Friedmann, E.I., and Onofri, S. (2005) Fungi at the edge of life: cryptoendolithic black fungi from Antarctic desert. *Stud Mycol* **51**: 1–32.

Shearer (1986) Teleomorph/Anamorph Connections of Fungi. In *The Biology of Marine Fungi*. Moss, S.T. (ed.). Cambridge University Press, p. 257.

Shenoy, S.K., and Lefkowitz, R.J. (2005) Receptor-specific ubiquitination of beta-arrestin directs assembly and targeting of seven-transmembrane receptor signalosomes. *J Biol Chem* **280**: 15315–24.

Sherman, F. (1997) Yeast genetics. In *The Encyclopedia of Molecular Biology and Molecular Medicine*. Meyers, R.A. (ed.). VCH Publisher, Weinheim. pp. 302–325.

Shoemaker, B. a, and Panchenko, A.R. (2007) Deciphering protein-protein interactions. Part I. Experimental techniques and databases. *PLoS Comput Biol* **3**: e42.

Simon, S.M. (2008) Golgi Governance : The Third Way. *Cell* **133**: 951–953.

Simons, K., and Ikonen, E. (1997) Functional rafts in cell membranes. *Nature* **387**: 569–72.

Singer, S.J., and Nicolson, G.L. (1972) The Fluid Mosaic Model of the Structure of Cell Membranes. *Science (80-)* **175**: 720–731.

Slaninová, I., Sesták, S., Svoboda, A., and Farkas, V. (2000) Cell wall and cytoskeleton reorganization as the response to hyperosmotic shock in *Saccharomyces cerevisiae*. *Arch Microbiol* **173**: 245–52.

Solinger, J.A., and Spang, A. (2013) Tethering complexes in the endocytic pathway: CORVET and HOPS. *FEBS J* **280**: 2743–57.

Sorkina, T., Doolen, S., Galperin, E., Zahniser, N.R., and Sorkin, A. (2003) Oligomerization of dopamine transporters visualized in living cells by fluorescence resonance energy transfer microscopy. *J Biol Chem* **278**: 28274–83.

Sotiriou, S., Gispert, S., Cheng, J., Wang, Y., Chen, A., Hoogstraten-Miller, S., *et al.* (2002) Ascorbic-acid transporter Slc23a1 is essential for vitamin C transport into the brain and for perinatal survival. *Nat Med* **8**: 514–7.

Springael, J.Y., Galan, J.M., Haguenauer-Tsapis, R., and André, B. (1999) NH4+-induced down-regulation of the *Saccharomyces cerevisiae* Gap1p permease involves its ubiquitination with lysine-63-linked chains. *J Cell Sci* **112**: 1375–83.

Springer, S., Malkus, P., Borchert, B., Wellbrock, U., Duden, R., and Schekman, R. (2014) Regulated oligomerization induces uptake of a membrane protein into COPII vesicles independent of its cytosolic tail. *Traffic* **15**: 531–545.

Stagljar, I., and Fields, S. (2002) Analysis of membrane protein interactions using yeast-based technologies. *Trends Biochem Sci* **27**: 559–63.

Starr, T.L., Pagant, S., Wang, C.-W., and Schekman, R. (2012) Sorting signals that mediate traffic of chitin synthase III between the TGN/endosomes and to the plasma membrane in yeast. *PLoS One* **7**: e46386.

Steinberg, G. (2007) On the move: endosomes in fungal growth and pathogenicity. *Nat Rev Microbiol* **5**: 309–16.

Stewart, M. (2001) Structural basis for bending tropomyosin around actin in muscle thin filaments. *Proc Natl Acad Sci U S A* **98**: 8165–6.

Stimpson, H.E.M., Lewis, M.J., and Pelham, H.R.B. (2006) Transferrin receptor-like proteins control the degradation of a yeast metal transporter. *EMBO J* **25**: 662–72.

Strádalová, V., Stahlschmidt, W., Grossmann, G., Blazíková, M., Rachel, R., Tanner, W., and Malinsky, J. (2009) Furrow-like invaginations of the yeast plasma membrane correspond to membrane compartment of Can1. *J Cell Sci* **122**: 2887–94.

Strochlic, T.I., Schmiedekamp, B.C., Lee, J., Katzmann, D.J., and Burd, C.G. (2008) Opposing activities of the Snx3-retromer complex and ESCRT proteins mediate regulated cargo sorting at a common endosome. *Mol Biol Cell* **19**: 4694–706.

Suarez, T., Queiroz, M.V. De, Oestreicher, N., and Scazzocchio, C. (1995) The sequence and binding specificity of UaY , the specific regulator of the purine utilization pathway in *Aspergillus nidulans* , suggest an evolutionary relationship with the PPR1 protein of *Saccharomyces cerevisiae*. *EMBO J* **14**: 1453–1467.

Sudakin, V. (2005) Identification of protein-protein interactions by conventional column chromatography. In *Protein-Protein Interactions: A Molecular Cloning Manual*. Golemis, E.A., and Adams, P.D. (eds). Cold Spring Harbor Press, New York. pp. 37–54.

Sullivan, J.A., Lewis, M.J., Nikko, E., and Pelham, H.R.B. (2007) Multiple Interactions Drive Adaptor-Mediated Recruitment of the Ubiquitin Ligase Rsp5 to Membrane Proteins In Vivo and In Vitro. *Mol Biol Cell* **18**: 2429–2440.

Swaminathan, S., Amerik, A.Y., and Hochstrasser, M. (1999) The Doa4 deubiquitinating enzyme is required for ubiquitin homeostasis in yeast. *Mol Biol Cell* **10**: 2583–94.

Szilágyi, A., Grimm, V., Arakaki, A.K., and Skolnick, J. (2005) Prediction of physical protein-protein interactions. *Phys Biol* **2**: S1–16.

Taheri-Talesh, N., Horio, T., Araujo-Bazán, L., Dou, X., Espeso, E. a, Peñalva, M. a, *et al.* (2008) The tip growth apparatus of *Aspergillus nidulans*. *Mol Biol Cell* **19**: 1439–49.

Takahashi, M., Malathi, P., Preiser, H., and Jung, C.Y. (1985) Radiation inactivation studies on the rabbit kidney sodium-dependent glucose transporter. *J Biol Chem* **260**: 10551–6.

Takeshita, N., Higashitsuji, Y., Konzack, S., and Fischer, R. (2008) Apical sterol-rich membranes are essential for localizing cell end markers that determine growth directionality in the filamentous fungus *Aspergillus nidulans*. *Mol Biol Cell* **19**: 339–351.

Tang, H., Xu, J., and Cai, M. (2000) Pan1p, End3p, and S1a1p, three yeast proteins required for normal cortical actin cytoskeleton organization, associate with each other and play essential roles in cell wall morphogenesis. *Mol Cell Biol* **20**: 12–25.

Tavoularis, S., Scazzocchio, C., and Sophianopoulou, V. (2001) Functional expression and cellular localization of a green fluorescent protein-tagged proline transporter in *Aspergillus nidulans*. *Fungal Genet Biol* **33**: 115–25.

Tazebay, U.H., Sophianopoulou, V., Scazzocchio, C., and Diallinas, G. (1997) The gene encoding the major proline transporter of *Aspergillus nidulans* is upregulated during conidiospore germination and in response to proline induction and amino acid starvation. *Mol Microbiol* **24**: 105–17.

Teige, M., Scheikl, E., Reiser, V., Ruis, H., and Ammerer, G. (2001) Rck2, a member of the calmodulin-protein kinase family, links protein synthesis to high osmolarity MAP kinase signaling in budding yeast. *Proc Natl Acad Sci U S A* **98**: 5625–30.

Thom, C., and Raper, K.B. (1945) *A Manual of the Aspergilli*. The Williams & Wilkins Company, Baltimore.

Tilburn, J., Scazzocchio, C., Taylor, G.G., Zabicky-Zissman, J.H., Lockington, R.A., and Davies, R.W. (1983) Transformation by integration in *Aspergillus nidulans*. *Gene* **26**: 205–21.

Timberlake, W.E. (1990) Molecular genetics of *Aspergillus development*. *Annu Rev Genet* **24**: 5–36.

Todd, R.B., Davis, M.A., and Hynes, M.J. (2007) Genetic manipulation of *Aspergillus nidulans*: meiotic progeny for genetic analysis and strain construction. *Nat Protoc* **2**: 811–21.

Tokarev, A.A., Alfonso, A., and Segev, N. (2009) Overview of Intracellular Compartments and Trafficking Pathways. In *Trafficking Inside Cells: Pathways, Mechanisms and Regulation*. Segev, N. (ed.). Landes Bioscience and Springer Science+Business Media, Chicago. pp. 1–12.

Tomás, M., Martínez-Alonso, E., Ballesta, J., and Martínez-Menárguez, J.A. (2010) Regulation of ER-Golgi intermediate compartment tubulation and mobility by COPI coats, motor proteins and microtubules. *Traffic* **11**: 616–25.

Torres, G.E., Carneiro, A., Seamans, K., Fiorentini, C., Sweeney, A., Yao, W.D., and Caron, M.G. (2003) Oligomerization and trafficking of the human dopamine transporter. Mutational analysis identifies critical domains important for the functional expression of the transporter. *J Biol Chem* **278**: 2731–9.

Trankle, J.H., and Herrmann, C. (2005) Calorimetry-based approaches in analysis of Protein-Protein interactions. In *Protein-Protein Interactions: A Molecular Cloning Manual*. Golemis, E., and Adams, P.D. (eds). Cold Spring Harbor Press, New York. pp. 229–252.

Traub, L.M. (2009) Tickets to ride: selecting cargo for clathrin-regulated internalization. *Nat Rev Mol Cell Biol* **10**: 583–96.

Valdez-Taubas, J., Diallinas, G., Scazzocchio, C., and Rosa, A.L. (2000) Protein expression and subcellular localization of the general purine transporter UapC from Aspergillus nidulans. *Fungal Genet Biol* **30**: 105–13.

Valdez-Taubas, J., Harispe, L., Scazzocchio, C., Gorfinkiel, L., and Rosa, A.L. (2004) Ammonium-induced internalisation of UapC, the general purine permease from *Aspergillus nidulans. Fungal Genet Biol* **41**: 42–51.

Vangelatos, I., Roumelioti, K., Gournas, C., Suarez, T., Scazzocchio, C., and Sophianopoulou, V. (2010) Eisosome organization in the filamentous ascomycete *Aspergillus nidulans. Eukaryot Cell* **9**: 1441–54.

Verveer, P.J., Rocks, O., Harpur, A.G., and Bastiaens, P. (2005) Imaging protein interactions by FRET Microscopy. In *Protein-Protein Interactions: A Molecular Cloning Manual*. Golemis, E.A., and Adams, P.D. (eds). Cold Spring Harbor Press, New York. pp. 609–636.

Vitale, A. (2002) Physical methods. *Plant Mol Biol* **50**: 825–36.

Vlanti, A., Amillis, S., Koukaki, M., and Diallinas, G. (2006) A novel-type substrate-selectivity filter and ER-exit determinants in the UapA purine transporter. *J Mol Biol* **357**: 808–19.

Vlanti, A., and Diallinas, G. (2008) The *Aspergillus nidulans* FcyB cytosine-purine scavenger is highly expressed during germination and in reproductive compartments and is downregulated by endocytosis. *Mol Microbiol* **68**: 959–77.

Wachtler, V., Rajagopalan, S., and Balasubramanian, M.K. (2003) Sterol-rich plasma membrane domains in the fission yeast Schizosaccharomyces pombe. *J Cell Sci* **116**: 867–74.

Walker, G.M. (2009) Yeasts. In *Desk Encyclopedia of Microbiology*. Schaechter, M. (ed.). Elsevier, London. pp. 1174–1187.

Walther, T.C., Brickner, J.H., Aguilar, P.S., Bernales, S., Pantoja, C., and Walter, P. (2006) Eisosomes mark static sites of endocytosis. *Nature* **439**: 998–1003.

Watanabe, R., and Riezman, H. (2004) Differential ER exit in yeast and mammalian cells. *Curr Opin Cell Biol* **16**: 350–5.

Wesp, A., Hicke, L., Palecek, J., Lombardi, R., Aust, T., Munn, A.L., and Riezman, H. (1997) End4p/Sla2p interacts with actin-associated proteins for endocytosis in *Saccharomyces cerevisiae*. *Mol Biol Cell* **8**: 2291–306.

Weyand, S., Shimamura, T., Yajima, S., Suzuki, S., Mirza, O., Krusong, K., *et al.* (2008) Structure and molecular mechanism of a nucleobase-cation-symport-1 family transporter. *Science* **322**: 709–13.

Wittig, I., and Schägger, H. (2009) Native electrophoretic techniques to identify protein-protein interactions. *Proteomics* **9**: 5214–23.

Wong, S., and Wolfe, K.H. (2005) Birth of a metabolic gene cluster in yeast by adaptive gene relocation. *Nat Genet* **37**: 777–82.

Yamashita, A., Singh, S.K., Kawate, T., Jin, Y., and Gouaux, E. (2005) Crystal structure of a bacterial homologue of Na+/Cl--dependent neurotransmitter transporters. *Nature* **437**: 215–23.

Yernool, D., Boudker, O., Jin, Y., and Gouaux, E. (2004) Structure of a glutamate transporter homologue from *Pyrococcus horikoshii*. *Nature* **431**: 811–8.

Yerushalmi, H., Lebendiker, M., and Schuldiner, S. (1996) Negative dominance studies demonstrate the oligomeric structure of EmrE, a multidrug antiporter from *Escherichia coli*. *J Biol Chem* **271**: 31044–8.

Yildirim, M. a, Goh, K. Il, Cusick, M.E., Barabási, A.L., and Vidal, M. (2007) Drug-target network. *Nat Biotechnol* **25**: 1119–26.

Yin, Y., He, X., Szewczyk, P., Nguyen, T., and Chang, G. (2006) Structure of the multidrug transporter EmrD from *Escherichia coli*. *Science (80-)* **312**: 741–4.

Zamyatnin, A.A., Solovyev, A.G., Bozhkov, P. V, Valkonen, J.P.T., Morozov, S.Y., and Savenkov, E.I. (2006) Assessment of the integral membrane protein topology in living cells. *Plant J* **46**: 145–54.

Zaragoza, O., and Gancedo, J.M. (2000) Pseudohyphal growth is induced in *Saccharomyces cerevisiae* by a combination of stress and cAMP signalling. *Antonie Van Leeuwenhoek* **78**: 187–94.

Zhang, N., Castlebury, L.A., Miller, A.N., Huhndorf, S.M., Schoch, C.L., Seifert, K.A., *et al.* (2006) An overview of the systematics of the Sordariomycetes based on a four-gene phylogeny. *Mycologia* **98**: 1076–87.

Zheng, C., Liu, H.-H., Yuan, S., Zhou, J., and Zhang, B. (2010) Molecular basis of LMAN1 in coordinating LMAN1-MCFD2 cargo receptor formation and ER-to-Golgi transport of FV/FVIII. *Blood* **116**: 5698–706.

8

Appendix

8.1 Abbreviations

AFM	Atomic Force Microscopy
ARTs	Arrestin-Related Trafficking adaptors
ATP	Adenosine-Triphosphate
bp	Base pairs
BiFC	Bifluorescence Complementation assay
BSA	Bovine Serum Albumin
°C	Celsius degrees
CFTR	Cystic Fibrosis Transmembrane Conductance Regulator
CM	Complete Media
CMAC	7-amino-4-chloromethyl coumarin
CoIP	Coimmunoprecipitation
COPI	Coat Protein Complex I
COPII	Coat Protein Complex II
CORVET	Class C Core Vacuole/Endosome Tethering Complex
ΔACZ	*uapAΔ uapCΔ azgAΔ*
Da	Dalton
DDM	Dodecyl-β-D-maltoside
DRM	Detergent-resistant Membranes
EE	Early Endosome
EDTA	Ethylenediaminetetraacetic Acid
ER	Endoplasmic Reticulum
ERAD	ER-Associated Degradation
ERES	ER Exit Site
ERGIC	ER-Golgi Intermediate Compartment

ERQC	ER-derived Quality Control Compartment
ESCRT	Endosomal Sorting Complex Required for Transport
EtBr	Ethidium Bromide
EtOH	Ethanol
FP	Fluorescent Protein
GEF	Guanine Nucleotide Exchange Factor
GFP	Green Fluorescent Protein
h	Hour
H_2O_{dist}	Distilled water
HOG	High-Osmolarity Glycerol
HOPS	Homotypic Fusion and Vacuole Protein Sorting
HRP	Horse Radish Peroxidase
K_m	Michaelis-Menten constant
Lat-B	Latrunculin B
LB	Luria-Bertani
LE	Late Endosome
MCC	Membrane Compartment occupied by Can1
MCP	Membrane Compartment occupied by Pma1
MFS	Major Facilitator Superfamily
min	Minute
MM	Minimal media
mRFP	Monomeric Red Fluorescent Protein
MT	Microtubules
MVB	Multivesicular Body
NAT	Nucleobase–Ascorbate Transporters
NCS1	Nucleobase Cation Symporter family 1
NCS2	Nucleobase Cation Symporter family 2
NEM	*N*-ethylmaleimide
paba	p-aminobenzoic acid
panto	D-pantothenic acid
PCR	Polymerase Chain Reaction
PIC	Protease inhibitors cocktail
PM	Plasma Membrane
PMA	Phorbol 12-Myristate 13-Acetate
PRT	Purine-Related Transporter family
PY	PPXY motif
pyro	Pyridoxine
ribo	Riboflavin
rpm	Rounds per minute
RT	Room Temperature
sec	Second
SDS	Sodium Dodecyl Sulfate
SDS-PAGE	Sodium Dodecyl Sulfate Polyacrylamide Gel Electrophoresis
SM	Sec1/Munc18 proteins
SNAP	Soluble NSF (NEM-sensitive fusion protein) Attachment Protein

SNARE Soluble NSF (NEM-sensitive fusion protein) Attachment Protein Receptor
SRP Signal Recognition Particle
suc Sucrose
T_m Melting temperature
TCA Trichloroacetic Acid
TEM Transmission Electron Microscopy
tER transitional ER
TGN *trans*-Golgi Network
TMR Transmembrane Receptor
TMS Transmembrane Segment
u Unit
UA Uric Acid
UBD Ubiquitin-Binding Domain
UPR Unfolded Protein Response
Ura Uracil
UV Ultraviolet
wt Wild type
X Xanthine
YAC Yeast Artificial Chromosome
YFP Yellow Fluorescent Protein
YNB Yeast Nitrogen Base

Amino Acids

A Ala Alanine
C Cys Cysteine
D Asp Aspartic acid
E Glu Glutamic acid
F Phe Phenylalanine
G Gly Glycine
H His Histidine
I Ile Isoleucine
K Lys Lysine
L Leu Leucine
M Met Methionine
N Asn Asparagine
P Pro Proline
Q Gln Glutamine
R Arg Arginine
S Ser Serine
T Thr Threonine
V Val Valine
W Trp Tryptophan
Y Tyr Tyrosine

8.2   Plasmids used in this study

8.2.1 List of Plasmids used in this study

Plasmid Name	Based on	References
pAN510$_{expXS}$	-	(Papageorgiou *et al.*, 2008)
pDV8	-	(Takeshita *et al.*, 2008)
pDV7	-	(Takeshita *et al.*, 2008)
pAN510$_{exp}$-YFP$_C$	pAN510$_{expXS}$	this study
pAN510$_{exp}$-YFP$_N$	pAN510$_{expXS}$	this study
pAN510$_{exp}$	-	(Vlanti and Diallinas, 2008; Papageorgiou *et al.*, 2008)
pBS-argB:alcA	-	(Gournas *et al.*, 2010)
pBS-argB:alcA-uapA-YFP$_N$	pBS-argB:alcA	this study
pAN520$_{exp}$:alcA-uapA-YFP$_C$	pAN510$_{exp}$-YFP$_C$	this study
pAN510$_{exp}$:alcA-N409D	pAN510$_{exp}$	this study
pAN520$_{exp}$:alcA-uapA^{-XbaI}	pAN520$_{exp}$:alcA-uapA-YFP$_C$	this study
pBS-argB:alcA-uapA^{-XbaI}	pBS-argB:alcA-uapA-YFP$_N$	this study
pAN520$_{exp}$:alcA-uapA-YFP$_C$^{fix}	pAN520$_{exp}$:alcA-uapA^{-XbaI}	this study
pBS-argB:alcA-uapA-YFP$_N$^{fix}	pBS-argB:alcA-uapA^{-XbaI}	this study
pAN520$_{exp}$:alcA-DYDY-YFP$_C$	pAN520$_{exp}$:alcA-uapA-YFP$_C$^{fix}	this study
pBS-argB:alcA-DYDY-YFP$_N$	pBS-argB:alcA-uapA-YFP$_N$^{fix}	this study
pAN520$_{exp}$:alcA-I74D-YFP$_C$	pAN520$_{exp}$:alcA-uapA-YFP$_C$	this study
pBS-argB:alcA-I74D-YFP$_N$	pBS-argB:alcA-uapA-YFP$_N$	this study
pAN520$_{exp}$:alcA-TMS14Δ-YFP$_C$	pAN520$_{exp}$:alcA-uapA-YFP$_C$^{fix}	this study
pBS-argB:alcA-TMS14Δ-YFP$_N$	pBS-argB:alcA-uapA-YFP$_N$^{fix}	this study
pBS-argB:alcA-ctailess-His	pBS-argB:alcA-uapA^{-XbaI}	this study
pBS-argB:alcA-DYDY/A-His	pBS-argB:alcA-ctailess-His	this study
pBS-argB:alcA-GGG/A-His	pBS-argB:alcA-ctailess-His	this study
pBS-argB:alcA-uapA-His	pBS-argB:alcA-ctailess-His	this study
pAN520$_{exp}$:alcA-DYDY/A-GFP	pAN520$_{exp}$:alcA-uapA^{-XbaI}	this study
pAN520$_{exp}$:alcA-GGG/A-GFP	pAN520$_{exp}$:alcA-uapA^{-XbaI}	this study

8.2.2 Description of plasmids constructed in this study

The construction process of the plasmids generated in this study is briefly described, followed by the corresponding plasmid maps. For a detailed description of the cloning procedure, please refer to Materials and Methods (section 2.6). For the references of the plasmids used as cloning vectors, please refer to the list of plasmids used in this study (section 8.2.1). For the sequences of the primers used for

amplifying the cloning inserts or for site-directed mutagenesis, please refer to the list of oligonucleotides used in this study (section 8.3).

pAN510$_{exp}$-YFP$_C$ & pAN510$_{exp}$-YFP$_N$

YFP$_C$ and YFP$_N$ fragments were amplified by PCR from plasmids pDV8 and pDV7 and using the primers YFPcF/YFPnR and YFPnF/YFPnR, respectively. Amplified fragments were digested with XbaI restriction endonuclease and were cloned in XbaI digested pAN510$_{expXS}$ cloning vector, generating plasmids pAN510$_{exp}$-YFP$_C$ and pAN510$_{exp}$-YFP$_N$.

pBS-argB:alcA-uapA-YFP$_N$

The fragment *uapA-YFP$_N$-3'UTR* was PCR amplified from plasmid pAN510$_{exp}$-YFP$_N$ with the primers expBamF/3'UTR BglIIR and was double digested with BamHI/BglII restriction endonucleases. The digested fragment was cloned to a BamHI digested pBS-argB:alcA cloning vector, thus generating plasmid pBS-argB:alcA-uapA-YFP$_N$.

pAN520$_{exp}$:alcA-uapA-YFP$_C$

Plasmid pAN510$_{exp}$-YFP$_C$ was digested with SalI restriction endonuclease and *argB* selection marker was replaced with *pabaA* selection marker. The resulting plasmid was then double digested with NotI/BamHI restriction endonucleases and the endogenous UapA promoter was replaced with *alcA$_p$*, which was recovered from the pBS-argB:alcA-uapA-YFP$_N$ plasmid with a NotI/BamHI double digestion, thus generating the plasmid pAN520$_{exp}$:alcA-uapA-YFP$_C$.

pAN510$_{exp}$:alcA-N409D

UapA-N409D ORF was amplified by PCR using the primers expBamF/uapAXbaR. The amplified fragment was double digested with BamHI and XbaI restriction endonucleases and was cloned in a BamHI/XbaI digested pAN510$_{exp}$ cloning vector. The resulting plasmid was then double digested with NotI/BamHI restriction endonucleases and the endogenous UapA promoter was replaced with *alcA$_p$*, which was recovered from the pBS-argB:alcA-uapA-YFP$_N$ plasmid with a NotI/BamHI double digestion, thus generating the plasmid pAN510$_{exp}$:alcA-N409D.

$pAN520_{exp}$:alcA-uapA-YFP$_C$^{fix} & pBS-argB:alcA-uapA-YFP$_N$^{fix}

To enable the exchange of UapA ORF with mutant versions of UapA in the $pAN520_{exp}$:alcA-uapA-YFP$_C$ and pBS-argB:alcA-uapA-YFP$_N$ with a simple BamHI/XbaI digestion, the two plasmids were NotI/BamHI digested and cloned with the *alcA$_p$*, which had been previously amplified with the primers alcANotIF/alcABamHIR and digested with the same pair of endonucleases. This way, the Xba restriction site of the pBS-argB:alcA multicloning site was removed. The plasmids were then XbaI digested and religated to ensure the removal of the YFP fragments, thus generating plasmids **$pAN520_{exp}$:alcA-uapA^{-XbaI}** and **pBS-argB:alcA-uapA^{-XbaI}**. Next, the resulting plasmids were BamHI/XbaI digested and cloned with *uapA-YFP$_C$* and *uapA-YFP$_N$* that had previously been amplified with primers expBamHIF/GFPSpeIR and expBamHIF/YFPnSpeIR, respectively, and digested with BamHI/SpeI. This way the YFP fragments were fixed to the respective cloning vectors and the final plasmids ($pAN520_{exp}$:alcA-uapA-YFP$_C$^{fix} and pBS-argB:alcA-uapA-YFP$_N$^{fix}) could be used as cloning vectors for several UapA mutants.

$pAN520_{exp}$:alcA-DYDY/A-YFP$_C$ & pBS-argB:alcA-DYDY/A-YFP$_N$

$pAN520_{exp}$:alcA-uapA-YFP$_C$^{fix} and pBS-argB:alcA-uapA-YFP$_N$^{fix} were BamHI/XbaI digested and cloned with *uapA-DYDY/A*, which had previously been amplified with primers expBamHIF/uapAXbaR NS and digested with BamHI/XbaI, thus generating the plasmids $pAN520_{exp}$:alcA-DYDY/A-YFP$_C$ and pBS-argB:alcA-DYDY/A-YFP$_N$, respectively.

$pAN520_{exp}$:alcA-I74D-YFP$_C$ & pBS-argB:alcA-I74D-YFP$_N$

$pAN520_{exp}$:alcA-I74D-YFP$_C$ and pBS-argB:alcA-I74D-YFP$_N$ were constructed by site-directed mutagenesis of the $pAN520_{exp}$:alcA-uapA-YFP$_C$ and pBS-argB:alcA-uapA-YFP$_N$, respectively, using the primers BamTMS1F/BamTMS1R.

$pAN520_{exp}$:alcA-TMS14Δ-YFP$_C$ & pBS-argB:alcA-TMS14Δ-YFP$_N$

$pAN520_{exp}$:alcA-uapA-YFP$_C$^{fix} and pBS-argB:alcA-uapA-YFP$_N$^{fix} were BamHI/XbaI digested and cloned with *uapA-TMS14Δ*, which had previously been amplified with primers expBamHIF/uapAXbaR NS and digested with BamHI/XbaI, thus generating

the plasmids pAN520$_{exp}$:alcA-TMS14Δ-YFP$_C$ and pBS-argB:alcA-TMS14Δ-YFP$_N$, respectively.

pBS-argB:alcA-ctailess-His

UapA-ctailess ORF was amplified by PCR using the primers expBamF/ Ctail His Spe R. This reverse primer contains the sequence coding for the His$_{10}$ tag, right after a XbaI restriction site. The amplified fragment was double digested with BamHI and SpeI restriction endonucleases and was cloned in a BamHI/XbaI digested pBS-argB:alcA-uapA^{-XbaI} cloning vector. This way the His$_{10}$ tag was fixed on the resulting plasmid (pBS-argB:alcA-ctailess-His) and the UapA-ctailess ORF could be easily replaced by any other ORF by a simple BamHI/XbaI digestion.

pBS-argB:alcA-DYDY/A-His, pBS-argB:alcA-GGG/A-His   & pBS-argB:alcA-uapA-His

pBS-argB:alcA-ctailess-His was BamHI/XbaI digested and cloned with the also BamHI/XbaI digested UapA-N-tail. The resulting plasmid was once again BamHI/XbaI digested and the UapA-N-tail was replaced by the *uapA-DYDY/A*, *uapA-GGG/A* or *uapA*, which had previously been amplified with primers expBamHIF/uapAXbaR NS II and digested with BamHI/XbaI, thus generating the plasmids pBS-argB:alcA-DYDY/A-His, pBS-argB:alcA-GGG/A-His and pBS-argB:alcA-uapA-His, respectively.

pAN520$_{exp}$:alcA-DYDY/A-GFP & pAN520$_{exp}$:alcA- GGG/A-GFP

pAN520$_{exp}$:alcA-uapA^{-XbaI} was BamHI/XbaI digested and cloned with the also BamHI/XbaI digested UapA-N-tail. The resulting plasmid was once again BamHI/XbaI digested and the UapA-N-tail was replaced by the *uapA-DYDY/A* or *uapA-GGG/A-GFP*, which had previously been amplified with primers expBamHIF/uapAXbaR NS II and expBamHIF/GFPXbaR, respectively, and double digested with BamHI/XbaI, thus generating the plasmids pAN520$_{exp}$:alcA-DYDY/A and pAN520$_{exp}$:alcA-GGG/A-GFP. pAN520$_{exp}$:alcA-DYDY/A was then XbaI digested and cloned with the GFP ORF, which had previously been amplified with primers GFP Xba F2/GFP SpeIR and XbaI/SpeI double digested, thus generating the plasmid pAN520$_{exp}$:alcA-DYDY/A-GFP.

8.3   Oligonucleotides used in this study

5' – 3' Sequence	Name
CG**TCTAGA**GGCCGACAAGCAGAAGAAC	YFPcF
CG**TCTAGA**GCTTGTACAGCTCGTCCATG	YFPcR
CG**TCTAGA**GGTGAGCAAGGGCGAGGAG	YFPnF
CG**TCTAGA**GCATGATATAGACGTTGTGGCTG	YFPnR
CGCG**GGATCC**CTCCATCCATTCAACCGAC	expBamF
GCTCTAGACTAAGCCTGCTTGCTCTGATAC	uapAXbaR
GC**AGATCT**GCAATAACTCAACCGCCTTCCC	3'UTR BglIIR
CGCG**GCGGCCGC**TAAGTCCCTTCGTATTTCTCC	alcANotIF
CG**GGATCC**ATTTTGAGGCGAGGTGATAG	alcABamHIR
CG**ACTAGT**TTACTTGTACAGCTCGTCCATG	GFPSpeIR
CGCG**ACTAGT**GCATGATATAGACGTTGTGGCTG	YFPnSpeIR
GC**TCTAGA**GCCTGCTTGCTCTGATACTC	uapAXbaR NS
GGCCTCAACGAGAAGGATCCCGTGCTGTTGGCGTTTATC	BamTMS1F
GATAAACGCCAACAGCACGGGATCCTTCTCGTTGAGGCC	BamTMS1R
CCG**ACTAGT**TTAATGATGATGATGATGATGGTGGTGGTGGTG**TCTAGA**GACTTCAGCAGGCATGATTGCG	Ctail His Spe R
GC**TCTAGA**AGCCTGCTTGCTCTGATACTC	uapAXbaR NS II
CGC**TCTAGA**TTACTTGTACAGCTCGTCC	GFPXbaR
CG**TCTAGA**ATGGTGAGCAAGGGCGAG	GFP Xba F2

PERSONAL INFORMATION

- Official name: Georgia – Maria Karachaliou
- Sex: Female | Date of birth: 25-03-1986 | Nationality: Greek
- *email:* mayiathebee@hotmail.com

EDUCATION & PROFESSIONAL EXPERIENCE

- *June 2003* – **High school Degree** – Hellenic American Educational Foundation, Athens, Greece (Final grade 19/20)

- *March 2009* – **B.Sc. Biology** – Faculty of Biology, University of Athens, Greece (Final grade 7.7/10), in the course of which:
  o Diploma thesis and research experience in Fungal Genetics Laboratory, Department of Applied Genetics and Cell Biology, Universität für Bodenkultur, Vienna, Austria, supervised by Univ. Doz. Dr. Joseph Strauss

  Subject: «Construction of Genetic and Molecular Tools for the Study of the Regulation of the Specific Transcription Factor NirA in the Filamentous Fungus *Aspergillus nidulans*»
  o Student helper for the organization of the 32nd «FEBS Congress on Molecular Machines» (2007), Vienna, Austria
  o Research on the role of uric acid in the eukaryotic model organism *Aspergillus nidulans*, Molecular Microbiology & Fungal Genetics Laboratory, Faculty of Biology, University of Athens, Greece, supervised by Assoc. Prof. George Diallinas

- *April 2012* – **M.Sc. Microbial Biotechnology** – Faculty of Biology, University of Athens, Greece (Final grade 9.1/10), in the course of which:
  o Master thesis in Molecular Microbiology & Fungal Genetics Laboratory, Faculty of Biology, University of Athens, Greece, supervised by Assoc. Prof. George Diallinas, in collaboration with Dr. Bernadette Byrne, Imperial College London, UK

  Subject:«Heterologous expression & functional characterization of nucleobase transporters in *Saccharomyces cerevisiae*»
  o Research on the mechanisms that control cellular expression and distribution of purine transporters in fungal model systems in the laboratory of Molecular Biotechnology, Center for Molecular Biology and Environmental Biology, Universidade do Minho, Braga, Portugal, supervised by Assoc. Prof. George Diallinas & Prof. Margarida Casal
  o Teaching assistant at the graduate student laboratories of "Genetics and Molecular Biotechnology" (MSc. Molecular Genetics, Center for Molecular Biology and Environmental Biology, Universidade do Minho, Braga, Portugal) coordinated by Assist. Prof. Tony Collins

- *April 2009 till present* – **Ph.D. Molecular Microbiology** – Faculty of Biology, University of Athens, Greece

  o PhD thesis in Molecular Microbiology & Fungal Genetics Laboratory, Faculty of Biology, University of Athens, Greece, supervised by Assoc. Prof. George Diallinas

  Subject: «Study of regulatory mechanisms of targeting and endocytosis of membrane purine transporters in a model genetic system»

  o Teaching assistant at the undergraduate student laboratories of "Microbiology" and of "Molecular and Applied Microbiology", (B. Sc. Biology, Faculty of Biology, University of Athens, Greece) coordinated by Assoc. Prof. George Diallinas

  o Teaching assistant at the graduate student laboratories of "Model microbial systems for the study of genes of medical, agricultural and industrial importance" (M.Sc. Microbial Biotechnology, Faculty of Biology, University of Athens, Greece) coordinated by Assoc. Prof. George Diallinas

PUBLICATIONS

- *Galanopoulou K., Scazzocchio C, Galinou M. E., Liu W., Borbolis F.,* **Karachaliou M.,** *Oestreicher N., Hatzinikolaou D. G., Diallinas G.* * *& Amillis S.* * Purine utilization proteins in the Eurotiales, intracellular localization, phylogenetic conservation and divergence. (2014) Fungal Genetics and Biology. In revision. * *Corresponding authors*

- **Karachaliou M.*,** *Amillis S.*, Evangelinos M., Kokotos A. C., Yalelis V. & Diallinas G.* The arrestin-like protein ArtA is essential for ubiquitination and endocytosis of the UapA transporter in response to both broad-range and specific signals. (2013) Mol Microbiol 88: 301-17 **Equal contribution*

- *Bitsikas V.*,* **Karachaliou M.*,** *Gournas C. & Diallinas G.* Hypertonic conditions trigger transient plasmolysis, growth arrest and blockage of transporter endocytosis in *Aspergillus nidulans* and *Saccharomyces cerevisiae.* (2011) Mol Membr Biol. 28: 54-68 **Equal contribution*

- *Leung J.,* **Karachaliou M.,** *Alves A., Diallinas G. & Byrne B.* Expression and purification of a functional uric acid – xanthine transporter (UapA). Protein Expr. Purif. (2010) Protein Expr. Purif. 72: 139-46

CONFERENCE ANNOUNCEMENTS & PRESENTATIONS

- **Karachaliou M.,** *Amillis S., Yialelis V. & Diallinas G.* Role of oligomerization in the trafficking and vacuolar turnover of a purine transporter in a model fungal system. (2014) 11th International Aspergillus Meeting –Asperfest, Seville, Spain.

- **Karachaliou M.,** *Amillis S., Yialelis V. & Diallinas G.* Role of oligomerization in the trafficking and vacuolar turnover of a purine transporter in a model fungal system. (2014) 12th European Conference on Fungal Genetics, Seville, Spain.

- **Karachaliou M.,** *Amillis S., Yialelis V. & Diallinas G.* Role of oligomerization in the trafficking and vacuolar turnover of a purine transporter in a model fungal system. (2014) EMBO Workshop – Signaling to and from endomembranes, Allensbach, Germany.

- **Karachaliou M.,** *Amillis S., Evangelinos M., Kokotos A., Yialelis V. & Diallinas G.* The arrestin-like protein ArtA is essential for ubiquitylation and endocytosis of the UapA

transporter in response to both broad-range & specific signals (2013) FEBS-EMBO Advanced Lecture Course – Biomembranes: Molecular Architecture Dynamics and Function, Cargèse, Corsica, France– *poster voted by participants for oral presentation*

- *Diallinas G., **Karachaliou M.**, Amillis S., Evangelinos M. & Kokotos A.* The arrestin-like protein ArtA is essential for ubiquitylation and endocytosis of the UapA transporter in response to both broad-range & specific signals (2013) 27th Fungal Genetics Conference, Asilomar, Pacific Grove, California, USA

- ***Karachaliou M.**, Amillis S., Yalelis V. & Diallinas G.* In search for a role of oligomerization of a purine transporter in a model fungal system (2012) FEBS Special meeting on protein quality control and ubiquitin systems in health and disease, Kusadasi, Turkey – *selected abstract for oral presentation*

- ***Karachaliou M.**, Amillis S., Evangelinos M., Kokotos A., Yialelis V. & Diallinas G.* The arrestin-like protein ArtA is essential for ubiquitylation and endocytosis of the UapA transporter in response to both broad-range & specific signals (2012) FEBS Special meeting on protein quality control and ubiquitin systems in health and disease, Kusadasi, Turkey

- ***Karachaliou M.**, Amillis S., Evangelinos M., Kokotos A., Yialelis V. & Diallinas G.* The arrestin-like protein ArtA is essential for ubiquitylation and endocytosis of the UapA transporter in response to both broad-range & specific signals (2012) EurofungBase Meeting, Berlin, Germany

- *Amillis S., **Karachaliou M.**, Yalelis V., Vlanti A., Gournas C. & Diallinas G.* Signals and mechanisms of membrane cargo trafficking and endocytosis in a model fungal system (2011) 62nd Conference of Hellenic Society of Biochemistry and Molecular Biology, Athens, Greece – *selected abstract for oral presentation*

- ***Karachaliou M**. & Diallinas G.* Oligomerization of the UapA transporter and its role in function and trafficking in *Aspergillus nidulans* (2011) 4th Panhellenic Conference of Microbiokosmos Scientific Society, Ioannina, Greece – *selected abstract for oral present*

- *Amillis S., **Karachaliou M.**, Yalelis V., Vlanti A., Gournas C. & Diallinas G.* Signals and mechanisms of transporter endocytosis in a model fungal system (2011) EMBO – Dynamic Endosomes: Mechanisms Controlling Endocytosis, Chania, Greece

- ***Karachaliou M.**, Bitsikas V., Gournas C. & Diallinas G.* Hypertonic conditions trigger transient plasmolysis, growth arrest and blockage of transporter endocytosis in *Aspergillus nidulans* and *Saccharomyces cerevisiae* (2010) 9th International Mycological Congress: The Biology of Fungi, Edinburgh, UK – *selected abstract for oral presentation*

- ***Karachaliou M.**, Leung J., Alves A., Byrne B. & Diallinas G.* Expression and purification of a functional uric acid – xanthine transporter (2010) 32nd Panhellenic Conference of the Hellenic Society of Biological Sciences, Karpenissi, Greece

- *Borbolis F., **Karachaliou M.**, Gournas C., Hatzinikolaou D., Pantazopoulou A. & Diallinas G.* A cryptic role of uric acid intercellular transport and catabolism in *Aspergillus nidulans* development (2008) 26th Small Meeting on Yeast Transport & Energetics (SMYTE), Braga, Portugal

- *Borbolis F., **Karachaliou M.**, Gournas C., Hatzinikolaou D., Pantazopoulou A. & Diallinas G.* A cryptic role of uric acid metabolism and intercellular redistribution in *Aspergillus nidulans* development (2008) Eurofungbase Meeting, Sant Feliu de Guixols, Spain.

AWARDS

- Award of excellence for the poster presented at the 11th International Aspergillus Meeting – Asperfest (2014), Seville, Spain.
- Travel grant by Society of Biology for the participation at the 12th European Conference on Fungal Genetics (2014), Seville, Spain.
- Travel grant by Society for Experimental Biology – Company of Biologists for the participation at the EMBO Workshop– Signaling to and from endomembranes (2014), Allensbach, Germany.
- Award of excellence for the poster presented at the FEBS-EMBO Advanced Lecture Course – Biomembranes: Molecular Architecture Dynamics and Function (2013), Cargèse, Corsica, France
- Travel grant by Boehringer Ingelheim Stiftung for the participation at the FEBS-EMBO Advanced Lecture Course – Biomembranes: Molecular Architecture Dynamics and Function (2013), Cargèse, Corsica, France
- FEBS Young Scientist Fellowship for the participation at the FEBS Special meeting on protein quality control and ubiquitin systems in health and disease (2012), Kusadasi, Turkey
- Travel bursary by the Congress Steering Committee of the International Mycological Congress (IMC) for the participation at the IMC 9: The Biology of Fungi (2010), Edinburgh, UK
- PhD scholarship from the research funding program Heracleitus II – Investing in knowledge society through the European Social Fund.
- PhD scholarship from the Special Account for Research Grants (ELKE), National and Kapodistrian University of Athens
- Highest final mark distinction for M.Sc. Molecular Biotechnology at the graduation ceremony of March 2012 – Awarded the privilege of pronouncing the Graduate Student Oath
- Masters scholarship from the A. G. Leventis Foundation Scholarships Program
- Highest final mark distinction for B.Sc. Biology at the graduation ceremony of April 2009 – Awarded the privilege of pronouncing the Graduate Student Oath

LANGUAGES

- **Greek** – *Native language*
- **English** – *Excellent use of written and oral speech*

  Certificate of Proficiency in English, University of Cambridge

  Official teaching permission for English by the Hellenic Ministry of Education

- **French** – *Very good use of written and oral speech*

  Diplôme d'Études en Langue Française (DELF) 1 & 2

  Diplôme Approfondi de Langue Française (DALF) – Unité B4

- **Portuguese** – *Intermediate use of written and oral speech*

  Diploma Intermédio De Português Língua Estrangeira (DIPLE), Universidade de Lisboa (CAPLE)

- **German**– *Intermediate use of written and oral speech*

COMPUTER SKILLS

- Microsoft Office tools – *very good command*
- Adobe Photoshop – *very good command*

## ADDITIONAL SCIENCE-RELATED COURSES

- «Genetics and Molecular Biotechnology» , MSc. Molecular Genetics, Center for Molecular Biology and Environmental Biology, Universidade do Minho, Braga, Portugal – Final grade 16/20 (February-April 2010)

- «Cellular and Functional Biology», MSc. Molecular Genetics, Center for Molecular Biology and Environmental Biology, Universidade do Minho, Braga, Portugal – Final grade 16/20 (October-November 2009)

- «Course on Recent Advances and Applications in Multidimensional Confocal Microscopy», Biomedical Research Foundation, Academy of Athens, Greece (26-28 May 2009)

- «History of Biology», interdepartmental course of Department of Philosophy and History of Science and Faculty of Biology, University of Athens, Greece – Final grade 5/10 (March-June 2009)

- «Teaching of Biology and Bioethics», interdepartmental course of School of Education and Faculty of Biology, University of Athens, Greece – Final grade 10/10 (March-June 2009)

Reprints of original publications

List of attached manuscripts

- *Leung J.,* **Karachaliou M.,** *Alves A., Diallinas G. & Byrne B.* Expression and purification of a functional uric acid – xanthine transporter (UapA). Protein Expr. Purif. (2010) Protein Expr. Purif. 72: 139-46

- *Bitsikas V.*,* **Karachaliou M.*,** *Gournas C. & Diallinas G.* Hypertonic conditions trigger transient plasmolysis, growth arrest and blockage of transporter endocytosis in *Aspergillus nidulans* and *Saccharomyces cerevisiae*. (2011) Mol Membr Biol. 28: 54-68 **Equal contribution*

- **Karachaliou M.*,** *Amillis S.*, Evangelinos M., Kokotos A. C., Yalelis V. & Diallinas G.* The arrestin-like protein ArtA is essential for ubiquitination and endocytosis of the UapA transporter in response to both broad-range and specific signals. (2013) Mol Microbiol 88: 301-17 **Equal contribution*

- *Galanopoulou K., Scazzocchio C, Galinou M. E., Liu W., Borbolis F.,* **Karachaliou M**., *Oestreicher N., Hatzinikolaou D. G., Diallinas G.[*] &* *Amillis S.[*]* Purine utilization proteins in the Eurotiales, intracellular localization, phylogenetic conservation and divergence. (2014) Fungal Genetics and Biology. In revision. ** Corresponding authors*
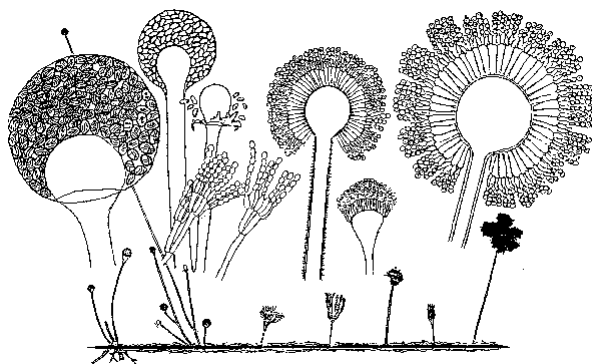
Έκφραση και καθαρισμός ενός λειτουργικού μεταφορέα ξανθίνης – ουρικού οξέος (UapA).

Leung J., Καραχάλιου Μ., Alves A., Διαλλινάς Γ. & Byrne B.

Περίληψη

Η οικογένεια μεταφορέων νουκλεοτιδικών βάσεων–ασκορβικού (NAT) περιλαμβάνει μεταφορείς με θεμελιώδη ρόλο στην πρόσληψη βασικών κυτταρικών μεταβολιτών, όπως το ουρικό οξύ και η βιταμίνη C. Ο πιο εκτενώς μελετημένος NAT μεταφορέας είναι ο μεταφορέας ουρικού– ξανθίνης (UapA) στον ασκομύκητα *Aspergillus nidulans*. Λεπτομερείς γενετικές και βιοχημικές αναλύσεις έχουν αποκαλύψει πολλά σε σχέση με το μηχανισμό δράσης αυτής της πρωτεΐνης. Ωστόσο, η δυσκολία χειρισμού μεμβρανικών πρωτεϊνών αποτελεί περιοριστικό παράγοντα στην προσπάθεια κατανόησης σχέσεων δομής–λειτουργίας μέσω κλασικών προσεγγίσεων δομικής βιολογίας (κρυσταλλογραφία, NMR). Στην εργασία αυτή περιγράφουμε την ετερόλογη υπερέκφραση λειτουργικών μορίων UapA σημασμένων με την πράσινη φθορίζουσα πρωτεΐνη (GFP) σε στελέχη του *Saccharomyces cerevisiae*. Συγκεκριμένα, η χιμαιρική πρωτεΐνη UapA–GFP εκφράστηκε σε συγκέντρωση 2.3 mg/L στο στέλεχος *pep4Δ*, στο οποίο έχει απενεργοποιηθεί μία βασική χυμοτοπιακή ενδοπεπτιδάση, και σε συγκέντρωση 3.8 mg/L στο στέλεχος *npi1-1*, το οποίο παρουσιάζει μειωμένη δράση της λιγάσης της ουβικουιτίνης, Rsp5p. Παράλληλα, παρατήρηση με μικροσκόπιο επιφθορισμού έδειξε ότι η UapA-GFP εντοπίζεται κατά κύριο λόγο στην πλασματική μεμβράνη και στα δύο στελέχη, με υψηλότερη ένταση φθορισμού στο στέλεχος *npi1-1*. Σε συμφωνία με αυτές τις παρατηρήσεις, το στέλεχος *npi1-1* έδειξε 5-πλάσια πρόσληψη [^{3}H]-ξανθίνης σε σύγκριση με το *pep4Δ*. Παρότι το στέλεχος *npi1-1* έδωσε καλύτερα αποτελέσματα σε επίπεδο λειτουργικής έκφρασης, η προερχόμενη από αυτό πρωτεΐνη UapA–GFP έδειξε αυξημένο βαθμό πρωτεόλυσης. Υπερέκφραση της πρωτεΐνης στο στέλεχος *pep4Δ* και επακόλουθος καθαρισμός της παρήγαγαν αξιόλογες (mg) ποσότητες καθαρής πρωτεΐνης, κατάλληλης για περαιτέρω δομικές και λειτουργικές μελέτες. Επιπλέον, η εργασία αυτή δημιούργησε ένα απλό ευκαρυωτικό σύστημα κατάλληλο για τη χρήση αντίστροφης γενετικής και άλλων στοχευμένων προσεγγίσεων, με σκοπό την περαιτέρω κατανόηση του μηχανισμού δράσης αυτής της σημαντικής πρωτεΐνης.

Expression and purification of a functional uric acid–xanthine transporter (UapA)

James Leung [a], Mayia Karachaliou [b], Claudia Alves [a,c], George Diallinas [b], Bernadette Byrne [a,*]

[a] Division of Molecular Biology, Imperial College London, London SW7 2AZ, UK
[b] Faculty of Biology, Department of Botany, University of Athens, Panepistimioupolis 15781, Athens, Greece
[c] Department of Biochemistry, University of Alberta, Edmonton, Canada

ARTICLE INFO

ABSTRACT

The Nucleobase–Ascorbate Transporters (NATs) family includes carriers with fundamental functions in uptake of key cellular metabolites, such as uric acid or vitamin C. The best studied example of a NAT transporter is the uric acid–xanthine permease (UapA) from the model ascomycete *Aspergillus nidulans*. Detailed genetic and biochemical analyses have revealed much about the mechanism of action of this protein; however, the difficulties associated with handling eukaryotic membrane proteins have limited efforts to elucidate the precise structure–function relationships of UapA by structural analysis. In this manuscript, we describe the heterologous overexpression of functional UapA as a fusion with GFP in different strains of *Saccharomyces cerevisiae*. The UapA–GFP construct expressed to 2.3 mg/L in a *pep4Δ* deletion strain lacking a key vacuolar endopeptidase and 3.8 mg/L in an *npi1-1* mutant strain with defective Rsp5 ubiquitin ligase activity. Epifluorescence microscopy revealed that the UapA–GFP was predominately localized to the plasma membrane in both strains, although a higher intensity of fluorescence was observed for the *npi1-1* mutant strain plasma membrane. In agreement with these observations, the *npi1-1* mutant strain demonstrated a ∼5-fold increase in uptake of [3H]-xanthine compared to the *pep4Δ* deletion strain. Despite yielding the best results for functional expression, in-gel fluorescence of the UapA–GFP expressed in the *npi1-1* mutant strain revealed that the protein was subject to significant proteolytic degradation. Large scale expression of the protein using the *pep4Δ* deletion strain followed by purification produced mg quantities of pure, monodispersed protein suitable for further structural and functional studies. In addition, this work has generated a yeast cell based system for performing reverse genetics and other targeted approaches, in order to further understand the mechanism of action of this important model protein.

Introduction

The ubiquitous Nucleobase–Ascorbate Transporter (NAT)[1] family includes carriers with fundamental functions in uptake of key cellular metabolites, such as uric acid or vitamin C [1–3]. These transporters are also responsible for mediating uptake of purine analogues used as antimicrobials, anticancer agents, antivirals [4] and as agents against parasitic diseases [5]. They are found in all organisms from bacteria (e.g. YgfO [6]), to plants [7,8] and humans [9]. Although highly related in structure, there are some key differences in substrate specificity among the members of the family. These differences can be used to subdivide the family into three distinct subgroups; some bacterial, the fungal and the plant NATs transport oxidized purines, xanthine or uric acid, some other bacterial transport only uracil, whereas the transporters from higher eukaryotes are specific to either L-ascorbic acid [1,2] or nucleobases in general [10]. In addition, the NATs from bacteria, fungi and plants are proton dependent, whereas the vertebrate transporters are sodium dependent. In common with several other carriers belonging to evolutionary distinct families, they are predicted to contain 12 α-helical transmembrane segments (TMS) and intracellular N and C termini [11]. NATs contain two specific motifs; the NAT signature motif, [Q/E/P]-N-X-G-X-X-X-X-T-[R/K/G] (where X is a hydrophobic amino acid residue) found in an amphipathic region just upstream of TM9 and the QH motif in the middle of TMS1, known to be critical for function of well-studied examples of this family [6,11–14]. The best characterized NAT is the uric acid–xanthine permease (UapA) from the model ascomycete *Aspergillus nidulans* [12,15–17]. Native UapA expression is developmentally activated early during germination of conidiospores and is subsequently dependent on the presence of environmental purines and/or nitrogen sources [15,17,18]. The UapA protein functions as a high-affinity, high-capacity transporter specific for uric acid and xanthine, but can also transport several xanthine analogues albeit with lower affinity. Extensive biochemical

and genetic analyses have made UapA a model for study of structure–function relationships of members of the NAT family. The long amphipathic loop linking TMS8–TMS9, which includes the NAT signature motif, was found to have a principal role in substrate translocation [11,19,20]. Four amino acid residues (E356, D388, Q408, N409) proved irreplaceable and several other affect UapA function, substrate affinity or specificity (A363, E371, R373, G411, T416, R417). Kinetic evidence is strongly supportive that the NAT motif in particular interacts with the imidazol moiety of xanthine, uric acid or other UapA ligands. In this interaction, Q408 is proposed to make a direct H bond with position N9 or C8=O of xanthine or uric acid, respectively, whereas N409 seems to be a dynamic element absolutely necessary for molecular movements associated with UapA-mediated transport. G411 and T416 are also important for narrowing the specificity of UapA to xanthine and uric acid, whereas R417 increases the affinity of UapA specifically for uric acid. Similar mutational analysis and Cys-scanning mutagenesis of YgfO, a bacterial NAT that is a functional homologue of UapA, confirmed the importance of the four irreplaceable for function amino acid residues found in UapA [6,21], revealing a very close relationship between the functional role of these individual residues in the two proteins.

Further studies have identified residues in TMS12 (T526, F528) with roles in the selectivity of UapA allowing binding and transport of uric acid and xanthine, but excluding other purines [20,22,23]. In contrast, the equivalent residues in YgfO have been found to be essential for function but not substrate selectivity, an observation highlighting subtle difference in the molecular make-up of the two transporters [24]. Furthermore, Cys-scanning mutagenesis in YgfO showed that these residues are probably in the vicinity of the binding site located in the TMS8–TMS9 region [24]. Finally, the QH motif in TMS1 (Q85, H86 in UapA) has also been shown to play an essential role in substrate transport and protein folding in both UapA [14] and YgfO [25], whereas the loop linking TMS1-TMS2 and several residues along TMS1 also affect UapA selectivity [20].

Despite the detailed studies of UapA and YgfO the understanding of this essential group of transporters is currently limited by the lack of high resolution structural data. One of the major hurdles to structural studies is the expression of high quality transporter protein. A recent study described the homologous expression of UapA in *A. nidulans* using the strong ethanol-inducible *alc*A promoter [26]. The protein produced was purified to near homogeneity and, based on circular dichroism, the purified UapA sample displayed a predominantly α-helical structure, as expected. However, the amounts produced were too low (0.6 mg/47 mg of membrane protein/2.5 g of dry mycelium/10 L).

Heterologous expression of membrane proteins in appropriate systems provides the best alternative for obtaining higher protein yields [27]. However, work on eukaryotic transporters has shown that one major hurdle to successful expression in heterologous systems is aberrant trafficking in the endoplasmic reticulum [28,29]. Some research has been done to develop specific *Saccharomyces cerevisiae* cell strains which optimize plasma membrane expression of eukaryotic transporters [30–32]. Most notably, *npi1*, a

mutation in *Rsp5*, the gene encoding a HECT ubiquitin ligase necessary for normal transporter turnover, proved the most promising modification [29]. This mutation is likely to reduce ubiquitination, therefore preventing transporter molecules being targeted to the vacuole for degradation, either via endocytosis or through direct sorting from the Golgi.

In this work, we describe the high-yield heterologous expression and purification of a functional uric acid–xanthine transporter (UapA) in *S. cerevisiae*. The system of *S. cerevisiae* used is designed for the large scale production of eukaryotic membrane proteins [33,34] and provides two important advantages. Firstly, it does not contain a NAT homologue [14] meaning that the functional expression of UapA can be assayed *in vivo* by directly measuring the uptake of xanthine or uric acid. Secondly, *S. cerevisiae* is not only the best studied simple eukaryotic system in respect to protein trafficking, but also provides unique genetic tools for modifying and improving the expression of a protein.

Materials and methods

Generation of S. cerevisiae expression construct and initial expression trials

The full-length UapA was amplified from a cDNA clone using the oligonucleotide primers 5′-TCGACGGATTCTAGAACTAGTGGAT CCCCCATGGATCCCTCCATCCATTCAAC-3′ and 5′-AAATTGACCTTGAA AATATAAATTTTCCCCAGCCTGCTTGCTCTGATACTCC-3′. These incorporate homologous recombination domains allowing direct incorporation into the pDDGFP-2 *S. cerevisiae* expression vector [34]. The expression vector generated was introduced by standard transformation and selection of complementation of a ura3⁻ auxotrophy (see Table 1 for details of the strains used in this study), into a standard wild-type strain (S288C), a *pep4Δ* deletion strain lacking a key vacuolar endopeptidase, which also leads to reduced levels of other vacuolar hydrolases [37], or an *npi1-1* mutant strain with a defective Rsp5 ubiquitin ligase activity [29]. Selected transformants were grown in an aerated 50 ml tube containing 5 ml-URA medium with 2% glucose overnight at 30 °C with shaking. The culture was then diluted in 10 ml-URA medium supplemented with 0.1% glucose to give a starting OD_{600} of 0.12. The cultures were then incubated with shaking at 30 °C to an OD_{600} of 0.6, and protein expression induced with a final concentration of 2% galactose. After 22 h of induction, the cells were harvested by centrifugation at 4000g and 4 °C for 5 min. The supernatant was decanted and the cell pellet resuspended in 200 μl yeast solubilization buffer (50 mM Tris–HCl (pH 7.6), 5 mM EDTA, 10% glycerol, 1 complete protease inhibitor cocktail tablet (Roche) per 50 ml buffer). Two hundred microliters of cell suspension was then transferred to a black Nunc 96-well optical bottom plate to examine the protein expression levels. GFP fluorescence emission was measured at 512 nm, by excitation at 488 nm, in a microplate spectrofluorometer (SpectraMax). The protein expression level was calculated from the relative fluorescent units, as described in Drew et al. [34].

Table 1
List of *S. cerevisiae* expression strains used in this study.

Strains	Description	Origin
MATa ura3-52 (Ura⁻)	A standard wild-type strain, uracil auxotroph	
MATa ura3-52 uapA-gfp (Ura⁻ UapA)	Ura⁻ transformed with plasmid pUapA-GFPH	This study
MATa ura3-52 npi1-1 (Npi1)	A Ura⁻ strain carrying mutation *npi1-1* which knocks-down Rsp5 ubiquitin ligase expression	[35]
MATa ura3-52 npi1-1 uapA-gfp (Npi1 UapA)	Npi1 transformed with plasmid pUapA-GFPH	This study
MATa ura3-52 lysΔ201 pep4Δ (Pep4Δ)	A strain carrying deletions of *pep4*, which encodes a vacuolar protease, and *lys*, a gene necessary for lysine prototrophy	[36]
MATa ura3-52 lysΔ201 pep4Δ uapA-gfp	The Pep4⁻ strain transformed with plasmid pUapA-GFPH	This study

Induction of UapA expression for uptake assays

YPD standard media were used for yeast growth. Minimal media (MM), used for induction conditions and growth tests, were made with Difco Yeast Nitrogen Base w/o amino acids and ammonium. Induction of UapA expression from the GAL1 promoter was achieved after 24 h of growth at 30 °C (OD$_{600 nm}$ 0.6–0.8) of appropriate strains, initiated from a single colony or from an o/n culture, in MM with urea (5 mM) as the sole nitrogen source, glucose (0.1%) as carbon source, galactose (2%) and appropriate auxotrophic supplements. Repression of UapA expression was achieved in MM supplemented with urea (5 mM) and glucose (2%). Standard drop tests were carried out at 30 °C. Purines (uric acid, xanthine) or purine analogues (oxypurinol) were used at 0.1 mg/ml final concentration.

Uptake assays

Kinetic analysis of UapA activity was measured by estimating uptake rates of [^{3}H]-xanthine uptake, as described in [18,38]. Briefly, [^{3}H]-xanthine uptake in MM was assayed in liquid cultures of *S. cerevisiae*, with optical density of 0.6–0.8, concentrated at 10^7 cells/100 μl, at 30 °C. Initial velocities were measured at 1 min of incubation with 0.2 μM radioactive substrate. Reactions were terminated by addition of an equal volume of ice-cold MM containing 1000-fold excess of non-radiolabelled substrate. Background uptake values were corrected by subtracting values obtained in the simultaneous presence of 1000-fold excess of non-radiolabelled substrate. The background uptake level did not exceed 15–20% of the total counts obtained in wild-type strains. $K_{m/i}$ and V_m values were obtained directly by performing and analyzing (Prism3) uptakes at various concentrations, as described previously [20]. All transport assays were carried out in at least two independent experiments, with three replicates for each concentration or time point. Radiolabelled [^{3}H]-xanthine (21.1 Ci/mmol) was purchased from Moravek Biochemicals, Brea, CA.

Epifluorescence microscopy

Liquid cultures of *S. cerevisiae* were inoculated in MM with urea (5 mM), glucose (0.1%), galactose (2%) and the appropriate auxotrophic supplements and were incubated for 24 h, protected from light, at 30 °C, 230 rpm. Samples were 10-fold concentrated (OD$_{600 nm}$ 3–6), a 7 μl aliquot was mixed with an equal volume of low melting agarose 1.2%, and observed on an Axioplan Zeiss phase-contrast epifluorescent microscope with appropriate filters. The resulting images were acquired with a Zeiss-MRC5 digital camera using the AxioVs40 V4.40.0 software and processed in the Adobe Photoshop CS2 V9.0.2 software.

Large scale expression and preparation of membranes

Large scale expression and preparation of membranes was performed as described in Drew et al. [34]. In brief, a starter culture was grown overnight at 30 °C in 5 ml of URA media supplemented with 2% glucose. This culture was used to inoculate a further 150 ml-URA media supplemented with 2% glucose, which was also then incubated overnight. This culture was then used to inoculate 10 L of URA media containing 0.1% glucose. The starter culture was diluted to give a starting OD$_{600}$ of 0.12. The cultures were then incubated with shaking at 30 °C to an OD$_{600}$ of 0.6, and protein expression was induced with a final concentration of 2% galactose for 20 h, at 30 °C. Cells were then harvested by centrifugation at 4000g and 4 °C for 5 min. The cells were resuspended in 300 ml of cold cell resuspension buffer (50 mM Tris–HCl (pH 7.6), 1 mM EDTA, 0.6 M sorbitol) supplemented with protease inhibitors (Roche). Cells were lysed using a Constant Systems (Constant Systems) cell disruptor at 4–10 °C. Unbroken cells and debris were removed by centrifugation at 15,000g at 4 °C for 10 min. The supernatant was further centrifuged at 150,000g at 4 °C for 60 min in order to isolate the membranes. The supernatant was discarded and the membrane pellet was resuspended in membrane resuspension buffer (20 mM Tris–HCl (pH 7.5) 0.3 M sucrose) to a final volume of 6 ml/L starting cell culture using a disposable 10 ml syringe with 21-gauge needle.

Solubilization and purification of UapA

The membranes were solubilized in membrane solubilization buffer (1 × PBS, 150 mM NaCl, 10% (v/v) glycerol, 1% (w/v) DDM$_{LA}$, and protease inhibitors) with constant stirring at 4 °C for 1 h. Unsolubilized membrane was pelleted by centrifugation at 150,000g and 4 °C for 45 min. Imidazole, pH 7.5, was added at a final concentration of 10 mM to the detergent solubilized sample and this was mixed with 20 ml of Ni^{2+}–NTA superflow resin (Qiagen) pre-equilibrated with Buffer A (1 × PBS, 150 mM NaCl, 10 mM imidazole pH 7.5, and 0.03% (w/v) DDM$_{LA}$). The resin and solubilized protein sample were incubated at 4 °C for 5 h with slow stirring. The mixture was applied onto a poly-prep/glass econo-column chromatography column (Bio-Rad) and washed with 20 CV of Buffer A supplemented with 20 mM imidazole followed by 20 CV of Buffer A supplemented with 30 mM imidazole and then 5 CV of Buffer B (20 mM Tris–HCl, pH 7.5, 150 mM NaCl, 0.03% (w/v) DDM$_{LA}$). The fusion protein was eluted in Buffer B supplemented with 250 mM imidazole. The GFP tag was removed from the fusion protein by treatment with an equimolar concentration of His-tagged TEV protease. The protein sample was then dialyzed overnight in Buffer B supplemented with 10% glycerol using 12 kDa molecular weight cut-off dialysis tubing (Spectrum Labs). The remaining protein sample was passed through a 0.22 μm filter (Millex) to remove any precipitation prior to loading onto a 5 ml His-trap column (GE Biosciences). The His-tagged GFP and TEV protease bind to the column, while the target UapA protein is found in the flow-through. The purified UapA was concentrated to 0.5 ml in 50 kDa molecular weight cut-off filters (Amicon). Aggregates were removed from the sample by centrifugation at 18,000g and 4 °C for 10 min. The sample was then loaded onto a superdex 200 10/300 gel filtration column equilibrated with Buffer B. The protein samples were collected and analyzed by SDS–PAGE.

SDS–PAGE and in-gel fluorescence analysis

The protein samples were separated on Novex 12% Tris-Gly gels (Invitrogen). The gels were rinsed with dH$_2$O and the protein bands visualized using Coomassie Blue stain, prior to detection of the fluorescent bands with a LAS-1000-3000 charge-coupled device (CCD) imaging system (Fujifilm). The gel was exposed to blue light (460 nm) for 20 s with a cut-off filter of 515 nm.

CD spectroscopy

Circular dichroism analysis was performed on a Chirascan™ Circular Dichroism Spectrometer. CD spectrum of protein samples (6.3 μM) were recorded in 20 mM Tris, pH 7.5, 150 mM NaCl, 0.03% DDM$_{LA}$ in a quartz cuvette of 1 mm path length at the wavelength range 260–180 nm at 0.5 nm intervals at 20 and 30 °C. The spectrum was corrected against the baseline.

Results

### UapA expressed in S. cerevisiae is functional

A full length cDNA corresponding to the ORF of *uapA* was cloned into the *S. cerevisiae* expression vector pDDGFP-2 [34], downstream from the *GAL1* promoter and in-frame with the GFP–His$_8$ epitope. This 2 μ vector harbors a *URA3* selection marker (see Materials and methods). The vector carrying *uapA* was used to transform mutant strains carrying either the *pep4Δ* deletion or the *npi1-1* mutation, as well as an isogenic standard wild-type strain (see Materials and methods). Several stable *ura3*[+] transformants were selected and tested for their ability to take up [³H]-xanthine, the standard radiolabelled substrate used for assaying UapA activity (Materials and methods). In comparative assays we noticed that transformants of all three different strains used showed saturable UapA-mediated [³H]-xanthine uptake (see later, Fig. 1E). We proceeded in a detailed kinetic analysis of UapA-mediated xanthine transport in the mutant carrying the *pep4Δ* deletion, which was eventually chosen for high-yield purification of UapA (see later). Fig. 1A shows that in the strain expressing UapA, [³H]-xanthine uptake increases linearly for 4 min and reaches a significant maximum plateau after 5 min, while an isogenic control strain (carrying an empty vector) has practically no ability for xanthine uptake, as expected. We performed a standard Michaelis–Menten kinetic analysis using increasing concentrations of [³H]-xanthine/xanthine or [³H]-xanthine/uric acid mixtures and found that: (i) UapA-mediated transport of xanthine (or binding of uric acid) is saturable and characteristic of a single carrier (Hill co-efficient −1), (ii) K_m (xanthine) or K_i (uric acid) values obtained are very similar to the ones obtained in *A. nidulans* (Fig. 1C) and characteristic of a high-affinity transport system, and (iii) The capacity (V_m value) for xanthine uptake is relatively high (Fig. 1C). We also tested the effect of known UapA competitive inhibitors, present in excess (1 mM), on [³H]-xanthine uptake (for experimental details see Materials and methods). Fig. 1B shows a competition profile, very similar to the one obtained in *A. nidulans* [11,13].

The similarity in transport kinetics and substrate specificity of UapA expressed in yeast and in *A. nidulans* shows that expression in yeast is fully functional.

Expression of UapA in S. cerevisiae does not lead to a detectable growth phenotype

Two stable *ura3*[+] transformants of mutant strains carrying either the *pep4Δ* deletion or the *npi1-1* mutations, as well as an isogenic standard wild-type strain, were phenotypically tested for their resistance/sensitivity on potentially toxic UapA substrates, such as high concentrations of uric acid (1–2 mM) or oxypurinol (50–100 μM) [11,20,23]. Sensitivity phenotypes would have permitted the direct selection of resistant mutants, a powerful genetic tool to approach structure–function relationships and trafficking mechanisms. Drop
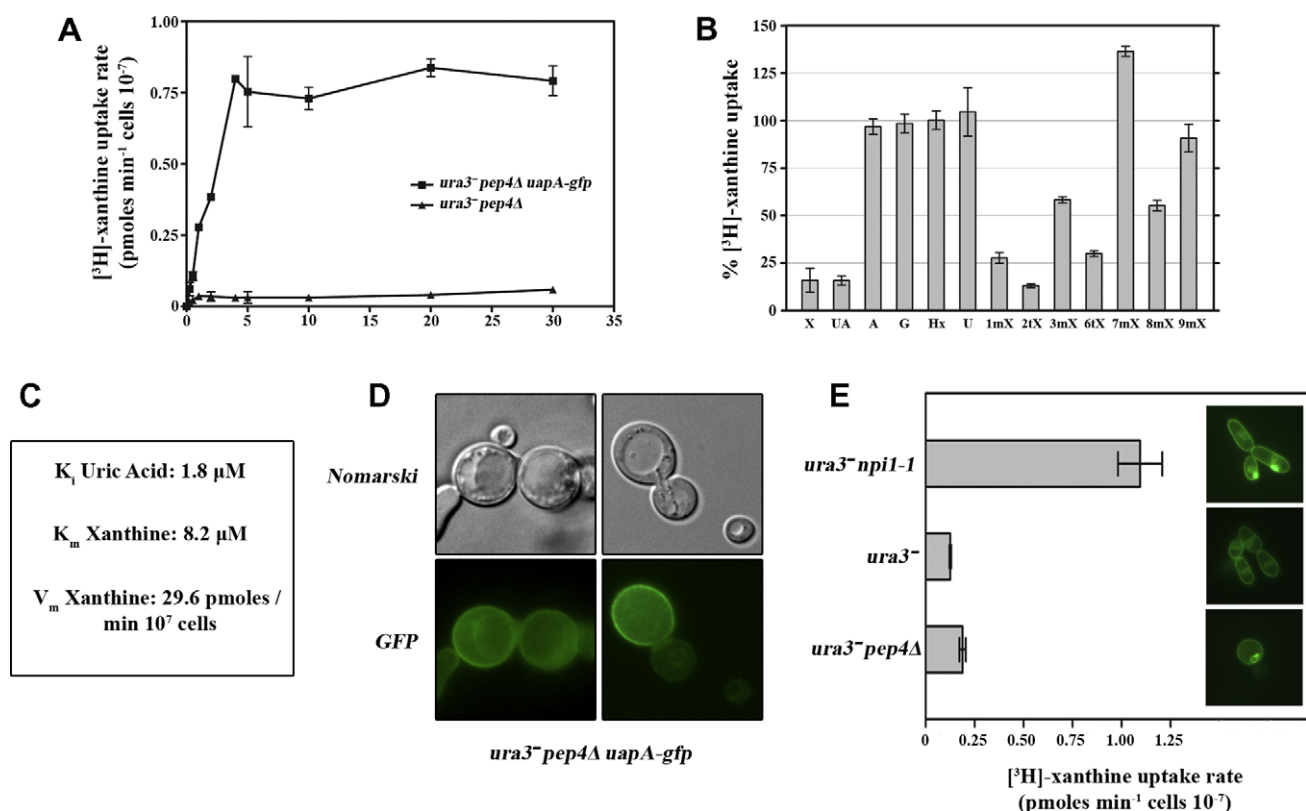
Fig. 1. (A) Time course of UapA–GFP-mediated [³H]-xanthine uptake rates in *S. cerevisiae* (FGY217). An isogenic strain lacking UapA (empty vector control) shows only very low background values of xanthine uptake. Results are averages of at least two independent experiments, each experiment carried out in triplicate. (B) UapA–GFP specificity profile. Estimation of relative [³H]-xanthine uptake in the presence of excess (1 mM) of non-labeled purines, pyrimidines and analogues. Measurements were carried out in the presence of 0.2 μM [³H]-xanthine. X, xanthine; UA, uric acid; A, adenine; G, guanine; Hx, hypoxanthine; U, uracil; 1mX, 1-methyl-xanthine; 2tX, 2-thio-xanthine; 3mX, 3-methyl-xanthine; 6tX, 6-thio-xanthine; 7mX, 7-methyl-xanthine; 8mX, 8-methyl-xanthine; 9mX, 9-methyl-xanthine. (C) Estimation of K_i (uric acid), K_m (xanthine) and V_m of UapA–GFP expressed in *S. cerevisiae* (FGY217). The values were estimated from a Michaelis–Menten kinetic analysis, using the Prism3 (http://pubs.acs.org/doi/abs/10.1021/ja025220m). (D) Sub-cellular topology of UapA–GFP. Nomarski and epifluorescence microscopy of a FGY217 (*pep4Δ*) transformant expressing UapA–GFP, after 24 h of galactose-induction. UapA–GFP is expressed principally on the plasma membrane, but is also detectable in the cytoplasm and the vacuolar membrane. (E) Comparison of UapA–GFP plasma membrane expression in different *S. cerevisiae* strains (*npi1-1*, *pep4Δ* and a standard control strain; see text). UapA-mediated transport rate of [³H]-xanthine (left) is also shown under identical conditions with the epifluorescence analysis (right). Notice the prominent pseudohyphal appearance of strain *npi1-1*, and to a less degree of the standard control strain (see text).

tests carried out on galactose media (inducing conditions) showed no evidence for sensitivity compared to an isogenic transformant hosting an empty vector (results not shown). The same negative result was obtained in liquid cultures, tested at regular intervals, for a period of 30 h (up to an OD of 1.5) (not shown). Given that UapA is functionally expressed in *S. cerevisiae*, these rather unexpected results suggested that uric acid or oxypurinol are not toxic in yeast, at least under the conditions tested.

*Localization of UapA–GFP in the plasma membrane of S. cerevisiae*

In several cases, overexpressed proteins may be susceptible to proteolysis. This might be due to improper folding, usually evident by retention in the ER, or problematic trafficking towards the plasma membrane and subsequent vacuolar degradation. Thus, proper subcellular targeting of transporters provides a good indication of their stability and functionality. We used the GFP tag to investigate the cellular topology of UapA–GFP using epifluorescence microscopy. Fig. 1D shows that UapA–GFP labels predominantly the plasma membrane of yeast cells and to a lesser extent some internal structures such as the vacuolar membrane or the ER. No evidence for UapA–GFP degradation in the vacuole was obtained. We also tested the sub-cellular localization of UapA–GFP in the two other yeast strains used in this work. In all cases UapA–GFP labels primarily the plasma membrane, but also internal structures that seem to be the ER and the vacuolar membrane. Interestingly, the intensity of fluorescence associated with the plasma membrane was significantly higher in the *npi1-1* genetic background, which is in perfect agreement with the fact that we detected ∼5-fold increase in the uptake of radiolabelled xanthine in this strain compared to standard strain or the one carrying *pep4Δ* (Fig. 1E). An increase in the total UapA protein level was also detected in the *npi1-1* (see below). These results were in agreement with previous reports showing that knocking-down Rsp5-dependent ubiquitination can be used to enhance the heterologous expression of transporters in *S. cerevisiae* [29]. However, we eventually selected the *pep4Δ* mutant for UapA purification for reasons associated with its reduced stability in the *npi1-1* genetic background, described below.

Selection of the appropriate S. cerevisiae genetic background for UapA purification

Preliminary analysis of the expression of UapA–GFP in the *pep4Δ* strain indicated an expression level of 2.3 mg/L (RFU = 25,000). The conditions and the *pep4Δ* strain used to functionally express UapA, constitute an appropriate system to purify good quality and significant amounts of pure UapA protein as described below. However, a further increase in the yield of the transporter might be eventually required for crystallization. For that, we also tried the expression of UapA through the same vector system in the *npi1-1* strain. In this case, we obtained a significantly increased expression level of 3.8 mg/L compared to that achieved with the *pep4Δ* strain. However, in-gel fluorescence (Fig. 2) of UapA–GFP expressed in *pep4Δ* and *npi1-1* cell strains indicated that the protein produced in *npi1-1* was subject to significant degradation, as indicated by the presence of a range of fluorescent lower molecular weight bands. In contrast, the protein expressed in *pep4Δ* was visible as a single band suggesting that in the case of UapA the lack of proteases was essential for expression of intact protein under the conditions tested.

Purification of UapA

UapA was isolated from *S. cerevisiae* membrane preparations using a three step purification protocol (Fig. 3). Following the first Ni^{2+}–NTA purification step the sample contains a major band of
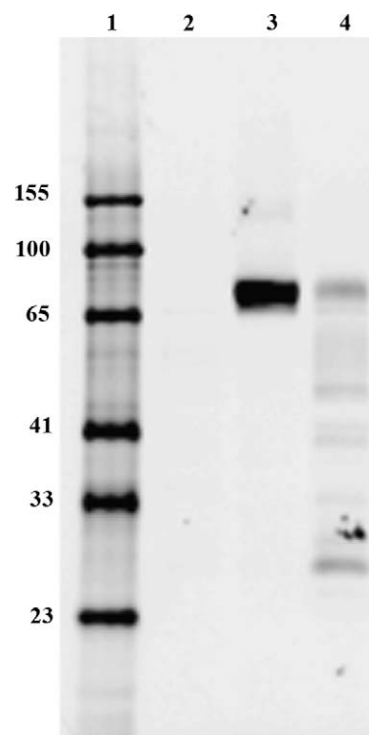
Fig. 2. In-gel fluorescence analysis of UapA–GFP expressed in *S. cerevisiae* expression strains *pep4Δ* (lane 3) and *npi1-1* (lane 4). The signal obtained from uninduced *pep4Δ* cells is shown in lane 2 and fluorescent molecular weight markers are shown in lane 1.

about 70 kDa on the denaturing gel (Fig. 3A). The same band is also visible by in-gel fluorescence (Fig. 3B) indicating that this band corresponds to UapA–GFP. After TEV cleavage to remove the GFP–His$_8$ tag and His trap purification the major band has shifted to approximately 55 kDa (Fig. 3A). The same protein band is not observed using in-gel fluorescence. In addition, the ∼70 kDa band corresponding to UapA–GFP is also not detected indicating cleavage of GFP is highly efficient. Following SEC the protein is visible as the one 55 kDa band and a larger band of approximately 110 kDa. It is possible that this larger band is a higher oligomeric form of the transporter. The chromatogram of the SEC profile shows a single monodispersed peak with no obvious aggregation (Fig. 4A). It is possible that the higher oligomeric form is an artifact of the SDS–PAGE, as often membrane proteins appear as several forms on a gel, but are revealed as one apparently monodispersed species by SEC. Since TEV cleavage removes both the GFP and the His$_8$ tag, it is not possible to confirm the identity of the protein by Western blot analysis. Therefore, the protein samples were analyzed by Mass Spectrometry, which confirmed the identity of the major band as UapA. The final yield of highly pure UapA was 0.15 mg/L.

CD spectroscopic analysis

CD spectroscopic analysis of the purified UapA yielded spectra characteristic of a highly α-helical protein as demonstrated by the absorbance minima at 208 and 222 nm [39]. Virtually identical spectra were obtained for the protein at 20 and 30 °C (Fig. 4). These results suggest that the protein maintains the same overall fold at the temperatures tested.

Discussion

Heterologous expression of eukaryotic transporters is in general very problematic. Yeast provides one of the most promising
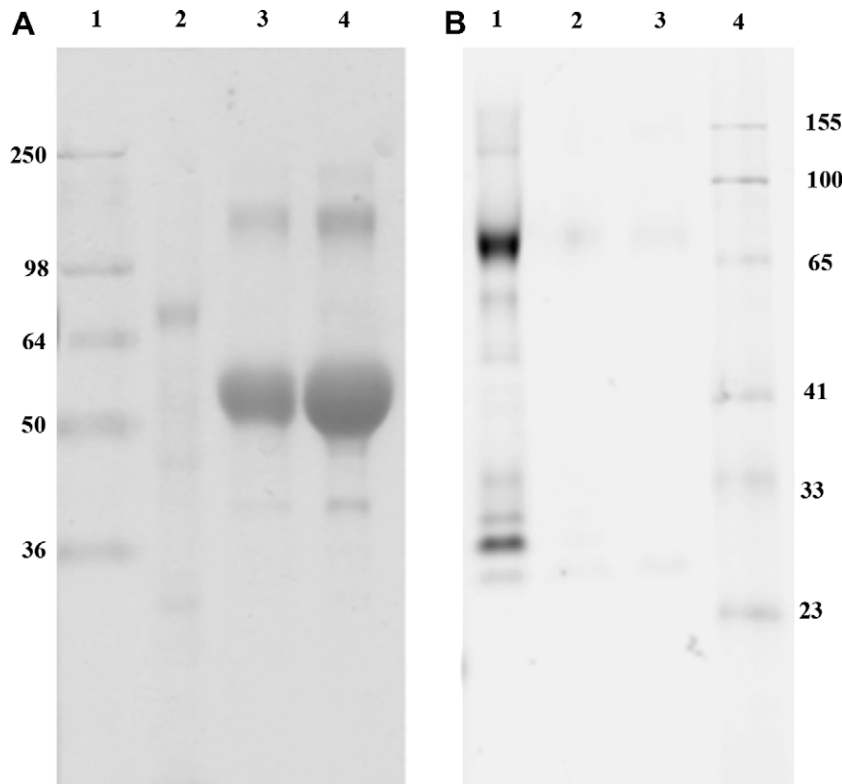
Fig. 3. SDS–PAGE (A) and in-gel fluorescence (B) analysis of samples of UapA taken at different points in the purification process. The SDS–PAGE (A) shows pre-stained molecular weight markers (lane 1), protein sample following Ni^{2+} affinity chromatography (lane 2), protein sample following TEV cleavage and reverse His trap chromatography (lane 3), protein sample following size exclusion chromatography (lane 4). The in-gel fluorescence shows protein sample following Ni^{2+} affinity chromatography (lane 1), protein sample following TEV cleavage and reverse His trap chromatography (lane 2), protein sample following size exclusion chromatography (lane 3) and fluorescent molecular weight markers (lane 4).

systems for production as, despite significant retention at the ER, a proportion of the expressed transporters find their way to the plasma membrane and show detectable activity (e.g. [28,40]). Here, we used a S. cerevisiae GFP expression system, specifically designed for the large scale production of eukaryotic membrane proteins [33,34], to express and purify the uric acid–xanthine transporter (UapA) of A. nidulans. The vector used, which carries the full length cDNA of the uapA ORF fused with a GFP–His$_8$ epitope, was introduced into three different S. cerevisiae strains; a standard ura3Δ (S288C) strain and two isogenic versions also carrying either a deletion of the PEP4 gene (encoding vacuolar protease) or a knock-down mutation (npi1-1) in NPI1 gene (encoding Rsp5 E3 HECT ubiquitin ligase). The rationale for the use of these strains was the following; pep4Δ might result in higher UapA yields as it lacks an efficient system for transporter turnover [41], whereas npi1-1 is expected to augment UapA expression at the plasma membrane as it lacks an efficient ubiquitination-dependent endocytic mechanism [29]. All strains expressed a fully functional UapA, as judged from transport kinetics and epifluorescence microscopy. Similarly to analogous UapA–GFP chimeras used in A. nidulans, the C-terminal fusion of a GFP with UapA seems to have no effect on transport activity in the yeast system. This is not always the case as several carriers fused with GFP affect transport activity, or most often trafficking of the carrier to the plasma membrane [42–45]. Despite the fact that we obtained higher expression of UapA in the npi1-1 mutant, the pep4Δ mutant proved more appropriate for production of the intact UapA, indicating that in our case at least the absence of the protease is more important than the absence of the pathway targeting protein for degradation. It may be that a strain containing both the npi1-1 and the pep4Δ mutants would improve the overall yield of UapA. The presence of a C-ter-

minal GFP–His$_8$ allowed accurate assessment of the expression level of the fusion protein by fluorescence, removed the need for Western blot analysis and allowed rapid detergent screening using fluorescent size exclusion chromatography (FSEC). In addition, we used a homologous recombination cloning methodology making plasmid generation very efficient and quick. We have optimized the functional expression of UapA and developed a protocol for the isolation of mg quantities of functional, highly stable, UapA from A. nidulans. The high quality protein produced is suitable for further functional and structural studies.

Starting with a 10 L culture volume we were able to isolate 1.5 mg of at least 95% pure UapA, a yield suitable for structural studies. The protein was concentrated to approximately 10 mg/ml with no significant losses due to aggregation, indicating that the protein is reasonably stable at the high concentrations typically required for crystallization trials. As mentioned, the starting expression level was 2.3 mg/L, indicating that we were losing significant amounts of the protein during solubilization and purification of the protein. One of the major advantages of the presence of the GFP is that it is very easy to monitor the recovery of the protein in the early stages of isolation, before TEV cleavage. Analysis has shown that the losses of UapA are incurred at several stages; the cell breakage step is only about 60% efficient, and while solubilization is close to 100% efficient, only about 50% of the protein binds to the Ni^{2+} resin. There are likely to be other losses due to unfolding and subsequent aggregation of some of the protein. However, the amounts of protein obtained are sufficient for further work. Earlier work has shown that it is possible to express UapA homologously in A. nidulans. CD spectroscopic analysis of the A. nidulans expressed protein confirmed that this was a largely α-helical protein. Comparison of the CD spectra obtained for the A. nidulans ex-
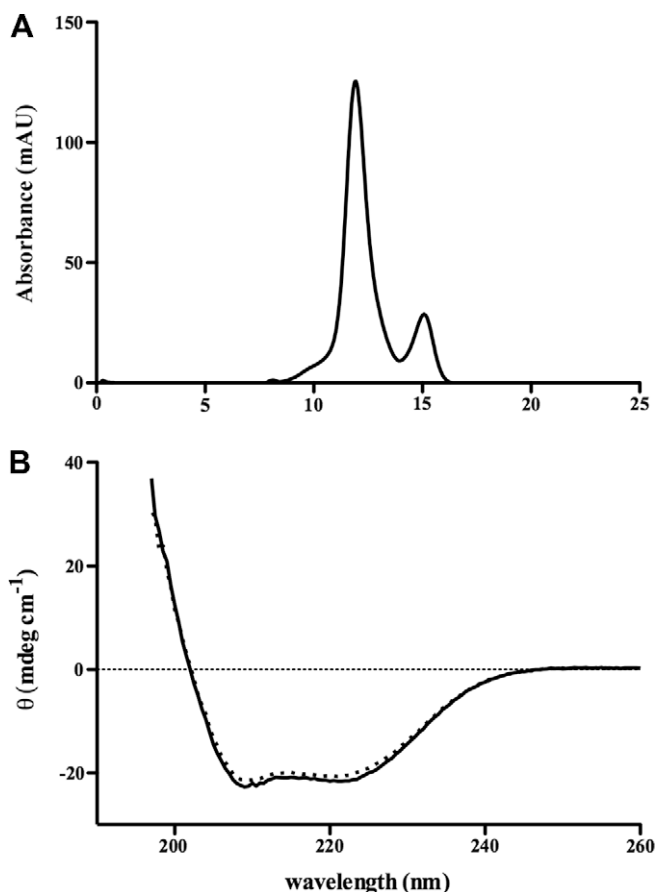
Fig. 4. Elution profile (A) for UapA separated on a superdex 200 10/300 gel filtration column. Far-ultraviolet CD spectra (B) of purified UapA in a buffer of 20 mM Tris–HCl, pH 7.5, 150 mM NaCl, 0.03% (w/v) DDM_{LA} recorded at 20 °C (solid line) and 30 °C (dashed line). Background values obtained with a buffer blank were negligible for the wavelength shown and were not subtracted.

pressed UapA with that obtained in this study indicated that both proteins were in a similar folded state, further confirming the suitability of the *S. cerevisiae* system for production of UapA.

Expression of UapA into *S. cerevisiae* will also provide a novel genetic system which will have all the advantages of yeast genetics and molecular biology for the analysis of NAT proteins. Unexpectedly, expression of UapA did not confer any visible growth phenotype in yeast. In *A. nidulans*, UapA-mediated uptake of uric acid in strains lacking uric acid oxidase (*uaZ⁻* mutants) is toxic [46]. Uric acid toxicity is a common observation in all kinds of cells, especially those lacking uric acid oxidase, connected with its pro-oxidant activity and low solubility. In addition, UapA-mediated uptake of oxypurinol also leads to toxicity in *A. nidulans*. We do not understand why none of these cytotoxic effects were detected in *S. cerevisiae* cells expressing UapA, despite the fact that these lack a uric acid oxidase. Unfortunately, the lack of UapA-dependent visible growth phenotypes does not allow the use of the system developed herein for the direct selection of mutants affected in UapA trafficking, function or specificity. In addition, signals triggering UapA endocytosis in *A. nidulans* do not seem to function in yeast cells (unpublished observations). However, yeast cells expressing UapA still provide an excellent system for performing reverse genetics and other targeted approaches in order to understand structure–function relationships in a prototype member of a very important transporter family, and also open the way for the functional analysis of several NAT members with unknown function from plants and animals.

References

[1] C. Gournas, I. Papageorgiou, G. Diallinas, The nucleobase–ascorbate transporter (NAT) family: genomics, evolution, structure–function relationships and physiological role, Mol. Biosyst. 4 (2008) 404–416.

[2] G. Diallinas, C. Gournas, Structure–function relationships in the nucleobase–ascorbate transporter (NAT) family: lessons from model microbial genetic systems, Channels 2 (2008) 363–372.

[3] H. de Koning, G. Diallinas, Nucleobase transporters, Mol. Membr. Biol. 17 (2000) 75–94.

[4] G. Elion, The purine path to chemotherapy, Science 244 (1989) 41–47.

[5] P. Maser, D. Vogel, C. Schmid, B. Raz, R. Kaminsky, Identification and characterization of trypanocides by functional expression of an adenosine transporter from *Trypanosoma brucei* in yeast, J. Mol. Med. 79 (2001) 121–127.

[6] P. Karatza, S. Frillingos, Cloning and functional characterization of two bacterial members of the NAT/NCS2 family in *Escherichia coli*, Mol. Membr. Biol. 22 (2005) 251–261.

[7] B. Gillissen, L. Burkle, B. Andre, C. Kuhn, D. Rentsch, B. Brandl, W.B. Frommer, A new family of high-affinity transporters for adenine, cytosine, and purine derivatives in *Arabidopsis*, Plant Cell 12 (2000) 291–300.

[8] V.G. Maurino, E. Grube, J. Zielinski, A. Schild, K. Fischer, U.I. Flugge, Identification and expression analysis of twelve members of the nucleobase–ascorbate transporter (NAT) gene family in *Arabidopsis thaliana*, Plant Cell. Physiol. 47 (2006) 1381–1393.

[9] H. Tsukaguchi, T. Tokui, B. Mackenzie, U.V. Berger, X.Z. Chen, Y. Wang, R.F. Brubaker, M.A. Hediger, A family of mammalian Na+-dependent L-ascorbic acid transporters, Nature 399 (1999) 70–75.

[10] S. Yamamoto, K. Inoue, T. Murata, S. Kamigaso, T. Yasujima, J.Y. Maeda, Y. Yoshida, K.Y. Ohta, H. Yuasa, Identification and functional characterization of the first nucleobase transporter in mammals: implication in the species difference in the intestinal absorption mechanism of nucleobases and their analogs between higher primates and other mammals, J. Biol. Chem. (2009) (Epub ahead of print).

[11] M. Koukaki, A. Vlanti, S. Goudela, A. Pantazopoulou, H. Gioule, S. Tournaviti, G. Diallinas, The nucleobase–ascorbate transporter (NAT) signature motif in UapA defines the function of the purine translocation pathway, J. Mol. Biol. 350 (2005) 499–513.

[12] G. Diallinas, J. Valdez, V. Sophianopoulou, A. Rosa, C. Scazzocchio, Chimeric purine transporters of *Aspergillus nidulans* define a domain critical for function and specificity conserved in bacterial, plant and metazoan homologues, EMBO J. 17 (1998) 3827–3837.

[13] C. Meintanis, A.D. Karagouni, G. Diallinas, Amino acid residues N450 and Q449 are critical for the uptake capacity and specificity of UapA, a prototype of a nucleobase–ascorbate transporter family, Mol. Membr. Biol. 17 (2000) 47–57.

[14] A. Pantazopoulou, G. Diallinas, Fungal nucleobase transporters, FEMS Microbiol. Rev. 31 (2007) 657–675.

[15] G. Diallinas, C. Scazzocchio, A gene coding for the uric acid–xanthine permease of *Aspergillus nidulans*: inactivational cloning, characterization, and sequence of a cis-acting mutation, Genetics 122 (1989) 341–350.

[16] G. Diallinas, L. Gorfinkiel, H.N. Arst Jr., G. Cecchetto, C. Scazzocchio, Genetic and molecular characterization of a gene encoding a wide specificity purine permease of *Aspergillus nidulans* reveals a novel family of transporters conserved in prokaryotes and eukaryotes, J. Biol. Chem. 270 (1995) 8610–8622.

[17] L. Gorfinkiel, G. Diallinas, C. Scazzocchio, Sequence and regulation of the uapA gene encoding a uric acid–xanthine permease in the fungus *Aspergillus nidulans*, J. Biol. Chem. 268 (1993) 23376–23381.

[18] S. Amillis, G. Cecchetto, V. Sophianopoulou, M. Koukaki, C. Scazzocchio, G. Diallinas, Transcription of purine transporter genes is activated during the isotropic growth phase of *Aspergillus nidulans* conidia, Mol. Microbiol. 52 (2004) 205–216.

[19] S. Goudela, P. Karatza, M. Koukaki, S. Frillingos, G. Diallinas, Comparative substrate recognition by bacterial and fungal purine transporters of the NAT/NCS2 family, Mol. Membr. Biol. 22 (2005) 263–275.

[20] I. Papageorgiou, C. Gournas, A. Vlanti, S. Amillis, A. Pantazopoulou, G. Diallinas, Specific interdomain synergy in the UapA transporter determines its unique specificity for uric acid among NAT carriers, J. Mol. Biol. 382 (2008) 1121–1135.

[21] P. Karatza, P. Panos, E. Georgopoulou, S. Frillingos, Cysteine-scanning analysis of the nucleobase–ascorbate transporter signature motif in YgfO permease of *Escherichia coli*: Gln-324 and Asn-325 are essential, and Ile-329-Val-339 form an alpha-helix, J. Biol. Chem. 281 (2006) 39881–39890.

[22] S. Amillis, M. Koukaki, G. Diallinas, Substitution F569S converts UapA, a specific uric acid–xanthine transporter, into a broad specificity transporter for purine-related solutes, J. Mol. Biol. 311 (2001) 765–774.

[23] A. Vlanti, S. Amillis, M. Koukaki, G. Diallina, A novel-type substrate-selectivity filter and ER-exit determinants in the UapA purine transporter, J. Mol. Biol. 357 (2006) 808–819.

[24] K. Papakostas, E. Georgopoulou, S. Frillingos, Cysteine-scanning analysis of putative helix XII in the YgfO xanthine permease: ILE-432 and ASN-430 are important, J. Biol. Chem. 283 (2008) 13666–13678.

[25] E. Karena, S. Frillingos, Role of intramembrane polar residues in the YgfO xanthine permease: HIS-31 and ASN-93 are crucial for affinity and specificity, and ASP-304 and GLU-272 are irreplaceable, J. Biol. Chem. 284 (2009) 24257–24268.

[26] N.D. Lemuh, G. Diallinas, S. Frillingos, G. Mermelekas, A.D. Karagouni, D.G. Hatzinikolaou, Purification and partial characterization of the xanthine–uric acid transport (UapA) of Aspergillus nidulans, Protein Expr. Purif. 63 (2009) 33–39.

[27] C.R. Midgett, D.R. Madden, Breaking the bottleneck: eukaryotic membrane protein expression for high-resolution structural studies, J. Struct. Biol. 160 (2007) 265–274.

[28] R. Wieczorke, S. Dlugai, S. Krampe, E. Boles, Characterisation of mammalian GLUT glucose transporters in a heterologous yeast expression system, Cell. Physiol. Biochem. 13 (2003) 123–134.

[29] H. Flegelova, R. Haguenauer-Tsapis, H. Sychrova, Heterologous expression of mammalian Na/H antiporters in Saccharomyces cerevisiae, Biochim. Biophys. Acta 1760 (2006) 504–516.

[30] R.A. Figler, H. Omote, R.K. Nakamoto, M.K. Al-Shawi, Use of chemical chaperones in the yeast Saccharomyces cerevisiae to enhance heterologous membrane protein expression: high-yield expression and purification of human P-glycoprotein, Arch. Biochem. Biophys. 376 (2000) 34–36.

[31] D. Zweytick, C. Hrastnik, S.D. Kohlwein, G. Daum, Biochemical characterization and subcellular localization of the sterol C-24(28) reductase, erg4p, from the yeast Saccharomyces cerevisiae, FEBS Lett. 470 (2000) 83–87.

[32] J. Makuc, C. Cappellaro, E. Boles, Co-expression of a mammalian accessory trafficking protein enables functional expression of the rat MCT1 monocarboxylate transporter in Saccharomyces cerevisiae, FEMS Yeast Res. 4 (2004) 795–801.

[33] S. Newstead, H. Kim, G. von Heijne, S. Iwata, D. Drew, High-throughput fluorescent-based optimization of eukaryotic membrane protein overexpression and purification in Saccharomyces cerevisiae, Proc. Natl. Acad. Sci. USA 104 (2007) 13936–13941.

[34] D. Drew, S. Newstead, Y. Sonoda, H. Kim, G. von Heijne, S. Iwata, GFP-based optimization scheme for the overexpression and purification of eukaryotic membrane proteins in Saccharomyces cerevisiae, Nat. Protoc. 3 (2008) 784–798.

[35] M. Grenson, Study of the positive control of the general amino-acid permease and other ammonia-sensitive uptake systems by the product of the NPR1 gene in the yeast Saccharomyces cerevisiae, Eur. J. Biochem. 133 (1983) 141–144.

[36] J. Kota, C.F. Gilstring, P.O. Ljungdahl, Membrane chaperone Shr3 assists in folding amino acid permeases preventing precocious ERAD, J. Cell Biol. 176 (2007) 617–628.

[37] C.A. Woolford, L.B. Daniels, F.J. Park, E.W. Jones, J.N. Van Arsdell, M.A. Innis, The PEP4 gene encodes an aspartyl protease implicated in the posttranslational regulation of Saccharomyces cerevisiae vacuolar hydrolases, Mol. Cell. Biol. 6 (1986) 2500–2510.

[38] G. Cecchetto, S. Amillis, G. Diallinas, C. Scazzocchio, C. Drevet, The AzgA purine transporter of Aspergillus nidulans. Characterization of a protein belonging to a new phylogenetic cluster, J. Biol. Chem. 279 (2004) 3132–3141.

[39] L.A. Compton, W.C. Johnson, Analysis of protein circular dichroism spectra for secondary structure using a simple matrix multiplication, Anal. Biochem. 155 (1986) 155–167.

[40] M.F. Vickers, R.S. Mani, M. Sundaram, D.L. Hogue, J.D. Young, S.A. Baldwin, C.E. Cass, Functional production and reconstitution of the human equilibrative nucleoside transporter (hENT 1) in Saccharomyces cerevisiae. Interaction of inhibitors of nucleoside transport with recombinant hENT 1 and a glycosylation-defective derivative (hENT 1/N48Q), Biochem. J. 339 (2001) 21–32.

[41] V. Westphal, E.G. Marcusson, J.R. Winther, S.D. Emr, H.B. van den Hazel, Multiple pathways for the vacuolar sorting of yeast proteinase A, J. Biol. Chem. 271 (1996) 11865–11867.

[42] S. Tavoularis, C. Scazzocchio, V. Sophianopoulou, Functional expression and cellular localization of a green fluorescent protein-tagged proline transporter in Aspergillus nidulans, Fungal Genet. Biol. 33 (2001) 115–125.

[43] I. Papageorgiou, H.P. De Koning, K. Soteriadou, G. Diallinas, Kinetic and mutational analysis of the Trypanosoma brucei NBT 1 nucleobase transporter expressed in Saccharomyces cerevisiae reveals structural similarities between ENT and MFS transporters, Int. J. Parasitol. 38 (2008) 641–653.

[44] A. Vlanti, G. Diallinas, The Aspergillus nidulans FcyB cytosine–purine scavenger is highly expressed during germination and in reproductive compartments and is downregulated by endocytosis, Mol. Microbiol. 68 (2008) 959–977.

[45] S. Amillis, Z. Hamari, K. Roumelioti, C. Scazzocchio, G. Diallinas, Regulations of expression and kinetic modeling of substrate interactions of a uracil transporter in Aspergillus nidulans, Mol. Membr. Biol. 24 (2007) 206–214.

[46] A.J. Darlington, C. Scazzocchio, J.A. Pateman, Biochemical and genetical studies of purine breakdown in Aspergillus, Nature 206 (1965) 599–600.

Οι υπερτονικές συνθήκες προκαλούν παροδική πλασμόλυση, μειωμένο ρυθμό αύξησης και αναστολή της ενδοκύτωσης των μεταφορέων στους *Aspergillus nidulans* και *Saccharomyces cerevisiae*

Μπίτσικας Β.*, Καραχάλιου Μ*., Γουρνάς Χ. & Διαλλινάς Γ.

*Ισάξια συνεισφορά

Περίληψη

Χρησιμοποιώντας στελέχη του *Aspergillus nidulans* που εκφράζουν διαμεμβρανικούς μεταφορείς σημασμένους με την πράσινη φθορίζουσα πρωτεΐνη (GFP) σε υπερτονικές συνθήκες, παρατηρήσαμε την άμεση εμφάνιση στατικών φθορίζουσων κηλίδων στο επίπεδο της πλασματικής μεμβράνης. Οι φθορίζουσες κηλίδες που παρατηρήθηκαν δεν αντιστοιχούν σε μικροπεριοχές της μεμβράνης ειδικές για μεταφορείς, καθώς συνεντοπίζονται με άλλες μεμβρανικές πρωτεΐνες όπως το πεπτίδιο ομόλογο της πλεξτρίνης (PH) και η SsoA t-SNARE, ή τους λιπόφιλους δείκτες FM4-64 και Φιλιπίνη. Επιπλέον, δεν εμφανίζουν χαρακτηριστικά λιπιδικών σχεδιών ή άλλων μεμβρανικών μικροπεριοχών. Εικόνες μικροσκοπίας που έχουν επεξεργαστεί με αλγόριθμους απο-αλληλεπικάλυψης (deconvolution) έδειξαν ότι οι φθορίζουσες αυτές κηλίδες αντιστοιχούν σε εκτεταμένες εγκολπώσεις της μεμβράνης. Οι μεταφορείς παραμένουν πλήρως λειτουργικοί κατά τη διάρκεια του φαινομένου της πλασμόλυσης. Η εμφάνιση αυτών των εγκολπώσεων συνοδεύεται από μειωμένο ρυθμό αύξησης και πλήρη αναστολή της ενδοκύτωσης μέσω κλαθρίνης, αλλά και της ενδοκύτωσης ρευστής φάσης. Τα παραπάνω φαινόμενα είναι παροδικά και άμεσα αναστρέψιμα με την απομάκρυνση των υπερτονικών διαλυμάτων. Το υπερτονικό στρες δεν επηρέασε την τοπολογία πρωίμων (SlaB-GFP) και όψιμων (AbpA-mRFP) παραγόντων του μηχανισμού ενδοκύτωσης, αλλά φαίνεται να τροποποιεί τον υποκυτταρικό εντοπισμό της τροπομυοσίνης (GFP-TpmA), υποδεικνύοντας ότι η παρεμπόδιση της ενδοκύτωσης των μεταφορέων και των λιπόφιλων χρωστικών γίνεται μέσω της τροποποίησης της δυναμικής οργάνωσης της ακτίνης. Το συμπέρασμα αυτό υποστηρίζεται και από τη δράση στην ενδοκύτωση των μεταφορέων της λατρουνκουλίνης Β, ενός παράγοντα που προκαλεί τον αποπολυμερισμό της ακτίνης. Παρόμοια φαινόμενα παρατηρήσαμε και στον *Saccharomyces cerevisiae*, γεγονός που υποδεικνύει ότι οι ασκομύκητες αποκρίνονται στις υπερτονικές συνθήκες χρησιμοποιώντας παρόμοιους μηχανισμούς. Τέλος, η εργασία αυτή δείχνεο ότι οι υπερτονικές συνθήκες μπορούν να χρησιμοποιηθούν σαν εργαλείο για τη μελέτη της ρύθμισης των μεταφορέων στον A. nidulans, όπου η πλήρης απενεργοποίηση γονιδίων σχετικών με την ενδοκύτωση είναι συνήθως θνησιγόνος.

informa
healthcare

Hypertonic conditions trigger transient plasmolysis, growth arrest and blockage of transporter endocytosis in *Aspergillus nidulans* and *Saccharomyces cerevisiae*

VASSILIS BITSIKAS[*], MAYIA KARACHALIOU[*], CHRISTOS GOURNAS & GEORGE DIALLINAS

Faculty of Biology, Department of Botany, University of Athens, Panepistimioupolis, Athens, Greece

Abstract

By using *Aspergillus nidulans* strains expressing functional GFP-tagged transporters under hypertonic conditions, we noticed the rapid appearance of cortical, relatively static, fluorescent patches (0.5–2.3 μm). These patches do not correspond to transporter microdomains as they co-localize with other plasma membrane-associated molecules, such as the pleckstrin homology (PH) domain and the SsoA t-Snare, or the lipophilic markers FM4-64 and filipin. In addition, they do not show characteristics of lipid rafts, MCCs or other membrane microdomains. Deconvoluted microscopic images showed that fluorescent patches correspond to plasma membrane invaginations. Transporters remain fully active during this phenomenon of localized plasmolysis. Plasmolysis was however associated with reduced growth rate and a dramatic blockage in transporter and FM4-64 endocytosis. These phenomena are transient and rapidly reversible upon wash-out of hypertonic media. Based on the observation that block in endocytosis by hypertonic treatment altered dramatically the cellular localization of tropomyosin (GFP-TpmA), although it did not affect the cortical appearance of upstream (SlaB-GFP) or downstream (AbpA-mRFP) endocytic components, we conclude that hypertonicity modifies actin dynamics and thus acts indirectly on endocytosis. This was further supported by the effect of latrunculin B, an actin depolymerization agent, on endocytosis. We show that the phenomena observed in *A. nidulans* also occur in *Saccharomyces cerevisiae*, suggesting that they constitute basic homeostatic responses of ascomycetes to hypertonic shock. Finally, our work shows that hypertonic treatments can be used as physiological tools to study the endocytic down-regulation of transporters in *A. nidulans*, as non-conditional genetic blocks affecting endocytic internalization are lethal or severely debilitating.

Keywords: *Fungi, patches, plasma membrane invaginations, microdomain/actin dynamics*

Introduction

Eukaryotic transporters respond to environmental and developmental signals at both the transcriptional and post-translational levels. Their tight control includes mostly rapid *de novo* synthesis and even more rapid down-regulation through endocytosis and vacuolar degradation (André and Haguenauer-Tsapis 2004, Dupré et al. 2004). The molecular mechanisms underlying endocytosis and vacuolar degradation are best understood in *Saccharomyces cerevisiae*. It has been shown that the principal signal for transporter endocytosis and entry into multivesicular bodies (MVBs),

which eventually fuse with the vacuole/lysosome and thus deliver the vesicles to degradative enzymes, is their ubiquitination (André and Haguenauer-Tsapis 2004, Dupré et al. 2004, Belgareh-Touze et al. 2008). Ubiquitination serves as a signal not only for transporter internalization from the plasma membrane, but also to redirect newly synthesized transporter molecules from the Golgi to endosomes (Soetens et al. 2001, Umebayashi and Nakano 2003) and for MVB sorting (Helliwell et al. 2001, Soetens et al. 2001, Reggiori and Pelham 2002, André and Haguenauer-Tsapis 2004, Blondel et al. 2004, Erpapazoglou et al. 2008).

Correspondence: Prof. George Diallinas, Faculty of Biology, Department of Botany, University of Athens, Panepistimioupolis, Athens 15781, Greece. Tel: +30 210 7274649. Fax: +30 210 7274702. E-mail: diallina@biol.uoa.gr

[*]These authors contributed equally to the paper.

The trafficking, function and turnover of *S. cerevisiae* transporters is also known to depend on their partitioning in lipid-rafts or plasma membrane compartments (MCs) with distinct lipid composition. Two such non-overlapping membrane compartments (MCs) have been distinguished, using GFP-tagged transporters as markers, as evenly distributed ~300 nm isolated patches (Grossmann et al. 2007). The first, MCC, contains permeases specific for arginine (Can1p), tryptophan (Tat2p) and uracil (Fur4p), whereas the second, MCP, contains the proton ATPase Pma1p (Malinska et al. 2004, Grossmann et al. 2006, 2007). MCCs contain a distinct lipid composition enriched in ergosterol, as visualized by staining with filipin, a fluorescent marker binding this lipid (Malinska et al. 2003, Grossmann et al. 2007), but also as supported by biochemical assays relating transporter extractability from membranes using Triton-X 100 (Grossmann et al. 2007). The compartmentation of the plasma membrane into MCC and MCP is highly stable (Malinska et al. 2004), but transporters dock within MCC patches in a reversible, membrane potential-dependent manner (Grossmann et al. 2007). Based on a number of observations relating to the rate of transporter endocytosis with localization in MCCs, it has been proposed that the biological function of MCCs is to protect therein embedded transporters and other proteins from internalization and turnover (Grossmann et al. 2008). This view is somehow contradicted by other studies showing that MCC organization is, at least in part, mediated by large protein complexes, termed eisosomes, which were proposed to mark static sites of endocytosis (Walther et al. 2006). One possible function of MCCs and eisosomes is to regulate protein and lipid abundance by sorting them into distinct, spatially separated pools where they are stabilized or from which they can be either endocytosed, or protected from internalization, selectively. Electron microscopy analysis suggested that MCC patches correspond to furrow-like invaginations in the plasma membrane of yeast (Strádalová et al. 2009).

Several transporters of the filamentous ascomycete *Aspergillus nidulans* have been studied (for reviews see Pantazopoulou and Diallinas 2007, Diallinas 2008). In most cases, transporters tagged with GFP remain fully functional, although in some cases the GFP tag led to increased instability and vacuolar turnover (Tavoularis et al. 2001, Pantazopoulou et al. 2007, Vlanti and Diallinas 2008). After transcriptional activation of the corresponding genes during conidiospore germination (Amillis et al. 2004), transporter proteins show a uniform distribution along the plasma membrane of germlings and developing mycelia. Often, GFP-tagged transporters also label the vacuoles, which is the site of their constitutive turnover (see Figure 1).

Transporter turnover is dramatically enhanced upon various physiological signals or stress conditions. For example, several transporters of purines (UapA, UapC), pyrimidines (FcyB, FurD) and amino acids (PrnB, AgtA) are rapidly turned-over in the presence of ammonium ions (Tavoularis et al. 2001, Valdez-Taubas et al. 2004, Pantazopoulou et al. 2007, Vlanti and Diallinas 2008, Apostolaki et al. 2009, Borbolis and Diallinas, unpublished). This is a typical example of down-regulation of transporters specific for nitrogenous compounds when a primary nitrogen source such as ammonium or glutamine is added in the media, a phenomenon very well studied in *S. cerevisiae*. Several *A. nidulans* transporters are also down-regulated by endocytosis and vacuolar degradation in the presence of their substrates (Vlanti and Diallinas 2008, Gournas et al. 2010, Borbolis, Pavlides and Diallinas, unpublished). An interesting aspect concerning the turnover of the UapA permease by its substrates is that endocytosis of inactive UapA molecules has been shown to occur *in trans* when co-expressed with active UapA versions, even if the latter cannot be endocytosed (Gournas et al. 2010). This last observation strongly suggested that UapA molecules might be organized in specific plasma membrane microdomains, either constitutively or prior to endocytosis.

In the course of previous work, we noticed that some *A. nidulans* transporters tagged with GFP form fluorescent cortical patches, when the samples were washed in buffers containing relatively high salt concentrations (Pavlides and Diallinas, unpublished). In the present work, we investigated the conditions eliciting the appearance of transporters as cortical patches, whether this phenomenon is specific to transporters and their turnover, and whether patches correspond to transporter-specific microdomains or membrane compartments similar to MCCs. We show that patches originally observed with transporters correspond to membrane invaginations rather than specific membrane microdomains, transiently elicited by hypertonic conditions. We further show that this phenomenon is associated with transient growth arrest and a total block of endocytic mechanisms in *A. nidulans*. Similar conclusions were reached in *S. cerevisiae*. We finally investigate aspects concerning the mechanism blocking endocytosis and discuss how conditions established herein can be used as physiological tools to study transporter trafficking and sorting in the MVB pathway in *A. nidulans*, where genetic blocks in relevant genes are usually lethal or debilitating

(Araujo-Bazán et al. 2008, Rodríguez-Galán et al. 2009, Abenza et al. 2010).

Methods

Strains, genetics, media and growth conditions

A. nidulans and *S. cerevisiae* strains used are listed in Table I. Newly-made *A. nidulans* strains were constructed with standard genetic crossing using auxotrophic markers for heterokaryon establishment. Standard complete (CM) and minimal media (MM) for *A. nidulans* were used (www.fgsc.net). Nitrogen sources were used at the following concentrations: urea 5 mM, $NaNO_3$ 10 mM, NH_4Cl 10 mM, uric acid 0.1 mg/ml. Induction of UapA expression from the *alcA* promoter was achieved after 14 h of growth in MM supplemented with urea (5 mM) and fructose (0.1%). Repression of UapA expressed from the *alcA* promoter ($alcA_p$) was achieved in MM supplemented with urea (5 mM) and glucose (1%). Growth tests were carried out at 25°C, at pH 6.8. Supplements were added when appropriate. In yeast, Jen1p-GFP expression was induced by 4 h growth in MM supplemented with 0.5% lactate (Paiva et al. 2009) and Fur4p-GFP by 16 h growth in MM with 2% galactose (Leung et al. 2010).

Epifluorescence and confocal microscopy

Samples for fluorescence microscopy were prepared as in Valdez-Taubas et al. (2004). In particular, the samples were incubated in 3 cm Petri dishes on cover slips, protected from light, in liquid MM supplemented with urea as nitrogen source and appropriate auxotrophies, at 25°C for 12–17 h and then shifted to various conditions for 2–4 h. Staining with FM4-64 (Molecular Probes, Inc, USA) was according to Penalva (2005). In particular, cover slips with germinated conidia were placed on top of plastic covers, covered with 0.1 ml of 10 μM FM4-64 in MM, incubated on ice for 15 min, washed in 5 ml MM, and transferred to fresh 3 ml medium for 0–30 min chase time. Staining with filipin (Sigma) was performed by addition of 0.1 ml MM supplemented with 25 μg/ml filipin on cover slips with germinated conidia, on top of plastic covers, 15 min prior to observation. Calcofluor white (Sigma) staining, used for detecting the presence and deposition of polysaccharides (chitin and b-1,3-glucan) in the cell walls of yeast and mycelial fungi, was performed according to Slaninová et al. (2000). Cells were stained for 5 min on coverslips with a solution of Calcofluor (0.001%w/v in relevant growth medium), washed and immediately observed in the fluorescence microscope. Lat-B was used as described (Taheri-Talesh et al. 2008), at a final concentration of 20–40 μg/ml (50–100 μM). The drug was added from a 10 mM stock in DMSO. For endocytosis, uric acid (0.1 mg/ml) or NH_4Cl (10–50 mM) was added for 1 h before observation. For hypertonic treatment, sucrose, NaCl or other agents were added as indicated in the relevant Figures. Samples were observed on an Axioplan Zeiss phase-contrast epifluorescent microscope with appropriate filters and the resulting images were acquired with a Zeiss-MRC5 digital camera using the AxioVs40 V4.40.0 software. Image

Table I. Strains used in this study.

Strains	Genotype	Origin
Aspergillus nidulans		
UapA-GFP	*pabaA1 ΔuapA ΔuapC ΔazgA argB2::argB uapA-gfp*	(Pantazopoulou et al. 2007)
$alcA_p$-UapA-GFP	*pabaA1 ΔuapA ΔuapC ΔazgA argB2::argB alcA_p-uapA-gfp*	(Gournas et al. 2010)
UapA-mRFP AzgA-GFP	*pabaA1 ΔuapA ΔuapC ΔazgA argB2 [uapA-mrfp]^{argB} [azgA-gfp]^{argB}*	This study
AzgA-GFP	*pabaA1 ΔuapA ΔuapC ΔazgA argB2::argB azgA-gfp*	(Pantazopoulou et al. 2007)
PrnB-GFP	*yA2 pabaA1 argB2 prn397::prnB-gfp-trpC_{C-term} prnC*	(Tavoularis et al. 2001)
FurD-GFP	*ΔuapA ΔuapC ΔazgA ΔfurD::riboB ΔcntA::riboB ΔnkuA::argB pantoB100 [furD-GFP]^{pantoB}*	(Borbolis and Diallinas unpublished)
GFP-PH domain	*yA2 pabaA1 argB2::argB^{BglII} gpdA_p-gfp-(PHdomainPLCΔ$_1$)$_2$*	(Pantazopoulou and Penalva 2009)
GFP-SsoA	*pyrG89 pyroA4 ΔnkuA::bar ssoA::[ssoA_p-gfp-ssoA]^{AfpyrG}*	(Taheri-Talesh et al. 2008)
SlaB-GFP	*pyrG89 pyroA4 argB2 ΔnkuA::argB slaB-gfp-AfpyrG*	(Araujo-Bazán et al. 2008)
SlaB-GFP UapA-mRFP	*pabaA1 ΔnkuA::argB slaB-gfp-AfpyrG argB2[uapA-mrfp]^{argB}*	This study
AbpA-GFP	*yA2 pabaA1 pyrG89[abpA-mrfp-AfpyrG]*	(Araujo-Bazán et al. 2008)
UapA-K572R-GFP	*pabaA1 ΔuapA ΔuapC ΔazgA argB2::argB alcA_p-K572R-gfp*	(Gournas et al. 2010)
GFP-TpmA	*fwA1 pyrG89 pyroA4 nicA2 ΔnkuA::argBAfpyG-mcherry-synA yA::AfpyroA tpmA_p-gfp-tpmA*	(Taheri-Talesh et al. 2008)
Saccharomyces cerevisiae		
Fur4p-GFP	*BY4742 MATa his3Δ1 leu2Δ0 lysΔ0 ura3Δ0/URA3 GAL-FUR4-GFP*	(Dupré and Haguenauer-Tsapis 2003)
Jen1p-GFP	*MATa ura3-52 JEN1-GFP*	(Paiva et al. 2009)

processing, contrast adjustment and color combining were made using Adobe Photoshop CS2 V9.0.2. Images were converted to 8-bit greyscale or RGB and annotated using Photoshop CS2 before being saved to TIFF. At CIB-CSIC (Madrid), an inverted Leica DMI6000B microscope with motorized z-focus and a Leica EL6000 external light source was used for epifluorescence excitation. The microscope was driven by Metamorph (Invitrogen, Carlsbad, CA, USA) software using a DMI6000-specific driver. Images were acquired using HCX ×63 1.4 numerical aperture (NA) or ×100 1.4 NA objectives and a Hamamatsu ORCA ER-II cooled-charge coupled device camera (Hamamatsu Photonics, Massy, France). The microscope was equipped with Semrock Brightline GFP-3035B and TXRED-4040B filter sets (Semrock, Rochester, NY, USA). Maximal intensity projections were obtained from z-stacks using the Metamorph 3D plugin. Images were converted to 8-bit greyscale or RGB and annotated using Photoshop CS2 before being saved to TIFF. When indicated (Figure 4), images were deconvoluted using the blind deconvolution algorithms of ImageJ 1.37 http://rsb.info.nih.gov/ij. For Laser Confocal Microscopy at the Medical School of Universidade do Minho, we used an inverted FLUOVIEW confocal laser scanning microscope, version FV1000 Viewer (Ver.2.0b) as described by the manufacturer (http://www.olympusfluoview.com/).

Transport assays

Radiolabelled xanthine (33.4 Ci/mmol) was from Moravek Biochemicals (Brea, CA, USA). [^{3}H]-xanthine uptake was assayed in conidiospores at 37°C as described previously (Koukaki et al. 2005, Papageorgiou et al. 2008). All experiments were carried out in triplicate. Initial velocities were corrected by subtracting background uptake values, measured in the *uapA⁻uapC⁻* mutant (Koukaki et al. 2005). The K_m (concentration for obtaining $V_m/2$) of UapA for xanthine was determined from full dose-response curves with a minimum of eight points spread over the relevant range. In all cases, the Hill coefficients were close to −1, consistent with competitive inhibition.

Western blot analysis

Protein extracts were prepared as in Pantazopoulou et al. (2007). In particular, liquid cultures were incubated for 12 h at 25°C before the addition of substrates or ammonium, or induction for the *alcA*$_p$-driven UapA expression. Protein concentrations were determined by the method of Bradford. In each case, 50 μg of protein were loaded for SDS PAGE. Samples were fractionated on a 10% SDS-page gel and electro-blotted (Mini PROTEAN^{TM} Tetra Cell, BIO-RAD) onto a PVDF membrane (Macherey-Nagel) for immunodetection. The membrane was treated with 2% non-fat dry milk or according to the manufacturer instructions and immunodetection was performed using a primary mouse anti-GFP monoclonal antibody (Roche) and a secondary goat anti-mouse IgG HRP-linked antibody (Cell Signaling). Blots were developed by the chemiluminescent method using the West Pico SuperSignal reagent (Pierce).

Determination of detergent resistance

This is basically as described in Grossmann et al. (2007). In brief, aliquots corresponding to 50 μg of membrane protein in 100 μl 50 mM Tris-HCl, pH 7.5, 150 mM NaCl, 5 mM EDTA, were treated with increasing concentrations of Triton X-100 (0–0.8%) at room temperature for 30 min. Non-solubilized material was pelleted by centrifugation (14,000 rpm at 4°C for 30 min) and washed by 100 μl of the corresponding buffers under the same conditions. The pellets were resuspended in 30 μl of sample buffer, dissociated at 37°C for 15 min and then resolved by SDS-PAGE, and UapA-GFP was detected by a specific anti-GFP antibody on a Western blot.

Results

Hypertonic media elicit a cortical patchy appearance of A. nidulans transporters

Using functional GFP-tagged versions of seven permeases belonging to four evolutionary distinct protein families (NAT/NCS2, NCS1, AzgA-like, APC; http://www.membranetransport.org/), we have found that after transcriptional activation of the corresponding genes during conidiospore germination, transporter polypeptides show a rather uniform distribution along the plasma membrane of germlings and developing mycelia. A similar picture of uniform plasma membrane partitioning was also observed in other *Aspergillus* transporters studied using GFP (Forment et al. 2006, Apostolaki et al. 2009, Ramon and Scazzocchio, personal communication). This contrasts the case of several *S. cerevisiae* transporters that appear to form discrete cortical foci, corresponding to MCCs or MCPs (see *Introduction*). A representative picture of transporter cellular expression in *A. nidulans* is shown in the upper panel of Figure 1a.
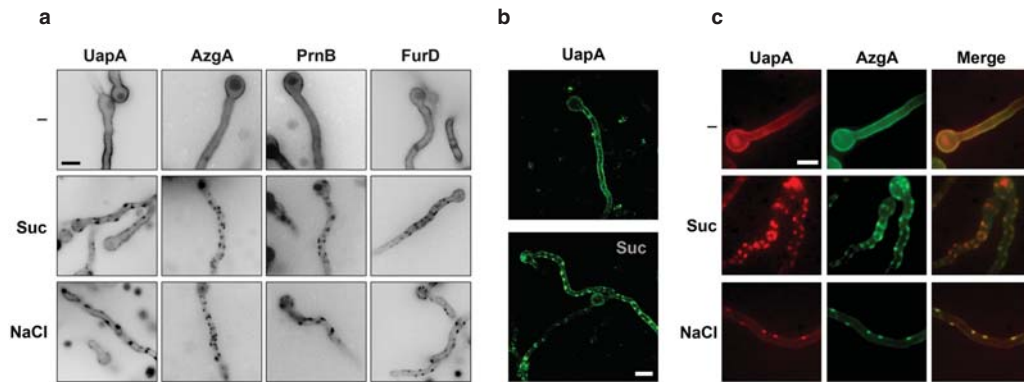
Figure 1. (a) Hypertonic media elicit a cortical patchy appearance of *A. nidulans* GFP-tagged transporters observed by epifluorescence microscopy. Upper panel: Control samples (–) were grown for 13 h in MM (urea 5 mM, glucose 1%) at 25°C, which permit the induction of transporters during conidiospore germination (Pantazopoulou and Diallinas 2007). Lower panels: Samples grown similarly as control samples, but then transferred to the same media containing 0.8 M Sucrose (Suc) or 0.5 M NaCl. Here and in several subsequent Figures, images were converted to 8-bit inverted grayscale. (b) Confocal laser scanning microscopy of UapA-GFP cellular expression in control media (–) or after 1 min exposure to 0.8 M Sucrose (Suc). (c) Epifluorescence microscopy of a strain expressing simultaneously UapA-mRFP and AzgA-GFP in control (–) or hypertonic (Suc, NaCl) media. Notice the overlap of red and green fluorescence (merge). Scale bars shown here and in subsequent figures correspond to 5 μm unless otherwise stated.

In this Figure, UapA is a carrier specific for uric acid-xanthine (Gorfinkiel et al. 1993) (NAT family), AzgA (Cecchetto et al. 2004) is a carrier specific for adenine-guanine-hypoxanthine (AzgA-like family), PrnB (Tazebay et al. 1997) is a proline permease (APC family) and FurD (Amillis et al. 2007) is a uracil permease (NCS1 family).

The cellular expression of the *A. nidulans* GFP-tagged transporters was also examined in samples treated for 1–5 min with NaCl or sucrose. Under these conditions, we observed the rapid appearance of cortical fluorescent patches, as those shown in the lower panels of Figure 1a and 1b. By using a strain simultaneously expressing two of these transporters,

UapA and AzgA, tagged with mRFP and GFP respectively, we showed that at least these permeases co-localize in the same patches (Figure 1c).

The kinetics of appearance of patches and most subsequent work were performed using a fully functional UapA-GFP transporter expressed from a strong controllable promoter (*alcA_p*) (Gournas et al. 2010). Patch appearance depended on the concentration of NaCl or sucrose (Figure 2a). The minimum concentrations of sucrose or NaCl eliciting the appearance of patches were determined to be >400 mM and > 200 mM, respectively, in agreement with the relative hypertonic strength of these two solutes. Patches formed by the two solutes looked identical
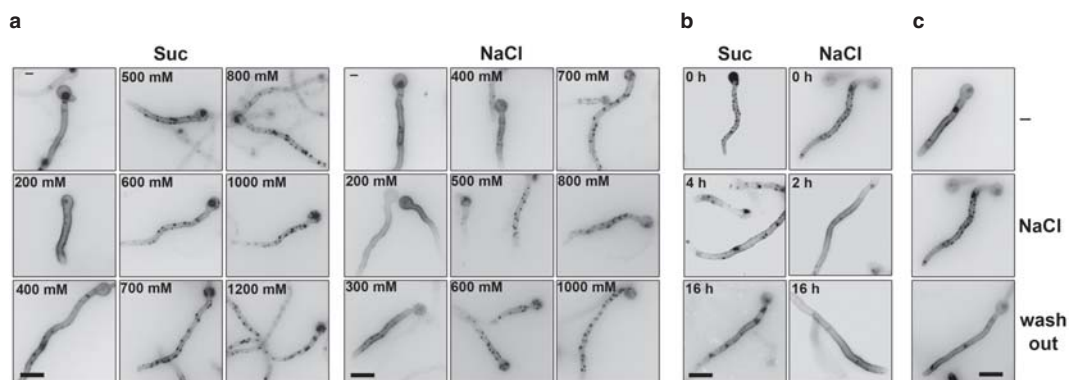

Figure 2. (a) Kinetics of appearance of cortical patches in a strain expressing UapA-GFP from the *alcA* promoter (*alcA_p*-UapA-GFP) in hypertonic media (1 min) in response to tonicity strength. Samples were grown for 14–15 h in mM (urea 5 mM, fructose 0.1%), at 25°C, which permits the induction of UapA-GFP from *alcA_p* (Gournas et al. 2010). (b) Disassembly of *alcA_p*-UapA-GFP fluorescent patches after prolonged growth (2, 4 or 16 h) in hypertonic media (Suc or NaCl). (c) Wash-out of *alcA_p*-UapA-GFP fluorescent patches (NaCl) after 10 min transfer to control (–) media. The figure shows epifluorescence microscopy images. Scale bars shown are 10 μM.

and their number and size depended on tonicity strength. The hypertonic effect imposed on mycelia was more evident at higher concentrations where hyphae became thinner, apparently due to water loss. The size of patches ranged from 0.5 through 2.3 μm. Patches were shown to appear transiently, as they disappeared in overnight cultures in hypertonic media (see Figure 2b). We estimated this recovery from the patchy appearance to take place after 4–8 h in sucrose (800 mM) or 2–4 h in NaCl (500 mM) (Figure 2b and not shown). Finally, patches disappeared rapidly (15 min) when sucrose or NaCl was washed-out (Figure 2c).

Several other hypertonic media (LiCl, KCl, Na_2PO_4, NH_4Cl, sorbitol or mannitol) led to patchy distribution of UapA, whereas other stress conditions such as the presence of most divalent ions or heavy metals, protein synthesis blockage (cycloheximide), proton gradient uncouplers or extreme pH, had no effect (Figure 3).

Patches correspond to plasma membrane invaginations rather than lipid raft-like microdomains specific for transporters

Some patches, especially those produced under stronger tonicity, although clearly plasma membrane-associated, seem to extend beyond the membrane towards the cytoplasm. This was more clearly seen in deconvoluted Z-stack images, which strongly supported that patches correspond to membrane invaginations (Figure 4). This observation is in full agreement with two reports in *S. cerevisiae* (Slaninová et al. 2000) and *Aspergillus repens* (Kelavkar et al. 1993) directly showing, using TEM, that hypertonic media lead to plasma membrane invaginations, that can be extended deeply in the cytoplasm (see also later).

We obtained independent evidence that fluorescent patches, initially observed using GFP-tagged transporters, are plasma membrane invaginations rather than specific transporter microdomains. This evidence is based on the following observations. Firstly, similar patches were observed using two other GFP-tagged plasma membrane associated polypeptides (Figure 5a). These are the pleckstrin homology (PH) domain of PLC-δ1, specifically recognizing the plasma membrane $PI(4,5)P_2$ lipids (Pantazopoulou and Penalva 2009) and the SsoA t-Snare, a protein that serves as a membrane-specific tag in the docking of transport vesicles to the plasma membrane (Taheri-Talesh et al. 2008). Secondly, similar patches were also observed in hypertonic conditions, using the lipophilic markers FM4-64 (Penalva 2005) or Filipin (Takeshita et al. 2008) (also Figure 5a). Importantly,
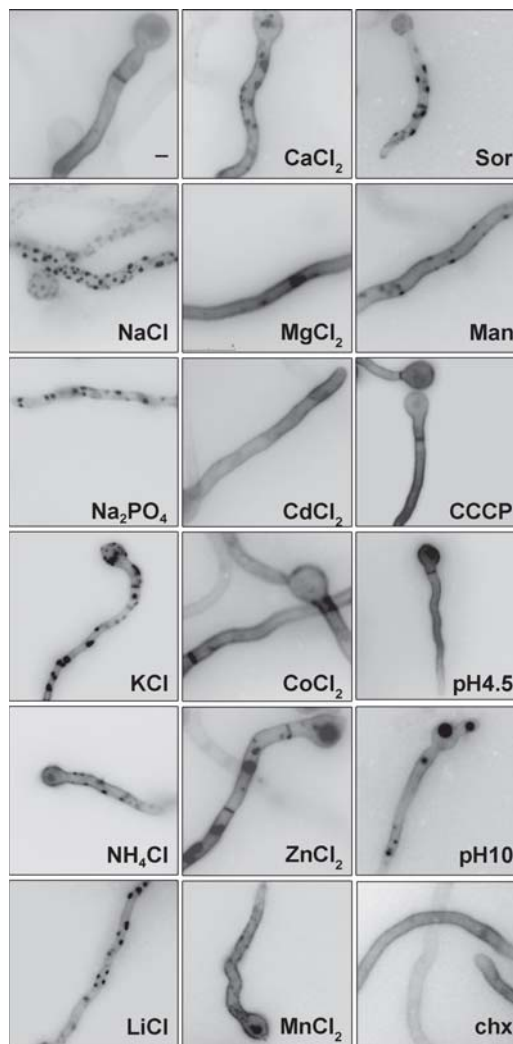

Figure 3. Examination by epifluorescence microscopy of UapA-specific fluorescent cortical patches after treatment with various salts (0.5 M), sugars (0.8 M), cycloheximide (chx, 20 μg/ml, 15 min prior to examination), different pH or the proton gradient uncoupler CCCP (30 μM, 15 min prior to examination). UapA-GFP is expressed from the the *alcA* promoter (*alcA_p*-UapA-GFP) as described in Figure 3. Sor and Man stand for Sorbitol and Mannitol, respectively. Notice that only monovalent ions and sugars (mostly Sor), which are known to produce hypertonic stress, lead to fluorescent patches.

FM4-64 patches co-localized with transporter (UapA) patches (see later in Figure 6f). Thirdly, as known plasma membrane microdomains have a distinct raft-like lipid composition, we tested the extractability of UapA by Triton X-100 from membranes. This biochemical approach is a standard assay used to detect partitioning of transporters in detergent resistant membranes (DRMs), which seems to be the biochemical equivalent of lipid-raft microdomains (Grossmann et al. 2007). Figure 5b shows that UapA extractability was identical in standard and hypertonic media. Fourthly,
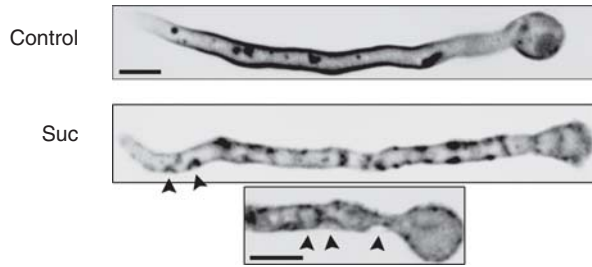
Control

Suc

Figure 4. Fluorescent, UapA-GFP specific (*alcA*$_p$-UapA-GFP), patches correspond to plasma membrane invaginations visible (highlighted with arrow heads) in deconvoluted images obtained with an inverted Leica microscope with motorized z-focus. Maximal intensity projections obtained from z-stacks using the Metamorph 3D are shown (see *Experimental* section). Two samples treated with sucrose (0.8 M) are shown compared with an untreated control.

direct transport measurements of radiolabeled ^{3}H-xanthine performed under hypertonic conditions (0.8 M sucrose or 0.5 NaCl) showed that UapA-GFP remains fully functional, showing a K_m value (8 μM) and transport capacity nearly identical to the one obtained in standard media (Figure 5c). Finally, using Calcofluor white staining, a marker of cell wall material such as chitin or b-1,3-glucan (see *Material and methods*), we showed that control samples exhibited a uniform blue fluorescence on their surfaces, whereas cells shifted to hyperosmotic medium (0.8 M sucrose) showed cortical fluorescent patches (Figure 5a, right panel). Several Calcofluor patches overlapped with UapA-GFP patches (highlighted with arrows). These results strongly suggest that invaginated areas of the plasma membrane are rapidly filled with cell wall material, either through *de novo* synthesis or reorganization of pre-existing peri-plasmic material. Similar observations were reported in yeast (Slaninová et al. 2000) and plants (Komis et al. 2002). The simplest explanation of all the above results is that fluorescent patches obtained with different markers represent plasma membrane invaginations, rather than specific microdomains with distinct lipid composition.
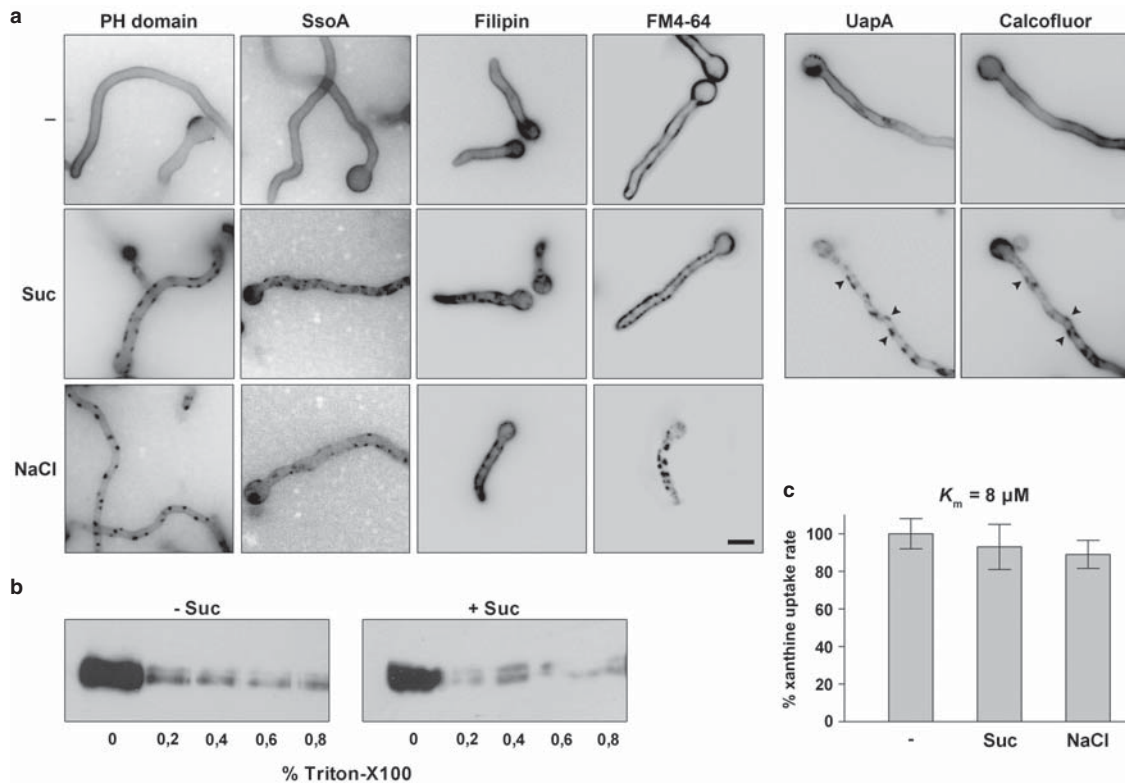

Figure 5. (a) Fluorescent patches detected with membrane-associated molecular markers other than transporters in hypertonic conditions. 'PH domain' is a GFP-tagged duplication of the PLC-δ1 PH domain which acts as an exclusive marker for the plasma membrane through its high affinity binding of PI(4,5)P$_2$ lipids. SsoA is a GFP-tagged t-Snare exocytic protein that attaches to the inner leaflet of the plasma membrane. Filipin and FM4-64 are fluorescent lipophilic markers labeling the plasma membrane under specific conditions (see *Experimental* section). Calcofluor white staining (see *Materials and methods*) showing overlap of UapA-GFP patches with deposition of cell wall material (highlighted with arrows). (b) Extractability of UapA-GFP by Triton X-100 from plasma membranes is identical in standard media and after exposure to hypertonic treatment (0.8 M sucrose, 10 min). (c) UapA-mediated (*alcA*$_p$-UapA-GFP) ^{3}H-xanthine transport capacity in standard media and after exposure to hypertonic treatment (0.8 M sucrose, 10 min). The K_m value of UapA-GFP (*alcA*$_p$-UapA-GFP) for xanthine, established in hypertonic media, is also shown (8 μM). For details of uptake studies, see *Experimental* section.

Hypertonic media elicit transient blockage of endocytosis and growth arrest

Sucrose has been reported to be a specific clathrin-dependent inhibitor of receptor and transporter endocytosis in mammalian cells (Heuser and Anderson 1989). We tested whether sucrose or other hypertonic media have an effect on endocytosis of UapA-GFP. We have recently showed the existence of two distinct, but converging endocytic pathways concerning the turnover of UapA in response to the presence of NH_4^+ ions or substrates (uric acid or xanthine). The process of endocytosis can be easily monitored by epifluorescence or confocal microscopy and Western blot analysis using an anti-GFP antibody.

We observed that the addition of sucrose (0.8 M) or NaCl (0.5 M) prior to ammonium or uric acid abolished the endocytosis and turnover of UapA-GFP (Figure 6a, 6b). As expected, we also observed that in the presence of sucrose or NaCl, UapA-GFP molecules appeared in plasma membrane patches described earlier. The block in transporter endocytosis and turnover was confirmed by Western blot analysis, which showed the absence of free GFP in samples grown for the last hour in the presence of ammonium ions (NH_4) or uric acid (UA) under
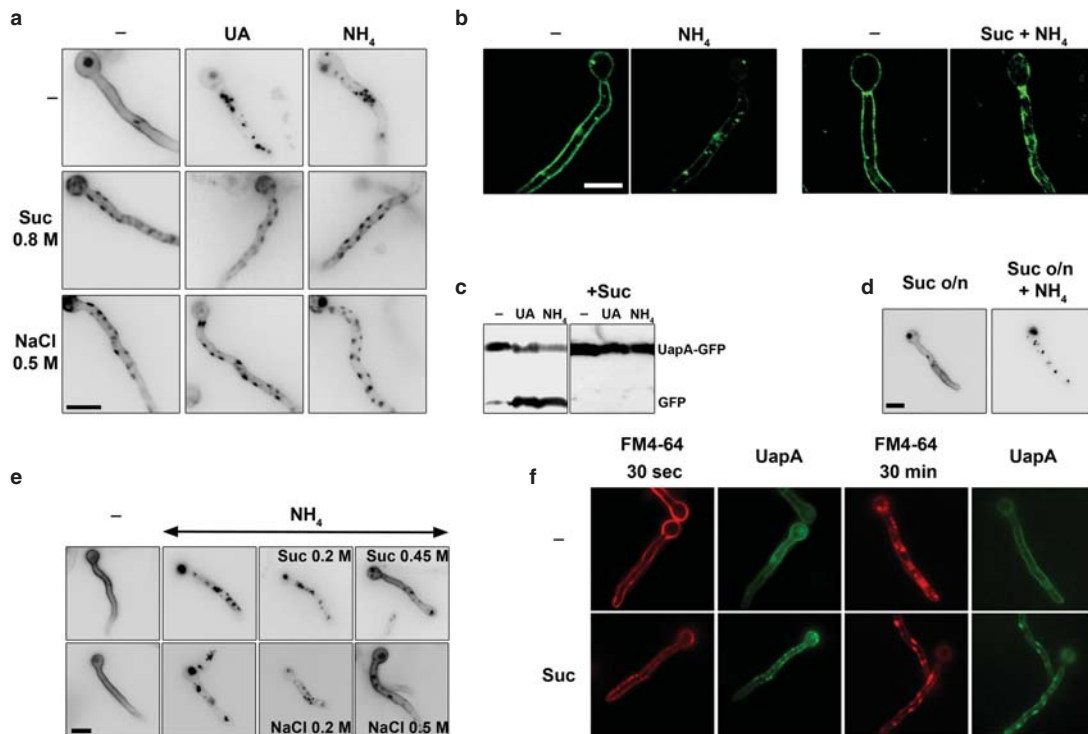

Figure 6. (a) Hypertonic media elicit a blockage of UapA-GFP endocytosis. In control samples UapA-GFP (*alcAp*-UapA-GFP) endocytosis is elicited upon transfer for 1h to standard media with either 1 mM uric acid (UA) or 20 mM ammonium ions (NH_4) (Gournas et al. 2010). Under these conditions, UapA-GFP is internalized and degraded in the vacuoles (appearing as prominent fluorescent granules in the cytoplasm) through sorting in the MBV pathway. Here and in all subsequent Figures, unless otherwise stated, hypertonic conditions are imposed by transfer to standard media with 0.8 M sucrose or 0.5 M NaCl. Notice that after hypertonic treatment there are UapA-GFP cortical fluorescent patches but no vacuoles visible in conditions that normally lead to UapA-GFP turnover. (b) UapA-GFP (*alcAp*-UapA-GFP) endocytosis by ammonium in a control sample and blockage of UapA-GFP endocytosis by ammonium after hypertonic treatment, as seen with inverted confocal laser microscopy in a single hypha. (c) Western blot analysis of membrane protein fractions corresponding to 2 h addition of UA or NH_4 and controls (–), probed with anti-GFP. The low mobility band corresponds to intact UapA-GFP (*alcAp*-UapA-GFP) and the high mobility band to free GFP produced through vacuolar degradation of UapA (see text). (d) Recovery of NH_4-elicited endocytosis of UapA-GFP (*alcAp*-UapA-GFP) after prolonged growth (16 h) in hypertonic media. (e) Minimal concentrations of sucrose or NaCl blocking endocytosis. (f) Effect of hypertonic treatment on FM4-64 internalization. The strain used is *alcAp*-UapA-GFP. Control and hypertonic samples were treated as previously. Upon 15 min of staining on ice and 30 sec transfer to 25°C, FM4-64 labels only the plasma membrane, which appears uniform in control media but patchy after sucrose treatment. A practically identical labeling was obtained with UapA-GFP (left panels). After 30 min of incubation at 25° in untreated samples, FM4-64 still labeled the plasma membrane but was mostly localized in endosomal compartments. In sharp contrast, in sucrose treated samples, FM4-64 still labeled cortical patches associated with plasma membrane and no sign of internalization was evident. The cortical fluorescent patches labeled with FM4-64 are identical with those labeled with UapA-GFP (right panels).

hypertonic treatment (Figure 6c). The appearance of free GFP is a well-established marker of endocytosis and vacuolar turnover of UapA-GFP and other GFP-tagged transporters (Gournas et al. 2010). The blockage in UapA-GFP endocytosis is transient, as its internalization recovers with kinetics practically identical to those of patch disassembly after longer exposures to hypertonic media (Figure 6d). In addition, the minimal concentration of hypertonic solutes blocking UapA-GFP endocytosis was practically identical to that leading to plasmolysis (~0.45 sucrose, ≥0.2 M NaCl) (Figure 6e).

Interestingly, Figure 6f shows that sucrose also blocked the constitutive internalization of the lipophilic marker FM4-64, strongly suggesting that tonicity has a global negative effect on both clathrin-mediated and fluid-phase endocytosis (discussed later).

In the course of the experiments described above, we noticed a significant delay in growth rate in samples exposed to hypertonicity. Figure 7a shows that this delay is maximal in media containing a non-catabolic carbon source such as fructose (0.1%) (40% reduction in colony radius), while it is more moderate in carbon catabolite repressing (1% glucose) media (20% reduction). Figure 7b shows a quantification of this growth arrest expressed as reduction in average hyphal length after hypertonic treatment (20–40% reduction in germ tube length). The delay in growth recovered after longer exposures to hypertonic media, as did the appearance of fluorescent patches and the block in endocytosis (not shown).

Hypertonicity affects actin dynamics and thus blocks endocytosis

A block in endocytosis can occur at several steps concerning the formation and internalization of the endocytic vesicle. To address this question we examined how basic elements of this process are affected by tonicity. In particular, we examined the cellular organization of well-characterized upstream (SlaB) and downstream (AbpA) endocytic factors, as well as that of tropomyosin (TpmA), tagged with either GFP or mRFP, under standard or hypertonic growth conditions. SlaB (Araujo-Bazán et al. 2008) is a Sla2p *S. cerevisiae* orthologue (Wesp et al. 1997), which acts as a well-characterized endocytosis regulator involved in the formation of early actin patch components (Newpher et al. 2005). In particular, Sla2p regulates the association of the clathrin endocytic machinery with actin polymerization (Newpher and Lemmon 2006). AbpA (Araujo-Bazán et al. 2008) is true homologue of Abp1p in *S. cerevisiae*, which is a late endocytic vesicle formation component. It appears near the end of Sla2p lifetime, is localized exclusively at cortical endocytic actin filaments/patches (Huckaba et al. 2004, Quintero-Monzon et al. 2005) and does not associate with actin cables (Huckaba et al. 2004). In *A. nidulans*, AbpA and SlaB are strongly polarized in hyphae, forming a ring that embraces the hyphal tip, leaving an area of exclusion at the apex (Araujo-Bazán et al. 2008). AbpA localizes at highly motile and transient peripheral foci overlapping with actin patches, which predominate in the tip (Taheri-Talesh et al. 2008). SlaB also localizes at peripheral foci, but these are markedly more abundant and cortical than those of AbpA (Araujo-Bazán et al. 2008). Based on SlaB and AbpA cellular dynamics, it has been proposed that spatial association of exocytosis with endocytosis at the fungal tip underlies hyphal growth. Interestingly and unlike the case in *S. cerevisiae*, SlaB is an essential gene revealing a major role of endocytosis in filamentous fungal growth. Tropomyosin (TpmA) is a major actin-binding protein that regulates actin mechanics (Stewart 2001). A GFP-TpmA fusion has been used to image actin cables, which was not feasible with
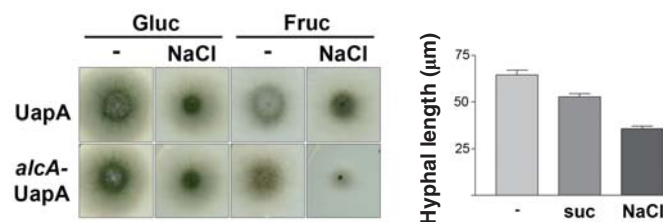

Figure 7. Hypertonic media elicit growth arrest of *A. nidulans*. (a) Growth tests of two isogenic strains expressing UapA-GFP from either its native promoter (used for Figure 1) or from the *alcA* promoter (used for all other Figures). 0.5 NaCl was used for hypertonic treatment and tests were carried out in MM with fructose (0.1%) or glucose (1%), as carbon sources. NaCl led to a reduction of both the diameter of colonies and conidiospore production. The reduction of growth was stronger in fructose media. (b) Reduction of hyphal length upon addition of either 0.8 M sucrose or 0.5 M NaCl for 4 h in the strain expressing *alcA_p*-UapA-GFP grown in fructose media.

GFP-actin fusions, in *A. nidulans* (Pearson et al. 2004, Taheri-Talesh et al. 2008). GFP-TpmA is concentrated near the apex and at forming septa (Pearson et al. 2004, Taheri-Talesh et al. 2008), labels actin cables along the hyphae, but does not seem to co-localize with endocytic actin patches.

Figure 8a (upper panels) shows that, as expected, SlaB and AbpA form cortical foci which are mostly concentrated at the tip of hyphae, whereas TpmA has a rather diffuse localization in the cytosol, but also clearly labels actin cables along the hyphal axis and the tip region. The lower panels in Figure 8a show that neither sucrose nor NaCl affected the cortical and polar appearance of SlaB-GFP or AbpA-mRFP foci, whereas hypertonic media dramatically modified the

cellular localization of GFP-TpmA. More specifically, fluorescence is not any longer associated with actin cables and the tips of hyphae, but is now apparent as diffuse cytosolic fluorescence and in scattered cortical foci along the axis of hyphae. This picture constitutes strong evidence that hypertonic media modify actin dynamics, rather than the formation of cortical endocytic complexes *per se*, probably through immediate actin depolymerization followed by rapid localized re-polymerization. A similar conclusion has been proposed for the effect of tonicity in plants (Komis et al. 2002).

We also tested how actin depolymerization triggered by Latrunculin B (Lat-B) (Taheri-Talesh et al. 2008) affects plasmolysis and transporter
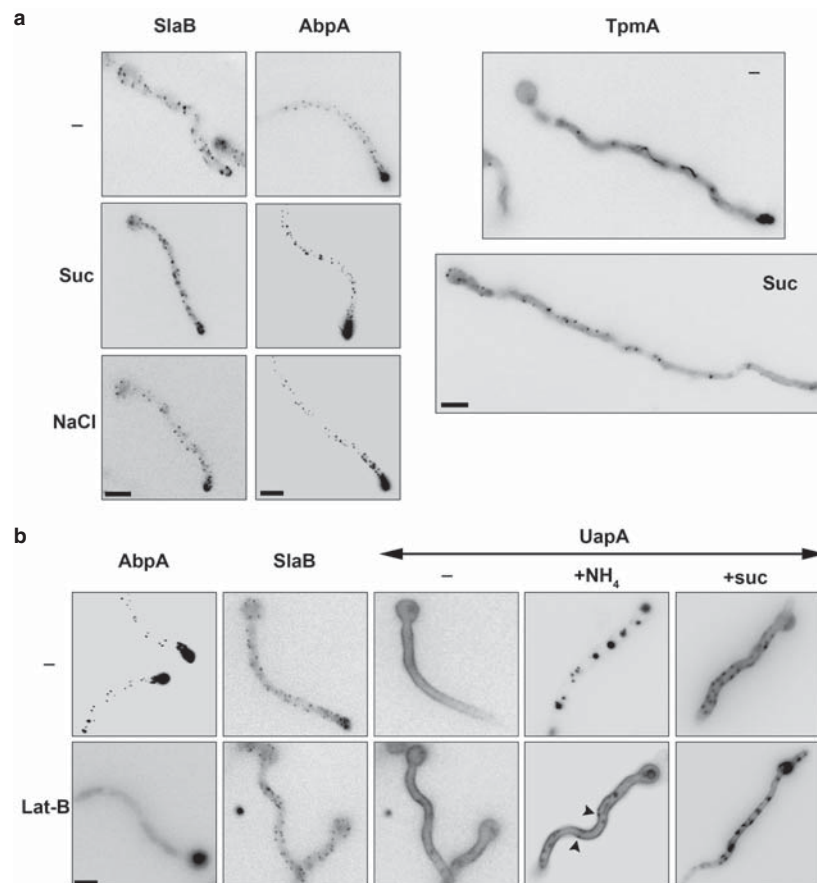

Figure 8. Hypertonicity and Lat-B effects on actin dynamics and the endocytic machinery. (a) Cellular localization of SlaB, AbpA and of TpmA, tagged with either GFP or mRFP, under standard or hypertonic growth conditions. Samples were treated as previously described. SlaB-GFP and AbpA-mRFP form cortical foci which predominate at the tip of hyphae under all conditions. GFP-TpmA in standard conditions (–) labels diffusely the cytocol and more strongly actin-like cables along the hyphal length and the tip. In hypertonic conditions (Suc) labeling of the actin cables and the tip disappears and scattered cortical patches appear along the hyphal length. (b) Effect of Lat-B (50 μM) on the cellular localization of UapA (-GFP or -mRFP tagged) in standard (–), endocytic (NH$_4$) or hypertonic (Suc) conditions. The effect of Lat-B on AbpA-GFP and SlaB-GFP was also examined as a control. Lat-B leads to the disassembly of all AbpA patches as expected (Araujo-Bazán et al. 2008), but has a minor effect on SlaB, as only the patches at the tip seem to disassemble. Lat-B has no effect on either the normal uniform localization of UapA in the plasma membrane in standard media (–) or on the appearance of UapA-specific fluorescent patches (plasmolysis) in hypertonic media (Lat-B + Suc and Lat-B + NaCl). In contrast, Lat-B blocked the internalization of UapA by NH$_4$. Note that in the latter case, UapA cortical foci are also visible (highlighted with arrows).

endocytosis. As a control of Lat-B action, we followed its effect on AbpA, but also on SlaB. Figure 8b shows that Lat-B led to complete disassembly of AbpA patches, as expected (Pantazopoulou and Penalva 2009), but had a moderate apparent effect on SlaB patches, more evident at the tip. This might be due to the fact that, unlike AbpA, SlaB regulates F-actin polymerization but contains a $PI(4,5)P_2$ binding domain that contributes to its plasma membrane localization. Lat-B had no effect on either the localization of UapA-GFP in the plasma membrane, or on the appearance of UapA-GFP cortical patches (plasmolysis), but blocked UapA-GFP endocytosis by ammonium (Figure 8b). Therefore, both hypertonicity and Lat-B blocked endocytosis, suggesting that hypertonicity, similarly to Lat-B, might act through an effect on actin dynamics.

Hypertonic conditions elicit similar phenomena in *S. cerevisiae* as in *A. nidulans*

We tried the effect of similar conditions and studied the response of *S. cerevisiae* to hypertonicity. In these studies, we used a strain expressing a functional GFP-tagged version of the lactate (Jen1p) permease, a transporter that in standard media labels uniformly the plasma membrane. Jen1p is endocytosed and degraded through the MVB pathway in response to the presence of a preferred carbon source such as glucose.

Figure 9 shows that both sucrose and NaCl lead to the appearance of prominent Jen1p-specific fluorescent patches. These patches are clearly distinguishable from the Fur4p-specific MCC foci observed in the standard media (see Introduction), the former being larger and extended towards the cytoplasm as expected for plasma membrane invaginations. In addition, Figure 9 also shows that under hypertonic conditions, the endocytosis of Jen1p by glucose is totally blocked. As in *A. nidulans*, patch appearance and blockage of endocytosis show similar kinetics and both phenomena recover after 10–14 h in hypertonic media (not shown). Finally, similarly to *A. nidulans*, hypertonic media elicited a growth arrest, which has also been observed by others (Slaninová et al. 2000, Hohmann et al. 2007). A notable difference between the response of the two fungi to hypertonicity was that *S. cerevisiae* proved more resistant than *A. nidulans* to tonicity, that is, two-fold higher concentrations of sucrose (1.6 M) or NaCl (1 M) were needed to elicit plasmolysis, blockage of endocytosis and growth arrest. Similar results were also obtained with a second *S. cerevisiae* transporter (Fur4p) (results not shown).
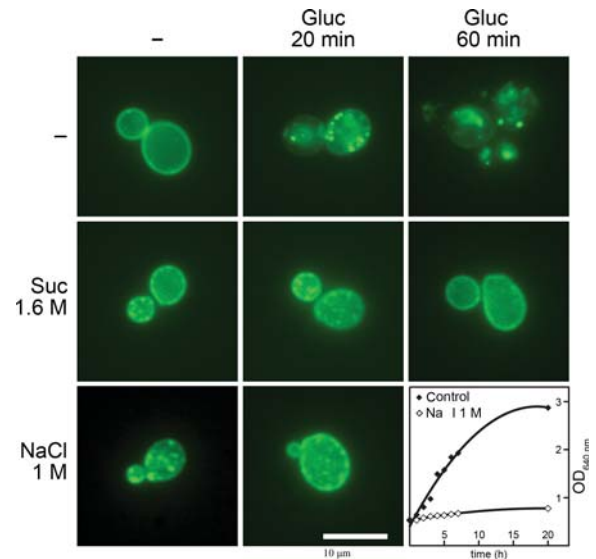

Figure 9. Hypertonic conditions elicit similar phenomena in *S. cerevisiae* as in *A. nidulans*. Epifluorescence microscopy images of a *S. cerevisiae* strain expressing a functional Jen1p-GFP chimeric transporter are shown. Jen1p-GFP is expressed uniformly in the plasma membrane under standard conditions of induction (–) but is rapidly internalized (20 min) and eventually degraded in the vacuole (60 min) upon addition of 1% glucose (Paiva et al. 2009). Hypertonic treatment (1.6 M sucrose or 1 M NaCl) for 1 min leads to the appearance of mostly cortical fluorescent patches and shows no evidence of internalization or degradation of Jen1p-GFP by glucose. The last panel shows the growth arrest elicited by addition of 1 M NaCl in the Jen1p-GFP strain at an $OD_{640\,nm}$ of 0.5. For more technical details, see the *Experimental* section.

Discussion

Using several transporters and other membrane-associated markers tagged with GFP or mRFP, but also fluorescent lipophilic probes, we directly showed that various moderate (within the osmoregulatory range) hypertonic media lead to rapid localized plasmolysis, growth arrest and blockage of endocytosis in *A. nidulans* and *S. cerevisiae*. These phenomena are reversed within minutes when the hypertonic media are washed-out. If the hypertonic media persist, deplasmolysis and recovery of endocytosis initiate after 2–8 h, depending on tonicity strength, although full reversal might take up to 14 h. Recovery to normal growth rate is slower, but this depends on the fungus and the agent used to elicit hypertonicity (not shown).

The effects of hypertonic treatment on fungi have been extensively studied before. Yeast cells respond to increased tonicity by water loss, cell shrinkage, cessation of growth associated with diminished translational capacity, rapid closure of the glycerol export channel Fps1, remodeling of the actin cytoskeleton

and a loss of cell polarity (for review, see Hohmann et al. 2007). The phenomena are transient and recover through gradual accumulation of solutes, mostly glycerol, as a consequence of the activation of genes of the so-called high-osmolarity glycerol (HOG) pathway. Similar responses have been observed in filamentous fungi, mostly *Neurosporra crassa* (Lew and Nasserifar 2009), but also in plants (Komis et al. 2002). A recent publication has shown that under extreme and persisting osmotic conditions (out of the osmoregulatory range) the plasma membrane of *S. cerevisiae* is functionally and structurally reorganized irreversibly, which in turn leads to cell death (Dupont et al. 2010). This work and two other publications in fungi (Kelavkar et al. 1993, Slaninová et al. 2000) have shown that responses to different degrees of hypertonic treatment include the rapid formation of deep plasma membrane invaginations or localized plasmolysis.

Our work strongly supports, by *in vivo* direct approaches, the previous findings concerning two major responses of fungi to moderate hypertonic media: first, the partial or localized plasmolysis and shrinkage of cells due to water loss, and second, growth arrest. It further investigates the specificity and kinetics of these effects, showing that plasmolysis is practically immediate (<1 min), tonicity-dependent rather than solute-dependent, never complete, reversible and transient, whereas growth arrest is also transient, but slower to recover than plasmolysis. Furthermore, we show for the first time, that the invaginated part of the membrane does not seem to have a distinct lipid composition, and that transporters embedded in it are fully functional. The first conclusion arises from *in vivo* microscopic evidence using specific lipophilic markers (Filipin, FM4-64 and the PI(4,5)P$_2$-binding marker (a duplication of the PH domain of PLC-δ1) and biochemical evidence showing that transporter membrane-extractability is not affected by hypertonic treatment. The second conclusion came from direct transport kinetics measurements using radiolabelled substrates. Furthermore, transporter-mediated uptake assays showed that there is no diffusion of radiolabelled substrates within the cells, a strong indication that the *A. nidulans* plasma membrane and lipid composition remain intact under the hypertonic treatment used. Thus, although the originally observed patches using GFP-tagged transporters resembled specific plasma membrane microdomains, such as the yeast MCC or MCP compartments, which all host transporters, they proved not to be so. The simplest explanation of the apparent fluorescence accumulation detected by using FM4-64, filipin, SsoA or the PH domain markers is an increase in plasma membrane surface due to infoldings.

We also directly showed that hypertonicity totally but transiently blocks the endocytosis of transporters. Several lines of evidence strongly support that this is due to a rapid effect of hypertonicity on actin dynamics, rather than due to the direct abolishment of clustering of cargoes in coated pits or the initial formation of membrane-associated endocytic complexes. Firstly, hypertonicity altered dramatically and rapidly the cellular localization of tropomyosin (GFP-TpmA), but not that of the endocytic cortical markers SlaB and AbpA, which act upstream from the pinching-off of endocytic vesicles. Using the GFP-TpmA marker, we detect the rapid disassembly of actin cables, which constitute the major machinery for the internalization of endocytic vesicles. Secondly, hypertonicity blocked the endocytosis of FM4-64, a marker of bulk fluid-phase endocytosis which, to our knowledge, operates by an actin-dependent but also a coated pit-independent mechanism (Vida and Emr 1995). In line with this observation, Dupont et al. (2010) have shown a similar block of FM4-64 endocytosis in yeast cells exposed to moderate hypertonic media. Thirdly, the abolishment of ammonium-elicited UapA-GFP endocytosis by Lat-B is also in line with an effect on actin dynamics. Despite the fact that this drug has a global effect on actin filament polymerization and thus the endocytic machinery, we noticed that in Lat-B treated cells exposed to ammonium ions, UapA-GFP, in addition to a uniform labeling of the plasma membrane, also appears in cortical foci. This observation suggests that UapA-GFP might well be clustered in upstream endocytic complexes/pre-vesicles, but these cannot be internalized. Thus, the simplest interpretation of our results is that hypertonicity elicits the modification of actin mechanics, rather than interfering with cargo clustering in cortical endocytic complexes. The observation that upon hypertonic treatment cables disappear and the actin patches redistribute over the cortex of hyphae has also been observed in *S. cerevisiae* (Slaninová et al. 2000) and plants (Komis et al. 2002). Evidently, the blockage of Jen1p endocytosis by hypertonic treatment in yeast, shown in Figure 9, should also take place through modification of actin dynamics.

Previous reports in vertebrate cells have shown that hypertonic media inhibit receptor-mediated endocytosis (Daukas et al. 1983, Larkin et al. 1986, Heuser and Anderson 1989). In polymorphonuclear leukocytes, hypertonic media inhibited receptor-mediated uptake of the chemotactic peptide N-formylnorleucylleucylphenylalanine. Furthermore, it was shown that hypertonic medium prevented the clustering of surface molecules as indicated by the inhibition of capping of fluorescent concanavalin A

(Daukas et al. 1983). In human and chicken fibro-blasts, TEM analysis has shown that hypertonic cells display empty clathrin 'microcages' rather than normal coated pit lattices, with concomitant loss of normally clustered low density lipoprotein (LDL) receptors observed in untreated cells. Upon return to normal medium, these changes reverse. The authors propose that hypertonic treatment causes coated pits to disintegrate, while clathrin becomes unavailable and endocytosis is blocked (Heuser and Anderson 1989). Clathrin is important for normal actin dynamics and progression of SlaB/Sla2p-containing patches during endocytosis in yeast (Newpher and Lemmon 2006). Thus, we cannot formally exclude that hypertonic media also have a negative effect on clathrin function in fungi. However, unlike vertebrate cells where fluid-phase endocytosis and endosome turnover, detected by FM4-64, is not blocked by hypertonicity, in *A. nidulans* FM4-64 internalization is totally blocked by both sucrose and NaCl, a result incompatible with a sole effect on clathrin. Of course, our results might also reflect differences in the molecular mechanisms employed by fungal (or plant) cells, compared to animal cells, to respond to hypertonicity.

Last but not least, this work establishes that moderate hypertonic treatment (within the osmo-regulatory range) constitutes a transient and reversible physiological inhibitor of fungal endocytosis. A similar block in endocytosis seems to occur in vertebrates and we predict that a similar situation might take place in plants. This is of primary importance for research in systems, such as *A. nidulans* and other filamentous fungi or even more complex cells, where genetic blocks in endocytosis and in cargo trafficking are usually lethal. Blocking endocytosis by sucrose or NaCl will permit us to ask novel questions on transporter trafficking, recycling and turnover through alternative pathways. We are currently using this approach for studying the direct sorting of transporters from the Golgi to the vacuole and how this is affected by lipid composition.

Acknowledgements

References

Abenza JF, Galindo A, Pantazopoulou A, Gil C, De Los Ríos V, Peñalva MA. 2010. *Aspergillus* RabBRab5 integrates acquisition of degradative identity with the long distance movement of early endosomes. Mol Biol Cell 21:2756–2769. PMID: 20534811.

Amillis S, Cecchetto G, Sophianopoulou V, Koukaki M, Scazzocchio C, Diallinas G. 2004. Transcription of purine transporter genes is activated during the isotropic growth phase of *Aspergillus nidulans* conidia. Mol Microbiol 52:205–216.

Amillis S, Hamari Z, Roumelioti K, Scazzocchio C, Diallinas G. 2007. Regulation of expression and kinetic modeling of substrate interactions of a uracil transporter in *Aspergillus nidulans*. Mol Membr Biol 24:206–214.

André B, Haguenauer-Tsapis R. 2004. Membrane trafficking of yeast transporters: Mechanisms and physiological control of downregulation. Top Curr Genet 273–323.

Apostolaki A, Erpapazoglou Z, Harispe L, Billini M, Kafasla P, Kizis D, Penalva MA, Scazzocchio C, Sophianopoulou V. 2009. AgtA, the dicarboxylic amino acid transporter of *Aspergillus nidulans*, is concertedly down-regulated by exquisite sensitivity to nitrogen metabolite repression and ammonium-elicited endocytosis. Eukaryot Cell 8:339–352.

Araujo-Bazán L, Penalva MA, Espeso EA. 2008. Preferential localization of the endocytic internalization machinery to hyphal tips underlies polarization of the actin cytoskeleton in *Aspergillus nidulans*. Mol Microbiol 67:891–905.

Belgareh-Touze N, Leon S, Erpapazoglou Z, Stawiecka-Mirota M, Urban-Grimal D, Haguenauer-Tsapis R. 2008. Versatile role of the yeast ubiquitin ligase Rsp5p in intracellular trafficking. Biochem Soc Trans 36:791–796.

Blondel MO, Morvan J, Dupré S, Urban-Grimal D, Haguenauer-Tsapis R, Volland C. 2004. Direct sorting of the yeast uracil permease to the endosomal system is controlled by uracil binding and Rsp5p-dependent ubiquitylation. Mol Biol Cell 15:883–895.

Cecchetto G, Amillis S, Diallinas G, Scazzocchio C, Drevet C. 2004. The AzgA purine transporter of *Aspergillus nidulans*. Characterization of a protein belonging to a new phylogenetic cluster. J Biol Chem 279:3132–3141.

Daukas G, Lauffenburger DA, Zigmond S. 1983. Reversible pinocytosis in polymorphonuclear leukocytes. J Cell Biol 96:1642–1650.

Diallinas G. 2008. Biochemistry. An almost-complete movie. Science 322:1644–1645.

Dupont S, Beney L, Ritt JF, Lherminier J, Gervais P. 2010. Lateral reorganization of plasma membrane is involved in the yeast resistance to severe dehydration. Biochim Biophys Acta 1798:975–985.

Dupré S, Haguenauer-Tsapis R. 2003. Raft partitioning of the yeast uracil permease during trafficking along the endocytic pathway. Traffic 4:83–96.

Dupré S, Urban-Grimal D, Haguenauer-Tsapis R. 2004. Ubiquitin and endocytic internalization in yeast and animal cells. Biochim Biophys Acta 1695:89–111.

Erpapazoglou Z, Froissard M, Nondier I, Lesuisse E, Haguenauer-Tsapis R, Belgareh-Touze N. 2008. Substrate- and ubiquitin-dependent trafficking of the yeast siderophore transporter Sit1. Traffic 9:1372–1391.

Forment JV, Flipphi M, Ramon D, Ventura L, Maccabe AP. 2006. Identification of the mstE gene encoding a glucose-inducible, low affinity glucose transporter in *Aspergillus nidulans*. J Biol Chem 281:8339–8346.

Gorfinkiel L, Diallinas G, Scazzocchio C. 1993. Sequence and regulation of the uapA gene encoding a uric acid-xanthine permease in the fungus *Aspergillus nidulans*. J Biol Chem 268:23376–2381.

Gournas C, Amillis S, Vlanti A, Diallinas G. 2010. Transport-dependent endocytosis and turnover of a uric acid-xanthine permease. Mol Microbiol 75:246–260.

Grossmann G, Opekarova M, Malinsky J, Weig-Meckl I, Tanner W. 2007. Membrane potential governs lateral segregation of plasma membrane proteins and lipids in yeast. EMBO J 26:1–8.

Grossmann G, Malinsky J, Stahlschmidt W, Loibl M, Weig-Meckl I, Frommer WB, Opekarová M, Tanner W. 2008. Plasma membrane microdomains regulate turnover of transport proteins in yeast. J Cell Biol 183:1075–1088.

Grossmann G, Opekarova M, Novakova L, Stolz J, Tanner W. 2006. Lipid raft-based membrane compartmentation of a plant transport protein expressed in *Saccharomyces cerevisiae*. Eukaryot Cell 5:945–953.

Helliwell SB, Losko S, Kaiser CA. 2001. Components of a ubiquitin ligase complex specify polyubiquitination and intracellular trafficking of the general amino acid permease. J Cell Biol 153:649–662.

Heuser JE, Anderson RG. 1989. Hypertonic media inhibit receptor-mediated endocytosis by blocking clathrin-coated pit formation. J Cell Biol 108:389–400.

Hohmann S, Krantz M, Nordlander B. 2007. Yeast osmoregulation. Methods Enzymol 428:29–45.

Huckaba TM, Gay AC, Pantalena LF, Yang HC, Pon LA. 2004. Live cell imaging of the assembly, disassembly, and actin cable-dependent movement of endosomes and actin patches in the budding yeast, *Saccharomyces cerevisiae*. J Cell Biol 167:519–530.

Kelavkar U, Rao KS, Ghhatpar HS. 1993. Sodium chloride stress induced morphological and ultrastructural changes in *Aspergillus repens*. Indian J Exp Biol 31:511–515.

Komis G, Apostolakos P, Galatis B. 2002. Hyperosmotic stress-induced actin filament reorganization in leaf cells of *Chlorophyton comosum*. J Exp Bot 53:1699–1710.

Koukaki M, Vlanti A, Goudela S, Pantazopoulou A, Gioule H, Tournaviti S, Diallinas G. 2005. The nucleobase-ascorbate transporter (NAT) signature motif in UapA defines the function of the purine translocation pathway. J Mol Biol 350:499–513.

Larkin JM, Donzell WC, Anderson RG. 1986. Potassium-dependent assembly of coated pits: New coated pits form as planar clathrin lattices. J Cell Biol 103:2619–2627.

Leung J, Karachaliou M, Alves C, Diallinas G, Byrne B. 2010. Expression and purification of a functional uric acid-xanthine transporter (UapA). Protein Expr Purif 72:139–146.

Lew RR, Nasserifar S. 2009. Transient responses during hyper-osmotic shock in the filamentous fungus *Neurospora crassa*. Microbiology 155:903–911.

Malinska K, Malinsky J, Opekarova M, Tanner W. 2003. Visualization of protein compartmentation within the plasma membrane of living yeast cells. Mol Biol Cell 14:4427–4436.

Malinska K, Malinsky J, Opekarova M, Tanner W. 2004. Distribution of Can1p into stable domains reflects lateral protein segregation within the plasma membrane of living *S. cerevisiae* cells. J Cell Sci 117:6031–6041.

Newpher TM, Lemmon SK. 2006. Clathrin is important for normal actin dynamics and progression of Sla2p-containing patches during endocytosis in yeast. Traffic 7:574–588.

Newpher TM, Smith RP, Lemmon V, Lemmon SK. 2005. In vivo dynamics of clathrin and its adaptor-dependent recruitment to the actin-based endocytic machinery in yeast. Dev Cell 9:87–98.

Paiva S, Vieira N, Nondier I, Haguenauer-Tsapis R, Casal M, Urban-Grimal D. 2009. Glucose-induced ubiquitylation and endocytosis of the yeast Jen1 transporter: Role of lysine 63-linked ubiquitin chains. J Biol Chem 284:19228–19236.

Pantazopoulou A, Diallinas G. 2007. Fungal nucleobase transporters. FEMS Microbiol Rev 31:657–675.

Pantazopoulou A, Lemuh ND, Hatzinikolaou DG, Drevet C, Cecchetto G, Scazzocchio C, Diallinas G. 2007. Differential physiological and developmental expression of the UapA and AzgA purine transporters in *Aspergillus nidulans*. Fungal Genet Biol 44:627–640.

Pantazopoulou A. Penalva MA. 2009. Organization and dynamics of the *Aspergillus nidulans* Golgi during apical extension and mitosis. Mol Biol Cell 20:4335–4347.

Papageorgiou I, Gournas C, Vlanti A, Amillis S, Pantazopoulou A, Diallinas G. 2008. Specific interdomain synergy in the UapA transporter determines its unique specificity for uric acid among NAT carriers. J Mol Biol 382:1121–1135.

Pearson CL, Xu K, Sharpless KE, Harris SD. 2004. MesA, a novel fungal protein required for the stabilization of polarity axes in *Aspergillus nidulans*. Mol Biol Cell 15:3658–3672.

Penalva MA. 2005. Tracing the endocytic pathway of *Aspergillus nidulans* with FM4-64. Fungal Genet Biol 42:963–975.

Quintero-Monzon O, Rodal AA, Strokopytov B, Almo SC, Goode BL. 2005. Structural and functional dissection of the Abp1 ADFH actin-binding domain reveals versatile in vivo adapter functions. Mol Biol Cell 16:3128–3139.

Reggiori F, Pelham HR. 2002. A transmembrane ubiquitin ligase required to sort membrane proteins into multivesicular bodies. Nat Cell Biol 4:117–123.

Rodríguez-Galán O, Galindo A, Hervás-Aguilar A, Arst HN Jr, Peñalva MA. 2009. Physiological involvement in pH signaling of

RIGHTSLINK

Vps24-mediated recruitment of Aspergillus PalB cysteine protease to ESCRT-III. J Biol Chem 284:4404–4412.

Slaninová I, Sestak S, Svoboda A, Farkas V. 2000. Cell wall and cytoskeleton reorganization as the response to hyperosmotic shock in *Saccharomyces cerevisiae*. Arch Microbiol 173:245–252.

Soetens O, De Craene JO, Andre B. 2001. Ubiquitin is required for sorting to the vacuole of the yeast general amino acid permease, Gap1. J Biol Chem 276:43949–43957.

Stewart M. 2001. Structural basis for bending tropomyosin around actin in muscle thin filaments. Proc Natl Acad Sci USA 98:8165–8166.

Strádalová V, Stahlschmidt W, Grossmann G, Blazikova M, Rachel R, Tanner W, Malinsky J. 2009. Furrow-like invaginations of the yeast plasma membrane correspond to membrane compartment of Can1. J Cell Sci 122:2887–2894.

Taheri-Talesh N, Horio T, Araujo-Bazán L, Dou X, Espeso EA, Penalva MA, Osmani SA, Oakley BR. 2008. The tip growth apparatus of *Aspergillus nidulans*. Mol Biol Cell 19:1439–1449.

Takeshita N, Higashitsuji Y, Konzack S, Fischer R. 2008. Apical sterol-rich membranes are essential for localizing cell end markers that determine growth directionality in the filamentous fungus *Aspergillus nidulans*. Mol Biol Cell 19:339–351.

Tavoularis S, Scazzocchio C, Sophianopoulou V. 2001. Functional expression and cellular localization of a green fluorescent protein-tagged proline transporter in *Aspergillus nidulans*. Fungal Genet Biol 33:115–125.

Tazebay UH, Sophianopoulou V, Scazzocchio C, Diallinas G. 1997. The gene encoding the major proline transporter of *Aspergillus nidulans* is upregulated during conidiospore germination and in response to proline induction and amino acid starvation. Mol Microbiol 24:105–117.

Umebayashi K, Nakano A. 2003. Ergosterol is required for targeting of tryptophan permease to the yeast plasma membrane. J Cell Biol 161:1117–1131.

Valdez-Taubas J, Harispe L, Scazzocchio C, Gorfinkiel L, Rosa AL. 2004. Ammonium-induced internalisation of UapC, the general purine permease from *Aspergillus nidulans*. Fungal Genet Biol 41:42–51.

Vida TA, Emr SD. 1995. A new vital stain for visualizing vacuolar membrane dynamics and endocytosis in yeast. J Cell Biol 128:779–792.

Vlanti A, Diallinas G. 2008. The *Aspergillus nidulans* FcyB cytosine-purine scavenger is highly expressed during germination and in reproductive compartments and is downregulated by endocytosis. Mol Microbiol 68:959–977.

Walther TC, Brickner JH, Aguilar PS, Bernales S, Pantoja C, Walter P. 2006. Eisosomes mark static sites of endocytosis. Nature 439:998–1003.

Wesp A, Hicke L, Palecek J, Lombardi R, Aust T, Munn AL, Riezman H. 1997. End4p/Sla2p interacts with actin-associated proteins for endocytosis in *Saccharomyces cerevisiae*. Mol Biol Cell 8:2291–2306.

Η ομοιάζουσα με αρρεστίνες πρωτεΐνη ArtA είναι απαραίτητη για την ουβικουιτινίωση και την ενδοκύτωση του μεταφορέα UapA ως απόκριση σε σήματα ευρέου φάσματος και εξειδικευμένα σήματα

Καραχάλιου Μ., Αμίλλης Σ.*,Ευαγγελινός Μ., Κοκοτός Α, Γιαλελής Β. & Διαλλινάς Γ.*

*Ισάξια συνεισφορά

Περίληψη

Στην εργασία αυτή μελετήσαμε το ρόλο όλων των πρωτεϊνών που ομοιάζουν με αρρεστίνες στον *Aspergillus nidulans*, σε σχέση με την ανάπτυξη, τη μορφολογία, την ευαισθησία σε φάρμακα και κυρίως την ενδοκύτωση του μεταφορέα ουρικού οξέος-ξανθίνης, UapA. Όλα τα στελέχη με απενεργοποιημένα τα γονίδια των αρρεστινών ήταν βιώσιμα και η ανάπτυξη και η μορφολογία τους ήταν αντίστοιχη με αυτή του στελέχους αγρίου τύπου, με εξαίρεση ένα, το οποίο παρουσίασε πρόβλημα στην παραγωγή κονιδιοσπορίων. Αρκετά όμως από αυτά παρουσίασαν τροποποιημένους φαινοτύπους σε σχέση με την χρήση διαφορετικών πηγών άνθρακα ή αζώτου, καθώς και με την ευαισθησία σε φάρμακα. Μία αρρεστίνη, η ArtA, βρέθηκε να είναι απαραίτητη για την εξαρτώμενη από τη HulA[Rsp5] ουβικουιτινίωση και ενδοκύτωση του UapA, ως απόκριση στην παρουσία αμμωνιακών ιόντων ή υποστρωμάτων. Περαιτέρω γενετική ανάλυση έδειξε ότι τα κατάλοιπα 545-563 του καρβοξυτελικού άκρου του UapA, που περιλαμβάνουν και ένα δισόξινο μοτίβο, είναι απαραίτητα για την ενδοκύτωση του UapA. Ανάλυση μέσω μεταλλαγών της ArtA έδειξε ότι η αμινοτελική περιοχή (κατάλοιπα 2-123), καθώς και τα δύο στοιχεία PY είναι απαραίτητα για τη λειτουργία της. Η ArtA ουβικουιτινιώνεται από τη HulA στη λυσίνη 343 και αυτή η τροποποίηση είναι σημαντική για την ουβικουιτινίωση και την ενδοκύτωση του UapA, ιδιαιτέρως ως απόκριση στην παρουσία αμμωνιακών ιόντων. Τέλος, δείχνουμε ότι η ArtA είναι απαραίτητη για την ενδοκύτωση και άλλων μεταφορέων, ειδικών για πουρίνες (AzgA) και προλίνη (PrnB), αλλά όχι για ασπαρτικό/γλουταμικό (AgtA). Τα αποτελέσματά μας σχολιάζονται στα πλαίσια πρόσφατα προταθέντων μηχανισμών για το πώς οι αρρεστίνες ενεργοποιούνται και στρατολογούνται για την ουβικουιτινίωση των μεταφορέων, ως απόκριση σε σήματα ευρέου φάσματος, αλλά ταυτόχρονα βάζουν τα θεμέλια για την κατανόηση του τρόπου με τον οποίο οι αρρεστίνες, όπως η ArtA, ρυθμίζουν τη ενδοκύτωση συγκεκριμένων μεταφορέων, ως απόκριση στην παρουσία των υποστρωμάτων τους.

The arrestin-like protein ArtA is essential for ubiquitination and endocytosis of the UapA transporter in response to both broad-range and specific signals

**Mayia Karachaliou,[†] Sotiris Amillis,[†]
Minoas Evangelinos, Alexandros C. Kokotos,
Vassilis Yalelis and George Diallinas***
*Faculty of Biology, University of Athens,
Panepistimiopolis 15784, Athens, Greece.*

Summary

We investigated the role of all arrestin-like proteins of *Aspergillus nidulans* in respect to growth, morphology, sensitivity to drugs and specifically for the endocytosis and turnover of the uric acid-xanthine transporter UapA. A single arrestin-like protein, ArtA, is essential for HulA[Rsp5]-dependent ubiquitination and endocytosis of UapA in response to ammonium or substrates. Mutational analysis showed that residues 545–563 of the UapA C-terminal region are required for efficient UapA endocytosis, whereas the N-terminal region (residues 2–123) and both PPxY motives are essential for ArtA function. We further show that ArtA undergoes HulA-dependent ubiquitination at residue Lys-343 and that this modification is critical for UapA ubiquitination and endocytosis. Lastly, we show that ArtA is essential for vacuolar turnover of transporters specific for purines (AzgA) or L-proline (PrnB), but not for an aspartate/glutamate transporter (AgtA). Our results are discussed within the frame of recently proposed mechanisms on how arrestin-like proteins are activated and recruited for ubiquitination of transporters in response to broad range signals, but also put the basis for understanding how arrestin-like proteins, such as ArtA, regulate the turnover of a specific transporter in the presence of its substrates.

Introduction

Plasma membrane transporters constitute primary targets of cellular regulatory circuits controlling cell communication and signalling (Dupré *et al.*, 2004; Sorkin and von Zastrow, 2009). Most transporters traffic to the plasma membrane embedded in exocytic vesicles, but under certain physiological conditions, stress stimuli, or in response to development signals, they can be re-routed to the vacuole/lysosome for degradation, either directly or through the MVB pathway (late endosome), or recycle between the Golgi, the endosome and the plasma membrane (Dupré *et al.*, 2004; Sorkin and von Zastrow, 2009; Foley *et al.*, 2011). Signals triggering transporter endocytosis include shifts in the nitrogen or carbon source availability of the growth medium, stress or the presence of excess substrate, (Hicke and Dunn, 2003; Dupré *et al.*, 2004; Sorkin and von Zastrow, 2009). Transporter endocytosis, recycling and direct sorting into the MVB/vacuolar pathway depend on alternating cycles of different types of ubiquitination and deubiquitination, named the 'ubiquitin code' (Belgareh-Touzé *et al.*, 2008; Risinger and Kaiser, 2008; Lauwers *et al.*, 2010).

In *S. cerevisiae*, in response to various physiological signals, several plasma membrane transporters are ubiquitinated by the HECT domain E3 ligase Rsp5 and subsequently removed from the cell surface, or directly diverted from the Golgi to the endovacuolar system (Hicke and Dunn, 2003; Dupré *et al.*, 2004; André and Haguenauer-Tsapis, 2004; Risinger *et al.*, 2006; Rubio-Texeira and Kaiser, 2006; Cain and Kaiser, 2011). Recent studies have contributed in the understanding of how Rsp5 recognizes a wide variety of substrates under various physiological signals. Rsp5 contains three WW domains, which recognize PY motifs with the typical sequence PPxY or LPxY. Several adaptor proteins containing such motifs have been shown to facilitate the ubiquitination of particular proteins or sets of proteins (Léon and Haguenauer-Tsapis, 2009). These adaptors include the membrane proteins Bsd2 (Hettema *et al.*, 2004), Tre1/2 (Stimpson *et al.*, 2006), Ear1 and Ssh4 (Léon *et al.*, 2008) or members of a family of soluble α-arrestins or arrestin-like proteins (Lin *et al.*, 2008; Léon and Haguenauer-Tsapis, 2009; Nikko and Pelham, 2009; Nikko *et al.*, 2009; Hatakeyama *et al.*, 2010; O' Donnell *et al.*, 2010; MacGurn *et al.*, 2011; Becuwe *et al.*, 2012) and their distant homologues Bul1 and Bul2 (Helliwell *et al.*, 2001; Soetens *et al.*, 2001; Merhi and André, 2012). All yeast α-arrestins, including Bul1 and Bul2, have been studied

systematically in respect to their role on the ubiquitination and endocytosis of several transporters and the general model emerging is that different arrestin-like proteins recognize different transporters, or the same transporter in response to different stimuli.

Recently, three reports (MacGurn *et al.*, 2011; Becuwe *et al.*, 2012; Merhi and André, 2012) put the basis on how arrestin-like proteins are post-translationally regulated in response to nutrient signalling. In the absence of preferred carbon or nitrogen sources, arrestin-like proteins Art4/Rod1, Bul1/2 or Art1, which control the ubiquitination and turnover of the acetate transporter Jen1p, the arginine transporter Can1p or the general amino acid permease Gap1p, respectively, are phosphorylated and remain inactive. In the case of Art4/Rod1 and Bul1/2, it was shown that under such poor nitrogen conditions the relevant arrestin-like proteins bind to 14-3-3 proteins, which inhibit their capacity to elicit Jen1p or Gap1p downregulation. Upon a shift to rich carbon or nitrogen sources, Art4/Rod1, Art1 or Bul1/2 are dephosphorylated, probably released from 14-3-3 proteins and recruited for catalysing the ubiquitination of Jen1p, Can1p or Gap1p respectively. In the case of the Art1 and Bul1/2, phosphorylation of the arrestin adaptors involves the Npr1 kinase, which is itself negatively regulated by the TOR pathway (MacGurn *et al.*, 2011), whereas in the case of Art4/Rod1, the AMPK homologue Snf1 seems to be implicated. Still, another arrestin-like protein, Aly2/Art3, which might localize in the endosomes, was recently found to be phosphorylated by Npr1 (Hatakeyama *et al.*, 2010). In the case of Bul1/2 and Art4, dephosphorylation of the arrestin-like proteins depends on the Sit4 and the PP1 phosphatases Glc7/Reg1 respectively.

Another aspect of the emerging mechanism underlying the control of transporter ubiquitination by specific arrestin-like protein adaptors is that the arrestins themselves are ubiquitinated, and this seems to be part of the mechanism regulating their action. In all cases tested (Art1, Art2, Art3/Aly2, Art4/Rod1, Art8/Rim8 and Art9), arrestin-like protein ubiquitination is Rsp5-dependent and essential for their function (Kee *et al.*, 2006; Nikko *et al.*, 2009; Hatakeyama *et al.*, 2010; Herrador *et al.*, 2010; MacGurn *et al.*, 2011; Becuwe *et al.*, 2012; Merhi and André, 2012; O'Donnell, 2012). Ubiquitination of PalF, an arrestin-like protein involved in pH sensing in the filamentous ascomycete *Aspergillus nidulans*, has been proposed to be the sole molecular trigger required for transmitting the alkaline pH signal to the downstream elements of the pathway (Hervás-Aguilar *et al.*, 2010). Studies on Art1, Art4/Rod1 and Bul1 revealed that this ubiquitination is required for proper permease downregulation and that there seems to be a cross-talk between the phosphorylation–dephosporylation status and the ubiquitination levels of arrestin-like proteins, but the mecha-

nisms controlling the ubiquitination of Art proteins and its exact role in transporter downregulation remain poorly known.

In some cases, specific transporters appear unaffected in single arrestin-like protein mutants, possibly because of functional redundancy of the arrestins (Léon and Haguenauer-Tsapis, 2009; Nikko and Pelham, 2009). In addition, it seems that not all α-arrestins regulate endocytosis, as described in a recent study, where two arrestin-like proteins, Aly1 and Aly2, regulate intracellular trafficking of the general amino acid permease Gap1 (O' Donnell *et al.*, 2010). Notably, Aly1 and Aly2 co-purify with clathrin and clathrin-adaptor protein (AP) complexes (McMahon and Boucrot, 2011) *in vivo* and interact directly with the γ-subunit of AP-1 *in vitro*, suggesting that, like their β-arrestin relatives (Goodman *et al.*, 1996), α-arrestins promote cargo incorporation into clathrin-coated vesicles (O' Donnell *et al.*, 2010).

Our lab has used the extensively studied uric acid-xanthine transporter UapA (reviewed in Diallinas and Gournas, 2008; Gournas *et al.*, 2008; Amillis *et al.*, 2011; Kosti *et al.*, 2011) of *A. nidulans* to approach questions concerning the mechanisms underlying endocytosis, triggered by ammonium or excess substrate (Gournas *et al.*, 2010). We have shown that either ammonium or substrates elicit the ubiquitination, by the HulA[Rsp5] E3 ligase, of a single Lys residue (Lys-572) in the C-terminal region of plasma membrane-localized UapA. Ubiquitinated UapA is internalized and is directed to the MVB/vacuolar pathway for degradation. We further showed that ammonium- and substrate-triggered UapA endocytosis recruit or activate distinct mechanisms, since the latter, unlike ammonium-elicited internalization, operates only for transport-active molecules. Using UapA mutants with modified function or altered substrate affinities and/or specificities, we showed that transport-dependent UapA endocytosis occurs through a mechanism which senses subtle conformational changes associated with the transport cycle (Gournas *et al.*, 2010). Interestingly, we have also demonstrated that in the presence of substrates, non-functional UapA versions can be endocytosed *in trans* if expressed in the simultaneous presence of active UapA versions, a result that suggests that UapA oligomerizes (Gournas *et al.*, 2010).

In this work we systematically knock-out all arrestin-like genes of *A. nidulans* and identify a single protein (ArtA) as being essential for the HulA[Rsp5]-dependent ubiquitination and subsequent endocytosis of UapA in response to apparently different signals. We provide strong evidence that ArtA interacts with a C-terminal region of UapA and show that the ArtA N-terminal region and both PPxY motives are necessary for its function. Furthermore, we show that ArtA is itself ubiquitinated at a single Lys residue and that ArtA ubiquitination is critical for UapA endocyto-

sis. Finally, we show that ArtA is specific for the turnover of some transporters but not of others. Our results are discussed in relation to how a single arrestin-like protein, ArtA, recognizes different substrates in response to broad-range or/and specific signals.

Results

Identification and in silico *analysis of genes encoding arrestin-like proteins in* A. nidulans

We investigated whether arrestin-like proteins have an analogous role in *A. nidulans* and if so, which proteins are specific for selected transporters and under which conditions. In this direction, we wanted to identify the arrestin-like protein(s) responsible for UapA endocytosis in response to different signals. A BlastP analysis showed that *A. nidulans* has 10 genes coding for putative arrestin-like proteins, most of which contain PY elements (see Fig. 1B). Three of them, *palF*, *creD* and *apyA*, have been previously described. PalF (gene: ANID_01844.1) is a positive-acting arrestin-like protein which, together with the seven-transmembrane receptor PalH, acts as a key molecular sensor that mediates activation of an intracellular signalling cascade by alkaline ambient pH in *A. nidulans* and other ascomycete fungi (Herranz *et al.*, 2005; Hervás-Aguilar *et al.*, 2010). PalF ubiquitination suffices to trigger alkaline pH signalling to downstream elements of the pathway (Hervás-Aguilar *et al.*, 2010). The *creD* gene (ANID_04170.1) has been genetically defined by a mutation (*creD34*) that suppresses the phenotypic effects of mutations in *creC* and *creB*, two genes encoding a de-ubiquitinating enzyme and a WD40-motif-containing protein, respectively, which form a complex essential for carbon catabolite regulation (Boase and Kelly, 2004). Finally, the *apyA* gene (ANID_03265.1) has been recognized as an arrestin-like protein through BlastP analysis, but its physiological role has not been studied. CreD and ApyA have been shown by a bacterial two-hybrid system to interact with the HulA ubiquitin ligase (Boase and Kelly, 2004). Seven more arrestin-like genes were identified herein and named *artA* (ANID_00056.1)*, artB* (ANID_01089.1)*, artC* (ANID_01743.1)*, artD* (ANID_09105.1), *artE* (ANID_02447.1), *artF* (ANID_03302.1), *artG* (ANID_05453.1). The genomes of other Aspergilli have 7–12 arrestin-like proteins (http://www.broadinstitute.org/annotation/genome/aspergillus_group/).

We compared the *A. nidulans* arrestin-like proteins with the arrestin-like proteins of *S. cerevisiae* and among themselves (Tables S2 and S3). ArtA is significantly more similar to the Art1p/Ldb19p/Cvs7p (21.4% identity) than to any other arrestin-like protein of *S. cerevisiae*. Art1p is an arrestin-like protein that is necessary for the endocytosis of several nitrogen-containing compounds, such as amino

acids and uracil (Lin *et al.*, 2008; Léon and Haguenauer-Tsapis, 2009; Nikko *et al.*, 2009; Nikko and Pelham, 2009; MacGurn *et al.*, 2011). CreD is mostly similar to Art4p/Rod1p and Art7p/Rog3p (24.1–26.7% identity), the former being involved in the endocytosis of the glucose transporter Htx6p and of the lactate permease Jen1 (Nikko and Pelham, 2009; Becuwe *et al.*, 2012). The remaining Art proteins of *A. nidulans* share less clear-cut similarities with the *S. cerevisiae* arrestin-like proteins (identities up to 19.1%). *A. nidulans* arrestin-like proteins share low similarity among themselves (< 18.9%), with a single exception being CreD and ApyA (26.3% identity). This contrasts the case in *S. cerevisiae*, where six out of the ten arrestin-like proteins can be classified in pairs (Art2-Art8, Art3-Art6, Art4-Art7), an indication of redundancy due to relatively recent duplication events. Thus, *A. nidulans* might prove to employ arrestin-like proteins in processes not present in yeasts.

Construction and phenotypic analysis of null mutants of genes encoding arrestin-like proteins

Using a standard gene knock-out procedure (see *Experimental procedures*), we constructed knock-out alleles of nine genes encoding arrestin-like proteins (*artA, artB, artC, artD, artE, artF, artG, apyA, creD*). The knock-out mutant of the tenth arrestin-like protein, *palFΔ*, was a gift from Prof. H. Arst. All knock-out null mutants were viable and could thus be tested directly for their morphology and rate of growth in different temperatures (25°C and 37°C), pH values, nitrogen or carbon sources and toxic analogues of purines, pyrimidines and amino acids. Highlights of this analysis are shown in Fig. 1A. Increased sensitivity towards toxic compounds has been used to identify arrestin-like genes in *S. cerevisiae* (Lin *et al.*, 2008; Nikko *et al.*, 2009). Among the ten arrestin-like protein knock-outs, *artEΔ* showed an inability to produce coloured asexual conidiospores decorating the surface of the colony. Several of the knock-out mutants showed different growth rates on various nitrogen or carbon sources and especially in respect to resistance or sensitivity to the toxic analogues tested.

In regard to UapA, which is the primary subject of this work, *artAΔ* showed increased sensitivity to allopurinol, a well established substrate of this transporter (Diallinas and Scazzocchio, 1989). *artAΔ* also showed increased sensitivity to 8-azaguanine, a substrate of the AzgA purine transporter (Cecchetto *et al.*, 2004). As will be shown below, ArtA is indeed responsible for the endocytic turnover of both UapA and AzgA, in full accordance with the increased sensitivity observed for the *artAΔ* mutant to allopurinol and 8-azaguanine (see Fig. 1A).

Based on the results shown in Fig. 1A, we also predicted possible relationships between arrestin-like
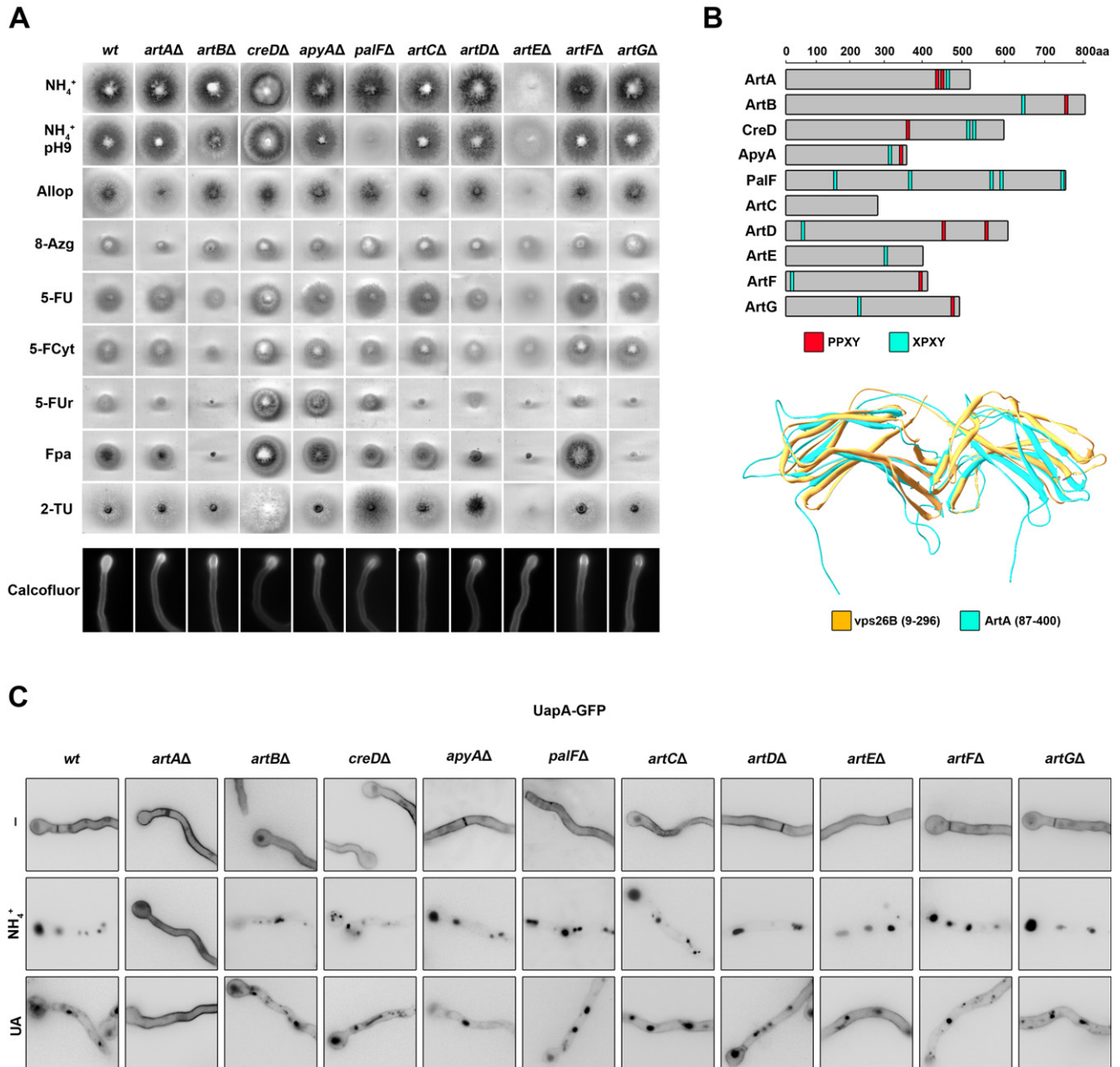
Fig. 1. Arrestin-like proteins in *A. nidulans*.

A. Growth phenotypes of arrestin null mutants. Complete genotypes are shown in Table S1. Supplemented minimal medium (MM) with 1% glucose as carbon source and 10 mM ammonium tartrate (NH$_4^+$) as nitrogen source was used as a growth rate control. Supplemented glucose MM with 10 mM sodium nitrate as nitrogen source was used with each of the following toxic analogues: allopurinol (Allop), 8-azaguanine (8-Azg), 5-fluorouracil (5-FU), 5-fluorocytosine (5-FCyt), 5-fluorouridine (5-FUr), p-fluorophenylalanine (FPA), 2-thiourea (2-TU). Growth tests were at 37°C and pH 6.8. In the lowest panel, vegetative microscopic samples of hyphal cells growing on MM with glucose as carbon source and ammonium tartrate as nitrogen source (16 h at 25°C) are shown after staining with Calcofluor white.

B. Upper panel: schematical representation of the actual positions of putative PY elements in the *A. nidulans* arrestin-like protein sequences. Noticeably, ArtC has no canonical PY elements. Lower panel: superimposition of the ArtA predicted structure, modelled on the crystal structure of the mouse vacuolar protein sorting-associated protein Vps26B (2r51_A), obtained from the RCSB PDB Protein Data Bank (http://www.pdb.org/pdb/home/home.do) and plotted with the SwissPdbViewer 4.0.1 software.

C. UapA subcellular localization in arrestin-like protein null mutants. Epifluorescence microscopy of UapA-GFP subcellular localization under non-endocytic (−) or endocytic conditions [NH$_4^+$ or uric acid (UA)] in isogenic arrestin-like protein null mutants. Growth conditions are described in *Experimental procedures*.

proteins and different transporters, summarized in Table S4. For example, the FurD (Amillis *et al.*, 2007) and FcyB (Krypotou *et al.*, 2012) nucleobase transporters, which belong to the NCS1 family (Pantazopoulou and Diallinas, 2007), might interact with arrestin-like proteins ArtB and ArtD, a conclusion based on the increased sensitivity of *artB*Δ and *artD*Δ mutants to 5-fluorouracil (5-FU) or 5-fluorocytosine (5-FC), respectively. The resistance/ sensitivity phenotypes on p-fluorophenylalanine (FPA) and 5-fluoruridine (5-FUd) or 2-thiourea (2-TU), which very probably reflect the apparent transport activities of a putative general amino acid permease, the unique *A. nidulans* nucleoside transporter CntA (Hamari *et al.*, 2009) and the major urea transporter UreA (Abreu *et al.*, 2010), respectively, seem to be affected by several arrestin-like proteins. It is also noticeable that *creD*Δ, *palF*Δ and mostly the *artB*Δ mutants show pleiotropic phenotypes. Furthermore, in some cases, some transporters seem to be affected negatively or positively by different arrestin knock-out mutations, such as the nucleoside transporter CntA. A similar situation has been observed before in *S. cerevisiae* and might be explained by the hypothesis that increased accumulation of some transporters might indirectly lead to reduced translocation of other transporters to the plasma membrane (Lin *et al.*, 2008). Finally, none of the arrestin-like protein knock-outs showed altered polar growth or hyphal morphology (Fig. 1A lowest panel).

A single arrestin-like protein, ArtA, is necessary for UapA endocytosis and vacuolar turnover in response to ammonium or excess substrate

In order to investigate the role of all arrestin-like proteins in the endocytosis and/or MVB sorting of UapA, we crossed all relevant null mutants with a strain expressing a fully functional UapA-GFP version from its endogenous promoter (Gournas *et al.*, 2010). The strain expressing UapA-GFP was deleted for the homologous *uapC* gene, encoding a secondary uric acid/xanthine transporter (Diallinas *et al.*, 1995), so that uric acid or xanthine uptake was solely mediated by UapA. Isogenic progeny was selected and analysed for UapA-GFP subcellular localization and endocytosis by epifluorescence microscopy. Results are summarized in Fig. 1C. None of the arrestin-like protein knock-out deletions had any effect on the expression or localization of UapA-GFP in the plasma membrane, visible in the hyphal periphery and in the septa, under control conditions. Under endocytic conditions, imposed by the presence of ammonium or excess substrate (uric acid), where UapA-GFP is normally internalized and sorted in MVBs/vacuoles (see wild-type control in Figs 1C and 2A), a single arrestin-like protein null mutant, *artA*Δ, showed no UapA-GFP vacuolar turnover. In all other

arrestin-like protein knock-out deletion mutants UapA-GFP was turned-over similarly to the wild-type control in the presence of ammonium or excess substrate. Given that we have previously concluded that UapA-GFP vacuolar turnover occurs exclusively via endocytosis and not through direct delivery to the vacuole from the Golgi (Gournas *et al.*, 2010), our results strongly suggest that lack of a functional ArtA blocks UapA internalization from the plasma membrane.

To show more rigorously that ArtA controls UapA endocytosis and vacuolar turnover, we constructed *artA*⁺ and *artA*Δ isogenic strains expressing UapA-GFP from the strong controllable *alcA*ₚ promoter (Gournas *et al.*, 2010; for details see *Experimental procedures*). These strains lack the genomic copies of *uapA* and *uapC* (i.e. *uapA*Δ *uapC*Δ) so that uric acid or xanthine uptake takes place through the plasmid borne *alcA*ₚ-UapA-GFP, expressed solely under de-repressed conditions (fructose as sole carbon source). In the presence of glucose (repressing carbon source) no UapA-GFP expression or transport activity can be detected. Using the *alcA*ₚ system had two advantages. First, we could uncouple ammonium-elicited repression of *uapA* transcription from UapA endocytic turnover (Pantazopoulou *et al.*, 2007), and second, we could regulate UapA *de novo* synthesis prior or after imposing endocytic conditions (Gournas *et al.*, 2010).

We examined the effect of ammonium or excess substrate into already synthesized UapA-GFP or to *de novo* made UapA-GFP in *artA*⁺ and *artA*Δ isogenic strains. In the first case, *alcA*ₚ-UapA-GFP expression was induced (4–6 h) in the presence of fructose/ethanol, then repressed by addition of glucose (1 hour), prior to ammonium or substrate addition. In the second case, ammonium or substrate was added to cultures in which *alcA*ₚ-UapA-GFP expression was repressed by glucose, and then (> 30 min) UapA-GFP expression was induced by shifting the cells in fructose/ethanol (4–6 h). In both conditions the result was identical, showing that lack of a functional ArtA blocked UapA-GFP sorting into early endosomes and abolished vacuolar turnover (Fig. 2A). Early endosomes marked with UapA-GFP were identified by their unique bidirectional motility observed in an inverted microscope and colocalization with FM4-64, whereas vacuoles marked with UapA-GFP were identified by FM4-64 and CMAC (not shown). A Western blot analysis confirmed that under both endocytic conditions UapA-GFP vacuolar turnover is significantly reduced in the *artA*Δ mutant (Fig. 2B).

Further evidence for the involvement of ArtA in UapA turnover was obtained by direct transport assays with radiolabelled xanthine. Figure 2C shows that, under endocytic conditions (presence of ammonium), in the wild-type control (*artA*⁺), the apparent xanthine uptake drops to 60%, whereas in the isogenic strain lacking ArtA (*artA*Δ) xanthine uptake remains close to 100%. We also obtained inde-
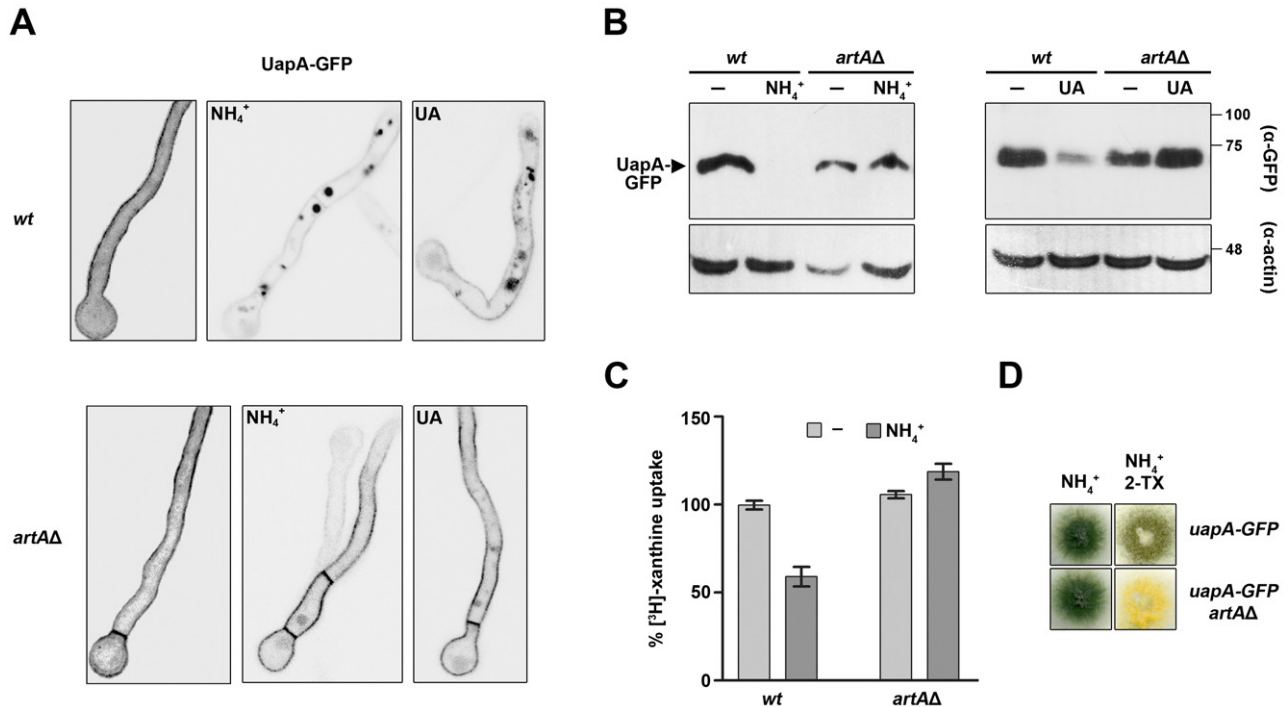
Fig. 2. ArtA is involved in UapA endocytosis and vacuolar turnover.
A. Confocal laser microscopy of UapA-GFP subcellular localization under non-endocytic (–) or endocytic conditions (NH₄⁺ or UA) in isogenic *artA⁺* (wt) and *artAΔ* strains expressing UapA-GFP. Growth conditions are described in *Experimental procedures*.
B. Western blot analysis of total protein extracts from *artA⁺* (wt) and *artAΔ* strains, expressing UapA-GFP from the *alcAₚ*, using anti-GFP antibody. Conditions were identical to (A).
C. Uptake rate of ³H-xanthine in *artA⁺* (wt) and *artAΔ* strains under non-endocytic (–) or endocytic conditions (NH₄⁺).
D. The 2-thioxanthine effect in the presence of NH₄⁺ as nitrogen source in *artA⁺* (wt) and *artAΔ* strains (see text).

pendent *in vivo* evidence for an apparent increase in UapA activity in an *artAΔ* genetic background under endocytic conditions by a simple growth test using 2-thioxanthine. This xanthine analogue is taken-up by UapA and is metabolized to 2-thiouric acid, which inhibits a laccase necessary for the conversion of yellow to green pigment in conidiospores (Darlington and Scazzocchio, 1967). As a result, strains expressing UapA from its native promoter produce yellow conidiospores in media containing 2-thioxanthine and a non-repressing nitrogen source (e.g. nitrate, L-proline). In the presence of NH₄⁺ however, UapA transcription is repressed and thus 2-thioxanthine is not taken up by the cells, and consequently conidiospores remain green. In media containing NH₄⁺ as a nitrogen source, a strain expressing UapA from the *alcAₚ* promoter, which is not repressible by ammonium, shows a leaky phenotype (i.e. mixture of green and yellow spores), apparently due to NH₄⁺-elicited UapA turnover by endocytosis. Figure 2D shows that in an *artAΔ* genetic background the effect of 2-thioxanthine is very strong (non-leaky appearance of yellow conidiospores) even in NH₄⁺-containing media, strongly suggesting that lack of ArtA reduces dramatically the turnover of UapA by endocytosis.

ArtA is essential for UapA ubiquitination

We investigated whether ArtA is involved in the ubiquitination of UapA, as all evidence predicted. For that, we performed Western blot analyses under conditions inhibiting the rapid de-ubiquitination of cargoes (see *Experimental procedures*). Figure 3A shows that in the *artA⁺* strain the anti-GFP antibody detects a less motile form of UapA-GFP only after a relatively short shift in media containing NH₄⁺ or substrate (uric acid), whereas in the isogenic *artAΔ* mutant such a form is not visible. Similar less motile UapA-GFP-specific molecules have been previously detected and shown to correspond to UapA-GFP/ubiquitin conjugates (Gournas *et al.*, 2010). To further confirm this, we purified UapA-His molecules, through Ni²⁺ affinity chromatography, expressed in isogenic strains *artA⁺* and *artAΔ* (see *Experimental procedures*) and the purified UapA-His fraction was immunoblotted with anti-His- and anti-ubiquitin-specific antibodies (Fig. 3B). Our results confirm that a functional ArtA is necessary for the formation of UapA-ubiquitin conjugates, similar to the need for a fully functional HulA ubiquitin ligase or the presence of Lys-572 in the tail of UapA (Gournas *et al.*, 2010).

A

B
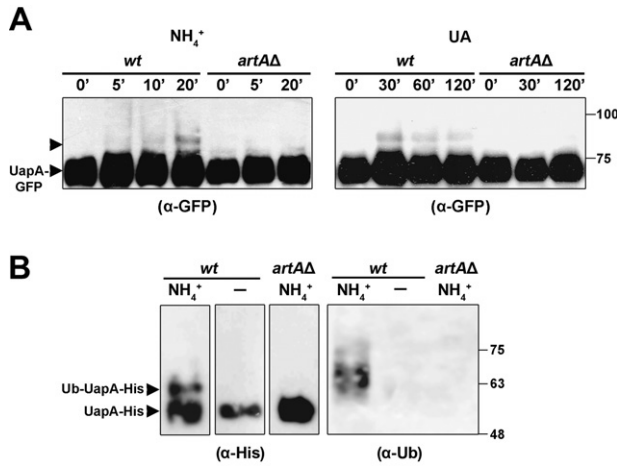
Fig. 3. ArtA is essential for UapA ubiquitination.
A. Western blot analysis of membrane-enriched protein extracts from $artA^+$ (wt) and $artA\Delta$ strains, expressing UapA-GFP from the $alcA_p$, using anti-GFP antibody, under conditions detecting ubiquitination of UapA (see *Experimental procedures*). Notice the ArtA-dependent appearance of less motile bands of UapA-GFP under endocytic conditions in membrane enriched fractions, which are not detected in the absence of a fully active HulA ubiquitin ligase ($hulA\Delta C2$) or with a UapA mutant lacking Lys-572 (K572R) (Gournas *et al.*, 2010).
B. The less motile ArtA-dependent UapA-GFP signals can also be detected with anti-Ub antibody in purified UapA-His after 20 min growth in NH_4^+ (+).

The N-terminus and the PPxY motives are essential for ArtA function

We constructed, by standard oligonucleotide mutagenesis, a series of mutations to test the function of specific regions, motives or residues of ArtA. The mutations made were the following: (i) a deletion of residues 2–123 corresponding to the ArtA N-terminus, which contains several putative Ser phosphorylation sites that might have a regulatory role analogous to that found for Art1 (Lin *et al.*, 2008). (ii) Ala substitutions of the two canonical PPxY motives. (iii) Ala substitutions of two well conserved residues (Gly185 and Phe191) within the arrestin motif, which have been shown to be critical for Art1 function in *S. cerevisiae* (Lin *et al.*, 2008). ArtA mutations were inserted to the genomic *artA* locus in a strain expressing UapA-GFP, through standard reverse genetics (see *Experimental procedures*). Corresponding mutants were viable showing wild-type growth and morphology, as expected, given that the *artA*Δ mutant shows no mutant phenotype.

All mutants were analysed microscopically in respect to $alcA_p$-UapA-GFP endocytosis by ammonium or substrate. Figure 4A shows that Ala substitutions of Gly185 and Phe191 had no significant effect on UapA stimulus-elicited endocytosis, whereas deletion of the N-terminus or either one of the two PPxY motives (PY1 or PY2) totally blocked UapA endocytosis, similar to an *artA*Δ mutation. *In vivo* evidence supporting the functionally essential role

of the two PPxY motives or the N-terminal region of ArtA was obtained using the 2-thioxanthine sensitivity test (not shown).
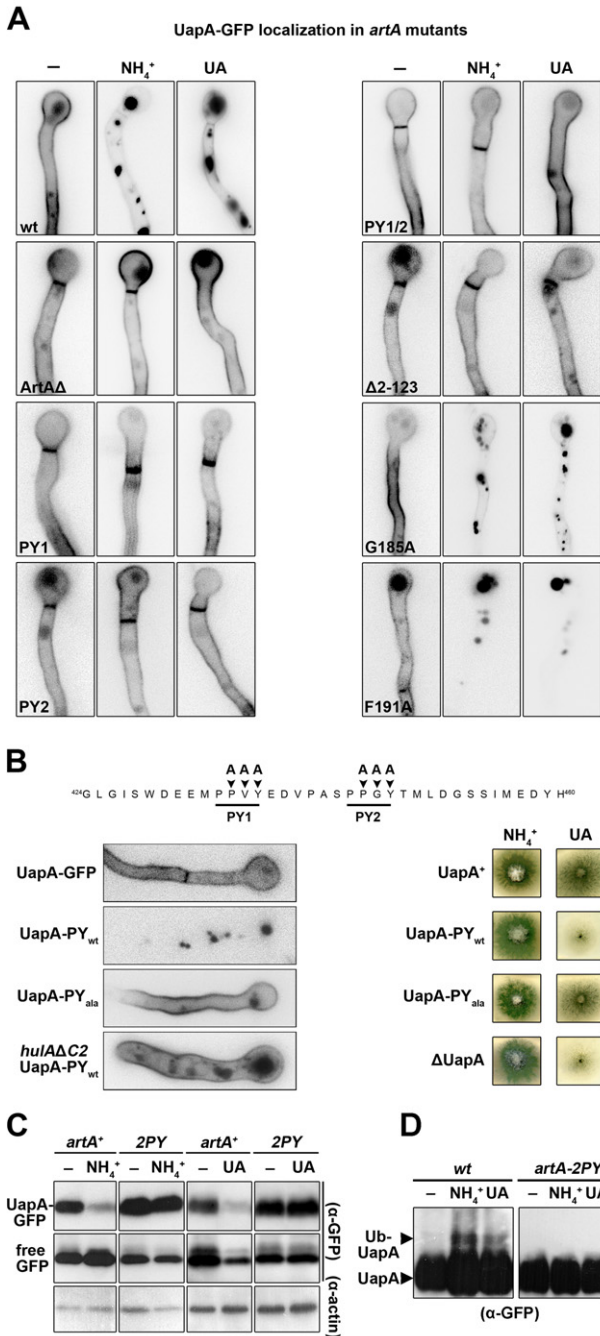
We obtained additional evidence that the PPxY motives are necessary and sufficient for HulA-dependent ubiquitination and subsequent turnover of UapA by constructing and analysing mutants expressing chimeric fusions of UapA with a conserved 38-amino-acid sequence of ArtA including the two PPxY motives, either in their wild-type (UapA-PY$_{wt}$) or in a mutated version (UapA-PY$_{ala}$). Figure 4B shows that a UapA-PY$_{wt}$ chimera is not functional (lack of growth on uric acid) due to constitutive targeting to the vacuole, whereas a UapA-PY$_{ala}$ chimera or UapA-PY$_{wt}$ chimera expressed in a $hulA\Delta C2$ background are functional (growth on uric acid), showing normal targeting to the plasma membrane.

The essentiality of the PPxY for ArtA-mediated UapA endocytosis was directly confirmed by Western blot analysis, which shows that, unlike the result obtained in $artA^+$ genetic background, UapA-GFP protein steady state levels were not reduced in the presence of either NH_4^+ or uric acid, an observation also associated with low level of UapA-GFP vacuolar turnover, similar to the level obtained under non-endocytic conditions, as judged by the low amount of free GFP detected (Fig. 4C). The requirement of the PPxY motives for HulA-dependent UapA ubiquitination was subsequently shown by an independent western analysis where no UapA-Ub conjugates could be detected in the strain expressing the *artA* allele mutated in its PPxY elements (Fig. 4D).

HulA-dependent ubiquitination of ArtA at Lys-343 is critical for ArtA function

We investigated whether ArtA itself is ubiquitinated and whether this has a role on UapA endocytosis. Figure 5A shows that anti-GFP antibody detects less motile forms of ArtA-GFP, which probably correspond to ArtA-ubiquitin conjugates. The steady state levels of ArtA-ubiquitin conjugates seemed moderately increased in response to ammonium, compared to control conditions or in response to substrates. The increase in ArtA ubiquitination levels in response to the presence of NH_4^+ for increasing periods of time was confirmed by quantitative measurements of the relative ratios of ArtA-Ub/ArtA (Fig. 5B). We subsequently showed that the less motile forms of ArtA-GFP, as expected, cross-react with anti-Ubiquitin antibody (Fig. 5C). Finally, we showed that ArtA ubiquitination requires an interaction with a fully functional HulA ligase, as judged by the non-appearance of ArtA-Ub forms in $hulA\Delta C2$ genetic background or when using an ArtA version mutated in its PPxY motives (see Fig. 5A).

Based on sequence alignments of ArtA and Art1, we predicted that Lys-343 might be the residue acting as an

A

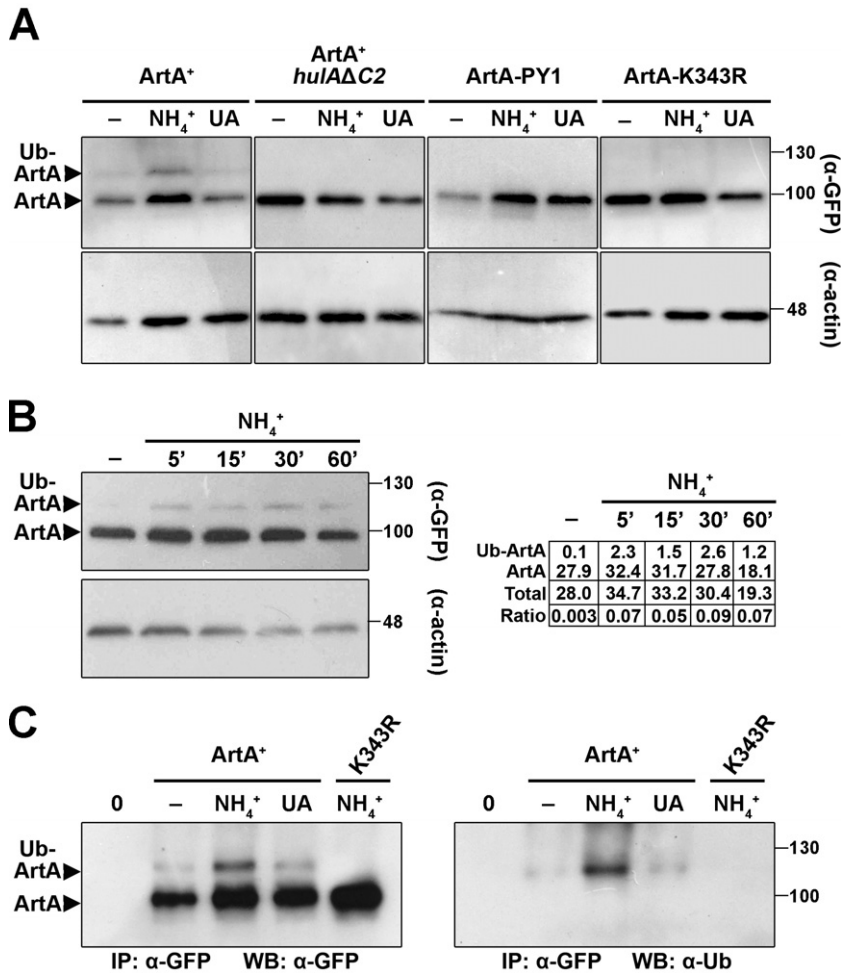**UapA-GFP localization in *artA* mutants**

B

C

D

Fig. 4. The N-terminus and the PY motives are essential for ArtA function.
A. Epifluorescence microscopy of UapA-GFP subcellular localization under non-endocytic (−) or endocytic conditions (NH_4^+ or UA) in isogenic *artA* mutants expressing UapA-GFP driven under the *alcA* regulable promoter. PY1 stands for ArtA P435A/V436A/Y437A and PY2 for ArtA P445A/G446A/Y447A. Δ2–123 stands for the N-terminal truncation of amino acids 2–123. Growth conditions are described in *Experimental procedures*.
B. Epifluorescence microscopy of UapA-PY$_{wt}$ and UapA-PY$_{ala}$ chimeras under non-endocytic conditions in *hulA*+ and in a *hulAΔC2* background, and UapA-mediated growth on UA as sole nitrogen source.
C. Western blot of total protein extracts of a wt (*artA*+) and an *artA* mutant strain carrying both PY1 and PY2 substitutions (2PY), expressing UapA-GFP under non-endocytic (−) or in the presence of UA or NH_4^+ for 2 h.
D. Western blot analysis of UapA-GFP ubiquitination in membrane enriched fractions of a wt (ArtA+) and an ArtA-2PY strain, grown under endocytic (30 min, NH_4^+) or control conditions.

genetic background. In this strain, mutation ArtA-K343R severely inhibited UapA endocytosis in response to both in NH_4^+ and substrates (Fig. 6A). Western blot analysis showed that ArtA-K343R is a practically loss-of function mutation in respect to UapA turnover, as intact UapA-GFP levels remain high under endocytic conditions. In addition the ratio of intact UapA-GFP/free vacuolar GFP is significantly higher to the ratio found in an *artA*+ background (Fig. 6B). Notably, however, some UapA-GFP turnover was observed in the ArtA-K343R background, suggesting that ArtA ubiquitination is critical, but not absolutely essential for some UapA turnover. This observation was in agreement with a subsequent Western blot analysis showing that, although UapA ubiquitination is significantly reduced in an ArtA-K343R mutant, some minor fraction of UapA can still be ubiquitinated (Fig. 6C).

The C-tail of UapA contains a region essential for ArtA binding

Previous studies have shown that the UapA C-tail includes the single Lys residue (Lys-572) necessary for HulA-dependent ubiquitination under endocytic conditions (Gournas *et al.*, 2010). This suggested that ArtA might interact with the C-terminal region of UapA. To investigate this assumption, the C-terminal region of UapA was fused into the C-terminal region of AzgA, a purine transporter, which is fairly insensitive to NH_4^+-triggered endocytosis (Pantazopoulou *et al.*, 2007), and the resulting chimeric molecule was used for testing whether the UapA C-terminal region confers ArtA-dependent internalization of AzgA. Results in Fig. 7A confirm that the UapA C-terminal region promotes enhanced ammonium-elicited AzgA endocytosis and that this phenomenon is dependent on a functional ArtA protein. This strongly suggested that the C-terminal region of UapA contains a domain necessary and sufficient for ArtA binding.

acceptor of ubiquitination in ArtA. To test this, we constructed a strain expressing ArtA-K343-GFP. Results, also shown in Fig. 5A, confirm that Lys-343 is indeed the acceptor residue for ubiquitination. These results show that HulA-dependent ArtA ubiquitination at a single Lys residue occurs through the involvement of its PPxY elements, very probably through a direct interaction with the WW motives of HulA.

To investigate the role of ArtA ubiquitination, we constructed a strain expressing UapA-GFP in an ArtA-K343R

Fig. 5. HulA-dependent ubiquitination of ArtA at Lys-343 is critical for ArtA function.
A. Western blots of total protein extracts in isogenic wt, *hulAΔC2* and *artA* mutants PY1 and K343R under non-endocytic (–) or endocytic conditions (NH$_4^+$ or UA).
B. Time-course (left) and ImageJ semi-quantitative estimation (right) of NH$_4^+$-dependent increase in ArtA ubiquitination.
C. Western blots of immunoprecipitated ArtA-GFP and ArtA-K343R-GFP under denaturing conditions in the presence (60 min, NH$_4^+$ or substrate) or absence (–) of endocytic stimuli, probed with anti-GFP (left panel) or anti-ubiquitin (right panel) antibodies.

To further identify the region responsible for ArtA binding, we searched for UapA residues upstream from Lys-572, which might prove necessary for UapA endocytosis. For this, we constructed several Ala substitutions in the region 545–571 and two deletions corresponding to residues 564–571 and 547–571 respectively (see upper part of panel B in Fig. 7). Microscopic analysis of corresponding mutants showed that solely the longer deletion (residues 547–571) or Ala substitutions of a di-acidic motif (E^{545}-V-E^{547}) led to a severe block of ammonium- or substrate-elicited UapA endocytosis (Fig. 7B). Interestingly, di-acidic motives are known to be involved in membrane cargo trafficking and in particular in ER-exit or Golgi-to-vacuole transfer (Bonifacino and Traub, 2003; Renard *et al.*, 2010; Starr *et al.*, 2012), but are not known to interact with arrestin-like proteins or be related to ubiquitination of cargoes. In this direction, we showed that an intact E^{545}-V-E^{547} element was necessary for UapA-GFP ubiquitination, and thus might be part of a putative ArtA binding site on the C-tail of UapA (Fig. 7C). On the whole, our results showed that the region corresponding to residues 545–563 is required for UapA endocytosis, which in turn suggested that it might host the ArtA binding site.

The function of ArtA is a prerequisite for the formation of UapA-specific, SagA-dependent, pre-endocytic cortical puncta

Considering that ArtA is involved in ubiquitination of UapA and that this modification constitutes the molecular signal for UapA endocytosis, we tested whether the effect of the *artAΔ* mutation is epistatic to a mutation blocking endocytosis at a step downstream from cargo ubiquitination.

For this, we decided to knock-out SagA (ANID_ 01023.1), the single End3 homologue of *A. nidulans* (38% amino acid identity). In *S. cerevisiae*, End3p belongs to the family of proteins possessing an EH domain, members of which are implicated in endocytosis, vesicle transport, and signal transduction. End3p is part of the coat module protein complex along with
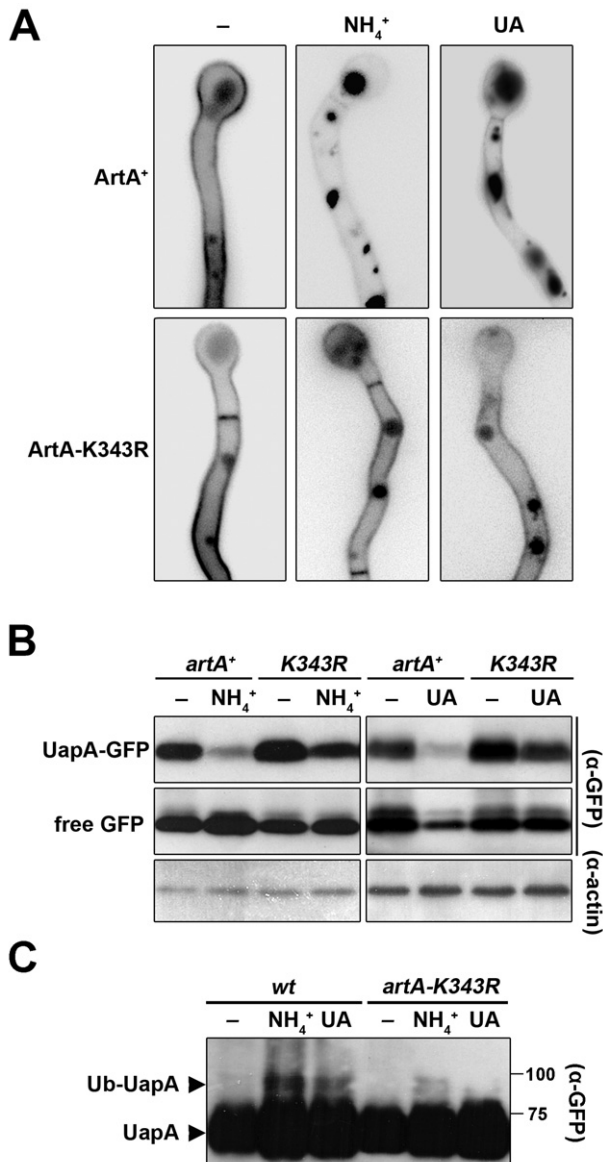
Fig. 6. Role of ArtA ubiquitination in UapA endocysis and turnover.
A. Epifluorescence microscopy of UapA-GFP subcellular localization under non-endocytic (−) or endocytic conditions (NH$_4^+$ or UA) in a wt or an ArtA-K343R mutant expressing UapA-GFP.
B. Western blot of total protein extracts of a wt (*artA*$^+$) and ArtA-K343R mutant strain, expressing UapA-GFP under non-endocytic (−) or in the presence of UA or NH$_4^+$ for 2 h.
C. Western blot analysis of UapA-GFP ubiquitination in membrane enriched fractions of a wt (ArtA$^+$) and an ArtA-K343R strain, grown under endocytic (30 min, NH$_4^+$) or control conditions.
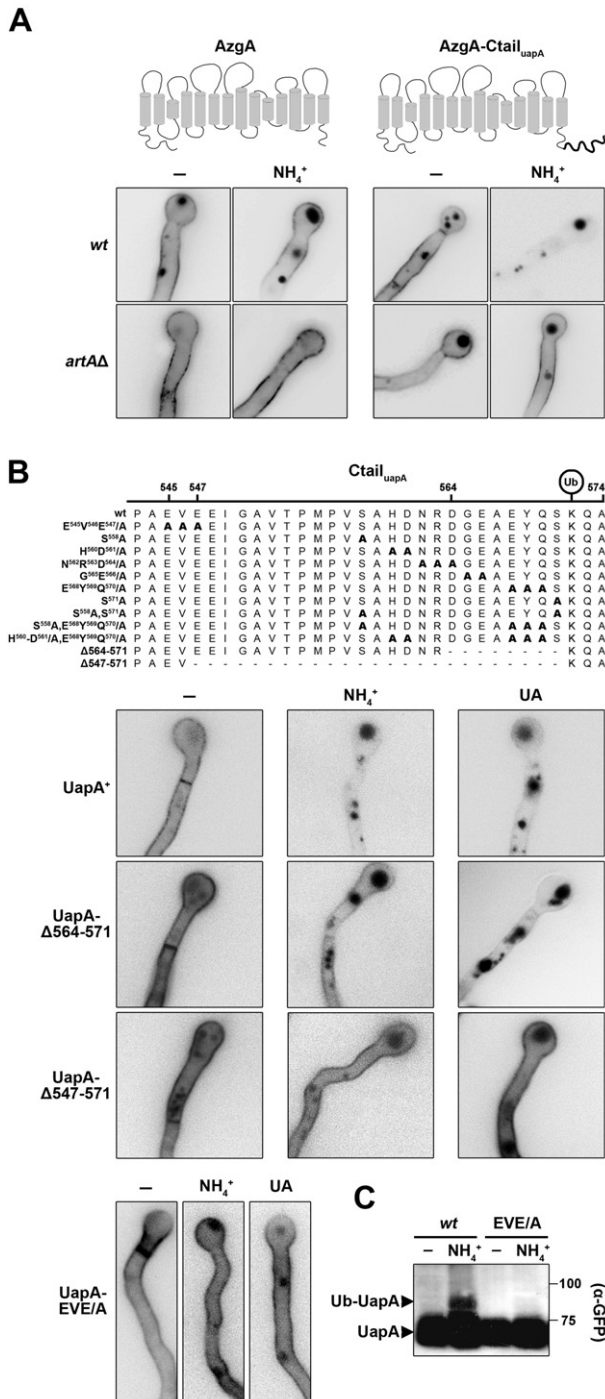
Pan1p, Sla1p and Sla2p, otherwise known as the Pan1 complex, which acts downstream of cargo ubiquitination, but upstream of actin organization at endocytic sites (Tang *et al.*, 2000). Furthermore, End3p has been shown to be necessary for the internalization of all transporters tested up-to date. The *sagA* gene has been genetically

identified as a gene that only affects sensitivity to DNA-damaging agents (Jones *et al.*, 1999). An apparent loss-of-function mutation in *sagA* has no detectable mutant phenotype, other than an increase in DNA alkylating agent sensitivity. A knock-out *sagA* mutant constructed for this work (see *Experimental procedures*) has a moderately delayed rate of growth, increased resistance to neomycin and enhanced frequency of bipolar emergence of germ tubes (Fig. S1A). Finally, a functional GFP-tagged SagA protein shows punctuate cortical subcellular localization (Fig. S1B), typical of other endocytic markers (Araujo-Bazán *et al.*, 2008).

We compared UapA-GFP expression in *artA*Δ, *sagA*Δ or *artA*Δ*sagA*Δ null mutants by constructing the appropriate isogenic strains (see *Experimental procedures*). Figure 8A shows that upon imposing an endocytic signal, either by NH$_4^+$ or substrates, there was a clear difference in the plasma membrane localization of UapA-GFP in the wild-type and in *artA*Δ, *sagA*Δ or *artA*Δ*sagA*Δ mutant backgrounds. In wild-type, as expected, UapA-GFP was internalized into mobile structures, apparently early endosomes, and sorted to the MVB/vacuole for degradation. As a consequence the amount of UapA-GFP remaining in the plasma membrane was reduced. In the *artA*Δ mutant UapA-GFP remained stable in the plasma membrane, marking the periphery of cells in a relatively homogeneous manner, similar to the picture obtained in all three strains under non-endocytic conditions. In the *sagA*Δ mutant, under endocytic conditions, UapA-GFP remained largely in or close to the plasma membrane, but in contrast to *artA*Δ, it also formed very distinctive cortical foci. Using an inverted fluorescent microscope we noticed that these puncta, which are very probably pre-endocytic membrane invaginations, are relatively static and remain attached to the plasma membrane, in mark contrast to the mobile early endosomes, seen in the wild-type strain. In the double mutant *artA*Δ *sagA*Δ, UapA-GFP remained stable in the plasma membrane, without forming cortical patches, similar to the single *artA*Δ mutant. This result strongly suggested that ArtA is implicated in UapA endocytosis at a step taking place in the plasma membrane, upstream of the action of SagA and the formation of pre-endocytic invaginations containing UapA-GFP.

To further confirm the above idea, we also tested whether blocking UapA ubiquitination by mutation K572R would have an effect on the formation of SagA-dependent, UapA-GFP-specific pre-endocytic invaginations. Figure 8B shows that blocking UapA ubiquitination also blocked the formation of pre-endocytic invaginations containing UapA-GFP in the *sagA*Δ background. Our results confirm that UapA ubiquitination takes place in the plasma membrane rather than in an early endosomal compartment, such as early endosomes.

Fig. 7. The C-tail of UapA contains a region essential for ubiquitination and endocytosis.
A. ArtA-dependent, NH₄⁺-elicited, endocytosis of an AzgA-GFP version including the C-terminus of UapA, as shown by epifluorescence microscopy.
B. Upper panel: schematic representation of UapA C-tail mutations analysed for UapA endocytosis. Lys-572 acting as ubiquitin acceptor is indicated. Lower panels: Epifluorescence microscopy of UapA C-terminal truncations (Δ564–571, Δ547–571) and mutation UapA-E545A/V546A/E547A (UapA-EVE/A) under non-endocytic (−) or endocytic conditions (NH₄⁺ or UA).
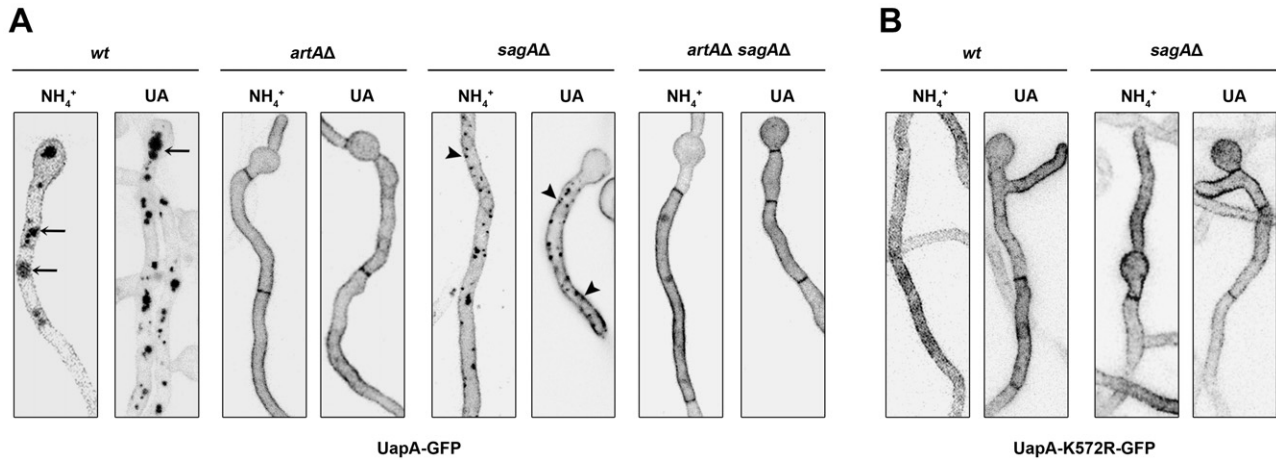C. Western blot analysis of UapA-GFP ubiquitination in membrane enriched fractions of a wt and a UapA-EVE/A strain, grown under endocytic (30 min, NH₄⁺) or control conditions.

triggered (AzgA; G. Diallinas, unpubl. obs.) endocytosis. Notably, all these transporters belong to structurally and evolutionary distinct transporter families (Diallinas, 2008). Figure 9 shows that ArtA is necessary for PrnB and AzgA endocytosis, but does not affect AgtA internalization (see also Fig. S2).

Discussion

Arrestin-like proteins have proved to be major adaptors of Rsp5/Nedd4-like ubiquitin ligases controlling the turnover of transporters through the control of the rate of ubiquitination, which is the primary molecular signal for cargo endocytosis (Lin *et al.*, 2008; Nikko *et al.*, 2009; Nikko and Pelham, 2009; Léon and Haguenauer-Tsapis, 2009; Hatakeyama *et al.*, 2010; MacGurn *et al.*, 2011; Becuwe *et al.*, 2012). Here we show that *A. nidulans* is not an exception. ArtA is involved in the endocytosis of UapA by mediating its ubiquitination via the HulA ubiquitin ligase, in response to the presence of ammonium or substrates. We further showed that a small fraction of ArtA is constitutively ubiquitinated and that ArtA ubiquitination is critical for efficient UapA ubiquitination and internalization from the plasma membrane. Furthermore, we have detected a small but repeatable increase in the fraction of ubiquitinated ArtA in response to NH₄⁺, but not in response to substrates.

The fact that ArtA controls UapA ubiquitination and endocytosis in response to both ammonium and substrates leads to an apparent paradox. Ammonium-elicited endocytosis is a broad range physiological response concerning probably all transporters involved in the uptake of nitrogenous compounds that can be used as secondary nitrogen sources, such as purines, amino acids or nitrate (Dupré *et al.*, 2004; Pantazopoulou and Diallinas, 2007). The physiological rationale for this is that when ammonium is present in the media as a primary nitrogen source, there is no need for taking up other nitrogenous compounds through their specific transporters, which are consequently internalized and turned-over. In contrast to ammonium-elicited endocytosis, substrate-elicited endo-

Specificity of ArtA in respect to transporter endocytosis

We also investigated the substrate specificity of ArtA by examining what is the effect of deleting the *artA* gene on other transporters. We constructed *artAΔ* mutants expressing GFP-tagged transporters for L-proline (PrnB), L-glutamate (AgtA) or purines (AzgA), proteins that undergo ammonium-elicited (PrnB and AgtA; Tavoularis *et al.*, 2001 and Apostolaki *et al.*, 2009) or substrate-

A

B

UapA-GFP

UapA-K572R-GFP

Fig. 8. SagA and ArtA block UapA internalization at distinct steps of endocytosis.
A. Confocal laser microscopy of UapA-GFP subcellular localization under endocytic conditions (NH_4^+ or UA) in isogenic wt, *artAΔ*, *sagAΔ* and *artAΔ/sagAΔ* strains expressing UapA-GFP.
B. Confocal laser microscopy of UapA-K572R-GFP subcellular localization under endocytic conditions (NH_4^+ or UA) in isogenic wt and *sagAΔ* strains expressing UapA-GFP. Arrows indicate vacuoles. Arrowheads indicate immobile cortical puncta associated with the PM, only visible in the *sagAΔ* genetic background.

cytosis is a highly specific signal, which seems to concern a single transporter in each case (Amillis *et al.*, 2007; Vlanti and Diallinas, 2008; Gournas *et al.*, 2010; G. Diallinas, unpubl. results). The presence of UapA substrates in the media does not affect the plasma localization of several transporters (e.g. PrnB, AgtA and AzgA) specific for other solutes, while UapA has never been observed to undergo endocytosis in response to other nitrogen-containing solutes, such as urea, nitrate, proline, aspartate, uracil, adenine, hypoxanthine or allantoin (G. Diallinas and S. Amillis, unpubl. obs.). The most interesting difference observed when comparing ammonium- to substrate-elicited UapA endocytosis is that the first operates on both active and inactive versions of the transporter, whereas the second is absolutely dependent on UapA activity (Gournas *et al.*, 2010). If arrestins respond to broad-range signals, like shifts in N or C sources or stress, through their dephosphorylation, ubiquitination, activation and recruitment to plasma membrane cargoes, as reported in a number of recent publications (MacGurn *et al.*, 2011; Becuwe *et al.*, 2012; Merhi and André, 2012), then how could this model account for the role of arrestin-like proteins in specific substrate-elicited endocytosis of a given transporter?

We have previously presented strong evidence that substrate-elicited endocytosis of UapA occurs through a mechanism, which senses subtle conformational changes associated with the transport cycle in the absence of any physiological or stress signal (Gournas *et al.*, 2010). Based on this, and results obtained with arrestin-like proteins in *S. cerevisiae* and in the present work, we propose a speculative model on how the same arrestin-like protein, ArtA, can operate in response to conditions that generate a broad-range signal concerning several transporters, but can also act specifically on UapA, when this protein is actively transporting its substrates.

The model proposed is the following. A small fraction of ArtA is constitutively ubiquitinated under conditions of relatively poor nitrogen supply. The level of ubiquitinated ArtA might be directly related to the level of cellular primary pools of nitrogen (e.g. NH_4^+) originating from the catabolism of secondary nitrogen sources (e.g. purines, amino acids, etc.). The ubiquitinated fraction of ArtA has increased capacity, relative to non-ubiquitinated ArtA, for recruiting HulA and is responsible for basal level endocytosis of several transporters specific for secondary nitrogen sources. Upon addition of a primary nitrogen source (e.g. NH_4^+) an increase in the levels of ubiquitinated ArtA takes place, probably via a dephosphorylation step as recent reports on other arrestin-like proteins have proposed (MacGurn *et al.*, 2011; Becuwe *et al.*, 2012; Merhi and André, 2012), leading to an increase in the rate of transporter endocytosis. Interestingly however, here we showed that although *artA* mutations in either the PPxY motives or K343 lead to total block of ArtA ubiquitination (see Fig. 5A), mutations in the former have a more severe effect on UapA-GFP turnover than K343R (compare Fig. 4C with Fig. 6C). This last observation suggests that non-ubiquitinated ArtA molecules, which however retain intact PPxY elements and thus are in principle able to interact with HulA, can still lead to moderate UapA ubiquitination and turnover. In other words, it seems that maximum ArtA activity, which is probably needed in response to a broad range physiological signal such as addition of NH_4^+, necessitates ArtA ubiquitination, but non-ubiquitinated ArtA might still conserve a minor activity in
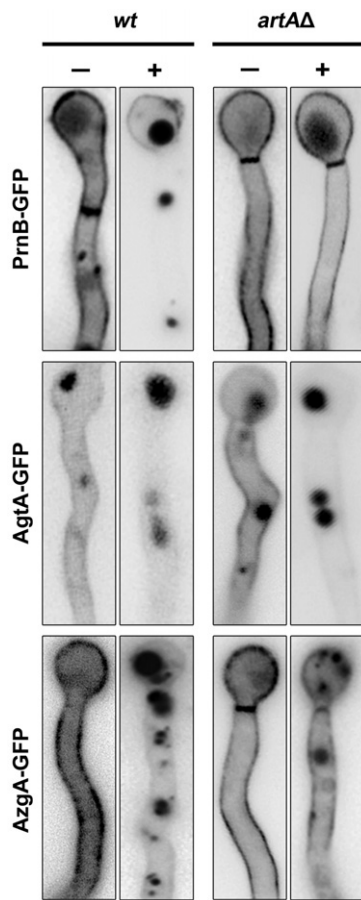
Fig. 9. Specificity of ArtA in respect to the endocytosis of different transporter cargoes. Epifluorescence microscopy of PrnB-GFP, AgtA-GFP, AzgA-GFP in *artAΔ* and *artA*+ (wt) backgrounds under non-endocytic (−) or endocytic conditions (+). Endocytic conditions for PrnB and AgtA indicate addition of NH$_4$+ and for AzgA addition substrate (Hypoxanthine) for 2 h. AgtA-GFP consistently gives a lower fluorescent signal compared to the other transporters tested. Notice that, unlike UapA-GFP or AzgA-GFP, AgtA-GFP and PrnB-GFP show a degree of constitutive turnover (appearance of GFP-labelled vacuoles) under non-endocytic conditions. For AgtA, this was recently shown to occur by direct sorting from the Golgi to the vacuole (S. Amillis, unpubl. obs.).

recruiting HulA on transporters. In the absence of a signal for activation (e.g. absence of NH$_4$+), ArtA remains probably phosphorylated and little ubiquitinated, showing very low affinity for cargoes. In the presence of a substrate however, when UapA becomes active, conformational changes associated with transport catalysis might increase the affinity of the transporter for non-ubiquitinated or/and for the small fraction of constitutively ubiquitinated ArtA, and thus elicit its enhanced ubiquitination and internalization.

This scenario also predicts that activation of ArtA is related to its ability to find its cargoes and not to a catalytic activation *per se*. In line with this, Lin *et al.* (2008) showed that Rsp5-mediated ubiquitination is required for the 'correct' plasma membrane subcellular localization of

Art1p in *S. cerevisiae*, while Hervás-Aguilar *et al.* (2010) showed that PalF ubiquitination is a key molecular trigger required for transmitting the alkaline pH signal from the plasma membrane to downstream elements of a pH-responding pathway in *A. nidulans*. Interestingly, overexpression of ArtA using the *alcA* promoter leads to relatively increased constitutive UapA endocytosis in the absence of ammonium or substrate (Fig. S3), an observation that is also in line with the idea that arrestin-like proteins can act on their cargoes in the absence of any physiological or stress signal.

We could not obtain any rigorous evidence of ArtA recruitment to the plasma membrane upon imposing endocytic conditions for UapA (not shown). We do not have an explanation on the reasons of the very low and diffuse fluorescent signal of ArtA-GFP expressed under native or strong promoters, but it seems that detecting the subcellular localization of arrestin-like proteins is not an easy task. To our knowledge, there is only a single case, that of Art1p in *S. cerevisiae*, where the subcellular localization of arrestin-like protein has been reported (Lin *et al.*, 2008; MacGurn *et al.*, 2011). In that case, Art1p was shown to be present in cytosolic foci colocalizing with a Golgi marker under control conditions, but associate transiently with the plasma membrane under endocytic conditions. We failed to obtain similar evidence for ArtA. However, ArtA ubiquitination does not take place in a HulA allele missing the C2 domain and thus unable to be recruited to the plasma membrane (*hulAΔC2*). This suggests that ArtA ubiquitination might occur in the plasma membrane.

At least two other *A. nidulans* transporters, specific for the uptake of nitrogenous compounds, PrnB (L-proline) and AzgA (purines) seem to be substrates of ArtA, either in response to ammonium (PrnB) or substrate (AzgA). The observation that overexpression of ArtA leads to reduced growth rates (not shown) suggests that several other transporters might also be substrates of this arrestin-like adaptor. Is there a recognizable common motif in these transporters that might act as a possible ArtA binding site? We showed that the ArtA putative binding site in UapA lies in its C-terminal region (residues 545–561), and interestingly, a di-acidic motif (E^{545}-V-E^{547}) in this region is essential for ArtA-dependent UapA ubiquitination and endocytosis. Similar di-acidic motives are present in the C- or N-terminal regions of other transporters under ArtA control, such as PrnB or AzgA.

Experimental procedures

Strains, classical and reverse genetics, media and growth conditions

Aspergillus nidulans strains used are listed in Table S1. Newly made null mutant strains and in locus gene tagging were constructed by transformation in an *nkuA* DNA helicase defi-

cient strain (TNO2A7; Nayak *et al.*, 2006), allowing only homologous recombination events, based on the *A. fumigatus* markers orotidine-5′-phosphate-decarboxylase (AF*pyrG*, Afu2g0836) or GTP-cyclohydrolase II (AF*riboB*, Afu1g13300), resulting in complementation of auxotrophies for uracil/uridine (*pyrG89*) or riboflavin (*riboB2*) respectively. Mutants of *uapA*-GFP were constructed by transformation of a strain lacking all major purine transporters *uapA*, *uapC* and *azgA* (ΔACZ) based on the *A. nidulans* ornithine-carbamoyltransferase (ANID_04409.3), complementing the arginine auxotrophic mutation *argB2*. Transformation of *A. nidulans* was performed according to Koukaki *et al.* (2003). Derivatives of mutant strains were made with standard genetic crossing using auxotrophic markers for heterokaryon establishment. Standard complete (CM) and minimal media (MM) for *A. nidulans* were used (http://www.fgsc.net). Auxotrophies were supplemented at the concentrations given in (http://www.gla.ac.uk/acad/ibls/molgen/aspergillus/supplement.html). Media and chemical reagents were obtained from Sigma-Aldrich (Life Science Chemilab SA) or AppliChem (Bioline Scientific SA). Nitrogen sources were used at the final concentrations: urea 5 mM, NaNO₃ 10 mM, ammonium L-(+)-tartrate 10 mM. Allantoin, purines and nucleosides were used at 0.5 mM. Amino acids were used at 5 mM. Nucleobase and nucleoside analogues were used at the final concentrations: 8-Aza-guanine 0.2-0.4 mM, 5-Fluoro-cytosine 20–50 μM, 5-Fluoro-uracil 40–100 μM, 5-Fluoro-uridine 5–10 μM, in the presence of NaNO₃ as sole nitrogen source. Allopurinol was used at 1–3 μM with hypoxanthine as sole nitrogen source. The amino acid toxic analogues D-serine and p-Fluoro-DL-phenylalanine were used at 2–5 mM and 25–50 μM respectively, in the presence of NaNO₃ as sole nitrogen source. 2-Thio-urea was used at 0.25–0.5 mM in the presence of NaNO₃ as sole nitrogen source. Neomycin sulphate was used at 2 mg ml⁻¹. Uracil and uridine were used at 5 mM and 10 mM respectively. Derepression of UapA expression from the *alcA_p* promoter was achieved after 14 h of growth in MM supplemented with urea or NaNO₃ and 0.1% (w/v) fructose as carbon source. Repression of UapA expressed was achieved in MM supplemented with urea or NaNO₃ and 1% (w/v) glucose. Induction of UapA expression from the *alcA_p* promoter was achieved by addition of 0.4% (v/v) ethanol in derepressing media.

DNA manipulations

Plasmid preparation from *Escherichia coli* strains was performed using the Qiagen Plasmid Mini Kit. DNA bands were purified from agarose gels using the MinElute Gel Extraction Kit (Qiagen GmbH, Hilden, Germany), or the Nucleospin Extract II kit (Macherey-Nagel, Lab Supplies Scientific SA) according to the manufacturer's instructions. High fidelity PCR reactions were carried out using the Phusion® Flash High-Fidelity PCR Master Mix (New England Biolabs GmbH, Frankfurt, Germany), or the KAPA HiFi HotStart ReadyMix (Kapa Biosystems, Lab Supplies Scientific SA). Conventional PCR reactions were carried out using the REDTaq® ReadyMix™ (Sigma-Aldrich Handels GmbH, Vienna, Austria), or the KAPATaq DNA polymerase (Kapa Biosystems, Lab Supplies Scientific SA). Restriction enzymes and T4-ligases used were purchased from Takara (Takara Bio Inc, Lab Supplies Scientific SA) and Fermentas (Fermentas GmbH, St.

Leon-Rot, Germany). [³²P]-dCTP labelled DNA molecules for Southern blots were prepared by a random hexanucleotide-primer Kit (New England Biolabs, Bioline Scientific SA) and purified on MicroSpin™ S-200 HR columns, following the supplier's instructions (Roche Diagnostics). Labelled [³²P]-dCTP (3000 Ci mmol⁻¹) was purchased from the Institute of Isotops Co., Ltd (Miklós, Budapest, Hungary). Primers were purchased by Sigma-Aldrich (Sigma-Aldrich Handels GmbH, Vienna, Austria), or VBC-Genomics (Vienna, Austria). DNA sequences were determined by VBC-Genomics (Vienna, Austria). Mutations were constructed by site-directed mutagenesis according to the instructions accompanying the Quik-Change® Site-Directed Mutagenesis Kit (Agilent Technologies, Stratagene). Targeted gene deletion and in locus gene tagging were carried out by transformation with linear cassettes containing upstream and downstream flanking regions of the corresponding ORFs and the *A. fumigatus* markers AF*pyrG* or AF*riboB* (see also Experimental procedures in Supporting Information, DNA manipulations and Table S5).

Microscopy

Preparations of samples for fluorescence microscopy and growth conditions are described in Gournas *et al.* (2010). Staining with FM4-64 and CMAC (7-amino-4-chloromethyl coumarin) (Life Technologies, Molecular Probes, Invitrogen, Antisel SA) was according to Gournas *et al.* (2010). Calcofluor white (Sigma-Aldrich, Life Science Chemilab SA) staining was performed according to Bitsikas *et al.* (2010). For endocytosis, uric acid (UA) or ammonium L-(+)-tartrate (NH₄⁺) were added at concentrations of 0.5 mM or 10–20 mM respectively for 2 h before observation. Samples were observed on an Axioplan Zeiss phase-contrast epifluorescent microscope and the resulting images were acquired with a Zeiss-MRC5 digital camera using the AxioVs40 V4.40.0 software. Image processing, contrast adjustment and colour combining were made using the Adobe Photoshop CS4 Extended version 11.0.2 software or the ImageJ software. Images were converted to 8-bit grayscale or RGB and annotated using Photoshop CS4 before being saved to TIFF. A confocal laser DMR upright microscope and a wide-field time-lapse Olympus IX-81 Cell-R imaging system for Live Cell Imaging System were also used (http://www.pasteur.gr). The Confocal system operates with the Image acquisition and analysis Leica Confocal Software LCS.

Transport assays

Radiolabelled [³H]-xanthine (33.4 Ci mmol⁻¹) was from Moravek Biochemicals (Brea, CA, USA). [³H]-xanthine uptake was assayed as described previously and was carried out in triplicate (Koukaki *et al.*, 2005; Papageorgiou *et al.*, 2008).

Protein manipulations

Total protein extracts were prepared from mycelium in liquid cultures incubated for 12–14 h at 25°C before the addition of substrates or NH₄⁺, or induction for the *alcA* driven UapA expression, as described in Apostolaki *et al.* (2012). UapA-

His purification was carried out as in Lemuh *et al.* (2009) using Protino Ni-NTA Columns (Macherey-Nagel GmbH, Lab Supplies Scientific SA). For immunoprecipitation under denaturing conditions, total protein extracts were first resuspended in extraction buffer, containing 50 mM Tris-HCl, pH 7.5, 2 mM EDTA, 100 mM NaCl, 2% SDS, protease inhibitor cocktail (PIC) (Sigma-Aldrich, Life Science Chemilab SA) and 20 mM *N*-ethylmaleimide (NEM). Immunoprecipitation buffer (IP: 50 mM Tris-HCl, pH 7.5, 2 mM EDTA, 150 mM NaCl, 1% Triton X-100, 0.5% sodium deoxycholate, PIC and 20 mM NEM) was added, and lysates were incubated with 4 µg anti-GFP with gentle rotation at 4°C for 2 h, followed by addition of A-Protein Sepharose CL-4B beads (Sigma-Aldrich, Life Science Chemilab SA) and incubation with gentle rotation at 4°C for 12 h. The beads were washed twice with IP buffer, once with a buffer containing 50 mM Tris-HCl, pH 7.5, 2 mM EDTA, 250 mM NaCl, 0.5% Triton X-100, 0.05% sodium deoxycholate, PIC and 20 mM NEM, once with a buffer containing 50 mM Tris-HCl, pH 7.5, 1 mM EDTA, 500 mM NaCl, 0.1% Triton X-100, PIC and 20 mM NEM and once with a buffer containing 50 mM Tris-HCl, pH 7.5, 1 mM EDTA, 100 mM NaCl, and PIC and were finally boiled for 5 min at 95°C in protein sample buffer. Detection of ubiquitinated UapA-GFP was achieved in membrane-enriched protein fractions according to Galan *et al.* 1996. Protein concentrations were determined by the method of Bradford. In each case 30–50 µg protein were fractionated on 8–10% SDS-PAGE gel and electroblotted (Mini PROTEAN™ Tetra Cell, BIO-RAD) onto a PVDF membrane (Macherey-Nagel GmbH, Lab Supplies Scientific SA). Immunodetection was performed using a primary mouse anti-GFP monoclonal antibody (Roche Diagnostics), a mouse anti-actin monoclonal (C4) antibody (MP Biomedicals Europe, Lab Supplies Scientific SA), an Anti-His (PentaHis HRP Conjugate; Qiagen, SafeBlood BioAnalytica SA), an Anti-Ubiquitin (Ub-P4D1 HRP Conjugate; Santa Cruz Biotechnology, SafeBlood BioAnalytica SA) and a secondary goat anti-mouse IgG HRP-linked antibody (Cell Signaling Technology Inc., Bioline Scientific SA) and detected by the chemiluminescent method using the LumiSensor Chemiluminescent HRP Substrate kit (GenScript USA Inc, Lab Supplies Scientific SA).

Acknowledgements

References

Abreu, C., Sanguinetti, M., Amillis, S., and Ramon, A. (2010) UreA, the major urea/H+ symporter in *Aspergillus nidulans*. *Fungal Genet Biol* **47:** 1023–1033.

Amillis, S., Hamari, Z., Roumelioti, K., Scazzocchio, C., and Diallinas, G. (2007) Regulation of expression and kinetic modeling of substrate interactions of a uracil transporter in *Aspergillus nidulans*. *Mol Membr Biol* **24:** 206–214.

Amillis, S., Kosti, V., Pantazopoulou, A., Mikros, E., and Diallinas, G. (2011) Mutational analysis and modeling reveal functionally critical residues in transmembrane segments 1 and 3 of the UapA transporter. *J Mol Biol* **411:** 567–580.

André, B., and Haguenauer-Tsapis, R. (2004) Membrane trafficking of yeast transporters: mechanisms and physiological control of downregulation. *Top Curr Genet* **9:** 273–323.

Apostolaki, A., Erpapazoglou, Z., Harispe, L., Billini, M., Kafasla, P., Kizis, D., *et al.* (2009) AgtA, the dicarboxylic amino acid transporter of *Aspergillus nidulans*, is concertedly down-regulated by exquisite sensitivity to nitrogen metabolite repression and ammonium-elicited endocytosis. *Eukaryot Cell* **8:** 339–352.

Apostolaki, A., Harispe, L., Calcagno-Pizarelli, A.M., Vangelatos, I., Sophianopoulou, V., Arst, H.N. Jr, *et al.* (2012) *Aspergillus nidulans* CkiA is an essential casein kinase I required for delivery of amino acid transporters to the plasma membrane. *Mol Microbiol* **84:** 530–549.

Araujo-Bazán, L., Peñalva, M.A., and Espeso, E.A. (2008) Preferential localization of the endocytic internalization machinery to hyphal tips underlies polarization of the actin cytoskeleton in *Aspergillus nidulans*. *Mol Microbiol* **67:** 891–905.

Becuwe, M., Vieira, N., Lara, D., Gomes-Rezende, J., Soares-Cunha, C., Casal, M., *et al.* (2012) A molecular switch on an arrestin-like protein relays glucose signaling to transporter endocytosis. *J Cell Biol* **23:** 247–259.

Belgareh-Touzé, N., Léon, S., Erpapazoglou, Z., Stawiecka-Mirota, M., Urban-Grimal, D., and Haguenauer-Tsapis, R. (2008) Versatile role of the yeast ubiquitin ligase Rsp5p in intracellular trafficking. *Biochem Soc Trans* **36:** 791–796.

Bitsikas, V., Karachaliou, M., Gournas, C., and Diallinas, G. (2010) Hypertonic conditions trigger transient plasmolysis, growth arrest and blockage of transporter endocytosis in *Aspergillus nidulans* and *Saccharomyces cerevisiae*. *Mol Membr Biol* **28:** 54–68.

Boase, N.A., and Kelly, J.M. (2004) A role for *creD*, a carbon catabolite repression gene from *Aspergillus nidulans*, in ubiquitination. *Mol Microbiol* **53:** 929–940.

Bonifacino, J.S., and Traub, L.M. (2003) Signals for sorting of transmembrane proteins to endosomes and lysosomes. *Annu Rev Biochem* **72:** 395–447.

Cain, N.E., and Kaiser, C.A. (2011) Transport activity-dependent intracellular sorting of the yeast general amino acid permease. *Mol Biol Cell* **22:** 1919–1929.

Cecchetto, G., Amillis, S., Diallinas, G., Scazzocchio, C., and Drevet, C. (2004) The AzgA purine transporter of *Aspergillus nidulans*. Characterization of a protein belonging to a new phylogenetic cluster. *J Biol Chem* **279:** 3132–3141.

Darlington, A.J., and Scazzocchio, C. (1967) Use of analogues and the substrate-sensitivity of mutants in analysis of purine uptake and breakdown in *Aspergillus nidulans*. *J Bacteriol* **93:** 937–940.

Diallinas, G. (2008) *Aspergillus* transporters. In *The Aspergilli. Genomics, Medical Applications, Biotechnology, and Research Methods*. Osmani, A., and Gustavo Goldman, H. (eds). Boca Raton, FL: CRC Press, pp. 297–316.

Diallinas, G., and Gournas, C. (2008) Structure-function relationships in the nucleobase-ascorbate transporter (NAT) family: lessons from model microbial genetic systems. *Channels* **2:** 363–372.

Diallinas, G., and Scazzocchio, C. (1989) A gene coding for the uric acid-xanthine permease of *Aspergillus nidulans*: inactivational cloning, characterization, and sequence of a *cis*-acting mutation. *Genetics* **122:** 341–350.

Diallinas, G., Gorfinkiel, L., Arst, H.N. Jr, Cecchetto, G., and Scazzocchio, C. (1995) Genetic and molecular characterization of a gene encoding a wide specificity purine permease of *Aspergillus nidulans* reveals a novel family of transporters conserved in prokaryotes and eukaryotes. *J Biol Chem* **270:** 8610–8622.

Dupré, S., Urban-Grimal, D., and Haguenauer-Tsapis, R. (2004) Ubiquitin and endocytic internalization in yeast and animal cells. *Biochim Biophys Acta* **169:** 89–111.

Foley, K., Boguslavsky, S., and Klip, A. (2011) Endocytosis, recycling, and regulated exocytosis of glucose transporter 4. *Biochemistry* **50:** 3048–3061.

Galan, J.M., Moreau, V., Andre, B., Volland, C., and Haguenauer-Tsapis, R. (1996) Ubiquitination mediated by the Npi1p/Rsp5p ubiquitin-protein ligase is required for endocytosis of the yeast uracil permease. *J Biol Chem* **271:** 10946–10952.

Goodman, O.B. Jr, Krupnick, J.G., Santini, F., Gurevich, V.V., Penn, R.B., Gagnon, A.W., *et al.* (1996) Beta-arrestin acts as a clathrin adaptor in endocytosis of the beta2-adrenergic receptor. *Nature* **383:** 447–450.

Gournas, C., Papageorgiou, I., and Diallinas, G. (2008) The nucleobase-ascorbate transporter (NAT) family: genomics, evolution, structure-function relationships and physiological role. *Mol Biosyst* **4:** 404–416.

Gournas, C., Amillis, S., Vlanti, A., and Diallinas, G. (2010) Transport-dependent endocytosis and turnover of a uric acid-xanthine permease. *Mol Microbiol* **75:** 246–260.

Hamari, Z., Amillis, S., Drevet, C., Apostolaki, A., Vágvölgyi, C., Diallinas, G., and Scazzocchio, C. (2009) Convergent evolution and orphan genes in the Fur4p-like family and characterization of a general nucleoside transporter in *Aspergillus nidulans*. *Mol Microbiol* **73:** 43–57.

Hatakeyama, R., Kamiya, M., Takahara, T., and Maeda, T. (2010) Endocytosis of the aspartic acid/glutamic acid transporter Dip5 is triggered by substrate-dependent recruitment of the Rsp5 ubiquitin ligase via the arrestin-like protein Aly2. *Mol Cell Biol* **30:** 5598–5607.

Helliwell, S.B., Losko, S., and Kaiser, C.A. (2001) Components of a ubiquitin ligase complex specify polyubiquitination and intracellular trafficking of the general amino acid permease. *J Cell Biol* **153:** 649–662.

Herrador, A., Herranz, S., Lara, D., and Vincent, O. (2010) Recruitment of the ESCRT machinery to a putative seven-transmembrane-domain receptor is mediated by an arrestin-related protein. *Mol Cell Biol* **30:** 897–907.

Herranz, S., Rodríguez, J.M., Bussink, H.J., Sánchez-Ferrero, J.C., Arst, H.N. Jr, Peñalva, M.A., and Vincent, O. (2005) Arrestin-related proteins mediate pH signaling in fungi. *Proc Natl Acad Sci USA* **102:** 12141–12146.

Hervás-Aguilar, A., Galindo, A., and Peñalva, M.A. (2010) Receptor-independent Ambient pH signaling by ubiquitin attachment to fungal arrestin-like PalF. *J Biol Chem* **285:** 18095–18102.

Hettema, E.H., Valdez-Taubas, J., and Pelham, H.R. (2004) Bsd2 binds the ubiquitin ligase Rsp5 and mediates the ubiquitination of transmembrane proteins. *EMBO J* **23:** 1279–1288.

Hicke, L., and Dunn, R. (2003) Regulation of membrane protein transport by ubiquitin and ubiquitin-binding proteins. *Annu Rev Cell Dev Biol* **19:** 141–172.

Jones, G.W., Hooley, P., Farrington, S.M., Shawcross, S.G., Iwanejko, L.A., and Strike, P. (1999) Cloning and characterisation of the *sagA* gene of *Aspergillus nidulans*: a gene which affects sensitivity to DNA-damaging agents. *Mol Gen Genet* **261:** 251–258.

Kee, Y., Muñoz, W., Lyon, N., and Huibregtse, J.M. (2006) The deubiquitinating enzyme Ubp2 modulates Rsp5-dependent Lys-63-linked polyubiquitin conjugates in *Saccharomyces cerevisiae*. *J Biol Chem* **281:** 36724–36731.

Kosti, V., Papageorgiou, I., and Diallinas, G. (2011) Dynamic elements at both cytoplasmically and extracellularly facing sides of the UapA transporter selectively control the accessibility of substrates to their translocation pathway. *J Mol Biol* **397:** 1132–1143.

Koukaki, M., Giannoutsou, E., Karagouni, A., and Diallinas, G. (2003) A novel improved method for *Aspergillus nidulans* transformation. *J Microbiol Methods* **55:** 687–695.

Koukaki, M., Vlanti, A., Goudela, S., Pantazopoulou, A., Gioule, H., Tournaviti, S., and Diallinas, G. (2005) The nucleobase-ascorbate transporter (NAT) signature motif in UapA defines the function of the purine translocation pathway. *J Mol Biol* **350:** 499–513.

Krypotou, E., Kosti, V., Amillis, S., Myrianthopoulos, V., Mikros, E., and Diallinas, G. (2012) Modeling, substrate docking, and mutational analysis identify residues essential for the function and specificity of a eukaryotic purine-cytosine NCS1 transporter. *J Biol Chem* **287:** 36792–36803.

Lauwers, E., Erpapazoglou, Z., Haguenauer-Tsapis, R., and André, B. (2010) The ubiquitin code of yeast permease trafficking. *Trends Cell Biol* **20:** 196–204.

Lemuh, N.D., Diallinas, G., Frillingos, S., Mermelekas, G., Karagouni, A.D., and Hatzinikolaou, D.G. (2009) Purification and partial characterization of the xanthine-uric acid transporter (UapA) of *Aspergillus nidulans*. *Protein Expr Purif* **63:** 33–39.

Léon, S., and Haguenauer-Tsapis, R. (2009) Ubiquitin ligase adaptors: regulators of ubiquitylation and endocytosis of plasma membrane proteins. *Exp Cell Res* **315:** 1574–1583.

Léon, S., Erpapazoglou, Z., and Haguenauer-Tsapis, R. (2008) Ear1p and Ssh4p are new adaptors of the ubiquitin ligase Rsp5p for cargo ubiquitylation and sorting at multivesicular bodies. *Mol Biol Cell* **19:** 2379–2388.

Lin, C.H., MacGurn, J.A., Chu, T., Stefan, C.J., and Emr, S.D. (2008) Arrestin-related ubiquitin-ligase adaptors regulate endocytosis and protein turnover at the cell surface. *Cell* **135:** 714–725.

Macgurn, J.A., Hsu, P.C., Smolka, M.B., and Emr, S.D. (2011) TORC1 regulates endocytosis via Npr1-mediated phosphoinhibition of a ubiquitin ligase adaptor. *Cell* **147:** 1104–1117.

McMahon, H.T., and Boucrot, E. (2011) Molecular mechanism and physiological functions of clathrin-mediated endocytosis. *Nat Rev Mol Cell Biol* **12:** 517–533.

Merhi, A., and André, B. (2012) Internal amino acids promote Gap1 permease ubiquitylation via TORC1/Npr1/14-3-3-dependent control of the Bul arrestin-like adaptors. *Mol Cell Biol* **32:** 4510–4522.

Nayak, T., Szewczyk, E., Oakley, C.E., Osmani, A., Ukil, L., Murray, S.L., *et al.* (2006) A versatile and efficient gene-targeting system for *Aspergillus nidulans*. *Genetics* **172:** 1557–1566.

Nikko, E., and Pelham, H.R. (2009) Arrestin-mediated endocytosis of yeast plasma membrane transporters. *Traffic* **10:** 1856–1867.

Nikko, E., Sullivan, J.A., and Pelham, H.R. (2009) Arrestin-like proteins mediate ubiquitination and endocytosis of the yeast metal transporter Smf1. *EMBO Rep* **9:** 1216–1221.

O' Donnell, A.F., Apffel, A., Gardner, R.G., and Cyert, M.S. (2010) Alpha-arrestins Aly1 and Aly2 regulate intracellular trafficking in response to nutrient signaling. *Mol Biol Cell* **21:** 3552–3566.

O'Donnell, A.F. (2012) The running of the Buls: control of permease trafficking by α-arrestins Bul1 and Bul2. *Mol Cell Biol* **32:** 4506–4509.

Pantazopoulou, A., and Diallinas, G. (2007) Fungal nucleobase transporters. *FEMS Microbiol Rev* **31:** 657–675.

Pantazopoulou, A., Lemuh, N.D., Hatzinikolaou, D.G., Drevet, C., Cecchetto, G., Scazzocchio, C., and Diallinas, G. (2007) Differential physiological and developmental expression of the UapA and AzgA purine transporters in *Aspergillus nidulans*. *Fungal Genet Biol* **44:** 627–640.

Papageorgiou, I., Gournas, C., Vlanti, A., Amillis, S., Pantazopoulou, A., and Diallinas, G. (2008) Specific interdomain synergy in the UapA transporter determines its unique specificity for uric acid among NAT carriers. *J Mol Biol* **382:** 1121–1135.

Renard, H.F., Demaegd, D., Guerriat, B., and Morsomme, P. (2010) Efficient ER exit and vacuole targeting of yeast Sna2p require two tyrosine-based sorting motives. *Traffic* **11:** 931–946.

Risinger, A.L., and Kaiser, C.A. (2008) Different ubiquitin signals act at the Golgi and plasma membrane to direct GAP1 trafficking. *Mol Biol Cell* **19:** 2962–2972.

Risinger, A.L., Cain, N.E., Chen, E.J., and Kaiser, C.A. (2006) Activity-dependent reversible inactivation of the general amino acid permease. *Mol Biol Cell* **17:** 4411–4419.

Rubio-Texeira, M., and Kaiser, C.A. (2006) Amino acids regulate retrieval of the yeast general amino acid permease from the vacuolar targeting pathway. *Mol Biol Cell* **17:** 3031–3050.

Soetens, O., De Craene, J.O., and Andre, B. (2001) Ubiquitin is required for sorting to the vacuole of the yeast general amino acid permease, Gap1. *J Biol Chem* **276:** 43949–43957.

Sorkin, A., and von Zastrow, M. (2009) Endocytosis and signalling: intertwining molecular networks. *Nat Rev Mol Cell Biol* **10:** 609–622.

Starr, T.L., Pagant, S., Wang, C.W., and Schekman, R. (2012) Sorting signals that mediate traffic of chitin synthase III between the TGN/endosomes and to the plasma membrane in yeast. *PLoS ONE* **7:** e46386.

Stimpson, H.E., Lewis, M.J., and Pelham, H.R. (2006) Transferrin receptor-like proteins control the degradation of a yeast metal transporter. *EMBO J* **25:** 662–672.

Tang, H.Y., Xu, J., and Cai, M. (2000) Pan1p, End3p, and S1a1p, three yeast proteins required for normal cortical actin cytoskeleton organization, associate with each other and play essential roles in cell wall morphogenesis. *Mol Cell Biol* **20:** 12–25.

Tavoularis, S., Scazzocchio, C., and Sophianopoulou, V. (2001) Functional expression and cellular localization of a green fluorescent protein-tagged proline transporter in *Aspergillus nidulans*. *Fungal Genet Biol* **33:** 115–125.

Vlanti, A., and Diallinas, G. (2008) The *Aspergillus nidulans* FcyB cytosine-purine scavenger is highly expressed during germination and in reproductive compartments and is downregulated by endocytosis. *Mol Microbiol* **68:** 959–977.

Supporting information

Additional supporting information may be found in the online version of this article at the publisher's web-site.

Ένζυμα καταβολισμού πουρινών στην τάξη Eurotiales: Ενδοκυτταρικός εντοπισμός, φυλογενετική συντήρηση και απόκλιση

Γαλανοπούλου Κ., Scazzocchio C., Γαληνού Μ. Ε., Liu W., Μπορμπόλης Φ.,Καραχάλιου Μ., Oestreicher N., Χατζηνικολάου Δ. Γ., Διαλλινάς Γ.* & Αμίλλης Σ.*

Περίληψη

Το μονοπάτι καταβολισμού των πουρινών έχει εκτενώς χαρακτηριστεί στον *Aspergillus nidulans.* Σε αυτή την εργασία περιγράφουμε τον υποκυτταρικό εντοπισμό επτά βασικών ενδοκυτταρικών ενζύμων, της αφυδρογονάσης της ξανθίνης (HxA), της οξειδάσης του ουρικού (UaZ), της υδρολάσης του 5-υδροξυ-ισο-ουρικού (UaX), της καρβοξυλάσης της 2-οξο-4-υδροξυ-4-καρβοξυ ουρεΐδο ιμιδαζολίνης (UaW), της αλλαντοϊνάσης (AlX), της αλλαντοϊκάσης (AaX), της λυάσης του ουρεϊδογλυκολικού οξέος (UglA) και την ειδική για τους μύκητες, σιδηρο Fe(II)-εξαρτώμενη διοξυγενάση του α-κετογλουταρικού οξέος (XanA). Τα ένζυμα HxA, AlX, AaX, UaW και XanA έχουν κυτταροπλασματικό εντοπισμό ενώ τα UaZ, UaX and UglA εντοπίζονται στα υπεροξεισώματα. Ο εντοπισμός στα υπεροξεισώματα επιβεβαιώθηκε από τη χρήση κατάλληλων *pex* μεταλλαγμένων στελεχών. Το μονοπάτι είναι ευρέως αλλά όχι εντελώς συντηρημένο στην κλάση Eurotiomycetes, ενώ σε κάποια είδη η AaX αντικαθίσταται από ένα εναλλακτικό ένζυμο, πιθανώς βακτηριακής προέλευσης. Επιπλέον, η UaZ και οι μεταφορείς ουρικού-ξανθίνης UapA και UapC εντοπίζονται σε ειδικά κύτταρα των κονιδιοφορέων. Στη παρούσα μελέτη δείχνουμε ότι η συσσώρευση μεταβολικά παραγόμενου ουρικού οξέος που παρατηρείται σε στελέχη με μεταλλαγές απενεργοποίησης στο γονίδιο *uaZ,* σχετίζεται με την αυξημένη συχνότητα εμφάνισης μορφολογικώς διακριτών τμημάτων σε αποικίες και τη διαφοροποιημένη απόκριση στο οξειδωτικό στρες, στην παραγωγή κονιδιοσπορίων και στην ανθεκτικότητα στη υπεριώδη ακτινοβολία, τα οποία πιθανώς αιτιολογούν τον εντοπισμό στους κονιδιοφορείς. Τέλος, ο ειδικός για το μονοπάτι μεταγραφικός παράγοντας UaY εντοπίζεται τόσο στο κυτταρόπλασμα όσο και στον πυρήνα σε συνθήκες μη-επαγωγής, ενώ υπό συνθήκες επαγωγής με ουρικό οξύ συσσωρεύεται άμεσα και κατ' αποκλειστικότητα στον πυρήνα.

Title: Purine utilization proteins in the Eurotiales: Cellular compartmentalization, phylogenetic conservation and divergence

Article Type: Regular Article

Corresponding Author: Dr. Sotiris Amillis, Ph.D.

Corresponding Author's Institution: National and Kapodistrian University of Athens

First Author: Katerina Galanopoulou

Order of Authors: Katerina Galanopoulou; Claudio Scazzocchio, Professor; Maria E Galinou; Weiwei Liu, Ph.D.; Fivos Borbolis; Mayia Karachaliou; Nathalie Oestreicher, Ph.D.; Dimitris G Hatzinikolaou, Ass. Professor; George Diallinas, Professor; Sotiris Amillis, Ph.D.

Abstract: The purine utilisation pathway has been thoroughly characterised in Aspergillus nidulans. We establish here the subcellular distribution of seven key intracellular enzymes, xanthine dehydrogenase (HxA), urate oxidase (UaZ), 5-hydroxy-isourate hydrolase (UaX), 2-oxo-4-hydroxy-4-carboxy ureido imidazoline carboxylase (UaW), allantoinase (AlX), allantoicase (AaX), ureidoglycolase lyase (UglA), and the fungal-specific α-ketoglutarate Fe(II)-dependent dioxygenase (XanA). HxA, AlX, AaX, UaW and XanA are cytosolic, while UaZ, UaX and UglA are peroxisomal. Peroxisomal localization was confirmed by using appropriate pex mutants. The pathway is largely, but not completely conserved in the Eurotiomycetes, noticeably in some species AaX is substituted by an alternative enzyme of probable bacterial origin. UaZ and the urate-xanthine UapA and UapC transporters, are also localised in specific cells of the conidiophore. We show that metabolic accumulation of uric acid occurring in null mutations in uaZ is associated with an increased frequency of morphologically distinct colony sectors and an altered response of A. nidulans to oxidation stress, conidiospore production and UV resistance, which may provide a rationale for the conidiophore-specific localisation. The pathway-specific transcription factor UaY is localized in both the cytoplasm and nuclei under non-inducing conditions, but it rapidly accumulates exclusively to the nuclei upon induction by uric acid.